

NMR Studies on the Structures and Mechanisms of Oxygenases

Noelle Goodyear

Exeter College, University of Oxford

Trinity Term 2025

A thesis submitted to the University of Oxford for the degree of Doctor of Philosophy

Abstract

NMR Studies on the Structures and Mechanisms of Oxygenases

Noelle Goodyear

University of Oxford, 2025

Oxygenases, that is enzymes that incorporate at least one oxygen atom from O_2 into their catalytic products, play important roles in many biological processes in animals, including oxygen sensing, epigenetic regulation, and metabolism. Despite extensive studies on their structures, principally using crystallography, relatively little research has been conducted to investigate oxygenase dynamics in solution. The work described in this thesis used protein nuclear magnetic resonance (NMR) spectroscopy to study Fe(II)- and 2-oxoglutarate-(2OG)-dependent dioxygenases in solution.

The primary focus of this work (described in **Chapter 2**) was to better understand the interactions of small molecules—including the 2-oxoglutarate and oxygen cosubstrates, metal ions, and inhibitors—with prolyl hydroxylase domain-containing protein 2 (PHD2), which acts as an oxygen sensor in the human hypoxia inducible factor (HIF) system. Studies on a marine-algae-derived Fe(II)- and 2OG-dependent halogenase, WelO5 (from *Hapalosiphon welwitschii UTEX B 1830*), which is of biocatalytic interest, are also described (**Chapter 3**).

Chapter 1 gives an introduction to the fields of 2OG-dependent dioxygenases and the hypoxic response. Upregulation of HIF-mediated transcription works to mitigate the effects of hypoxia, while PHD catalysed HIF-α prolyl hydroxylation signals for degradation of HIF-α. Mutations of pathways involving the HIF system are linked to diseases such as anaemia, diabetes, and cancer. PHD2 is proposed to be the most important sensor of chronic hypoxia. WelO5 is also described, which is of interest as a biocatalyst to enable late-stage halogenation during medicinal chemistry research. **Chapter 1** also introduces methods of protein NMR and the challenges of working with paramagnetic species in NMR studies.

Chapter 2 describes protein-observed NMR studies of PHD2. Components of the PHD2 reaction involved in catalysis were studied, including its metal cofactor, cosubstrate 2OG, its HIF-α substrate, and inhibitors. Importantly, the NMR studies informed on how the PHD2:Fe(II):2OG complex reacts with O_2. Exposure of the PHD2:Fe(II):2OG complex to dioxygen in the absence of HIF-α results in specific changes in the NMR spectrum, corresponding to formation of a new complex. Related changes were found to occur with the PHD2:Fe(II):2OG:HIF-1α complex on exposure to dioxygen, though these changes were

more difficult to interpret, likely due to turnover of 2OG and HIF-1α. These studies led to the discovery that the shielded methyl region (the region below 0 ppm) in the ^{1}H-NMR spectrum is a useful indicator of structural changes at the PHD2 active site. Through study of the shielded methyl region of the ^{1}H-NMR spectra of PHD2, it was discovered that changes in the PHD2:Fe(II):2OG complex in the presence of dioxygen lead to a new form of the PHD2:Fe:2OG complex, which is stable to inhibition involving competition with 2OG. Combined with other studies, the complex formed in the presence of dioxygen is assigned as a PHD2:Fe(III):2OG complex. This complex is highly stable and can reversibly bind HIF-α, which does not undergo reaction. If any component of this PHD2:Fe(III):2OG complex were removed, the resistance to inhibition by 2OG competitors was abolished. These findings open up the possibility of a new interface between the PHDs and O_2 that may be relevant to the oxygen-sensing mechanism of PHD2 in cells. Studies on O_2 interaction with the PHD2:Fe(II):2OG complex also revealed the presence of two unique states of the complex in the absence of dioxygen, as characterised by two sets of peaks in the ^{1}H,^{15}N-HSQC spectrum. These states may be attributed to two distinct protein conformations, a change in the oxidation state or spin state of the active site metal, or some other feature, as described in **Chapter 2**.

As described in **Chapter 3**, a second focus of the work was studies on the Fe(II)- and 2OG-dependent halogenase, WelO5, which has a similar proposed mechanism to that of PHD2 but carries out halogenation. The dynamics of WelO5 in solution have not been previously studied, so methods similar to those carried out on PHD2 were utilised. The results revealed important differences in the structures and dynamics of PHD2 and WelO5 that may be related to their hydroxylation and halogenation potentials, respectively. These include reduced stability of the WelO5:Fe(II):2OG and WelO5:Zn(II):2OG complexes compared to the PHD2 counterparts; notably the ^{1}H,^{15}N-HSQC spectrum of the anoxic WelO5:Fe(II):2OG complex indicated no changes on addition of O_2, contrasting with the PHD2:Fe(II):2OG complex.

The overall results further demonstrate that protein NMR is a useful tool for analysing structural changes in the active site of Fe- and 2OG-dependent dioxygenases. These results also reveal a new potential interface between the PHDs and O_2 and support the proposal that the catalytic properties of the PHDs are unusual compared to other 2OG-dependent dioxygenases.

Table of Contents

Abstract ..... *ii*

Contents ..... *iv*

Acknowledgements ..... *v*

Abbreviations ..... *vi*

Chapter 1: Introduction *1-1*

Chapter 2: Studies on the Structure and Dynamics of PHD2 ..... *2-1*

Chapter 3: Studies on the Structure and Dynamics of WelO5 ..... *3-1*

Chapter 4: Appendix *4-1*

Chapter 5: Methods *5-1*

Chapter 6: Summary and Future Work *6-1*

Acknowledgements

First, I would like to thank my supervisors, Professor Timothy Claridge and Professor Christopher Schofield for being the most amazing supervisor duo. They have had a profound impact on my work, on how I've developed as a chemist and researcher, and on my understanding of how to offer compassionate guidance in a professorship role. They, and the Oxford environment, have helped me develop as a person far beyond what I thought possible and have furthered my resolve to become a professor. I would like to thank Martine Abboud, whose strength and knowledge I will never forget. Thanks for not giving up on me when I was learning and struggling with new biology knowledge and concepts.

I would also like to thank the Schofield and Claridge groups for becoming my families away from home, and all the wild and fascinating conversations we've had throughout the years. Thanks to my fellow basement gremlins, who learned to live without sun and who were the silliest group of people. You taught me a lot of useful NMR knowledge through our casual conversations. Thanks to Patrick Rabe and Jos Kamps, who were my first friends in the UK and who have been some of the absolute kindest people I have ever met. I appreciate you both for your guidance and friendship. Thanks to Sam Atwal and Jimmy Wang for bringing fun and conversation to my late night and weekend NMR runs, and for your friendship as well.

I would like to dedicate this thesis to my parents and brother, Madison, who have never given up on me through troubled times and have always been the foundation that has kept me standing. I wouldn't have made it this far without your enduring love and support. You will always be the most important people in my life and I can't imagine a world without you. And thanks to all my family, who has been rooting for me since the beginning. I hope I have done you all proud; I love you all.

Abbreviations

1-D	1 dimensional
2-D	2 dimensional
2HG	(R)-2-hydroxyglutarate
2OG	2-oxoglutarate
3-D	3 dimensional
ACV	δ-(L-α-aminoadipyl)-L-cysteinyl-D-valine
AlkB	bacterial protein involved in cellular recovery from alkylation damage
apo	without bound ion/metal
asc	ascorbate
CODD	C-terminal oxygen dependent degradation domain
comp. 84	compound 84 (a possible PHD2 enhancer)
CPMG	Carr-Purcell-Meiboom-Gill
DMSO	dimethyl sulphoxide
EDTA	ethylenediaminetetraacetic acid
EPO	erythropoitin
EPR	electron paramagnetic resonance spectroscopy
FG-4592	a clinically approved PHD2 inhibitor
FIH	factor inhibiting HIF
fum	fumarate
GLUT1	glucose transporter 1
HIF	hypoxia induceable factor
His tag	an amino acid sequence of at least 6 histidines at the C or N terminal of a protein used in purification
HMQC	heteronuclear multiple quantum coherence
H_N	region of the hydrogen spectrum where hydrogens connected to nitrogens are found
HNCA	describes a transfer of resonance from hydrogen to nitrogen to alpha carbon
HNCACB	describes a transfer of resonance from hydrogen to nitrogen to alpha carbon to beta carbon
HNCACO	describes a transfer of resonance from hydrogen to nitrogen to alpha carbon to carbonyl
HNCO	describes a transfer of resonance from hydrogen to nitrogen to carbonyl
HNCOCA	describes a transfer of resonance from hydrogen to nitrogen to carbonyl to alpha carbon

HNCOCACB	describes a transfer of resonance from hydrogen to nitrogen to carbonyl to alpha carbon to beta carbon
HSQC	heteronuclear single quantum coherence
INEPT	insensitive nuclei enhanced by polarisation transfer
IPNS	isopenicillin N synthase
IPTG	isopropyl B-D-1-thiogalactopyranoside
K_D	dissociation constant
k_{on}	the rate of formation of the protein:ligand complex
k_{off}	the rate of dissociation of the protein:ligand complex
MYND	myeloid, Nervy, and DEAF-1
NaAsc	sodium ascorbate
NMR	nuclear magnetic resonance
NO	nitric oxide
NODD	N-terminal oxygen dependent degradation domain
NOG	N-oxalyl glycine
NUS	non-uniform sampling
PDB	protein data bank
PHD	prolyl hydroxylase domain containing protein
PHD2	prolyl hydroxylase domain containing protein 2
ppm	parts per million
PRE	paramagnetic relaxation enhancement
PROJECT	Periodic Refocusing of J Evolution by Coherence Transfer
rHuEPO	recombinant human erythropoietin
SDS-PAGE	sodium dodecylsulfate polyacrylamide gel electrophoresis
SHIFTX2	methyl shift prediction program
SOFAST	selective optimised flip angle short transient
SNR	signal-to-noise ratio
succ	succinate
T1	longitudinal relaxation time constant
T2	transverse relaxation time constant
Tris	tris(hydroxymethyl)aminomethane
Tris-D_{11}	tris(hydroxymethyl) aminomethane with deuterated protons
VEGF	vascular endothelial growth factor
VHL	Von Hippel Lindau tumour suppressing protein
VO	vanadium oxide
WelO5	halogenation enzyme derived from the marine algae Hapalosiphon welwitschii UTEX B 1830
wt	wild-type

Chapter 1:

Introduction

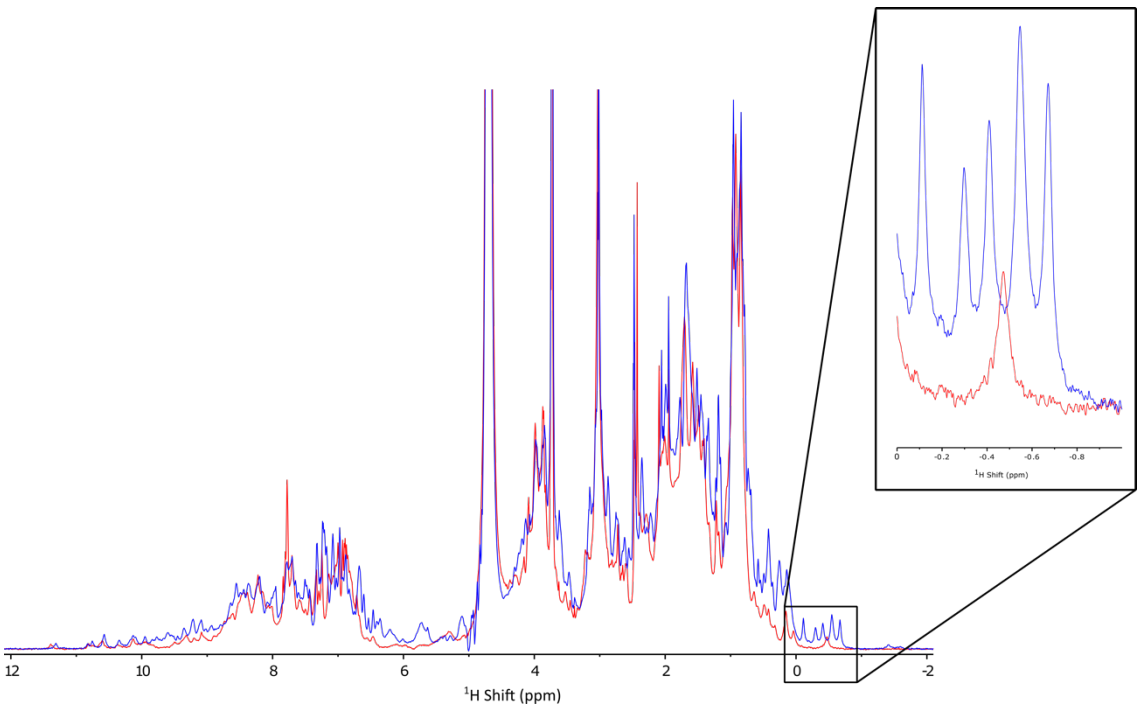


Table of Contents

Chapter 1: 1-1

1.1 Biological Systems Studied 1-3
1.1.1 Overview 1-3
1.1.2 Prolyl Hydroxylase Domain-Containing Protein 2 (PHD2) 1-3
1.1.2.1 Biological Function of PHD2 1-5
1.1.2.2 Catalytic Mechanism of PHD2 and Other 2OG-Dependent Dioxygenases 1-8
1.1.2.3 The Proposed Oxygen Sensing Mechanism of PHD2 1-11
1.1.2.4 Inhibition of PHD2 1-14
1.1.2.5 CODD/NODD Interactions with PHD2 1-15
1.1.3 WelO5 1-17
1.1.3.1 Biocatalysis in Drug Synthesis 1-17
1.1.3.2 Biological Function of WelO5 1-18
1.1.3.3 Mechanism of WelO5 1-19

1.2 Protein NMR 1-20
1.2.1 Overview 1-20
1.2.2 ^{1}H NMR 1-22
1.2.2.1 Ligand-Observed ^{1}H NMR 1-22
1.2.2.1.1 Carr-Purcell-Meiboom-Gill (CPMG)-Edited ^{1}H Experiments 1-22
1.2.2.2 Protein-Observed ^{1}H NMR 1-27
1.2.3 ^{1}H, ^{15}N-HSQC NMR 1-28
1.2.3.1 Protein:Ligand ^{1}H,^{15}N-HSQC 1-29
1.2.3.1.1 Slow, Intermediate, and Fast Ligand Exchange 1-30
1.2.3.2 Protein Peak Shift Mapping 1-31
1.2.4 Three-Dimensional NMR 1-32
1.2.5 Paramagnetic Effects 1-38
1.2.5.1 Paramagnetic Dipolar Relaxation Enhancements (PRE) 1-38
1.2.5.2 Paramagnet-Induced Shifts 1-39

1.3 Overall Aims of the Work Described in this Thesis 1-41

1.4 References 1-44

1.1 Biological Systems Studied

1.1.1 Overview

Dioxygen (O_2, hereafter oxygen) is an essential energy source for all aerobic lifeforms, including humans. Complex multicellular organisms have established systems to deliver oxygen to cells and mechanisms for responding when oxygen supply becomes limiting, a situation termed hypoxia. It has long been known that limiting oxygen availability, for example on going to high altitude, can induce physiological responses in humans, such as increased red blood cell production (erythropoiesis). [1] Until relatively recently, however, the cellular details of how humans and other animals respond to hypoxia in order to elicit physiological responses were not well understood. [1] Work over the last three decades or so has defined key elements of the hypoxic response in humans, though many details remain to be defined. [2] Indeed, the available evidence is that pathways through which biology interacts with oxygen are highly complex; furthermore, although dioxygen is essential for aerobic lifeforms, excessive oxygen can be damaging. [3] This thesis describes molecular studies on prolyl hydroxylase domain-containing protein 2 (PHD2), which is a key player in human oxygen homeostasis. The ultimate aim of the research was to inform on the details of the hypoxic response in humans and providing a better understanding of how oxygen interacts with proteins.

1.1.2 Prolyl Hydroxylase Domain-Containing Protein 2 (PHD2)

A breakthrough in understanding the hypoxic response in humans came with the discovery of the α,β-hypoxia inducible transcription factor (HIF). [4] HIF works to promote the expression of genes that oppose the negative effects of hypoxia, including those encoding for erythropoietin (EPO), which promotes red blood cell production, and vascular endothelial growth factor (VEGF), which promotes blood vessel formation. [5]

Crucially, levels of HIF-α but not HIF-β were shown to be negatively regulated by oxygen availability, providing a mechanism for oxygen dependent regulation of transcription. [5] A key process in HIF-α mediated degradation was shown to involve its post-translational prolyl hydroxylation, an oxygen-availability-limited process that signals for HIF-α degradation by the ubiquitin-proteasome system. [1] [6]

Prolyl hydroxylase domain-containing protein 2 (PHD2) is an Fe(II)- and 2-oxoglutarate (2OG)-dependent oxygenase that catalyses the post-translational C-4 prolyl hydroxylation of α–subunits of HIF. [1] There are approximately seventy human 2OG-dependent oxygenases, [7] and PHD2 is one of three PHD isoforms (PHD 1-3) that are involved in the humans hypoxic response. [1] PHD2 is distinguished from PHD1 and PHD3 by the presence of an N-terminal MYND type zinc finger domain, which is reported to help recruit its HIF-α substrates. [8] Whereas PHD1 and PHD3 are reported to be found in specific tissues (e.g. PHD1 in the testes and PHD3 predominantly in the heart), PHD2 is ubiquitously present in the bodily tissues of humans and, unlike PHD1 and PHD3 is conserved throughout the animal kingdom. [1] [6] [9] This introduction summarises the biological roles and importance of PHD2 as well as methods used to inhibit its function.

A view of the PHD2 active site and the reaction that it catalyses is provided in **Figure 1.1**. Like most other 2OG dependent oxygenases, PHD2 contains a core distorted jelly-roll, double stranded beta-helix (DSBH), or cupin fold, which is comprised of eight strands (one of which is often distorted). [10] Together with surrounding elements, the core cupin fold of the 2OG oxygenases supports binding of a single Fe(II) ion at the active site. [11] The Fe(II) of the PHDs is coordinated by a conserved His-X-Asp…His motif that is present in most, but not all, studied 2OG oxygenases. [11] The cupin fold also supports the binding of 2OG, which coordinates the Fe(II) in a bidentate manner via its

C1 carboxylate and C-2 ketone groups. All three of the human PHDs catalyse the *trans* C-4 prolyl hydroxylation of their HIF-α substrates; such hydroxylation promotes a change in the preferred conformation of the proline substrates, that is from the C4 *endo* to the C4 *exo* conformation in the *trans* C-4 prolyl hydroxylated products (**Figure 1.1**). [12]

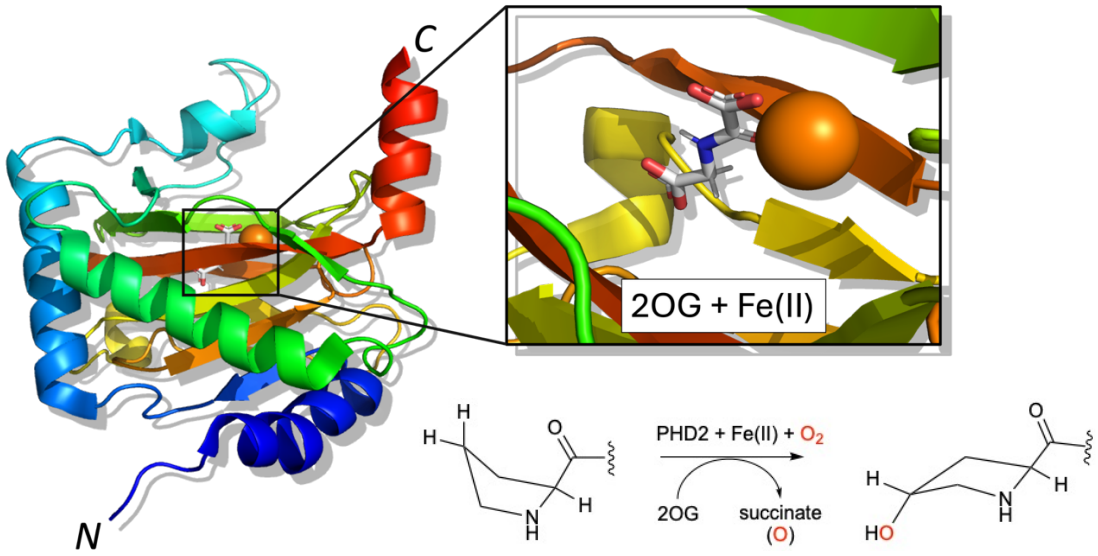


Figure 1.1 *View from a crystal structure of PHD2 in complex with Fe(II) and N-oxalylglycine (NOG, which is a structural mimic of 2OG)(PDB: 5L9R). A close-up view of the active site of PHD2 is shown in the inset. C4 prolyl hydroxylation of HIF-α substrates proceeds through the C4 endo conformation of the prolyl residue which, on hydroxylation, is predominately observed in the C4 exo conformation. [12]*

1.1.2.1 Biological Function of PHD2

There is extensive evidence, including from genetic and inhibition studies, that the PHDs play important cellular roles in the hypoxic response in human biology. [1] [2] [6] [13] Under normoxic conditions (normal oxygen levels), the PHDs efficiently catalyse hydroxylation of the *C*-terminal and *N*-terminal oxygen-dependent degradation domains (NODD at Pro-402 of HIF-1α and CODD at Pro-564 of HIF-1α, respectively) of hypoxia-inducible factor α (HIF-α) isoforms, of which there are three in humans (HIF-1-3α). [1] [6] Whereas PHD3 acts preferentially on the CODD domains, PHD1 and

PHD2 catalyse prolyl-hydroxylation of both the NODD and CODD domains of HIF-1α and HIF-2α and the CODD domain of HIF-3α, the latter of which does not contain a NODD domain. [6]

PHD catalysed HIF-α prolyl-hydroxylation promotes binding of HIF-α to VHL (the Von Hippel Lindau tumour suppressing protein), which is a targeting component of a ubiquitin-ligase system for protein degradation via proteasome catalysed hydrolysis. [1] [6] [13] The VHL:ubiquitin-ligase complex adds ubiquitin to lysine residues in prolyl-hydroxylated HIF-α isoforms, leading to their hydrolytic degradation by proteasomes. [14]

When oxygen levels become low (hypoxia), PHD catalysis decreases and HIF-α levels rise, leading to the translocation of HIF-α to the nucleus. In the nucleus, HIF-α combines with HIF-β. The α,β-HIF complex then binds to hypoxia response elements in promoter regions of HIF target genes, promoting their transcription (**Figure 1.2**). [1] [5] [6] α,β-HIF has the capacity to promote upregulation of multiple genes, including those encoding for EPO (erythropoietin), VEGF (vascular endothelial growth factor), and GLUT1 (glucose transporter 1), which have roles in the regulation of erythropoiesis, angiogenesis, and glucose uptake into cells respectively. [5] [15] [16] [17] The actions of these genes/proteins help to compensate for the effects of hypoxia. It is important to appreciate that the factors regulating HIF target genes expression depend on the context—in a manner that is poorly understood. For example, whether and how the PHDs differentially regulate the various HIF-α isoforms (HIF-1-3α) is unclear.

Interestingly, another 2OG oxygenase, factor inhibiting HIF (FIH), is reported to regulate HIF mediated expression by catalysing asparagine hydroxylation of HIF-1/2α, a post translational modification reported to hinder interaction of HIFα with histone acetyl transferases [1] [6]: enzymes that promote transcription by transfer of acetyl

groups to lysine residues at the N-terminal region of histones in order to weaken histone-DNA and nucleosome-nucleosome interactions. [18] Aside from the role of the HIF system in a healthy hypoxic response, the HIF system is also involved in diseases such as anaemia, diabetes, and cancer, especially a form of kidney cancer where the *VHL* gene is mutated. [13]

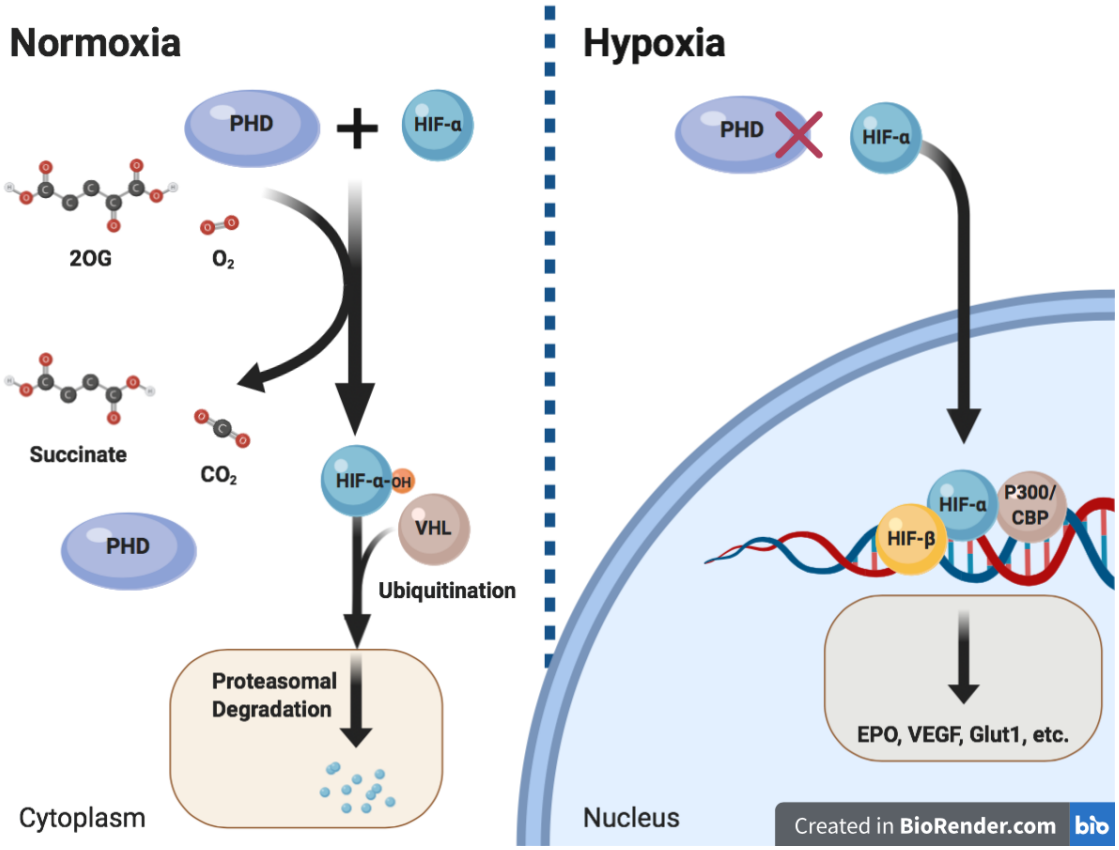


Figure 1.2 *Summary of the biological function of the PHDs. Under normoxia (normal oxygen conditions), the PHDs catalyse the C4 trans-hydroxylation of specific prolyl residues in the CODD or NODD domains of HIF-α isoforms. This causes ubiquitination and, subsequently, proteasomal degradation of HIF-α. Under hypoxic (low oxygen) conditions, HIF-α escapes degradation and enters the nucleus where it binds with HIF-β to form a transcriptionally active α,β-HIF which promotes expression of genes such as EPO, VEGF, and GLUT1.*

1.1.2.2 Catalytic Mechanism of PHD2 and Other 2OG-Dependent Dioxygenases

Studies extending over decades have led to a consensus mechanism for the Fe(II)- and 2OG-dependent oxygenases, of which the key elements are thought to be applicable to the catalytic mechanisms of the PHDs, in particular the mechanism of PHD2. [10] [19] [20] [21] At the start of the catalytic cycle, the active site Fe(II) is coordinated by a facial triad of residues (consisting of two histidyl residues and one aspartyl residue) and two or three water molecules (**Figure 1.3**). 2OG then binds to the active site Fe(II) in a bidentate manner, causing displacement of two of the bound water molecules. The substrate, HIF-α in the case of the PHDs, then binds to the active site with the prolyl residue in close proximity to the Fe(II). In some, but not necessarily all, cases, substrate binding weakens binding of the remaining ligated water molecule, opening a vacant site for triplet state O_2 to bind to the Fe(II) and be activated for reaction with 2OG. [11] There is, however, evidence that displacement of the Fe-coordinating water does not necessarily occur in the case of PHD2, potentially reflecting its unusually slow reaction with O_2, a property proposed to reflect its role as a hypoxia/O_2 availability sensor. [22] Reaction of O_2 with the active site Fe(II) likely forms an Fe(III)-superoxide complex. There is recently reported crystallographic evidence for an Fe(III)-superoxide intermediate from studies on isopenicillin N synthase (IPNS), which is structurally and mechanistically related to the Fe(II) and 2OG-dependent dioxygenases, [23] [24] but which does not employ 2OG as a cosubstrate. In the case of 2OG-dependent dioxygenases, the Fe(III)-superoxide can then react with the keto group of 2OG to give a peroxysuccinate intermediate and CO_2, the latter of which likely leaves the active site. The peroxysuccinate intermediate then fragments to give a Fe(IV)=O (ferryl) intermediate and succinate, the latter adopting a monodentate binding mode. The Fe(IV)=O intermediate then stereoselectively abstracts a hydrogen from the prolyl residue, forming a prolyl radical and reducing the Fe(IV) to

an Fe(III). [25] The prolyl radical then abstracts the hydroxyl group from the Fe(III)-OH intermediate in a rebound process, forming the hydroxylated HIF-α product and reducing Fe(III) to Fe(II). Succinate and product are released to regenerate the enzymatic activity. [26]

As further evidenced by the research described later in this thesis, there is evidence that PHD2 may not completely follow the current consensus mechanism for 2OG-dependent dioxygenases; this may be in a manner related to its slow reaction with O_2, something in turn proposed to reflect its oxygen sensing role. [27] [28] [29] Notably, PHD2 forms an unusually tight complex with Fe(II) and 2OG, and the Fe(II) coordinated water is present even when HIF-α is complexed with PHD2, [30] [31] thus may affect the mode of oxygen binding.

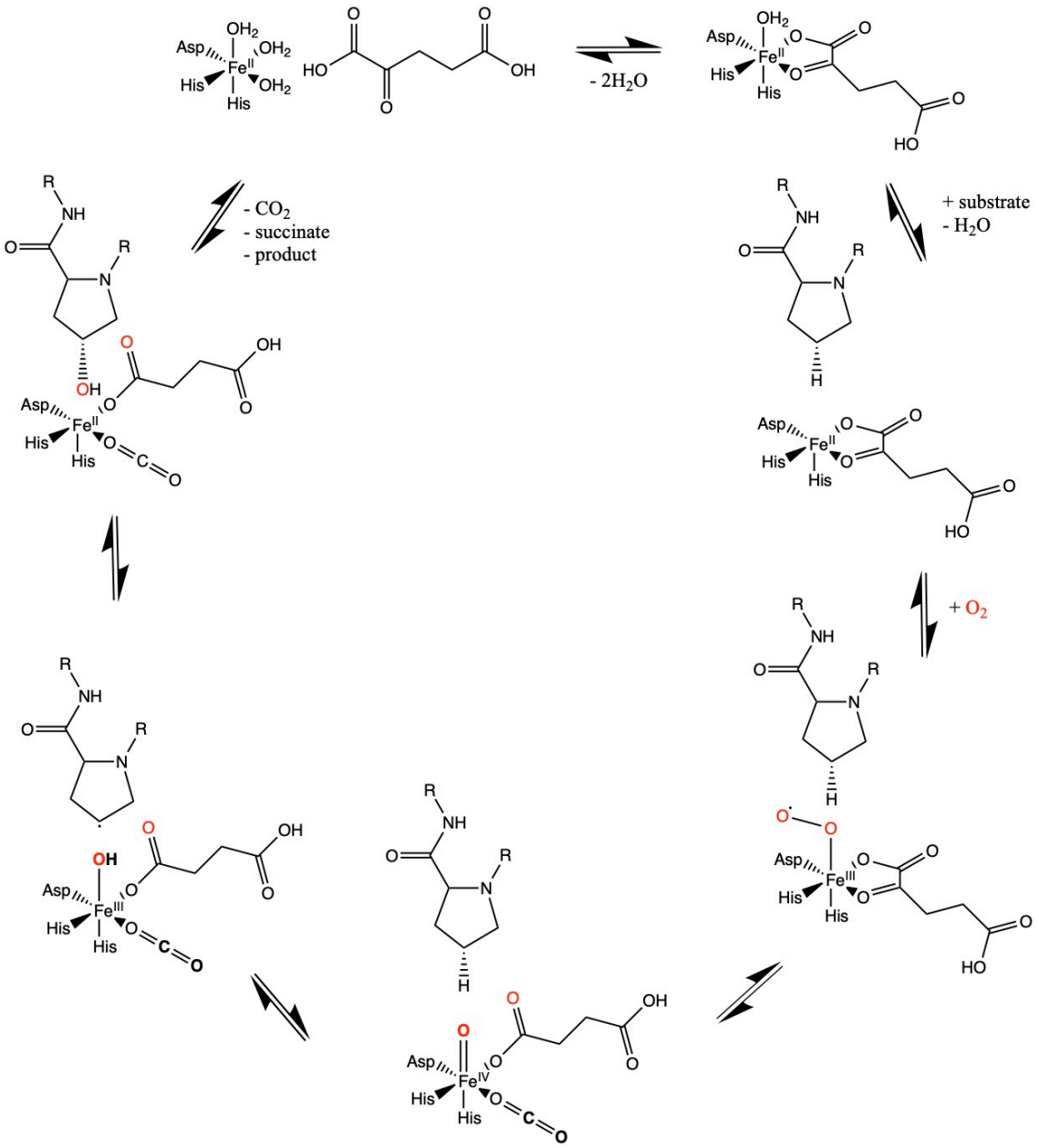


Figure 1.3 *Consensus mechanism for 2OG-dependent dioxygenases as applied to PHD catalysis for prolyl hydroxylation of HIF-α. Note that the rates of each steps may be different and variations on the consensus may occur (in particular the possibility of a peroxysuccinate intermediate [26]); note that the Fe-complexed water may remain after HIF-α substrate binding to the PHD2 active site. [32]*

Although crystallographic and other biophysical studies reveal that PHD2 contains the key elements present in other 2OG-dependent dioxygenases, [33] these studies have not revealed information on exactly how oxygen binds at the active site of the PHDs or why PHD2 reacts unusually slowly with oxygen. [32]

1.1.2.3 The Proposed Oxygen Sensing Mechanism of PHD2

Dioxygen is a unique diatomic molecule that is ubiquitous in the aerobic natural world and has shaped the progression of life on earth. The importance of oxygen in biology is likely, in part, due to its water solubility, preferred triplet electronic state, and capacity to act as an energy source. PHD2, as is the case for all oxygenases, is dependent on oxygen for its function (as described in Section **1.1.2.1**). The reaction of PHD2 with oxygen is unusually slow; [27] [28] [29] the nature of catalysis by PHD2 may be key to its role as an oxygen sensing enzyme. Little is currently known, however, about the chemical details of how oxygen initially interacts with PHD2. Elucidating the step at which PHD2 catalysis is rate-limited may provide insight into the oxygen sensing mechanism.

There are several factors that may impact the rate of oxygen reaching the active site of PHD2 and, therefore, impact its function as an oxygen sensor. One such factor is the hydrophobicity or hydrophilicity of channels leading to the active site; there is potential for oxygen to interact both with hydrophobic and polar groups (e.g. OH or NH groups). Computational analyses suggest that oxygen molecules may easily pass from solvent through the protein matrix of PHD2, but its progress may be slowed at the junction between the oxygen passage channel and the active site. [32] The PHD2 active site contains both hydrophobic and hydrophilic groups (including residues from the substrate) that may interact with the oxygen and slow its progression towards active-site binding, possibly contributing to the oxygen sensing property of PHD2.

Another factor that may impact the speed of oxygen binding to the PHD2 active site is the position of other Fe-ligands at the active site. Though the consensus 2OG-dependent dioxygenase mechanism suggests that HIF-α binding might help to displace an Fe(II)-bound water molecule, which frees up a space for oxygen binding, it is also

possible that the initially bidentate-bound 2OG switches to monodentate binding (briefly) to allow for oxygen binding. Some experimental results described in this thesis suggest a non-consensus mechanism for PHD2 (see Chapter 2, **Figure 2.95**). [32]

A third factor that may impact the rate of oxygen binding to, and reaction at, the PHD active site is the oxidation state and properties of the active site Fe metal. [34] [35] This is an important factor in understanding metal binding since triplet state oxygen is paramagnetic and will interact more strongly with other paramagnetic species than diamagnetic species (a description of paramagnetic strengths of various transition metals is provided in **Table 1.1**). Further discussion of the properties of various metalloprotein:metal complexes [36] [37] [38] [39] will be discussed, including PHD2 and WelO5 complexes in **Chapter 2** and **Chapter 3** of this thesis respectively.

Metal	d^n	S	μ_{eff} (BM)
Sc(III)	0	0	0
Ti(III)	1	½	1.7-1.8
V(III)	2	1	2.7-2.9
Cr(III)	3	3/2	3.7-3.9
Mn(III)	4	2	4.8-4.9
Fe(III)	5	5/2	5.7-6.0
Fe(II)	6	2	5.0-5.6
Co(II)	7	3/2	4.3-5.2
Ni(II)	8	1	2.9-3.5
Cu(II)	9	½	1.8-2.1
Zn(II)	10	0	0

Table 1.1 *The paramagnetic strength of 3d orbital transition metals. d^n indicates the number of 3d orbital electrons, S indicates the overall spin of the electrons, and μeff indicates the effective magnetic moment. The higher the effective magnetic moment, the more paramagnetic the species and, therefore, the more effect it will have on nearby nuclei. [40]*

The paramagnetism of oxygen is important to consider in the case of PHD2, which hosts an Fe(II) ion at its active site. Depending on the spin state of the Fe(II), it can either be diamagnetic (low spin) or paramagnetic (high spin). Once dioxygen binds, Fe(II) is likely oxidized to an Fe(III) superoxide complex, which can be in either a high or low spin paramagnetic state (***Figure 1.4***). Understanding both the magnetic state and spin state of the metal at the protein active site is important for understanding how dioxygen binds to PHD2.

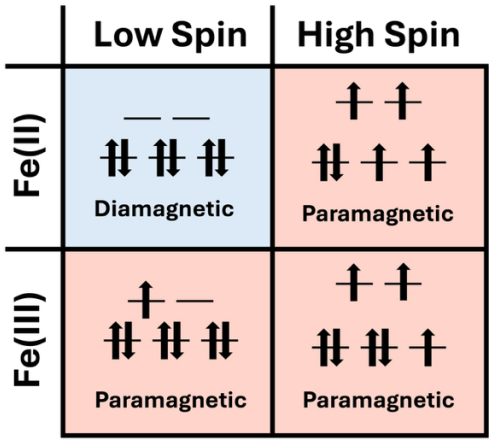


Figure 1.4 *Possible spin states and oxidation states of Fe(II) and Fe(III) in the PHD2:Fe(II):2OG:±O_2 complex. Columns indicate spin states and rows indicate oxidation states. Low spin Fe(II) is diamagnetic while all other spin/oxidation state combinations yield paramagnetic species.*

1.1.2.4 Inhibition of PHD2

Inhibition of the PHDs is a useful tool for treatment of anaemia patients. Though anaemia can have many causes, the result is insufficient levels of oxygen carried to the tissues. An important drug that has been useful in the treatment of anaemia is rHuEPO (recombinant human erythropoietin), [41] which was developed in the 1980s. Though useful in the treatment of anaemia, issues such as high blood pressure, high blood viscosity, and platelet-activation-caused cardiovascular complications are problems with rHuEPO. [42] Small molecule inhibitors of the PHDs offer an alternative, orally active method of treating anaemia, possibly with fewer complications. [22] [33] [43]

Though diseases such as anaemia benefit from the upregulation of HIF-1/2α due to their roles in the upregulation of genes involved in EPO and heme red blood cell production, treatment of other diseases, including cancer, may respond uniquely to regulation of PHD activity. [44] [45] Since some tumours grow rapidly, formation of vasculature throughout the tumour is important for the survival and proliferation of tumour cells, which need oxygen to survive. Upregulation of HIF-1/2α can lead to the

upregulation of VEGF, which is responsible for the formation of vasculature and, therefore, is proposed to promote tumour survival and growth. [46] [47] Enhancers—as opposed to inhibitors—of PHD2 might help stop tumour proliferation by decreasing HIF-1/2α levels; PHD enhancers that act directly have not been reported.

PHD inhibitors developed for treatment of anaemia in chronic kidney disease typically contain a metal chelating group that can interact with the active site metal in a bidentate binding mode, similarly to 2OG binding (**Figure 1.5**). [22] [33] [43] Commonly employed functional groups in 2OG-dependent dioxygenase inhibitors include the 1,3-carbonyl moiety, which is thought to bind to the Fe(II) in its enolate form, and glycinamide side-chain groups, [48] [49] which are present in some PHD inhibitors that are currently in clinical use or in clinical trials (**Figure 1.5**). [50] [51] [52] The three most important interactions explored in PHD inhibitors to date are the bidentate binding mode to the Fe(II) centre [53] and polar interactions with PHD2 Tyr329 and Arg383, [22] [54] [55] which are involved in binding the C5 carboxylic acid of 2OG.

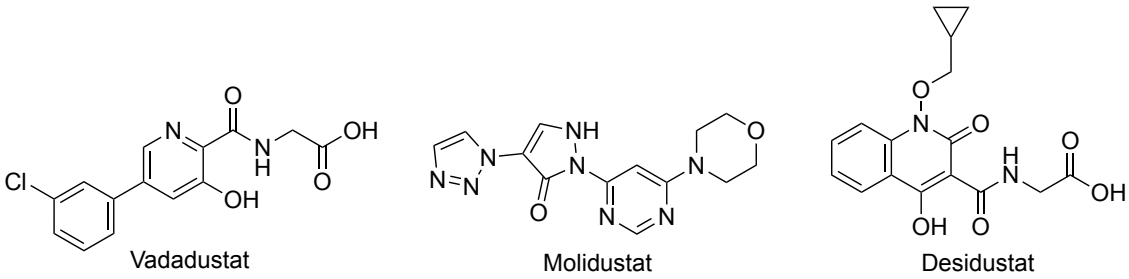


Figure 1.5 *Examples of PHD inhibitors in clinical use. All these inhibitors bind to the active site Fe(II) in a bidentate manner and compete with 2OG for binding.*

1.1.2.5 CODD/NODD Interactions with PHD2

As stated earlier, hydroxylation of prolyl residues in HIF-1/2α occurs at two different sites which are denoted as NODD and CODD (on residues Pro-402 and Pro-564 in HIF-1α, respectively). [1] [6] Though hydroxylation can occur at both NODD and CODD sites, it is important to consider the differences between the sites and how these

differences may impact proteasomal degradation. A factor that differentiates CODD and NODD hydroxylation in cells is the oxygen level at which hydroxylation occurs. CODD is thought to be hydroxylated at oxygen levels as low as 0.5% whereas NODD is only hydroxylated at levels greater than 2%. [56] This difference is possibly, at least in part, due to the greater binding strength of CODD to PHD2 as opposed to NODD/PHD2 binding; [56] the greater binding strength possibly leading to stronger protein:substrate interactions.

The binding of NODD and CODD to PHD2 involves an induced fit mechanism, but the regions in which structural changes of PHD2 occur differs somewhat for the NODD and CODD domains. [31] On CODD and NODD binding, a loop region located between the β2/β3 strands folds over the substrate to help lock the substrate in a catalytically productive manner. [13] [31] [57] Inward movement of the C-terminal α-helix is induced on both CODD and NODD binding, but the available evidence is that a more functionally interesting interaction might occur in the case of CODD. [13] Mutation studies indicate that the presence of L574 of HIF-1α is necessary for CODD binding, but an analogous Leu residue is not present with the NODD of HIF-1α. There is evidence that NODD binding may involve interactions with the R370-R371 residues of PHD2. [31]

Interestingly, the VHL protein also interacts more strongly with the hydroxylated CODD than the hydroxylated NODD, [31] suggesting CODD hydroxylation may be more important for HIF-α proteasomal degradation compared to NODD hydroxylation; this hypothesis is consistent with the observation that CODD in more conserved than NODD during animal evolution. [31]

1.1.3 WelO5

WelO5, derived from the marine algae *Hapalosiphon welwitschii UTEX B 1830*, is a 2OG- and Fe(II)-dependent halogenase with a mechanism related to that of 2OG dependent hydroxylases such as PHD2 (**Figure 1.1**). [58] WelO5 is one of five enzymes responsible for the stepwise conversion of 12-*epi*-fischerindole U into welwitindolinone C, where its role is to convert the starting material to 12-*epi*-fischerindole G, the chlorinated product and an intermediate step in the complete synthesis. [58] The reaction catalysed by WelO5 is shown in **Figure 1.6**. Due to the mild nature of the enzyme catalysed oxidative chlorination of WelO5, as compared to many chemical methods of oxidative chlorination, WelO5 may be a useful catalyst for chlorination of medicinally relevant / biologically active molecules. [59] In the text below, studies on WelO5 will be described in relation to PHD2 to outline the value of working with these two proteins in tandem.

1.1.3.1 Biocatalysis in Drug Synthesis

There are several advantages to employing biocatalysis in drug and agrochemical production. Whereas chemical catalysis often uses harsh conditions and toxic chemicals to achieve the desired reactions, these means are often not viable in living organisms and, therefore, enzymes have evolved to carry out the same molecular mechanisms under more mild conditions. [60] [61] Benefits of biocatalysis over chemical catalysis include the use of lower reaction temperatures (therefore, requiring less energy), the stability of enzymes as reusable catalysts, use of aqueous solvents (which limit waste and associated costs), and the ability to functionalise compounds at positions which are often inaccessible by chemical means. [62] Because of the specific shape of the enzyme active site pockets, stereoselectivity of functionalisation is also commonly achieved. [63]

One often encountered disadvantage of biocatalysis is the narrow substrate scope of enzymes as compared to chemical catalysts. The shape of the active site of an enzyme is often tailored to fit a specific substrate or substrate type, because specificity is important in biological systems. To allow for a broader range of substrates, mutation of active site residues can be useful. These mutations can be carried out systematically (separately mutating each active-site residue) with the specific shape and polarity of the substrate in mind or can be carried out empirically via random mutagenesis (targeted to specific regions). [64] With a larger substrate scope, these enzymes can be used for modification of a greater range of molecules.

1.1.3.2 Biological Function of WelO5

Chlorine is present in many drugs, as it can enhance the electronegativity of the attached carbon and increase bioactivity. Many drugs—used in the treatment of cancers, AIDS, and other major diseases—have been either naturally produced by an intermediate with a chloro-group or are synthesized with a chloro-group. [65] The stereoselective oxidative installation of chlorine atoms under mild conditions is a challenge, and further research into methods to achieve this may be beneficial to the discovery of new, biologically active molecules.

What differentiates WelO5 from similar halogenases is its ability to stereo-specifically chlorinate its substrate at an unactivated, sp^3 hybridised carbon without the aid of a carrier protein—something commonly used by halogenases. [66] Very little information is reported on the solution-state dynamics and structure of WelO5.

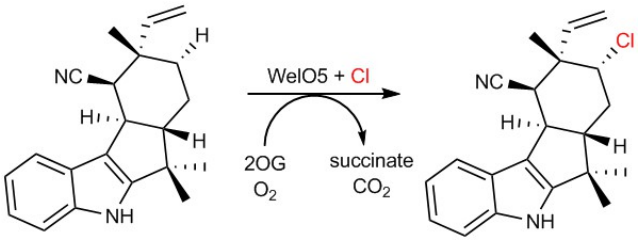


Figure 1.6 *The chlorination reaction catalysed by WelO5.*

1.1.3.3 Mechanism of WelO5

Like other 2OG-dependent halogenases, WelO5 uses two histidine residues to coordinate its active site Fe(II) (**Figure 1.7**). [58] The WelO5 active site thus differs from 2OG-dependent hydroxylases, like PHD2, which have an additional aspartate/glutamate residue coordinated (where the two histidine residues and one glutamate/aspartate residue make up a facial triad) (**Figure 1.1**). The absence of a third active site coordinating residue makes space for chloride ion binding to the WelO5 active site Fe(II), along with two histidine residues and a water. The mechanism of WelO5 halogenation is inferred from the consensus mechanism of both 2OG-dependent hydroxylases (**Figure 1.3**) and non-heme iron 2OG-dependent halogenases. 2OG complexes to the Fe(II) in a bidentate manner along with one water molecule. [66] Substrate then binds, leading to dioxygen binding, which displaces the Fe(II) coordinated water (possibly with the help of substrate). [67] [68] The Fe-coordinated dioxygen then reacts with 2OG, forming succinate and carbon dioxide, and oxidising Fe(III) to Fe(IV). The oxygen atom of the Fe(IV)=O (ferryl) intermediate then abstracts a hydrogen from the position where chlorination will occur. At this stage, rather than transferring a hydroxyl group as occurs with a hydroxylase such as PHD2 (**Figure 1.3**), the Fe-coordinated chlorine atom is transferred to the radical. The difference in reaction is thought to be related to the position of the substrate in the active site pocket, [69] but the precise reasons for chlorine atom transfer over hydroxyl group transfer in the course of hydroxylation remain unclear. This has led to interest in modifying the active site residues of WelO5 to try and observe preference for hydroxylation over halogenation in some mutants. This may lead to a better understanding of hydroxylation and halogenation mechanisms for medicinal chemistry purposes.

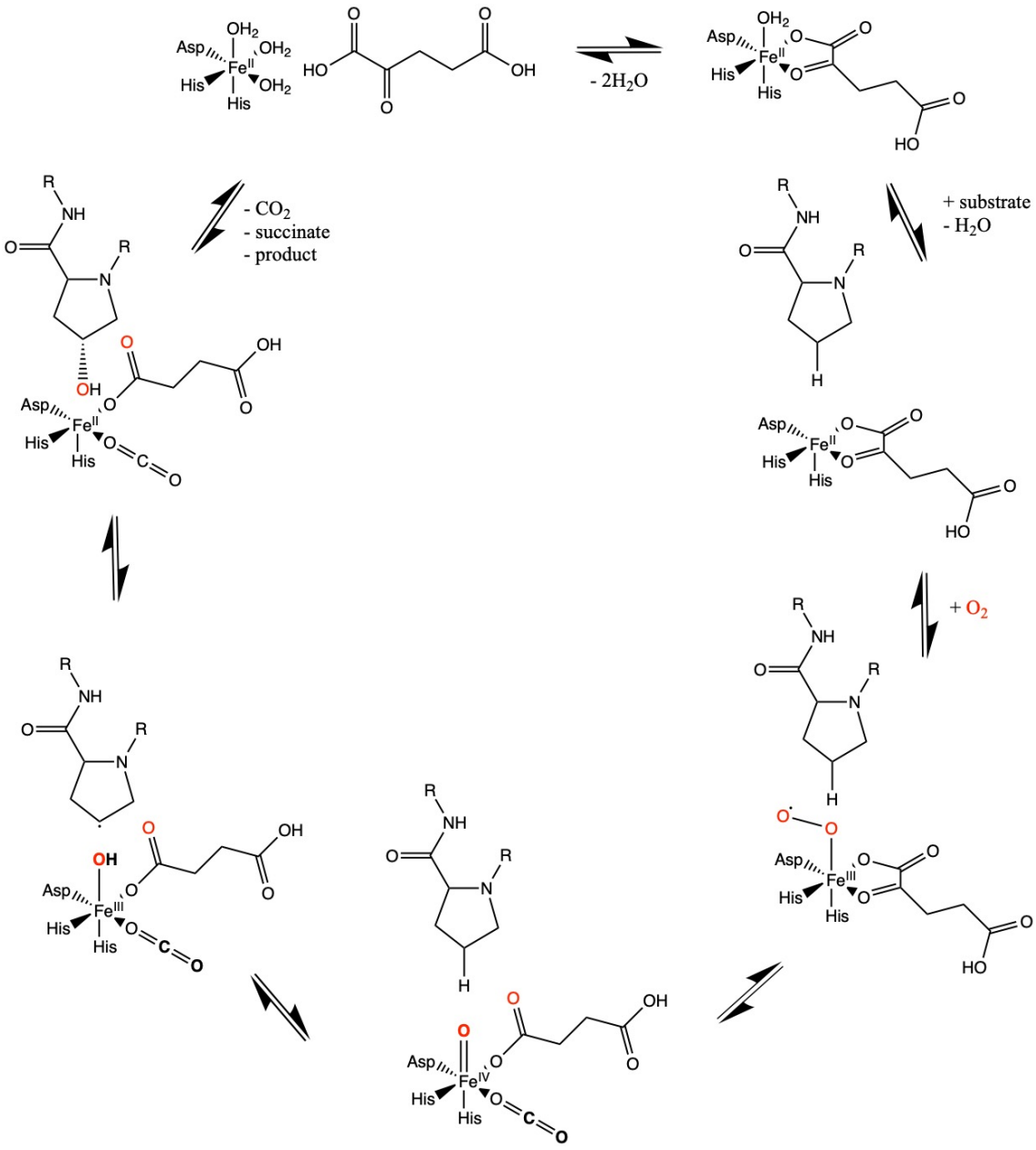


Figure 1.7 *Consensus mechanism for chlorination by 2OG dependent halogenases as shown for WelO5. [66]*

1.2 Protein NMR

1.2.1 Overview

The process of enzymatic catalysis has long been a subject of interest in the scientific community yet it has been difficult to study at atomic resolution. Some factors that may impact our ability to study enzymatic catalysis include internal protein motions

and conformational substates (notably reactive intermediates). [70] The process of catalysis and the observed conformational/catalytic states may be impacted by factors such as temperature, pH, buffer conditions, and a host of other parameters. Disruption of the native conditions may alter the mechanism, leading to misrepresentation of the native mechanism. For this reason, careful consideration must be taken when choosing biophysical methods to study enzymatic catalysis.

Of the various available biophysical methods, nuclear magnetic resonance (NMR) spectroscopy was chosen for my work on PHD2 and WelO5 in part due to its robustness and physiological relevance. NMR started out as a tool to probe the fundamental properties of matter but has since evolved into a key method for understanding phenomena across many scientific fields. Magnetic resonance describes a phenomenon in which a nucleus emits a frequency indicative of the nucleus' identity as well as its magnetic environment (while located in a strong magnetic field) when it is perturbed from equilibrium. This perturbation is achieved through a series of pulses—known as a pulse sequence—where variations of the pulse widths, locations in time, and frequencies can be applied. This makes NMR a very useful tool for probing a variety of structures, features, and functions of the analyte of interest. [71]

The benefits of NMR in investigating enzyme structure and function stem from its ability to observe molecular motion on the atomic scale, in solution, and for extended durations. [71] These properties of NMR enable a variety of measurements including laboratory-frame spin-relaxation studies, sensitivity to pico/nanosecond-scale reorientation motions, rotating frame relaxation-dispersion measurements, and micro/millisecond-sensitivity to chemical exchange processes, [72] [73] [74] all of which contribute to an understanding of the molecular motions and structures of the analyte. By contrast, other commonly used biophysical methods such as protein X-ray

crystallography and cryo-electron microscopy are normally performed at low temperatures with solid-state measurements and are, therefore, restricted in terms of analysis of dynamic motions, though some new developments may mediate these losses (e.g. room temperature protein crystallography). Methods such as fluorescence resonance energy transfer, atomic force microscopy, and stop-flow fluorescence spectroscopy image individual site dynamics and overall enzyme motion but cannot follow the motions of multiple residues site specifically and simultaneously as can be achieved with NMR. [72] Despite the limitations of NMR analysis (including the substantial time cost of many NMR experiments) it is a very useful method for investigating enzymes in solution. [75]

1.2.2 ^{1}H NMR

One of the simplest NMR-based methods to track changes in a protein under varied conditions is through ^{1}H spectra. ^{1}H NMR experiments can be carried out by observation of either the protein or ligand ^{1}H signals. ^{1}H-observed experiments are common in NMR since the sensitivity of ^{1}H nuclei to perturbation is high due to the large magnitude of its gyromagnetic ratio, making it an, often, ideal nucleus for NMR observations. [76] [77] [78]

1.2.2.1 Ligand-Observed ^{1}H NMR

Ligand-observed ^{1}H NMR is a commonly used method for qualitative determination of the binding strength between proteins and small molecules. [79] [80] [81] [82] Depending on the precise method used, protein signals may either be deselected or cancelled out by the selective placement of pulses within a pulse sequence without significantly affecting small molecule signals. Several ligand-observed methods can be used in tandem to control for the weaknesses of each method. [83] [84] [85]

1.2.2.1.1 Carr-Purcell-Meiboom-Gill (CPMG)-Edited ^{1}H Experiments

Carr-Purcell-Meiboom-Gill (CPMG)-edited NMR is a method that relies on the size discrepancy between small molecules and proteins. [80] Large molecules tumble

more slowly in solution, allowing for longer and a greater number of interactions with surrounding molecules and, therefore, faster T2 relaxation rates (transverse relaxation is the predominant method of relaxation in large molecules like proteins); small molecules, which more rapidly tumble in solution, see fewer of these interactions and will retain their magnetisation longer. [81] This difference can be utilised to selectively edit out protein signals while retaining ligand signals so that changes in the state of the ligand can be observed. [81]

To select small molecule resonances, a delay period is placed at the beginning of the pulse sequence to allow for protein signal relaxation *before* acquisition (**Figure 1.8**). This takes the form of a spin echo that refocuses the signals along the transverse axis repeatedly (as a series of spin echo loops) until the protein signal has sufficiently decayed. [79] The number of loops and the spin echo period are adjusted to maximize ligand signal and minimize the protein signal. These parameters are highly system dependent, and the total delay period commonly ranges from 10-100 ms. [79]

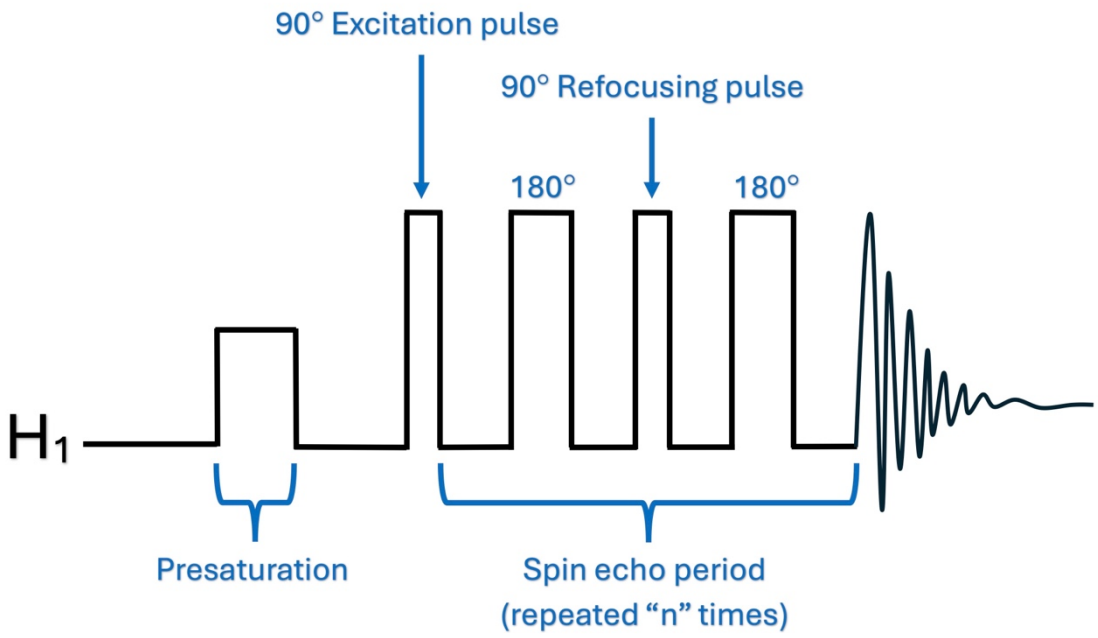


Figure 1.8 *Diagram of a typical NMR CPMG-PROJECT (Periodic Refocusing of J Evolution by Coherence Transfer) pulse sequence (Bruker: cpmg_project with*

presaturation). [86] The CPMG pulse program used in this research (with water signal suppression by presaturation) involves a 90° excitation pulse followed by a series of 180° refocusing pulses that are repeated "n" number of times (loops) during the spin echo period. An additional 90° refocusing pulse is added during each loop in the CPMG-PROJECT pulse sequence for suppression of J modulations.

There are two major methods through which ligand binding affinity can be qualitatively determined by ligand observed NMR that will be discussed in this section: cofactor displacement assays and competition assays. Such assays rely on protein-bound ligand tumbling much slower than free ligand, since the protein-bound ligand will adopt the same tumbling rate as the protein. [81] [82] Protein-bound-ligand signals will be broadened due to slower tumbling, while free-ligand signals will be sharp. By measuring the peak intensity of the ligand before and after protein binding, one can approximate the fraction of ligand in the protein-bound state and, therefore, the binding strength of the ligand.

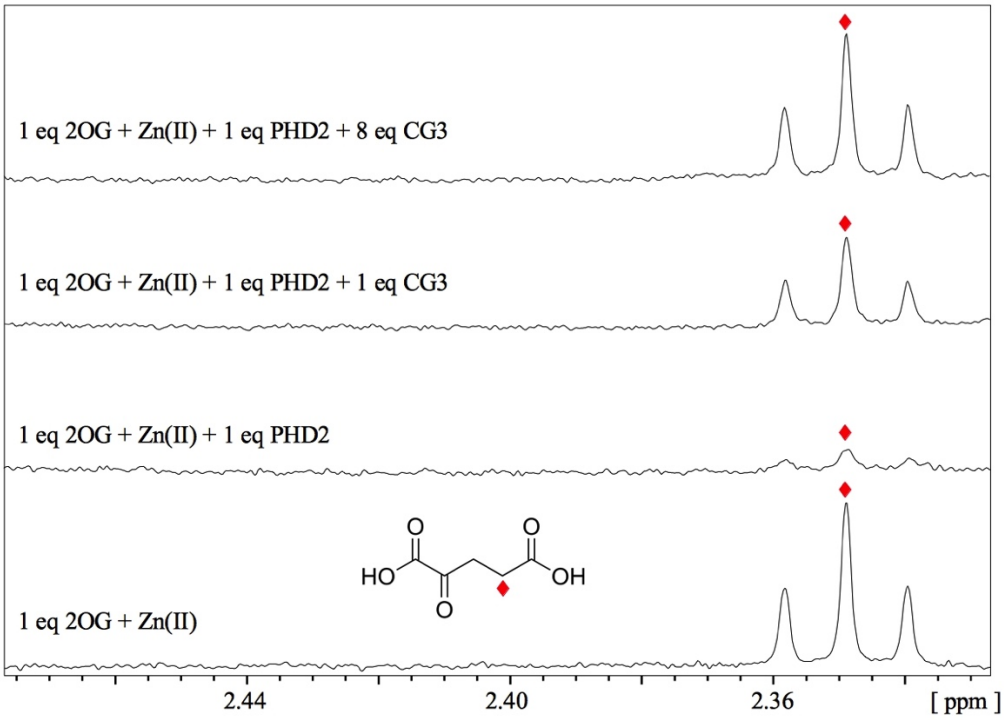


Figure 1.9. *Example of an NMR monitored cofactor displacement assay showing the displacement of 2OG from PHD2 binding by an inhibitor (see Chapter 5,* ***Section 5.2.4.2.2****). The resonance at 2.35 ppm is the diamond labelled methylene signal of 2OG. 2OG binds strongly to PHD2 in the absence of inhibitor but is almost completely displaced by the inhibitor (CG3) when the inhibitor is present in excess.*

Cofactor displacement assays are helpful in measuring the propensity for inhibitors to displace natural cosubstrate/cofactors (e.g. 2OG) or substrates from a protein. [82] Displacement is commonly observed as either direct competition at the active site or by allosteric binding (**Figure 1.9**). In the case of slow exchange (as discussed in **Section 1.2.3.1.1**), addition of an appropriate protein causes a reduction or loss of the cofactor signal. The inhibitor is then added, often initially in an equimolar concentration with respect to the cofactor, and the change in the intensity of the cofactor peak is observed. A minimal or no change in the cofactor peaks likely indicates that the ligand is either a moderate or poor cofactor competitive binder (this assay is not ideal for determining the binding strength of moderate binders). If the cofactor peak intensity

significantly recovers, then the inhibitor is likely a strong enough binder to displace the natural cofactor. [82]

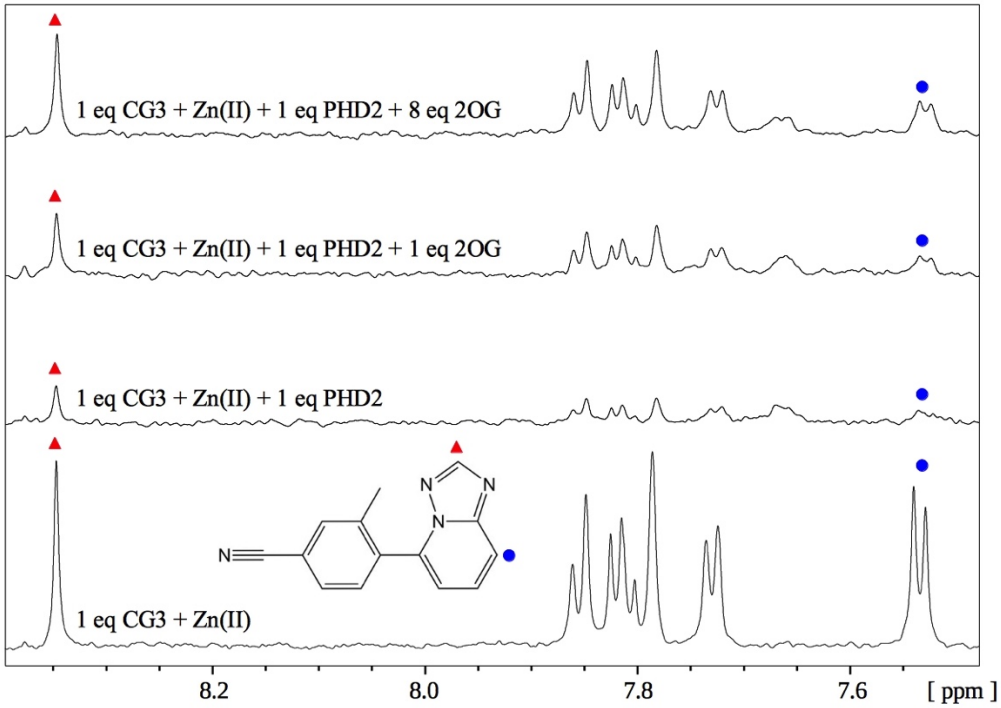


Figure 1.10 *Example of an assay showing displacement of an inhibitor from PHD2 binding by 2OG (see Chapter 5,* ***Section 5.2.4.2.1****). The inhibitor binds strongly to PHD2 in the absence of 2OG but is partially displaced by 2OG when 2OG is present in excess.*

The order of addition of assay components is crucial in studying enzyme systems; with addition of an inhibitor before the cofactor new information can be gleaned. Initially, spectra are taken of the inhibitor in the presence and absence of protein. The cofactor is added to the solution and change in the inhibitor peak intensities is observed (**Figure 1.10**). If the inhibitor peak intensities increase significantly on natural cofactor addition, then the inhibitor is likely a moderate to weak binder because it is easily displaced. This method is especially useful in determining if a cofactor, substrate, or other analyte molecule is a strong binder to the protein of interest. These methods can also be adapted to study cooperative ligand binding. [87] Binding affinities determined from by these

assays may be used to find the K_D values for strong binders, [88] though the method was used for qualitative studies in this thesis.

1.2.2.2 Protein-Observed ^{1}H NMR

Changes in small molecule signals are often good indicators of ligand-protein interactions, but direct protein signal observation is often needed to understand protein interactions in further detail. Therefore, one may consider that direct observation of the ^{1}H protein signals is a preferred choice for evaluating protein interactions. one-dimensional (1-D) ^{1}H protein NMR is a useful tool for achieving a broad understanding of protein conformation but can be complicated and difficult to analyse. There are two main reasons why 1-D ^{1}H spectral analysis is challenging for proteins: (1) the protein peak widths are broadened due to slow tumbling rates and (2) the ^{1}H spectra are complex from the thousands of magnetically inequivalent protons within the protein. [89] To glean useful information from ^{1}H protein spectra, it is often desirable to find regions of minimal peak overlap.

One region of the ^{1}H spectrum with minimal overlap is the region below zero, which is referred to as the "shielded methyl region" in this thesis. The resonances that appear in this region tend to be methyl groups that are either shielded by the inductive effects of nearby aromatic rings or shifted by paramagnetic species (see **Section 1.2.5**). These peaks are often useful in determining if the protein is in the correct conformational state as compared to a control spectrum since the peaks: 1) are typically well dispersed and easy to track, 2) are from methyl-containing residues buried within the protein, and 3) often reflect a change in local environment, e.g. if the protein is in a different conformational fold, causing a change in the shift values. [90] Though matching the whole ^{1}H spectrum to a control provides the best information on the overall protein fold, the shielded methyl region can provide a relatively clear indication of specific elements

of the overall protein conformation. Previous work on the AlkB and PHD2, observing the shielded methyl regions by ^{1}H NMR, may inform on the unique nature of this spectral region. [91]

A second region of minimal overlap in the ^{1}H spectrum is the region from about 9 ppm to 12 ppm, which will be referred to as the "deshielded H_N region" in this thesis. Peaks in this region are more deshielded than other ^{1}H peaks, separating them from the bulk of the H_N signals, because they are usually ^{1}H peaks of hydrogens that are directly attached to backbone nitrogen atoms. Due to this separation from the rest of the spectrum, deshielded H_N peaks can be especially useful as they can be correlated back to ^{1}H,^{15}N-HSQC peaks (an NMR method discussed in the next section).

1.2.3 ^{1}H, ^{15}N-HSQC NMR

To achieve higher resolution, 2-dimensional (2D) techniques such as ^{1}H,^{15}N-labelled heteronuclear single-quantum coherence spectroscopy (^{1}H,^{15}N-HSQC) are applied (an example of an ^{1}H,^{15}N-HSQC spectrum is shown in **Figure 1.11**).

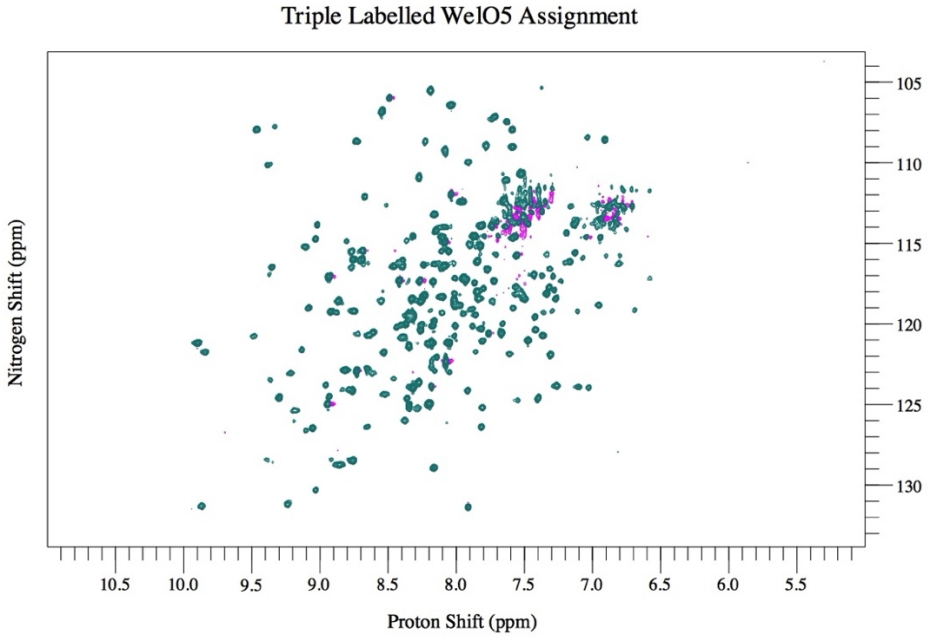


Figure 1.11 *^{1}H,^{15}N-HSQC of WelO5 in the presence of Zn(II) and 2OG. Each peak represents a correlation between an ^{15}N nucleus and an attached ^{1}H nucleus. The spectrum was produced using CCPNMR Analysis.*

Of the various 2-D NMR techniques, $^{1}H,^{15}N$-HSQC spectra are particularly useful for protein spectral assignment and analysis. As with all 2-D spectra, higher resolution is achieved by separating peaks into two dimensions based on correlations between two types of nuclei. An additional advantage of the $^{1}H,^{15}N$-HSQC technique is that most amino acids in a protein chain contain *only one* N-H bond within the "backbone" (or main chain) of the protein structure. It is important to note that, under most circumstances, because only one signal arises from each amino acid, this method provides a means to track structural changes site-specifically by observing changes in single or groups of N-H peaks. The chemical shifts of the nitrogen and hydrogen in this bond are relatively stable with respect to random motions and are often more structurally correlated than other regions of the protein. N-H backbone signals are, therefore, sensitive to conformational change as they are (often) locked by the protein conformational fold, partially due to the influence of hydrogen bonding. [92] This makes the N-H bond an ideal reporter of protein conformation and conformational changes induced by environmental influences such as ligand binding, degradation, or other physical processes.

1.2.3.1 Protein:Ligand $^{1}H,^{15}N$-HSQC

There are a few ways in which changes in a $^{1}H,^{15}N$-HSQC spectrum can be interpreted. In the case of protein-ligand binding, it is often useful to observe the type of peak shifts that are occurring on addition of ligand. These shifts occur because binding of the ligand causes a change in the electronic environment of nuclei near ligand atoms and, in some cases, may induce conformational change in the protein. [93] Based on the strength of the interaction between protein and ligand, these shifts will fall into either slow or fast exchange regimes. [74] [94] Gradual titration of the ligand into the protein solution in necessary to fully observe which type of exchange is taking place.

1.2.3.1.1 Slow, Intermediate, and Fast Ligand Exchange

In the slow exchange regime, peak shifts will occur as the gradual broadening of the initial protein peaks—but only in peaks which are affected by ligand binding—and the growth of a new peak from the same residue. [95] Therefore, in an intermediate state, before all the protein has bound the ligand, peaks corresponding to ligated and non-ligated protein will be visible. Slow exchange is observed in the case of ligand binding and dissociation timescales within the timeframe of a single scan. This means that over many scans, both states will be observed. [96] Peaks of ligands in slow exchange with protein will often be difficult to track since several residues will experience change and the new peaks that appear will be difficult to assign to a specific residue. This drawback is why peaks indicative of fast exchange can be useful for tracking protein conformational changes on ligand binding. Despite this drawback, some NMR methods only work with strongly interacting molecules in slow exchange, so the method of choice depends on what is being studied. [97]

Fast exchange is a process that is observed when a ligand is rapidly binding and dissociating with a protein in an NMR time regime faster than experimental acquisition. [95] Since both states are present before acquisition, the peak that is observed is an average of the ligand bound and unbound protein states. [95] [96] Titration of a ligand into the protein solution will allow the peak trajectory to be tracked as the ligand shifts from one state to the other. This works because, at low ligand concentrations, most of the protein is not interacting with ligand and, therefore, the average state favours the position of the non-interacting peak. As excess ligand is added, the balance will be tilted towards the ligand-bound protein state. Since the trajectory can be tracked, it is easy to assign the ligand-bound protein spectrum from the unbound protein spectrum, or vice versa.

Another way to describe ligand exchange in NMR is with its dissociation constant (K_D), where a $K_D > 1$ μM indicates medium to weak binders and a $K_D < 1$ μM indicates tight binders; typical NMR assays probe the former. [98] The dissociation constant can be used to describe the relationship between the on-rate (the rate of formation of the protein (P):ligand (L) complex (k_{on})) to the off-rate (the rate of dissociation of the protein:ligand complex (k_{off})). [85] The relationship between these variables is as follows: [99]

$$P + L \underset{k_{off}}{\overset{k_{on}}{\rightleftharpoons}} PL$$

The dissociation constant can be defined in terms of the rate constants as follows:

$$K_D = \frac{[P][L]}{[PL]} = \frac{k_{off}}{k_{on}}$$

where [P], [L], and [PL] indicate concentrations of the respective molecules/complexes.

The off-rate (k_{off}) may also be useful in estimating the strength of protein:ligand binding (see **Section 1.2.2.1.1**), with Δω (chemical shift difference of the ligand in the bound and free states [Hz]) greater than k_{off} in the case of slow exchange, equivalent to k_{off} in the case of intermediate exchange, and smaller than k_{off} in the case of fast exchange. [99] These tools help to add to the rigour of the use of NMR in describing protein:ligand interactions.

1.2.3.2 Protein Peak Shift Mapping

In most cases, new $^{1}H,^{15}N$-HSQC spectra are assigned from an initial spectrum using a nearest neighbour approach, which assumes that a peak with shift values most similar to a peak in an adjacent spectrum is from the same protein residue, considering best fit for all peaks across the spectrum and not only individual peak shifts. [93] This method may suffer in accuracy depending on the complexity of the spectrum and the

flexibility of the protein of interest, but is necessary to avoid full spectral assignment of each spectrum collected across various protein environments and/or conditions (the cost and complications of full spectral assignment are described in **Section 1.2.4**). Newer approaches have utilised computational methods for this purpose. [100] [101]

When determining if the magnitude of change in peak position between two spectra is of interest for further analysis, a positional averaging approach is favoured. In this approach, the following equation is used, [93]

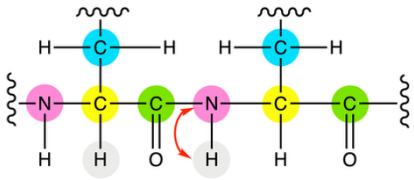
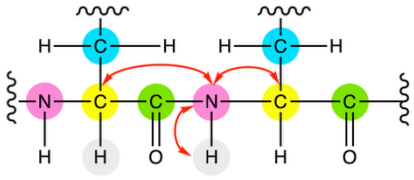
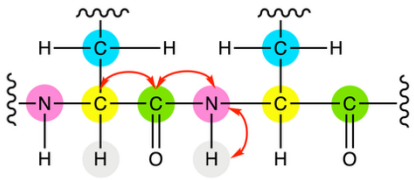
$$d = \sqrt{\frac{1}{2}({\delta_H}^2 + \alpha * {\delta_N}^2)}$$

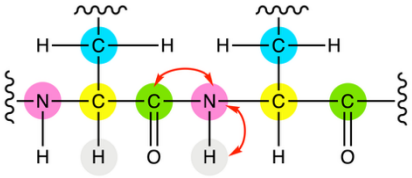
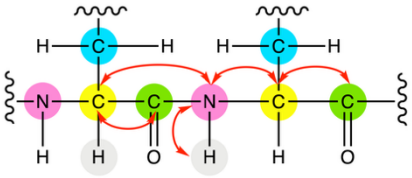
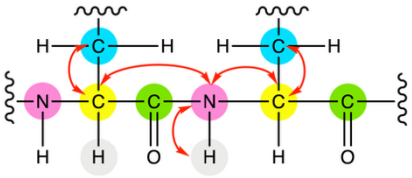
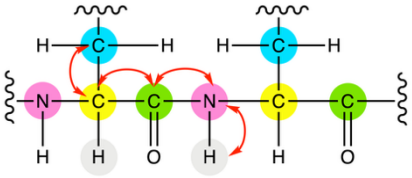
where d is the Euclidian distance shift, δ is the chemical shift, and α defines the scaling factor for the nitrogen shift (0.2 was used for glycine residues and 0.14 was used for all other residues). [93] The importance placed on Euclidian weighting is determined by an iterative approach. To evaluate which residues undergo substantial chemical shift changes, the standard deviation of the Euclidian distance values is calculated, and any shift outside three standard deviations is excluded. This process is iterated until no more distance values can be excluded by this process. The standard deviation value at which no more distance values are excluded is used as the cut-off: meaning that anything above this standard deviation value is considered significant. [93]

1.2.4 Three-Dimensional NMR

Three-dimensional (3-D) spectral assignment is a necessary step towards $^{1}H,^{15}N$-HSQC analysis. Though $^{1}H,^{15}N$-HSQC spectra can be analysed independently of spectral assignment, this type of analysis is limited to qualitative structural changes: which provide a narrow window of information on protein conformation changes such as ligand binding, degradation, aggregation, and degree of overall environmental or conformational changes. [102] 3-D assignment data allows for residue-specific

conformational changes to be understood. The 3-D spectra correlate the amide N-H chemical shifts to other nearby nuclei throughout the residue and throughout neighbouring residues, providing both identity and positional information (pathways described in **Table 1.2**). [103] Though $^{1}H,^{15}N$-HSQC assignment can be time-consuming, costly, and require the production of both $^{1}H,^{15}N$- and $^{2}H,^{13}C,^{15}N$-labelled protein, [104] once assigned, the spectra can be used to assign new spectra of closely related protein conformations as described above in **Section 1.2.3.2**.

NMR Experiment	Transfer Pathway	Description
$^{1}H,^{15}N$-**HSQC**		$^{1}H,^{15}N$-HSQC spectra are templates for mapping conformational changes of proteins. The purpose of most 3-D experiments are to assign the peaks of $^{1}H,^{15}N$-HSQC spectra to their corresponding amino acid residues in the protein sequence.
HNCA		HNCA spectra are useful in determining Cα carbon shifts of both the Xaa_i residue and the neighbouring Xaa_n residue relative to the backbone ^{1}H and ^{15}N amide resonances of Xaa_i
HNCOCA		HNCOCA spectra are often used in conjunction with HNCA spectra (above). HNCOCA spectra are useful in determining the Cα carbon shift of the neighbouring Xaa_n residue relative to the backbone ^{1}H and ^{15}N amide resonances of Xaa_i.

		It is not always necessary to collect HNCOCA spectra when HNCA spectra are available.
HNCO		HNCO spectra are useful in determining the carbonyl carbon shift of the neighbouring Xaa_n residue relative to the backbone ^{1}H and ^{15}N amide resonances of the Xaa_i residue. It is not always necessary to collect HNCO spectra when HNCACO spectra are available.
HNCACO		HNCACO spectra are often used in conjunction with HNCO spectra (above). HNCACO spectra are useful in determining Cα carbon shifts of both the Xaa_i residue and the neighbouring Xaa_n residue relative to the backbone ^{1}H and ^{15}N amide resonances of Xaa_i.
HNCACB		HNCACB spectra are useful in determining Cα carbon and Cβ carbon shifts of both the Xaa_i residue and the neighbouring Xaa_n residue relative to the backbone ^{1}H and ^{15}N amide resonances of Xaa_i.
HNCOCACB		HNCOCACB spectra are often used in conjunction with HNCACB spectra (above). HNCOCACB spectra are useful in determining Cα carbon and Cβ carbon shifts of

	the neighbouring Xaa_n residue relative to the backbone ^{1}H and ^{15}N amide resonances of Xaa_i. It is not always necessary to collect HNCOCACB spectra when HNCACB spectra are available.
H_N Hydrogen, Backbone Nitrogen, Carbonyl Carbon Cα Carbon, Cβ Carbon, Transfer Pathway	

Table 1.2 *Transfer pathways and pulse programs for each of the main spectra for 3-D spectral assignment. [105] [106] As discussed in* **Figure *1.12***, *the amino acid at the beginning of the transfer pathway will be referred to as the Xaa_i residue and the neighbouring residue linked to the Xaa_i amide bond will be referred to as the Xaa_n residue.*

As with all NMR techniques, the transfer pathway—and therefore efficacy of the experiment—is dependent on the proper placement of pulses in the pulse sequence. Two amino acid residues will be involved in this transfer pathway; the residue at the beginning of the magnetisation transfer pathway, which is referred to as the initial (Xaa_i) residue and the residue with which the backbone ^{15}N nitrogen of the Xaa_i residue shares an amide bond, referred to as the Xaa_n residue.

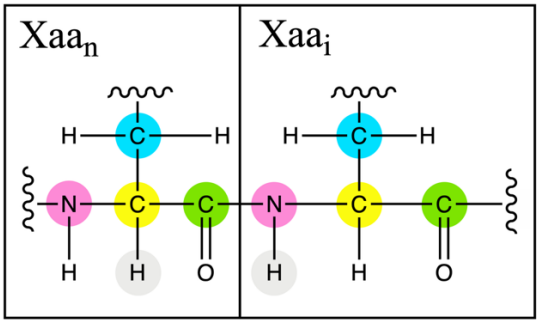


Figure 1.12 *Naming scheme for amino acids involved in the magnetisation transfer pathway of the 3-D protein NMR pulse sequences. The amino acid residue at the beginning of the transfer pathway will be referred to as the initial (Xaa_i) amino acid*

residue and the residue with which the Xaa_i residue shares an amide bond will be referred to as the neighbouring (Xaa_n) amino acid residue.

For protein assignment work, most types of 3-D pulse sequences come in sets of two: one with a linear transfer pathway, and another proceeding from the ^{15}N nitrogen of the Xaa_i residue through both nearby Cα carbons, splitting the transfer pathway (as indicated in **Figure 1.13**). [103] The splitting of the transfer pathway is due to the similarity in the J-coupling between the: 1) ^{15}N nitrogen of the Xaa_i residue and the neighbouring Cα carbon (7 Hz) when compared to the J-coupling between the 2) ^{15}N nitrogen and Cα carbon of the Xaa_i residue (11 Hz) (**Figure 1.13**). Therefore, both transfer pathways are explored. [107] Collecting a set of spectra utilising both the linear and branched types of transfer pathways (e.g. obtaining both HNCO and HNCACO spectra) can be useful for several reasons. First, having separate data on neighbouring residue peak shifts (e.g., obtaining an HNCO spectrum even though the HNCACO spectrum contains much of the same information) makes it easier to differentiate between the resonances of the Xaa_i and neighbouring Xaa_n residues, which are both associated with the same ^{15}N resonance of the Xaa_i residue due to the direction of the transfer pathway. Second, obtaining both spectra can be useful in the case of poor signal to noise; a spectrum with a shorter magnetisation transfer pathway (e.g. an HNCO spectrum in comparison to an HNCACO spectrum) may exhibit greater sensitivity, which aids in protein assignment for spectra with poor signal to noise.

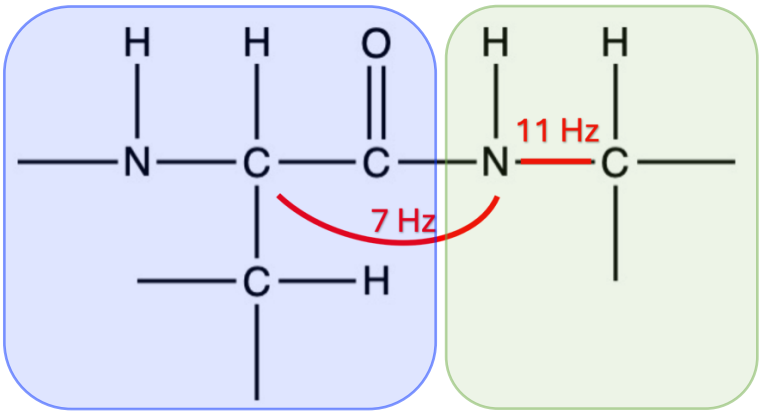


Figure 1.13 *J-coupling values for magnetisation transfer across protein backbone and side-chain. Transfer from the ^{15}N nitrogen of the Xaa_i residue (indicated in green) to the Cα carbons always proceeds via transfer the Cα carbons of both Xaa_i and neighbouring Xaa_n (indicated in blue) residues due to the similarity in J-coupling values (7 and 11 Hz). [108]*

The HNCO and HNCACO spectral pair help to relate an ^{15}N initial resonance to the carbonyl carbon of both Xaa_i and neighbouring Xaa_n residues (as shown in **Table 1.2**). The transfer pathway for an HNCACO pulse sequence proceeds in the following order: 1) the H_N proton of the Xaa_i residue (most 3-D acquisitions begin with the H_N proton due to the large magnitude of the hydrogen gyromagnetic ratio), 2) the ^{15}N nucleus of the Xaa_i residue, 3) the Cα nuclei of both the Xaa_i and neighbouring Xaa_n residues, 4) the carbonyl carbon of both the Xaa_i and neighbouring Xaa_n residues (respective to steps (3), and 5) back to the H_N proton of the Xaa_i residue (where it is detected) via steps 4 → 3 → 2 → 1. The transfer pathway for an HNCO pulse sequence is much the same, proceeding through steps 1 → 2 → 4 → 2 → 1, excluding transfer through either Cα carbon (step 3) and without magnetisation transfer to the carbonyl carbon of the Xaa_i residue. [103] It should be noted that the names of NMR pulse sequences for 3-D protein assignment are often describing one direction of the magnetisation transfer pathway: for example in the HNCACO, steps 1 → 2 → 3 → 4 could be written as H_N → N → CA →

CO, where CO denotes a carbonyl carbon and CA denotes a Cα carbon. This naming scheme holds for the other 3-D spectral sets described in this thesis (HNCA, HNCOCA, HNCACB, and HNCOCACB) as well as other important 3-D NMR pulse sequences that are useful for understanding protein folding and secondary structure but are not utilised in the research described in this thesis (HCCH-TOCSY and NOESY-HSQC). [109]

1.2.5 Paramagnetic Effects

Paramagnetism was initially perceived as a potential limitation for NMR studies but has since developed into a useful tool in the NMR toolbox. [110] [111] [112] [113] Whereas paramagnetic species were once avoided in NMR research, they are now often used as probes to aid in structural analysis, act as gas binding indicators, and even to give more far-reaching distance restraints than NOEs (which are limited to <6 Å distances). [110] [111] The commonly observed effects of paramagnets in protein solutions are described briefly below.

1.2.5.1 Paramagnetic Dipolar Relaxation Enhancements (PRE)

One of the major effects paramagnetic species have on nuclei is via paramagnetic dipolar relaxation enhancement (PRE). [112] These relaxation effects are due to the magnet-like properties of paramagnets. [114] Within the magnetic field of an NMR instrument, paramagnets, acting as miniature magnets in solution, tumble at arbitrary orientations relative to the main magnetic field and nearby nuclei. This causes the nearby nuclei to experience inconsistent magnetic fields across the sample and a scatter of magnetic environments, leading to broadening of NMR peaks. [114] These effects are observed in both longitudinal and transverse directions. The following equations are used to describe these relaxation effects. [115] [116]

Longitudinal relaxation rate:

$$R_1 = \frac{2}{15}\left(\frac{\mu_0}{4\pi}\right)^2 \frac{{\gamma_I}^2 (g_e \mu_B)^2 S(S+1)}{r^6}\left(\frac{3\tau_c}{1+{\omega_I}^2{\tau_c}^2} + \frac{7\tau_c}{1+{\omega_S}^2{\tau_c}^2}\right)$$

Transverse relaxation rate:

$$R_2 = \frac{1}{15}\left(\frac{\mu_0}{4\pi}\right)^2 \frac{{\gamma_I}^2 (g_e \mu_B)^2 S(S+1)}{r^6}\left(4\tau_c + \frac{3\tau_c}{1+{\omega_I}^2{\tau_c}^2} + \frac{13\tau_c}{1+{\omega_S}^2{\tau_c}^2}\right)$$

where R_1 and R_2 represent the longitudinal and transverse relaxation rates respectively, μ_0 is the permeability in a vacuum, γ_I is the gyromagnetic ratio of the nucleus of interest, g_e is the Landé factor (g-factor or gyromagnetic ratio of the electron), μ_B is the Bohr magneton (a constant), S is the total angular momentum of the paramagnetic centre, τ_c is the effective correlation time, ω_I is the nuclear Larmor frequency, and ω_S is the electronic Larmor frequency. [115] [116]

These equations indicate that an increase in the relaxation rate will occur with a large gyromagnetic ratio of the nucleus, more unpaired electrons (as defined by the g-factor and total angular momentum), and a shorter distance between the nucleus and paramagnetic species. [110] [115] [116] Though the paramagnetic broadening decrease rapidly with distance due to the $1/r^6$ term, the large gyromagnetic ratio of the electron makes the interaction much stronger than interactions observed between nuclei. Whereas NOE effects only reach under 6 Å distances, [110] PRE broadening effects can be commonly observed at greater than 15 Å. [117] This factor makes paramagnetic species increasingly popular in distance restraint determination. Though the effect of transverse relaxation is more easily apparent (as the broadening of peak widths), longitudinal relaxation can also be observed in the form of quicker magnetisation recovery.

1.2.5.2 Paramagnet-Induced Shifts

Another effect caused by paramagnets in solution is paramagnetic shifts, which are observed as changes in peak positions as a consequence of altering the electronic environment of the nuclei. Paramagnetic shifts can be more useful than the relaxation effects described above because, unlike signal broadening, the intensities of the peaks are preserved. Both relaxation and shifts may result from the addition of a paramagnetic

species, so a paramagnetic probe must be chosen wisely for the desired effect. These effects can be classified as contact or pseudocontact shifts. [118] The following equations are used to describe paramagnetic shifts. [119] [120]

Contact Shifts:

$$\delta_C = -\frac{2\pi}{\gamma_I} g_e \mu_B A \frac{S(S+1)}{3k_B T}$$

Pseudocontact Shifts:

$$\delta_{PC} = \frac{1}{12\pi r^3}\left[\Delta\chi_{ax}(3\cos^2\theta - 1) + \frac{3}{2}\Delta\chi_{rh}(\sin^2\theta\cos 2\phi)\right]$$

where δ_C and δ_{PC} represent the contact and pseudo contact shifts respectively, γ_I is the gyromagnetic ratio of the nucleus of interest, g_e is the Landé factor (g-factor or gyromagnetic ratio of the electron), μ_B is the Bohr magneton (a constant), A is the hyperfine coupling constant, S is the total angular momentum of the paramagnetic centre, $k_B T$ is the thermal energy, r is the distance between the nucleus and paramagnetic centre, $\Delta\chi_{ax}$ and $\Delta\chi_{rh}$ are the axial and rhombic components (respectively) of the magnetic susceptibility tensor due to anisotropy, and θ and ϕ describe the angles of the nucleus of interest relative to the principle axes of the magnetic susceptibility tensor. [119] [120]

Contact shifts are induced by spin polarisation and delocalisation of electrons through nearby molecular orbitals (hence the term "contact") and can be considered as comparable to "through-bond" interactions observed between nuclei. Unlike pseudocontact shifts (described in the next paragraph), contact shifts only occur within a small proximity to the paramagnet, and the effects reach across few bonds: since nuclei must experience a non-zero electron spin density to exhibit contact shifts. [121] These types of shifts are highly dependent on the angle between the paramagnet/nucleus bond and the magnetic field as well as the spin magnetisations. Contact shifts are of interest

for observation of gas-protein interactions since key gases like oxygen act as paramagnets in solution (this topic is explored further in Chapter 6, **Section 6.1.1**).

If contact shifts can be likened to "through-bond" interactions, pseudocontact shifts can be likened to "through-space" interactions, with a reach of 50 Å or greater [118] (this effect drops off as $1/r^3$, as shown in the equation above). Pseudocontact shifts are caused by a change in the *effective* magnetic field, resultant from dipolar coupling between the nuclear magnetic moment and the anisotropic component of the unpaired electron. [118] Despite considerable reach, high sensitivity, and versatility of pseudocontact shifts, this tool suffers from many of the same drawbacks as described for other methods utilising paramagnetic species [122] and only more recently have software tools like ROSETTA bridged that gap to allow for more complex analysis such as full 3-D protein structural determination without the use of other tools/methods. [123]

1.3 Overall Aims of the Work Described in this Thesis

The research literature describing the properties of 2OG-dependent dioxygenases—such as PHD and WelO5—covers a range of properties from structural changes on substrate interactions to kinetic profiles of the enzymatic processes, yet lacks rigorous studies on protein solution dynamics—internal protein motions, conformational substates, atomic scale molecular motions, etc.—and dioxygen-metal interactions at the active site. These dynamics and interactions are important to explore as they may enable a better understanding of the biological functions of 2OG oxygenases, including the details of hypoxia sensing by PHD2; they may also be useful in developing improved 2OG-dependent dioxygenase biocatalysts, e.g. engineered halogenases based on WelO5. A consistent theme of the research described in this thesis involves the use of NMR spectroscopy to investigate the solution dynamics of PHD2 and WelO5 and how they interact with their substrates, cosubstrates, and inhibitors, including investigations on

conformational changes. The work on the catalytic domain of PHD2, including with respect to substrate binding, was built on a report concerning the NMR assignment of the relevant PHD2 residues. [31]

The broad aims of the work described in this thesis are as summarized below

(1) **Chapter 2** initially describes investigations concerning PHD2:metal complexes with the specific goals of: 1) obtaining an improved understanding of the specificity with which PHD2 reacts *only* with oxygen in the presence of Fe(II), 2) investigating PHD2:metal complexes that may be mimics of reactive intermediates in the PHD2 catalysis, 3) studies investigating PHD2 inhibition by metal ions such as Co(II), and 4) studies utilising the paramagnetic nature of oxygen and PHD2-binding transition metals to investigate interactions at the PHD2 active site.

(2) **Chapter 2** also describes investigations concerning the structure and stability of PHD2 in the presence and absence of oxygen with the goals of: 1) evaluating the efficacy of NMR methods in tracking oxygen binding to PHD2 through paramagnetic effects at both the PHD2 active site and the channel leading to the active site, 2) mapping changes in the PHD2 conformation on reaction with oxygen, and 3) investigating changes in the stabilities of various PHD2 complexes (with and without 2OG/inhibitors) in the presence and absence of oxygen. A discussion is given regarding how these PHD2:O_2 interactions may relate to the slow reaction of oxygen with PHD2.

(3) **Chapter 3** describes investigations into the structure and dynamics of WelO5 with the specific goals of: 1) carrying out $^{1}H,^{15}N$-HSQC spectral assignment of WelO5 by 3-D NMR methods, 2) establishing a baseline understanding of the in-solution dynamics of WelO5 and further exploring features of WelO5 catalysis, and 3) comparing the structures of PHD2 and WelO5 (especially with respect to metal-protein and gas-

protein interactions) to better understand the halogenation mechanism of WelO5 and what causes its preference for halogenation over hydroxylation.

A discussion of potential future research building off the progress described in this thesis is given in **Chapter 6**.

1.4 References

[1] C. J. Schofield and P. J. Ratcliffe, "Oxygen sensing by HIF hydroxylases," *Nature Reviews Molecular Cell Biology,* vol. 5, p. 343, 2004.

[2] C. Liao and Q. Zhang, "Understanding the Oxygen-Sensing Pathway and Its Therapeutic Implications in Diseases," *American Journal of Pathology,* vol. 190, no. 8, pp. 1584-1595, 2020.

[3] M. M. Briehl, "Oxygen in human health from life to death – An approach to teaching redox biology and signaling to graduate and medical students," *Redox Biology,* vol. 5, pp. 124-139, 2015.

[4] G. L. Semenza, "Hypoxia-inducible factor 1 (HIF-1) pathway," *Science's STKE : signal transduction knowledge environment,* no. 407, 2007.

[5] G. L. Semenza and G. L. Wang, "A nuclear factor induced by hypoxia via de novo protein synthesis binds to the human erythropoietin gene enhancer at a site required for transcriptional activation," *Mollecular and Cellular Biology,* vol. 12, no. 12, p. 447–5454, 1992.

[6] W. G. Kaelin and P. J. Ratcliffe, "Oxygen Sensing by Metazoans: The Central Role of the HIF Hydroxylase Pathway," *Molecular Cell,* vol. 30, pp. 393-402, 2008.

[7] I. J. Clifton, M. A. McDonough, D. Ehrismann, N. J. Kershaw, N. Granatino and C. J. Schofield, "Structural studies on 2-oxoglutarate oxygenases and related double-stranded beta-helix fold proteins," *Journal of Inorganic Biochemistry,* vol. 100, no. 4, pp. 644-669, 2006.

[8] P. R. Arsenault, D. Song, M. Bergkamp, A. M. Ravaschiere, B. E. Navalsky, P. M. Lieberman and F. S. Lee, "Identification of Small-Molecule PHD2 Zinc Finger Inhibitors that Activate Hypoxia Inducible Factor," *ChemBioChem,* vol. 17, no. 24, pp. 2316-2323, 2016.

[9] K. Lippl, A. Boleininger, M. A. McDonough, M. I. Abboud, H. Tarhonskaya, R. Chowdhury, C. Loenarz and C. J. Schofield, "Born to sense: biophysical analyses of the oxygen sensing prolyl hydroxylase from the simplest animal Trichoplax adhaerens," *Hypoxia (Auckl),* vol. 6, pp. 57-71, 2018.

[10] S. Martinez and R. P. Hausinger, "Catalytic Mechanisms of Fe(II)- and 2-Oxoglutarate-dependent Oxygenases," *Journal of Biological Chemistry,* vol. 290, no. 34, pp. 20702-20711, 2015.

[11] M. A. McDonough, C. Loenarz, R. Chowdhury, I. J. Clifton and C. J. Schofield, "Structural studies on human 2-oxoglutarate dependent oxygenases," *Current Opinion in Structural Biology,* vol. 20, no. 6, pp. 659-672, 2010.

[12] C. Loenarz, J. Mecinović, R. Chowdhury, L. McNeill, E. Flashman and C. J. Schofield, "Evidence for a Stereoelectronic Effect in Human Oxygen Sensing," *Angewandte Chemie International Edition,* vol. 48, no. 10, pp. 1784-1787, 2009.

[13] S. E. Wilkins, M. I. Abboud, R. L. Hancock and C. J. Schofield, "Targeting Protein–Protein Interactions in the HIF System," *ChemMedChem,* vol. 11, no. 8, p. 773–786, 2016.

[14] P. Jaakkola, D. R. Mole, Y.-M. Tian, M. I. Wilson, J. Gielbert, S. J. Gaskell, A. v. Kriegsheim, H. F. Hebestreit, M. Mukherji, C. J. Schofield, P. H. Maxwell, C. W. Pugh and P. J. Ratcliffe, "Targeting of HIF-α to the von Hippel-Lindau

Ubiquitylation Complex by O2-Regulated Prolyl Hydroxylation," *Science,* vol. 292, no. 5516, pp. 468-472, 2001.

[15] J. Lopez-Barneo, R. Pardal and P. Ortega-Sáenz, "Cellular mechanism of oxygen sensing," *Annual Review of Physiology,* vol. 63, pp. 259-287, 2001.

[16] T. Acker and K. H. Plate, "A role for hypoxia and hypoxia-inducible transcription factors in tumor physiology," *Journal of Molecular Medicine,* vol. 80, no. 9, pp. 562-575, 2002.

[17] G.-H. Fong and K. Takeda, "Role and regulation of prolyl hydroxylase domain proteins," *Cell Death & Differentiation,* vol. 15, p. 635–641, 2008.

[18] D. E. Sterner and S. L. Berger, "Acetylation of Histones and Transcription-Related Factors," *Microbiology and Molecular Biology Reviews,* vol. 64, no. 2, p. 435–459, 2000.

[19] M. A. McDonough, V. Li, E. Flashman, R. Chowdhury, C. Mohr, B. M. R. Liénard, J. Zondlo, N. J. Oldham, I. J. Clifton, J. Lewis, L. A. McNeill, R. J. M. Kurzeja, K. S. Hewitson, E. Yang, S. Jordan, R. S. Syed and C. J. Schofield, "Cellular oxygen sensing: Crystal structure of hypoxia-inducible factor prolyl hydroxylase (PHD2)," *Proc Natl Acad Sci U S A,* vol. 103, no. 26, pp. 9814-9819, 2006.

[20] G. Fiorini and C. J. Schofield, "Biochemistry of the hypoxia-inducible factor hydroxylases," *Current Opinion in Chemical Biology,* vol. 79, p. 102428, 2024.

[21] M. S. Islam, T. M. Leissing, R. Chowdhury, R. J. Hopkinson and C. J. Schofield, "2-Oxoglutarate-Dependent Oxygenases," *Annual Review of Biochemistry,* vol. 87, pp. 585-620, 2018.

[22] W. D. Figg, M. A. McDonough, R. Chowdhury, Y. Nakashima, Z. Zhang, J. P. Holt-Martyn, A. Krajnc and C. J. Schofield, "Structural Basis of Prolyl Hydroxylase Domain Inhibition by Molidustat," *ChemMedChem,* vol. 16, p. 2082, 2021.

[23] P. Rabe, J. J. A. G. Kamps and C. J. Schofield, "X-ray free-electron laser studies reveal correlated motion during isopenicillin N synthase catalysis," *Science Advances,* vol. 7, no. 34, 2021.

[24] C. J. Schofield and Z. Zhang, "Structural and mechanistic studies on 2-oxoglutarate-dependent oxygenases and related enzymes," *Current Opinion in Structural Biology,* vol. 9, no. 6, pp. 722-731, 1999.

[25] J. M. Bollinger, W.-c. Chang, M. L. Matthews, R. J. Martinie, A. K. Boal and C. Krebs, "Mechanisms of 2-Oxoglutarate-Dependent Oxygenases: The Hydroxylation Paradigm and Beyond," in *2-Oxoglutarate-Dependent Oxygenases*, The Royal Society of Chemistry, 2015, pp. 95 - 122.

[26] A. J. Mitchell, N. P. Dunham, R. J. Martinie, J. A. Bergman, C. J. Pollock, K. Hu, B. D. Allen, W.-c. Chang, A. Silakov, J. M. B. Jr., C. Krebs and A. K. Boal, "Visualizing the Reaction Cycle in an Iron(II)- and 2-(Oxo)-glutarate-Dependent Hydroxylase," *Journal of the American Chemical Society,* vol. 139, no. 39, p. 13830–13836, 2017.

[27] H. Tarhonskaya, A. P. Hardy, E. A. Howe, N. D. Loik, H. B. Kramer, J. S. O. McCullagh, C. J. Schofield and E. Flashman, "Kinetic Investigations of the Role of Factor Inhibiting Hypoxia-inducible Factor (FIH) as an Oxygen Sensor," *Journal of Biological Chemistry,* vol. 290, no. 32, pp. 19726-19742, 2015.

[28] H. Tarhonskaya, R. Chowdhury, I. K. H. Leung, N. D. Loik, J. S. O. McCullagh, T. D. W. Claridge, C. J. Schofield and E. Flashman, "Investigating the contribution of the active site environment to the slow reaction of hypoxia-inducible factor prolyl hydroxylase domain 2 with oxygen," *Biochemical Journal,* vol. 463, no. 3, pp. 363-372, 2014.

[29] E. Flashman, L. M. Hoffart, R. B. Hamed, J. M. Bollinger, C. Krebs and C. J. Schofield, "Evidence for the slow reaction of hypoxia-inducible factor prolyl hydroxylase 2 with oxygen," *The FEBS Journal,* vol. 277, no. 19, pp. 4089-4099, 2010.

[30] L. A. McNeill, E. Flashman, M. R. G. Buck, K. S. Hewitson, I. J. Clifton, G. Jeschke, T. D. W. Claridge, D. Ehrismann, N. J. Oldhama and C. J. Schofield, "Hypoxia-inducible factor prolyl hydroxylase 2 has a high affinity for ferrous iron and 2-oxoglutarate," *Molecular Biosystems,* vol. 1, no. 4, pp. 321-324, 2005.

[31] R. Chowdhury, I. K. H. Leung, Y.-M. Tian, M. I. Abboud, W. Ge, C. Domene, F.-X. Cantrelle, I. Landrieu, A. P. Hardy, C. W. Pugh, P. J. Ratcliffe, T. D. W. Claridge and C. J. Schofield, "Structural basis for oxygen degradation domain selectivity of the HIF prolyl hydroxylases," *Nature Communications,* vol. 7, p. 12673, 2016.

[32] C. Domene, C. Jorgensen and C. Schofield, "Mechanism of Molecular Oxygen Diffusion in a Hypoxia-Sensing Prolyl Hydroxylase Using Multiscale Simulation," *Journal of the American Chemical Society,* vol. 142, no. 5, pp. 2253-2263, 2020.

[33] M. C. Chan, J. P. Holt-Martyn, C. J. Schofield and P. J. Ratcliffe, "Pharmacological targeting of the HIF hydroxylases – A new field in medicine development," *Molecular Aspects of Medicine,* Vols. 47-48, pp. 54-75, 2016.

[34] X. Huang and J. T. Groves, "Oxygen Activation and Radical Transformations in Heme Proteins and Metalloporphyrins," *Chemical Reviews,* vol. 118, no. 5, p. 2491–2553, 2017.

[35] T. L. Olson, J. C. Williams and J. P. Allen, "Influence of protein interactions on oxidation/reduction midpoint potentials of cofactors in natural and de novo metalloproteins," *Biochimica et Biophysica Acta (BBA) - Bioenergetics,* vol. 1827, no. 8-9, pp. 914-922, 2013.

[36] M. L. Kennedy and B. R. Gibney, "Metalloprotein and redox protein design," *Current Opinion in Structural Biology,* vol. 11, no. 4, pp. 485-490, 2001.

[37] S. E. J. Bowman, J. Bridwell-Rabb and C. L. Drennan, "Metalloprotein Crystallography: More than a Structure," *Accounts of Chemical Research,* vol. 49, no. 4, p. 695–702, 2016.

[38] C. J. Wilson, D. Apiyo and P. Wittung-Stafshede, "Role of cofactors in metalloprotein folding," *Quarterly Reviews of Biophysics,* vol. 37, no. 3-4, pp. 285-314, 2004.

[39] Y. Lu, N. Yeung, N. Sieracki and N. M. Marshall, "Design of functional metalloproteins," *Nature,* vol. 460, p. 855–862, 2009.

[40] M. Dalal, A Textbook of Inorganic Chemistry - Volume 1, Dalal Institute, 2017.

[41] J. D. Cody and E. M. Hodson, "Recombinant human erythropoietin versus placebo or no treatment for the anaemia of chronic kidney disease in people not requiring dialysis," *Cochrane Database of Systematic Reviews,* vol. 1, p. CD003266, 2016.

[42] A. Raine, "Hypertension, blood viscosity, and cardiovascular morbidity in renal failure: implications of erythropoietin therapy," *The Lancet,* vol. 331, no. 8577, pp. 97-100, 1988.

[43] T.-L. Yeh, T. M. Leissing, M. I. Abboud, C. C. Thinnes, O. Atasoylu, J. P. Holt-Martyn, D. Zhang, A. Tumber and e. al., "Molecular and cellular mechanisms of HIF prolyl hydroxylase inhibitors in clinical trials," *Chemical Science,* vol. 8, no. 11, pp. 7651-7668, 2017.

[44] A. M. Meneses and B. Wielockx, "PHD2: from hypoxia regulation to disease progression," *Hypoxia (Auckland, N.Z.),* vol. 4, p. 53–67, 2016.

[45] K. Takeda, H. L. Aguila, N. S. Parikh, X. Li, K. Lamothe, L.-J. Duan, H. Takeda, F. S. Lee and G.-H. Fong, "Regulation of adult erythropoiesis by prolyl hydroxylase domain proteins," *Blood,* vol. 111, no. 6, p. 3229–3235, 2008.

[46] M. Lemus-Varela, M. Flores-Soto, R. Cervantes-Munguía, B. Torres-Mendoza, G. Gudiño-Cabrera, V. Chaparro-Huerta, D. Ortuño-Sahagún and C. Beas-Zárate, "Expression of HIF-1α, VEGF and EPO in peripheral blood from patients with two cardiac abnormalities associated with hypoxia," *Clinical Biochemistry,* vol. 43, no. 3, pp. 234-239, 2010.

[47] A. Weidemann and R. Johnson, "Biology of HIF-1α," *Cell Death & Differentiation,* vol. 15, p. 621–627, 2008.

[48] A. Zuk, Z. Si, S. Loi, S. Bommegowda, D. Hoivik, S. Danthi, G. Molnar, V. Csizmadia and M. Rabinowitz, "Preclinical Characterization of Vadadustat (AKB-6548), an Oral Small Molecule Hypoxia-Inducible Factor Prolyl-4-Hydroxylase Inhibitor, for the Potential Treatment of Renal Anemia," *Journal of Pharmacology and Experimental Therapeutics,* vol. 383, no. 1, pp. 11-24, 2022.

[49] T. P. Corner, A. Tumber, E. Salah, M. Jabbary, Y. Nakashima, L. I. Schnaubelt, S. Basak, F. M. Alshref, L. Brewitz and C. J. Schofield, "Derivatives of the Clinically Used HIF Prolyl Hydroxylase Inhibitor Desidustat Are Efficient Inhibitors of Human γ-Butyrobetaine Hydroxylase," *Journal of Medicinal Chemistry,* vol. 68, no. 9, p. 9777–9798, 2025.

[50] S. Dhillon, "Desidustat: First Approval," *Drugs,* vol. 82, p. 1207–1212, 2022.

[51] J. L. Ariazi, K. J. Duffy, D. F. Adams, D. M. Fitch, L. Luo, M. Pappalardi, M. Biju, E. H. DiFilippo, T. Shaw, K. Wiggall and C. Erickson-Miller, "Discovery and Preclinical Characterization of GSK1278863 (Daprodustat), a Small Molecule Hypoxia Inducible Factor-Prolyl Hydroxylase Inhibitor for Anemia," *Journal of Pharmacology and Experimental Therapeutics,* vol. 363, no. 3, pp. 336-347, 2017.

[52] P. E. Pergola, B. S. Spinowitz, C. S. Hartman, B. J. Maroni and V. H. Haase, "Vadadustat, a novel oral HIF stabilizer, provides effective anemia treatment in nondialysis-dependent chronic kidney disease," *Kidney International,* vol. 90, no. 5, pp. 1115-1122, 2016.

[53] A. Singh, J. W. Wilson, C. J. Schofield and R. Chen, "Hypoxia-inducible factor (HIF) prolyl hydroxylase inhibitors induce autophagy and have a protective effect in an in-vitro ischaemia model," *Scientific Reports,* vol. 10, p. 1597, 2020.

[54] J. Chandrasekaran and J. Balasubramaniam, "A computational evaluation of FDA medicines' ability to inhibit hypoxia-inducible factor prolyl hydroxylase-2 (PHD-2) for acute respiratory distress syndrome," *Structural Chemistry,* vol. 33, p. 1391–1407, 2022.

[55] A. M. Sayaf, S. U. Khalid, J. A. Hameed, A. Alshammari, A. Khan, A. Mohammad, S. Alghamdi, D.-Q. Wei and K. Yeoh, "Exploring the natural products chemical space through a molecular search to discover potential inhibitors that target the hypoxia-inducible factor (HIF) prolyl hydroxylase domain (PHD)," *Frontiers in pharmacology,* vol. 14, p. 1202128, 2023.

[56] D. A. Chan, P. D. Sutphin, S. E. Yen and A. J. Giaccia, "Coordinate regulation of the oxygen-dependent degradation domains of hypoxia-inducible factor 1 alpha," *Molecular and cellular biology,* vol. 25, no. 15, p. 6415–6426, 2005.

[57] E. Flashman, E. A. L. Bagg, R. Chowdhury, J. Mecinović, C. Loenarz, M. A. McDonough, K. S. Hewitson and C. J. Schofield, "Kinetic rationale for selectivity toward N- and C-terminal oxygen-dependent degradation domain substrates mediated by a loop region of hypoxia-inducible factor prolyl hydroxylases," *Journal of Biological Chemistry,* vol. 283, no. 7, pp. 3808-3815, 2008.

[58] M. L. Hillwig and X. Liu, "A new family of iron-dependent halogenases acts on freestanding substrates," *Nature Chemical Biology,* vol. 10, p. 921–923, 2014.

[59] M. Z. Hernandes, S. M. T. Cavalcanti, D. R. M. Moreira, W. F. d. Azevedo and A. C. L. Leite, "Halogen Atoms in the Modern Medicinal Chemistry: Hints for the Drug Design, Current Drug Targets," *Current Drug Targets,* vol. 11, no. 3, pp. 303-314, 2010.

[60] P. N. Devine, R. M. Howard, R. Kumar, M. P. Thompson, M. D. Truppo and N. J. Turner, "Extending the application of biocatalysis to meet the challenges of drug development," *Nature Reviews Chemistry,* vol. 2, p. 409–421, 2018.

[61] A. Fryszkowska and P. N. Devine, "Biocatalysis in drug discovery and development," *Current Opinion in Chemical Biology,* vol. 55, pp. 151-160, 2020.

[62] E. M. M. Abdelraheem, H. Busch, U. Hanefeld and F. Tonin, "Biocatalysis explained: from pharmaceutical to bulk chemical production," *Reaction Chemistry & Engineering,* vol. 4, pp. 1878-1894, 2019.

[63] G. Li, J.-b. Wang and M. T. Reetz, "Biocatalysts for the pharmaceutical industry created by structure-guided directed evolution of stereoselective enzymes," *Bioorganic & Medicinal Chemistry,* vol. 26, no. 7, pp. 1241-1251, 2018.

[64] E. L. Bell, W. Finnigan, S. P. France, A. P. Green, M. A. Hayes, L. J. Hepworth, S. L. Lovelock, H. Niikura, S. Osuna, E. Romero, K. S. Ryan, N. J. Turner and S. L. Flitsch, "Biocatalysis," *Nature Reviews Methods Primers,* vol. 1, p. 46, 2021.

[65] D. Chiodi and Y. Ishihara, ""Magic Chloro": Profound Effects of the Chlorine Atom in Drug Discovery," *Journal of Medicinal Chemistry,* vol. 66, no. 8, 2023.

[66] A. J. Mitchell, Q. Zhu, A. O. Maggiolo, N. R. Ananth, M. L. Hillwig, X. Liu and A. K. Boal, "Structural basis for halogenation by iron- and 2-oxo-glutarate-dependent enzyme WelO5," *Nature Chemical Biology,* vol. 12, p. 636–640, 2016.

[67] C. Crowe, S. Molyneux, S. V. Sharma, Y. Zhang, D. S. Gkotsi, H. Connaris and R. J. M. Goss, "Halogenases: a palette of emerging opportunities for synthetic biology–synthetic chemistry and C–H functionalisation," *Chemical Society Reviews,* vol. 50, no. 17, p. 9443–9481, 2021.

[68] M. L. Matthews, C. M. Krest, E. W. Barr, F. H. Vaillancourt, C. T. Walsh, M. T. Green, C. Krebs and J. M. B. Jr., "Substrate-Triggered Formation and Remarkable Stability of the C−H Bond-Cleaving Chloroferryl Intermediate in the Aliphatic Halogenase, SyrB2," *Biochemistry,* vol. 48, no. 20, p. 4331–4343, 2009.

[69] E. Hegarty, J. Büchler and R. M. Buller, "Halogenases for the synthesis of small molecules," *Current Opinion in Green and Sustainable Chemistry,* vol. 41, p. 100784, 2023.

[70] P. K. Agarwal, "A Biophysical Perspective on Enzyme Catalysis," *Biochemistry,* vol. 58, no. 6, p. 438–449, 2019.

[71] G. P. Lisia and J. P. Loriaa, "Using NMR spectroscopy to elucidate the role of molecular motions in enzyme function," *Progress in Nuclear Magnetic Resonance Spectroscopy,* Vols. 92-93, pp. 1-17, 2016.

[72] A. G. Palmer, "Enzyme Dynamics from NMR Spectroscopy," *Accounts of Chemical Research,* vol. 48, no. 2, 2015.

[73] Y. Hu, K. Cheng, L. He, X. Zhang, B. Jiang, L. Jiang, C. Li, G. Wang, Y. Yang and M. Liu, "NMR-Based Methods for Protein Analysis," *Analytical Chemistry ,* vol. 93, no. 4, 2021.

[74] A. K. Mittermaier and L. E. Kay, "Observing biological dynamics at atomic resolution using NMR," *Trends in Biochemical Sciences,* vol. 34, no. 12, pp. 601-611, 2009.

[75] P. Markwick, T. Malliavin and M. Nilges, "Structural biology by NMR: structure, dynamics, and interactions," *PLOS Computational Biology,* vol. 4, no. 9, 2008.

[76] Y. H. Cheng, L. H. Zhang, B. Jiang, L. Jiang, C. Li, G. Wang, Y. Yang and M. Liu, "NMR-Based Methods for Protein Analysis," *Analytical Chemistry,* vol. 93, no. 4, pp. 1866-1879, 2021.

[77] A. M. Gronenborn and T. Polenova, "Introduction: Biomolecular NMR Spectroscopy," *Chemical Reviews,* vol. 122, no. 10, pp. 9265-9266, 2022.

[78] T. D. W. Claridge, High-Resolution NMR Techniques in Organic Chemistry, Third Edition, Elsevier Science, 2016.

[79] E. R. Jenista, A. M. Stokes, Rosa Tamara Branca and W. S. Warrena, "Optimized, unequal pulse spacing in multiple echo sequences improves refocusing in magnetic resonance," *Journal of Chemical Physics,* vol. 131, no. 20, p. 204510, 2009.

[80] A. Mittermaier and L. E. Kay, "New Tools Provide New Insights in NMR Studies of Protein Dynamics," *Science,* vol. 312, pp. 224-228, 2006.

[81] G. D. Fullerton, J. L. Potter and N. C. Dornbluth, "NMR relaxation of protons in tissues and other macromolecular water solutions," *Magnetic Resonance Imaging,* vol. 1, no. 4, pp. 209-226, 1982.

[82] I. K. H. Leung, M. Demetriades, A. P. Hardy, C. Lejeune, T. J. Smart, A. Szöllössi, A. Kawamura, C. J. Schofield and T. D. W. Claridge, "Reporter Ligand NMR Screening Method for 2-Oxoglutarate Oxygenase Inhibitors," *Journal of Medicinal Chemistry,* vol. 56, no. 2, p. 547–555, 2013.

[83] A. D. Gossert and W. Jahnke, "NMR in drug discovery: A practical guide to identification and validation of ligands interacting with biological macromolecules," *Progress in Nuclear Magnetic Resonance Spectroscopy,* vol. 97, pp. 82-125, 2016.

[84] O. Cala, F. Guillière and I. Krimm, "NMR-based analysis of protein–ligand interactions," *Analytical and Bioanalytical Chemistry,* vol. 406, p. 943–956, 2014.

[85] C. Dalvit, I. Gmür, P. Rößler and A. D. Gossert, "Affinity measurement of strong ligands with NMR spectroscopy: Limitations and ways to overcome them,"

Progress in Nuclear Magnetic Resonance Spectroscopy, Vols. 138-139, pp. 52-69, 2023.

[86] J. A. Aguilar, M. Nilsson, G. Bodenhausen and G. A. Morris, "Spin echo NMR spectra without J modulation," *Chemical Communications,* vol. 48, no. 6, pp. 811-813, 2012.

[87] R. K. Leśniak, A. M. Rydzik, J. J. A. G. Kamps, A. Kahn, T. D. W. Claridge and C. J. Schofield, "19F NMR studies on γ-butyrobetaine hydroxylase provide mechanistic insights and suggest a dual inhibition mode," *Chemical Communications,* vol. 55, no. 98, pp. 14717-14720, 2019.

[88] L. Fielding, "NMR methods for the determination of protein–ligand dissociation constants," *Progress in Nuclear Magnetic Resonance Spectroscopy,* vol. 51, no. 4, pp. 219-242, 2007.

[89] A. Bax, "Multidimensional nuclear magnetic resonance methods for protein studies," *Current Opinion in Chemical Biology,* vol. 4, pp. 738-744, 1994.

[90] B. Bleijlevens, T. Shivarattan, K. S. v. d. Boom, A. d. Haan, G. v. d. Zwan, P. J. Simpson and S. J. Matthews, "Changes in Protein Dynamics of the DNA Repair Dioxygenase AlkB upon Binding of Fe2+ and 2-Oxoglutarate," *Biochemistry,* vol. 51, no. 16, p. 3334–3341, 2012.

[91] B. Bleijlevens, T. Shivarattan, E. Flashman, Y. Yang, P. J. Simpson, P. Koivisto, B. Sedgwick, C. J. Schofield and S. J. Matthews, "Dynamic states of the DNA repair enzyme AlkB regulate product release," *EMBO Reports,* vol. 9, no. 9, p. 872–877, 2008.

[92] D. Idiyatullin, I. Nesmelova, V. A. Daragan and K. H. Mayo, "Comparison of 13CαH and 15NH backbone dynamics in protein GB1," *Protein Science,* vol. 12, no. 5, pp. 914-922, 2003.

[93] M. P. Williamson, "Using chemical shift perturbation to characterise ligand binding," *Progress in Nuclear Magnetic Resonance Spectroscopy,* vol. 73, pp. 1-16, 2013.

[94] M. P. Latham, G. R. Zimmermann and A. Pardi, "NMR Chemical Exchange as a Probe for Ligand-Binding Kinetics in a Theophylline-Binding RNA Aptamer," *Journal of the American Chemical Society,* vol. 131, no. 14, p. 5052–5053, 2009.

[95] I. R. Kleckner and M. P. Foster, "An introduction to NMR-based approaches for measuring protein dynamics," *Biochimica et Biophysica Acta,* vol. 1814, no. 8, p. 942–968, 2011.

[96] A. D. Bain, "Chemical exchange in NMR," *Progress in Nuclear Magnetic Resonance Spectroscopy,* vol. 43, no. 3-4, pp. 63-103, 2003.

[97] W. Becker, K. C. Bhattiprolu, N. Gubensäk and K. Zangger, "Investigating Protein–Ligand Interactions by Solution Nuclear Magnetic Resonance Spectroscopy," *ChemPhysChem,* vol. 19, no. 8, p. 895–906, 2018.

[98] C. Dalvit, I. Gmür, P. Rößler and A. D. Gossert, "Affinity measurement of strong ligands with NMR spectroscopy: Limitations and ways to overcome them," *Progress in Nuclear Magnetic Resonance Spectroscopy,* Vols. 138-139, pp. 52-69, 2023.

[99] B. Meyer and T. Peters, "NMR Spectroscopy Techniques for Screening and Identifying Ligand Binding to Protein Receptors," *Angewandte Chemie International Edition,* vol. 42, no. 8, pp. 864-890, 2003.

[100] H. Wetton, P. Klukowski, R. Riek and P. Güntert, "Chemical shift transfer: an effective strategy for protein NMR assignment with ARTINA," *Frontiers in Molecular Biosciences,* vol. 10, p. 1244029, 2023.

[101] P. Klukowski, R. Riek and P. Güntert, "Machine learning in NMR spectroscopy," *Progress in Nuclear Magnetic Resonance Spectroscopy,* Vols. 148-149, p. 101575, 2025.

[102] B. Brutscher, I. C. Felli, S. Gil-Caballero, T. Hošek, R. Kümmerle, A. Piai, R. Pierattelli and Z. Sólyom, "NMR Methods for the Study of Instrinsically Disordered Proteins Structure, Dynamics, and Interactions: General Overview and Practical Guidelines," in *Intrinsically Disordered Proteins Studied by NMR Spectroscopy*, vol. 870, Springer, Cham, 2015.

[103] M. J. Sattler, *Progress in NMR Spectroscopy,* vol. 34, pp. 93-158, 1999.

[104] B. Rowlinson, E. Crublet, R. Kerfah and M. J. Plevin, "Specific isotopic labelling and reverse labelling for protein NMR spectroscopy: using metabolic precursors in sample preparation," *Biochemical Society Transactions,* vol. 50, no. 6, p. 1555–1567, 2022.

[105] A. Bax and M. Ikura, "An efficient 3D NMR technique for correlating the proton and 15N backbone amide resonances with the α-carbon of the preceding residue in uniformly 15N/13C enriched proteins," *Journal of Biomolecular NMR ,* vol. 1, p. 99–104, 1991.

[106] L. E. Kay, M. Ikura, R. Tschudin and A. Bax, "Three-dimensional triple-resonance NMR spectroscopy of isotopically enriched proteins," *Journal of Magnetic Resonance,* vol. 89, no. 3, pp. 496-514, 1990.

[107] F. Inagaki, "Protein NMR Resonance Assignment," in *Roberts, G.C.K. (eds) Encyclopedia of Biophysics*, Berlin, Heidelberg, Springer, 2013, p. 2033–2037.

[108] M. Sattler, J. Schleucher and C. Griesinger, "Heteronuclear multidimensional NMR experiments for the structure determination of proteins in solution employing pulsed field gradients," *Progress in Nuclear Magnetic Resonance Spectroscopy,* vol. 34, no. 2, pp. 93-158, 1999.

[109] C. Redfield, "Assignment of Protein NMR Spectra Using Heteronuclear NMR—A Tutorial," in *Protein NMR*, vol. 32, Boston, MA, Springer, 2015, p. 1–42.

[110] G. M. Clore, C. Tang and J. Iwahara, "Elucidating transient macromolecular interactions using paramagnetic relaxation enhancement," *Current Opinion in Structural Biology,* vol. 17, no. 5, p. 603–616, 2007.

[111] M. J. Howard, "Protein NMR spectroscopy," *Current Biology,* vol. 8, no. 10, pp. R331-R333, 1998.

[112] Q. Miao, C. Nitsche, H. Orton, M. Overhand, G. Otting and M. Ubbink, "Paramagnetic Chemical Probes for Studying Biological Macromolecules," *Chemical Reviews,* vol. 122, no. 10, p. 9571–9642, 2022.

[113] I. B. Trindade, A. Coelho, F. Cantini, M. Piccioli and R. O. Louro, "NMR of paramagnetic metalloproteins in solution: Ubi venire, quo vadis?," *Journal of Inorganic Biochemistry,* vol. 234, p. 111871, 2022.

[114] V. Kocman, G. M. D. Mauro, G. Veglia and A. Ramamoorthy, "Use of paramagnetic systems to speed-up NMR data acquisition and for structural and dynamic studies," *Solid State Nuclear Magnetic Resonance,* vol. 102, pp. 36-46, 2019.

[115] I. Solomon, "Relaxation Processes in a System of Two Spins," *Physical Review,* vol. 99, p. 559–565, 1955.

[116] X. Guo, L. Zhang, J. Hu, B. Szilágyi, M. Yu, S. Chen, G. Tircsó, X. Zhou and J. Tao, "Improving the potential of paraCEST through magnetic-coupling induced line sharpening," *Chemical Science,* vol. 14, pp. 14157-14165, 2023.

[117] B. Liang, J. H. Bushweller and L. K. Tamm, "Site-Directed Parallel Spin-Labeling and Paramagnetic Relaxation Enhancement in Structure Determination of Membrane Proteins by Solution NMR Spectroscopy," *Journal of the American Chemical Society,* vol. 128, no. 13, p. 389–4397, 2011.

[118] K. Zimmermann, D. Joss, T. Müntener, E. S. Nogueira, M. Schäfer, L. Knörr, F. W. Monnard and D. Häussinger, "Localization of ligands within human carbonic anhydrase II using 19F pseudocontact shift analysis," *Chemical Science,* vol. 10, pp. 5064-5072, 2019.

[119] T. Müntener, D. Joss, D. Häussinger and S. Hiller, "Pseudocontact Shifts in Biomolecular NMR Spectroscopy," *Chemical Reviews,* vol. 122, no. 10, 2022.

[120] A. G. Nobile, D. Trummer, Z. J. Berkson, M. Wörle, C. Copéret and P.-A. Payard, "Assigning 1H chemical shifts in paramagnetic mono- and bimetallic surface sites using DFT: a case study on the Union Carbide polymerization catalyst," *Chemical Science,* vol. 14, no. 9, pp. 2361-2368, 2023.

[121] G. Parigi and C. Luchinat, "NMR Consequences of the Nucleus–Electron Spin Interactions," in *Paramagnetism in Experimental Biomolecular NMR*, Royal Society of Chemistry, 2018, pp. 1-41.

[122] I. Bertini, C. Luchinat and G. Parigi, "Magnetic susceptibility in paramagnetic NMR," *Progress in Nuclear Magnetic Resonance Spectroscopy,* vol. 40, no. 3, pp. 249-273, 2002.

[123] C. Schmitz, R. Vernon, G. Otting, D. Baker and T. Huber, "Protein Structure Determination from Pseudocontact Shifts Using ROSETTA," *Journal of Molecular Biology,* vol. 416, no. 5, pp. 668-677, 2012.

[124] J. Lopez-Barneo, R. Pardal and P. Ortega-Sáenz, "Cellular mechanism of oxygen sensing," *Annual Review of Physiology,* vol. 63, pp. 259-287, 2001.

[125] W. D. Figg, M. A. McDonough, R. Chowdhury, Y. Nakashima, Z. Zhang, J. P. Holt-Martyn, A. Krajnc and C. J. Schofield, "Structural Basis of Prolyl Hydroxylase Domain Inhibition by Molidustat," *ChemMedChem,* vol. 16, p. 2082, 2021.

[126] W. D. F. Jr., G. Fiorini, R. Chowdhury, Y. Nakashima, A. Tumber, M. A. McDonough and C. J. Schofield, "Structural basis for binding of the renal carcinoma target hypoxia-inducible factor 2α to prolyl hydroxylase domain 2," *Proteins,* vol. 91, no. 11, pp. 1510-1524, 2023.

Chapter 2:

Studies on the Structure and Dynamics of PHD2

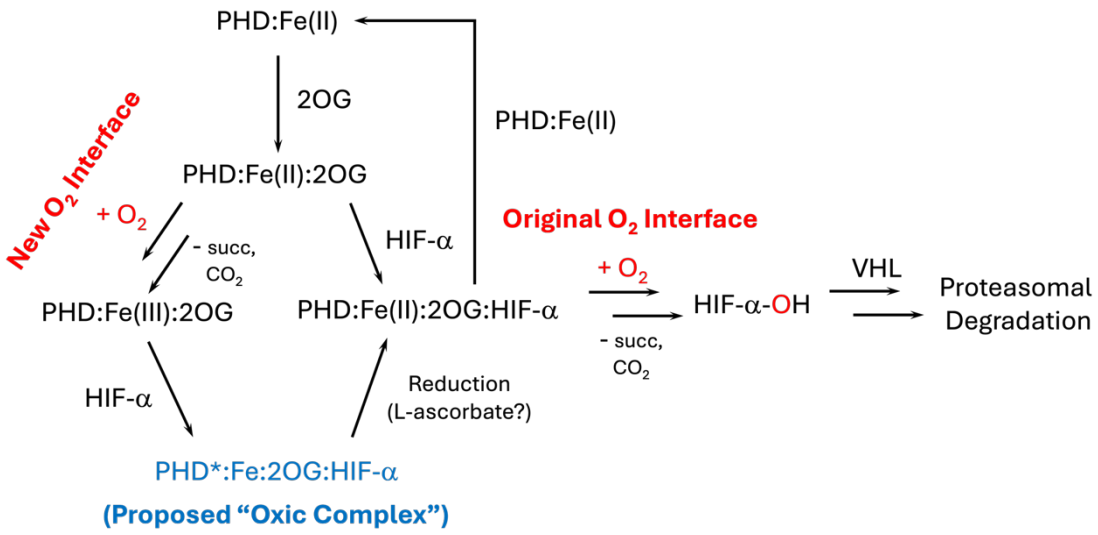


Table of Contents

Chapter 2: 2-1

2.1 Introduction 2-4

2.2 Results 2-4

2.2.1 PHD2 $^{1}H,^{15}N$-HSQC Optimization 2-4

2.2.1.1 Non-Uniform Sampling Studies 2-4

2.2.1.2 Expanded Window Spectral Studies 2-6

2.2.1.3 Variable Temperature Studies 2-9

2.2.1.4 Substrate Studies 2-13

2.2.1.5 Summary of Analyses 2-19

2.2.2 PHD2 Oxygen Binding Studies 2-20

2.2.2.1 Development of Sample Conditions for PHD2-Oxygen Interaction Studies 2-20

2.2.2.1.1 Metal Analysis 2-21

2.2.2.1.2 Oxic and Anoxic Complex Metal Studies 2-28

2.2.2.1.3 Oxic and Anoxic Complex Ligand Analysis 2-38

2.2.2.1.4 Oxic and Anoxic Complex Gas Analysis 2-47

2.2.2.1.5 Oxic and Anoxic Complex Substrate Analysis 2-48

2.2.2.1.6 Summary of Analyses 2-51

2.2.2.2 Further Analysis of the Oxic and Anoxic PHD2:Fe(II):2OG Complexes 2-51

2.2.2.2.1 Shielded Methyl Analysis 2-51

2.2.2.2.2 Analysis of the T387 Shielded Methyl Peak by Mutagenesis 2-55

2.2.2.2.3 Controlled Oxygen Pressure Experiments 2-66

2.2.2.2.4 Investigating Effects of Ascorbate/Glutathione on the Oxic PHD2 Complex .. 2-68

2.2.2.2.5 EPR Studies on the Oxic and Anoxic PHD2:Fe(II):2OG Complexes 2-76

2.2.3 PHD2 Further Metal Studies 2-79

2.2.3.1 Studies of the Effects of Metals on Free 2OG Shifts 2-79

2.2.3.2 Studies of PHD2:Metal Complexes 2-85

2.2.3.2.1 PHD2:Metal Complexes in the Presence or Absence of Oxygen, 2OG, and CODD 2-85

2.2.3.2.2 Studies on the Competition Between Co(II) and Zn(II) for PHD2 Binding 2-97

2.2.3.2.3 Vanadium Oxide Binding Studies 2-102

2.2.4 PHD2: Oxic and Anoxic Complex Stabilities 2-105

2.2.4.1 Studies on the Stabilities of PHD2:Fe(II):Inhibitor Complexes..... 2-108

2.2.4.2 Studies on the Stabilities of the PHD2:Fe(II):Ligand:Substrate Complexes 2-133

2.2.4.3 Studies on the Stabilities of the PHD2:Fe(III):Ligand Complexes..... 2-150

2.2.4.4 Studies on the Stabilities of PHD2:Fe(III):Ligand:Substrate Complexes 2-169

2.2.4.5 Summary of Results..... 2-185

2.3 Conclusions.....2-187

2.4 References.....2-191

2.1 Introduction

Interest in PHD2 stems from its role in the human hypoxic response as well as the connections between PHD and HIF activities and various forms of cancer. [1] [2] [3] Despite previous studies investigating the mechanism of PHD2, little is understood about how oxygen approaches and interacts with the active site, processes which are proposed to be related to its function as an oxygenase and hypoxia sensor. [4] [5] The research described in this chapter utilised NMR methods to investigate the role of oxygen in the activity of PHD2 from a mechanistic and dynamics perspective. Initial experiments aimed to investigate what conditions would be suitable for carrying out the NMR studies—including variable factors such as temperature, PHD2 construct, appropriate metal ion, cosubstrate/ligand, and the gas. Once the conditions had been established, paramagnetic interactions were used to investigate oxygen-protein interactions and ^{15}N-HSQC analyses were used to investigate structural changes.

2.2 Results

2.2.1 PHD2 ^{1}H,^{15}N-HSQC Optimization

The first step was to determine what pulse sequence and parameters were best suited to the intended experiments, as well as the conditions for PHD2 protein studies. Previous NMR studies of PHD2:Zn(II):2OG helped to inform on these decisions, as described in the D. Phil theses of Martine Abboud and Ivanhoe Leung. [6] [7]

2.2.1.1 Non-Uniform Sampling Studies

Non-uniform sampling (NUS) is an NMR acquisition method that works by decreasing the sampling of NMR data points along the indirect dimension in multi-dimensional experiments, therefore, decreasing the acquisition time. [8] [9] Using

predictive methods, a complete dataset can be extrapolated. [8] [9] The NUS acquisition method is a useful way to save time with minimal loss in data quality. A major drawback of the NUS method is that spectra with less defined peaks of lower intensity can manifest a significant drop-off in data quality, potentially leading to loss of weaker peaks.

A $^{1}H,^{15}N$-HSQC spectrum of PHD2:Zn(II):2OG was recorded with parameters and conditions similar to previous NMR studies, but using lower concentrations (to test the limits of NUS sampling under less favourable protein conditions that may occur under some sample conditions) (**Figure 2.1**, blue). On acquisition, utilising NUS at 50% sampling (**Figure 2.1**, red), several peaks in the characteristic regions of the protein spectrum (above 8.5 ppm) were lost. Higher protein concentrations would yield better results with NUS acquisition but would likely not be feasible at the ~100 μM protein concentrations planned for these studies. PHD2 protein samples at these concentrations lack the signal-to-noise ratio (SNR) required, which can lead to issues of sampling artifacts (due to reconstruction of data), loss of weaker peaks, and greater consideration for the parameters and reconstruction schemes will be needed. [10] [11] [12]

Peaks of interest for the research described in this thesis are expected to be affected by: 1) non-native/active PHD2 complexes leading to lower protein complex stability; 2) paramagnetic relaxation and shift effects (as discussed in **Section 1.2.5**) which may broaden peaks; and 3) populations of different PHD2 protein exchange complexes, which may decrease the sensitivity of the experiments. Due to these factors, NUS sampling was not chosen as a method for $^{1}H,^{15}N$-HSQC data acquisition.

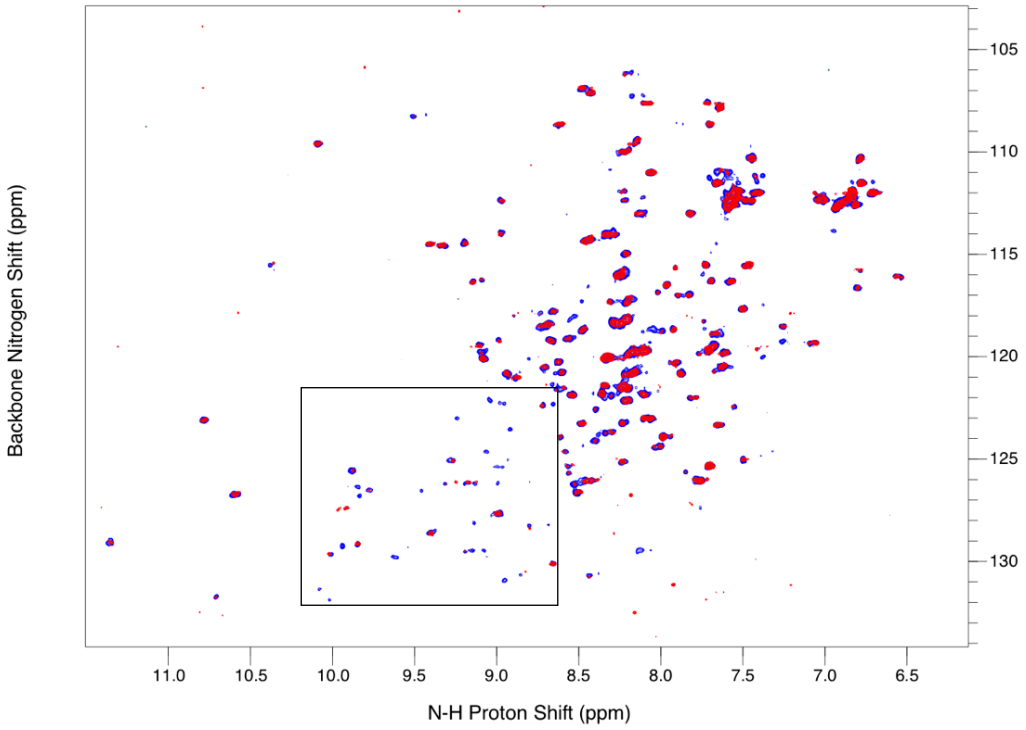


Figure 2.1 *^{1}H,^{15}N-HSQC spectral comparison of PHD2:Zn(II):2OG spectra in the presence and absence of non-uniform sampling (NUS) acquisition methods under oxic conditions (i.e. under aerobic conditions). The experiment was carried out at 0% (blue) and 50% (red) NUS. The results suggested that the NUS method would not be viable for further studies due to considerable loss of weaker intensity signals, especially in the 8.5-10.0 ppm region (as indicated by the black box). The standard concentrations of each component were: 73 µM PHD2, 195 µM Zn(II), 195 µM 2OG, room pressure O_2. Buffer conditions were 10% D_2O and 90% 50 mM Tris-D_{11} pH 6.6.*

2.2.1.2 Expanded Window Spectral Studies

The next preliminary study was to investigate which of the ^{1}H,^{15}N-HSQC peaks of PHD2 belong to side-chain residues. Side-chain residue peaks tend to be more mobile than backbone peaks, as they are not locked into the backbone of the protein. Protein residues containing N-H side chain groups with characteristic shifts in the ^{1}H,^{15}N-HSQC spectrum include asparagine and glutamine (typically seen as a strong cluster of peaks around 6.5-7.5 ppm, depending on solution pH and other factors), tryptophan (often found in the most deshielded region of the ^{1}H dimension), arginine, and lysine. [13] Both

arginine and lysine peaks can be found aliased or folded into the bulk of the ^{1}H,^{15}N-HSQC peaks and identifying them can be challenging. [14] To better characterise these side-chain peaks, the peaks were identified through expansion of the spectral window. This method unaliases/unfolds the peaks so that they can be observed at their true chemical shift values.

On expansion of the PHD2:Zn(II):2OG window (**Figure 2.2**, blue), a set of peaks falling around 85 ppm in the ^{15}N dimension was observed; these peaks may be attributed to the side-chains of arginine and lysine residues once aliasing was removed. The corresponding peaks in the unaliased spectrum (**Figure 2.2**, red peaks) would be expected to be absent from the expanded window spectrum (**Figure 2.2**, blue peaks) in the regions between 105 and 132 ppm in the ^{15}N dimension,, therefore, are identifiable as the red coloured peaks with an identical ^{1}H shift to the corresponding, unaliased, blue peaks in the ^{15}N region below 90 ppm.

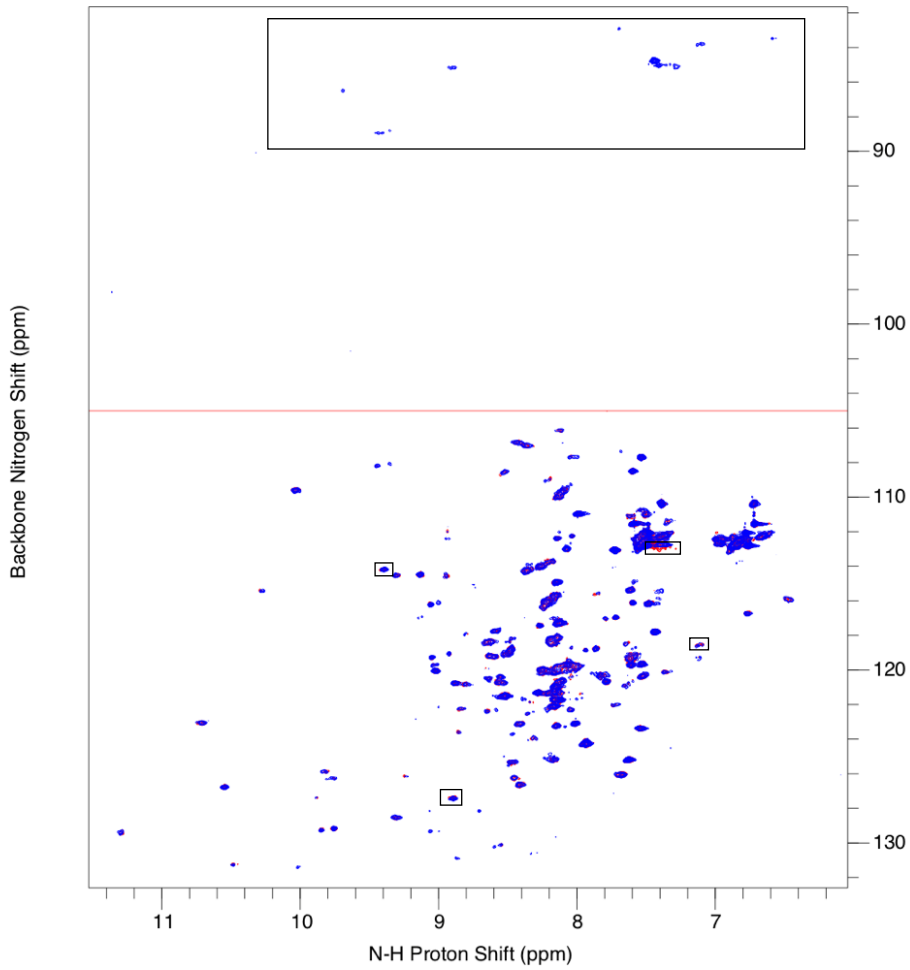


Figure 2.2 *$^{1}H,^{15}N$-HSQC spectral comparison of oxic PHD2:Zn(II):2OG with and without an expanded ^{15}N spectral window. The expanded window (blue) and normal window (red) spectra were compared. A set of peaks were observed around 85 ppm in the ^{15}N dimension that can be attributed to arginine (~7 ppm in ^{1}H) and lysine (~9-10 ppm in ^{1}H) residues, indicated within the black box at the top of the figure. Positions where the aliased peaks may fall in the $^{1}H,^{15}N$-HSQC spectrum without an expanded window are indicated within the smaller black boxes. Some aliased peaks that were observed with an expanded spectral window (blue) could not be tracked in the typical spectral window (red) due to peak overlap and, possibly, broadening. Standard concentrations of each component were: 73 µM PHD2, 195 µM Zn(II), 195 µM 2OG, room pressure O_2. Buffer conditions were 10% D2O and 90% 50 mM Tris-D_{11} pH 6.6.*

The lack of visibility of the unaliased peaks in the typical window size (**Figure 2.2**, red) indicates these peaks may have considerable overlap with peaks of interest or aren't sensitive enough to be detected over the noise. Regions where the unaliased peaks

are predicted to be found (as indicated by the small black boxes in **Figure 2.2**) generally contain clusters of peaks. Movement of peaks in these regions during further NMR studies should take into account that these side chain resonances are flexible (rather, shifts in these regions may be due to minor environmental changes and may not reflect catalytically relevant changes).

2.2.1.3 Variable Temperature Studies

Next, peak shifts and broadening in the PHD2:Zn(II):2OG complex were investigated as a function of temperature variation. It should be noted that part of the deshielding effect on the spectrum as a whole as the temperature is increased may be attributed to the effect of temperature on the pH of tris(hydroxymethyl)aminomethane (tris), the buffer used in this experiment (**Figure 2.3**). The subsequent change in pH is likely, at least partially, responsible for the uniform shifts in the $^{1}H,^{15}N$-HSQC spectrum.

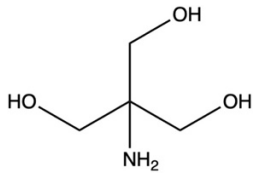


Figure 2.3 *Structure of tris(hydroxymethyl)aminomethane (tris "buffer").*

Beyond uniform, linear shifting of the spectrum as the temperature is increased, as expected in a temperature series, [15] less uniform shifts and broadening may be observed that are indicative of local changes in conformation, flexibility of residues, protein solubility, and/or disordered protein regions. [16] [17] [18] In the $^{1}H,^{15}N$-HSQC spectrum of PHD2:Zn(II):2OG at 278 K (**Figure 2.4**, black), considerable loss of the more deshielded—or "ordered"—peaks was observed. Protein tumbling in solution is slowed as the temperature decreases, leading to less averaging of signals and, therefore, broader peaks, which may partially explain this effect. The region around 6 to 8.5 ppm is also where partially precipitated or folded protein peaks are typically observed, and

variable temperature studies can be useful tools for teasing out these disordered regions. [18]

As the temperature is increased, a wider range of chemical shifts across the protein backbone resonances is observed, with faster tumbling and therefore, sharper peaks. [16] The spectral properties of 1) sharper peaks and 2) greater range of peak shifts made relatively high temperature $^{1}H,^{15}N$-HSQC spectra potentially useful for understanding the oxygen sensing mechanism of PHD2 from structural and functional perspectives, with the drawbacks of 1) faster reaction speeds that are harder to record and 2) instability—precipitation and changes in protein fold—of some proteins at higher temperatures.

As temperatures were increased step-wise from 278 K to 310 K for the PHD2:Zn(II):2OG complex (**Figure 2.4**), the major change observed was sharpening of the amide peaks; several peaks that weren't visible above the noise at temperatures below 288 K became sharp. No evidence for precipitation was observed at 310 K. These observations indicated that temperatures around 310 K could be preferred for NMR experiments on PHD2. Temperatures of 308 K were used going forward as the standard for ^{1}H,15N-HSQC spectra described in this thesis to enable correlation with previous data. [19] [20] The pH of samples for $^{1}H,^{15}N$-HSQC experiments was 6.5 for ease of comparison with previously published data on PHD2 (ranging from 6.5-6.8). [6] [7]

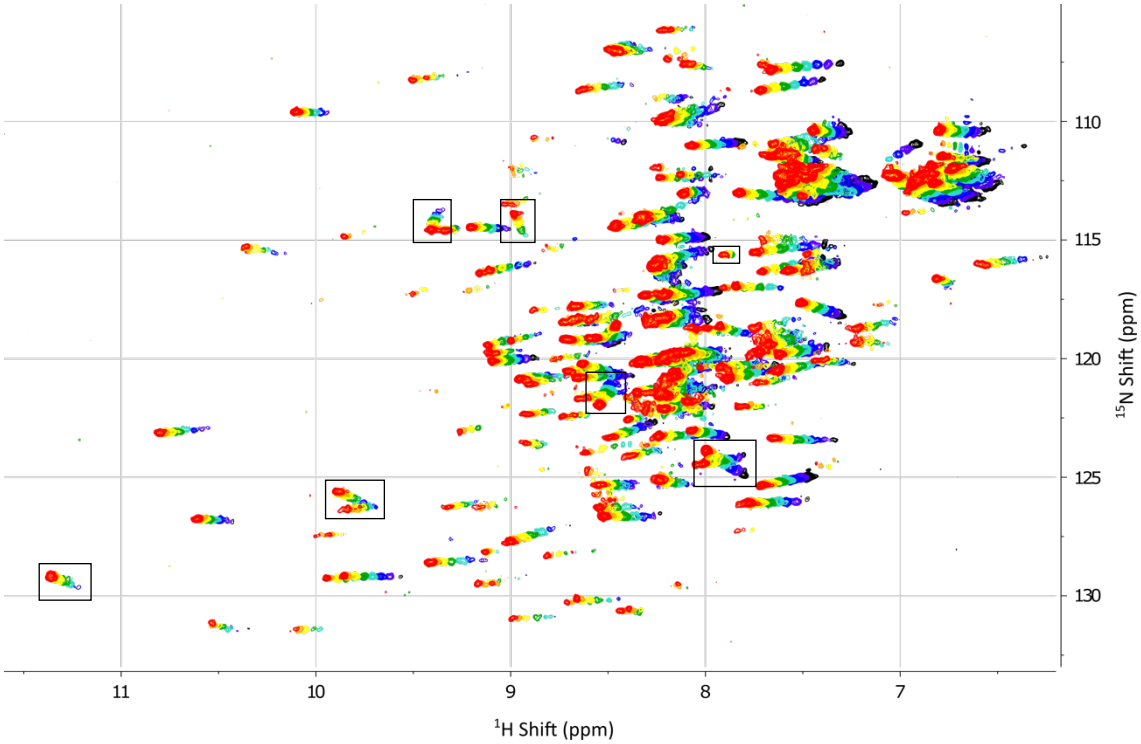


Figure 2.4 *^{1}H,^{15}N-HSQC spectra of the oxic PHD2:Zn(II):2OG complex at various temperatures. The temperatures explored were 278 K (black), 283 K (purple), 288 K (blue), 293 K (cyan), 298 K (green), 303 K (yellow), 308 K (orange), and 310 K (red). Analysis of peaks exhibiting differences in ^{15}N and ^{1}H peak shift compared to the majority of peaks hint at flexibilities of the related residues. Examples of some of the more distinct peak shifts impacted by increasing temperatures are shown within the black boxes. Standard concentrations of each component were: 100 µM unlabelled PHD2, 300 µM Zn(II), 500 µM 2OG, and room pressure O_2. Buffer conditions were 10% D_2O, and 90% 50 mM Tris-d_{11} pH 6.5.*

Distances between subsequent peaks for each interval in the temperature series were compared and outliers were analysed. Peaks with different broadening patterns or distinctive shifts in the ^{1}H dimension were also analysed. From this set of data, four peak areas were identified as being of particular interest. Two of the areas of interest (**Figure 2.5**, a) and c)) correspond to the region of the β2β3 loop of PHD2, which is important in the catalytic mechanism. [2] [21] [22] The other two areas of interest (**Figure 2.5**, b) and d)) are in predicted flexible regions, with region d) showing two conformations in PHD2 crystal structures.

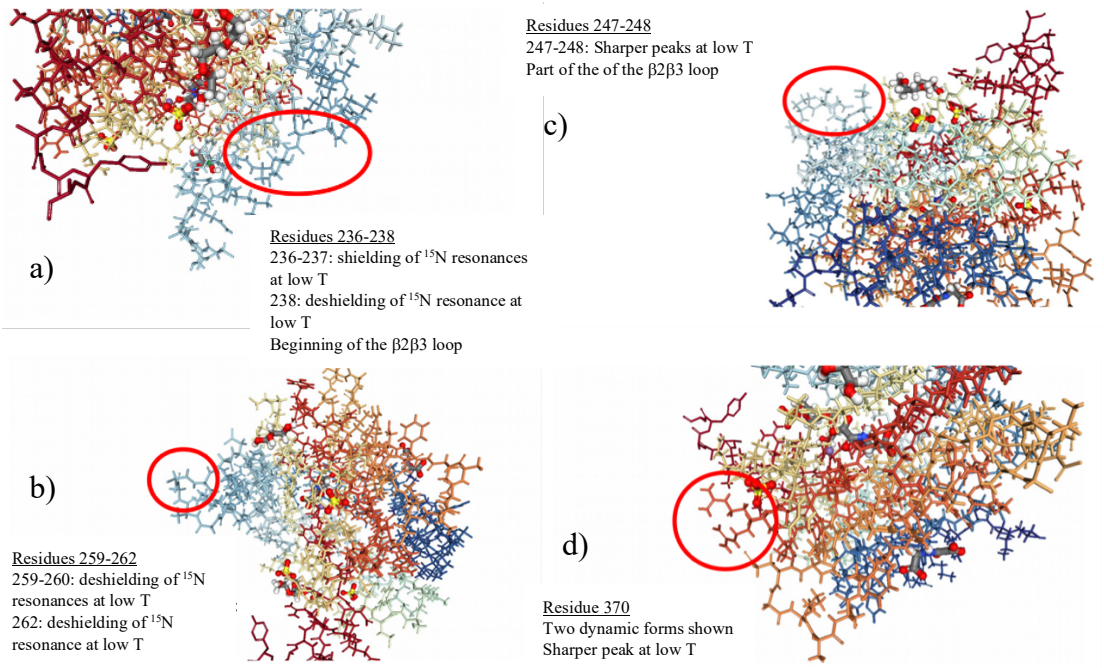


Figure 2.5 *Site-specific analysis of PHD2 showing four regions of interest as observed from variable temperature studies. These regions (a, b, c, and d), exhibit different shielding and deshielding patterns under variable temperature conditions as compared to the majority of the PHD2 peaks. From analysis of uniquely shifted peaks assigned by the nearest neighbour approach, it was proposed that these peaks may be attributed to regions of the protein that are expected to be more flexible, including flexible side chains and regions of the β2β3 loop (residues 237-254). These observations indicate that temperature variation may be a useful tool for understanding the flexibility of PHD2 in various complexes and under a variety of conditions (PDB:5L9R).*

Studies on regions of the ^{1}H,^{15}N-HSQC spectrum with unique chemical shifts and broadening patterns over a series of temperatures can help to elucidate flexible and structurally interesting regions of the protein surface. Temperature studies may also help to inform on which regions of the protein surface are more likely to respond to changes in the protein environment. Similar methods have been used in a paper I coauthored involving isopencillin N synthase (see Chapter 4, **Section 4.1**) [23] and are likely to be valuable in further PHD2 studies.

2.2.1.4 Substrate Studies

The next stage was to understand the stability and binding of the three HIF CODD substrates [24] [25] [26] in the presence of PHD2, Zn(II), and 2OG. The three substrates used were as follows (all prepared with C-terminal amides):

HIF-1α CODD = 2254 g/mol (^{556}DLDLEMLAPYIPMDDDFQL^{574})
HIF-2α CODD = 2309 g/mol (^{518}DLDLE**T**LAPYIPMD**GE**DFQL^{537})
HIF-3α CODD = 2315 g/mol (^{484}**A**LDLEMLAPYI**S**MDDDFQLN^{503})

It was considered that NMR investigations on all three types of human HIF-α CODD substrates (HIF-1α, HIF-2α and HIF-3α CODD) would inform analyses on differences in substrate binding modes and selectivity. [27] [28]

To build a baseline understanding of the interactions between PHD2 and its HIF-1α substrate, ^{1}H,^{15}N-HSQC spectra of PHD2:Zn(II):2OG with (red) and without (blue) HIF-1α CODD binding were compared (**Figure 2.6**). Zn(II) was used as catalytically inert substitute for the active Fe(II). As observed previously, [22] significant shift differences were observed on HIF-1α CODD binding. These shift differences will be compared to the shifts observed in the presence of HIF-2α and HIF-3α CODD, as apparent in the subsequently described figures, to investigate how sequence differences impact on the three PHD2:HIF-α complex structures.

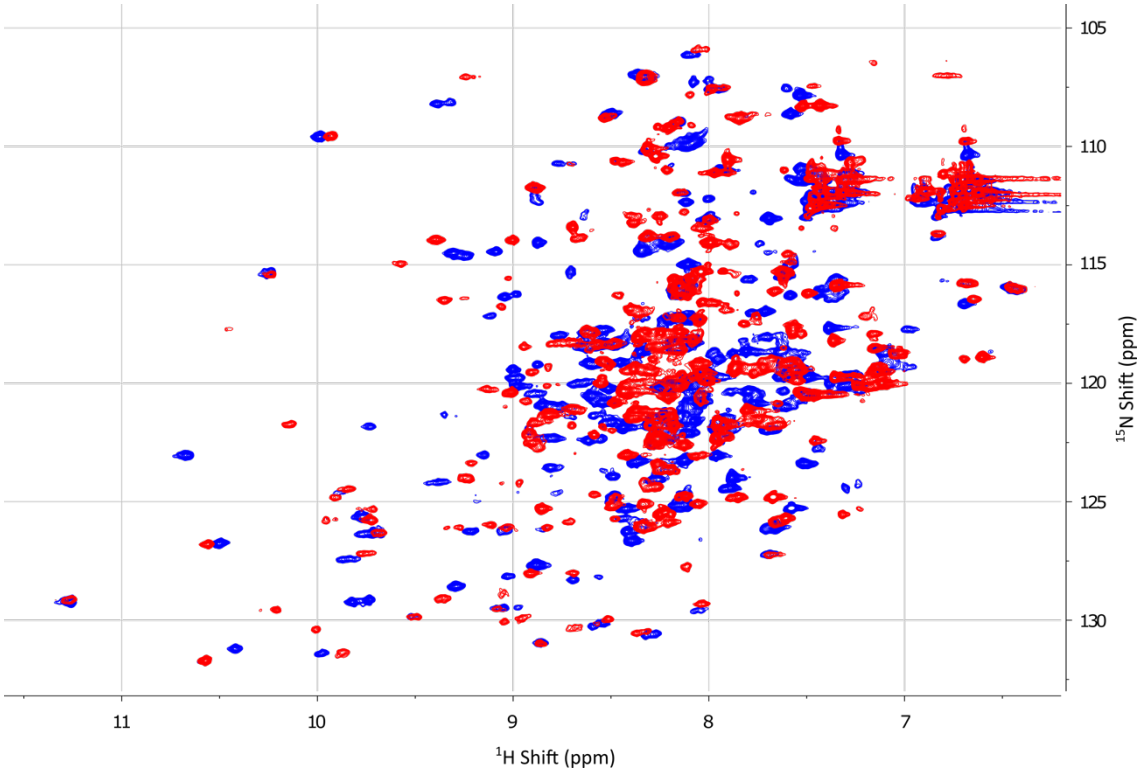


Figure 2.6 *$^{1}H,^{15}N$-HSQC spectral comparison of the oxic PHD2:Zn(II):2OG complex in the presence (red) or absence (blue) of HIF-1α CODD. Substantial shift differences occur on addition of HIF-1α CODD. Standard concentrations of each component were: 100 μM ^{15}N-labelled PHD2, 300 μM Zn(II), 500 μM 2OG, 500 μM HIF-1 CODD, and room pressure O_2. Buffer conditions were 10% D_2O, and 90% 50 mM Tris-d_{11} pH 6.5.*

Next, the $^{1}H,^{15}N$-HSQC spectra of PHD2:Zn(II):2OG in the presence (green) and absence (blue) of HIF-2α CODD (**Figure 2.7**) and the $^{1}H,^{15}N$-HSQC spectra of PHD2:Zn(II):2OG in the presence (pink) and absence (blue) of HIF-3α CODD (**Figure 2.8**) were collected. As with the HIF-1α CODD complex (**Figure 2.6**), significant changes across the spectra were observed on addition of substrate; many of the peak shifts on addition of HIF-1α CODD appeared to correspond with those observed on addition of HIF-2α and HIF-3α CODD to the PHD2:Zn(II):2OG complex (**Figure 2.7** and **Figure 2.8** respectively). These observations indicate that the differences in amino acid sequences between the substrates may not drastically impact the structure of these non-native (Zn(II)-bound) complexes and that the binding modes of the HIF-α CODD

substrates are similar. Further studies of these complexes in the presence of Fe(II) and NOG—to ensure the complexes are catalytically inactive—may be useful to start to investigate the importance of the substrate sequence in: 1) affecting active site conformation and 2) regulating interactions with gases and, in particular, oxygen to get a better understanding of the importance of the active site structure in oxygen interactions.

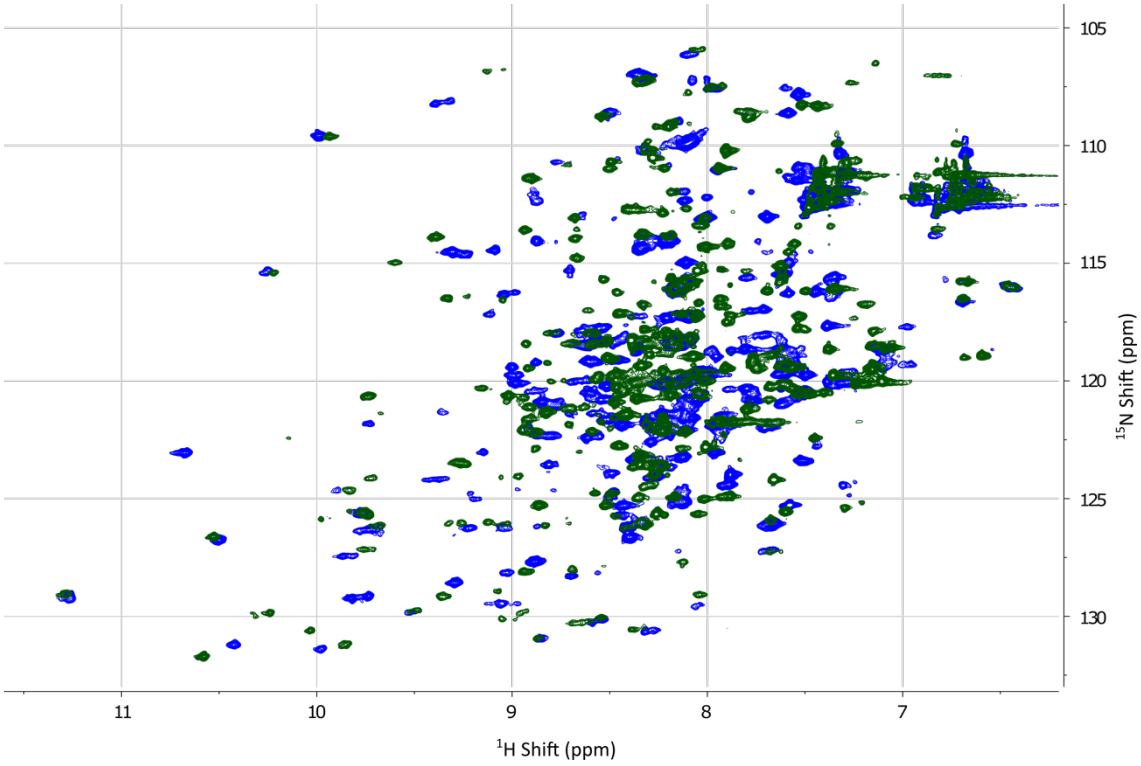


Figure 2.7 *^{1}H,^{15}N-HSQC spectral comparison of the oxic PHD2:Zn(II):2OG complex in the presence (green) or absence (blue) of HIF-2α CODD. Substantial shift differences occur on addition of HIF-2α CODD. Standard concentrations of each component were: 100 μM ^{15}N-labelled PHD2, 300 μM Zn(II), 500 μM 2OG, 500 μM HIF-2α CODD, and room pressure O_2. Buffer conditions were 10% D_2O, and 90% 50 mM Tris-d_{11} pH 6.5.*

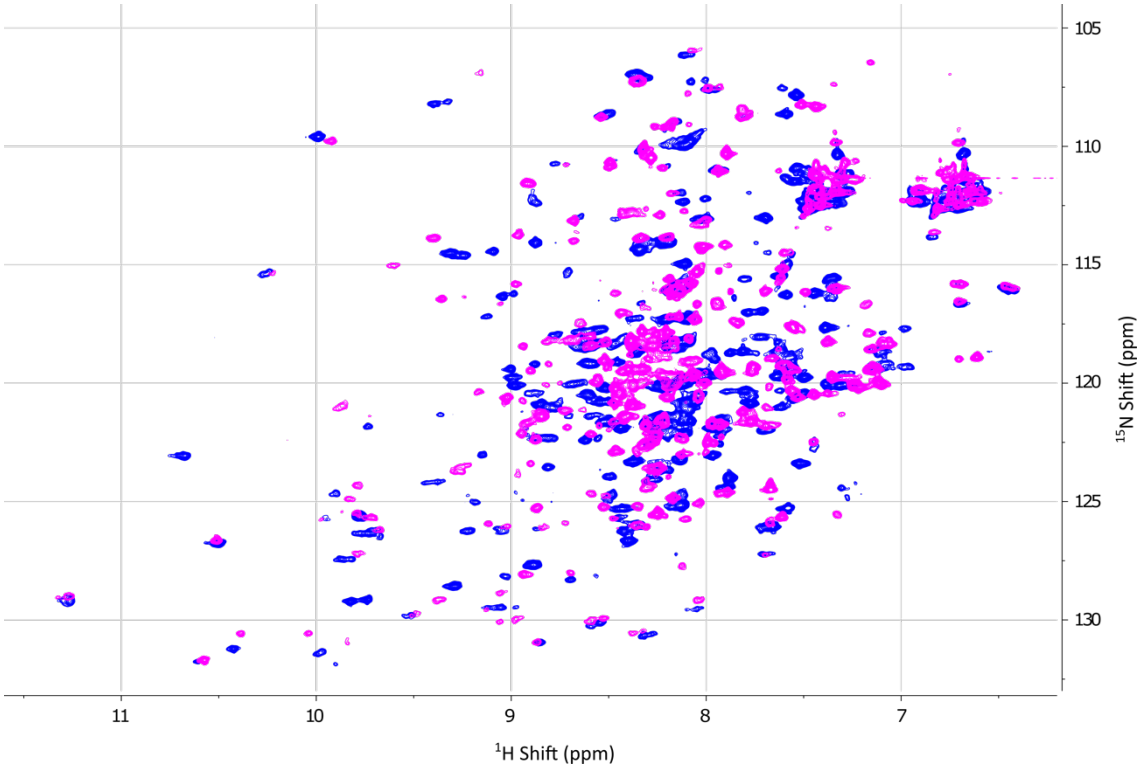


Figure 2.8 *^{1}H,^{15}N-HSQC spectral comparison of the oxic PHD2:Zn(II):2OG complex in the presence (pink) or absence (blue) of HIF-3α CODD. Substantial shift differences occur on addition of HIF-3α CODD. Standard concentrations of each component were: 100 μM ^{15}N-labelled PHD2, 300 μM Zn(II), 500 μM 2OG, 500 μM HIF-3α CODD, and room pressure O_2. Buffer conditions were 10% D_2O, and 90% 50 mM Tris-d_{11} pH 6.5.*

Figure 2.9 shows an overlay of the PHD2:Zn(II):2OG:HIF-1α, PHD2:Zn(II):2OG:HIF-2α, and PHD2:Zn(II):2OG:HIF-3α CODD complexes (**Figure 2.9** red, green, and pink respectively), indicating the level of overlap in the peak shifts. Peaks of interest with clear peak shift differences across the different substrates are in black boxes.

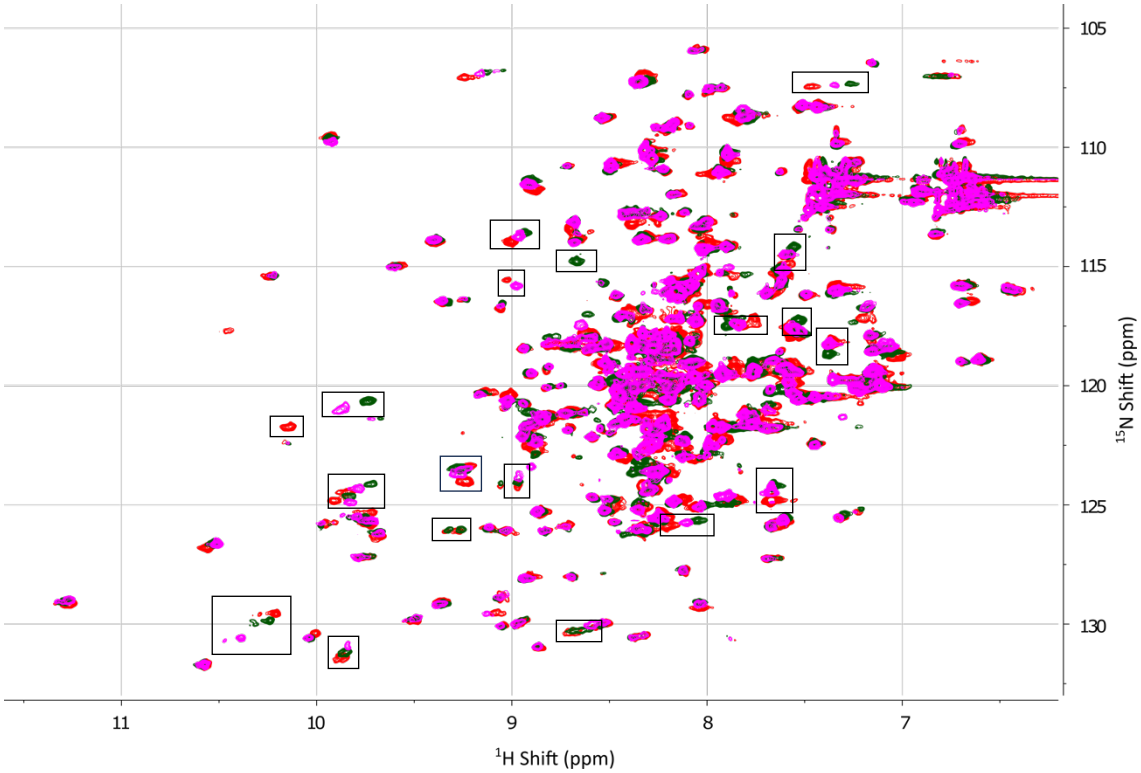


Figure 2.9 *$^{1}H,^{15}N$-HSQC spectral comparison of the oxic PHD2:Zn(II):2OG:CODD complexes for the HIF-1α (red), HIF-2α (green), and HIF-3α (pink) CODD variants. Relatively minor shift differences are observed between the variants. The peaks within the black boxes indicate peaks in less crowded areas of the spectrum that may show slightly greater variation in shifts across substrate complexes, as observed qualitatively. Standard concentrations of each component were: 100 μM ^{15}N-labelled PHD2, 300 μM Zn(II), 500 μM 2OG, 500 μM CODD, and room pressure O_2. Buffer conditions were 10% D_2O, and 90% 50 mM Tris-d_{11} pH 6.5.*

Quantitative comparison of the PHD2:Zn(II):2OG:HIF-1α, PHD2:Zn(II):2OG:HIF-2α, and PHD2:Zn(II):2OG:HIF-3α CODD complexes (Error! Reference source not found. blue, orange, and yellow respectively) mirrors the qualitative analysis above (**Figure 2.9**), indicating that there are no large shift differences between the PHD2 complexes in the presence of the three HIF-α CODD substrates. Minor shift differences are observed, mainly in regions of greater protein flexibility and regions that have been previously found to be affected by substrate binding, [20] including at the βIVβV loop and the C-terminal helix. In regions that differ across substrate complexes

(as indicated by residues within black boxes in **Figure 2.10**), the HIF-1α CODD substrate (**Figure 2.10**, blue) complex exhibits the smallest magnitude of peak shifts relative to the PHD2:Zn(II):2OG complex, differentiating it from the HIF-2α and HIF-3α CODD complexes (**Figure 2.10**Error! Reference source not found., orange and yellow respectively), which share similar, larger magnitudes of peak shifts in these regions. This effect may be, in part, due to destabilisation of complexes involving non-native substrates. Interestingly, the β2β3 loop did not show significant peak shift variation across substrate complexes, as may have been expected from previous substrate complex studies involving CODD and NODD complexes. [20]

Comparison of the shift differences of the $PHD2_{181-402}$:Zn(II):2OG:HIF-1α CODD complex (from previous work on PHD2; Error! Reference source not found.**,** green) [6] [7] to that of the $PHD2_{181-407}$:Zn(II):2OG:HIF-1α CODD complex (Error! Reference source not found.**,** blue), shows larger peak shifts for the smaller ($PHD2_{181-402}$) construct. These shift differences may be due to slight differences in protein stability or structure due to a shortened C-terminal helix. Overall, the similarity in shifts indicates that data is comparable across the two constructs.

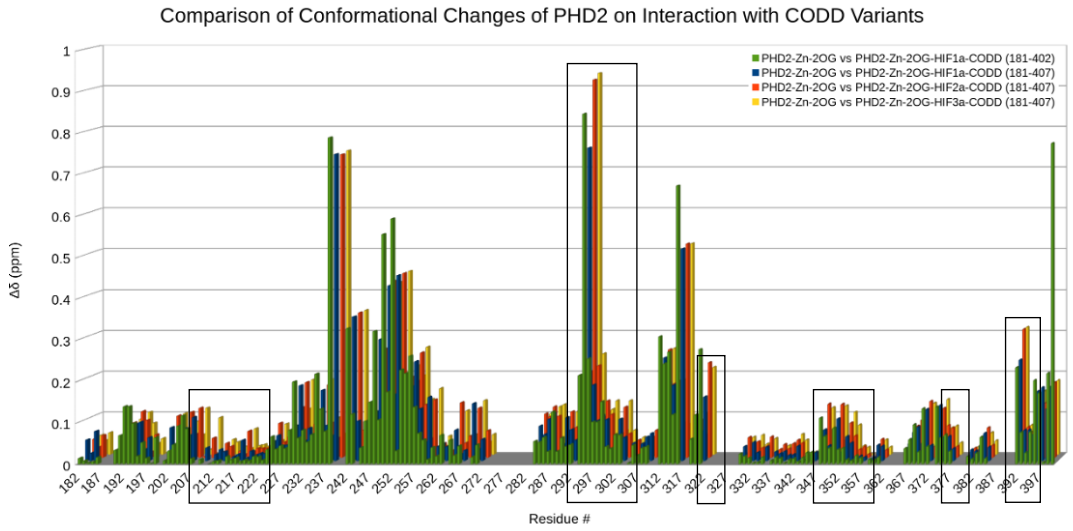


Figure 2.10 *Comparison of the shift differences between the $^{1}H,^{15}N$-HSQC spectra of the oxic PHD2:Zn(II):2OG:CODD complexes and the oxic PHD2:Zn(II):2OG complexes. The complexes investigated were: PHD2:Zn(II):2OG:HIF-1α CODD (blue), PHD2:Zn(II):2OG:HIF-2α CODD (orange), PHD2:Zn(II):2OG:HIF-3α CODD (yellow), and PHD2:Zn(II):2OG:HIF-1α CODD for a shorter PHD2 construct previously studied* ***[6]*** *(green, $PHD2_{181\text{-}402}$). The four spectra show very similar peak shift patterns on CODD binding. The black boxes indicate regions of variation between peak shifts of $PHD2_{181\text{-}407}$ substrate complexes. Shift differences were calculated using the equation given in Chapter 1,* ***Section 1.2.3.2****.*

2.2.1.5 Summary of Analyses

From the $^{1}H,^{15}N$-HSQC optimisation experiments carried out with PHD2, it was determined that: 1) NUS is not a viable methods for the experiments of interest, 2) some PHD2 sidechain peaks fall in regions detrimental to following peaks of interest, 3) flexible regions of interest on the protein surface are affected by temperature variation, include a region containing, or around, the β2β3 loop of PHD2, and 4) all the tested HIF-α CODD substrates appear to give similar shifts in relation to the PHD2:Zn(II):2OG complex, despite not having the same amino acid sequences. From this preliminary analysis of PHD2 complex properties, a standard for NMR conditions and analysis was established.

2.2.2 PHD2 Oxygen Binding Studies

As discussed in Chapter 1, analysis of the interaction between PHD2 and oxygen is important for understanding the mechanism of its role in oxygen sensing. The research described in this chapter systematically evaluated each component of the active site of PHD2, aiming to tease out which components contribute to the unusually slow reaction of PHD2 with oxygen [4] [29] [30] and which are important in the PHD2 catalytic structure, [31] [32] factors which are important in understanding the oxygen sensing mechanism.

Initial studies focused on investigating the impact of oxygen binding on chemical shifts and broadening of the $^{1}H,^{15}N$-HSQC spectrum of PHD2, with later studies relying on ^{1}H NMR methods for fast and sensitive analysis of changes in ^{1}H resonances with unique shifts, attributed to proximity to paramagnetic species or other unique protein environments. These approaches aimed to investigate: 1) shifts and broadening due to protein conformational changes induced by oxygen binding, 2) site-specific changes in NMR peaks due to interactions between amino acid side chains and oxygen, and 3) paramagnetic-induced changes in NMR peaks from changes in the oxidation or spin state of the active site metal.

The first step was to develop a stable and biologically relevant set-up for analysing oxygen binding using $^{1}H,^{15}N$-HSQC NMR spectroscopy.

2.2.2.1 Development of Sample Conditions for PHD2-Oxygen Interaction Studies

Four major components of PHD2 catalysis chemistry that were considered when developing the system for study were the: 1) active site metal, 2) cosubstrate/ligand, 3) gas molecule, and 4) substrate used. To analyse the importance of each component in forming the active site and protein conformation, each component was systematically

replaced by a structurally similar—yet inactive—alternative to give an inactive PHD2 complex that might still respond to oxygen. Such complexes are necessary to measure changes in PHD2 structure over the long $^{1}H,^{15}N$-HSQC spectral acquisition times required. They also need to retain an ability to bind oxygen to be used as model complexes for analysis of the oxygen sensing mechanism of PHD2. The following described studies were initially carried out in the absence of the substrate to simplify conditions.

2.2.2.1.1 Metal Analysis

The first step was to explore the PHD2:Zn(II):2OG complex by NMR. This complex has been extensively studied by $^{1}H,^{15}N$-HSQC NMR spectral analysis, as previously discussed, [6] [7] but had yet to be explored in the presence and absence of oxygen. Zn(II) has been previously used as an inert metal of choice for studies of PHD2 due to its diamagnetism and single protein-bound oxidation state. [33] [34] [35] These properties facilitate NMR analyses by simplifying the spectrum (paramagnetism creates more complicated analysis through shifting and broadening of peaks). [36]

The spectrum of the oxic PHD2:Zn(II):2OG complex, as was explored previously in this chapter, is shown in **Figure 2.11**.

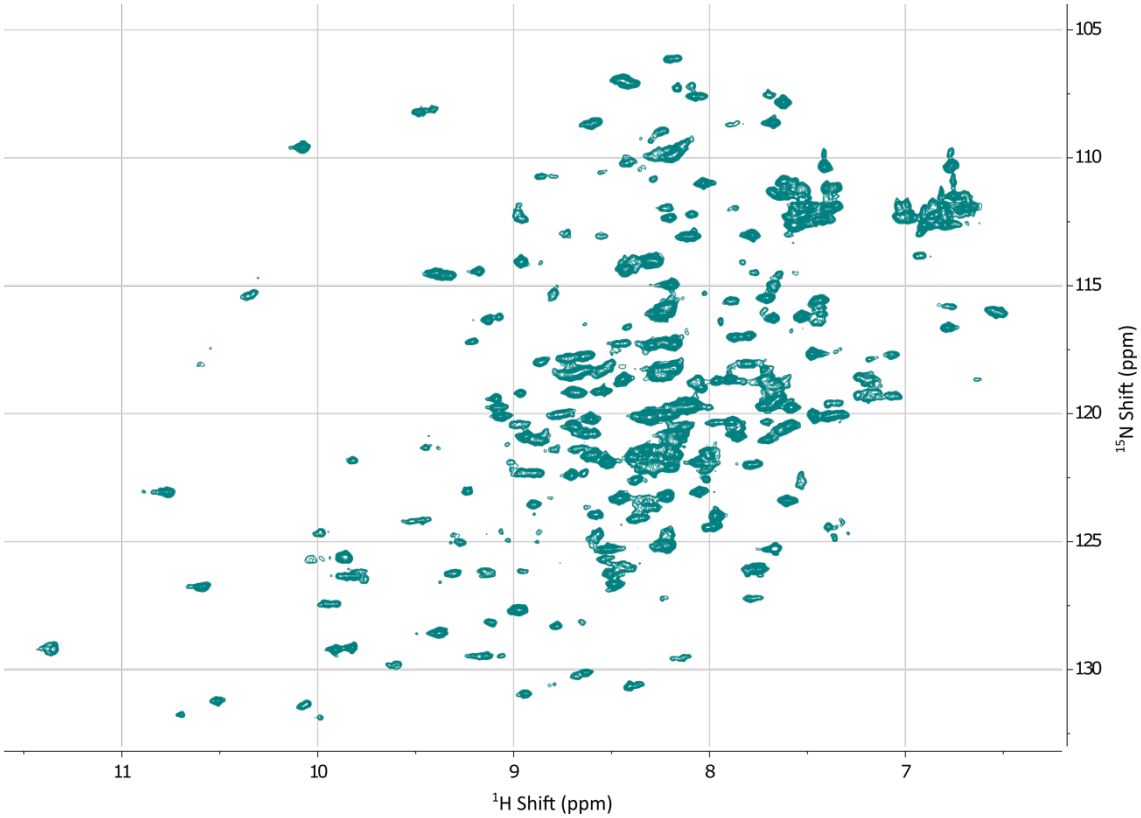


Figure 2.11 *$^{1}H,^{15}N$-HSQC spectrum of the oxic PHD2:Zn(II):2OG complex. Standard concentrations of each component were: 100 µM ^{15}N-labelled PHD2, 300 µM Zn(II), 500 µM 2OG, and room pressure O_2. Buffer conditions were 10% D_2O, and 90% 50 mM Tris-d_{11} pH 6.5.*

Though Zn(II) is a useful choice for general NMR analyses of PHD2, the Zn(II) complex is not expected to react with O_2—at least not in a catalytically productive manner—when oxygen is at the active site due to a lack of alternative, accessible Zn-oxidation states. [33]

Next, the PHD2:Ni(II):2OG complex was explored. Unlike with Zn(II), more than one oxidation state (Ni(I), Ni(II), and Ni(III)) has commonly been observed in nickel-based metalloproteins. [38] [39] [40] Ni(II) may act as a useful Fe(II) surrogate due to its weak paramagnetism (see Chapter 1, **Table 1.1**), which is less than some other transition metals, but which is enough to induce greater interactions with oxygen than diamagnetic Zn(II). The paramagnetism of Ni(II) also means that small changes in the

region around the active-site Ni(II) may potentially cause changes in the Ni(II) paramagnetic state and manifest more globally across the protein. This makes Ni(II) a potentially useful, catalytically inactive probe for changes in the PHD2 active site that may be caused by oxygen binding.

The PHD2:Ni(II):2OG complex NMR spectrum revealed similarities to the PHD2:Zn(II):2OG complex spectrum, with slight shift differences (**Figure 2.12**). Interestingly, the peaks of the PHD2:Ni(II):2OG complex were sharper and less irregular than the analogous PHD2:Zn(II):2OG peaks, an observation which may indicate a difference in flexibility of the protein conformation. Less crowding in the 8-8.5 ppm region of the $^{1}H,^{15}N$-HSQC spectrum was also observed, making it easier to analyse than its Zn(II) counterpart. These changes in the $^{1}H,^{15}N$-HSQC spectrum likely indicate binding of nickel to the PHD2 active site, though further studies may be useful to confirm if this is the case. The utility of the PHD2:Ni(II):2OG complex will be described later in this chapter.

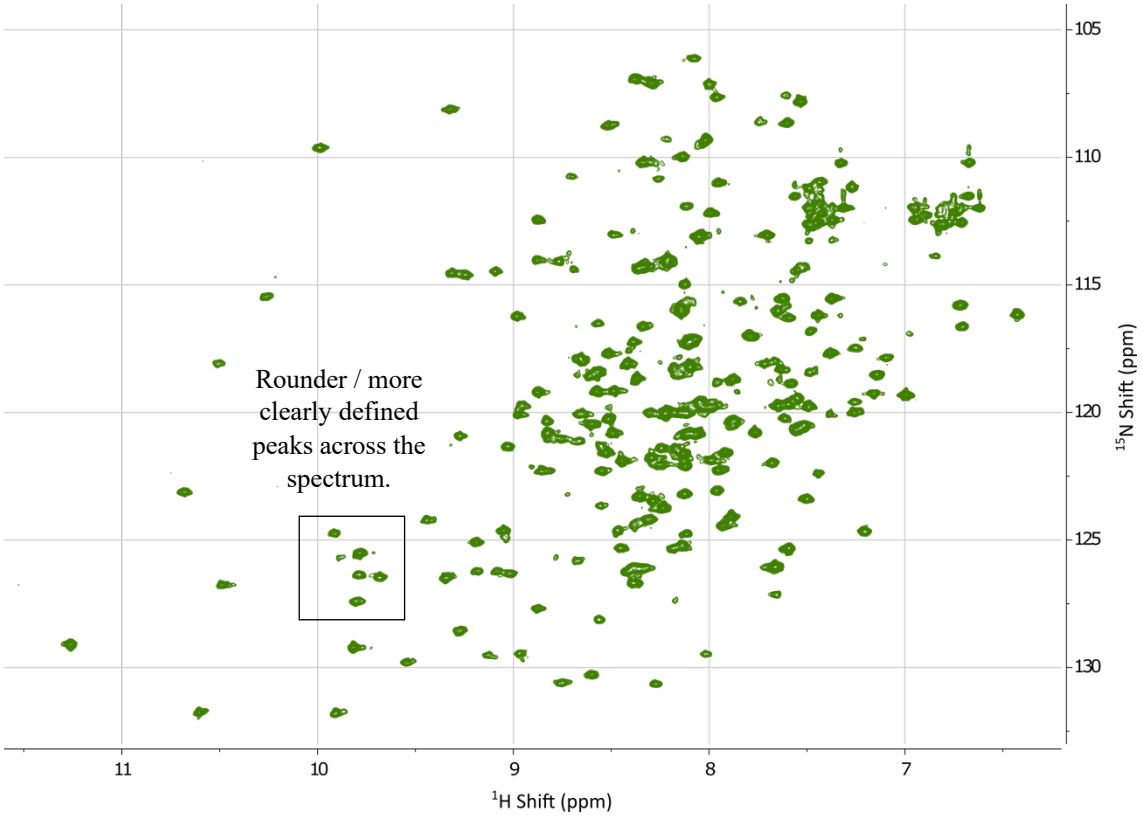


Figure 2.12 *$^{1}H,^{15}N$-HSQC spectrum of the oxic PHD2:Ni(II):2OG complex. The Ni(II) complex exhibits more well defined peaks than seen in the diamagnetic Zn(II) complex (Figure 2.11). Paramagnetic broadening is not observed. Standard concentrations of each component were: 100 μM ^{15}N-labelled PHD2, 300 μM Ni(II), 500 μM 2OG, and room pressure O_2. Buffer conditions were 10% D_2O, and 90% 50 mM Tris-d_{11} pH 6.5.*

The next metal of interest investigated was Co(II), which forms the PHD2:Co(II):2OG complex. Like Ni(II), Co(II) has been thought to induce hypoxia-like behaviours through interactions with enzymes involved in human oxygen sensing pathways by displacement of native Fe(II). [41] Co(II) was investigated as an Fe(II) surrogate in the PHD2 complex for several reasons. The most relevant of these is its ability to bind to oxygen at the active sites of some Fe(II)-based metalloproteins [42] and to be oxidised to Co(III) in some similar oxygen-interacting proteins like haemoglobin. [43] [44] Co(II) is also most similar in terms of the position in the periodic table to Fe(II) and has a spin-only magnetic moment that is similar to that of Fe(II). [45] [46] The latter property potentially enables larger paramagnetic effects than the transition metals

previously mentioned. The last property of note is that Co(II) has been observed to block the catalytic activity of PHD2 through an unknown mechanism, likely through competition with Fe(II). [47] These properties make Co(II) an exceptionally interesting metal of study even beyond just oxygen sensing analysis.

Under oxic conditions, the PHD2:Co(II):2OG complex gave a large spread of peaks (from paramagnetic shifts), but did not give substantial paramagnetic broadening (**Figure 2.13**). This is a useful attribute as the shifted peaks can still be analysed whereas broadened peaks are more difficult to observe. It should be noted that, due to the extent of paramagnetic shifts in this spectrum, it will not be possible to confidently assign, at least many, peaks by comparison with peaks in the PHD2:Zn(II):2OG spectrum by the nearest neighbour approach. Additionally, it appears as if more than one set of peaks is present, though possibly not enough to indicate two stable protein conformations. This is not expected to be a result of the disordered (8-8.5 ppm) and side-chain (6.9 and 7.6 ppm) regions manifesting greater differentiation in peak shifts, but this hypothesis cannot be entirely ruled out.

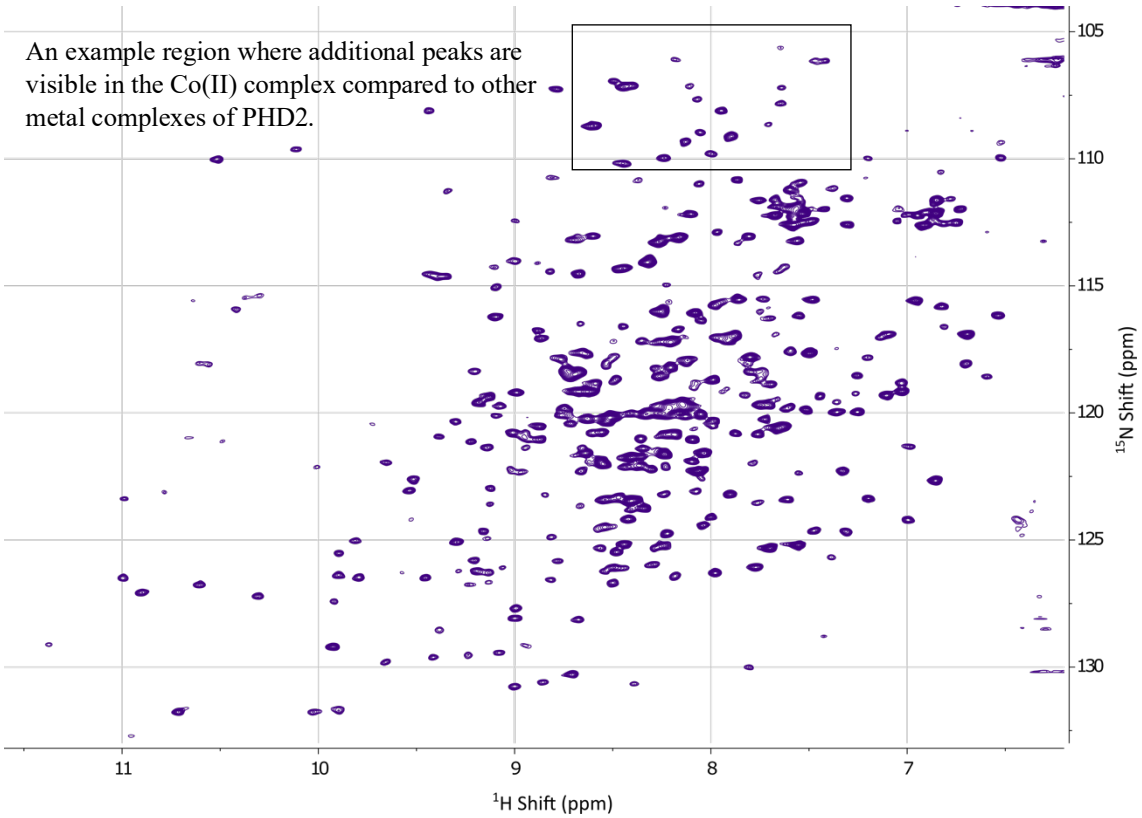


Figure 2.13 *$^{1}H,^{15}N$-HSQC spectrum of the oxic PHD2:Co(II):2OG complex. More peaks are observed in the Co(II) complex than any other PHD2:metal:2OG complex discussed in this thesis. Significant paramagnetic shifts are observed with minimal, if any, paramagnetic broadening. Standard concentrations of each component were: 100 µM ^{15}N-labelled PHD2, 300 µM Co(II), 500 µM 2OG, and room pressure O_2. Buffer conditions were 10% D_2O, and 90% 50 mM Tris-d_{11} pH 6.5.*

Finally, the oxic PHD2:Fe(II):2OG complex was analysed in comparison to the other metal surrogates. As this complex is most similar to the catalytically active complex, it was considered the most desirable complex for analysis. A potential concern with the PHD2:Fe(II):2OG complex was prime-substrate-uncoupled turnover of 2OG, which may lead to undesired additional components of the solution and an uncertain state of the active site. [32] Note, however, that PHD2 is reported to catalyse such uncoupled turnover poorly. [48]

Interestingly, the $^{1}H,^{15}N$-HSQC spectrum of oxic PHD2:Fe(II):2OG complex (**Figure 2.14**) revealed similar peak shifts to the Ni(II) complex (**Figure 2.12**), with

additional broadening observed in the 9-10 ppm region (which can be a characteristic region for a well-folded protein and broadening in this region may indicate some level of disorder). The peak shapes in this spectrum were found to be less irregular than the Zn(II) spectrum (**Figure 2.11**) and the region around 8-8.5 ppm showed greater crowding than the Ni(II) spectrum (**Figure 2.12**). Despite having an even greater spin-only magnetic moment than the Co(II) complex (see **Table 1.1** in Chapter 1) (**Figure 2.13**), the Fe(II) complex shows weaker paramagnetic shift effects, an observation that may be due to the difference in strength or orientation of metal binding. Alternatively, the observation could, in part, reflect a difference in the Co oxidation state (perhaps involving the partial presence of Co(III)).

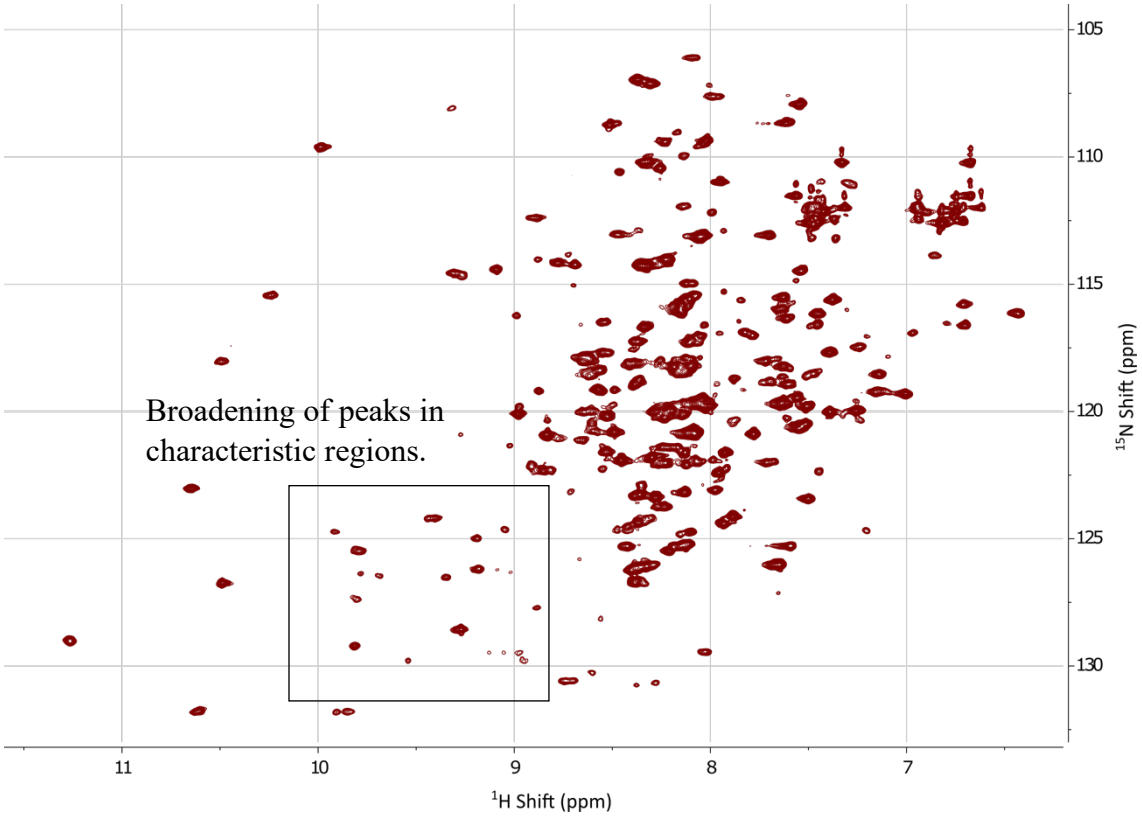


Figure 2.14 *^{1}H,^{15}N-HSQC spectrum of the oxic PHD2:Fe(II):2OG complex. Paramagnetic shifts exhibited in the oxic Fe(II) complex matched the paramagnetic shifts of the Ni(II) complex (Figure 2.12), with greater paramagnetic broadening in the case of oxic Fe(II). Standard concentrations of each component were: 100 µM ^{15}N-labelled*

PHD2, 300 μM Fe(II), 500 μM 2OG, and room pressure O_2. Buffer conditions were 10% D_2O, and 90% 50 mM Tris-d_{11} pH 6.5.

The last metal of interest to be considered was Cu(II), which may react to form an oxic PHD2:Cu(II):2OG complex, since Cu(II) has been shown to bind oxygen in other metalloproteins. [49] Difficulty with solution solubility of the Cu(II) metal when tested with the WelO5 complex (data not published in this thesis due to lack of a spectrum) led to no further exploration with PHD2:Cu(II) complexes. Studies of Cu(II) may be of interest in the future following optimisation of conditions.

From these studies, it was found that Zn(II), Ni(II), Co(II), and Fe(II) all showed reasonable binding affinities to PHD2 in the presence of 2OG and could be suited for further analysis of metal binding and gas studies of PHD2. Initial gas binding studies of PHD2 will focus on the PHD2:Zn(II):2OG (diamagnetic control) and the PHD2:Fe(II):2OG (less reactive, near-native) complexes.

2.2.2.1.2 Oxic and Anoxic Complex Metal Studies

Once the various PHD2:metal:2OG complexes had been explored, the effects of oxygen on these complexes could be studied. As the surrogate Zn(II) metal in the PHD2:Zn(II):2OG complex active site is not expected to react with oxygen, it was used as a diamagnetic control in the following studies. To ensure oxygen is not present at the protein active site during anoxic experiments, each component of the PHD2 complex was purged with N_2 gas before forming the complex (methods to purge oxygen from the solution are described in Chapter 5 **Section 5.2.3**). [50]

Addition of oxygen to the anoxic PHD2:Zn(II):2OG complex showed no substantial changes in the $^{1}H,^{15}N$-HSQC spectrum (**Figure 2.15**). The slight increase in noise in the spectrum from 8-8.5 ppm for the anoxic sample may be due to the harsher sample preparation conditions used in order to ensure the sample is anoxic, and/or due to

the higher temperature and higher airflow environments in the glovebox (Chapter 5, **Section 5.2.3**). These observations are consistent with a lack of strong interaction between the PHD2:Zn(II):2OG complex and O_2 gas, as was expected with the Zn(II) complex. From these findings, the PHD2:Zn(II):2OG complex was determined to be a useful control complex for further O_2 interaction studies.

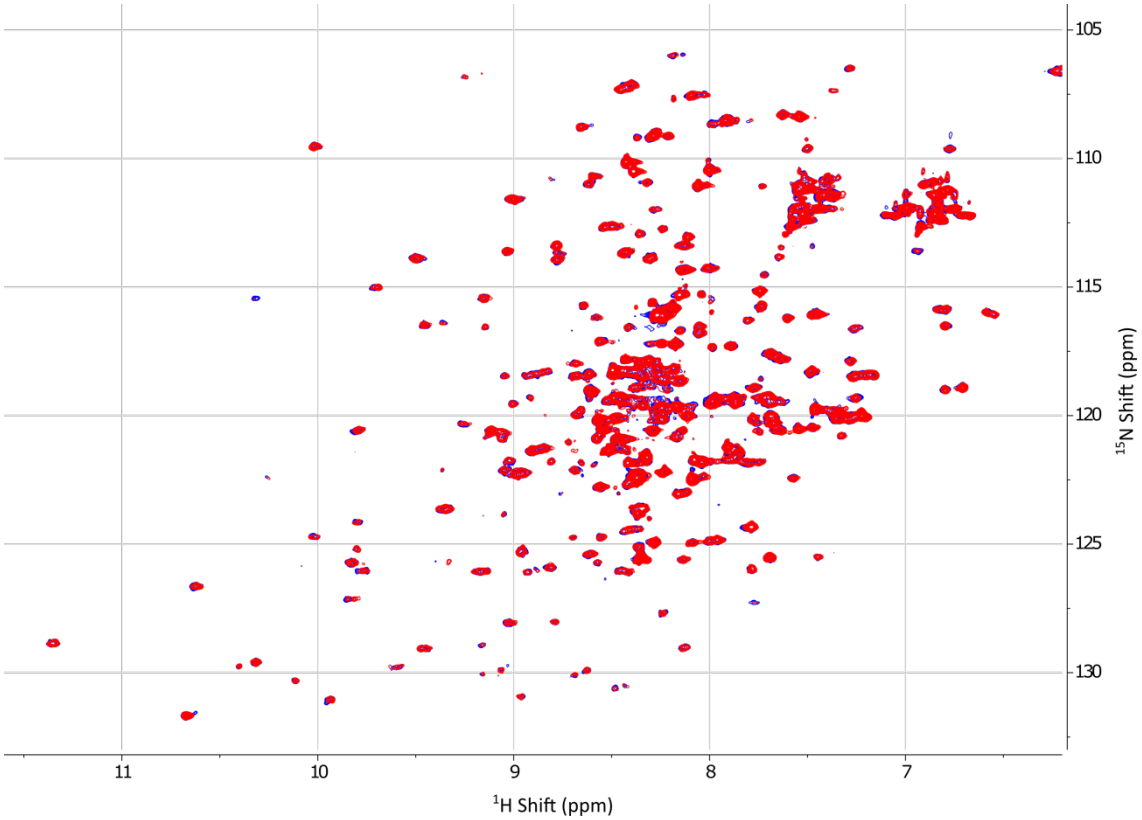


Figure 2.15 *^{1}H,^{15}N-HSQC spectra of the oxic (red) and anoxic (blue) PHD2:Zn(II):2OG complexes. There was no observed difference between oxic and anoxic spectra. Standard concentrations of each component were: 100 µM unlabelled PHD2, 300 µM Zn(II), 500 µM 2OG, <2 ppm O_2 pressure (anoxic), and room pressure O_2 (oxic). Buffer conditions were 10% D_2O, and 90% 50 mM Tris-d_{11} pH 6.5.*

Addition of HIF-1α CODD to the oxic and anoxic PHD2:Zn(II):2OG complexes also yielded no oxygen-dependent changes (**Figure 2.16**). Minor shifts in the side-chain peaks in the region around 7-8 ppm, (**Figure 2.16)** were observed, likely due to slight temperature/acidity differences. As with the PHD2:Zn(II):2OG complex (**Figure 2.15**),

the PHD2:Zn(II):2OG:HIF-1α CODD complex may be a useful control for further PHD2:metal:cofactor:substrate studies with the purpose of following oxygen binding.

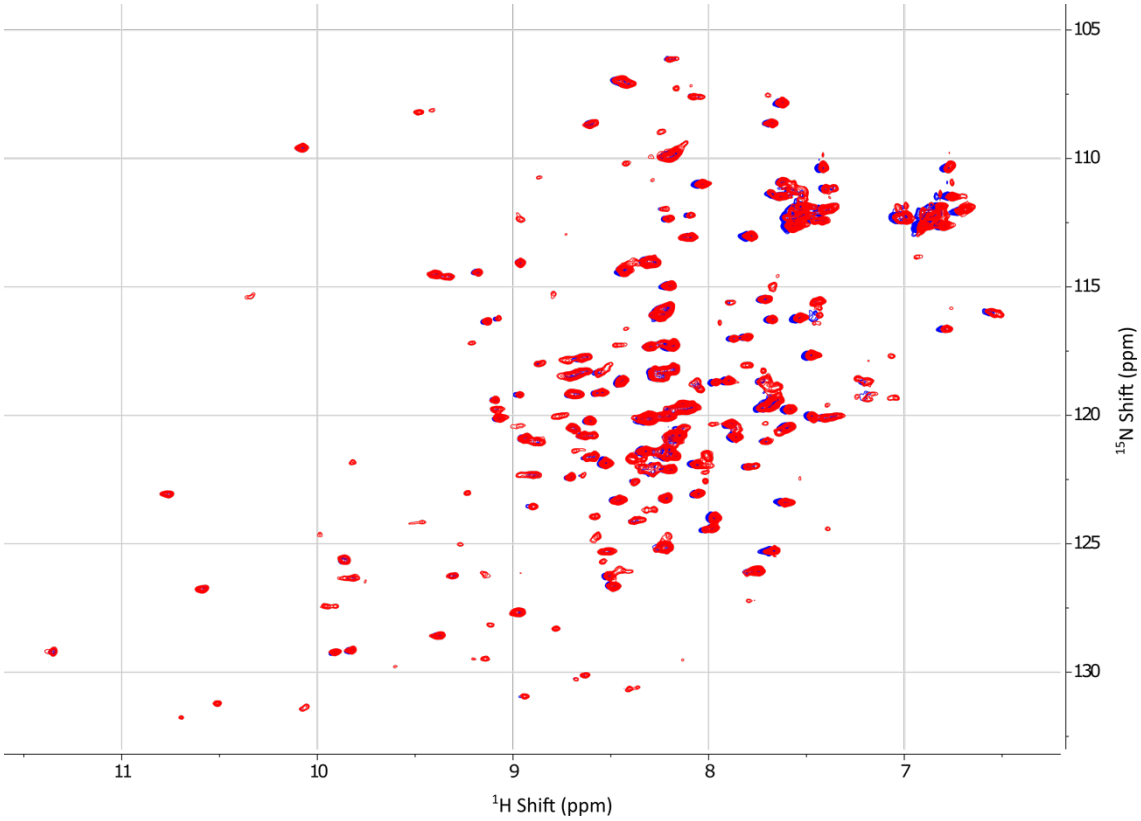


Figure 2.16 *^{1}H,^{15}N-HSQC spectra of the oxic (red) and anoxic (blue) PHD2:Zn(II):2OG:HIF-1α CODD complexes. There was no observable difference between oxic and anoxic spectra. Standard concentrations of each component were: 100 μM unlabelled PHD2, 300 μM Zn(II), 500 μM 2OG, 800 μM CODD, <2 ppm O_2 pressure (anoxic), and room pressure O_2 (oxic). Buffer conditions were 10% D_2O, and 90% 50 mM Tris-d_{11} pH 6.5.*

Once the Zn(II) complexes had been shown to manifest no indications of substantial structural or paramagnetic changes on oxygen exposure, the PHD2:Fe(II):2OG complex was explored. As has been discussed previously, this complex involves additional complications due to uncoupled turnover of 2OG [32] [48] and, therefore, the oxidation state of the active site metal and the bound ligand may not be Fe(II) and 2OG, respectively.

On analysis of the PHD2:Fe(II):2OG complex under oxic and anoxic conditions (**Figure 2.17**), clear differences between the two complexes were observed. These differences were surprising both in their scale and variability. The most notable change was that the anoxic spectrum contained twice as many peaks as the oxic spectrum and that the additional peaks were especially concentrated in the region around 9-10 ppm; deshielding of these peaks may be an indication of paramagnetic effects as has been seen for the Co(II) complex (**Figure 2.13**). Two other unique features of the anoxic PHD2:Fe(II):2OG complex were: 1) the anoxic spectrum peaks are of lower intensity, hinting that they may have been split into two separate sets of peaks and 2) the anoxic spectrum peaks are more regularly shaped, which may indicate a difference in the dynamics of the PHD2:Fe(II):2OG complex under oxic and anoxic conditions. These findings were of interest as they can be considered the first evidence of changes in the structure of the PHD2 complex in the presence of oxygen (as discussed in this thesis). Long term storage of these samples indicated that the complexes are stable to both degradation and changes in the spectra over time.

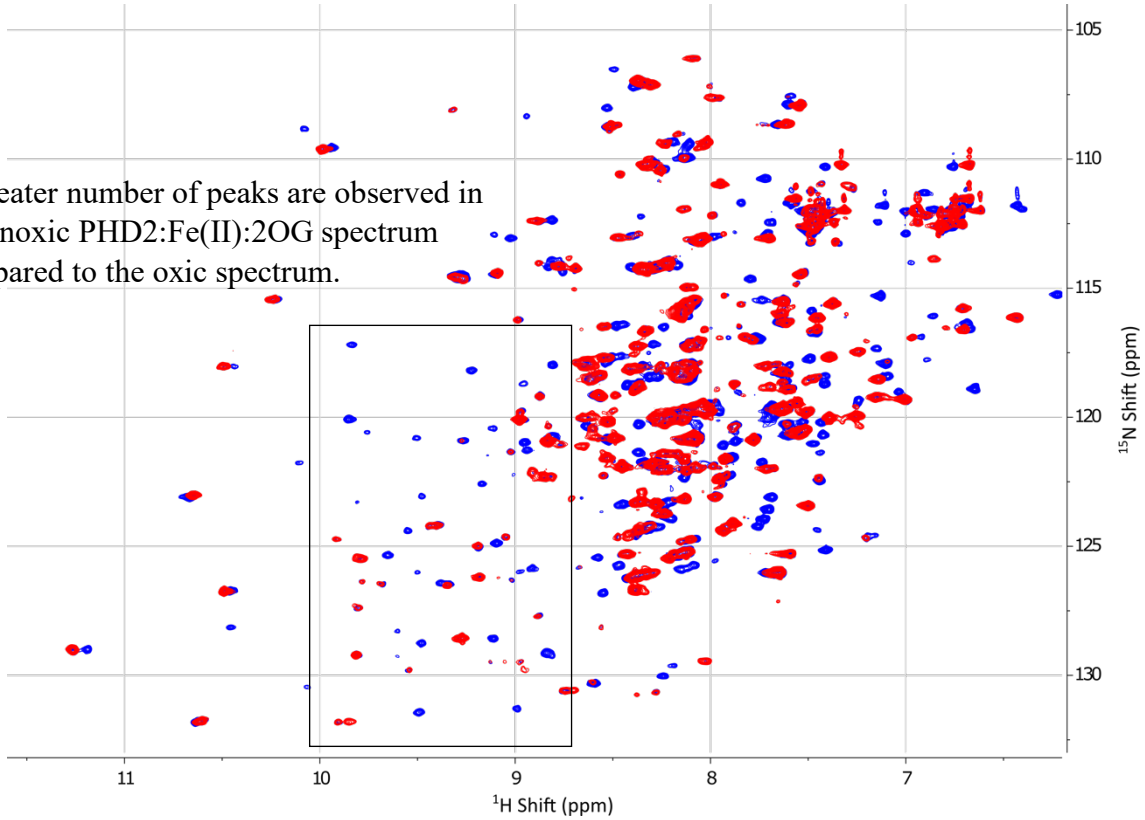


Figure 2.17 *$^{1}H,^{15}N$-HSQC spectra of the oxic (red) and anoxic (blue) PHD2:Fe(II):2OG complexes. The anoxic complex exhibited two sets of peaks, approximately half of which were similar in shift to peaks in the oxic spectrum and half that exhibited more unique shifts. Standard concentrations of each component were: 100 μM unlabelled PHD2, 300 μM Fe(II), 500 μM 2OG, <2 ppm O_2 pressure (anoxic), and room pressure O_2 (oxic). Buffer conditions were 10% D_2O, and 90% 50 mM Tris-d_{11} pH 6.5.*

Observation of the PHD2:Fe(II):2OG spectra from an alternative view (**Figure 2.18**) reveals that one set of the anoxic PHD2:Fe(II):2OG peaks matches closely with the oxic PHD2:Fe(II):2OG spectrum. This observation indicates that about half of the anoxic protein is adopting a conformation/state similar to the oxic protein and another half is adopting an alternative conformation/state. There are several possible causes for the two unique sets of peaks in the anoxic spectrum. The anoxic complex may have: 1) multiple metal oxidation states, 2) multiple metal spin states, 3) multiple orientations of the 2OG substrate, 4) multiple binding modes of the 2OG cofactor at the active site metal, or 5) an

otherwise altered conformation of the protein (e.g. involving the β2β3 loop). These possibilities were investigated.

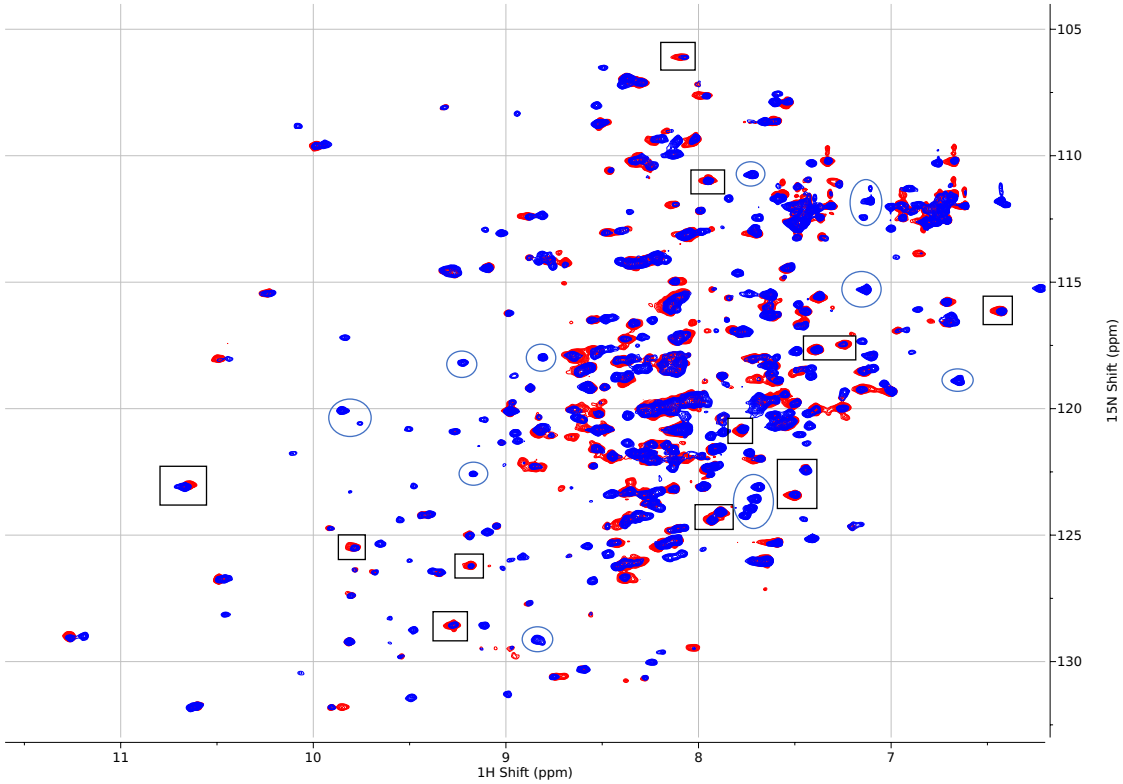


Figure 2.18 *^{1}H,^{15}N-HSQC spectra of the oxic (red) and anoxic (blue) PHD2:Fe(II):2OG complexes, alternative view. Most of the oxic spectrum peaks (red) approximately match the peak shifts of the anoxic spectrum (blue). A second set of peaks in the anoxic spectrum does not align with oxic spectrum peaks. Some examples of peaks with similar shifts in the anoxic and oxic spectra are indicated in black boxes; examples of peaks that are only found in the anoxic spectrum are indicated within blue circles. Standard concentrations of each component were: 100 μM unlabelled PHD2, 300 μM Fe(II), 500 μM 2OG, <2 ppm O_2 pressure (anoxic), and room pressure O_2 (oxic). Buffer conditions were 10% D_2O, and 90% 50 mM Tris-d_{11} pH 6.5.*

Following from the ^{1}H,^{15}N-HSQC oxic and anoxic PHD2:Fe(II):2OG spectral studies, ^{1}H NMR analysis seemed to indicate additional regions of sensitivity to the addition of oxygen in the PHD2:Fe(II):2OG complex (**Figure 2.19**). These differences were especially apparent in the region below 0 ppm (subsequently referred to as the

shielded methyl region) and the region above 9 ppm (subsequently referred to as the deshielded H_N region).

Peaks in the shielded methyl region typically arise from proximity between a methyl group on an amino acid and an aromatic ring in a neighbouring residue. [51] This proximity (with an appropriate orientation) leads to shielding of the methyl electrons by an altered flow of electrons in the aromatic ring. [51] Methyl peaks that would typically fall around 1 ppm can be shifted to negative values due to shielding effects. Analysis of the shielded methyl region can be useful in protein NMR to check for indications of a proper protein fold, as shielded methyls are often found in more protected regions in order to promote a stable enough interaction between the methyl and aromatic residues to exhibit strong shielding effects. [52] Methyl groups are commonly enclosed in hydrophobic regions near the active site or hydrophobic pockets, which are important regions for protein folding and function. [53] [54] [55] For the purposes of exploring interactions with PHD2, it was considered that analysis of the shielded methyl region may be a valuable tool for probing less accessible regions of PHD2, including the active site pocket.

Though one set of the anoxic PHD2:Fe(II):2OG peaks in the ^{1}H,^{15}N-HSQC spectrum appears to match the peaks of the oxic PHD2:Fe(II):2OG spectrum (**Figure 2.18**), it is interesting to note that this isn't the case for the ^{1}H spectra (**Figure 2.19**), especially in the shielded methyl region. This may indicate that it is small, local changes that cause the shielded methyl pattern differences rather than overall protein conformational changes.

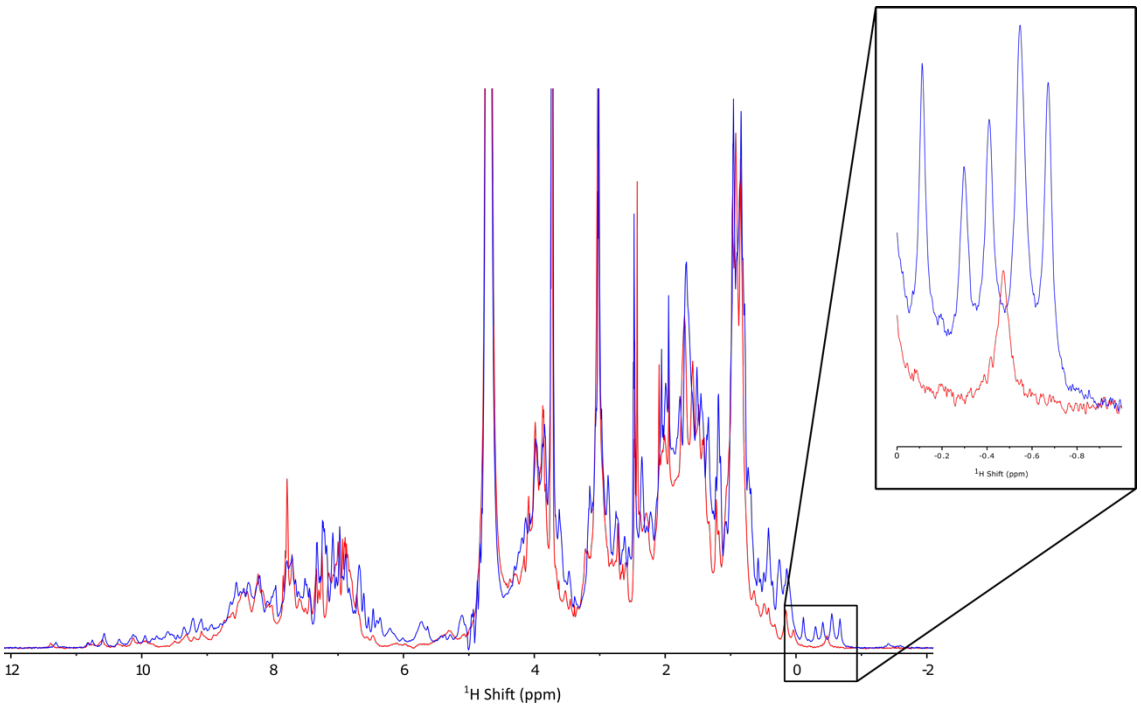


Figure 2.19 *^{1}H spectral overlay of the oxic (red) and anoxic (blue) PHD2:Fe(II):2OG complexes. The shielded methyl region (<0 ppm) shows very characteristic differences between the oxic and anoxic complexes. Standard concentrations of each component were: 100 μM unlabelled PHD2, 300 μM Fe(II), 500 μM 2OG, <2 ppm O_2 pressure (anoxic), and room pressure O_2 (oxic). Buffer conditions were 135 mM NaCl, 10% D_2O, and 90% 50 mM Tris-d_{11} pH 7.5.*

Once analysis of the shielded methyl region was identified as an efficient method of analysing oxic and anoxic PHD2 spectra, this method was used to study the interactions in other PHD2:metal complexes. It was considered that use of the ^{1}H spectra for analysis of ligand binding-induced changes in the protein may be an efficient screening tool to compliment ^{1}H,^{15}N-HSQC analysis.

Comparison of the oxic and anoxic ^{1}H spectra of the PHD2:Fe(II):2OG, PHD2:Zn(II):2OG, PHD2:Co(II):2OG, and PHD2:Ni(II):2OG complexes (**Figure 2.20**) revealed differences between the complex peak patterns in the shielded methyl region—these seemed to be more sensitive to the particular metal ion complex than had been observed in the overall ^{1}H,^{15}N-HSQC spectra (**Figure 2.11, Figure 2.12, Figure 2.13,**

Figure 2.14), which may indicate that the shielded methyls of interest are in a region adjacent to the active site metal. The observations were explored further as described below.

The ^{1}H NMR spectra of the PHD2:Fe(II):2OG, PHD2:Zn(II):2OG, and PHD2:Ni(II):2OG complexes (**Figure 2.20** a, b, and c, respectively) span from -1 ppm to 11.7 ppm, whereas the PHD2:Co(II):2OG complex had a greater spread of peak shifts that extended outside of the region of -2 ppm to 12 ppm (**Figure 2.20 d**), as had been previously observed for the AlkB:Co(II):2OG complex [56] (note, the exact limits cannot be stated since spectra were not acquired beyond the -2 ppm to 12 ppm range). The oxic PHD2:Fe(II):2OG and PHD2:Ni(II):2OG complexes shared the approximate positions of their most shielded and deshielded peaks, which reflects the ^{1}H,^{15}N-HSQC spectral similarity between the oxic PHD2:Fe(II):2OG and PHD2:Ni(II):2OG complexes, with more extensive broadening observed for the oxic PHD2:Fe(II):2OG complex.

One other substantial observation was that only the PHD2:Fe(II):2OG complexes showed differences between the oxic and anoxic conditions (**Figure 2.20** a), further indicating that the use of metals other than Fe(II) does not lead to complexes that bind to / react with oxygen. Note, the Fe oxidation state in the oxic PHD2:Fe(II):2OG complexes is uncertain—it could be Fe(II), Fe(III), or a mixture of these.

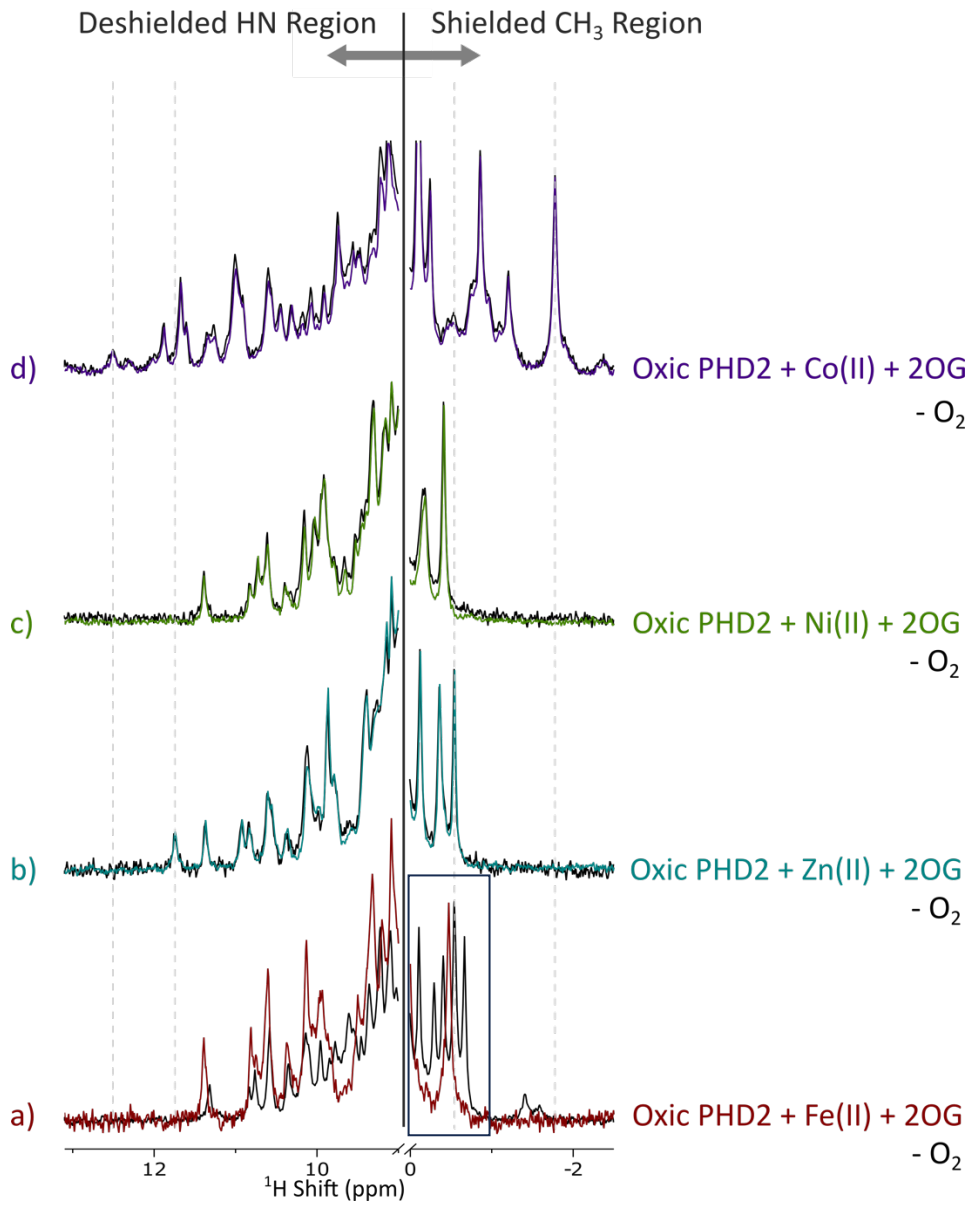


Figure 2.20 *^{1}H spectra of the competition between oxic and anoxic conditions for various PHD2:metal:2OG complexes. a) PHD2:Fe(II):2OG (red) overlayed with PHD2:Fe(II):2OG:O_2 (black), b) PHD2:Zn(II):2OG (blue) overlayed with PHD2:Zn(II):2OG:O_2 (black), c) PHD2:Ni(II):2OG (green) overlayed with PHD2:Ni(II):2OG:O_2 (black), and d) PHD2:Co(II):2OG (red) overlayed with PHD2:Co(II):2OG:O_2 (black). The dotted grey lines are used to help differentiate shifts. The black, vertical separating line indicates the position where the region from 0 to 9 ppm of the spectrum was removed for simplicity. Only in the presence of Fe(II) are there substantial differences between oxic and anoxic spectra. The shielded methyl region of the PHD2:Fe(II):2OG spectrum that differs between the oxic and anoxic spectra is indicated within the black box. Standard concentrations of each component were: 100*

μM unlabelled PHD2, 300 μM Fe(II),300 μM Zn(II), 300 μM Ni(II), 300 μM Co(II), 500 μM 2OG, <2 ppm O_2 pressure (anoxic), and room pressure O_2 (oxic). Buffer conditions were 135 mM NaCl, 10% D_2O, and 90% 50 mM Tris-d_{11} pH 7.5.

From the results of these studies, it was determined that the PHD2:Fe(II):2OG complex would be the subject of further studies investigating the mechanism of PHD2.

2.2.2.1.3 Oxic and Anoxic Complex Ligand Analysis

After establishing favourable conditions for studying PHD2:Fe(II):2OG complexes, alternative cosubstrate mimics of 2OG binding to PHD2 were of interest. The goal was to determine if the close—but not active—2OG mimic, N-oxalylglycine (NOG), could give similar oxygen-sensitive conformational changes as had been shown with the PHD2:Fe(II):2OG complex, but without the complications of prime substrate uncoupled turnover.

The first NOG complexes to be explored were the oxic and anoxic PHD2:Fe(II):NOG complexes in the absence of HIF-1α CODD (**Figure 2.21**). On addition of oxygen to the anoxic complex, there were very minor shift differences observed between the oxic and anoxic $^{1}H,^{15}N$-HSQC spectra. The shifted peaks appeared to be mainly N-H side-chain peaks and peaks close in intensity to the noise level; these peaks are unlikely to be significant in analysis of oxygen-binding-induced changes.

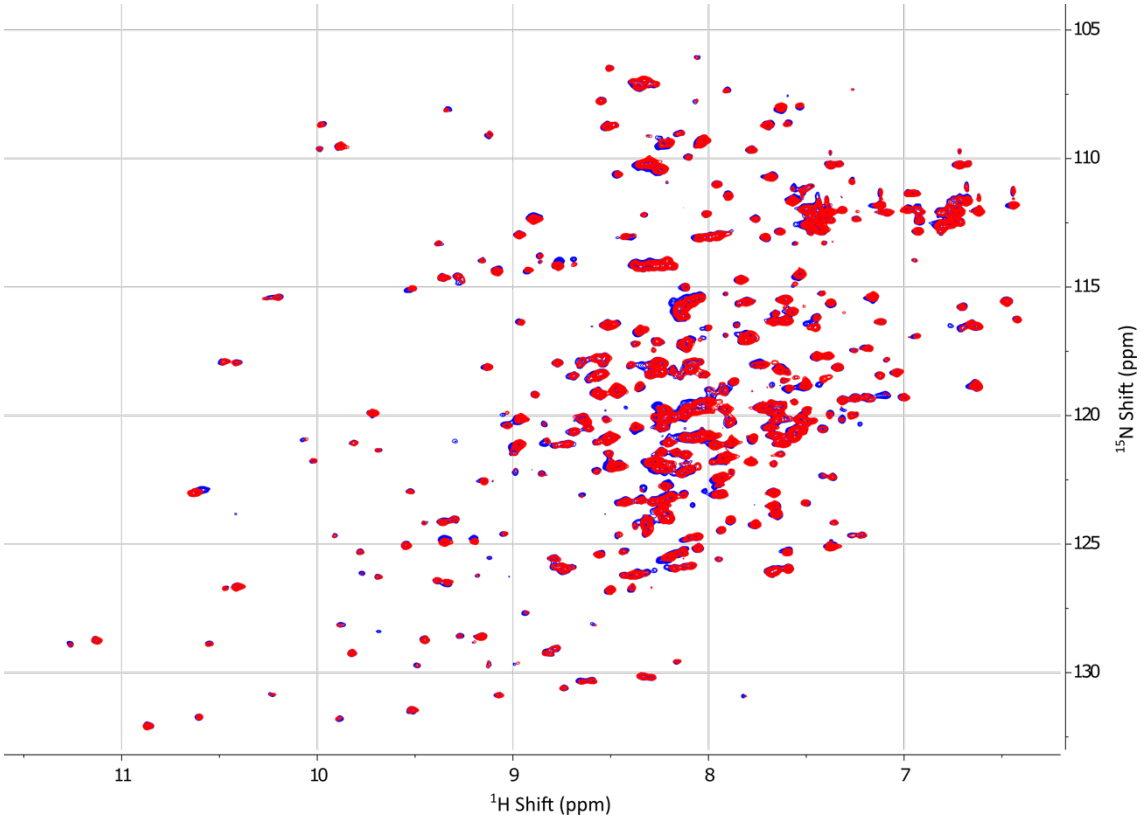


Figure 2.21 *$^{1}H,^{15}N$-HSQC spectra of the oxic (red) and anoxic (blue) PHD2:Fe(II):NOG complexes. There was no substantial shift or broadening differences between the oxic and anoxic spectra. Both spectra exhibited approximately two sets of peaks. Standard concentrations of each component were: 100 μM unlabelled PHD2, 300 μM Fe(II), 500 μM NOG, <2 ppm O_2 pressure (anoxic), and room pressure O_2 (oxic). Buffer conditions were 10% D_2O, and 90% 50 mM Tris-d_{11} pH 6.5.*

More interestingly, as had been similarly observed in the anoxic PHD2:Fe(II):2OG spectrum (**Figure 2.17**), there appeared to be two sets of peaks in both the anoxic and oxic PHD2:Fe(II):NOG spectra (**Figure 2.21**). The two sets of peaks in the oxic and anoxic PHD2:Fe(II):NOG complexes are also similar in shift to the two sets of peaks in the anoxic PHD2:Fe(II):2OG complex (**Figure 2.22**). Since both the NOG complexes and the anoxic complexes would not be expected to exhibit uncoupled turnover, uncoupled turnover of the oxic complex is the most likely explanation for why the oxic PHD2:Fe(II):2OG complex differs: having only one set of peaks. The process of uncoupled turnover may have changed the oxidation state or spin state of the active site

metal, altered the way in which the 2OG cofactor bound at the active site, or changed the protein conformation. Since the $^{1}H,^{15}N$-HSQC spectrum of the oxic PHD2:Fe(II):2OG complex (**Figure 2.14**) more closely matches other PHD2:metal complexes, including the oxic and anoxic spectra of PHD2:Zn(II):2OG and PHD2:Ni(II):2OG complexes (**Figure 2.11** and **Figure 2.12**, respectively), it can be inferred that the PHD2:Fe(II):2OG and PHD2:Fe(II):NOG complexes in the absence of uncoupled turnover have unique structures or properties that should be further explored.

Comparison of the spectrum of the anoxic PHD2:Fe(II):2OG with the spectrum of the anoxic PHD2:Fe(II):NOG complexes (shown from two different perspectives in **Figure 2.22** and **Figure 2.23**) revealed broader peaks in the case of the NOG complex and minor shift differences, which may be attributed to the way in which the cofactor is bound. This observation indicates that the conformations of the anoxic PHD2:Fe(II):2OG and oxic/anoxic PHD2:Fe(II):NOG are similar, but not identical. Considering that the crystal structures of 2OG- and NOG-bound PHD2 show ligand binding in the same position at the active site, another possibility is that the slight differences in $^{1}H,^{15}N$-HSQC spectral peak shifts are due to differences in the Fe(II) metal oxidation state or spin state, though differences in NOG and 2OG coordination cannot be ruled out. Overall, this and earlier results imply that under the tested conditions, oxygen does not form stable complexes or interact with most PHD2:metal:2OG/NOG complexes and that reaction only occurs with the PHD2:Fe(II):2OG complex.

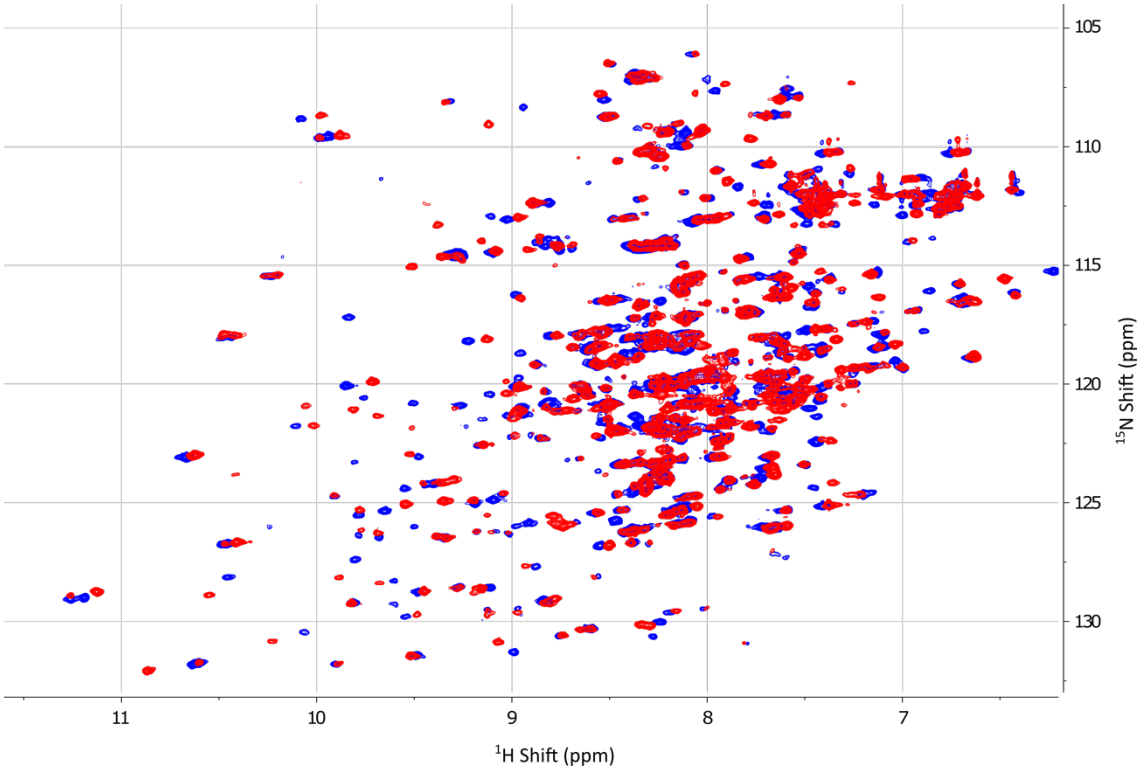


Figure 2.22 *Comparison of the $^{1}H,^{15}N$-HSQC spectra of anoxic PHD2:Fe(II):2OG (blue) and anoxic PHD2:Fe(II):NOG (red) complexes. Both spectra exhibited approximately two sets of peaks, and the differences between them were mild shift differences. Standard concentrations of each component were: 100 μM unlabelled PHD2, 300 μM Fe(II), 500 μM 2OG or NOG, and <2 ppm O_2 pressure. Buffer conditions were 10% D_2O, and 90% 50 mM Tris-d_{11} pH 6.5.*

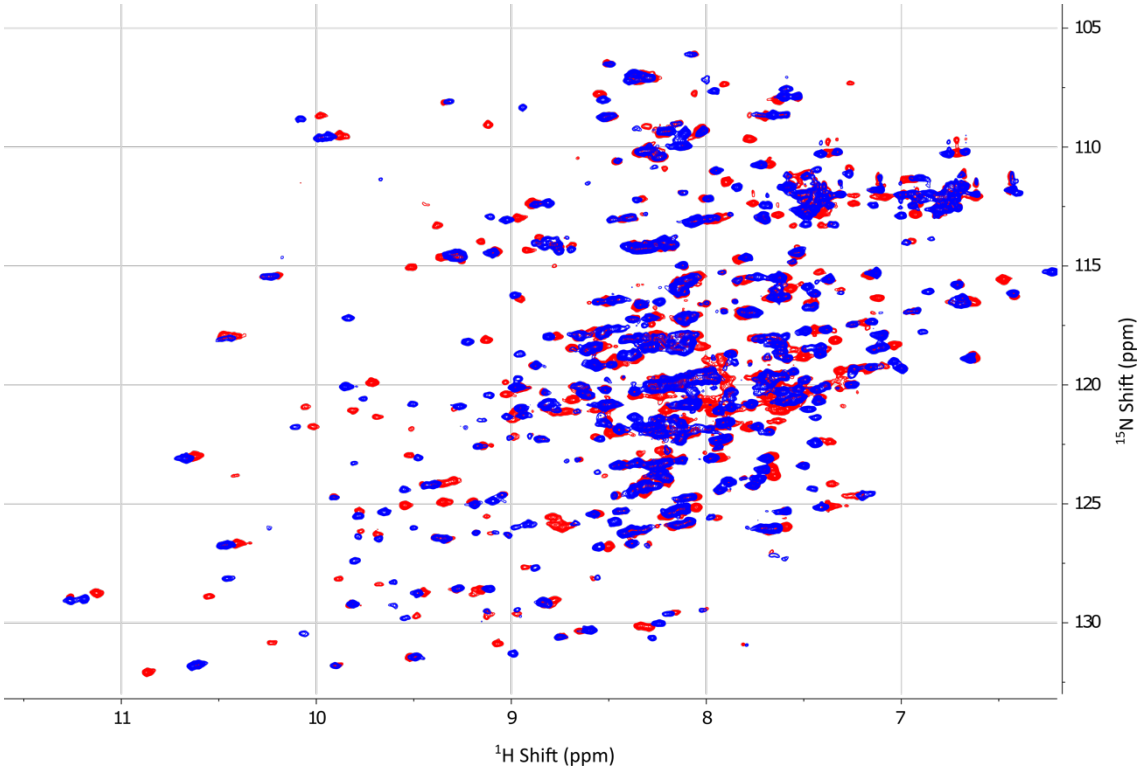


Figure 2.23 *Comparison of the $^{1}H,^{15}N$-HSQC spectra of anoxic PHD2:Fe(II):2OG (blue) and anoxic PHD2:Fe(II):NOG (red) complexes, alternative view (with the NOG complex in the back). Standard concentrations of each component were: 100 μM unlabelled PHD2, 300 μM Fe(II), 500 μM 2OG or NOG, and <2 ppm O_2 pressure. Buffer conditions were 10% D_2O, and 90% 50 mM Tris-d_{11} pH 6.5.*

Another possible explanation for the difference in peak shifts between the anoxic PHD2:Fe(II):2OG and anoxic PHD2:Fe(II):NOG spectra could be differences in interactions of the two small molecules with the residues of the active site pocket, especially involving the shielded methyl groups. This could explain why there are shift differences between the ^{1}H shielded methyl regions of the two spectra (***Figure 2.24***).

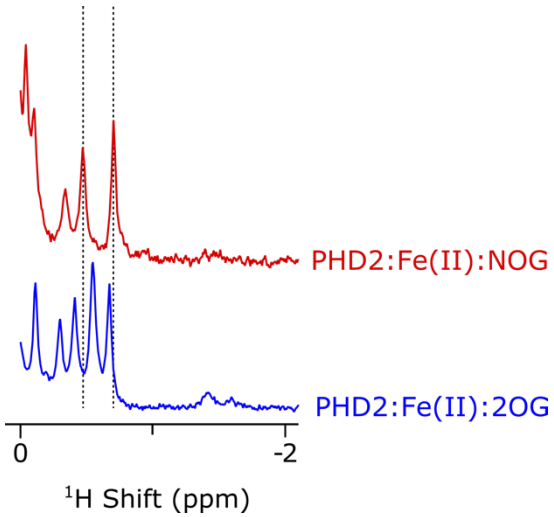


Figure 2.24 *Comparison of the ^{1}H spectra of anoxic PHD2:Fe(II):2OG (blue) and anoxic PHD2:Fe(II):NOG (red) complexes. The PHD2:Fe(II):2OG spectrum exhibits more shielded methyl peaks than the PHD2:Fe(II):NOG spectrum, though both have more complex shielded methyl regions than typical ^{1}H PHD2 spectra. Standard concentrations of each component were: 100 μM unlabelled PHD2, 300 μM Fe(II), 500 μM 2OG or NOG, and <2 ppm O_2 pressure. Buffer conditions were 135 mM NaCl, 10% D_2O, and 90% 50 mM Tris-d_{11} pH 7.5.*

In order to test if the anoxic PHD2:Fe(II):NOG complex was stable over time, a ^{1}H,^{15}N-HSQC spectrum was taken again after 10 hours at 308 K to investigate if any changes in the complex could be observed **(Figure 2.25).** The results showed that there were no changes in the spectrum, which indicated that the PHD2:Fe(II):NOG complex is reasonably stable.

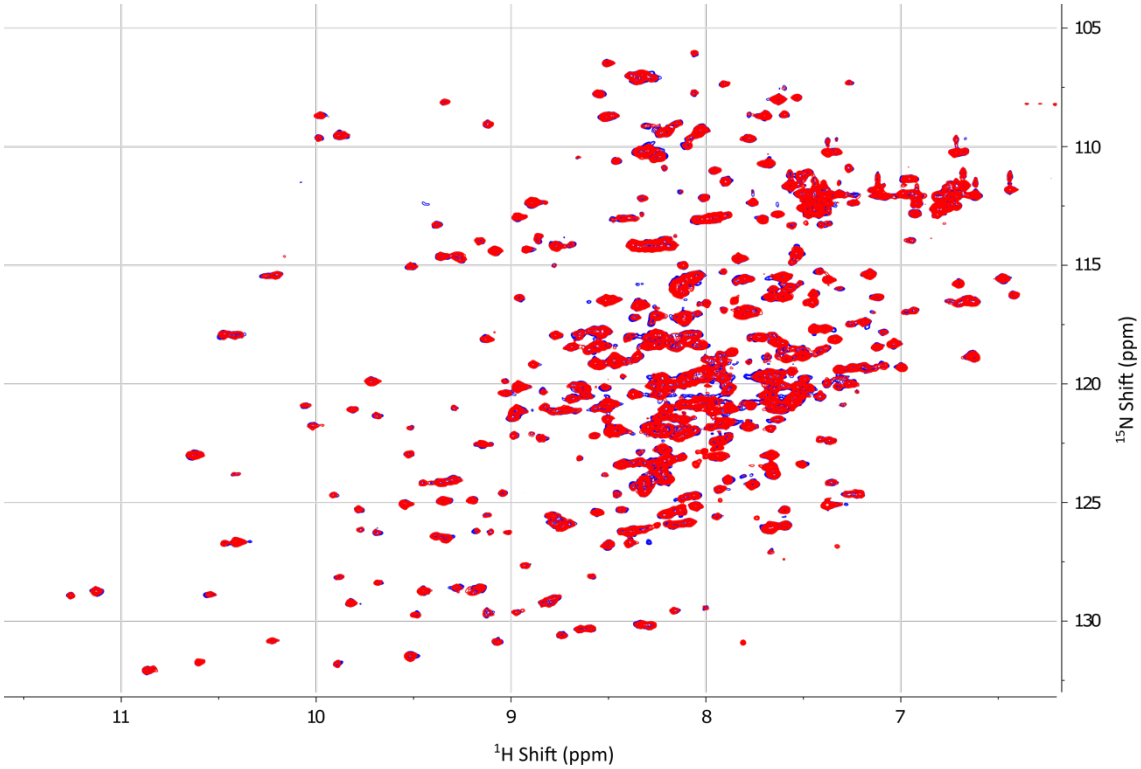


Figure 2.25 *$^{1}H,^{15}N$-HSQC spectra of the anoxic PHD2:Fe(II):NOG complex before (blue) and after (red) 10 hours. The sample was very stable over time at 308 K. Standard concentrations of each component were: 100 μM unlabelled PHD2, 300 μM Fe(II), 500 μM NOG, <2 ppm O_2 pressure (anoxic), and room pressure O_2 (oxic). Buffer conditions were 10% D_2O, and 90% 50 mM Tris-d_{11} pH 6.5.*

The next goal was to investigate if addition of NOG to the oxic PHD2:Fe(II):2OG complex leads to changes in the $^{1}H,^{15}N$-HSQC spectrum that would indicate displacement of the 2OG with NOG at the active site (**Figure 2.26**). The spectrum after NOG addition exhibited only minor shift differences that cannot be attributed to formation of the PHD2:Fe(II):NOG complex due to the appearance of only one set of peaks. This observation is consistent with 2OG being a stronger binder to the PHD2:Fe(II) complex than NOG. Note, again, the oxidation state of the Fe in the oxic PHD2:Fe:2OG complex is uncertain.

The shifts observed on NOG addition may reflect a partial disordering of the protein structure, as a majority of the changes are observed in the crowded, less

characteristic region of the $^{1}H,^{15}N$-HSQC spectrum around 8-8.5 ppm. Additionally, the presence of 2OG and NOG together in a PHD2:Fe(II) solution was observed to result in instability and formation of an unknown, broad peak at around 8 ppm (data not shown). The cause of instability of the PHD2:Fe(II)2OG complex in the presence of both 2OG and NOG is unclear but usually occurs at high cofactor concentrations.

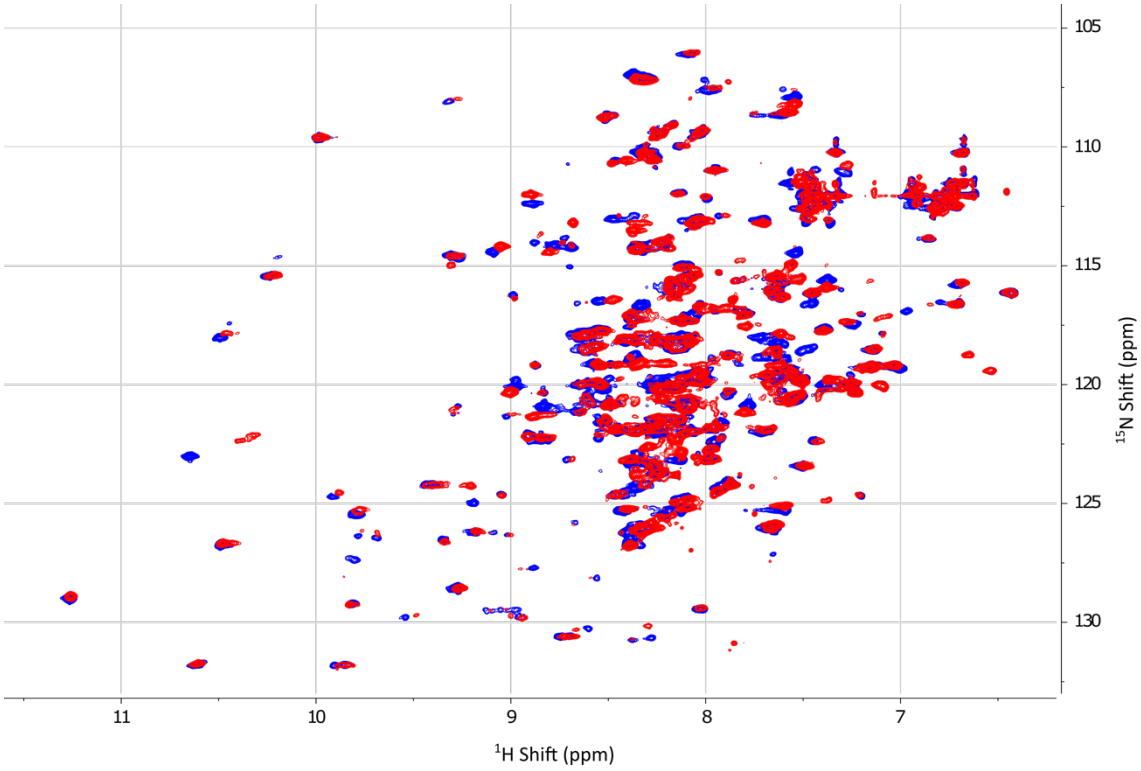


Figure 2.26 *$^{1}H,^{15}N$-HSQC spectra of oxic PHD2:Fe(II):2OG before (blue) and after (red) NOG addition. The 2OG complex remains majorly unperturbed in regions other than side chains. NOG addition did cause some additional precipitation, as predicted from the crowding of peaks in the 8-8.5 ppm region. Standard concentrations of each component were: 100 µM unlabelled PHD2, 300 µM Fe(II), 500 µM 2OG, 1 mM NOG, and room pressure oxygen. Buffer conditions were 10% D_2O, and 90% 50 mM Tris-d_{11} pH 6.5.*

When these steps were carried out in reverse, that is starting with the oxic PHD2:Fe(II):NOG complex and adding 2OG (**Figure 2.27**), there was a clear transition to the oxic PHD2:Fe(II):2OG complex. As discussed later in this chapter, under oxic conditions, the 2OG is likely locked into the Fe(III) oxidation state on formation of the

oxic PHD2:Fe:2OG complex, making the complex resistant to inhibitor binding. The displacement of NOG by 2OG is especially apparent when observing the disappearance of the extra set of peaks in the 9-10 ppm region of the $^{1}H,^{15}N$-HSQC spectrum of the PHD2:Fe(II):NOG complex (**Figure 2.27**, from blue to red). This result is perhaps expected, as 2OG is a stronger binder than NOG.

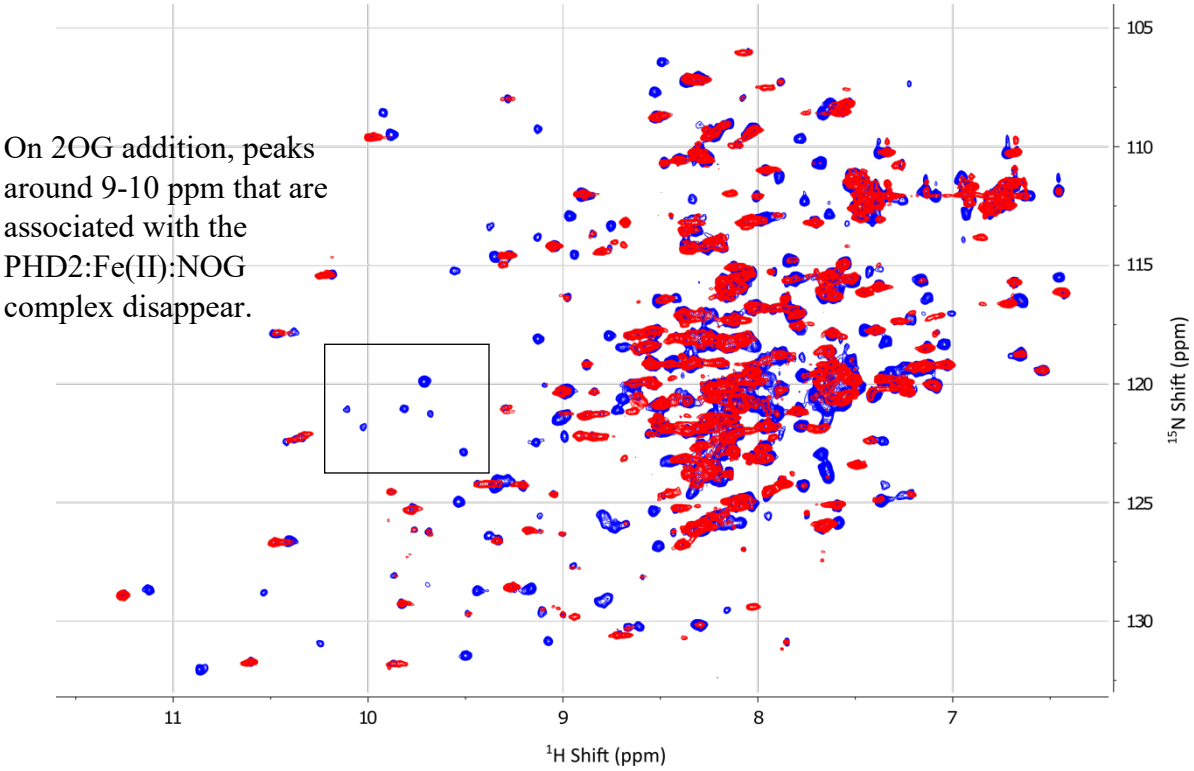


Figure 2.27 *$^{1}H,^{15}N$-HSQC spectra of oxic PHD2:Fe(II):NOG before (blue) and after (red) 2OG addition. The NOG complex appears to be completely displaced by 2OG binding on addition of 2OG. One region where peaks from the initial PHD2:Fe(II):NOG complex are lost on 2OG addition is indicated within the black box. Standard concentrations of each component were: 100 µM unlabelled PHD2, 300 µM Fe(II), 500 µM 2OG, 1 mM NOG, and room pressure oxygen. Buffer conditions were 10% D_2O, and 90% 50 mM Tris-d_{11} pH 6.5.*

From these studies, it was considered that NOG is not a viable surrogate for 2OG in terms of investigating the reaction of oxygen with PHD2.

2.2.2.1.4 Oxic and Anoxic Complex Gas Analysis

The next component for analysis was the gas molecule. Replacement of oxygen gas with a surrogate gas molecule would allow for study of the native PHD2:Fe(II):2OG and PHD2:Fe(II):2OG:HIF-1α CODD complexes in the presence of an Fe(II)-binding gas without the concern of coupled or uncoupled turnover. Studies with surrogate gases could help to uncover if the differences in the $^{1}H,^{15}N$-HSQC spectra of the oxic and anoxic PHD2:Fe(II):2OG complexes was due to reversible oxygen gas binding or due to other processes.

Three most viable candidates for this study were considered to be carbon monoxide (CO), nitric oxide (NO), and xenon (Xe), all of which are similar in size to oxygen. Xenon is unlikely to bind the active site metal but may be useful for other studies, like high pressure Xe-observed NMR studies of the hydrophobic tunnel that leads to the active site (see Chapter 6, **Section 6.1.1**). Carbon monoxide and nitric oxide could be viable candidates for such studies, but nitric oxide was used due to its higher binding affinity for Fe(II) [57].

On addition of 1,000 ppm nitric oxide to the anoxic PHD2:Fe(II):2OG complex (**Figure 2.28**, where the anoxic complex was prepared under N_2), there was no substantial change in the PHD2 ^{1}H spectrum. Slight differences in the extent of water suppression were observed likely due to thicker NMR tube walls (used for anoxic samples) or the presence of paramagnetic nitric oxide. This observation indicates that no nitric oxide is bound to PHD2. This result is consistent with the literature studies [58]; the cause of unfavourable nitric oxide binding despite the similarity of nitric oxide to oxygen is unclear, but may relate to the precise active site chemistry of the PHDs in relation to other 2OG-dependent dioxygenases.

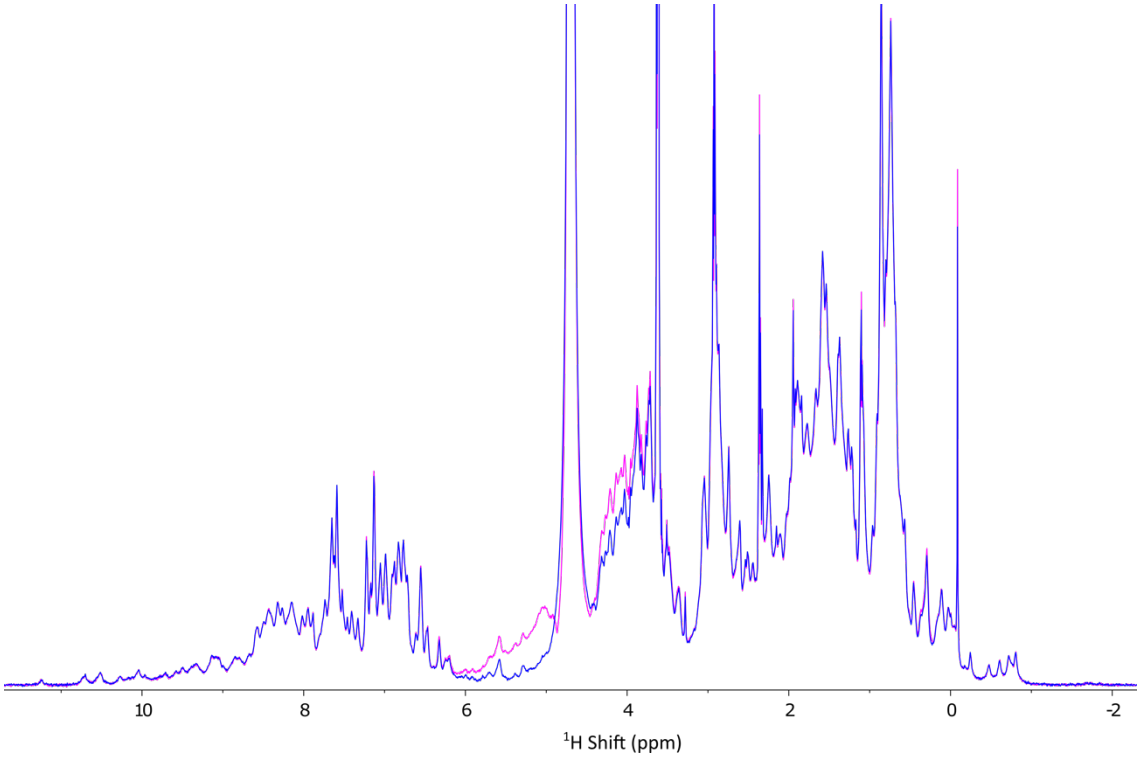


Figure 2.28 *^{1}H spectral overlay of the PHD2:Fe(II):2OG complex in the presence (pink) and absence (blue) of nitric oxide (NO). No difference in the spectra can be observed. Standard concentrations of each component were: 200 μM unlabelled PHD2, 400 μM Fe(II), 1 mM 2OG, <2 ppm O_2 pressure (anoxic), and 1,000 ppm NO. Buffer conditions were 135 mM NaCl, 10% D_2O, and 90% 50 mM Tris-d_{11} pH 7.5.*

Further studies into the conditions for nitric oxide binding, in the presence and absence of substrate, as well as the interactions between the PHD2:Fe(II):2OG complex and carbon monoxide should be explored.

The results further imply that nitric oxide does not appear to be a viable surrogate for oxygen in probing the process of oxygen binding to PHD2. The available evidence indicates that the PHD2:Fe(II):2OG complex may have evolved not to interact with NO as a protection mechanism to help preserve its focused role as a hypoxia / oxygen sensor.

2.2.2.1.5 Oxic and Anoxic Complex Substrate Analysis

The last component of the PHD2 catalytic complex to study was the substrate, HIF-1α CODD. Though the oxic PHD2:Fe(II) complex (+/- CODD) is expected to react

with 2OG under conditions suitable for coupled turnover, it was considered that analysis of the oxic and anoxic complexes may help shed light on what is observed in the case of oxic PHD2:Fe(II):2OG.

Alternative substrates were considered for the analysis, but the only available substrates with reasonable homology to HIF-1α CODD were the HIF-2α and HIF-3α CODD substrates, which had been explored previously by observing the ^{1}H,^{15}N-HSQC spectra of the PHD2:Zn(II):2OG:CODD complexes for HIF-1α, HIF-2α, and HIF-3α CODD (**Figure 2.9**). Though analysis of these substrates in the PHD2 complex would be valuable, turnover would still be an issue and the differences in amino acid sequence between the HIF CODD substrates may disrupt the function of the complex of interest. The alternative HIF CODD substrates should be considered for study in the future. [59] For the remainder of this section CODD refers to HIF-1α CODD.

In the case of the oxic and anoxic PHD2:Fe(II):2OG:CODD complexes, complications arose. Though the oxic and anoxic PHD2:Fe(II):2OG complexes were observed to be exceptionally stable, addition of CODD to these complexes caused severe precipitation. This is manifested in the spectra as a loss of ^{1}H,^{15}N-HSQC peaks in the region above 9 ppm and additional peaks around 8-8.5 ppm (**Figure 2.29**). Previous studies have shown that PHD2 undergoes complicated changes on CODD binding. Because of the loss of PHD2 protein in solution for both the oxic and anoxic PHD2:Fe(II):2OG:CODD complexes, it was difficult to analyse the differences between oxic and anoxic conditions. It does appear that the anoxic PHD2:Fe(II):2OG:CODD spectrum has additional peaks not present in the oxic PHD2:Fe(II):2OG:CODD spectrum, but this may be due to the greater loss of protein in the oxic sample (which had been run after exposing the anoxic sample to oxygen). This experiment was repeated with the same result.

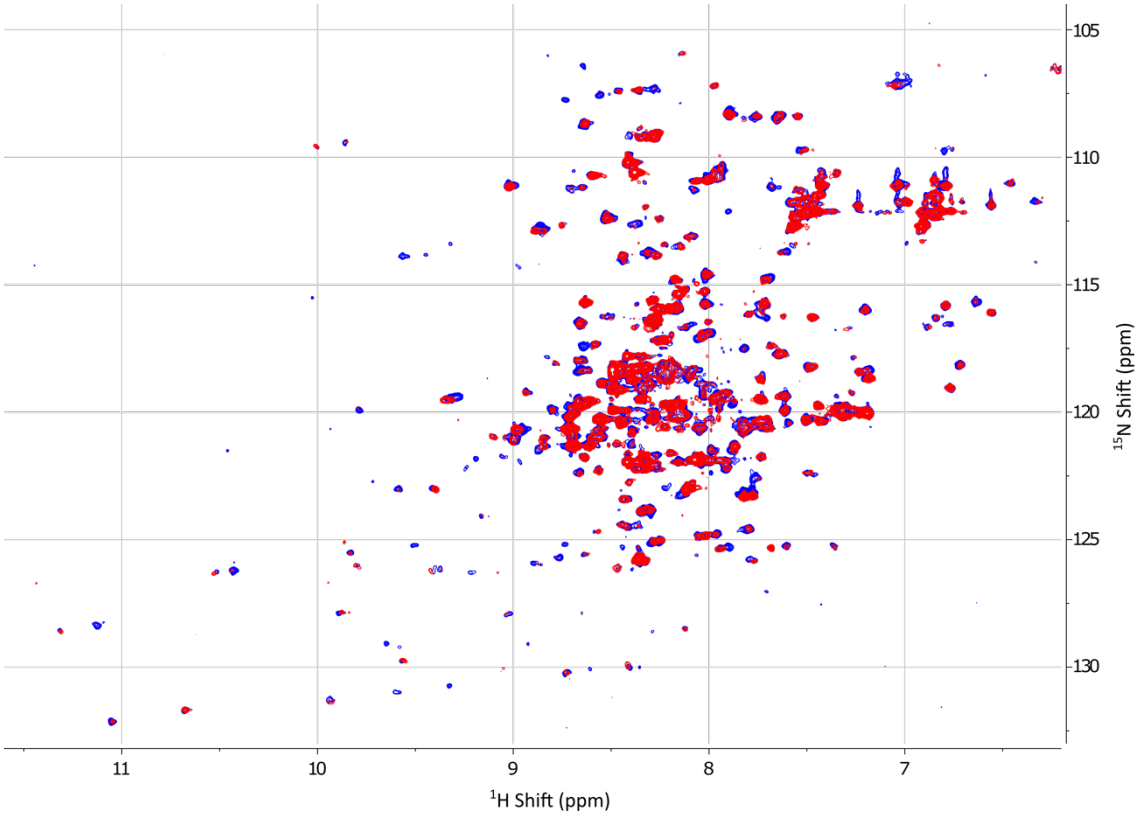


Figure 2.29 *$^{1}H,^{15}N$-HSQC spectra of the oxic (red) and anoxic (blue) PHD2:Fe(II):2OG:CODD complexes. Substantial shift differences between oxic and anoxic spectra seem to be indicated, but due to heavy precipitation of protein leading to poor spectral quality, no firm inferences can be made. Standard concentrations of each component were: 100 μM unlabelled PHD2, 300 μM Fe(II), 500 μM 2OG, 800 μM CODD, and room pressure O_2. Buffer conditions were 10% D_2O, and 90% 50 mM Tris-d_{11} pH 6.5.*

It is uncertain if the precipitation observed on CODD binding to the PHD2:Fe(II):2OG complex related to mechanistically relevant changes—further work is required. It is interesting to note that this destabilisation does not occur in the presence of Zn(II) (**Figure 2.6**), an observation which seems to add another facet to the PHD2:Fe(II) complex (alongside the appearance of multiple sets of peaks observed in anoxic PHD2:Fe(II):2OG and oxic/anoxic PHD2:Fe(II):NOG complexes).

2.2.2.1.6 Summary of Analyses

From these findings it was determined that the most viable complex for further studying the oxygen sensing mechanism of PHD2 was the PHD2:Fe(II):2OG complex.

2.2.2.2 Further Analysis of the Oxic and Anoxic PHD2:Fe(II):2OG Complexes

2.2.2.2.1 Shielded Methyl Analysis

Since the shielded methyl region of PHD2 complexes appeared to be highly susceptible to changes at the active site (as had been seen with the variation of number and shift of peaks in this region when substituting in various metals and cosubstrate/mimics), it was considered that the shielded methyl region of ^{1}H spectra may be a useful tool for understanding the oxygen sensing mechanism and how the state of the active site may be involved.

The first step was to predict which methyl residues are highly shielded due to the protein conformation alone. SHIFTX2 was used for this purpose. [60] The SHIFTX2 predictions are affected by the rigid crystal structure that is input into the algorithm and cannot predict values below 0 ppm, but can be used to approximate which methyl-containing residues might be most useful to explore first (with shifts closest to 0 ppm). When this algorithm was applied to the PHD2:Fe(II):2OG crystal structure (PDB ID: 5L9R), 8 residues were predicted to have shift values low enough (<0.5 ppm) to initially consider them as possible shielded methyl residues (**Table 2.1**).

Num	RES	HB	HB2	HB3	HD1	HD2	HG	HG1	HG12	HG13	HG2
198	I	1.6516	****	****	0.6275	****	****	****	1.3958	1.2009	0.3071
214	L	****	1.6114	1.3375	0.3611	0.1379	1.0675	****	****	****	****
226	V	1.7925	****	****	****	****	****	0.4961	****	****	0.8076
272	L	****	1.5809	1.4119	0.3003	0.4386	1.0983	****	****	****	****
280	I	1.6707	****	****	0.2687	****	****	****	1.0124	0.9439	0.4946
345	I	1.4907	****	****	0.2731	****	****	****	0.9201	0.8931	0.3846
363	L	****	1.4318	1.213	0.3265	0.0557	1.0953	****	****	****	****
376	V	1.9616	****	****	****	****	****	0.4485	****	****	0.7892

Table 2.1 *Lowest values for predicted chemical shifts of PHD2 side-chain ^{1}H peaks from SHIFTX2* ***[60]****. The columns indicate: 1) the residue number, 2) the residue type, and 3-12) ^{1}H shifts for each hydrogen along the amino acid residue. The boxes are coloured on a green-red spectrum with the lowest values highlighted in green and the highest values highlighted in red. Asterisks indicate values that could not be given. The side-chain ^{1}H RMSD in this study was ~0.12-0.40.*

The PHD2:Mn(II):NOG crystal structure was then evaluated for residues that could contain the shielded methyl groups. Only residues within the jellyroll core fold, which is relatively less solvent exposed, were used. From this analysis, 5 candidate shielded methyls and 4 adjacent aromatic residues were identified—these methyls were Ile256, Thr325, Ile327, Ile345, and Thr387. The majority of these potential shielded methyl causing residues did not match the shielded methyls predicted from the SHIFTX2 studies. It is possible that the shielded methyl observations involve paramagnetic effects due to the active site Fe.

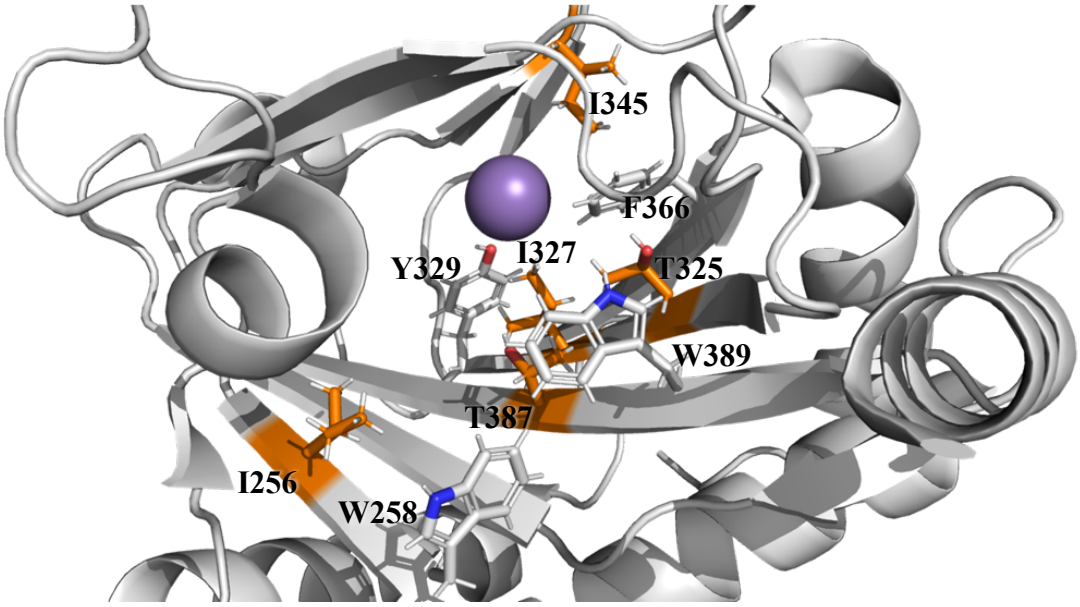


Figure 2.30 *View from a PHD2:Mn(II):2OG crystal structure. The residues shown in orange sticks are methyl-containing residues that are near to aromatic groups: Ile256, Thr325, Ile327, Ile345, and Thr387. The residues shown in grey sticks are aromatic-ring-containing residues that are near to methyl-containing groups: Trp258, Tyr329, Trp389, and Phe366. (The figure was made using PDB ID: 5L9R).*

Analysis of the active site complex of PHD2 as observed in crystal structures indicates a potentially shielded methyl patch adjacent to the active site Fe(II) and in the position close to where oxygen is expected to bind (**Figure 2.31**). This observation suggests that measuring changes in these shielded methyl peaks will give direct evidence of changes in the state of the active site. Some possible changes that could be observed through this method are changes in: 1) the oxidation state of the metal, 2) the spin state of the metal, 3) the orientation of 2OG binding, 4) the position of any residue within the shielded methyl patch, and 5) the position of the substrate. If the methyls observed in the shielded methyl region of the ^{1}H spectrum of PHD2 belong to this region, it would explain why small changes in the state of the protein have led to substantial changes in the ^{1}H shielded methyl region. Further studies were carried out to investigate the identities of these shielded methyls.

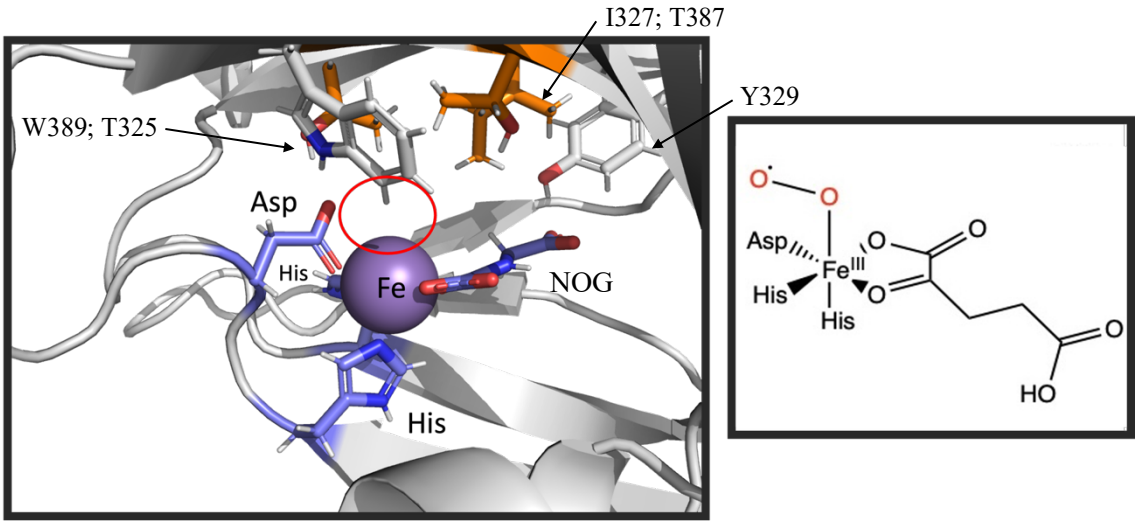


Figure 2.31 *Hypothesised mode of oxygen binding to PHD2. View from a crystal structure showing the active site of PHD2 (complexed with NOG) with the hypothesised position of oxygen binding circled in red (left). Proposed oxygen binding mode (right). The potential shielded methyl patch is close to the metal so may provide valuable information on the state of the active site. Note more than one mode of oxygen binding to PHD2 has been proposed.* ***[5]*** *(The Figure was made using PDB ID: 5L9R).*

To further evaluate the identities of the shielded methyls in the anoxic PHD2:Fe(II):2OG complex, a $^{1}H,^{13}C$-HMQC spectrum was recorded. From this spectrum at least 5 shielded methyl peaks (2 overlapping) were observed. These peaks were indicative of leucine, isoleucine, and valine residues [51].

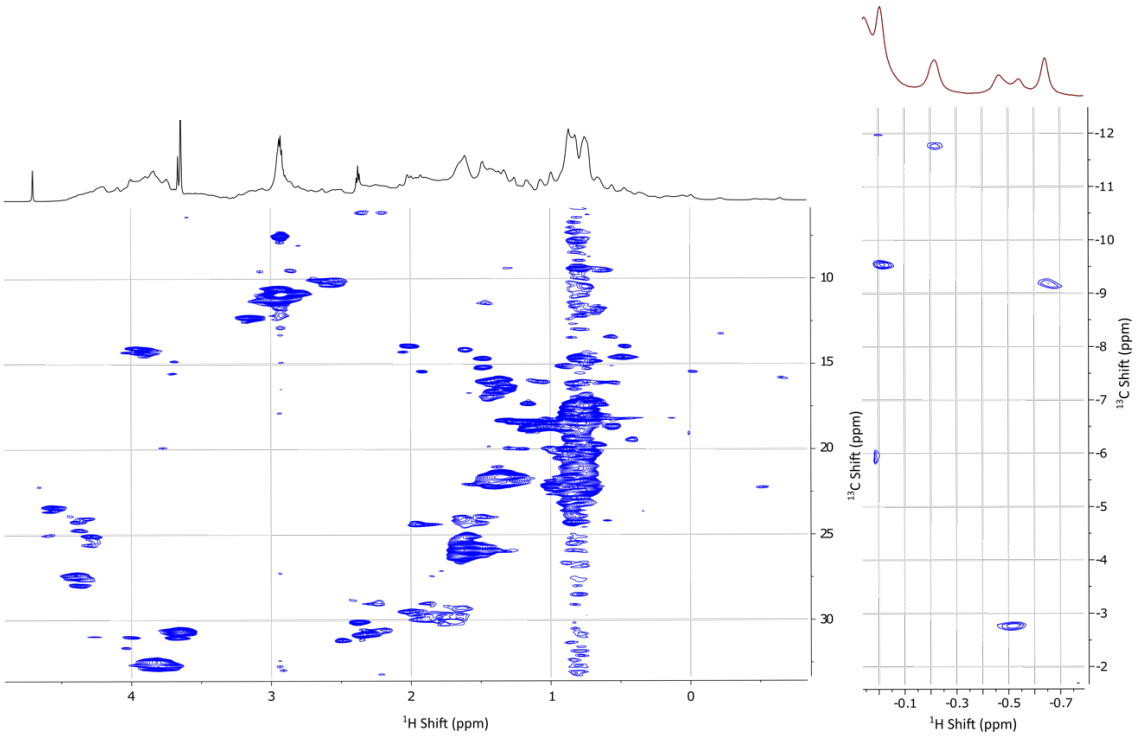


Figure 2.32 *^{13}C-HMQC spectrum of the anoxic PHD2:Fe(II):2OG spectrum (left) and an expanded view of the shielded methyl region (right). All 5 shielded methyl peaks are observed (with 2 overlapping). Standard concentrations of each component were: 200 μM unlabelled PHD2, 400 μM Zn(II), 600 μM 2OG, and room pressure O_2. Buffer conditions were 50 mM Tris-d_{11} in 100% D_2O at pH 6.5. The pulse sequence was a standard Bruker hmqcetgp at 950 scans with 256 F1 increments and 512 F2 increments. The experiment was recorded at 298 K.*

The above-described studies have led to a greater understanding of the identities of the shielded methyl region of the anoxic PHD2:Fe(II):2OG complex. Further studies into the identities of the shielded methyl peaks could involve site-selective mutagenesis of residues of interest.

2.2.2.2.2 Analysis of the T387 Shielded Methyl Peak by Mutagenesis

Once possible identities for the shielded methyls peaks in the PHD2:Fe(II):2OG spectra were compiled, existing mutants of these methyl residues were explored. Luckily, one of the potential shielded methyls in the hydrophobic patch beneath the Fe(II) active

site metal had two existing mutants: T387, with mutations to alanine and serine (position shown in **Figure 2.30**). These proteins were prepared by Giorgia Fiorini.

Previous interest in mutants of the T387 protein stemmed from the evidence that this residue may act as a gatekeeper residue for the entrance of oxygen into the PHD2 active site pocket (Giorgia Fiorini, University of Oxford, D.Phil thesis). [61] This led to studies on the T387A and T387S mutants, both of which could be useful for understanding if this residue is responsible for any of the shielded methyl peaks seen in the oxic and anoxic PHD2:Fe(II):2OG ^{1}H spectra. The T387A mutant was proposed to provide insight on how altering the position of the methyl on this residue may affect the peak positions in the shielded methyl region. In contrast, the T387S mutant is more similar in structure to the native T387 residue and could reveal if removing a methyl from the shielded methyl patch under the active site Fe(II) causes a loss of a peak in the shielded methyl region of the ^{1}H spectrum.

In order to carry out studies on changes in the shielded methyl region of the PHD2:Fe(II):2OG complex with the T387 mutants, an important factor to determine was the number of relevant peaks in each ^{1}H spectrum. This is difficult (especially in the presence of a paramagnetic metal like Fe(II)) due to weak / overlapping signals and substantial broadening effects in the shielded methyl region. It was considered that a variable that may help in separating out the shielded methyl peaks may be to vary the sample temperature.

The first set of ^{1}H spectra to be explored were the wild-type anoxic PHD2:Fe(II):2OG complexes under various temperature conditions (**Figure 2.33**). From these studies, 5 shielded methyl peaks were observed that moved to about the same degree with increasing temperature. All 5 peaks were fully separated at 308 K.

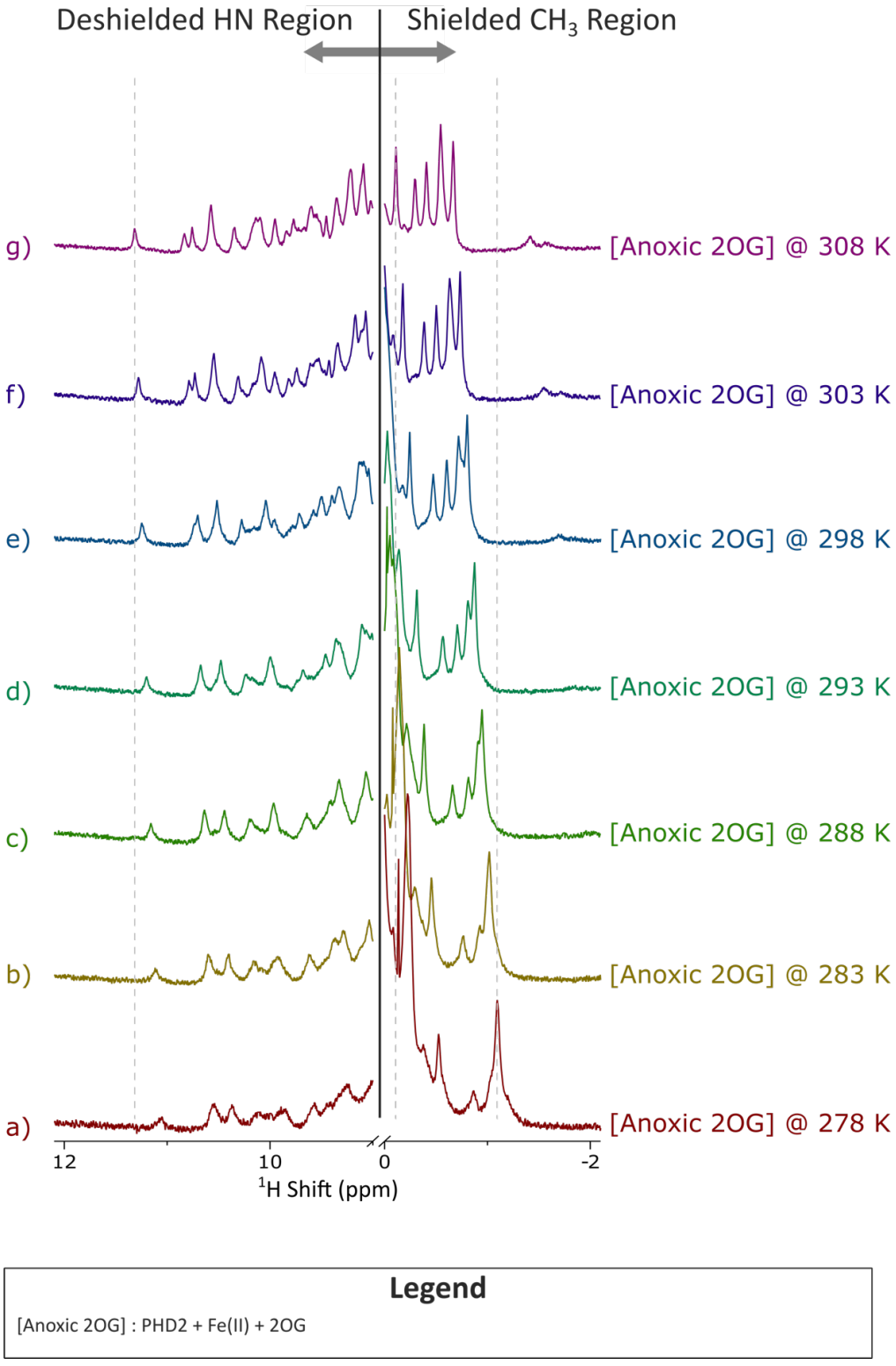


Figure 2.33 *^{1}H spectral comparison of the anoxic PHD2:Fe(II):2OG complex under various temperature conditions. Data were collected at the following temperatures: 278 K (a), 283 K (b), 288 K (c), 293 K (d), 298 K (e), 303 K (f), and 308 K (g). The shielded methyl region (<0 ppm) is most suitable to be observed between temperatures ranging*

from 303-308 K. The deshielded H_N region also benefitted from temperatures around 303-308 K, especially in the region above 10 ppm. The dotted grey lines are used to help differentiate shifts. Standard concentrations of each component were: 100 μM unlabelled PHD2, 300 μM Fe(II), 500 μM 2OG, and <2 ppm O_2 pressure. Buffer conditions were 135 mM NaCl, 10% D_2O, and 90% 50 mM Tris-d_{11} pH 7.5.

Next, the number of peaks in the wild-type oxic PHD2:Fe(II):2OG ^{1}H spectrum shielded methyl region was analysed at different temperatures (**Figure 2.34**). These studies manifested only one major peak in the shielded methyl region, with a small shoulder observed at lower temperatures that may be another broad peak.

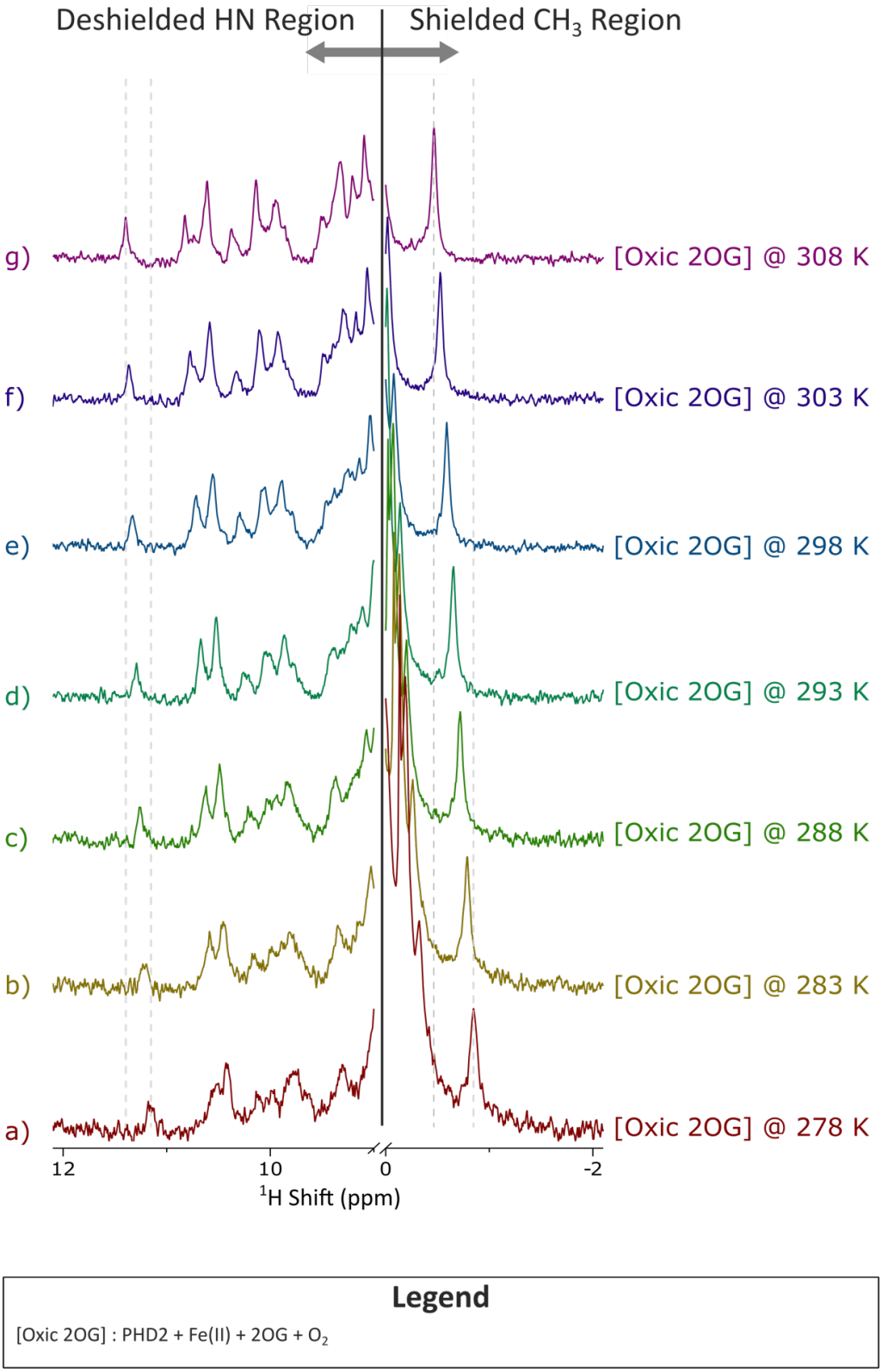


Figure 2.34 *^{1}H spectral comparison of the oxic PHD2:Fe(II):2OG complex under various temperature conditions. Data were collected at the following temperatures: 278 K (a), 283 K (b), 288 K (c), 293 K (d), 298 K (e), 303 K (f), and 308 K (g). The shielded*

methyl region (<0 ppm) is suitable for observations at any of the tested temperatures, whereas the deshielded H_N region can be best resolved from 293 to 308 K. The oxic methyl peak positions generally appear to be less influenced by temperature than the anoxic peak positions. The dotted grey lines are used to help differentiate shifts. Standard concentrations of each component were: 100 μM unlabelled PHD2, 300 μM Fe(II), 500 μM 2OG, and <2 ppm O_2 pressure. Buffer conditions were 135 mM NaCl, 10% D_2O, and 90% 50 mM Tris-d_{11} pH 7.5.

The next complex to be studied under various temperature conditions was the anoxic PHD2(T387S):Fe(II):2OG complex (**Figure 2.35**). This complex was unstable, giving poor quality spectra that made it difficult to analyse at low temperatures. At high temperatures the shielded methyl peaks were not well resolved. There appeared to be 5-6 shielded methyl peaks, which is equal to or greater than the number of peaks found in the analogous wild-type protein complex. This indicated that removal of the T387 methyl by substitution with a serine residue does not decrease the number of methyl peaks in the ^{1}H shielded methyl region.

Differences in the shifts of methyls in the shielded methyl region were observed for the mutant in comparison to the wild-type protein, which may indicate that T387 is near to, or linked to, residues containing the shielded methyl peaks. This hypothesis is further supported by the observation that threonine methyl ^{1}H peaks tend to be too deshielded to appear in the shielded methyl region. [51]

Further exploration of this complex may require more stable protein conditions, as the instability of the T387S protein made it difficult to acquire oxic PHD2(T387S):Fe(II):2OG spectra at various temperatures, therefore, these studies were not carried out.

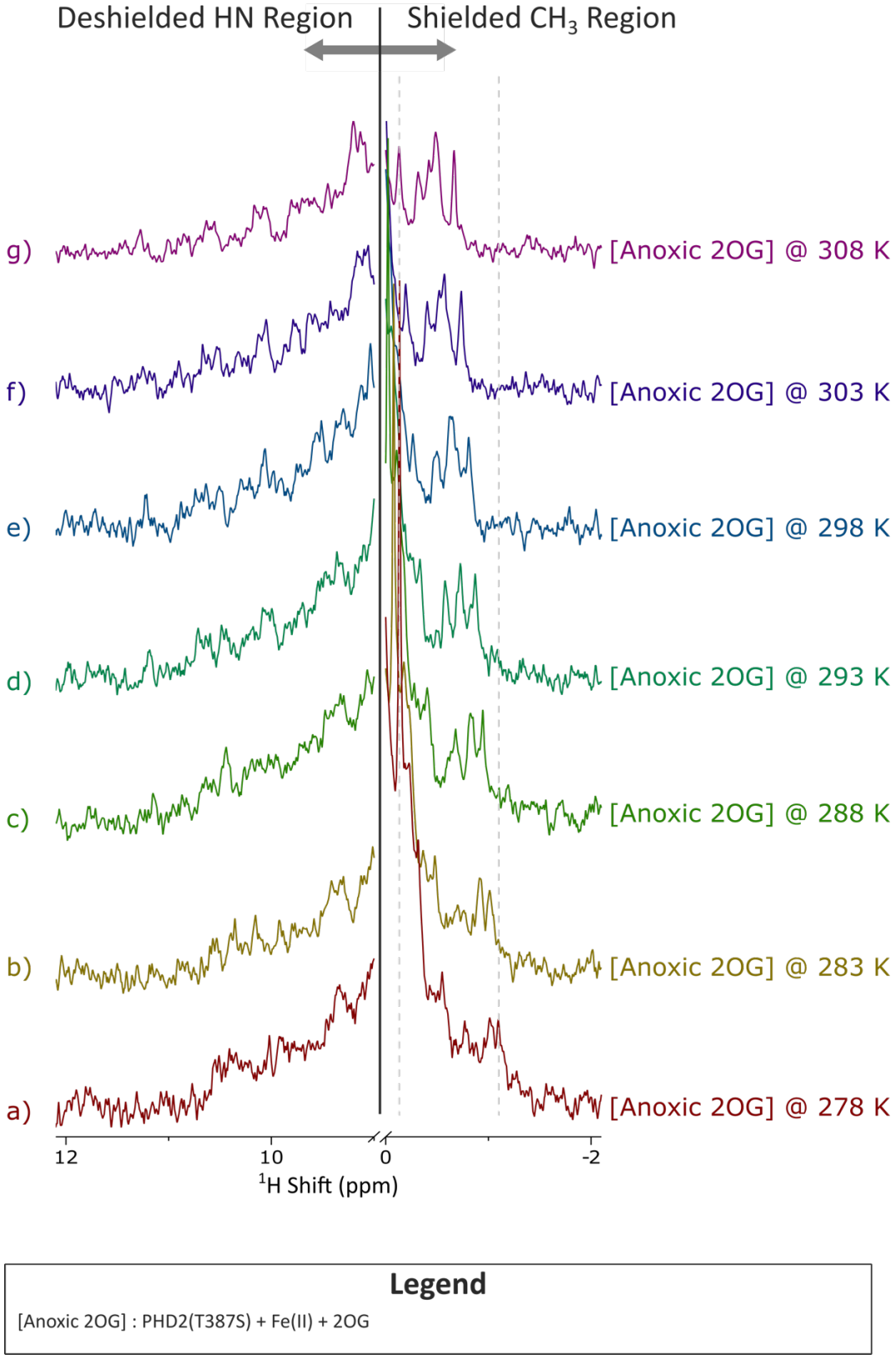


Figure 2.35 *^{1}H spectral comparison of the anoxic PHD2(T387S):Fe(II):2OG complex at different temperatures. Data was collected at the following temperatures: 278 K (a), 283 K (b), 288 K (c), 293 K (d), 298 K (e), 303 K (f), and 308 K (g). Severe precipitation led*

to poor data quality. Both the shielded methyl region (<0 ppm) and the deshielded H_N region cannot be well characterised under these conditions, though the shielded methyl region does appear to have at least 5 shielded methyl peaks as has been observed in the wild-type protein. This may indicate that residue T387 is not one of the shielded methyls observed below 0 ppm. The dotted grey lines are used to help differentiate shifts. Standard concentrations of each component were: 50 μM unlabelled PHD2(T387S), 300 μM Fe(II), 500 μM 2OG, and <2 ppm O_2 pressure. Buffer conditions were 135 mM NaCl, 10% D_2O, and 90% 50 mM Tris-d_{11} pH 7.5.

The last complex of interest studied under various temperature conditions was the anoxic PHD2(T387A):Fe(II):2OG complex (**Figure 2.36**). This protein appeared to be more stable than the T387S mutant giving clearer peaks.

In variable temperature studies, the PHD2(T387A) complex exhibited clear signs of an additional shielded methyl peak, where 6 shielded methyl peaks were counted in total. These observations indicate that converting the T387 residue to an alanine has either: 1) further shielded a methyl group that was already present in the protein or 2) has been shielded to an extent where the alanine methyl is responsible for the new shielded methyl peak. Another alternative could be that a broad shielded methyl peak has been sharpened due to a change in the paramagnetic effects acting on it.

Despite better stability than the T387S mutant protein complex, study of the oxic PHD2(T387A):Fe(II):2OG complex across variable temperatures still exhibited unresolved complications.

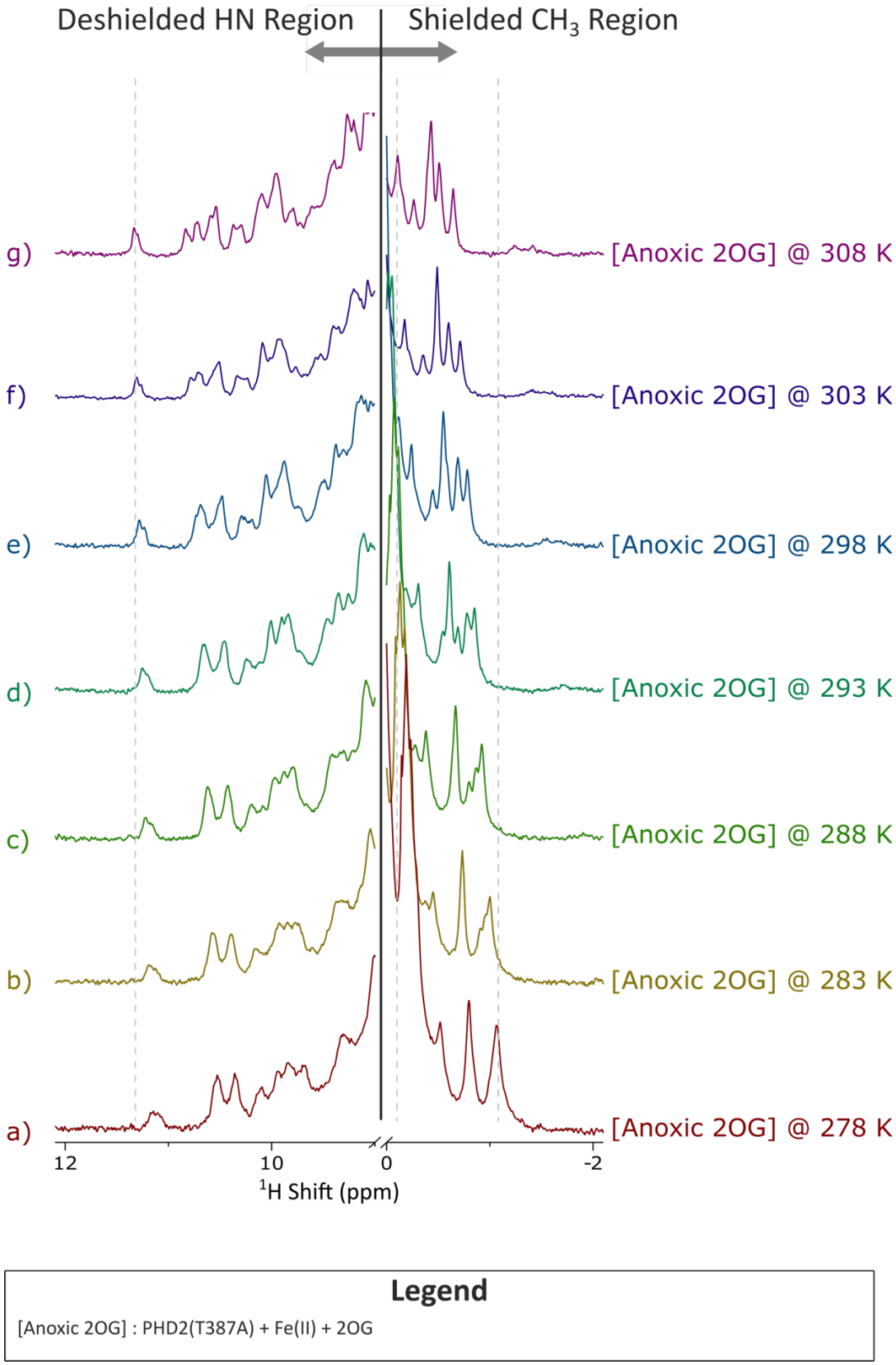


Figure 2.36 *^{1}H spectral comparison of the anoxic PHD2(T387A):Fe(II):2OG complex at different temperatures. Data was collected at the following temperatures: 278 K (a),*

283 K (b), 288 K (c), 293 K (d), 298 K (e), 303 K (f), and 308 K (g). Some precipitation occurred, but quality data was still obtained. Both the shielded methyl region (<0 ppm) and the deshielded H_N region can be well characterised under these conditions. The shielded methyl region appears to have at least 6 shielded methyl peaks, a greater number than observed in the wild-type protein. This may indicate that T387 is not one of the shielded methyl peaks below 0 ppm. The dotted grey lines are used to help differentiate shifts. Standard concentrations of each component were: 50 μM unlabelled PHD2(T387A), 300 μM Fe(II), 500 μM 2OG, and <2 ppm O_2 pressure. Buffer conditions were 135 mM NaCl, 10% D_2O, and 90% 50 mM Tris-d_{11} pH 7.5.

Comparison of the wild-type and mutant PHD2:Fe(II):2OG variable temperature studies show that the anoxic wild-type complex manifested 5 shielded methyl peaks whereas the anoxic T387S complex manifested 5-6 shielded methyl peaks, and the anoxic T387A complex manifested 6 shielded methyl peaks. These observations suggest that the threonine methyl peak(s) of T387 may not contribute to the shielded methyl region. Since shifts could be observed in the two mutant complexes relative to the wild-type complex, it is likely that mutation of the T387 residue affects the shielding of some shielded methyl peaks which may indicate that T387 is adjacent to shielded methyl-containing residues. Additionally, the T387S mutant contained an extra methyl peak that appeared to be in the shielded methyl region. This may imply that the native threonine does experience the effects of shielding but is not shielded enough to fall in the shielded methyl region.

Analysis of the oxic wild-type and T387A PHD2:Fe(II):2OG complexes shows that both seem to contain only one shielded methyl peak, which is only slightly affected by the mutation.

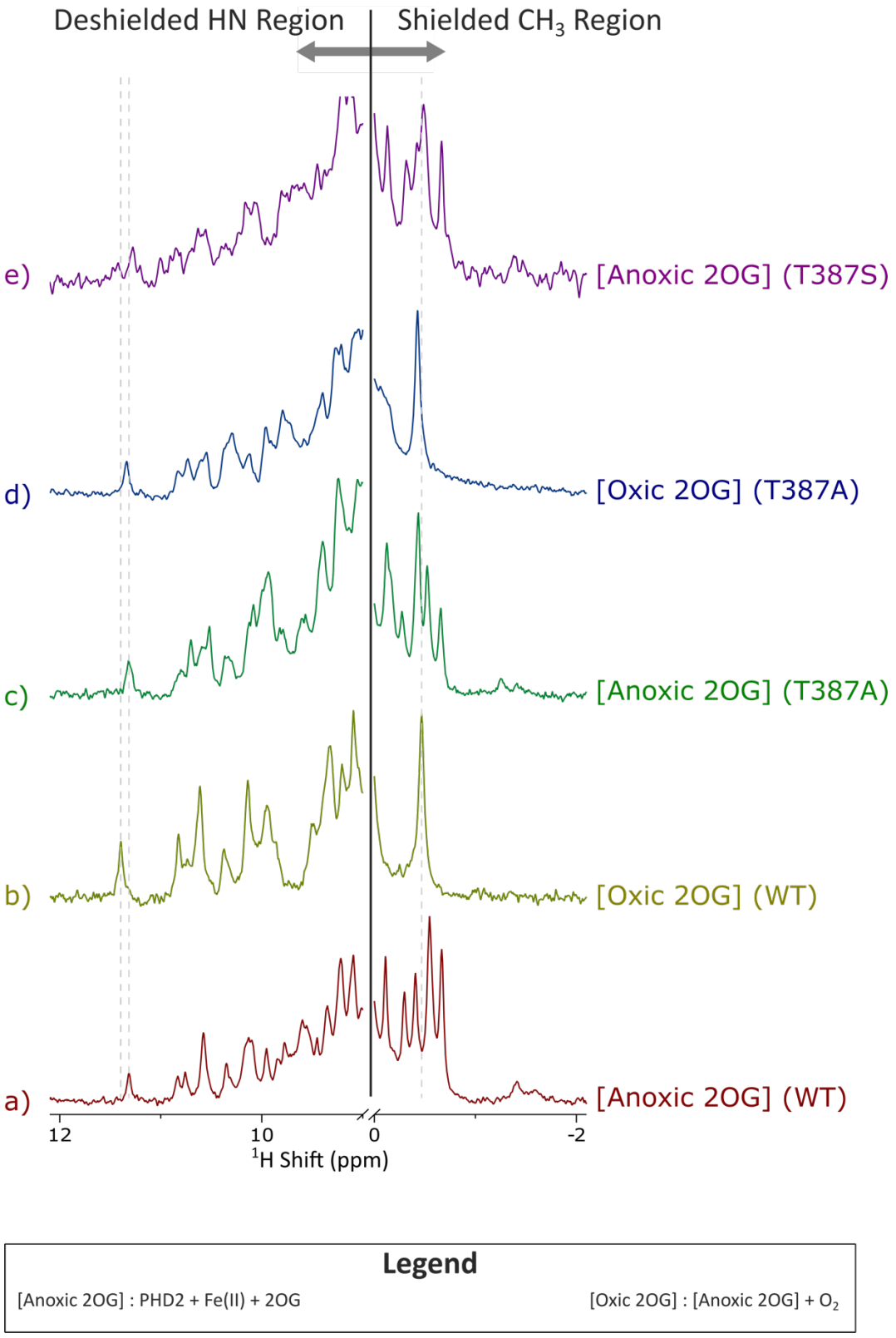


Figure 2.37 *^{1}H spectral comparison of oxic and anoxic PHD2:Fe(II):2OG complexes for wild-type, T387S, and T387A variants. Variations of the T387 residue do not appear to cause substantial changes in the shielded methyl and deshielded H_N regions of the ^{1}H*

spectrum. The oxic PHD2(T387S):Fe(II):2OG complex was not available due to heavy precipitation. The dotted grey lines are used to help differentiate shifts. The black, vertical separating line indicates the position where the region from 0 to 9 ppm of the spectrum was removed for simplicity. Standard concentrations of each component were: 100 μM unlabelled PHD2(WT), 50 μM unlabelled PHD2(T387S or T387A), 300 μM Fe(II), 500 μM 2OG, 500 μM CODD, <2 ppm O_2 pressure (anoxic), and room pressure O_2 (oxic). Buffer conditions were 135 mM NaCl, 10% D_2O, and 90% 50 mM Tris-d_{11} pH 7.5.

These studies imply T387 has a role linked to the shielded methyl region of the ^{1}H spectrum. From these studies it was determined that analysis of all shielded-methyl- and aromatic-ring-containing residues in the hydrophobic patch close to the active site Fe(II) should be studied further.

2.2.2.2.3 Controlled Oxygen Pressure Experiments

A key aspect of the role of the PHDs in hypoxia sensing is that their reactivity is affected in a graded way by oxygen availability. Turnover of CODD in cells, however, may occur at values as low as 0.2% atmospheric oxygen. [62] The work described in this section explored the amount of oxic complex formed from anoxic complex exposure to various oxygen concentrations, a variable that might relate to the cellular role of the PHDs as hypoxia sensors.

Step-wise addition of increasing oxygen to the anoxic PHD2:Fe(II):2OG complex shows immediate turnover of 2OG at oxygen concentrations as low as 0.1-0.2% (**Figure 2.38**), and appears to continue until substantial amounts of 2OG had reacted. Below 0.8% oxygen the reaction appears to only reach a certain level of turnover before stalling. This may be due to the lack of ascorbate, which is proposed to complete uncoupled reaction cycles, possibly by reducing inactive Fe(III)/Fe(IV) forms.

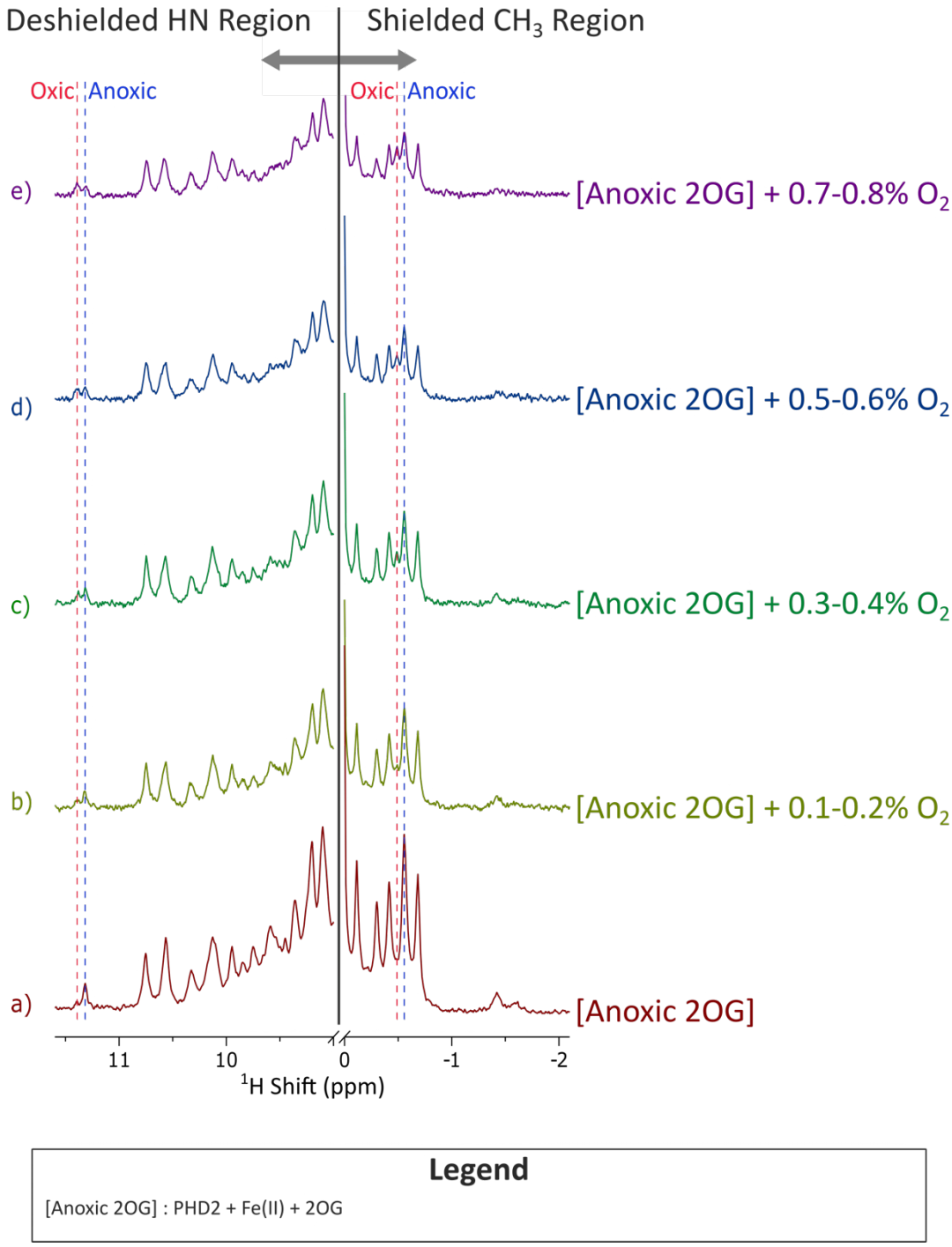


Figure 2.38 *Step-wise titration of oxygen into the anoxic PHD2:Fe(II):2OG complex. PHD2 complex at 0% (red), 0.1-0.2% (red), 0.3-0.4% (green), 0.5-0.6% (pink), and 0.7-0.8% (black) oxygen concentrations. Loss of 5 anoxic shielded methyl peaks and growth of an oxic shielded methyl peak is observed. All oxygen exposed conditions included 2.2% CO_2. Standard concentrations of each component were: 100 µM unlabelled PHD2, 300 µM Fe(II), 500 µM 2OG, and <2 ppm O_2 pressure (anoxic). Buffer conditions were 10% D_2O, and 90% 50 mM Tris-d_{11} pH 6.5.*

Observation of the $^{1}H,^{15}N$-HSQC spectrum indicates a complex corresponding in nature to the oxic PHD2:Fe(II):2OG complex (**Figure 2.39**) obtained at 4% oxygen.

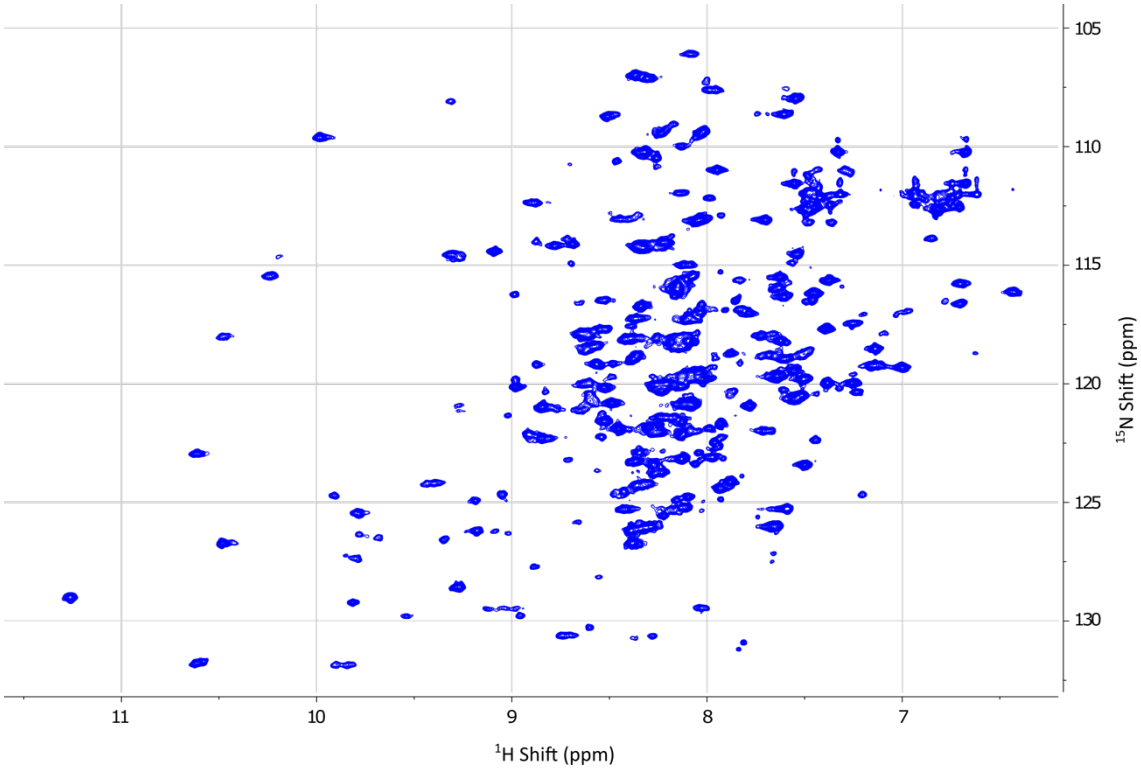


Figure 2.39 *$^{1}H,^{15}N$-HSQC spectrum of PHD2:Fe(II):2OG under 4% O_2 and 2.2% CO_2 conditions. At 4% oxygen, the spectrum already mirrors the spectrum of a fully oxic(~20 % oxygen pressure) sample. Standard concentrations of each component were: 100 µM unlabelled PHD2, 300 µM Fe(II), 500 µM 2OG, 4% O_2 concentrations, and 2.2% CO_2 concentrations. Buffer conditions were 10% D_2O, and 90% 50 mM Tris-d_{11} pH 6.5.*

Further studies on oxygen titration with the anoxic PHD2:Fe(II):2OG:CODD complex should be explored to investigate reactivity of the catalytically productive enzyme-substrate complex.

2.2.2.2.4 Investigating Effects of Ascorbate/Glutathione on the Oxic PHD2 Complex

Regeneration of the active PHD2 complex after 2OG turnover under substrate uncoupled conditions is of interest. Studies on PHD2 catalytic activity show ascorbate apparently promotes and perpetuates catalysis, [63] yet the mechanism(s) through which ascorbate carries out these roles is not understood. A possible explanation is that

ascorbate acts as a reducing agent, converting the PHD2 active site Fe(III) (or Fe(IV)) back to Fe(II) at the end of the uncoupled reactions. The work described in this section aimed to investigate how ascorbate interacts with PHD2.

In the absence of ascorbate and the presence of small amounts of oxygen (**Figure 2.40** a), the PHD2:Fe(II):2OG complex slowly converts to a fully oxic complex over a few days (**Figure 2.40** b-d). This complex did not revert to the anoxic complex over time. When CODD was introduced to this complex after the complex reached the fully oxic state, no turnover and no change in the ^{1}H spectrum were observed (**Figure 2.40** e). These observations show that the (oxic) complex, formed by reaction of the PHD2:Fe(II):2OG complex with oxygen, is inactive (likely in the Fe(III) state).

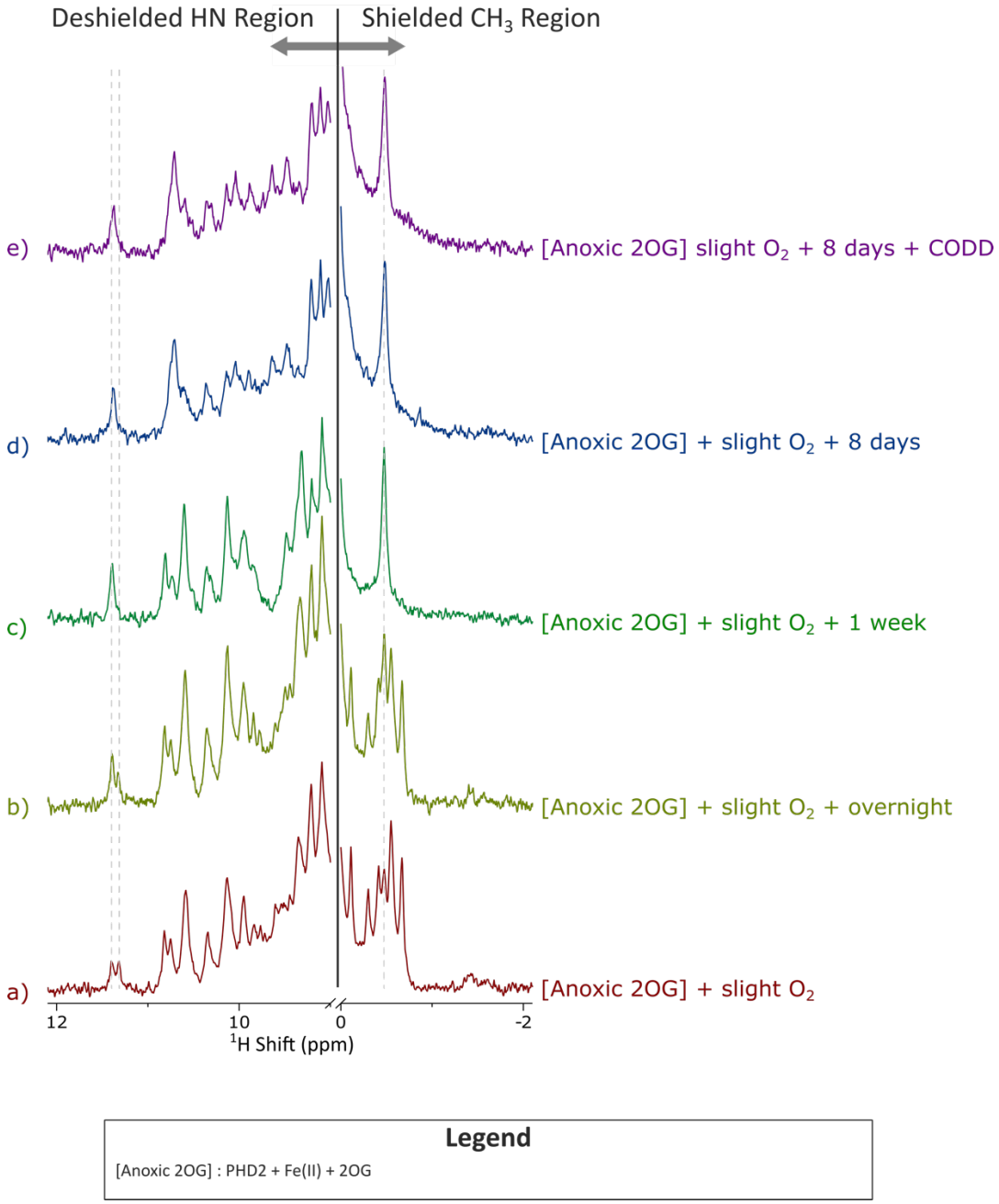


Figure 2.40 *^{1}H spectrum timecourse of the briefly oxic PHD2:Fe(II):2OG complex in the absence of ascorbate. The sample was mixed while oxic, left for 3 minutes, then quickly purged of oxygen. After 2 hours of purging, the sample was monitored over time: a) 0 days, b) ~15 hours, c) 7 days, d) 8 days, e) 8 days + addition of CODD. On initial observation (a), no reversal of the oxic state was observed. After 8 days without reversal (d), CODD was added to the solution (e) to observe if this state was still catalytically active. No activity was observed. The dotted grey lines are used to help differentiate shifts. Standard concentrations of each component were: 100 µM unlabelled PHD2, 300*

μM Fe(II), 2 mM 2OG, and variable O_2 pressures. Buffer conditions were 135 mM NaCl, 10% D_2O, and 90% 50 mM Tris-d_{11} pH 7.5.

When ascorbate was added to the briefly oxic PHD2:Fe(II):2OG complex, the formation of the oxic complex was halted and reversed over the span of a few hours (**Figure 2.41**). This newly formed fully anoxic complex was stable and did not further convert to the oxic complex. These observations indicate that ascorbate can reverse the effects oxygen has on the PHD2:Fe(II):2OG complex through an unknown mechanism. This seems to support the proposal that ascorbate is acting to revert the active site to its initial state, possibly through direct or indirect reduction of Fe(III) to Fe(II).

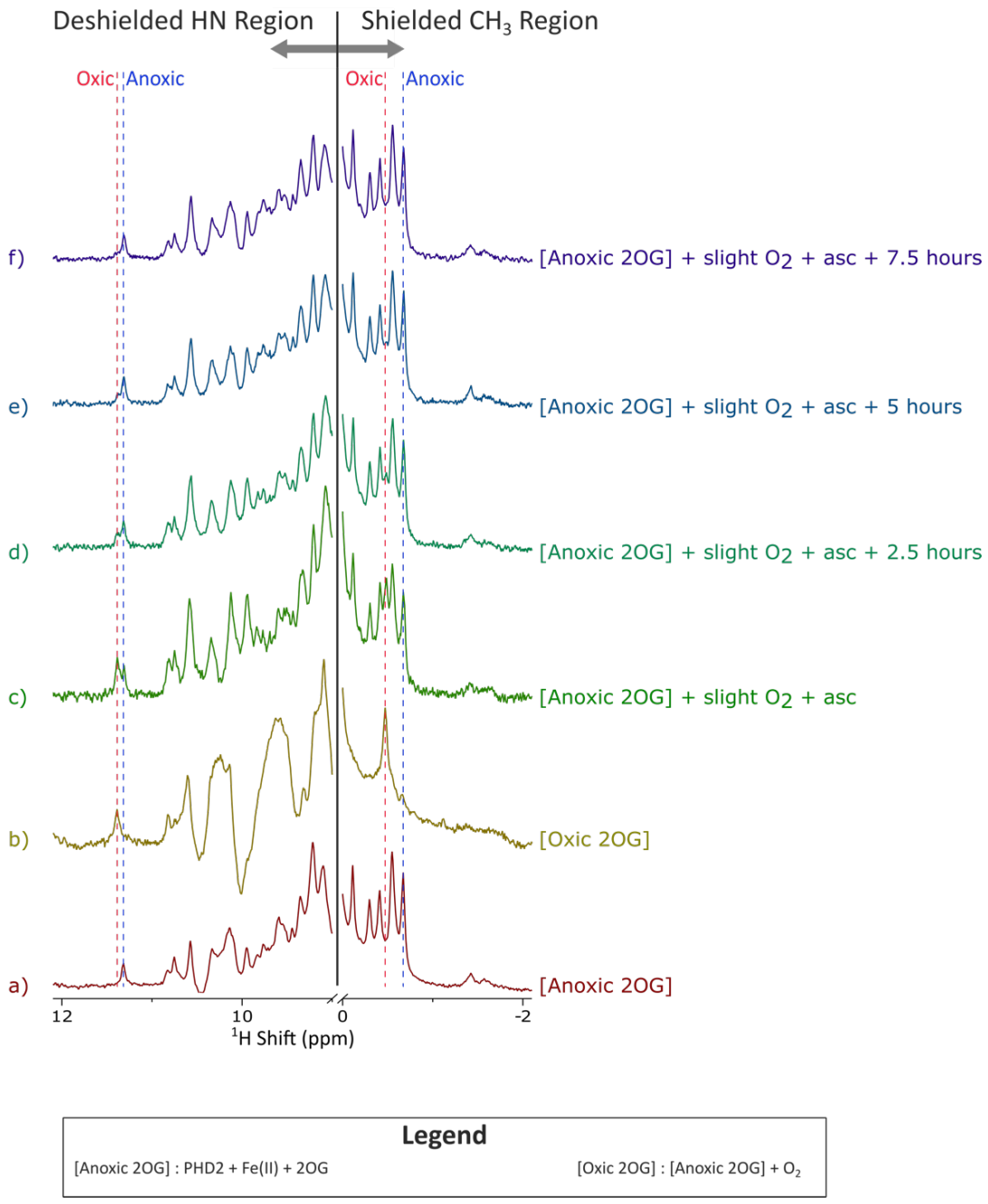


Figure 2.41 *^{1}H spectrum timecourse of the briefly oxic PHD2:Fe(II):2OG complex in the presence of ascorbate. An initial spectrum of the oxic complex was taken (b). The sample was mixed whilst oxic, left for 3 minutes, then quickly purged of oxygen. After 2 hours of purging (a), ascorbate and excess Fe(II) were added and the sample was monitored over time: c) 0 hours, d) 2.5 hours, e) 5 hours, f) 7.5 hours. Reversal of the oxic state was observed. The spectrum (b) indicates poor water suppression, but this did not affect the quality of data in the regions of interest. Standard concentrations of each component were: 100 μM unlabelled PHD2, 300 μM Fe(II) (plus an additional 300 μM after*

purging), 2 mM 2OG, 1 mM ascorbate, and variable O_2 pressures. Buffer conditions were 135 mM NaCl, 10% D_2O, and 90% 50 mM Tris-d_{11} pH 7.5.

After following the effects of ascorbate on the state of the briefly oxic PHD2:Fe(II):2OG complex, it was important to probe what—if any—effect the presence of ascorbate may have on the anoxic PHD2:Fe(II):2OG complex. Addition of ascorbate to the anoxic PHD2:Fe(II):2OG complex yielded no substantial changes in the $^{1}H,^{15}N$-HSQC spectrum (**Figure 2.42**). As had been expected, in the absence of an O_2 source in solution, ascorbate does not appear to affect the structure or dynamics of the anoxic PHD2:Fe(II):2OG complex, as observed by NMR.

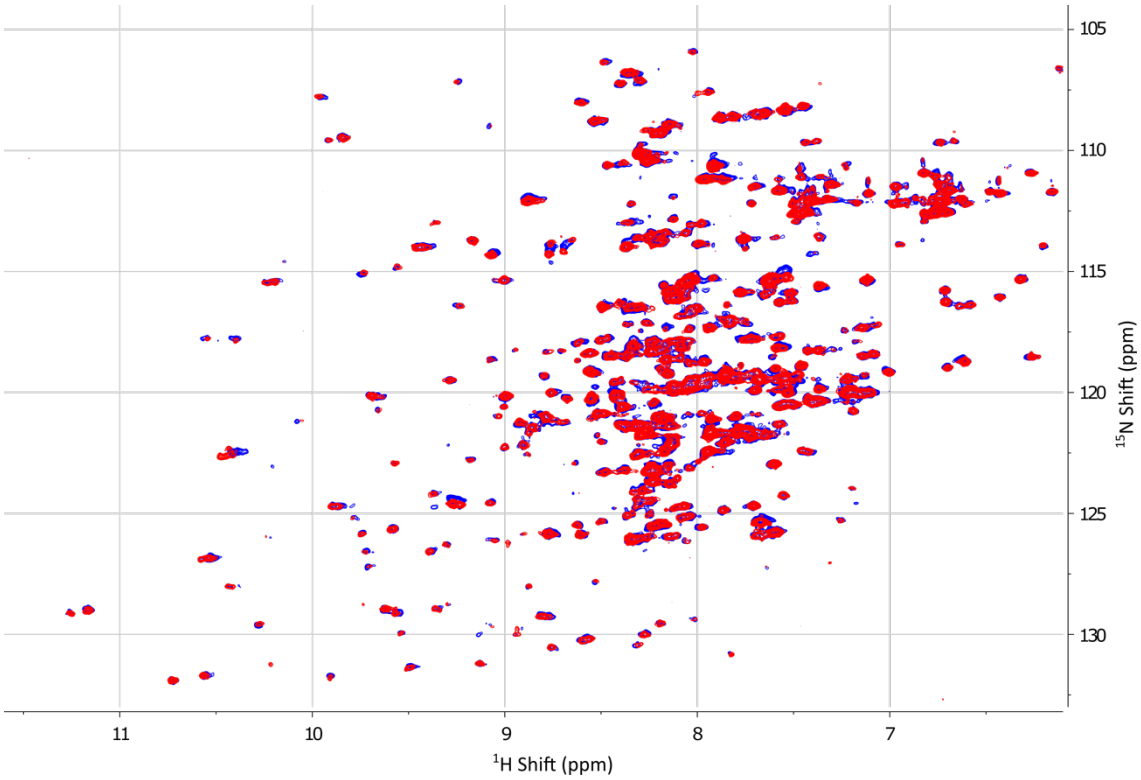


Figure 2.42 *$^{1}H,^{15}N$-HSQC spectra of the anoxic PHD2:Fe(II):2OG complex in the presence (red) and absence (blue) of ascorbate. There is no substantial change in the anoxic spectrum on ascorbate addition. Standard concentrations of each component were: 100 μM unlabelled PHD2, 200 μM Fe(II), 400 μM 2OG, 400 μM ascorbate, and <2 ppm O_2 pressure. Buffer conditions were 10% D_2O, and 90% 50 mM Tris-d_{11} pH 6.5.*

Next, the impact of glutathione on the formation of the oxic PHD2:Fe(II):2OG complex under slightly oxic conditions was observed, with glutathione apparently having a similar reducing function to ascorbate in biological systems. The presence of glutathione has been found to stimulate PHD2 activity. [64]

Addition of glutathione to the briefly oxic PHD2:Fe(II):2OG complex led to slow reversal of the oxic state and full recovery of the anoxic state (**Figure 2.43**). This occurred more slowly than with ascorbate, despite starting with slightly lower oxygen concentrations (as is evident from the smaller oxic complex peak in the shielded methyl region at timepoint zero). This indicates that glutathione does appear to act on the PHD2 oxic complex in a similar manner to ascorbate, consistent with prior studies. [64]

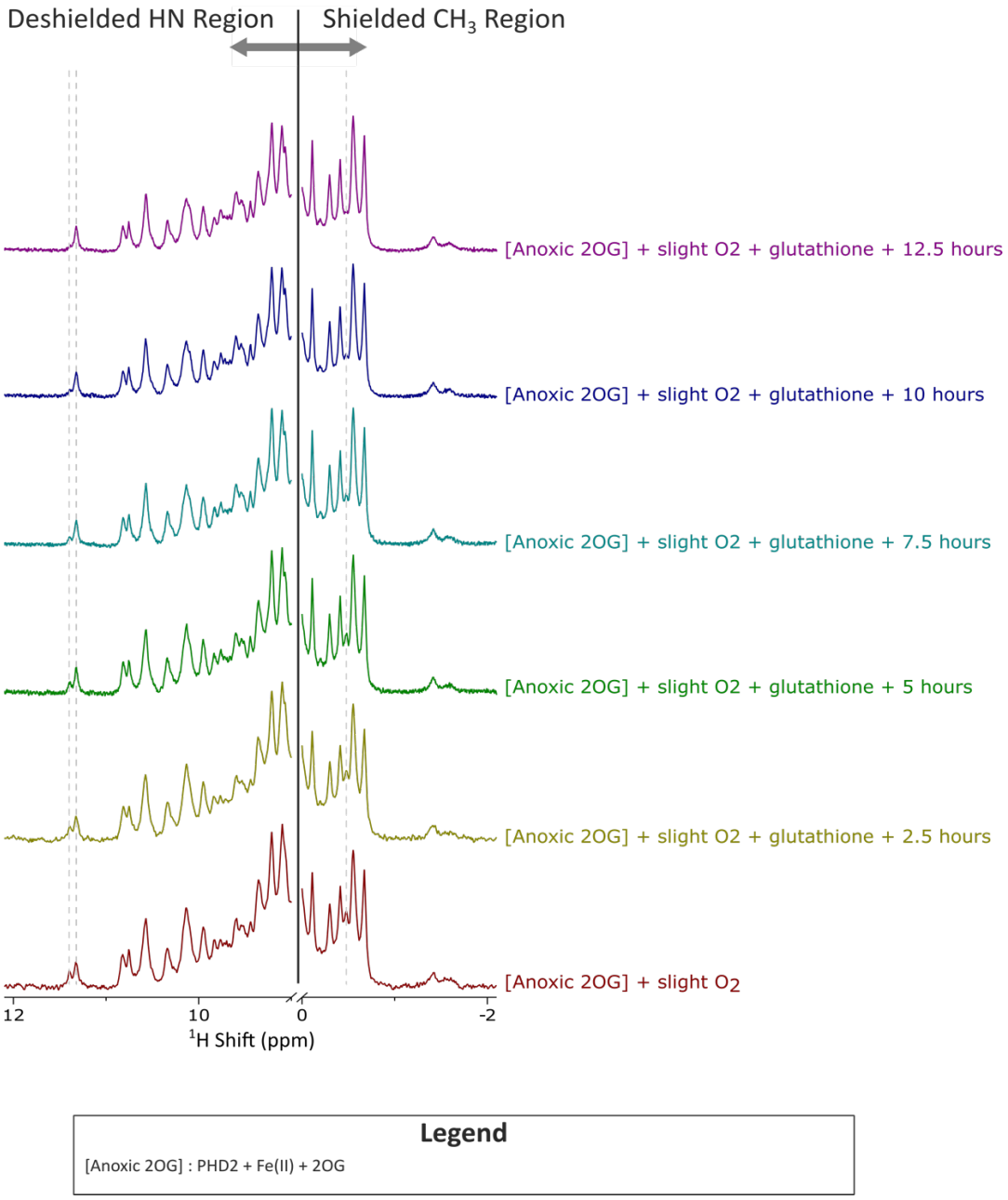


Figure 2.43 *^{1}H spectrum timecourse of the briefly oxic PHD2:Fe(II):2OG complex in the presence of glutathione. The sample was mixed while oxic, left for 3 minutes, then quickly purged of oxygen. After 2 hours of purging, glutathione and excess Fe(II) was added and the sample was monitored over time (2.5 hour increments). Reversal of the oxic state was observed. The trend observed in the presence of glutathione mirrored what is observed in the presence of ascorbate. The dotted grey lines are used to help differentiate shifts. Standard concentrations of each component were: 100 μM unlabelled PHD2, 300 μM Fe(II) (plus an additional 300 μM after purging), 2 mM 2OG, 1 mM glutathione, and*

variable O_2 pressures. Buffer conditions were 135 mM NaCl, 10% D_2O, and 90% 50 mM Tris-d_{11} pH 7.5.

From these studies, it can be conclude that: 1) ascorbate does not impact the structure of the anoxic PHD2:Fe(II):2OG complex, 2) ascorbate both slows the formation of, and acts to reverse the oxic PHD2:Fe(II):2OG complex to its anoxic state, and 3) glutathione can acts similarly to ascorbate, but on a longer timescale.

2.2.2.2.5 EPR Studies on the Oxic and Anoxic PHD2:Fe(II):2OG Complexes

Previously, the differences in the spectra of oxic and anoxic PHD2:Fe(II):2OG were described (**Figure 2.17, Figure 2.18,** and **Figure 2.19**). One explanation for the set of two peaks in the anoxic PHD2:Fe(II):2OG spectra was the presence of more than one spin state and/or oxidation state. Possible spin state / oxidation state pairs include: 1) low spin / diamagnetic Fe(II), 2) high spin / paramagnetic Fe(II), 3) low spin / paramagnetic Fe(III), and 4) high spin / paramagnetic Fe(III).

One set of the anoxic PHD2:Fe(II):2OG peaks in the $^{1}H,^{15}N$-HSQC spectrum matches the chemical shifts of the $^{1}H,^{15}N$-HSQC spectrum of the oxic PHD2:Fe(II):2OG complex, while the other set of peaks are unique. One initial hypothesis was that one set may adopt the same spin/oxidation state as the oxic complex and the other may take on a different spin/oxidation state. These two sets of peaks in the anoxic spectrum may be due to two protein conformations, but a possibly more likely explanation is multiple binding modes of the cosubstrate, 2OG, leading to a change in the paramagnetic properties of the active site Fe(II). Electron paramagnetic resonance (EPR) spectroscopy is a tool useful in elucidation of these possible paramagnetic species and has been previously used to study PHD2. [58]

Details of the process of preparing and running EPR experiments are given in Chapter 5, **Section 5.4**. It was notable that upon cryogenic freezing, the oxic

PHD2:Fe(II):2OG complex was observed to be a deep blue colour and the anoxic PHD2:Fe(II):2OG complex was observed to be a light purple (**Figure 2.44**). The blue colour did not fade on melting, and ^{1}H NMR spectra appeared identical to typical PHD2:Fe(II):2OG spectra.

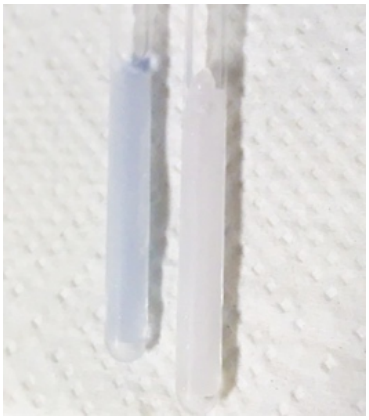
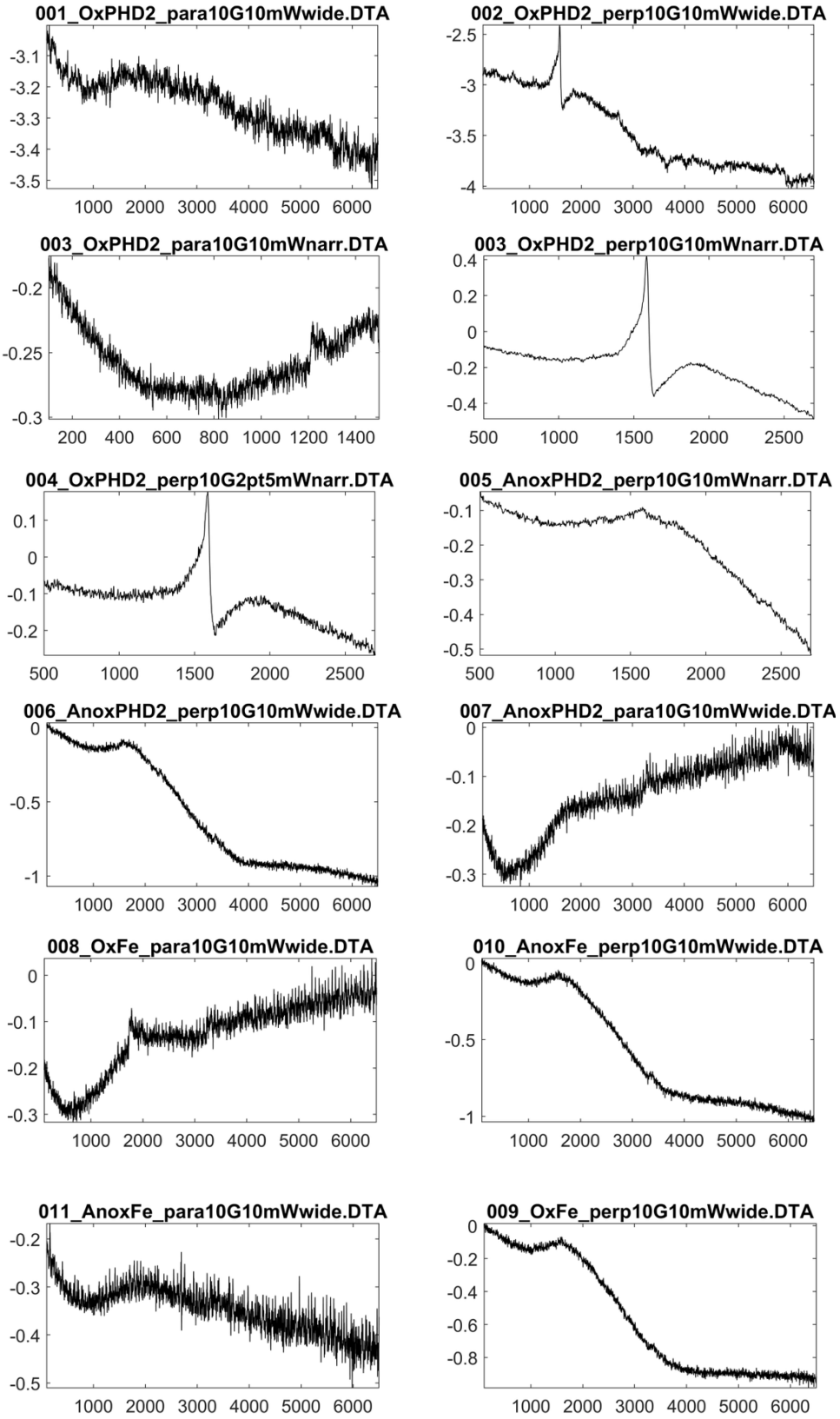


Figure 2.44 *EPR samples of oxic and anoxic PHD2:Fe(II):2OG complexes (left and right respectively) after cryogenic freezing. The oxic sample was observed to be dark blue and the anoxic sample was observed to be light purple. Sample colours did not fade on defrosting. Standard concentrations of each component were: 100 μM unlabelled PHD2, 150 μM Fe(II), and 500 μM 2OG. Buffer conditions were 10% D_2O, and 90% 50 mM Tris-d_{11} pH 7.5.*

The experiments were run in parallel mode EPR studies carried out with Dr. William Myers (Chemistry Department, Oxford University). Metal free comparison samples were prepared with oxic and anoxic Fe(II):2OG in order to rule out signals due to oxidation of the metal in solution through a nonenzymatic process. Measurements of the oxic and anoxic Fe(II):2OG metal free control samples indicated no paramagnetic EPR signals (**Figure 2.45,** 009 and 010 respectively). Additionally, measurement of the anoxic PHD2:Fe(II):2OG sample revealed no signals (**Figure 2.45**, 005 and 006), suggesting an Fe(II) oxidation state. The oxic PHD2:Fe(II):2OG sample alternatively showed a strong peak in the region indicative of an Fe(III) complex (**Figure 2.45**, 002, 003, and 004).


001_OxPHD2_para10G10mWwide.DTA
002_OxPHD2_perp10G10mWwide.DTA
003_OxPHD2_para10G10mWnarr.DTA
003_OxPHD2_perp10G10mWnarr.DTA
004_OxPHD2_perp10G2pt5mWnarr.DTA
005_AnoxPHD2_perp10G10mWnarr.DTA
006_AnoxPHD2_perp10G10mWwide.DTA
007_AnoxPHD2_para10G10mWwide.DTA
008_OxFe_para10G10mWwide.DTA
010_AnoxFe_perp10G10mWwide.DTA
011_AnoxFe_para10G10mWwide.DTA
009_OxFe_perp10G10mWwide.DTA

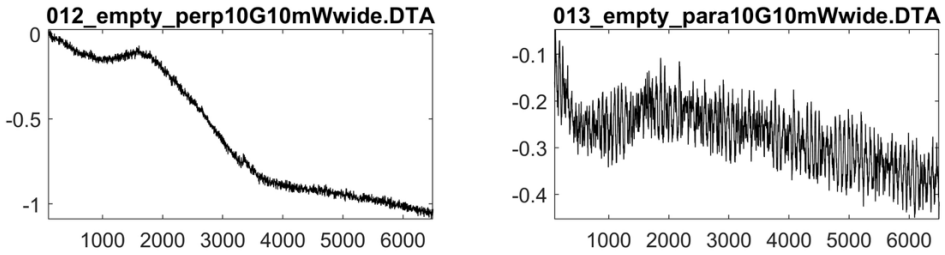


Figure 2.45 *Parallel Mode EPR spectra for PHD2 oxygen studies. The following spectra were recorded in perpendicular: the oxic PHD2:Fe(II):2OG (002, 003, and 004) spectra, the anoxic PHD2:Fe(II):2OG (005 and 006) spectra, the oxic Fe(II):2OG (009) spectrum, and the anoxic Fe(II):2OG (010) spectrum. The following spectra were recorded in parallel: the oxic PHD2:Fe(II):2OG (001 and 003) spectra, the anoxic PHD2:Fe(II):2OG (007) spectrum, the oxic Fe(II):2OG (008) spectrum, and the anoxic Fe(II):2OG (011) spectrum. One oxic and one anoxic spectrum were taken for baseline measures of the perpendicular and parallel phases (012 and 013 respectively). The x-and y-axes of these spectra represent B_o (G) and intensity respectively.*

From these studies, the presence of both Fe(II) and Fe(III) species simultaneously in the anoxic PHD2:Fe(II):2OG complex can be ruled out; it is likely that only the Fe(II) species is present. Additionally, the oxic PHD2:Fe(II):2OG complex likely contains Fe(III) at the active site, and the oxidation of the metal is PHD2-complex dependent (no Fe(III) was observed in the oxic Fe(II):2OG complex in the absence of enzyme).

2.2.3 PHD2 Further Metal Studies

2.2.3.1 Studies of the Effects of Metals on Free 2OG Shifts

As paramagnetism has an important role in my research on PHD2, effects of paramagnetic metals on 2OG in solution were investigated. This work was also of interest with respect to whether Fe(II) enters the active site as an independent metal ion or as a metal-ion-2OG complex.

The first metal of interest studied was Zn(II) as a diamagnetic comparator. Addition of Zn(II) at low concentration to a 2OG solution resulted in no paramagnetic

shifting or broadening (**Figure 2.46**). Higher concentrations of Zn(II) also did not cause changes in the ^{1}H 2OG triplet peaks.

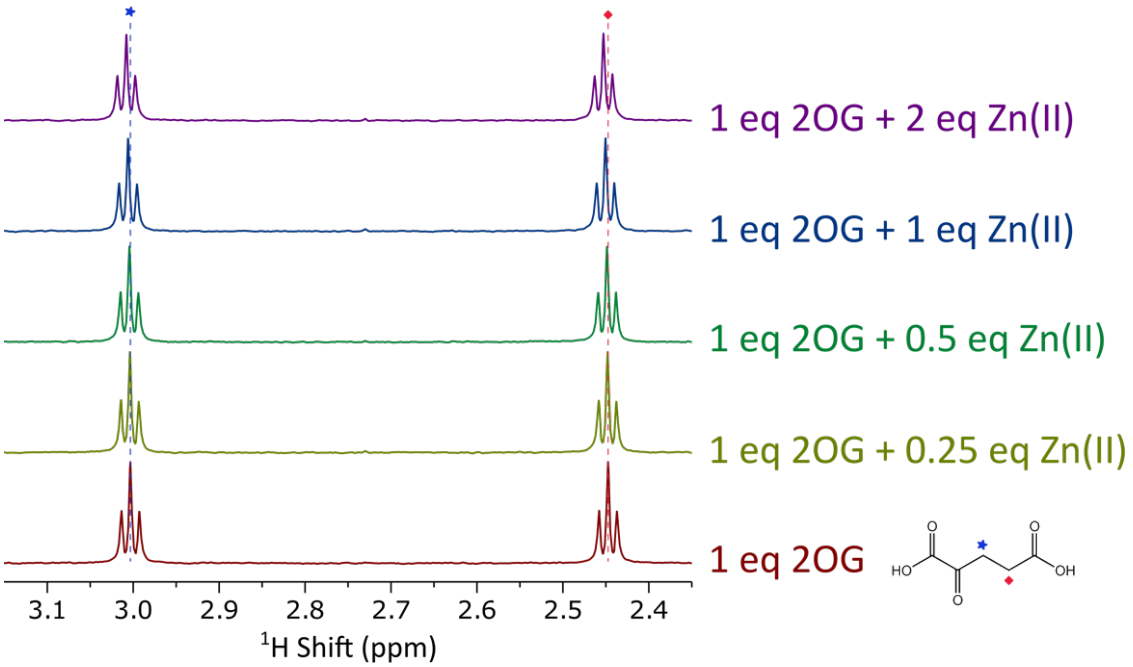


Figure 2.46 *^{1}H spectral comparison of 2OG peaks with varied Zn(II) concentrations. The dotted red lines indicate the initial positions of the 2OG CH_2 triplets in the absence of metal. The identities of these CH_2 hydrogens are denoted by red diamond and blue star symbols in positions both above their respective peaks and next to their locations in the 2OG structure. 1 eq (equivalent) is equal to 200 µM. The peak positions have not been adjusted relative to a standard since only relativistic positions between metal and no-metal conditions were required. With increasing Zn(II) concentrations, there is little to no change in the broadening or shifting of 2OG CH_2 triplets. Buffer conditions were 135 mM NaCl, 10% D_2O, and 90% 50 mM Tris-d_{11} pH 7.5.*

The next metal of interest studied was Fe(II), which had been shown to cause both paramagnetic shifts and broadening in PHD2 protein solution analyses. Addition of small concentrations of Fe(II) to a 2OG solution resulted in the broadening and shifting of both of the 2OG triplet peaks (**Figure 2.47**), with the C5 carboxylic acid-adjacent methylene protons experiencing greater paramagnetic effects than the ketone-adjacent protons. Addition of higher Fe(II) concentrations further shifts and broadens both 2OG ^{1}H methyl

peaks, but at high Fe(II):2OG ratios the relative broadening of the triplets is reversed and the ketone-adjacent methylene protons experience greater paramagnetic broadening. Despite this, the paramagnetic shifts remain greater for the carboxyl-adjacent protons, perhaps reflecting their adjacent nature to an Fe(II) chelating C5 carboxylate, whereas the other (C3) methylene is separated from the C1 carboxylate by the C2 ketone. Interestingly, the two triplets experienced different shift effects, where the C5 carboxylic-adjacent triplet experienced deshielding and the ketone-adjacent methylene triplet experienced shielding.

These changes are likely a result of the formation of 2OG complex(es) in solution, though the components of that complex are uncertain. A large triplet (likely ammonium from the added Fe(II) salt) and a large, broad singlet appear in the region above 8 ppm, which further suggests some water- or buffer-related complex is formed.

The experiment was repeated with an alternate form of Fe(II) (absent of ammonium) with the same observations, without the deshielded ammonium peak.

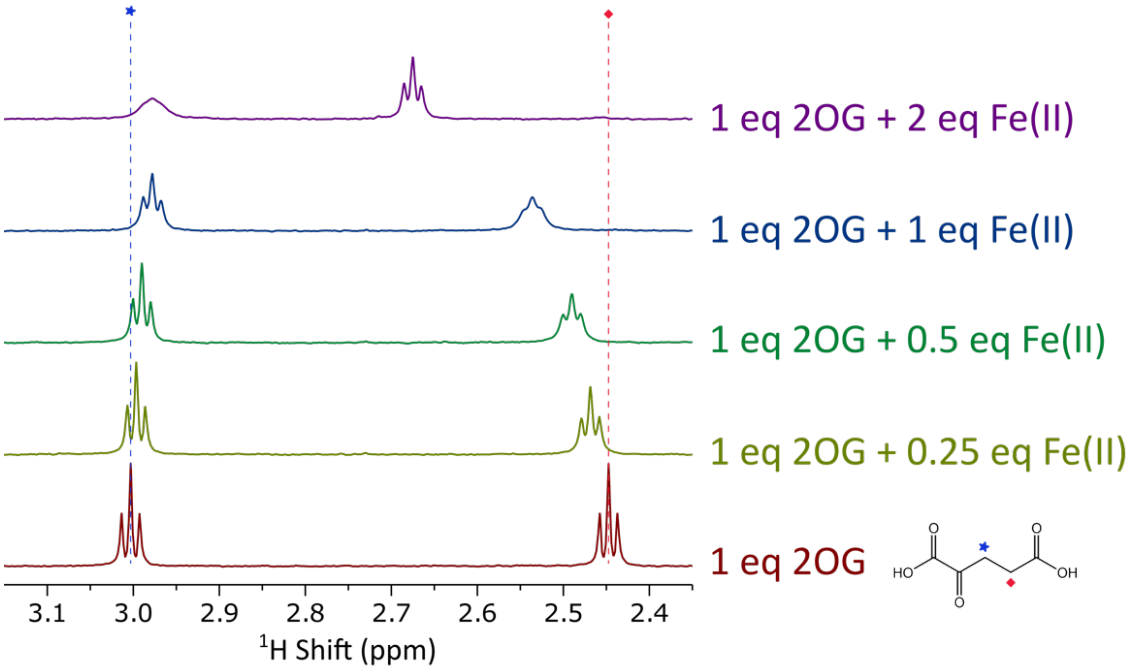


Figure 2.47 *^{1}H spectral comparison of 2OG peaks with varied Fe(II) concentrations. The dotted red lines indicate the initial positions of the 2OG CH_2 triplets in the absence of metal. The identities of these CH_2 hydrogens are denoted by red diamond and blue star symbols in positions both above their respective peaks and next to their locations in the 2OG structure. 1 eq (equivalent) is equal to 200 µM. The peak positions have not been adjusted relative to a standard since only relativistic positions between metal and no-metal conditions were required. With increasing Fe(II) concentrations, there is an "inward" shift of both 2OG CH_2 triplets as well as broadening of both triplets. Initial broadening is most severe on the protons closest to the ketone (blue star) but the trend flips around 400 µM Fe(II). This odd behaviour should be explored in the future. Buffer conditions were 135 mM NaCl, 10% D_2O, and 90% 50 mM Tris-d_{11} pH 7.5.*

Studies with Ni(II) led to observation of slight paramagnetic shifts and no paramagnetic broadening in the protein complex (**Figure 2.48**). The paramagnetic broadening affected the 2OG methyl peaks to a similar magnitude, with slightly greater broadening on the carboxyl-adjacent protons. This trend continues as more Ni(II) was added to solution.

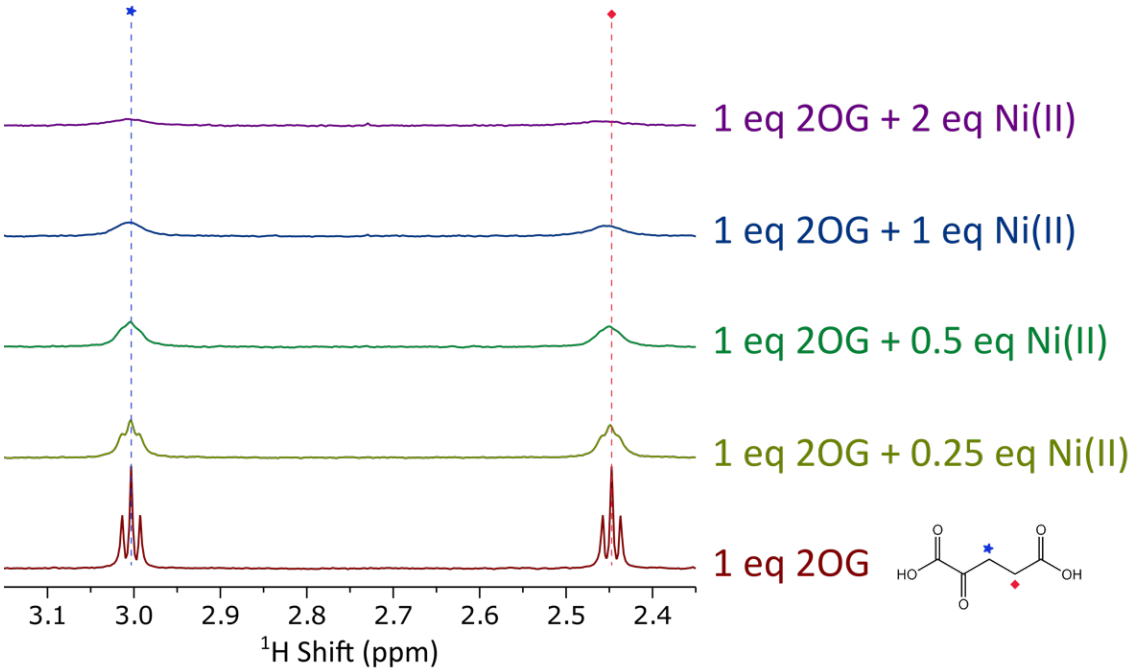


Figure 2.48 *^{1}H spectral comparison of 2OG peaks with varied Ni(II) concentrations. The dotted red lines indicate the initial positions of the 2OG CH_2 triplets in the absence of metal. The identities of these CH_2 hydrogens are denoted by red diamond and blue star symbols in positions both above their respective peaks and next to their locations in the 2OG structure. 1 eq (equivalent) is equal to 200 µM. The peak positions have not been adjusted relative to a standard since only relativistic positions between metal and no-metal conditions were required. With increasing Ni(II) concentrations, there is no substantial shift of the 2OG CH_2 triplets. Broadening occurs to an almost equal extent on both 2OG CH_2 triplets. Buffer conditions were 135 mM NaCl, 10% D_2O, and 90% 50 mM Tris-d_{11} pH 7.5.*

When tested, Co(II) was found to cause major paramagnetic shifts throughout the PHD2 spectrum, but minor/no broadening (**Figure 2.13**). On addition of small amounts of Co(II) to a 2OG solution, both paramagnetic shifting and broadening were observed. As with Fe(II), the effects of paramagnetic broadening were greatest on the C5 carboxylic acid-adjacent methylene triplet, and the effects of paramagnetic shifting were greatest on the ketone-adjacent methylene triplet. As the concentration of Co(II) was increased, this

trend continued. By contrast with Fe(II), both triplets experienced a deshielding effect from interactions with Co(II).

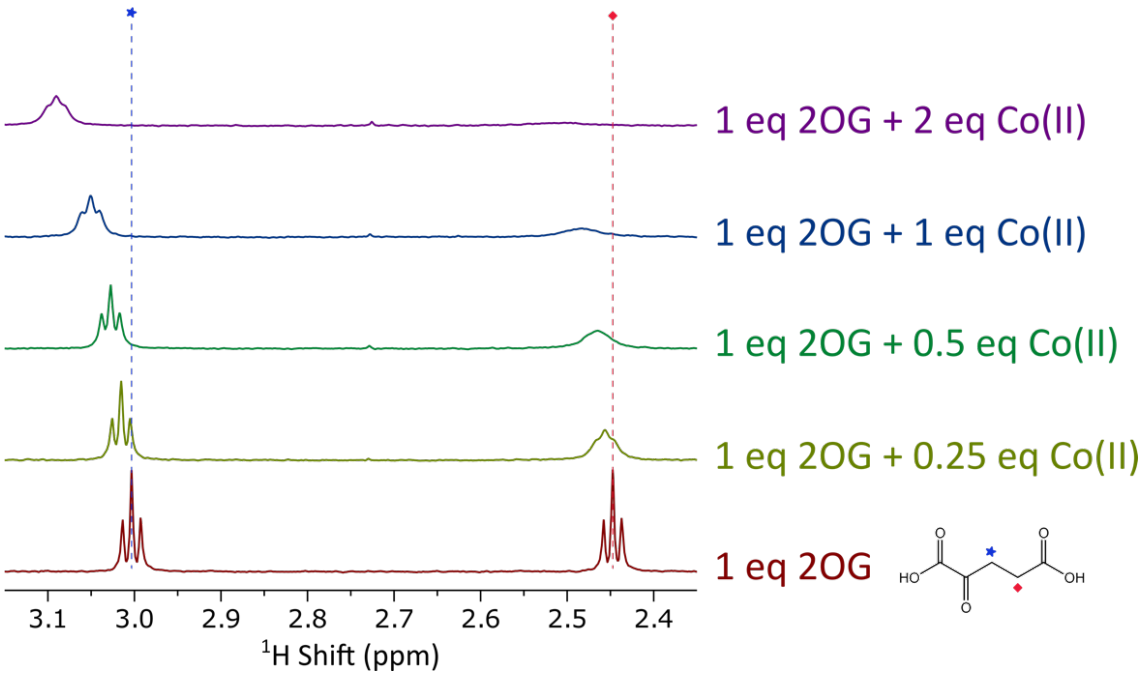


Figure 2.49 *^{1}H spectral comparison of 2OG peaks with varied Co(II) concentrations. The dotted red lines indicate the initial positions of the 2OG CH_2 triplets in the absence of metal. The identities of these CH_2 hydrogens are denoted by red diamond and blue star symbols in positions both above their respective peaks and next to their locations in the 2OG structure. 1 eq (equivalent) is equal to 200 µM. The peak positions have not been adjusted relative to a standard since only relativistic positions between metal and no-metal conditions were required. With increasing Co(II) concentrations, there is a deshielding shift of both 2OG CH_2 triplets as well as broadening to unequal extents, where the protons further from the ketone (red diamond) are broadened the most. Buffer conditions were 135 mM NaCl, 10% D_2O, and 90% 50 mM Tris-d_{11} pH 7.5.*

The overall results show that the paramagnetic effects on 2OG in solution vary depending on the metal ion added. Future studies may include addition of HIF-α substrate to the metal-2OG solution to see if the mode of binding changes as well as to study whether, and if so how, the 2OG metal ion complexes bind to PHD2 and other 2OG-dependent dioxygenases.

2.2.3.2 Studies of PHD2:Metal Complexes

2.2.3.2.1 PHD2:Metal Complexes in the Presence or Absence of Oxygen, 2OG, and CODD

In order to further probe the interactions between various metal ions within the active site of PHD2, oxic/anoxic PHD2:metal ion complexes were observed in the presence and absence of 2OG and CODD. Previously no differences between the oxic and anoxic PHD2:metal:2OG complexes were observed except in the presence of Fe(II) (**Figure 2.20**). These studies aimed to investigate if other complexes may reveal oxic vs. anoxic differences in the PHD2:metal spectra.

On further exploring the various complexes of PHD2:Fe(II) with and without oxygen, ligand, and substrate, it was found that only in the presence of 2OG was a difference in the oxic and anoxic complexes observed (**Figure 2.50**). This is important because only in the presence of 2OG is the complex active (in the cases of both coupled and uncoupled turnover). This may imply that some reversible change(s) caused by the presence of oxygen may also cause the variation observed between oxic and anoxic PHD2:Fe(II):2OG complexes.

This difference between oxic and anoxic conformations extends to the PHD2:Fe(II):2OG:CODD complex, which exhibits a set of peaks unique from the PHD2:Fe(II):2OG complex in both oxic and anoxic states (**Figure 2.50** d and f, where the differences in the oxic PHD2:Fe(II):2OG and oxic PHD2:Fe(II):2OG:CODD complexes can be observed mainly in the deshielded H_N region). This feature should be further explored as the protein complex after both coupled and uncoupled turnover exhibits oxygen-dependent changes in the spectra. It is also interesting that in the anoxic spectrum, in the presence of CODD, appears to further shield some methyl groups, as

evidenced by at least one additional shielded methyl in the shielded methyl region (**Figure 2.50** e).

The following figure captions will indicate what complexes were expected to have formed under the given conditions, with "+ O_2" in a product indicating that there was no evidence of oxygen interaction with the complex of interest, based on the ^{1}H spectra.

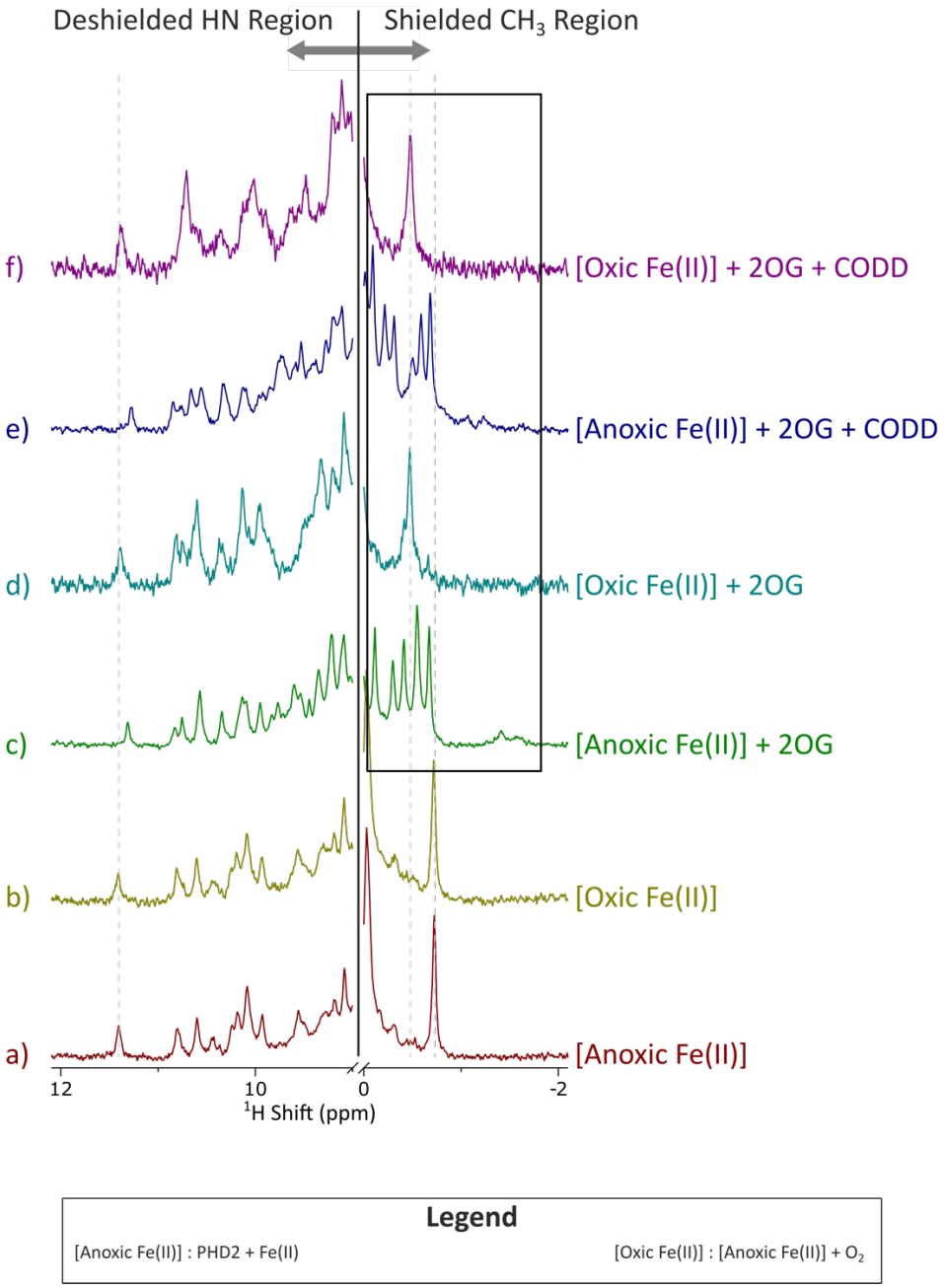


Figure 2.50 *^{1}H spectral comparison of oxic and anoxic conditions for various PHD2:Fe(II) complexes. Only in the PHD2:Fe(II):2OG and PHD2:Fe(II):2OG:CODD complexes does addition of O_2 cause changes in the ^{1}H spectra. The labels in the figure for each spectrum above indicates the starting complex, whereas each component after a "+" is added to solution in the order written from left to right. The reaction components (separated by "+" signs) and proposed major complex formed are given as follows. a) PHD2:Fe(II), b) PHD2:Fe(II) + O_2, c) PHD2:Fe(II) + 2OG → PHD2:Fe(II):2OG, d) PHD2:Fe(II):O_2 + 2OG → PHD2:Fe(II):2OG:O_2, e) PHD2:Fe(II) + 2OG + CODD →*

PHD2:Fe(II):2OG:CODD, and f) PHD2:Fe(II) + O_2 + 2OG + CODD → PHD2:Fe(II):2OG:CODD:O_2. The dotted grey lines are used to help differentiate shifts. The black, vertical separating line indicates the position where the region from 0 to 9 ppm of the spectrum was removed for simplicity. Standard concentrations of each component were: 100 μM unlabelled PHD2, 300 μM Fe(II), 500 μM 2OG, 500 μM CODD, <2 ppm O_2 pressure (anoxic), and room pressure O_2 (oxic). Buffer conditions were 135 mM NaCl, 10% D_2O, and 90% 50 mM Tris-d_{11} pH 7.5.

Next, this set of PHD2:Fe(II) complexes were observed in the presence of ascorbate (**Figure 2.51)**. If taken at early timepoints, as carried out for the **Figure 2.51** spectra, the oxic and anoxic PHD2:Fe(II):2OG complexes appear identical, though the typical peak shifts commonly observed for the oxic complex develop over time in the presence of oxygen when ascorbate is added. In contrast, the oxic and anoxic PHD2:Fe(II):2OG:CODD complexes are easily differentiable even at early timepoints, likely due to fast catalytic activity in the presence of ascorbate (**Figure 2.51** e-f), where catalytic activity has been associated with formation of the oxic complexes in the work described in this thesis.

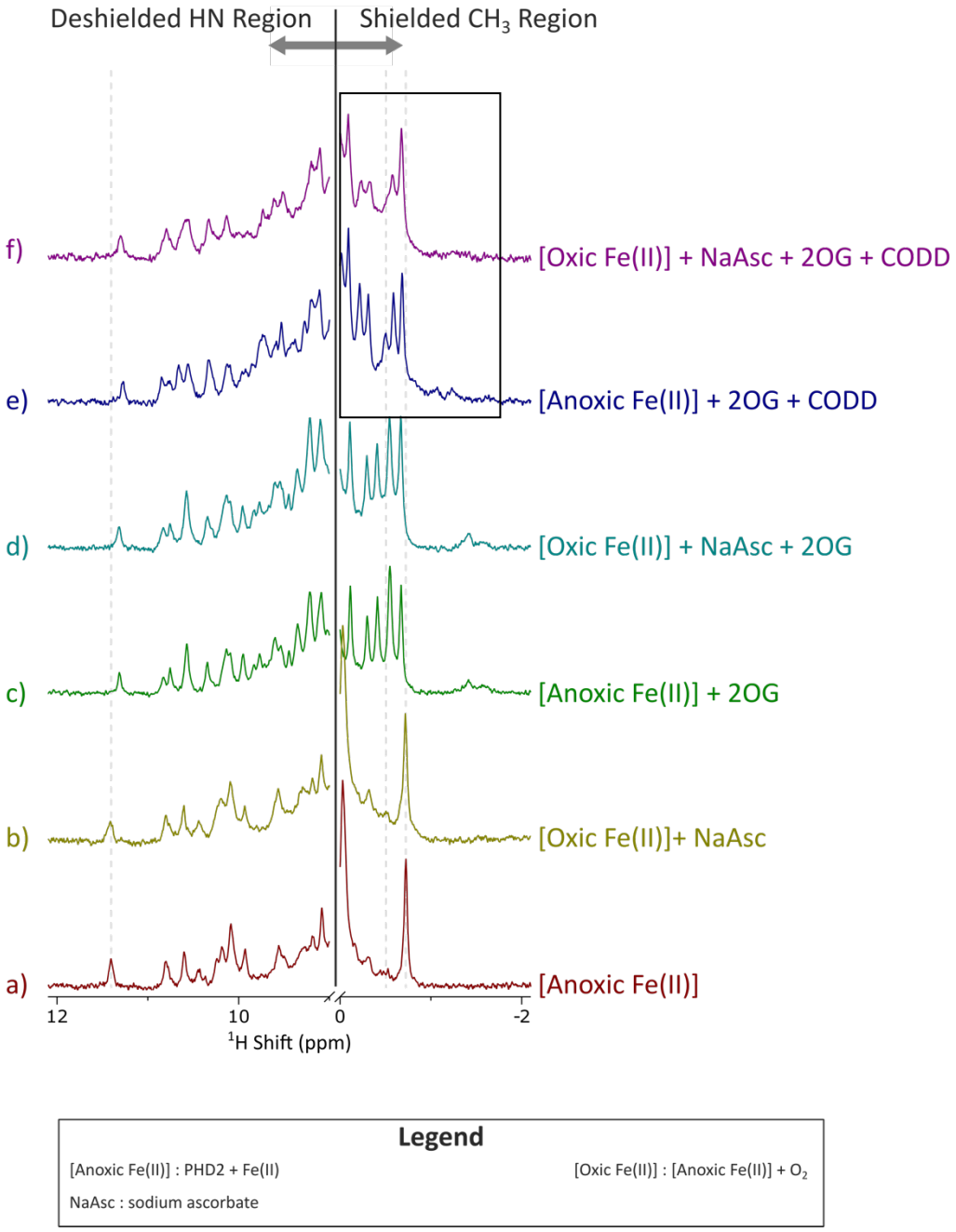


Figure 2.51 *^{1}H spectral comparison of oxic and anoxic conditions for various PHD2:Fe(II) +/- ascorbate complexes. The goal is to determine if ascorbate protects against the formation of the oxic complex. Only in the case of the PHD2:Fe(II):2OG:CODD complex (with ascorbate present) are changes in the ^{1}H spectrum observed on addition of O_2. This is likely due to fast turnover of 2OG; the PHD2:Fe(II):2OG complex spectra would likely show similar results at a later timepoint. The labels indicates the starting complex, whereas each component after a "+" is added to solution in the order written from left to right. The reaction components (separated by*

"+" signs) and proposed major complex formed are given as follows. a) PHD2:Fe(II), b) PHD2:Fe(II) + O_2, c) PHD2:Fe(II) + 2OG → PHD2:Fe(II):2OG, d) PHD2:Fe(II) + O_2 + 2OG → PHD2:Fe(II):2OG:O_2 (most likely complex), e) PHD2:Fe(II) + 2OG + CODD → PHD2:Fe(II):2OG:CODD, and f) PHD2:Fe(II) + O_2 + 2OG + CODD → PHD2:Fe(II):2OG:CODD:O_2. The dotted grey lines are used to help differentiate shifts. The black, vertical separating line indicates the position where the region from 0 to 9 ppm of the spectrum was removed for simplicity. Standard concentrations of each component were: 100 μM unlabelled PHD2, 300 μM Fe(II), 500 μM 2OG, 500 μM CODD, <2 ppm O_2 pressure (anoxic), and room pressure O_2 (oxic). Buffer conditions were 135 mM NaCl, 10% D_2O, and 90% 50 mM Tris-d_{11} pH 7.5.

The next complexes of interest to be studied were the PHD2:Zn(II) complexes in the presence and absence of oxygen, 2OG, and CODD. As expected, no differences between oxic and anoxic spectra were observed for any PHD2:Zn(II) complexes, as oxygen is not expected to bind Zn(II) (**Figure 2.52**). As observed in the Fe(II) complexes, binding of the oxic and anoxic PHD2:Zn(II):2OG complexes to CODD can be easily distinguished as a change in both the shielded methyl and deshielded H_N regions of the ^{1}H spectrum (**Figure 2.52**, c-f).

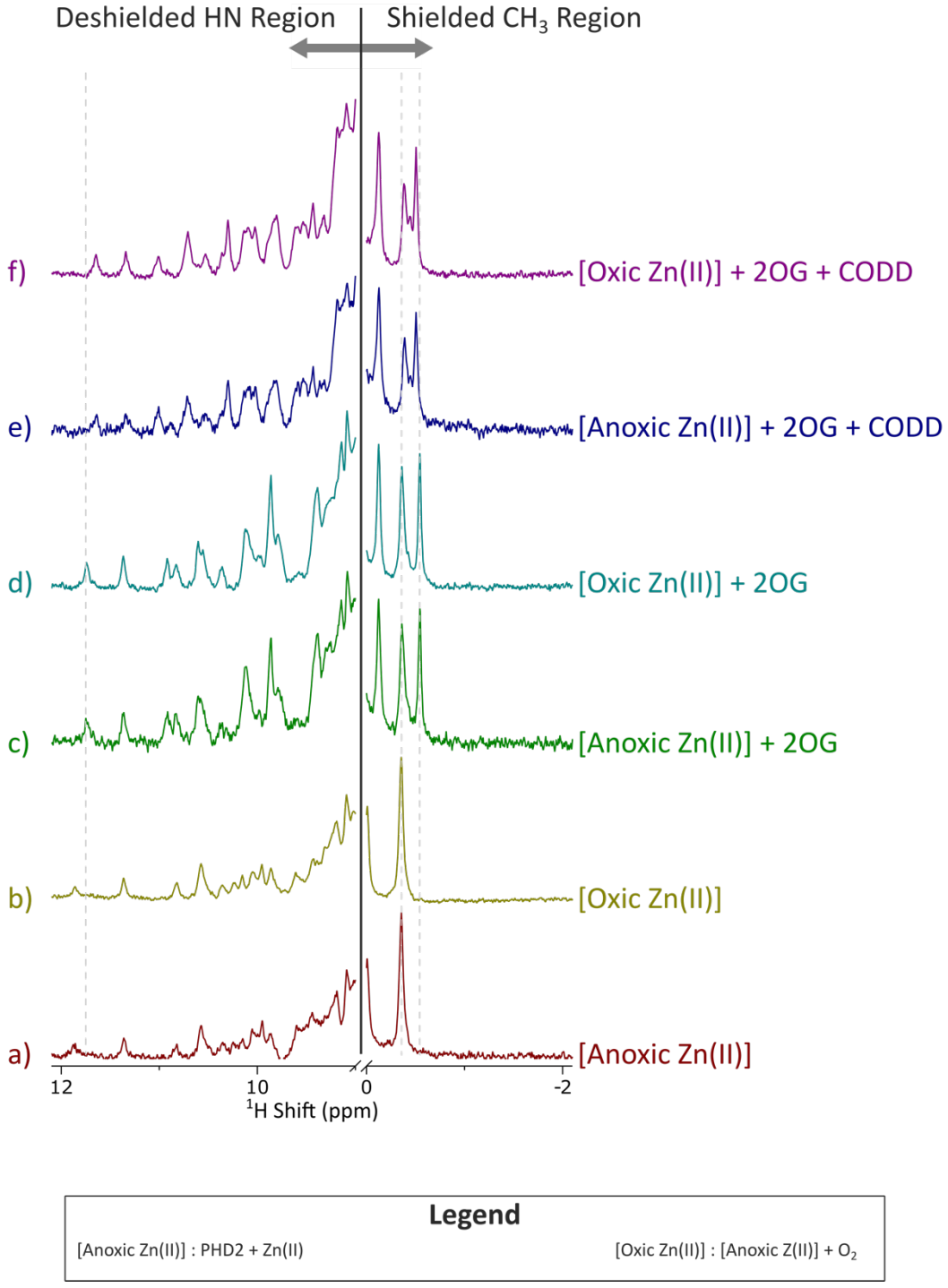


Figure 2.52 *^1H spectral comparison of oxic and anoxic conditions for various PHD2:Zn(II) complexes. Changes in the spectra were observed on 2OG and CODD addition but not observed on addition of O_2. The labels in the figure for each spectrum above indicates the starting complex, whereas each component after a "+" is added to solution in the order written from left to right. The reaction components (separated by "+" signs) and proposed major complex formed are given as follows. a) PHD2:Zn(II),*

b) PHD2:Zn(II) + O_2, c) PHD2:Zn(II) + 2OG → PHD2:Zn(II):2OG, d) PHD2:Zn(II) + O_2 + 2OG → PHD2:Zn(II):2OG + O_2, e) PHD2:Zn(II) + 2OG + CODD → PHD2:Zn(II):2OG:CODD, and f) PHD2:Zn(II) + O_2 + 2OG + CODD → PHD2:Zn(II):2OG:CODD + O_2. The dotted grey lines are used to help differentiate shifts. The black, vertical separating line indicates the position where the region from 0 to 9 ppm of the spectrum was removed for simplicity. Standard concentrations of each component were: 100 μM unlabelled PHD2, 300 μM Zn(II), 500 μM 2OG, 500 μM CODD, <2 ppm O_2 pressure (anoxic), and room pressure O_2 (oxic). Buffer conditions were 135 mM NaCl, 10% D_2O, and 90% 50 mM Tris-d_{11} pH 7.5.

Exploration of the various PHD2:Ni(II) complexes in the presence or absence of oxygen, 2OG, and CODD also revealed very few oxygen-dependent changes (**Figure 2.53**). As with the three previous cases, the PHD2:Ni(II) complex does appear to bind 2OG and CODD, but the observed changes in the ^{1}H spectrum on 2OG and CODD binding are minimal. This is interesting to consider in comparison to the oxic PHD2:Ni(II):2OG complex ^{1}H,^{15}N-HSQC spectrum discussed previously (**Figure 2.12**), which was found to give more sharp, uniform peaks than observed with any of the other metal complexes. No changes in the ^{1}H spectra of the PHD2:Ni(II) complexes are observed on O_2 addition.

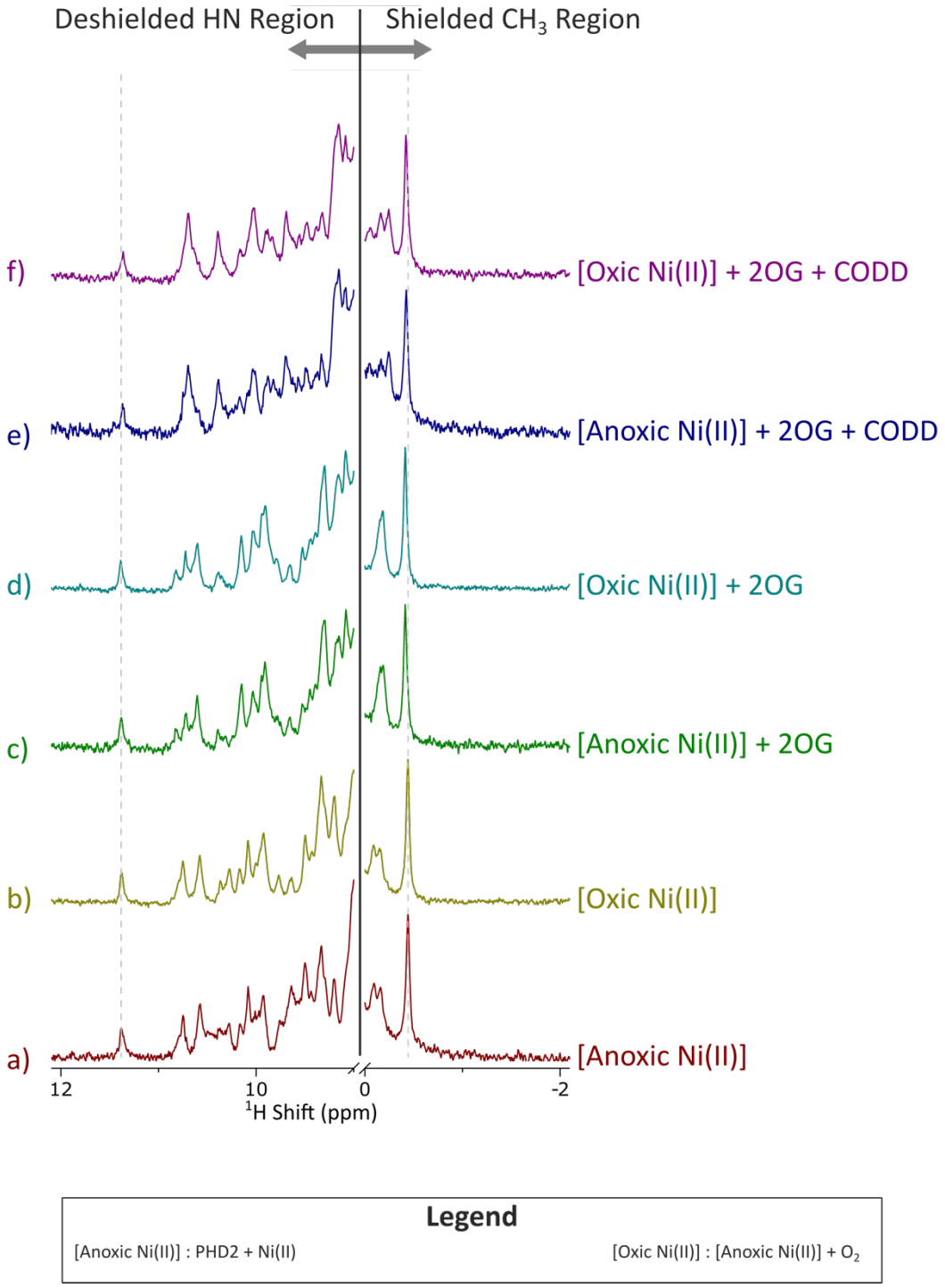


Figure 2.53 *^{1}H spectral comparison of oxic and anoxic conditions for various PHD2:Ni(II) complexes. Minor changes in the ^{1}H spectra of the PHD2:Ni(II) complexes are observed on addition of 2OG and CODD; No changes are observed on addition of O_2. The labels in the figure for each spectrum above indicates the starting complex, whereas each component after a "+" is added to solution in the order written from left to right. The reaction components (separated by "+" signs) and proposed major complex*

formed are given as follows. a) PHD2:Ni(II), b) PHD2:Ni(II) + O_2, c) PHD2:Ni(II) + 2OG → PHD2:Ni(II):2OG, d) PHD2:Ni(II) + O_2 + 2OG → PHD2:Ni(II):2OG + O_2, e) PHD2:Ni(II) + 2OG + CODD → PHD2:Ni(II):2OG:CODD, and f) PHD2:Ni(II) + O_2 + 2OG + CODD → PHD2:Zn(II):2OG:CODD + O_2. The dotted grey lines are used to help differentiate shifts. The black, vertical separating line indicates the position where the region from 0 to 9 ppm of the spectrum was removed for simplicity. Standard concentrations of each component were: 100 μM unlabelled PHD2, 300 μM Ni(II), 500 μM 2OG, 500 μM CODD, <2 ppm O_2 pressure (anoxic), and room pressure O_2 (oxic). Buffer conditions were 135 mM NaCl, 10% D_2O, and 90% 50 mM Tris-d_{11} pH 7.5.

The last metal complex of interest studied was the PHD2:Co(II) complex in the presence and absence of oxygen, 2OG, and CODD. Co(II)-substituted Fe(II)-dependent metalloproteins with oxygen artificially ligated to the active site metal in molecular dynamics simulations have suggested unique Co-O-O binding characteristics relative to Fe-O-O binding and was of substantial interest. [65] Yet, as with the other non-catalytic metal ions explored, there was no difference between the oxic and anoxic ^{1}H spectra under any of the observed conditions (**Figure 2.54**).

The observation that the relatively poor quality PHD2:Co(II) spectra were improved by the presence of 2OG (**Figure 2.54** a-d) may indicate that Co(II) is not a strong *apo*-PHD2 binder in the absence of 2OG, a property of note when considering the role of Co(II) as a PHD2 inhibitor.

Addition of CODD to the PHD2:Co(II):2OG complex gives a distinct set of peaks which indicates that CODD is binding (**Figure 2.54** c-f). The CODD complex is interesting as it shows indications of greater paramagnetic effects than the PHD2:Co(II):2OG complex alone, as evidenced by the observed peaks across a larger spectral range. This may indicate that the addition of CODD locks the active site into a more stable conformation, since paramagnetic metals exhibit greater paramagnetic

effects when more tightly bound (due less averaging of the paramagnetic interactions with protein residues).

The unique stability characteristics of PHD2:Co(II) complexes should be further explored to understand how these interesting traits may relate to the Co(II)-mediated inhibition of PHD activity in vivo.

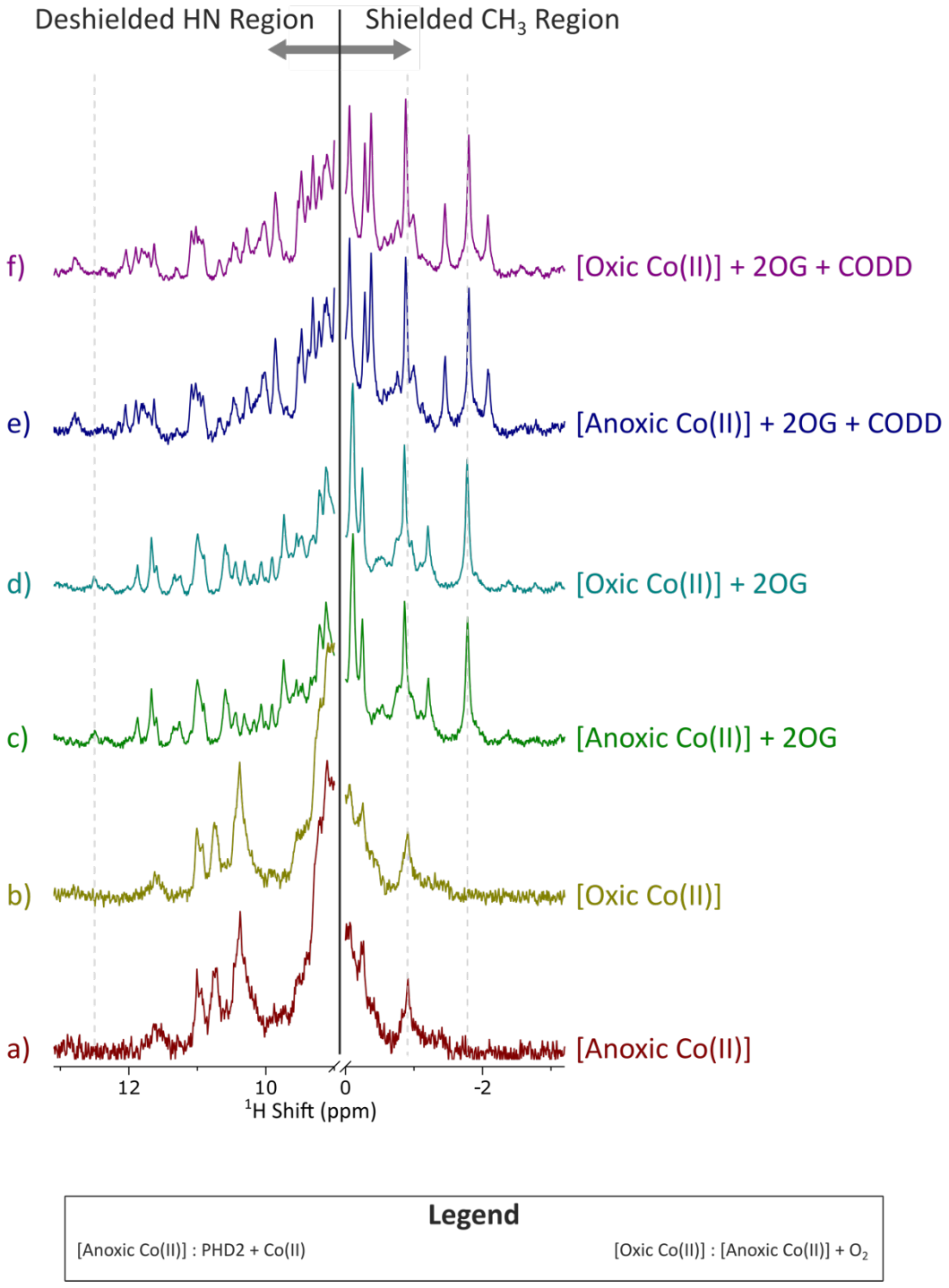


Figure 2.54 *^1H spectral comparison of oxic and anoxic conditions for various PHD2:Co(II) complexes. Additions of 2OG and CODD to the PHD2:Co(II) complex cause paramagnetic shifts and sharpening of the ^1H NMR spectra. No evidence of changes in the spectra are observed on addition of O_2. The labels in the figure for each spectrum above indicates the starting complex, whereas each component after a "+" is added to solution in the order written from left to right. The reaction components*

(separated by "+" signs) and proposed major complex formed are given as follows. a) PHD2:Co(II), b) PHD2:Co(II) + O_2, c) PHD2:Zn(II) + 2OG → PHD2:Co(II):2OG, d) PHD2:Co(II) + O_2 + 2OG → PHD2:Co(II):2OG + O_2, e) PHD2:Co(II) + 2OG + CODD → PHD2:Co(II):2OG:CODD, and f) PHD2:Co(II) + O_2 + 2OG + CODD → PHD2:Co(II):2OG:CODD + O_2. The dotted grey lines are used to help differentiate shifts. The black, vertical separating line indicates the position where the region from 0 to 9 ppm of the spectrum was removed for simplicity. Standard concentrations of each component were: 100 μM unlabelled PHD2, 300 μM Co(II), 500 μM 2OG, 500 μM CODD, <2 ppm O_2 pressure (anoxic), and room pressure O_2 (oxic). Buffer conditions were 135 mM NaCl, 10% D_2O, and 90% 50 mM Tris-d_{11} pH 7.5.

2.2.3.2.2 Studies on the Competition Between Co(II) and Zn(II) for PHD2 Binding

Due to the unique properties observed in the PHD2:Co(II):2OG complexes and inhibition of PHD2 by Co(II) in the literature, the interactions between PHD2 complexes and Co(II) were explored further. The goal of these experiments was to see if Co(II) could displace Zn(II) in the PHD2:Zn(II):2OG complexes and if, conversely, Zn(II) could displace Co(II) in the PHD2:Co(II):2OG complexes. Zn(II) rather than Fe(II) was used in these studies in order to rule out paramagnetic effects from the control metal (Zn(II) in this case). Further studies involving competition between Co(II) and Fe(II) would be useful.

Comparison of the oxic PHD2:Zn(II):2OG and oxic PHD2:Co(II):2OG spectra showed substantial differences in the chemical shifts of the two complexes (**Figure 2.55**), which was ideal for differentiating the complexes in this study.

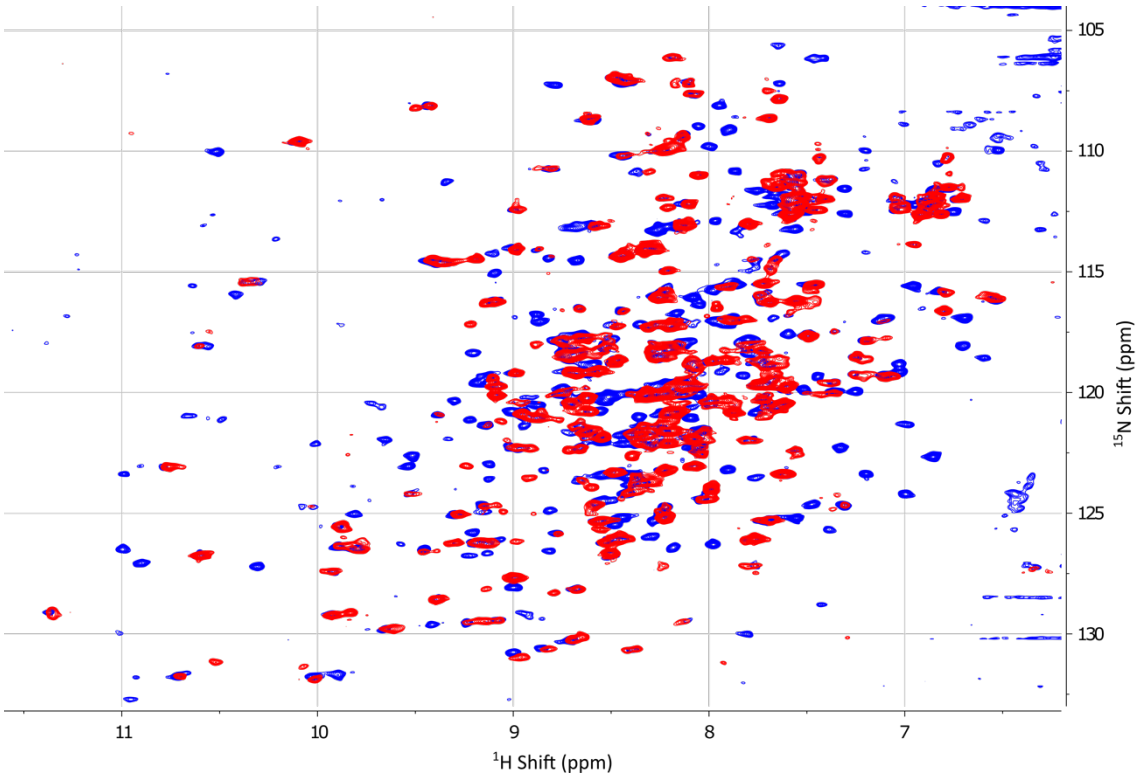


Figure 2.55 *Comparison of the $^{1}H,^{15}N$-HSQC spectra of PHD2:Co(II):2OG (blue) and PHD2:Zn(II):2OG (red). Large shift differences are observed in the PHD2:Co(II):2OG vs the PHD2:Zn(II):2OG complex spectra. Standard concentrations of each component were: 100 μM unlabelled PHD2, 150 μM Co(II) or Zn(II), 200 μM 2OG, and room pressure O_2. Buffer conditions were 10% D_2O, and 90% 50 mM Tris-d_{11} pH 6.5.*

Stepwise addition of increasing Co(II) concentrations to the PHD2:Zn(II):2OG complex showed little to no change in the $^{1}H,^{15}N$-HSQC spectrum (**Figure 2.56**). This result indicates that the PHD2:Zn(II):2OG complex is resistant to Co(II) binding, even at high Co(II) concentrations.

As observed with studies on PHD2:Co(II) complexes in the presence and absence of 2OG and CODD (**Figure 2.54**), Co(II) in solution may not be a strong enough binder to *apo*-PHD2 to displace a metal:2OG complex from the PHD2 active site, as PHD2:Co(II) complexes have been shown to require 2OG or 2OG:CODD binding for stability. It is unknown if this property translates to the PHD2:Fe(II):2OG complex.

Nonetheless, these results highlight the role of 2OG in stabilising PHD2:metal ion complexes, especially in the case of Co(II).

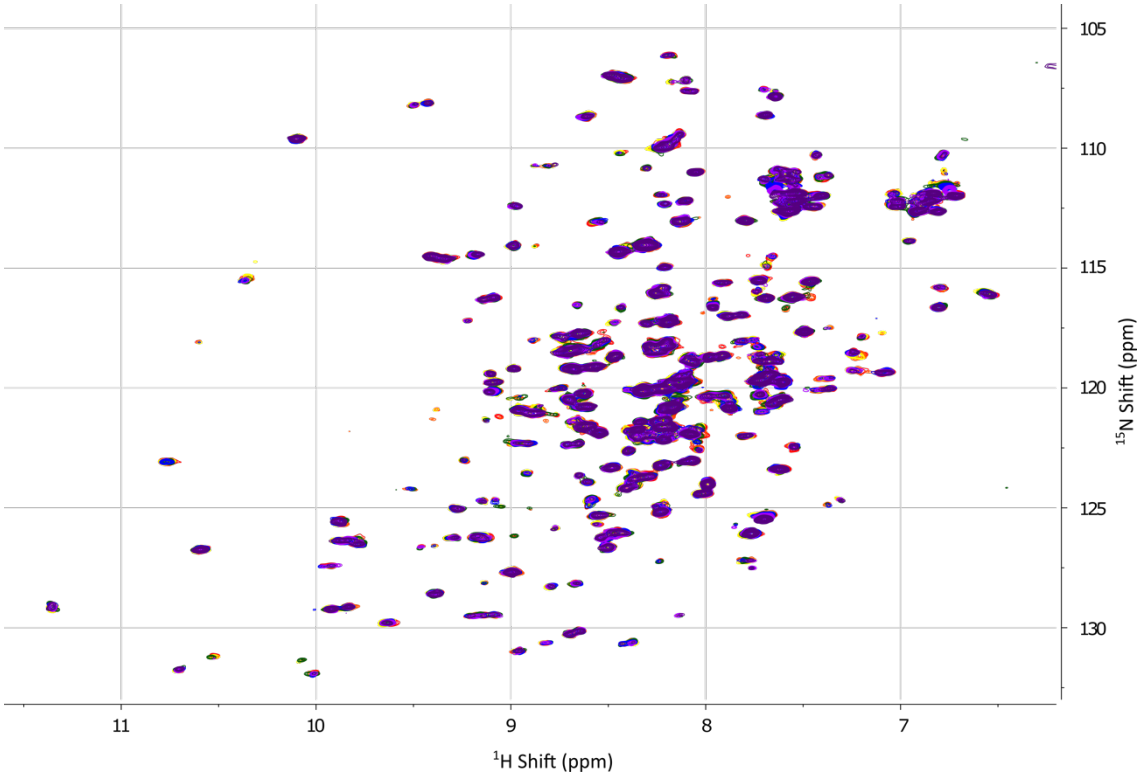


Figure 2.56 *^{1}H,^{15}N-HSQC spectrum of PHD2:Zn(II):2OG during stepwise Co(II) addition. From these studies, it was observed that Co(II) addition to a PHD2:Zn(II):2OG complex does not lead to displacement of Zn(II) and does not lead to any substantial changes in the spectrum. Standard concentrations of each component were: 100 µM unlabelled PHD2, 150 µM Zn(II), 200 µM 2OG, and room pressure O_2. The Zn(II):Co(II) ratio in each sample was 1:0 (red), 1:1/3 (yellow), 1:2/3 (green), 1:4/3 (blue), and 1:8/3 (purple) respectively. Buffer conditions were 10% D_2O, and 90% 50 mM Tris-d_{11} pH 6.5.*

Comparison of the PHD2:Zn(II):2OG spectrum before and after addition of > 2 equivalents of Co(II) showed no substantial Zn(II) displacement (**Figure 2.57),** as described above. Some peak shifts and broadening are observed.

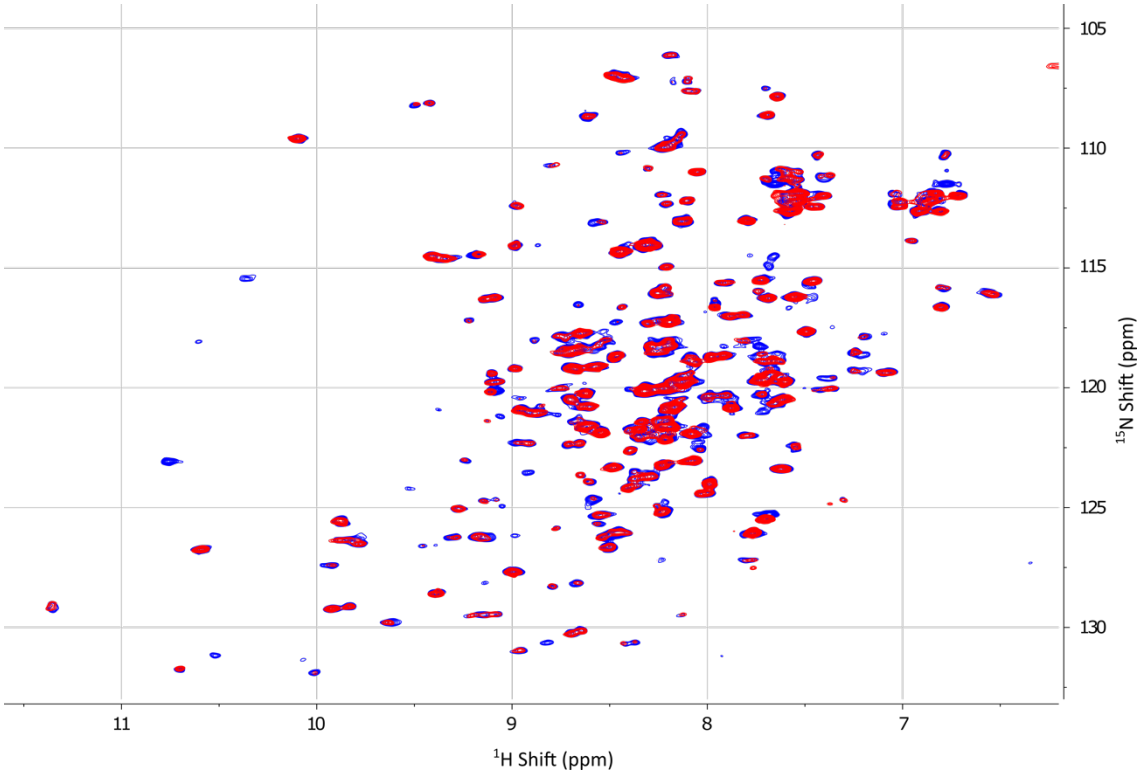


Figure 2.57 *^{1}H,^{15}N-HSQC spectra of PHD2:Zn(II):2OG before (blue) and after (red) excess Co(II) addition. Standard concentrations of each component were: 100 µM unlabelled PHD2, 150 µM Zn(II), 200 µM 2OG, and room pressure O_2. The Zn(II):Co(II) ratio in each sample was 1:0 (blue) and 1:8/3 (red) respectively. Buffer conditions were 10% D_2O, and 90% 50 mM Tris-d_{11} pH 6.5.*

When Zn(II) was added to the PHD2:Co(II):2OG complex, substantial changes in the ^{1}H,^{15}N-HSQC spectrum were observed (**Figure 2.58**). Loss of Co(II) complex peaks was observed, but interestingly the resultant ^{1}H,^{15}N-HSQC spectrum was not identical to the PHD2:Zn(II):2OG complex spectrum. This may indicate that Co(II) was only partially displaced or that there is an allosteric position on PHD2 where Co(II) binds. Like the anoxic PHD2:Fe(II):2OG complex, the oxic PHD2:Co(II):2OG complex appears to have two sets of peaks. Addition of Zn(II) to the PHD2:Co(II):2OG complex caused changes in the ^{1}H,^{15}N-HSQC spectrum that led to the loss of this second set of peaks. This observation may be of interest for gaining a better understanding of the origin

of these additional PHD2 peaks. It should be noted that the full PHD2:Co(II):2OG complex is maintained with up to 1/3 equivalent of Zn(II) in solution.

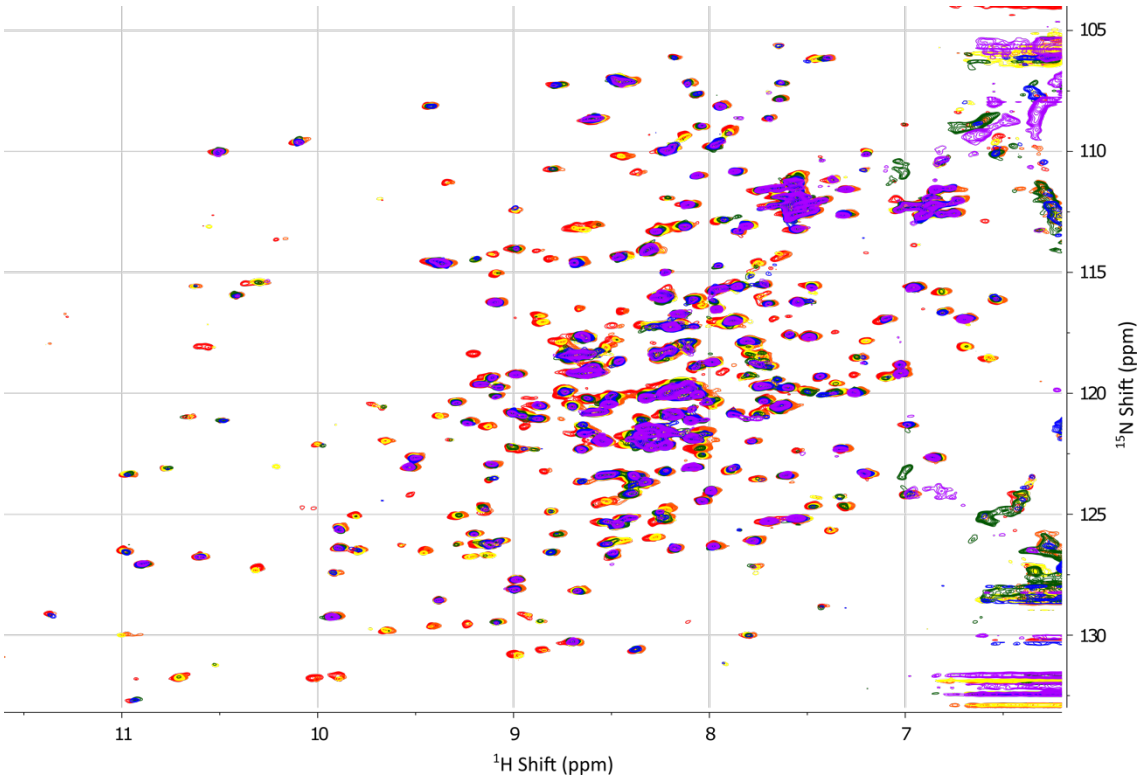


Figure 2.58 *^{1}H,^{15}N-HSQC spectra of PHD2:Co(II):2OG during stepwise Zn(II) addition. Standard concentrations of each component were: 100 µM unlabelled PHD2, 150 µM Co(II), 200 µM 2OG, and room pressure O_2. The Co(II):Zn(II) was 1:0 (red), 1:1/3 (yellow), 1:2/3 (green), 1:4/3 (blue), and 1:8/3 (purple) respectively. From these studies, it was observed that Zn(II) addition to a PHD2:Co(II):2OG complex led to the loss of one set of the PHD2:Co(II):2OG complex ^{1}H,^{15}N-HSQC spectral peaks. Buffer conditions were 10% D_2O, and 90% 50 mM Tris-d_{11} pH 6.5.*

Comparison of the PHD2:Co(II):2OG spectrum before and after addition of > 2 equivalents of Zn(II) showed substantial changes in the spectrum. As can be shown in **Figure 2.59**, some shift differences were observed, but the most prominent change was the loss of peaks.

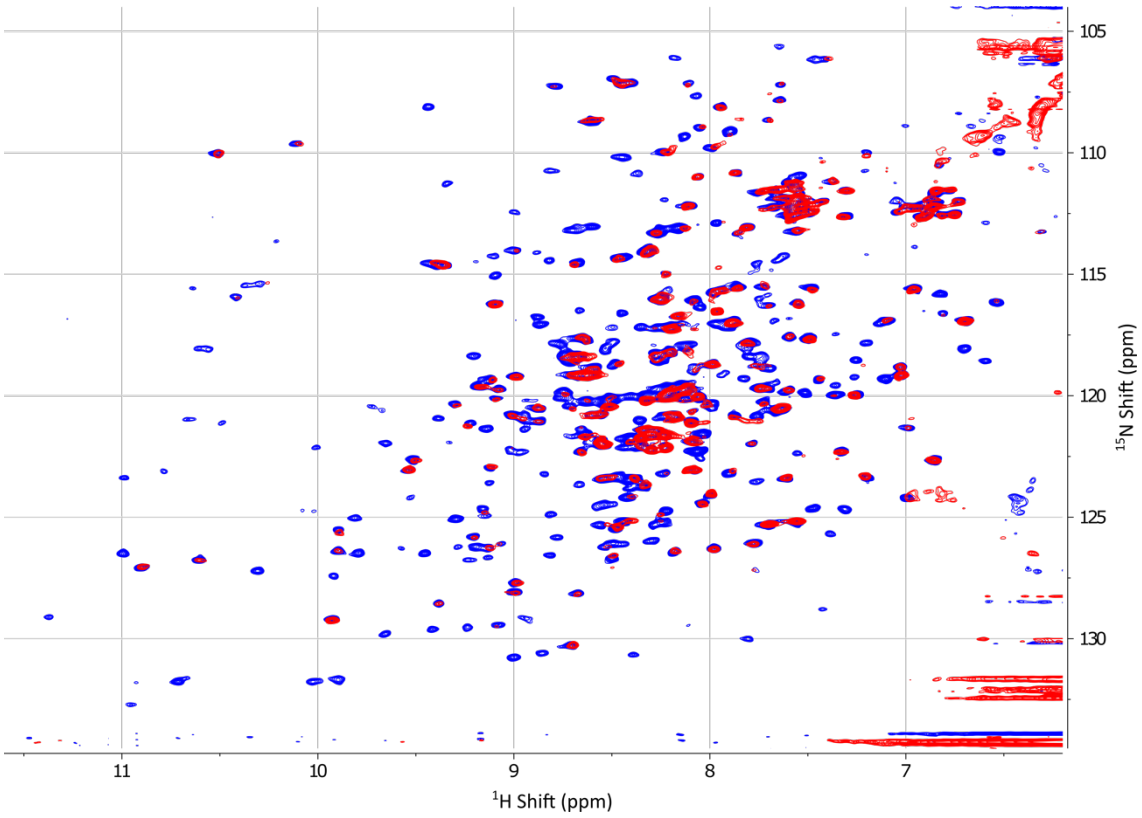


Figure 2.59 *$^{1}H,^{15}N$-HSQC spectra of PHD2:Co(II):2OG before (blue) and after (red) excess Zn(II) addition. Standard concentrations of each component were: 100 µM unlabelled PHD2, 150 µM Co(II), 200 µM 2OG, and room pressure O_2. The Co(II):Zn(II) ratio in each sample was 1:0 (blue) and 1:8/3 (red) respectively. Buffer conditions were 10% D_2O, and 90% 50 mM Tris-d_{11} pH 6.5.*

These studies show that Co(II) is incapable of (efficiently) displacing Zn(II) from the PHD2:Zn(II):2OG complex, but Zn(II) may partially displace Co(II) from the PHD2:Co(II):2OG complex. Further exploration into the PHD2:Co(II):2OG complex and the effects of Co(II) on other PHD2 complexes (including the oxic and anoxic PHD2:Fe(II):2OG complexes) is of interest.

2.2.3.2.3 Vanadium Oxide Binding Studies

Formation of the PHD2:Fe(II):2OG:O_2 complex is valuable for understanding the oxygen sensing mechanism of PHD2 but is exceptionally difficult to lock in a steady state due to uncoupled turnover. Nitric oxide has been used as an oxygen mimic for PHD2, but without success due to the inability of nitric oxide to bind concurrently with 2OG (**Figure**

2.28). Therefore, in order to further probe a catalytic-like complex of PHD2 without turnover, vanadium oxide studies were explored. Vanadium oxide is a proposed surrogate for oxygen binding as it takes the place of both metal and oxygen in the active site, mimicking the proposed Fe=O intermediate. When vanadium oxide was added to PHD2, it appeared to form a new complex, likely a PHD2:V(IV)O complex (**Figure 2.60** blue). Addition of 2OG to this complex caused shifts in the ^{1}H,^{15}N-HSQC spectrum peaks (**Figure 2.60**), indicating 2OG binding.

It is interesting to note that the complex formed after 2OG binding to the PHD2:V(IV)O complex appears similar, but not identical, to the oxic PHD2:Fe(II):2OG complex. It would be interesting to find a metal ion surrogate that does not have an attached oxygen atom to see if a complex reminiscent of the anoxic PHD2:Fe(II):2OG complex could be formed.

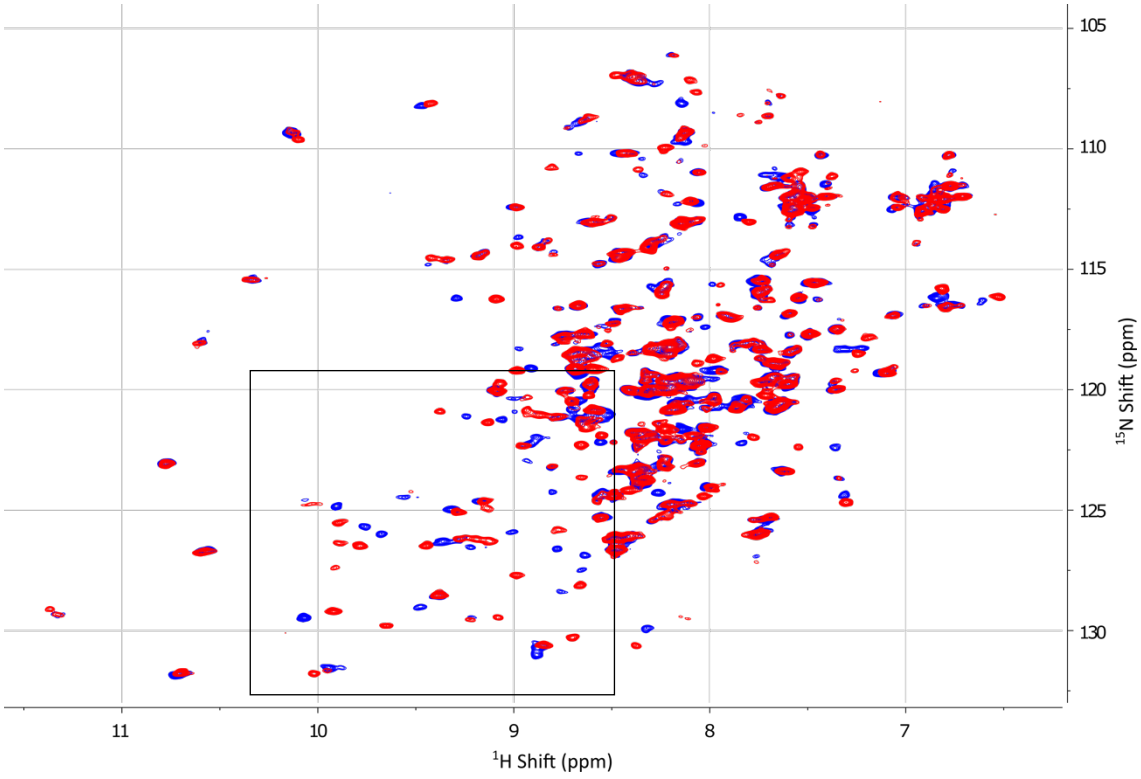


Figure 2.60 *^{1}H,^{15}N-HSQC spectra of anoxic PHD2:V(IV)O before (blue) and after (red) 2OG addition. The majority of peaks were not perturbed by 2OG addition, whereas peaks*

in the region characteristic of the protein fold (~9-10 ppm, indicated in the black box) exhibited larger peak shifts, likely reflecting 2OG binding. Standard concentrations of each component were: 100 µM unlabelled PHD2, 200 µM V(IV)O, 400 µM 2OG, and <2 ppm O_2 pressure. Buffer conditions were 10% D_2O, and 90% 50 mM Tris-d_{11} pH 6.5.

The same experiment was performed in the presence of succinate rather than 2OG; on addition of succinate to the PHD2:V(IV)O complex, less prevalent changes in the $^{1}H,^{15}N$-HSQC spectrum were observed (**Figure 2.61**). This is likely due to the weak binding affinity of succinate to PHD2 complexes.

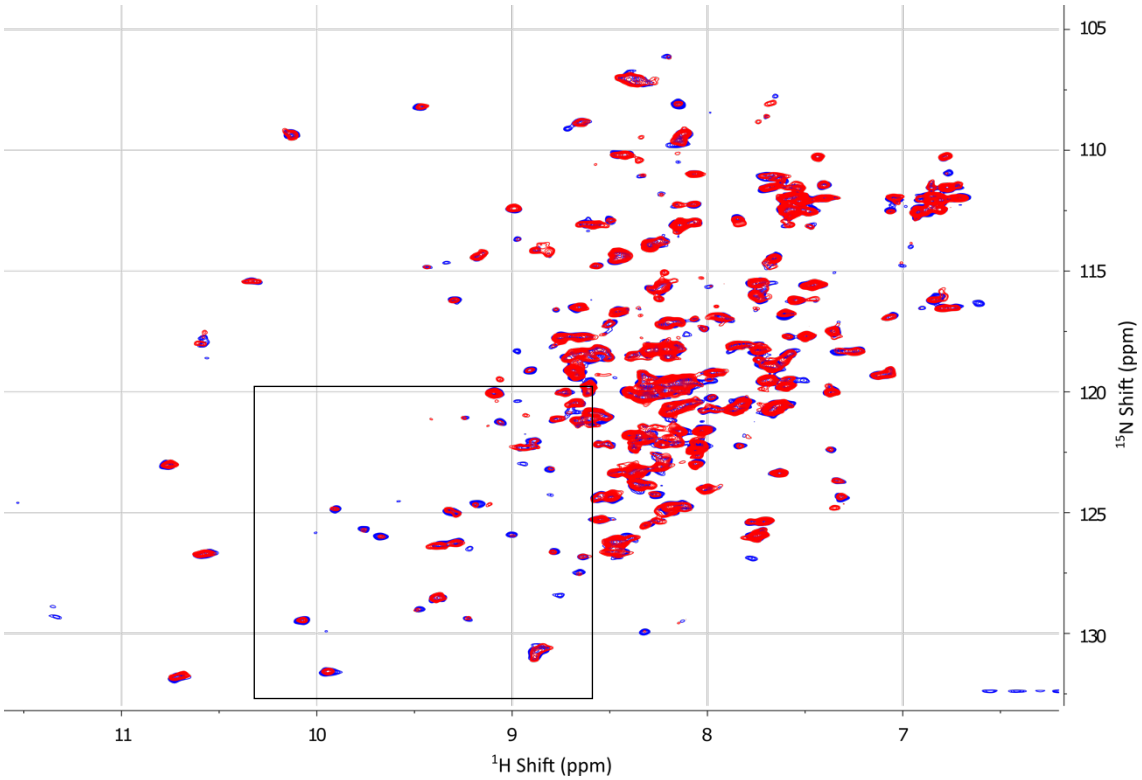


Figure 2.61 *$^{1}H,^{15}N$-HSQC spectra of anoxic PHD2:V(IV)O before (blue) and after (red) succinate addition. The majority of peaks were not perturbed by succinate addition. Peaks in the ~9-10 ppm region of the spectrum were slightly broadened (as shown within the black box). Standard concentrations of each component were: 100 µM unlabelled PHD2, 200 µM V(IV)O, 1 mM succinate, and <2 ppm O_2 pressure. Buffer conditions were 10% D_2O, and 90% 50 mM Tris-d_{11} pH 6.5.*

These results indicate that vanadium oxide may be a partial mimic of the Fe:O complexes at the active site of PHD2 and should be explored further both in PHD2 and

in ligand/substrate solutions. It may also be valuable to observe the crystal structure of the vanadium complex to see where the vanadium-bound oxygen atom is oriented in the PHD2 active site to determine if this matches with the position that oxygen is thought to bind.

2.2.4 PHD2: Oxic and Anoxic Complex Stabilities

$^{1}H,^{15}N$-HSQC studies revealed clear differences between the oxic and anoxic PHD2:Fe(II):2OG complexes. To further probe these differences, with the additional goal of helping to elucidate the components of the oxic complex, competition studies were carried out between each complex of interest and an inhibitor. The stabilities of the complexes in the following sections will be determined by resistance of the analyte complex of interest (PHD2:Metal ± Cofactor ± Substrate ± Inhibitor) to displacement/replacement by other complexes.

The inhibitors chosen were FG-4592 (**Figure 2.62**), a clinically approved PHD2 inhibitor, and N-oxalyl glycine (NOG, **Figure 2.63**), which is a good mimic of 2OG and a weaker binder. Both inhibitors have been evaluated for PHD2 binding previously. [66]

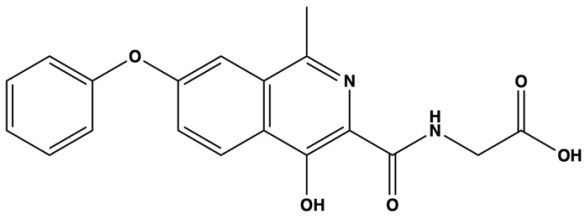


Figure 2.62 *Structure of FG-4592. A strong inhibitor of PHD2.*

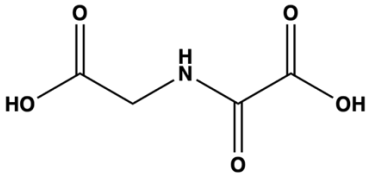


Figure 2.63 *Structure of N-oxalylglycine (NOG). An inhibitor of PHD2 and a closer mimic of 2OG than FG-4592.*

Comparison of the oxic/anoxic PHD2:Fe(II) spectra with oxic/anoxic PHD2:Fe(II):2OG, PHD2:Fe(II):NOG, and PHD2:Fe(II):FG-4592 spectra reveal clear differences in the shielded methyl and the deshielded H_N regions. These results suggest that acquisition of ^1H spectra could be a feasible method of distinguishing between different protein:metal:inhibitor:ligand complexes. ^1H analysis was a preferred method due to the time and quantity of material required for such studies compared to more complex NMR analyses. On addition of O_2 to the PHD2:Fe(II), PHD2:Fe(II):NOG, and PHD2:Fe(II):FG-4592 complexes, there are no substantial changes in the ^1H spectra (**Figure 2.64)**.

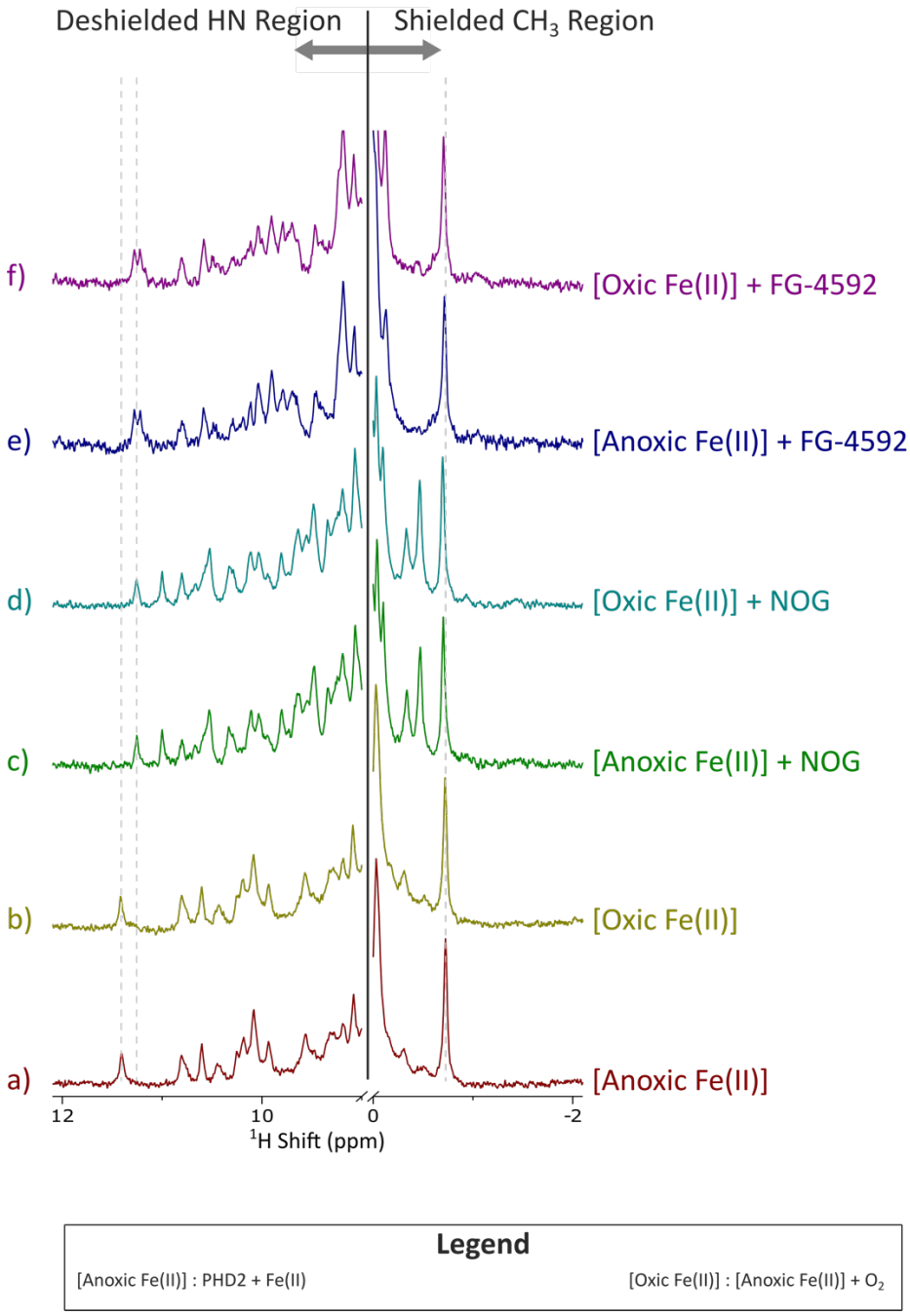


Figure 2.64 *Comparison of oxic/anoxic PHD2:Fe(II) ^{1}H spectra with oxic/anoxic PHD2:Fe(II):NOG and PHD2:Fe(II):FG-4592 inhibitor spectra. The labels for each spectrum in the figure above indicate the starting complex, whereas each component after a "+" is added to solution in the order written from left to right. The dotted grey lines are used to help differentiate shifts. The black, vertical separating line indicates the region from 0 to 9 ppm of the spectrum which was removed for clarity. The standard concentration of each component was 100 μM unlabelled PHD2, 300 μM Fe(II), 500 μM*

NOG, 500 μM FG-4592, <2 ppm O_2 pressure (anoxic), and room pressure O_2 (oxic). Buffer conditions were 135 mM NaCl, 10% D_2O, and 90% 50 mM Tris-d_{11} pH 7.5.

These spectra will be used as controls in the study of PHD2 inhibitor complexes. It should be noted that the simplicity of the shielded methyl region of the PHD2:Fe(II):FG-4592 complexes may aid in NMR analysis, in comparison to the complicated shielded methyl region of the PHD2:Fe(II):NOG complexes. Both inhibitors appear to bind to the PHD2:Fe(II) complex.

2.2.4.1 Studies on the Stabilities of PHD2:Fe(II):Inhibitor Complexes

Initial studies were carried out to determine if FG-4592 or NOG would be the preferred inhibitor for further studies. This was investigated by studying which inhibitor: 1) gave characteristic peaks that are at different chemical shifts than the peaks of the PHD2:Fe(II) and PHD2:Fe(II):2OG complexes, 2) exhibited sufficient inhibition to enable the analysis of relative PHD2 complex strengths (isn't too strong or too weak of an inhibitor), and 3) is sufficiently stable in solution so that solubility is not a factor. Four samples were used in these initial studies, consisting of the two possible ligand complexes (PHD2:metal:ligand +/- O_2) and two possible inhibitor complexes (PHD2:metal:inhibitor +/- O_2). A general scheme for these experiments is shown below in **Figure 2.65** (in the absence of substrate) and in **Figure 2.79** (in the presence of substrate).

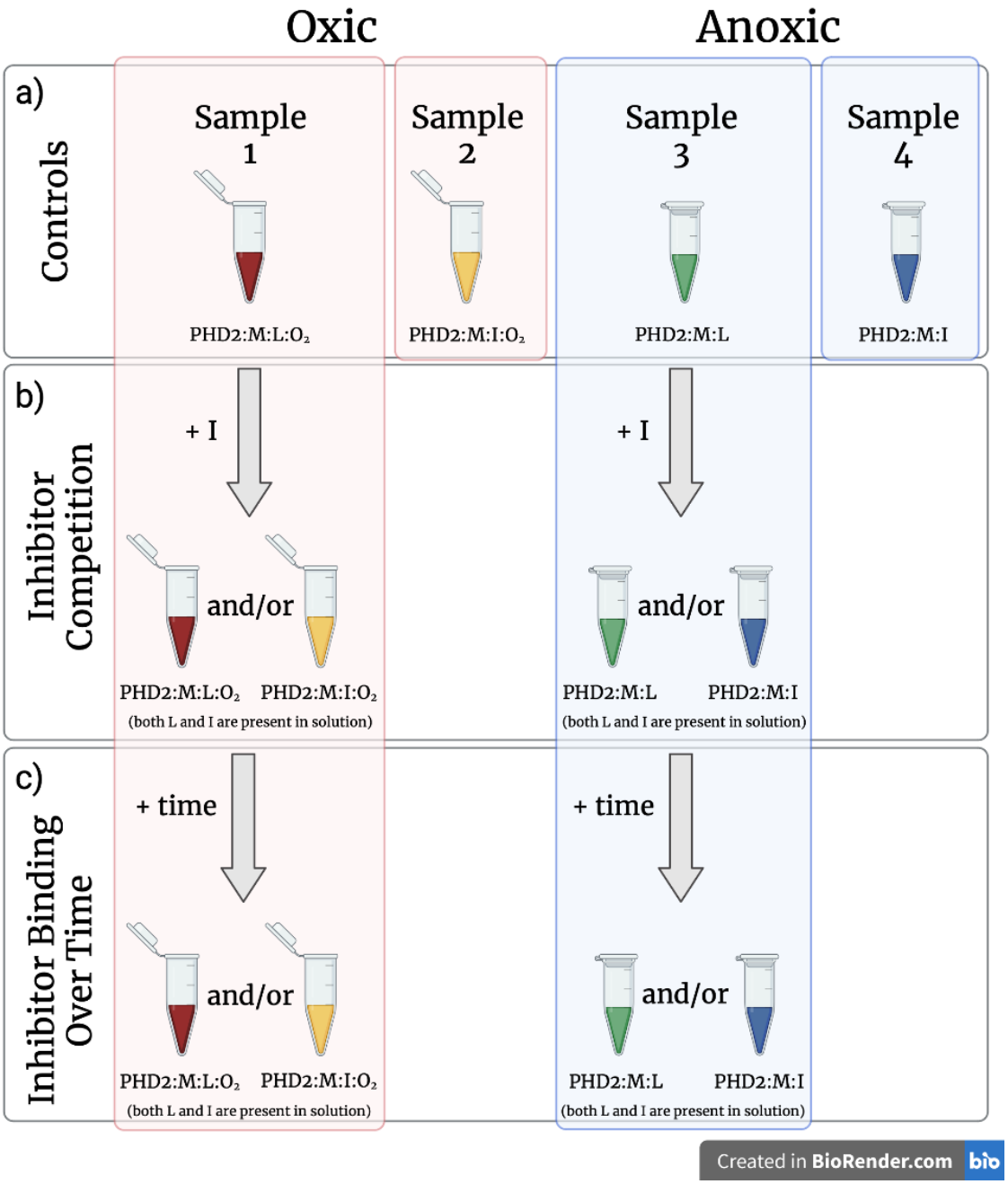


Figure 2.65 *General scheme for ^{1}H NMR oxic/anoxic PHD2 complex stability studies. M denotes metal, L denotes ligand, and I denotes inhibitor. Components connected by a colon ":" form a complex. The left side of the figure, enclosed in pink, shows experiments carried out under oxic conditions (room pressure oxygen concentration) and the right side of the figure, enclosed in blue, are experiments carried out under anoxic conditions (<2 ppm oxygen concentrations). a) The four starting samples used as controls: oxic/anoxic PHD2:M:L (+/- O_2) and oxic/anoxic PHD2:M:I (+/- O_2). b) Inhibitor (I) was added to the oxic/anoxic ligand (L) complexes and the level of incorporation of the inhibitor into the PHD2:M:C complexes was observed. The relative inhibitor*

incorporation as a function of 2OG ligand displacement was measured as a change in characteristic ^{1}H peak intensities for each complex. In the figure above, it is illustrated as a mixture of PHD2:M:L and PHD2:M:I complexes (which each vary in the relative concentration from 0 to 100% of the mixture). c) The sample was left overnight (~15 hours) to determine if the preferred complex (either ligand or inhibitor complex) would change over time. Again, this is illustrated as a mixture of PHD2:M:L and PHD2:M:I complexes. The figure was created using Biorender.com.

Initial studies were carried out to investigate the effect of inhibitors on the oxic/anoxic PHD2:Fe(II):2OG complexes. It was thought that the oxic and anoxic complexes may have different properties, considering the substantial ^{1}H,^{15}N-HSQC spectral differences between them. Initial studies were carried out with an Fe(II) solution prepared in Milli-Q H_2O, but this was changed to 20 mM HCl in Milli-Q H_2O due to the appearance of evidence for oxidised metal (PHD2:Fe(III)) in the oxic spectra. This was considered to be of interest in the future, but limiting non-catalytic Fe(III) formation in initial studies was desired. The concentrations of each component in these studies were chosen to match the standard conditions used in oxic/anoxic ^{1}H,^{15}N-HSQC spectra studies (100 μM PHD2, 300 μM metal, 500 μM ligand, 500 μM substrate (when used), and 500 μM inhibitor), where ligand and inhibitor concentrations could be varied to ensure ligand binding in the initial complex and inhibitor binding at levels conducive to determining PHD2:metal:ligand complex stability and resistance to displacement (as described previously).

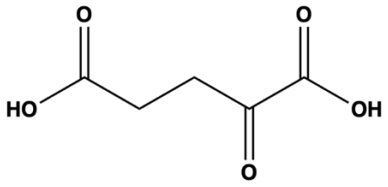


Figure 2.66 *2-Oxoglutarate (2OG), the natural cosubstrate of PHD2.*

Starting with FG-4592 and the PHD2:Fe(II):2OG complex, it was observed that the ^{1}H peaks of the PHD2:Fe(II):FG-4592 complex could be easily distinguished from the PHD2:Fe(II):2OG peaks, both under oxic and anoxic conditions (**Figure 2.67** a-d). On addition of FG-4592 to the oxic/anoxic PHD2:Fe(II):2OG complexes (**Figure 2.67** e-f), FG-4592 binding (and, therefore, displacement of 2OG binding) did not occur to the same extent on the oxic complex as it did the anoxic complex. This was an interesting result. The oxic PHD2:Fe(II):2OG complex showed substantial stability against FG-4592 treatment (though minor formation of the PHD2:Fe(II):FG-4592 complex was observed), whereas the anoxic PHD2:Fe(II):2OG complex manifested complete displacement by FG-4592 (no evidence of the PHD2:Fe(II):2OG complex was observed). This observation seems to indicate that the oxic PHD2:Fe(II):2OG complex is more resistant than the anoxic complex to inhibitor binding. This was an important result because it could indicate the formation of an oxygen-derived PHD2 complex (that may or may not be related to the catalytic cycle) that is stable against perturbation. Such a complex may slow down the catalytic mechanism of PHD2 under oxic conditions (see below).

After the samples were left for ~15 hours at room temperature (**Figure 2.67** g-h), low levels of displacement of the oxic PHD2:Fe(II):2OG complex by FG-4592 was observed over time, whereas no displacement of the anoxic PHD2:Fe(II):FG-4592 complex (which had previously been the anoxic PHD2:Fe(II):2OG complex before displacement by FG-4592) by 2OG was observed.

These observations seem to indicate that titration of FG-4592 (at equimolar concentrations to 2OG) into a PHD2:metal:ligand complex would provide a useful tool for probing the stability of PHD2:metal:ligand complexes.

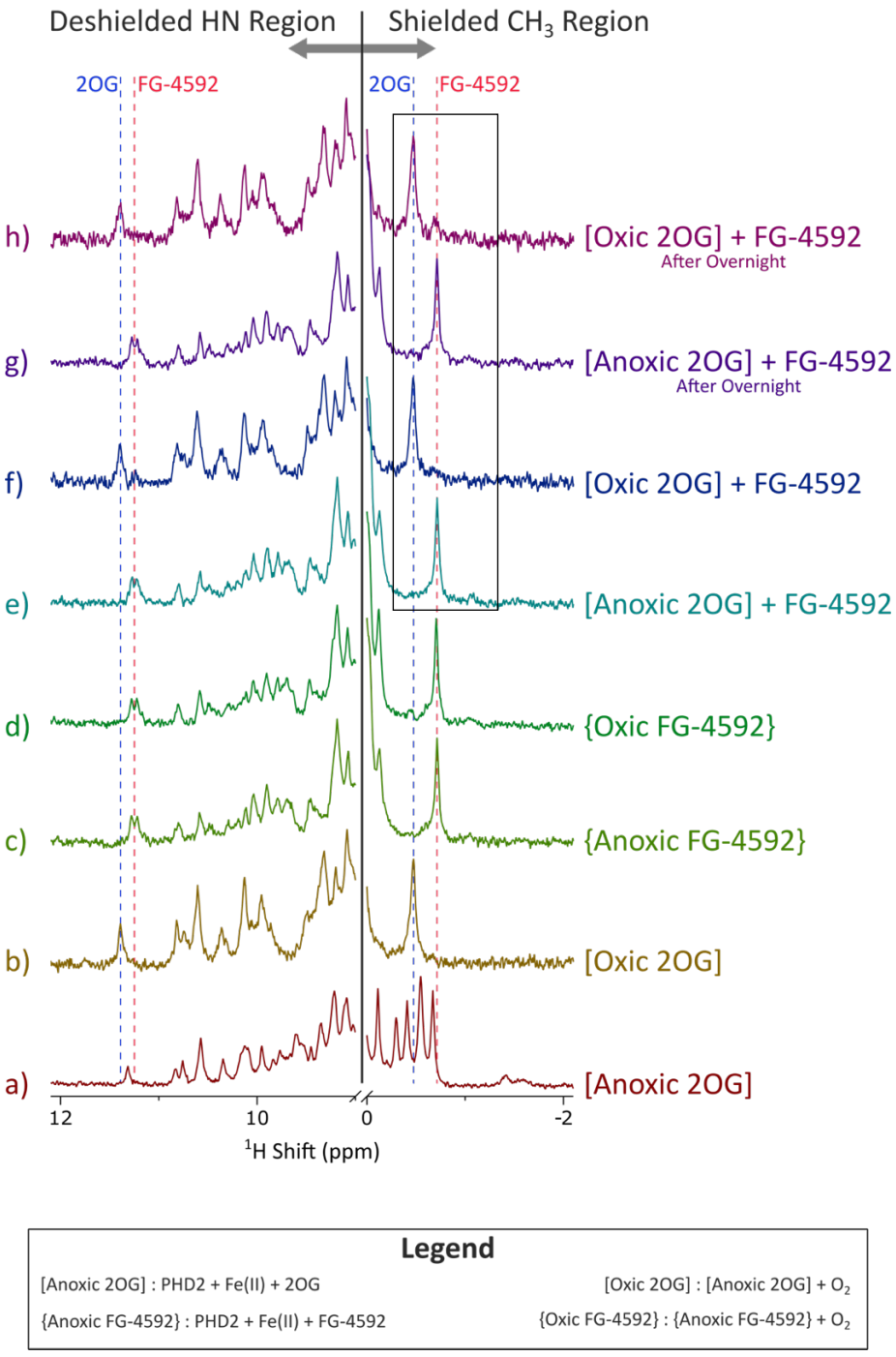


Figure 2.67 *^{1}H spectra of the competition between 2OG and FG-4592 for PHD2:Fe(II) binding. The labels in the figure above each spectrum indicate the starting complex. Each component after a "+" was added to solution in the order written from left to right. The reaction components (separated by "+" signs) and proposed major complexes formed are given as follows. Controls: a) PHD2:Fe(II):2OG, b) PHD2:Fe(II):2OG:O_2, c) PHD2:Fe(II):FG-4592, d) PHD2:Fe(II):FG-4592 + O_2. Inhibitor competition: e)*

PHD2:Fe(II):2OG + FG-4592 → PHD2:Fe(II):FG-4592, f) PHD2:Fe(II):2OG:O_2 + FG-4592 → PHD2:Fe(II):2OG:O_2. Inhibitor binding over time: g) PHD2:Fe(II):FG-4592 + 2OG → PHD2:Fe(II):FG-4592 after ~15 hours at room temperature, h) PHD2:Fe(II):2OG:O_2 + FG-4592 → PHD2:Fe(II):2OG:O_2 after ~15 hours at room temperature. The dotted red lines indicate the characteristic shifts of the FG-4592 complex, and the dotted blue lines indicate the characteristic shifts of the 2OG complex. These shifts were used to investigate the identity of the bound species (ligand or inhibitor). The black, vertical separating line indicates the position where the region from 0 to 9 ppm of the spectrum was removed for simplicity. The black box indicates a region of interest, where the anoxic PHD2:Fe(II):2OG complex was displaced by FG-4592 binding but the oxic PHD2:Fe(II):2OG complex was not. Standard concentrations of each component were: 100 μM unlabelled PHD2, 300 μM Fe(II), 500 μM 2OG, 500 μM FG-4592, <2 ppm O_2 pressure (anoxic), and room pressure O_2 (oxic). Buffer conditions were 135 mM NaCl, 10% D_2O, and 90% 50 mM Tris-d_{11} pH 7.5.

Next, NOG was investigated to see if it merited further inhibitor studies for the purpose of probing oxygen interactions with PHD2 complexes. Since NOG is reported to be a weaker PHD2 inhibitor than FG-4592, it was titrated at 2 eq NOG to 1 eq 2OG to ensure reasonable competition with 2OG for protein binding.

The same set of experiments as described in **Figure 2.67** were carried out in the presence of NOG as shown in **Figure 2.68**. As was the case with competition of FG-4592 with the oxic PHD2:Fe(II):2OG complex, competition of the oxic PHD2:Fe(II):2OG complex with NOG yielded no displacement of 2OG (**Figure 2.68** f). This observation is further evidence of the stability of the oxic PHD2:Fe(II):2OG complex against inhibitor binding. In the case of NOG competing with 2OG for binding the anoxic PHD2:Fe(II):2OG complex (**Figure 2.68** e), 2OG in the anoxic complex is only partially displaced by NOG binding. This observation is consistent with the data indicating NOG is a weaker PHD2 inhibitor than FG-4592.

After the samples were left at room temperature for ~15 hours, both the oxic and anoxic complexes (**Figure 2.68** g-h) showed no difference from when inhibitor had been initially added (**Figure 2.68** e-f).

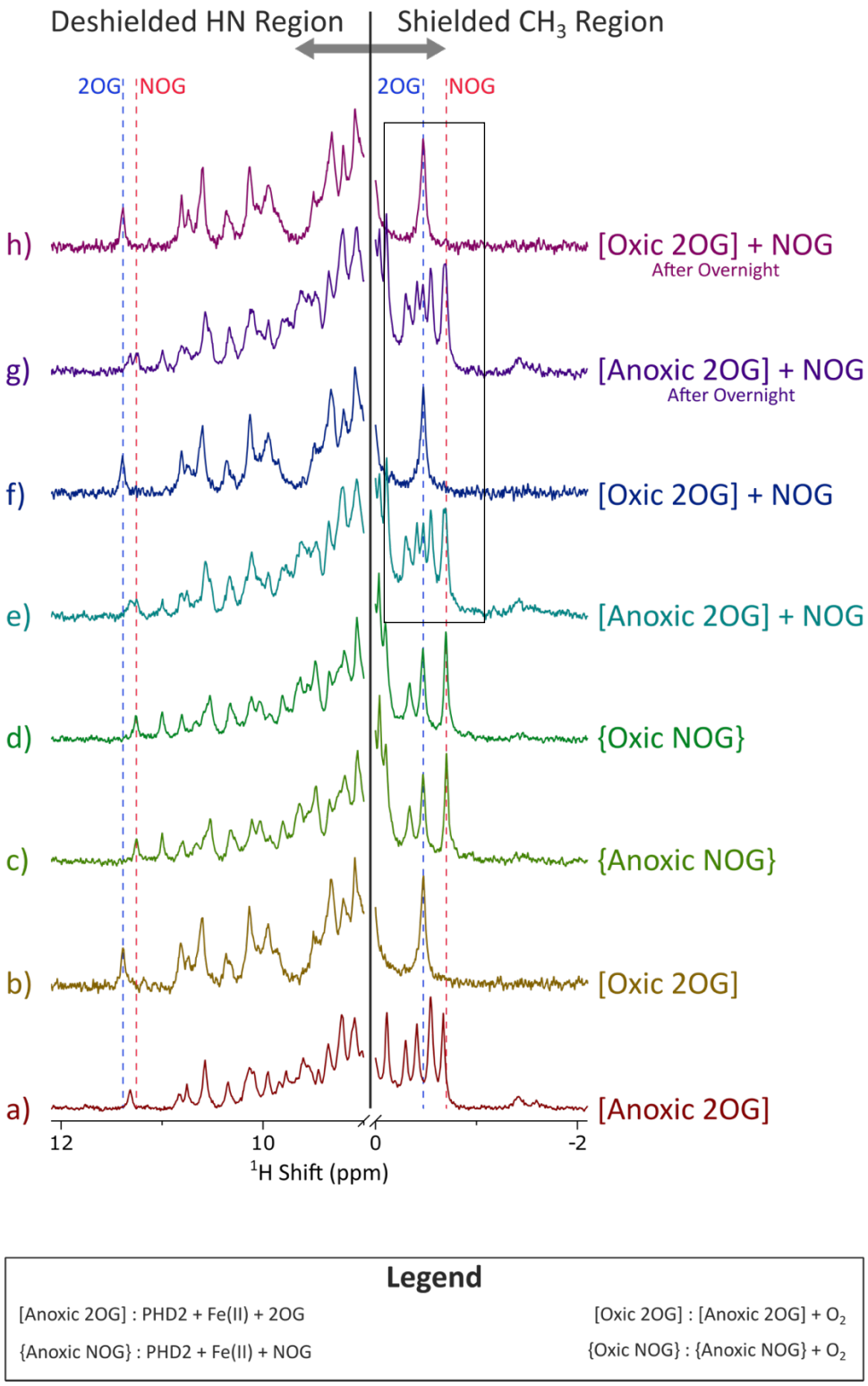


Figure 2.68 *^{1}H spectra of competition between 2OG and NOG for PHD2:Fe(II) binding. The labels in the figure above each spectrum indicate the starting complex. Each component after a "+" was added to solution in the order written from left to right. The reaction components (separated by "+" signs) and proposed major complex formed are*

given as follows. Controls: a) PHD2:Fe(II):2OG, b) PHD2:Fe(II):2OG:O_2, c) PHD2:Fe(II):NOG, d) PHD2:Fe(II):NOG + O_2. Inhibitor competition: e) PHD2:Fe(II):2OG + NOG → PHD2:Fe(II):2OG + PHD2:Fe(II):NOG, f) PHD2:Fe(II):2OG:O_2 + NOG → PHD2:Fe(II):2OG:O_2. Inhibitor binding over time: g) PHD2:Fe(II):2OG + NOG → PHD2:Fe(II):2OG + PHD2:Fe(II):NOG after ~15 hours at room temperature, h) PHD2:Fe(II):2OG:O_2 + NOG → PHD2:Fe(II):2OG:O_2 after ~15 hours at room temperature. The dotted red lines indicate the characteristic shifts of the NOG complex and the dotted blue lines indicate the characteristic shifts of the 2OG complex. These shifts were used to investigate the identity of the bound species (ligand or inhibitor). The black, vertical separating line indicates the position where the region from 0 to 9 ppm of the spectrum was removed for simplicity. The black box indicates a region of interest where the anoxic PHD2:Fe(II):2OG complex is partially displaced by NOG binding. To displacement of the oxic PHD2:Fe(II):2OG complex is observed. Standard concentrations of each component were: 100 μM unlabelled PHD2, 300 μM Fe(II), 500 μM 2OG, 1 mM NOG, <2 ppm O_2 pressure (anoxic), and room pressure O_2 (oxic). Buffer conditions were 135 mM NaCl, 10% D_2O, and 90% 50 mM Tris-d_{11} pH 7.5. This study indicated that large differences between the stability of PHD2:Fe(II):2OG:O_2 and PHD2:Fe(II):2OG could be observed.

The pattern of retention/displacement of 2OG in the PHD2:Fe(II):2OG complex on addition of inhibitor is similar for that of NOG **(Figure 2.68**) and FG-4592 **(Figure 2.67**). NOG, however, indicated weaker binding affinity to the PHD2:Fe(II) complex than FG-4592, with more complicated peak patterns in the shielded methyl and deshielded H_N ^1H spectral regions, making it less useful for ^1H NMR studies. After ~15 hours, not all of the 2OG in the anoxic PHD2:Fe(II):2OG complex was displaced (**Figure 2.68** e, g) and none of the oxic PHD2:Fe(II):2OG complex was displaced (**Figure 2.68** f, h).

From inhibitor studies, FG-4592 exhibited full displacement of 2OG in the anoxic PHD2:Fe(II):2OG complex immediately on measurement (**Figure 2.67** e, g) whereas NOG only exhibited partial displacement of 2OG in the anoxic PHD2:Fe(II):2OG complex (**Figure 2.68** e, g). Both NOG and FG-4592 failed to displace 2OG in the oxic

PHD2:Fe(II):2OG complexes, with only minimal 2OG displacement in by FG-4592 after ~15 hours (**Figure 2.67** f, h; **Figure 2.68** f, h). From these findings, it was determined that FG-4592 would be the preferred inhibitor for ^{1}H spectral studies on oxic and anoxic PHD2:Fe(II):2OG and related complexes.

Once the most viable experimental conditions had been determined, studies were carried out in the presence of a variety of alternative ligands of interest. The first molecule tested after 2OG was NOG (a close structural analogue of 2OG). The oxic/anoxic PHD2:Fe(II):NOG complex was also shown to give similar ^{1}H,^{15}N-HSQC spectra to the anoxic PHD2:Fe(II):2OG complex, which made it a preferred substitute for 2OG in trying to understand the stability of the PHD2:Fe(II):2OG complexes (**Figure 2.17**, **Figure 2.18**, and **Figure 2.21**).

On addition of FG-4592 to the oxic/anoxic PHD2:Fe(II):NOG complexes (**Figure 2.69** e-f), NOG was completely displaced. After the samples were left for ~15 hours at room temperature, there was no change in relative NOG/FG-4592 binding, indicating that NOG does not displace FG-4592 at the PHD2:Fe(II) active site over time (**Figure 2.69** g-h). These results support observations of the unusual nature of the PHD2:Fe(II):2OG oxic complex.

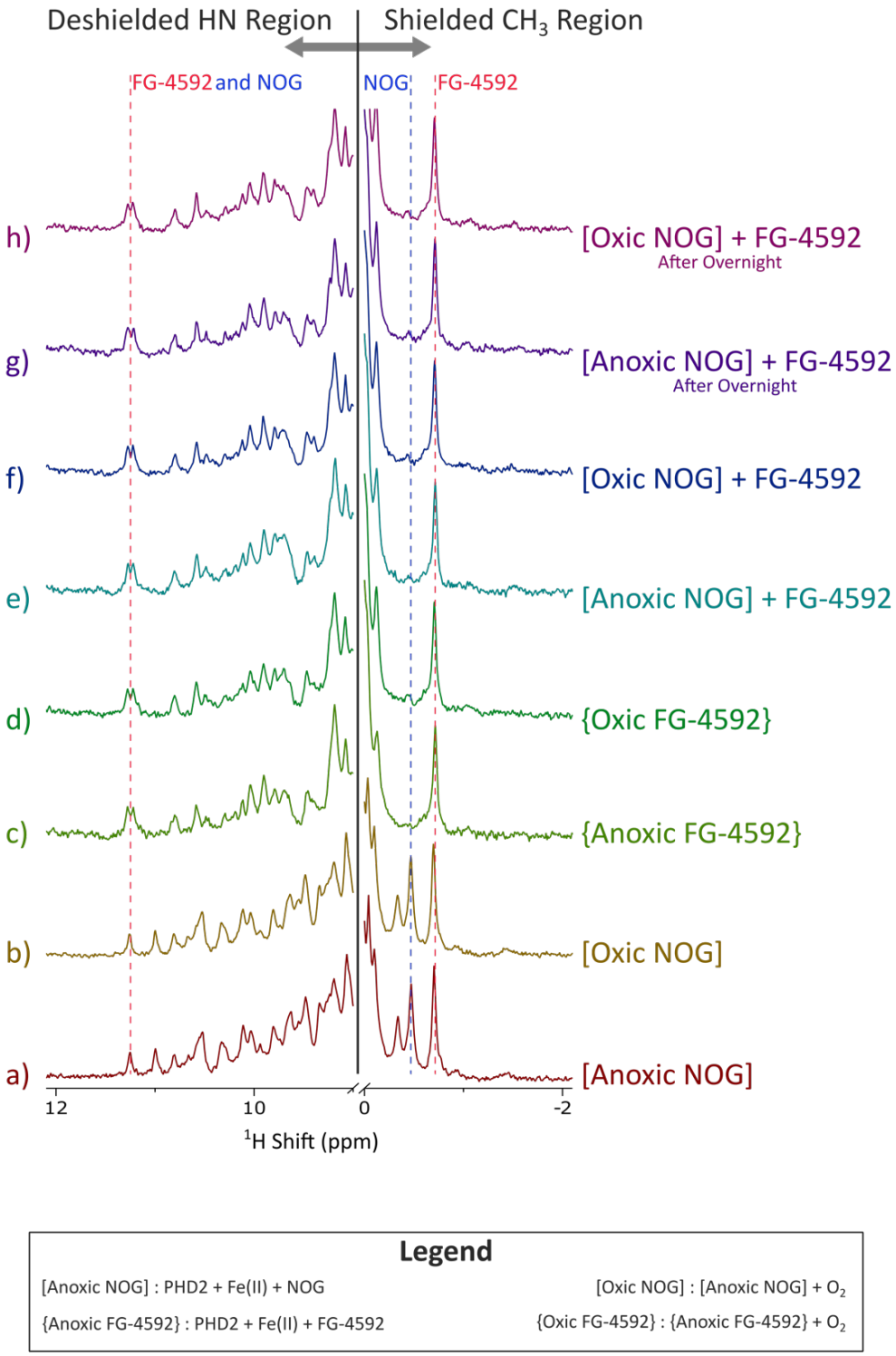


Figure 2.69 *^{1}H spectra for competition between NOG and FG-4592 for PHD2:Fe(II) binding. The labels in the figure above each spectrum indicates the starting complex. Each component after a "+" was added to solution in the order written from left to right. The reaction components (separated by "+" signs) and proposed major complex formed are given as follows. Controls: a) PHD2:Fe(II):NOG, b) PHD2:Fe(II):NOG + O_2, c) PHD2:Fe(II):FG-4592, d) PHD2:Fe(II):FG-4592 + O_2. Inhibitor competition: e)*

PHD2:Fe(II):NOG + FG-4592 → PHD2:Fe(II):FG-4592, f) PHD2:Fe(II):NOG + O_2 + FG-4592 → PHD2:Fe(II):FG-4592 + O_2. Inhibitor binding over time: g) PHD2:Fe(II):NOG + FG-4592 → PHD2:Fe(II):FG-4592 after ~15 hours at room temperature, h) PHD2:Fe(II):NOG + O_2 + FG-4592 → PHD2:Fe(II): FG-4592 + O_2 after ~15 hours at room temperature. The dotted red lines indicate the characteristic shifts of the FG-4592 complex and the dotted blue line indicates the characteristic shift of the NOG complex. These shifts were used to investigate the identity of the bound species (ligand or inhibitor). The dotted red line on the far-left is in the position of both the NOG complex and the FG-4592 complex, but FG-4592 can still be differentiated as it has two equal intensity peaks on either side of this line (and the assumptions can be corroborated with shielded methyl peak data). The black, vertical separating line indicates the position where the region from 0 to 9 ppm of the spectrum was removed for simplicity. FG-4592 was found to displace NOG in both the oxic and anoxic PHD2:Fe(II):NOG complexes. Standard concentrations of each component were: 100 μM unlabelled PHD2, 300 μM Fe(II), 500 μM NOG, 500 μM FG-4592, <2 ppm O_2 pressure (anoxic), and room pressure O_2 (oxic). Buffer conditions were 135 mM NaCl, 10% D_2O, and 90% 50 mM Tris-d_{11} pH 7.5.

The above observations imply the binding of anoxic 2OG and NOG is similar. However, due to uncoupled turnover, the oxic PHD2:Fe(II):2OG complex is stabilised, likely as the PHD2:Fe(III):2OG complex. This proposed PHD2:Fe(III):2OG complex may bind CODD to give a catalytically inert complex (likely the PHD2:Fe(III):2OG.CODD complex) which can be activated by reduction. Whether this process is relevant in cells can be explored in future work, but this hypothesis describes a potential method of bringing four of the five components of the catalytically relevant PHD2 complex together (oxygen being the fifth), albeit with Fe in the inert Fe(III) form.

The next ligand of interest to be explored was *(R)*-2-hydroxyglutarate (2HG), which is similar in structure to 2OG, but with an alcohol at the C-2 position. 2HG is a 2OG analogue and an assigned oncometabolite with two enantiomers (the D enantiomer was used for these studies due to its connection with certain types of cancer). [67]

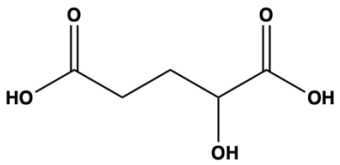


Figure 2.70 *Structure of (R)-2-hydroxyglutarate (2HG). There are two possible enantiomers of 2HG.*

In both the oxic/anoxic PHD2:Fe(II):2HG complexes, the characteristic peak in the shielded methyl region matched the shift of both the oxic/anoxic PHD2:Fe(II) complexes (**Figure 2.71** a-d), making the spectra difficult to interpret. The presence of 2HG did, however, cause differences in the deshielded H_N region of the ^1H spectrum, which varied from the observed oxic/anoxic PHD2:Fe(II) and PHD2:Fe(II):FG-4592 deshielded H_N peaks. Another notable observation about the oxic/anoxic PHD2:Fe(II):2HG peaks in the shielded methyl region was that the oxic spectrum seems to form an Fe(III) complex (either as PHD2:Fe(III):2HG or PHD2:Fe(III)), as characterised by the broad peak appearing around -0.4 ppm. This Fe(III) peak may indicate that 2HG is weakly binding and, therefore, not inhibiting active site metal oxidation, releasing the active site Fe(III) into solution over time. This was not observed in the anoxic 2HG spectrum since O_2 is not present.

As might be expected of a weakly binding ligand, on addition of FG-4592 to the oxic/anoxic PHD2:Fe(II):2HG complexes, 2HG was immediately displaced by FG-4592 (**Figure 2.71** e-f) and remained displaced after ~15 hours at room temperature (**Figure 2.71** g-h). Although further work is required, the protein complex in the presence of 2HG, thought to be in the form of either PHD2:Fe(III):2HG or PHD2:Fe(III), seemed to be further protected from FG-4592 binding since the broad Fe(III) peak was visible both before and after the ~ 15 hour incubation.

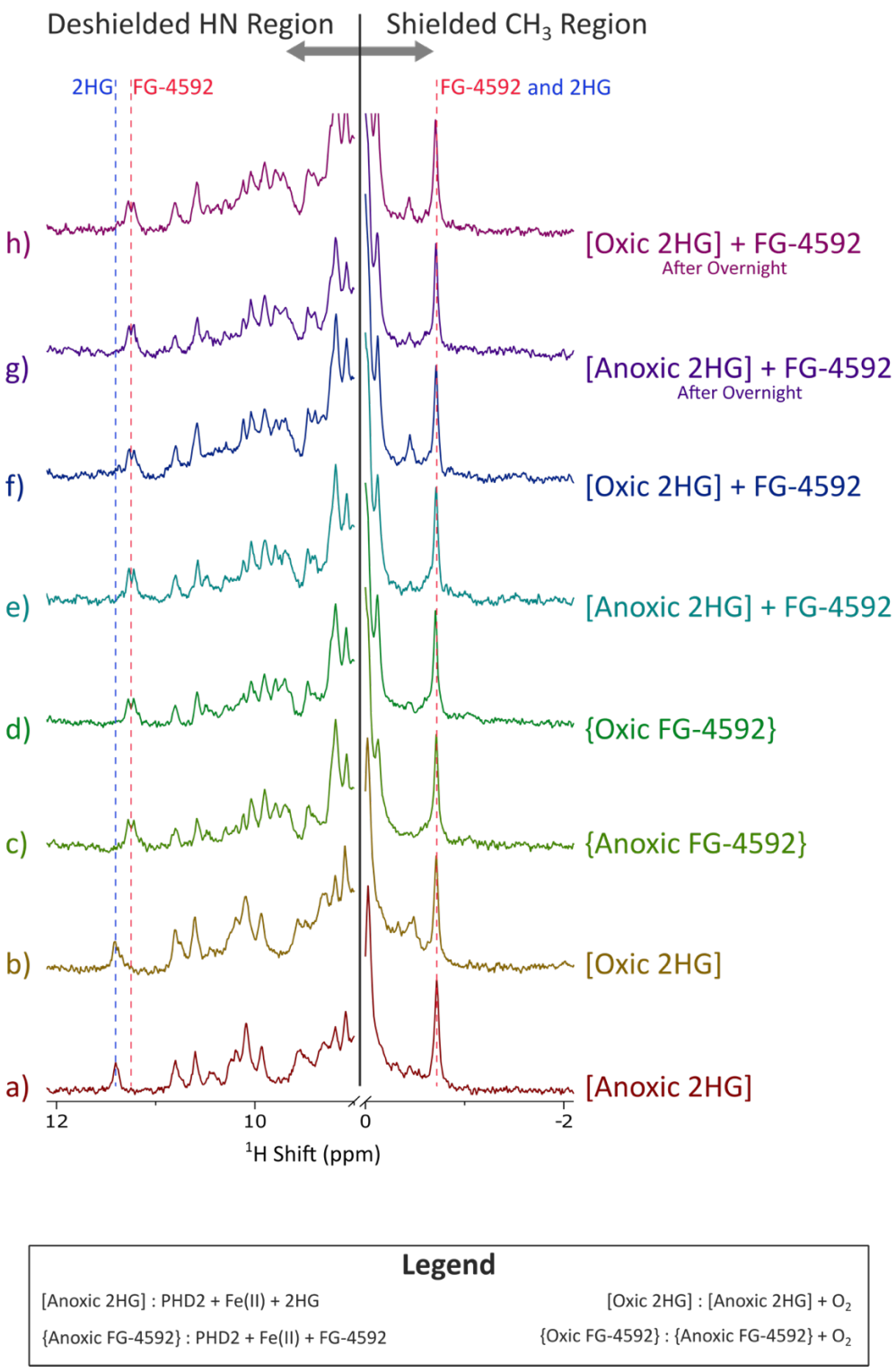


Figure 2.71 *^{1}H spectra of the competition between 2HG and FG-4592 for PHD2:Fe(II) binding. The labels in the figure above each spectrum indicates the starting complex. Each component after a "+" was added to solution in the order written from left to right. The reaction components (separated by "+" signs) and proposed major complex formed are given as follows. Controls: a) PHD2:Fe(II):2HG, b) PHD2:Fe(II):2HG + O_2*

(possibly a PHD2:Fe(III) complex as well), c) PHD2:Fe(II):FG-4592, d) PHD2:Fe(II):FG-4592 + O_2. Inhibitor competition: e) PHD2:Fe(II):2HG + FG-4592 → PHD2:Fe(II):FG-4592, f) PHD2:Fe(II):2HG + O_2 + FG-4592 → PHD2:Fe(II):FG-4592 + O_2. Inhibitor binding over time: g) PHD2:Fe(II):2HG + FG-4592 → PHD2:Fe(II):FG-4592 after ~15 hours at room temperature, h) PHD2:Fe(II):2HG + O_2 + FG-4592 → PHD2:Fe(II):FG-4592 + O_2 after ~15 hours at room temperature. The dotted red lines indicate the characteristic shifts of the FG-4592 complex and the dotted blue line indicates the characteristic shift of the 2HG complex. These shifts were used to investigate the identity of the bound species (ligand or inhibitor). The dotted red line on the far-right is in the position of both the 2HG complex and the FG-4592 complex, since both have similar shielded methyl shifts to that which is observed for the PHD2:Fe(II) complex. They can only be differentiated by deshielded H_N peaks. The black, vertical separating line indicates the position where the region from 0 to 9 ppm of the spectrum was removed for simplicity. Both anoxic and oxic PHD2:Fe(II):2HG complexes were displaced by FG-4592 binding. Standard concentrations of each component were: 100 μM unlabelled PHD2, 300 μM Fe(II), 1 mM 2HG, 500 μM FG-4592, <2 ppm O_2 pressure (anoxic), and room pressure O_2 (oxic). Buffer conditions were 135 mM NaCl, 10% D_2O, and 90% 50 mM Tris-d_{11} pH 7.5.

Succinate is thought to be a weak binder of PHD2 that adopts a monodentate binding mode. [19] The necessity for release of succinate following catalysis to refresh the catalyst for the next reaction may be reason for its weak binding. Despite weak interactions between PHD2 and succinate, it was of interest to understand: 1) how succinate binds to PHD2, 2) how this PHD2-succinate interaction may impact catalysis and 3) if succinate interactions with PHD2 differ under Fe(II) and Fe(III) conditions (as described later in this chapter).

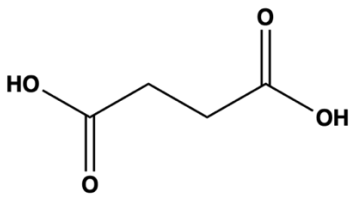


Figure 2.72 *Structure of succinate, a coproduct of PHD2 catalysis.*

As was observed for binding of 2HG to PHD2:Fe(II), succinate binds weakly and was displaced by FG-4592 (**Figure 2.73** e-f). This displacement by FG-4592 was not reversed over time (**Figure 2.73** g-h). The presence of succinate also appears to allow for the formation of Fe(III) complexes (**Figure 2.73** b), observed as a broad peak around -0.4 ppm. The observations for succinate under these conditions correlate with the observations on 2HG addition to the PHD2:Fe(II) complex.

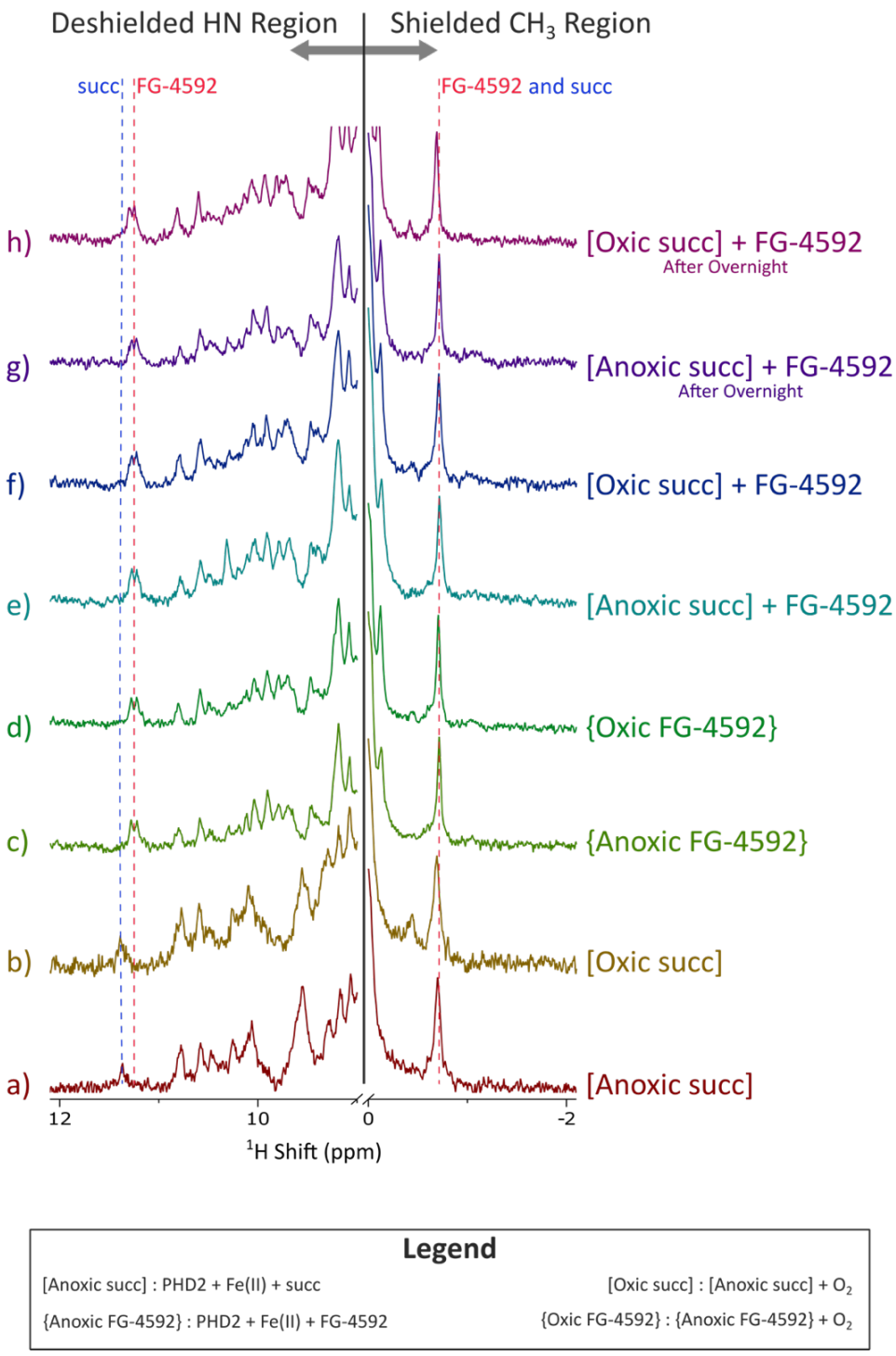


Figure 2.73 *^{1}H spectra of the competition between succinate (succ) and FG-4592 for PHD2:Fe(II) binding. The labels in the figure above each spectrum indicates the starting complex. Each component after a "+" was added to solution in the order written from left to right. The reaction components (separated by "+" signs) and proposed major complex formed are given. Controls: a) PHD2:Fe(II):succ, b) PHD2:Fe(II):succ + O_2 (possibly a PHD2:Fe(III) complex as well), c) PHD2:Fe(II):FG-4592, d)*

PHD2:Fe(II):FG-4592 + O_2. Inhibitor competition: e) PHD2:Fe(II):succ + FG-4592 → PHD2:Fe(II):FG-4592, f) PHD2:Fe(II):succ + O_2 + FG-4592 → PHD2:Fe(II):succ:FG-4592 + O_2. Inhibitor binding over time: g) PHD2:Fe(II):succ + FG-4592 → PHD2:Fe(II):FG-4592 after ~15 hours at room temperature, h) PHD2:Fe(II):succ + O_2 + FG-4592 → PHD2:Fe(II):FG-4592 + O_2 after ~15 hours at room temperature. The dotted red lines indicate the characteristic shifts of the FG-4592 complex and the dotted blue line indicates the characteristic shift of the succinate complex. The dotted red line on the far-right is in the position of both the succinate complex and the FG-4592 complex, since both have similar shielded methyl shifts to that which is observed for the PHD2:Fe(II) complex. They can only be differentiated by deshielded H_N peaks. These shifts were used to investigate the identity of the bound species (ligand or inhibitor). The black, vertical separating line indicates the position where the region from 0 to 9 ppm of the spectrum was removed for simplicity. The oxic and anoxic PHD2:Fe(II):succ complexes were easily displaced by FG-4592 binding, as indicated by the deshielded H_N region of the spectra. Standard concentrations of each component were: 100 μM unlabelled PHD2, 300 μM Fe(II), 1 mM 2HG, 500 μM FG-4592, <2 ppm O_2 pressure (anoxic), and room pressure O_2 (oxic). Buffer conditions were 135 mM NaCl, 10% D_2O, and 90% 50 mM Tris-d_{11} pH 7.5.

The observation of fewer shielded methyl peaks for the PHD2:Fe(II):succinate complexes (as compared to the PHD2:Fe(II):2OG complexes) aligns with what has been previously observed in the Fe(II)- and 2OG-dependent dioxygenase, AlkB. Preliminary studies on the PHD2:Co(II):succinate / PHD2:Fe(II):succinate and PHD2:Co(II):2OG / PHD2:Fe(II):2OG complexes were reported, which showed the same trend in the shielded methyl region. [56]

The last ligand of this series that was explored was fumarate, levels of which have been reported to be upregulated in some cases of mutations of fumarate hydratase. [68]

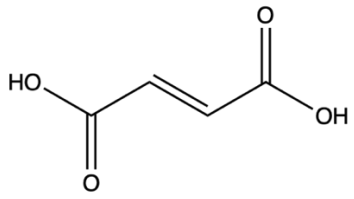


Figure 2.74 *Structure of fumarate.*

Fumarate, like 2HG and succinate, has been observed to be a weak PHD2 binder and exhibited binding characteristics similar to what was observed for 2HG and succinate (**Figure 2.71** and **Figure 2.73**, respectively). [68] On addition of FG-4592 to the oxic/anoxic PHD2:Fe(II):fumarate complexes, fumarate was displaced (**Figure 2.75** e-f) and this displacement was not reversed with time (**Figure 2.75** g-h).

The consistency between the interactions of each weak binder with PHD2 indicates that the ^{1}H NMR assay method is likely robust in differentiating binding modes but may not provide any additional quantitative information on weak interactions.

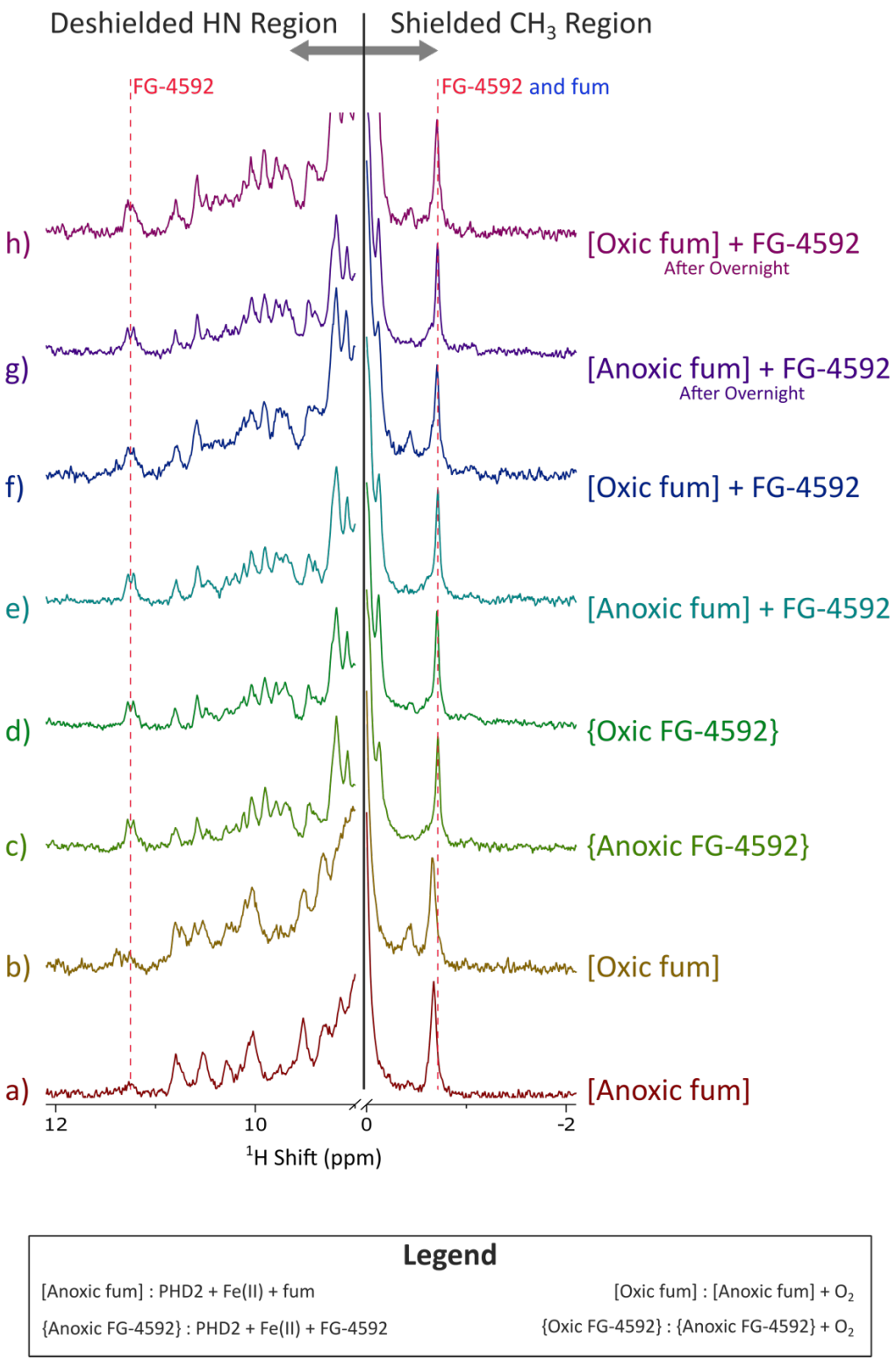


Figure 2.75 *^{1}H spectra of the competition between fumarate (fum) and FG-4592 for PHD2:Fe(II) binding. The labels in the figure above each spectrum indicates the starting complex. Each component after a "+" was added to solution in the order written from left to right.* ***[68]*** *Controls: a) PHD2:Fe(II):fum, b) PHD2:Fe(II):fum + O_2, c)*

PHD2:Fe(II):FG-4592, d) PHD2:Fe(II):FG-4592 + O_2. Inhibitor competition: e) PHD2:Fe(II):fum + FG-4592 → PHD2:Fe(II):FG-4592, f) PHD2:Fe(II):fum + O_2 + FG-4592 → PHD2:Fe(II):FG-4592 + O_2. Inhibitor binding over time: g) PHD2:Fe(II):fum + FG-4592 → PHD2:Fe(II):FG-4592 after ~15 hours at room temperature, h) PHD2:Fe(II):fum + O_2 + FG-4592 → PHD2:Fe(II):FG-4592 + O_2 after ~15 hours at room temperature. The dotted red lines indicate the characteristic shifts of the FG-4592 complex. The dotted red line on the far-right is in the position of both the fumarate complex and the FG-4592 complex, since both have similar shielded methyl shifts to that observed for the PHD2:Fe(II) complex. They can only be differentiated the deshielded H_N peaks. These shifts were used to investigate the identity of the bound species (ligand or inhibitor). It should be noted that broad peaks across all spectra may indicate disordering or misfolding of the protein due to instability. The black, vertical separating line indicates the position where the region from 0 to 9 ppm of the spectrum was removed for simplicity. As with 2HG and succinate, the oxic and anoxic PHD2:Fe(II):fumarate complexes were displaced by FG-4592 binding. Standard concentrations of each component were: 100 μM unlabelled PHD2, 300 μM Fe(II), 1 mM fum, 500 μM FG-4592, <2 ppm O_2 pressure (anoxic), and room pressure O_2 (oxic). Buffer conditions were 135 mM NaCl, 10% D_2O, and 90% 50 mM Tris-d_{11} pH 7.5.

Analysis of the binding of 2HG, succinate, and fumarate to the oxic/anoxic PHD2:Fe(II) complexes further illustrates that: 1) 2OG in the PHD2:Fe(II):2OG complex may play a vital role in both the formation of a stable PHD2 complex and in the unique interactions between PHD2 complexes and O_2 and 2) 2OG-like ligands, e.g. NOG, bind PHD2:Fe(II) complexes in a mode distinct from other ligands, which may bring insight to the nature of the oxic and anoxic PHD2:Fe(II):2OG complexes.

Next, a possible PHD2 enhancer / HIF inhibitor compound developed by James Holt-Martyn (Department of Chemistry, University of Oxford) labelled compound 84 (comp.84 or cpd 84) was studied (**Figure 2.76**). The goal of these studies was to determine if compound 84 can alter 2OG binding, possibly allosterically, and determine how strongly comp. 84 binds to the PHD2:Fe(II) complex.

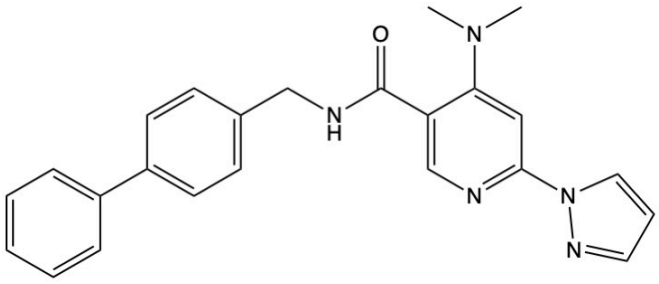


Figure 2.76 *Structure of compound 84.*

On addition of FG-4592 to the PHD2:Fe(II):comp. 84 complex, under oxic and anoxic conditions, comp.84 was fully displaced, as determined by observation of the deshielded H_N region of the spectra; the characteristic peaks in the shielded methyl region for both oxic and anoxic PHD2:Fe(II):FG-4592 and PHD2:Fe(II):comp.84 overlap, which may be indicative of similar binding modes (**Figure 2.77** h-g). It should be noted that substantial precipitation of PHD2 and comp. 84 occurred during these studies, which may have impacted the results.

Comp.84 was then added to the PHD2:Fe(II):2OG complex under oxic and anoxic conditions—no displacement of 2OG was observed (**Figure 2.77** i-j). The lack of spectral change when comp.84 was added to the PHD2:Fe(II):2OG complexes may indicate that it binds at a position of the PHD2 complex that does not disturb the binding of 2OG (as may be the case for activators, since 2OG binding is required), or that compound 84 is not interacting with this complex.

FG-4592 was then added to the oxic and anoxic PHD2:Fe(II):2OG:comp.84 complexes (**Figure 2.77** k-l). Displacement of 2OG by FG-4592 in the PHD2:Fe(II):2OG:comp.84 complex was observed under anoxic but not oxic conditions. These complexes behaved similar to how the oxic and anoxic PHD2:Fe(II):2OG complexes have been shown to respond to FG-4592 addition (**Figure 2.67**), which may

indicate: 1) comp. 84 is not binding or 2) comp. 84 binding does not affect the PHD2:Fe(II):2OG complex or the displacement of 2OG in this complex.

After the oxic and anoxic complexes containing PHD2, Fe(II), 2OG, comp.84 and FG-4592 had been left overnight (**Figure 2.77** m-n), the anoxic spectrum indicated no change (either the PHD2:Fe(II):comp.84:FG-4592 or the PHD2:Fe(II):FG-4592 complex was present). The oxic complex indicated some displacement of 2OG (or 2OG:comp.84) to give the PHD2:Fe(II):FG-4592 (or the PHD2:Fe(II):comp.84:FG-4592) complex. This 2OG displacement occurred more rapidly than has previously been observed in the absence of comp.84 (**Figure 2.67**), which may indicate: 1) the presence of comp.84 destabilises the oxic PHD2:Fe(II):2OG complex, or 2) the precipitation of comp.84 in solution destabilises the system (possibly through non-enzymatic means) disordering the protein structure and leaving it more vulnerable than typical to displacement by FG-4592.

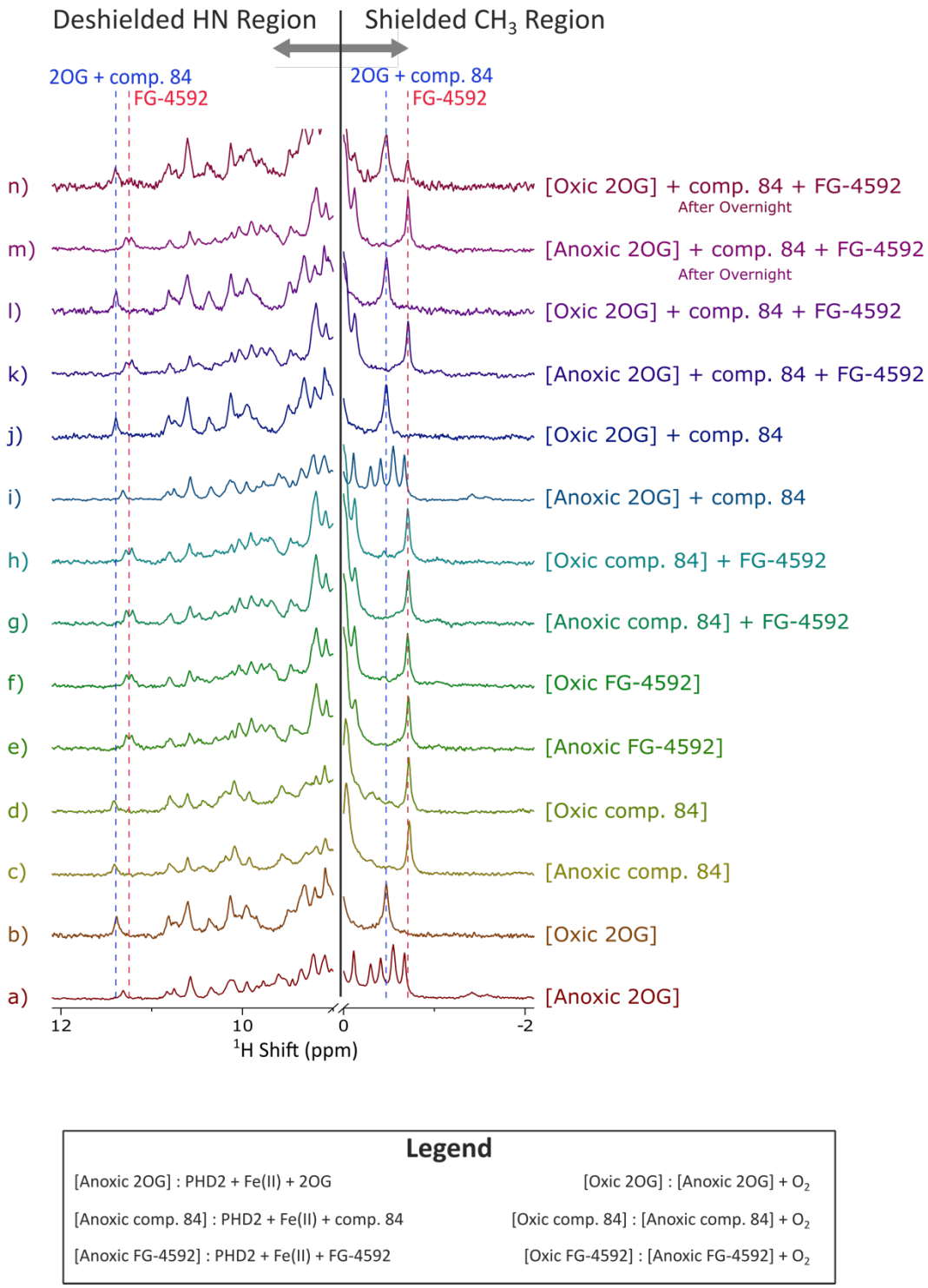


Figure 2.77 *^{1}H NMR spectra of the competition between the 2OG:comp.84 complex and FG-4592 for PHD2:Fe(II) binding. The labels in the figure above each spectrum indicates the starting complex. Each component after a "+" was added to solution in the order written from left to right. The reaction components (separated by "+" signs) and proposed major complex formed are given as follows. Controls: a) PHD2:Fe(II):2OG, b) PHD2:Fe(II):2OG:O_2, c) PHD2:Fe(II):comp.84, d) PHD2:Fe(II):comp.84 + O_2. , e) PHD2:Fe(II):FG-4592, f) PHD2:Fe(II):FG-4592 + O_2. Inhibitor and enhancer*

competition: g) PHD2:Fe(II):comp.84 + FG-4592 → PHD2:Fe(II):FG-4592, h) PHD2:Fe(II):comp.84 + O_2 + FG-4592 → PHD2:Fe(II):FG-4592 + O_2, i) PHD2:Fe(II):2OG + comp.84 → PHD2:Fe(II):2OG:comp.84 (or PHD2:Fe(II):2OG), j) PHD2:Fe(II):2OG + O_2 + comp.84 → PHD2:Fe(II):2OG:comp.84:O_2 and/or PHD2:Fe(II):2OG:O_2, , k) PHD2:Fe(II):2OG:comp.84 + FG-4592 → PHD2:Fe(II):FG-4592, l) PHD2:Fe(II):2OG:comp.84:O_2 + FG-4592 → PHD2:Fe(II):2OG:comp.84:O_2 and/or PHD2:Fe(II):2OG:O_2. Inhibitor binding over time: m) PHD2:Fe(II):2OG:comp.84 + FG-4592 → PHD2:Fe(II):FG-4592 after ~15 hours at room temperature, n) PHD2:Fe(II):2OG:comp.84:O_2 + FG-4592 → PHD2:Fe(II):2OG:comp.-84:O_2 and/or PHD2:Fe(II):2OG:O_2 and PHD2:Fe(II):FG-4592:O_2 after ~15 hours at room temperature. The dotted red lines indicate the characteristic shifts of the FG-4592 complex. The dotted blue lines indicate the characteristic shifts of the 2OG:comp.-84? complex. The question marks after comp.-84 in some instances indicates uncertainty of if the enhancer is binding. The black, vertical separating line indicates the position where the region from 0 to 9 ppm of the spectrum was removed for simplicity. Though it is unknown if comp.84 is binding, addition of comp.84 to the oxic PHD2:Fe(II):2OG complex led to destabilisation, which caused partial displacement of 2OG by FG-4592. Standard concentrations of each component were: 100 μM unlabelled PHD2, 300 μM Fe(II), 500 μM 2OG, 500 μM comp.-84, 500 μM FG-4592, <2 ppm O_2 pressure (anoxic), and room pressure O_2 (oxic). Buffer conditions were 135 mM NaCl, 10% D_2O, and 90% 50 mM Tris-d_{11} pH 7.5.

Without a method to further stabilise binding of comp.84 in solution, it is difficult to conclude anything from these studies. Interestingly, if comp.84 is found to interact with the protein at an allosteric site without causing displacement of 2OG, the subsequent destabilisation of the oxic PHD2:Fe(II):2OG complex may lead to higher turnover rates, as would be expected of a PHD2 enhancer. It has been previously shown that the oxic PHD2:Fe(II):2OG complex is extremely stable against 2OG displacement by FG-4592 (**Figure 2.67** e-h) and has been hypothesised that this stabilisation may be involved in the oxygen sensing mechanism (explored at the end of the chapter).

From the studies on the oxic/anoxic PHD2:Fe(II):ligand complexes, the main findings were: 1) the oxic PHD2:Fe(II):2OG complex is unusual in its stability, 2) no other tested ligand shows the same level of stability against FG-4592 as 2OG, and 3) weak binding ligands may allow for partial oxidation of the Fe(II) centre, which may make these PHD2:Fe(III) complexes more stable against binding of FG-4592. The table

below gives a summary of the levels of stability of the complexes in the presence of FG-4592 as analysed by ^{1}H NMR (**Table 2.2**).

Fe(II) Ligand Complexes				
Ligand	*Oxygen?*	*PHD2:Fe(II):L*	*PHD2:Fe(II):L + I*	*PHD2:Fe(II):L +I (overnight)*
2OG	anoxic	100% L	100% I	100% I
	oxic	100% L	100% L	100% L
NOG	anoxic	100% L	100% I	100% I
	oxic	100% L	100% I	100% I
2HG	anoxic	100% L	100% I	100% I
	oxic	100% L	100% I	100% I
succ	anoxic	100% L	100% I	100% I
	oxic	100% L	100% I	100% I
fum	anoxic	100% L	100% I	100% I
	oxic	100% L	100% I	100% I

Table 2.2 *Summary of PHD2:Fe(II):ligand complex stabilities in the presence of FG-4592. The ligands are defined by L and the inhibitor (FG-4592) is defined by I. Green indicates almost full retention of the ligand complex, yellow indicates approximately equal retention of ligand complex and displacement by inhibitor, and red indicates almost complete ligand displacement by the inhibitor. Oxic and anoxic results are differentiated. All numeric values are estimated.*

2.2.4.2 Studies on the Stabilities of the PHD2:Fe(II):Ligand:Substrate Complexes

Once oxic and anoxic Fe(II)-ligand complex stabilities had been explored, the next step was to understand the stabilities of these complexes in the presence of a fragment of the native (HIF-1α) substrate, CODD. This step is relevant to probing the role of CODD in the binding of oxygen, since CODD is thought to be involved in displacement or loosening of a water molecule at the active site of PHD2 to allow for oxygen binding. [69] CODD may also affect the lifetimes of weak ligand complexes since it narrows the channel through which small molecules can enter and leave the active site pocket. The focus of these studies was on the substrate fragment, CODD (from HIF-1α), but future work may include analysis of alternative, biologically relevant substrates including CODD and NODD regions of HIF1-3α.

The first step was to ensure any peaks in the areas of interest (from about -4 ppm to 0 ppm and from about 9 ppm to 12 ppm) are due to bound CODD (in PHD2 complexes) rather than CODD in solution. The CODD spectrum was compared to the anoxic PHD2:Fe(II):2OG:CODD complex (**Figure 2.80** g). The results indicated that the peaks in the areas of interest were not due to CODD in solution (**Figure 2.78**).

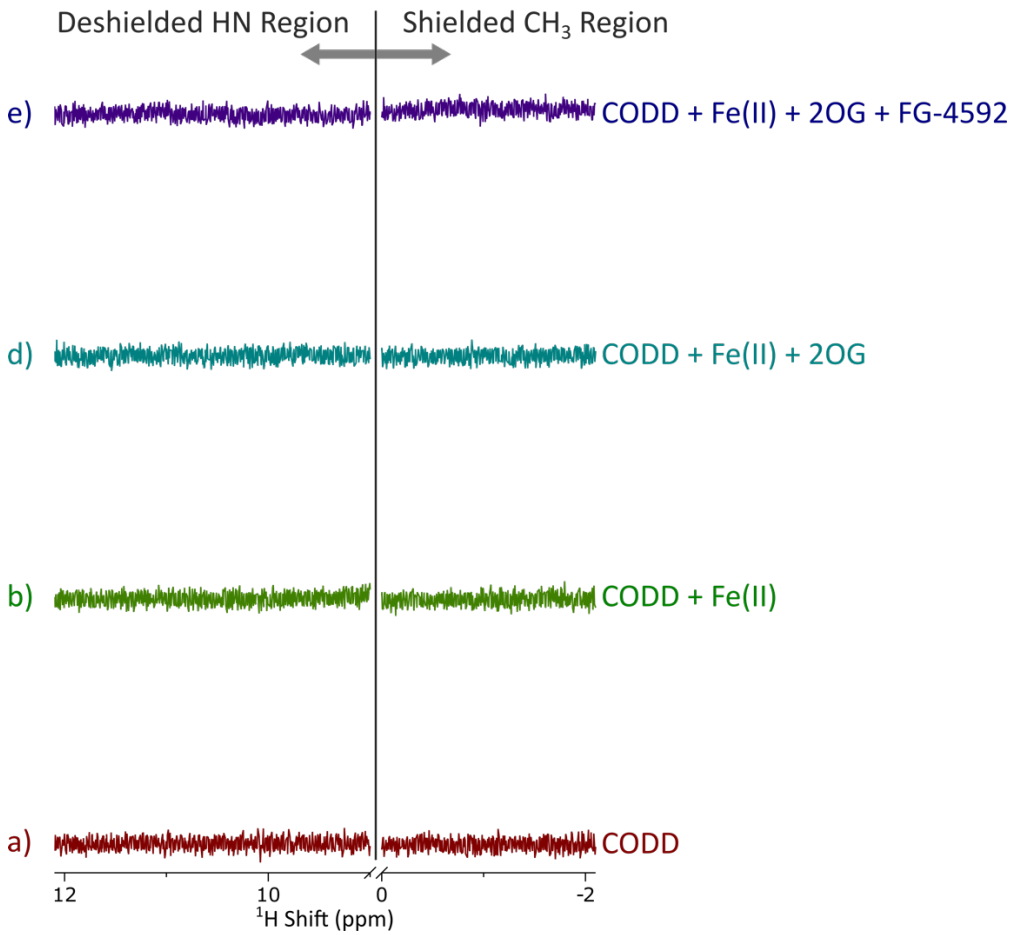


Figure 2.78 *Comparison of oxic CODD spectra in the absence of PHD2. The black, vertical separating line indicates the position where the region from 0 to 9 ppm of the spectrum was removed for simplicity. No CODD peaks are observed in ^1H regions of interest in the absence of PHD2. Standard concentrations of each component were: 300 µM Fe(II), 500 µM 2OG, 500 µM FG-4592, and room pressure O_2. Buffer conditions were 135 mM NaCl, 10% D_2O, and 90% 50 mM Tris-d_{11} pH 7.5.*

Next, an assay was designed to analyse the stability of PHD2:Fe(II):ligand:substrate complexes with respect to inhibitor binding. This assay

matches the set-up described in **Figure 2.65**, except with CODD as a component of the control samples. The general description for the sample preparations is shown in **Figure 2.79**.

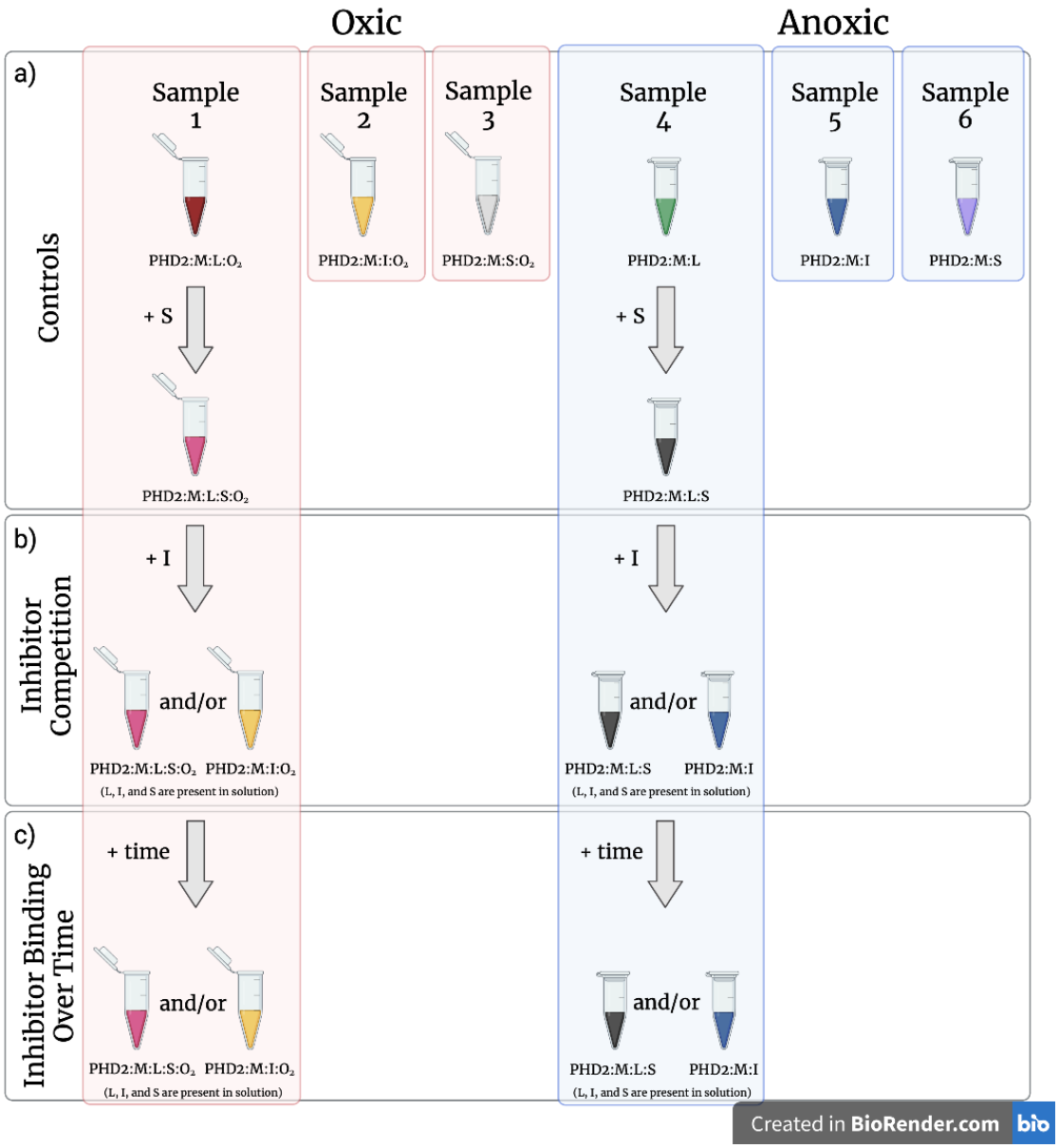


Figure 2.79 *General scheme for ^{1}H NMR oxic/anoxic PHD2:CODD complex stability studies. M denotes metal, L denotes ligand, S denotes substrate, and I denotes inhibitor. Components connected by a colon ":" form a complex. The left side of the figure, enclosed in pink, reflects experiments carried out under oxic conditions (room pressure oxygen concentration) and the right side of the figure, enclosed in blue, are experiments carried out under anoxic conditions (<2 ppm oxygen). a) The six starting samples used as controls were: oxic(red)/anoxic(green) PHD2:M:L (+/- O_2),*

oxic(yellow)/anoxic(blue) PHD2:M:I (+/- O_2), and oxic(silver)/anoxic(purple) PHD2:M:S (+/- O_2). To the oxic/anoxic PHD2:M:L (+/- O_2) samples, CODD substrate (S) was added to form oxic(pink)/anoxic(black) PHD2:M:L:S (+/- O_2), and these new complexes were also used as controls. b) Inhibitor (I) was added to the oxic/anoxic ligand/substrate (L:S) complexes and the level of incorporation of the inhibitor into the PHD2:M:L:S complexes was observed. In the figure above, the product after inhibitor incorporation is illustrated as a mixture of PHD2:M:L:S and PHD2:M:I complexes (which each vary in the relative concentration from 0 to 100% of the mixture). Formation of the oxic/anoxic PHD2:M:L and oxic/anoxic PHD2:M:S complexes was not shown as a possible product since this was not observed in these studies. c) The sample was left overnight (~15 hours) to investigate if the preferred complex (either ligand or inhibitor complex) would change over time. Again this is illustrated as a mixture of PHD2:M:L:S and PHD2:M:I complexes. The figure was created using Biorender.com.

As with the ligand studies, substrate studies were carried out in the presence of each of the following ligands: 2OG, NOG, 2HG, succinate, and fumarate. The goal was to compare the stability of each of these complexes in the absence and presence of substrate.

Starting with studies on the stability of the 2OG complexes against FG-4592 binding, the control samples used were oxic/anoxic PHD2:Fe(II):2OG, oxic/anoxic PHD2:Fe(II):2OG:CODD, oxic/anoxic PHD2:Fe(II):CODD, and oxic/anoxic PHD2:Fe(II):FG-4592 (**Figure 2.80** a-h). Whereas in the ligand studies, each of the control samples were prepared separately, in the substrate studies the oxic/anoxic PHD2:Fe(II):2OG:CODD controls were prepared by addition of CODD to the oxic/anoxic PHD2:Fe(II):2OG control samples.

On addition of FG-4592 to the oxic/anoxic PHD2:Fe(II):2OG:CODD samples, both samples were observed to be stable against FG-4592 binding (**Figure 2.80** i-j), with small amounts of the anoxic PHD2:Fe(II):2OG:CODD complex being converted to the PHD2:Fe(II):FG-4592 complex by 2OG displacement. After ~15 hours, the 2OG in the

anoxic PHD2:Fe(II):2OG:CODD complex was displaced by FG-4592, yet the oxic PHD2:Fe(II):2OG:CODD complex remained stable (**Figure 2.80** k-l). This observation indicates that the anoxic PHD2:Fe(II):2OG complex is resistant to displacement of 2OG by FG-4592 in the presence of CODD (**Figure 2.67** e-f), which may hint at a mechanism where CODD locks the ligand in place.

After ~15 hours, the oxic PHD2:Fe(II):2OG:CODD complex remained largely resistant to FG-4592 binding, but the anoxic PHD2:Fe(II):2OG:CODD complex was almost completely displaced by FG-4592. This observation indicated that, despite the increased stability of the anoxic complex in the presence of CODD, the complex remains less stable than both the oxic PHD2:Fe(II):2OG and the oxic PHD2:Fe(II):2OG:CODD complexes.

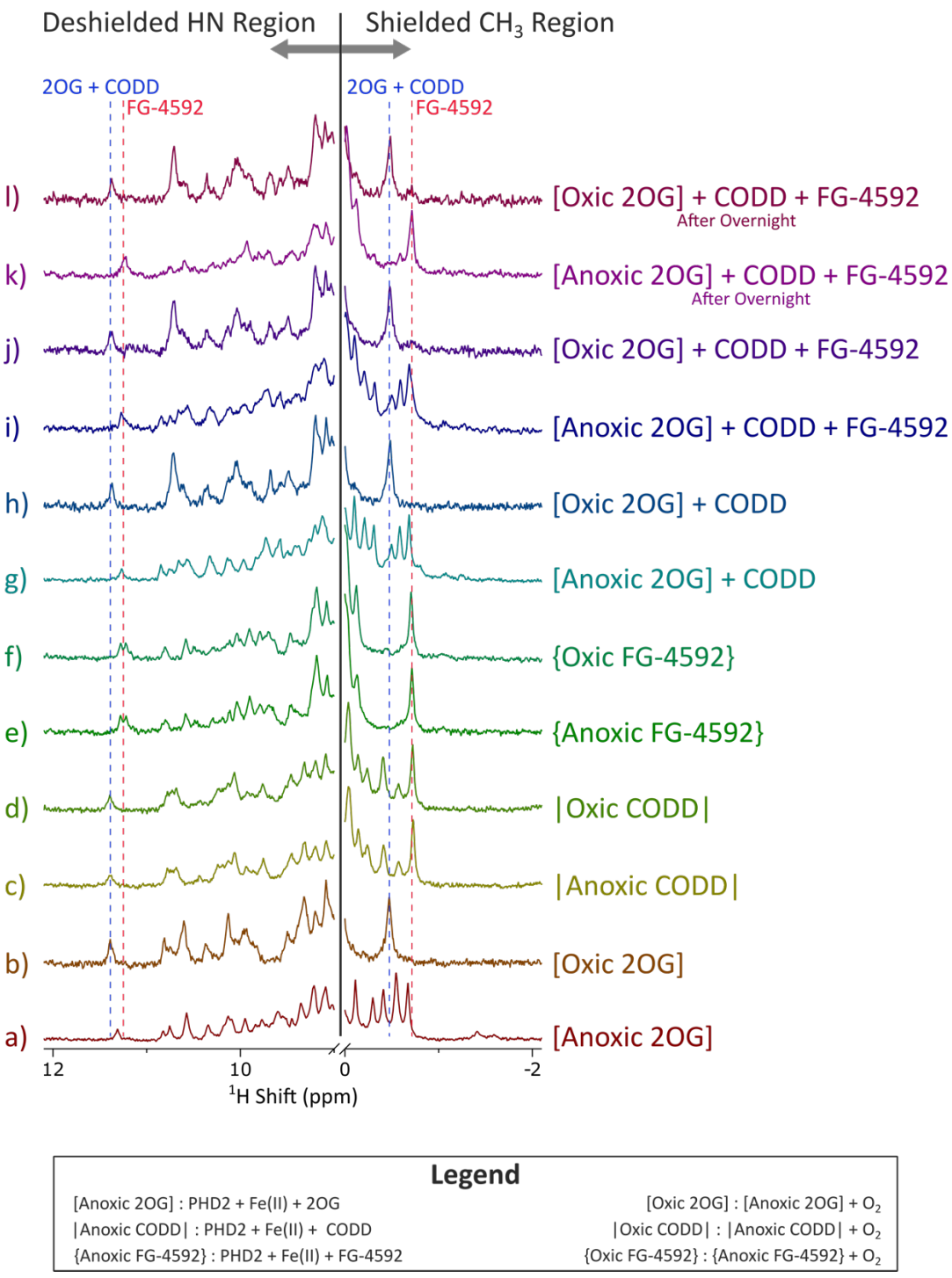


Figure 2.80 *^{1}H spectra of the competition between 2OG:CODD and FG-4592 for PHD2:Fe(II) binding. The labels in the figure above each spectrum indicates the starting complex. Each component after a "+" was added to solution in the order written from left to right. The reaction components (separated by "+" signs) and proposed major complex formed are given as follows. Controls: a) PHD2:Fe(II):2OG, b) PHD2:Fe(II):2OG:O_2, c) PHD2:Fe(II):CODD, d) PHD2:Fe(II):CODD:O_2 e) PHD2:Fe(II):FG-4592, f) PHD2:Fe(II):FG-4592 + O_2, g) PHD2:Fe(II):2OG + CODD → PHD2:Fe(II):2OG:CODD, h) PHD2:Fe(II):2OG:O_2 + CODD → PHD2:Fe(II):2OG:CODD:O_2. Inhibitor competition: i) PHD2:Fe(II):2OG:CODD +*

FG-4592 → PHD2:Fe(II):2OG:CODD, j) PHD2:Fe(II):2OG:CODD:O_2 + FG-4592 → PHD2:Fe(II):2OG:CODD:O_2. Inhibitor binding over time: k) PHD2:Fe(II):2OG:CODD + FG-4592 → PHD2:Fe(II):FG-4592 after ~15 hours at room temperature, and l) PHD2:Fe(II):2OG:CODD:O_2 + FG-4592 → PHD2:Fe(II):2OG:CODD:O_2 after ~15 hours at room temperature. The dotted red lines indicate the characteristic shifts of the FG-4592 complex and the dotted blue lines indicate the characteristic shifts of the 2OG:CODD complex. It should be noted that the line denoting the 2OG:CODD characteristic shifts follows the oxic peaks. These shifts were used to investigate the identity of the bound species (ligand:substrate or inhibitor). The black, vertical separating line indicates the position where the region from 0 to 9 ppm of the spectrum was removed for simplicity. The presence of CODD stabilises both the oxic and anoxic PHD2:Fe(II):2OG complexes against FG-4592 binding. Standard concentrations of each component were: 100 μM unlabelled PHD2, 300 μM Fe(II), 500 μM 2OG, 500 μM CODD, 500 μM FG-4592, <2 ppm O_2 pressure (anoxic), and room pressure O_2 (oxic). Buffer conditions were 135 mM NaCl, 10% D_2O, and 90% 50 mM Tris-d_{11} pH 7.5.

Next, the NOG:CODD complex was evaluated by ^{1}H NMR spectral analysis. On addition of FG-4592 to the oxic/anoxic PHD2:Fe(II):NOG:CODD complexes, only about a third of the complex was displaced by FG-4592 binding (Figure **2.81** i-j). This observation indicates greater stability of the oxic/anoxic PHD2:Fe(II):NOG:CODD complexes than the oxic/anoxic PHD2:Fe(II):NOG complexes (**Figure 2.69** e-f), which matches what was observed for the 2OG complexes. This result is interesting because it indicates that CODD may stabilise binding of ligands other than 2OG, or may stabilise all ligands equally (CODD may block movement in and out of the active site once the complex has formed), whereas ligand preference is more nuanced. This observation supports previous theories concerning the mechanisms of the PHDs.

After ~15 hours, both the oxic/anoxic PHD2:Fe(II):NOG:CODD complexes were perturbed by FG-4592 binding (**Figure 2.81** k-l). This observation matches the behaviour of the anoxic PHD2:Fe(II):2OG:CODD complex (**Figure 2.80**), with the exception that the NOG complex is less stable against FG-4592 than the 2OG complex.

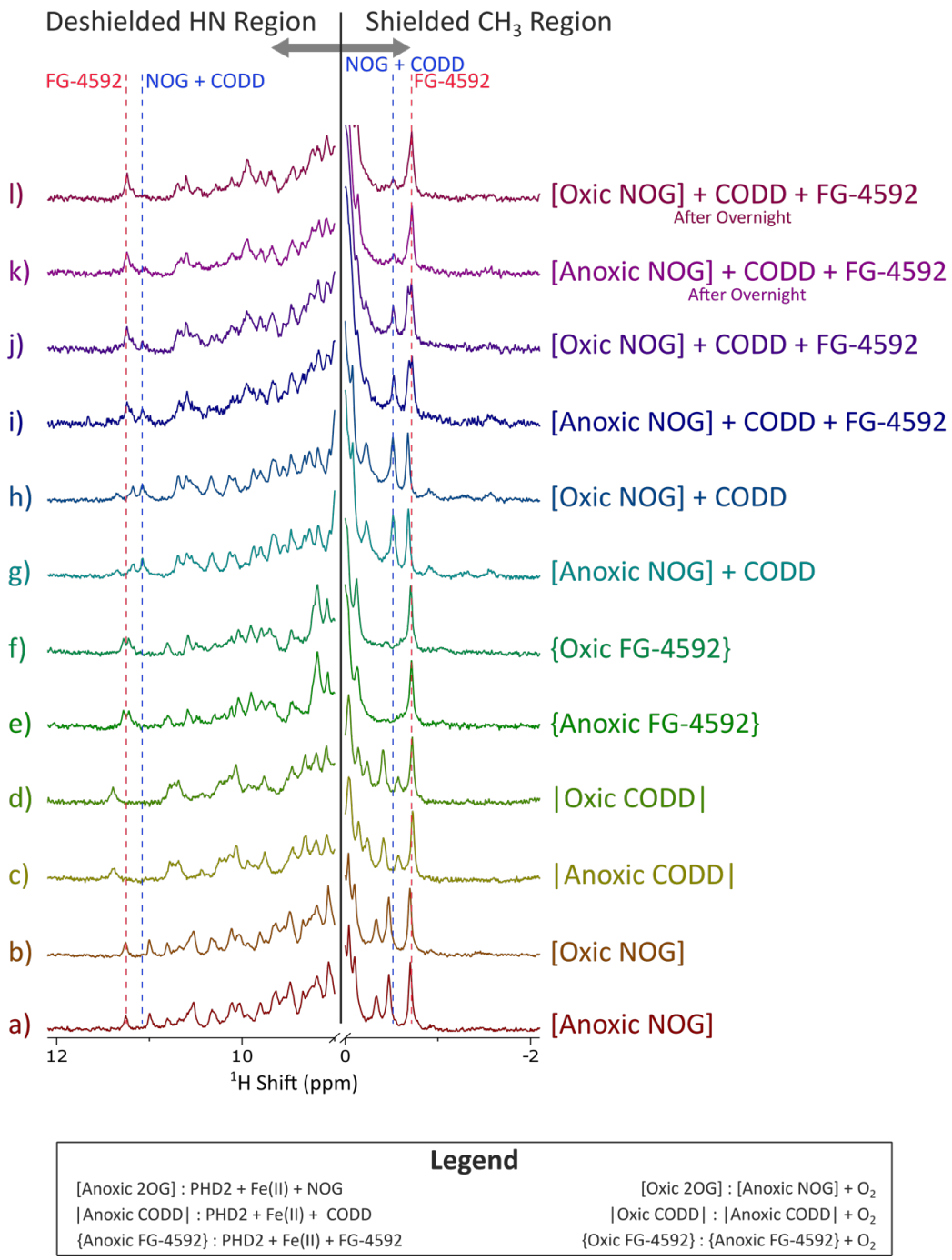


Figure 2.81 *^{1}H spectra of the competition between NOG:CODD and FG-4592 for PHD2:Fe(II) binding. The labels in the figure above each spectrum indicates the starting complex. Each component after a "+" was added to solution in the order written from left to right. The reaction components (separated by "+" signs) and proposed major complex formed are given as follows. Controls: a) PHD2:Fe(II):NOG, b) PHD2:Fe(II):NOG + O_2, c) PHD2:Fe(II):CODD, d) PHD2:Fe(II):CODD + O_2 e) PHD2:Fe(II):FG-4592, f) PHD2:Fe(II):FG-4592 + O_2, g) PHD2:Fe(II):NOG + CODD → PHD2:Fe(II):NOG:CODD, h) PHD2:Fe(II):NOG + O_2 + CODD → PHD2:Fe(II):NOG:CODD + O_2. Inhibitor competition: i) PHD2:Fe(II):NOG:CODD + FG-4592 → PHD2:Fe(II):NOG:CODD + PHD2:Fe(II):FG-4592, j)*

PHD2:Fe(II):NOG:CODD + O_2 + FG-4592 → PHD2:Fe(II):NOG:CODD + O_2 + PHD2:Fe(II):FG-4592. Inhibitor binding over time: k) PHD2:Fe(II):NOG:CODD + FG-4592 → PHD2:Fe(II):FG-4592 ~15 hours at room temperature, and l) PHD2:Fe(II):NOG:CODD + O_2 + FG-4592 → PHD2:Fe(II):FG-4592 + O_2 after ~15 hours at room temperature. The dotted red lines indicate the characteristic shifts of the FG-4592 complex and the dotted blue lines indicate the characteristic shifts of the NOG:CODD complex. These shifts were used to investigate the identity of the bound species (ligand:substrate or inhibitor). The black, vertical separating line indicates the position where the region from 0 to 9 ppm of the spectrum was removed for simplicity. CODD binding stabilises the oxic and anoxic PHD2:Fe(II):NOG complexes against displacement by FG-4592. Standard concentrations of each component were: 100 μM unlabelled PHD2, 300 μM Fe(II), 1 mM NOG, 500 μM CODD, 500 μM FG-4592, <2 ppm O_2 pressure (anoxic), and room pressure O_2 (oxic). Buffer conditions were 135 mM NaCl, 10% D_2O, and 90% 50 mM Tris-d_{11} pH 7.5.

The 2HG:CODD complex stability was then tested. On CODD addition to form the oxic/anoxic PHD2:Fe(II):2HG:CODD complexes (**Figure 2.82** g-h), it was noted that a complex set of peaks was observed in the shielded methyl region. This complexity is similar to what is observed in the anoxic PHD2:Fe(II):2OG:CODD complex (**Figure 2.80** g, ~ 5-6 shielded methyl peaks were observed in both cases). This may indicate that the same shielded methyl residues are perturbed at the active site in these complexes. Interestingly, this similarity in shielded methyl pattern is not observed when comparing the oxic/anoxic PHD2:Fe(II):2HG (**Figure 2.82** a) complex to the anoxic PHD2:Fe(II):2OG complex (**Figure 2.67** a), where the 2HG complex does not exhibit a complex peak pattern. This may indicate that the shielded methyls involved in this complex peak pattern are only perturbed from the stronger ligand binding induced by formation of a CODD substrate complex.

It should also be noted that the broad peak/peaks found at -0.3 ppm on the oxic PHD2:Fe(II):2HG complex, the oxic PHD2:Fe(II):2HG:CODD complex, and the PHD2:Fe(II):2HG:CODD complex in the presence of FG-4592 (**Figure 2.82** b, h, and j respectively) have been attributed to oxidation of Fe(II) to Fe(III), as will be shown later

in this chapter. This is likely caused by weak ligand binding leaving the active site Fe(II) susceptible to oxidation.

When FG-4592 was added to the oxic/anoxic PHD2:Fe(II):2HG:CODD complexes, the anoxic complex was completely displaced by FG-4592 addition (**Figure 2.82** i), while the oxic complex maintained some stability, as evidenced by observation of the most deshielded peak (**Figure 2.82** j). After ~15 hours, the anoxic complex remained FG-4592 bound and the oxic complex remained partially 2HG:CODD bound and partially FG-4592 bound (**Figure 2.82** k-l).

These findings indicate that CODD binding increases the stability of the oxic 2HG complex so that it became partially stable against FG-4592 inhibitor binding (as compared to the lack of stability in the absence of CODD as seen in **Figure 2.71** f). Notably, the presence of CODD did not afford additional stability to the anoxic complex (**Figure 2.71** e as compared to **Figure 2.82** i).

The last point of note is that increased stability on CODD binding was observed in both oxic NOG and oxic 2HG complexes. Though 2HG is a weaker binder than NOG, both ligands have similar structures to 2OG. This may hint that CODD increases overall ligand binding but has a greater impact on 2OG-like binder complex stabilities. This relationship was further explored with weak, 2OG-dissimilar ligands as will be discussed below.

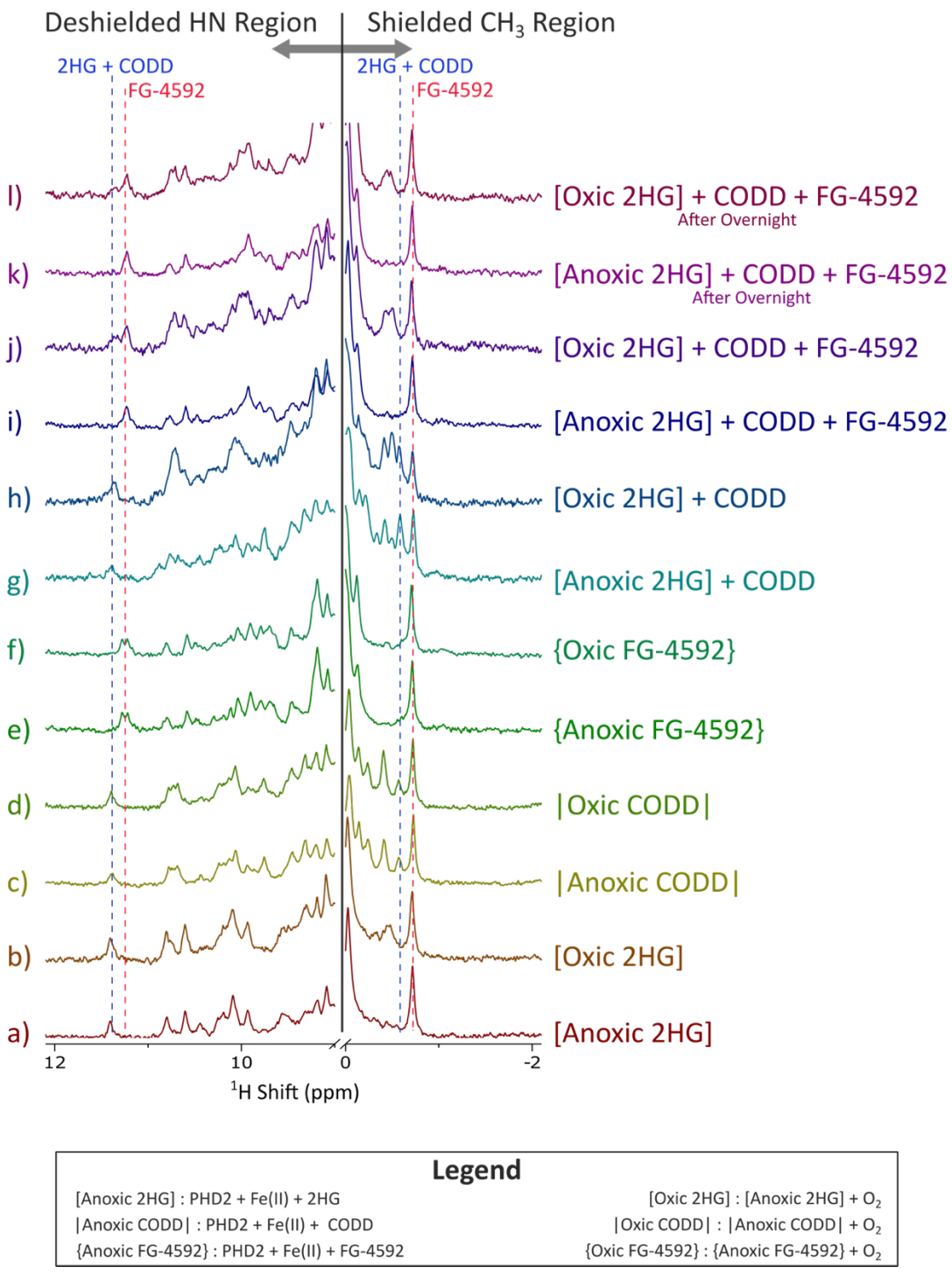


Figure 2.82 *^{1}H spectra of the competition between 2HG:CODD and FG-4592 for PHD2:Fe(II) binding. The labels in the figure above each spectrum indicates the starting complex. Each component after a "+" was added to solution in the order written from left to right. The reaction components (separated by "+" signs) and proposed major complex formed are given as follows. Controls: a) PHD2:Fe(II):2HG, b) PHD2:Fe(II):2HG + O_2, c) PHD2:Fe(II):CODD, d) PHD2:Fe(II):CODD + O_2 e) PHD2:Fe(II):FG-4592, f) PHD2:Fe(II):FG-4592 + O_2, g) PHD2:Fe(II):2HG + CODD → PHD2:Fe(II):2HG:CODD, h) PHD2:Fe(II):2HG + O_2 + CODD →*

PHD2:Fe(II):2HG:CODD + O_2. Inhibitor competition: i) PHD2:Fe(II):2HG:CODD + FG-4592 → PHD2:Fe(II):FG-4592, j) PHD2:Fe(II):2HG:CODD + O_2 + FG-4592 → PHD2:Fe(II):2HG:CODD + O_2. + PHD2:Fe(II):FG-4592 + O_2. Inhibitor binding over time: k) PHD2:Fe(II):2HG:CODD + FG-4592 → PHD2:Fe(II):FG-4592 ~15 hours at room temperature, and l) PHD2:Fe(II):2HG:CODD + O_2 + FG-4592 → PHD2:Fe(II):2HG:CODD + O_2. + PHD2:Fe(II):FG-4592 + O_2. after ~15 hours at room temperature. One of the broad peaks in j) and l) at around -0.4 ppm was assumed to be due to oxidation of Fe(II) to Fe(III), as had been shown in the ligand study of 2HG. The dotted red lines indicate the characteristic shifts of the FG-4592 complex and the dotted blue lines indicate the characteristic shifts of the 2HG:CODD complex. These shifts were used to investigate the identity of the bound species (ligand:substrate or inhibitor). The black, vertical separating line indicates the position where the region from 0 to 9 ppm of the spectrum was removed for simplicity. A unique set of shielded methyl peaks are observed in the oxic and anoxic PHD2:Fe(II):2HG:CODD complexes. Displacement is observed in both complexes on addition of FG-4592, though the oxic complex may show some stabilisation in the presence of CODD. Standard concentrations of each component were:: 100 μM unlabelled PHD2, 300 μM Fe(II), 1 mM 2HG, 500 μM CODD, 500 μM FG-4592, <2 ppm O_2 pressure (anoxic), and room pressure O_2 (oxic). Buffer conditions were 135 mM NaCl, 10% D_2O, and 90% 50 mM Tris-d_{11} pH 7.5.

Succinate, a product of PHD2 catalysis, was the next ligand to be added to the PHD2:Fe(II) complex in the presence of CODD. Understanding the binding stability of succinate under oxic, anoxic, and substrate conditions may give insight into PHD2 catalysis and the process of succinate release. Succinate's role in PHD2 catalysis has been difficult to study (due to poor binding affinity) but it has potential to be involved in the mechanism of oxygen sensing, as it may remain proximate to the protein after catalysis. From studies of the PHD2:Fe(II):2OG complex (**Figure 2.67** and most sections after), it has been inferred that there may be a secondary form of the PHD2 complex that is inactive and, therefore, removed from the catalytic cycle. It is possible that this complex is related to succinate either directly or indirectly.

On CODD binding, the oxic/anoxic PHD2:Fe(II):succ:CODD complexes appear to be formed, the evidence for which comes from a deshielding of the shielded methyl peak when CODD binds (comparison of **Figure 2.83** a-b to g-h). On FG-4592 addition, the oxic/anoxic PHD2:Fe(II):succ:CODD complexes are immediately displaced by FG-

4592 binding (**Figure 2.83** i-j). After ~15 hours the complexes still have FG-4592 bound (**Figure 2.83** k-l).

Again it should be noted that oxidation of Fe(II) to Fe(III) in the PHD2 complex likely occurs for the oxic PHD2:Fe(II):succ, the oxic PHD2:Fe(II):succ:CODD, and the oxic PHD2:Fe(II):succ:CODD (with FG-4592) complexes (**Figure 2.83** b, h, and j respectively) due to weak ligand binding.

These results seem to indicate that increased stabilisation of the ligand complexes by CODD binding may be related to the precise nature of the complexes rather than, or in addition to, binding strength, since 2HG was a weak binder that exhibited benefits from CODD binding, whereas succinate was a weak binder that showed no additional protection (where 2HG is a 2OG-like binder and succinate is not). No concrete inferences can be made on the role of succinate in the PHD2 mechanism or oxygen sensing mechanism from these results, but the free movement of succinate out of the active site in the presence of CODD may be related to the necessity for succinate release after catalysis.

Further studies with Fe(III), which may better elucidate succinate interactions with PHD2, may be useful in gaining further insight and are described later in this chapter.

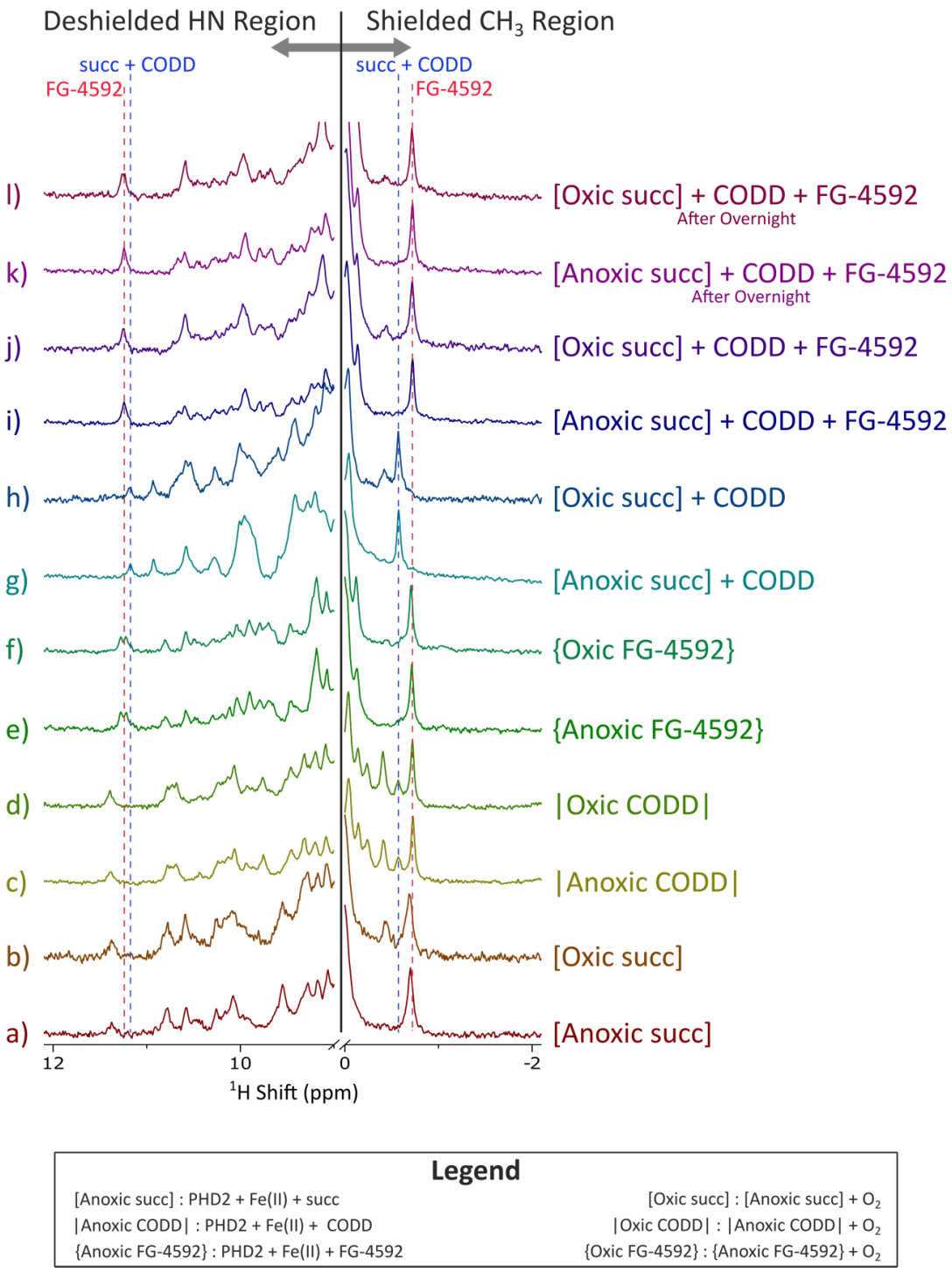


Figure 2.83 *^{1}H spectra of the competition between succinate(succ):CODD and FG-4592 for PHD2:Fe(II) binding. The labels in the figure above each spectrum indicate the starting complex. Each component after a "+" was added to solution in the order written from left to right. The reaction components (separated by "+" signs) and proposed major complex formed are given as follows. Controls: a) PHD2:Fe(II):succ, b) PHD2:Fe(II):succ + O_2, c) PHD2:Fe(II):CODD, d) PHD2:Fe(II):CODD + O_2 e) PHD2:Fe(II):FG-4592, f) PHD2:Fe(II):FG-4592 + O_2, g) PHD2:Fe(II):succ + CODD → PHD2:Fe(II):succ:CODD, h) PHD2:Fe(II):succ + O_2 + CODD →*

PHD2:Fe(II):succ:CODD + O_2. Inhibitor competition: i) PHD2:Fe(II):succ:CODD + FG-4592 → PHD2:Fe(II):FG-4592, j) PHD2:Fe(II):succ:CODD + O_2 + FG-4592 → PHD2:Fe(II):FG-4592 + O_2. Inhibitor binding over time: k) PHD2:Fe(II):succ:CODD + FG-4592 → PHD2:Fe(II):FG-4592 ~15 hours at room temperature, and l) PHD2:Fe(II):succ:CODD + O_2 + FG-4592 → PHD2:Fe(II):FG-4592 + O_2 after ~15 hours at room temperature. The dotted red lines indicate the characteristic shifts of the FG-4592 complex and the dotted blue lines indicate the characteristic shifts of the succ:CODD complex. These shifts were used to investigate the identity of the bound species (ligand:substrate or inhibitor). The black, vertical separating line indicates the position where the region from 0 to 9 ppm of the spectrum was removed for simplicity. No stabilisation of the PHD2:Fe(II):succ: complex against FG-4592 binding was observed in the presence of CODD. Standard concentrations of each component were: 100 μM unlabelled PHD2, 300 μM Fe(II), 1 mM succ, 500 uM CODD, 500 μM FG-4592, <2 ppm O_2 pressure (anoxic), and room pressure O_2 (oxic). Buffer conditions were 135 mM NaCl, 10% D_2O, and 90% 50 mM Tris-d_{11} pH 7.5.

Fumarate (fum) binding was then explored in the presence of CODD. On addition of CODD to the oxic/anoxic PHD2:Fe(II):fum complexes (**Figure 2.84** g-h), there was a characteristic shift in the shielded methyl peaks, as had been observed for succinate. The remaining steps also seemed to mirror what had been observed for the succinate:CODD studies. On FG-4592 addition, the oxic/anoxic PHD2:Fe(II):fum:CODD complexes were completely displaced by FG-4592 binding (**Figure 2.84** i-j). These complexes remained displaced by FG-4592 after ~15 hours (**Figure 2.84** k-l). As with succinate, this observation seems to indicate fumarate is a weak binder and so CODD binding does not help to protect the fumarate complex against FG-4592 binding.

Again, it should be noted that oxidation of Fe(II) to Fe(III) in the PHD2 complex occurs for the oxic PHD2:Fe(II):fum, the oxic PHD2:Fe(II):fum:CODD, and the oxic PHD2:Fe(II):fum:CODD (in the presence of FG-4592) complexes (**Figure 2.84** b, h, and j respectively) due to weak ligand binding.

These observations support the idea that the structure of the cosubstrate mimic is important in determining the extent of stabilisation by CODD binding. Next it was considered of interest to understand if this relationship extends to the Fe(III) complexes.

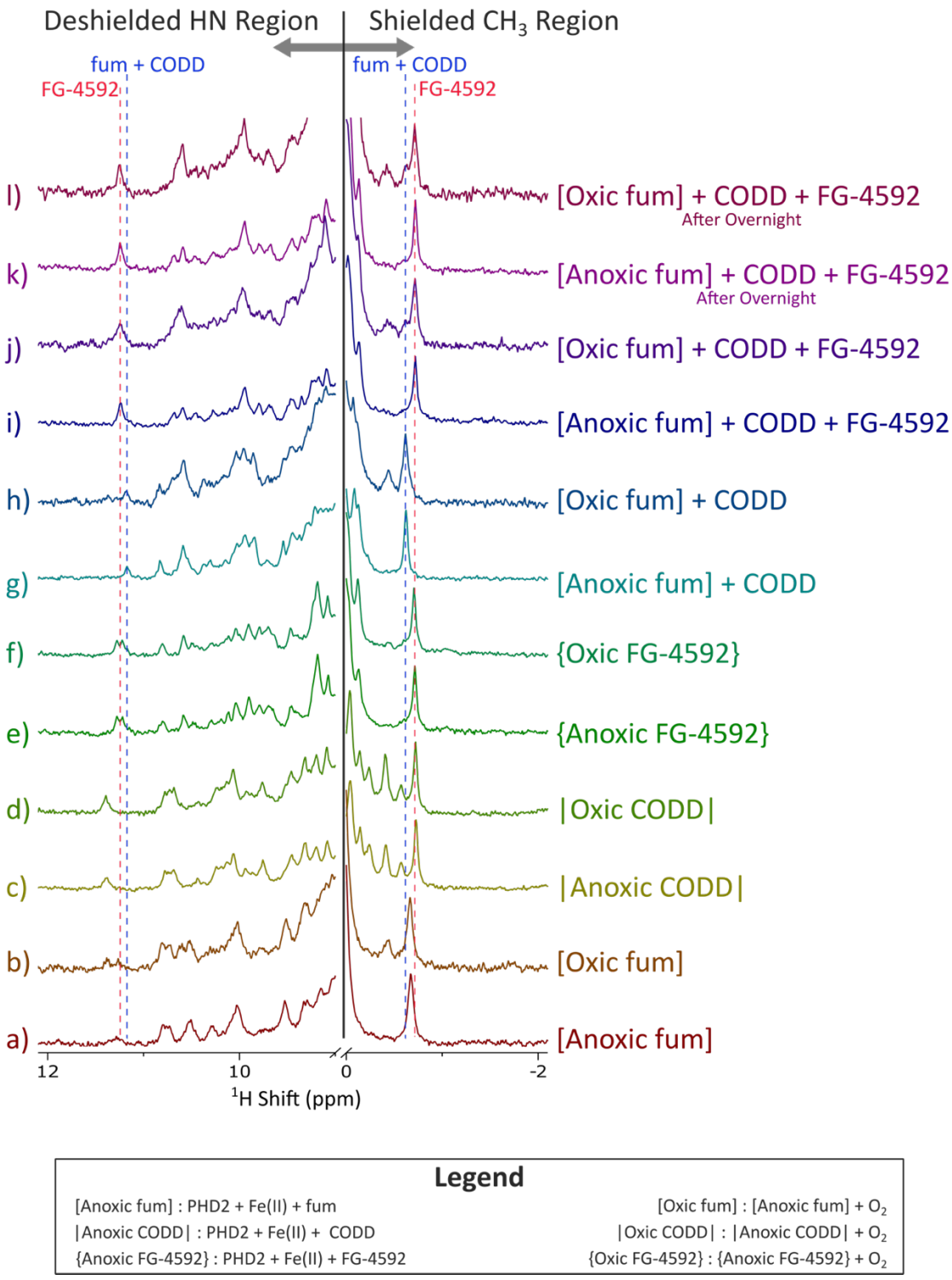


Figure 2.84 *^{1}H spectra of the competition between fumarate(fum):CODD and FG-4592 for PHD2:Fe(II) binding. The labels in the figure above each spectrum indicates the starting complex. Each component after a "+" was added to solution in the order written from left to right. Controls: a) PHD2:Fe(II):fum, b) PHD2:Fe(II):fum + O_2, c) PHD2:Fe(II):CODD, d) PHD2:Fe(II):CODD + O_2 e) PHD2:Fe(II):FG-4592, f)*

PHD2:Fe(II):FG-4592 + O_2, g) PHD2:Fe(II):fum + CODD → PHD2:Fe(II):fum:CODD, h) PHD2:Fe(II):fum + O_2 + CODD → PHD2:Fe(II):fum:CODD + O_2. Inhibitor competition: i) PHD2:Fe(II):fum:CODD + FG-4592 → PHD2:Fe(II):FG-4592, j) PHD2:Fe(II):fum:CODD + O_2 + FG-4592 → PHD2:Fe(II):FG-4592 + O_2. Inhibitor binding over time: k) PHD2:Fe(II):fum:CODD + FG-4592 → PHD2:Fe(II):FG-4592 ~15 hours at room temperature, and l) PHD2:Fe(II):fum:CODD + O_2 + FG-4592 → PHD2:Fe(II):FG-4592 + O_2 after ~15 hours at room temperature. In spectra j) and l), it appears that there is some oxic PHD2:Fe(II):fum:CODD complex bound (shoulder of the peak) but it is difficult to tell. The dotted red lines indicate the characteristic shifts of the FG-4592 complex and the dotted blue lines indicate the characteristic shifts of the fum:CODD complex. These shifts were used to investigate the identity of the bound species (ligand:substrate or inhibitor). The black, vertical separating line indicates the position where the region from 0 to 9 ppm of the spectrum was removed for simplicity. No stabilisation of the PHD2:Fe(II):fum complex against FG-4592 binding was observed in the presence of CODD. Standard concentrations of each component were: 100 μM unlabelled PHD2, 300 μM Fe(II), 1 mM fum, 500 μM CODD, 500 μM FG-4592, <2 ppm O_2 pressure (anoxic), and room pressure O_2 (oxic). Buffer conditions were 135 mM NaCl, 10% D_2O, and 90% 50 mM Tris-d_{11} pH 7.5.

The main findings from these studies were that. the: 1) oxic/anoxic PHD2:Fe(II):2OG:CODD, oxic/anoxic PHD2:Fe(II):NOG:CODD, and oxic/anoxic PHD2:Fe(II):2HG:CODD complexes are more stable against FG-4592 than the 2OG, NOG, or 2HG complexes in the absence of CODD, an observation which might reflect the 2OG-like structures of the latter 3 ligands, 2) complexes formed with weak, less 2OG-like, ligands like succinate and fumarate are not/minimally stabilised by the presence of CODD, and 3) the oxic/anoxic PHD2:Fe(II):2HG:CODD complex has a unique shielded methyl peak pattern that might further hint at the locations of the shielded methyls in the protein complex. Comparisons of the levels of ligand displacement by inhibitor are shown below in **Table 2.3**.

Fe(II) Ligand:Substrate Complexes				
Ligand	*Oxygen?*	*PHD2:Fe(II):L:S*	*PHD2:Fe(II):L:S + I*	*PHD2:Fe(II):L:S +I (overnight)*
2OG	anoxic	100% L:S	100% L:S	5% L:S, 95% I
	oxic	100% L:S	95% L:S, 5% I	95% L:S, 5% I
NOG	anoxic	100% L:S	50% L:S, 50% I	5% L:S, 95% I
	oxic	100% L:S	50% L:S, 50% I	5% L:S, 95% I
2HG	anoxic	100% L:S	100% I	100% I
	oxic	100% L:S	50% L:S, 50% I	50% L:S, 50% I
succ	anoxic	100% L:S	100% I	100% I
	oxic	100% L:S	100% I	100% I
fum	anoxic	100% L:S	100% I	100% I
	oxic	100% L:S	10% L:S, 90% I	10% L:S, 90% I

Table 2.3 *Compiled description of PHD2:Fe(II):ligand:substrate complex stabilities against inhibitor binding. Green indicates almost full retention of the ligand complex, yellow indicates approximately equal retention of ligand complex and displacement by inhibitor, and red indicates almost complete ligand displacement by inhibitor. Oxic and anoxic results are differentiated.*

2.2.4.3 Studies on the Stabilities of the PHD2:Fe(III):Ligand Complexes

From the above described studies on the stabilities of the oxic/anoxic PHD2:Fe(II): ligand :(+/-)substrate complexes, it was found that only the Fe(II):2OG complexes are stable against FG-4592 binding in the absence of CODD, and only the Fe(II):2OG-like ligand complexes are stable in the presence of CODD. Generally, the oxic forms of these complexes manifested the greatest stability.

With this understanding, the next step in understanding the PHD2 complexes was to observe these complexes in the presence of Fe(III) to investigate if the increased stability of oxic complexes is due to the formation of Fe(III) (Fe(III) is formed from Fe(II) in the presence of oxygen). It was considered that such studies may also help elucidate: 1) if the oxic complexes of 2OG have Fe(III) bound and if the structures of the catalytically converted Fe(III) complexes match those where Fe(III) is directly added, 2) whether Fe(III) at the active site has a stabilising effect on the complexes, as may be indicated by increased stability of some of the oxic complexes over the anoxic complexes, and 3) whether the Fe(III) complexes interact differently with succinate, compared to the

Fe(II) complexes, and how such differences might relate to the PHD2 mechanism, including release of succinate.

The theory that Fe(III) may be, at least in part, responsible for the greater stability of the oxic PHD2:Fe(II):2OG complex stems from EPR studies (**Figure 2.45**), which indicate that the oxic PHD2:Fe(II):2OG complex contains Fe(III) that is formed enzymatically. Further exploration of the Fe(III) complexes may be key to understanding the greater oxic PHD2:Fe(II):2OG complex stability and, possibly, gain key insights into the oxygen sensing mechanism of PHD2.

It should be noted that these experiments may be less robust than their Fe(II) counterparts as: 1) binding of Fe(III) to some components of the complex may be weak and 2) the presence of Fe(III) in an NMR solution causes paramagnetic broadening and shifting of peaks (see Chapter 1, **Section 1.2.5**), which complicates the data. It is likely that PHD2 in the presence of Fe(III) is not fully metal-bound and that ligands and inhibitors will also have a more challenging time binding to these complexes. It should also be noted that the Fe(III) solution was left exposed to oxygen for a month before use to ensure no Fe(II) contamination.

As observed in the Fe(II) studies, peaks for the Fe(II) complexes tend to appear around -0.8 ppm in cases of single, major shielded methyl peaks (as was seen with the PHD2:Fe(II) complex, PHD2:Fe(II):FG-4592 complex, and several others). Fe(III) complexes tend to exhibit shielded methyls around -0.4 ppm, as was observed 1) passively over time under oxic conditions with weak binding ligands (2HG, succinate, fumarate) bound to the PHD2 complexes (**Figure 2.71** b, **Figure 2.73** b, and **Figure 2.75** b), 2) in the oxic PHD2:Fe(II):2OG (**Figure 2.67** b) complex, 3) and in the oxic

PHD2:Fe(II):2OG:CODD (**Figure 2.80** b) complex. Note the first two instances reflect substrate uncoupled turnover and last instance coupled turnover.

On initial studies of the Fe(III) complexes in the presence of 2OG or FG-4592, it was clear that there were complications. Addition of 2OG to the oxic/anoxic PHD2:Fe(III) complex gave several, overlapping shielded methyl peaks in the -0.4 ppm region (**Figure 2.85** a-b). This differs from the oxic PHD2:Fe(II):2OG complex that has a single shielded methyl peak in this region, so it can be proposed that the oxic PHD2:Fe(II):2OG complex (thought to be a PHD2:Fe(III):2OG complex that formed by exposure of the PHD2:Fe(II):2OG complex to oxygen) is not the same as a PHD2:Fe(III):2OG complex formed from PHD2:Fe(III) and 2OG. If we were to assume the oxic PHD2:Fe(II):2OG complex is an Fe(III) complex (as EPR studies indicate), it is likely that Fe(III) added to solution binds differently than Fe(III) that has formed at the active site through turnover. This would explain the difference in behaviour between what has been observed in oxic PHD2:Fe(II):2OG complexes that are thought to contain Fe(III) and PHD2:Fe(III):2OG complexes (discussed in this section): there is more than one type of Fe(III) complex formed on Fe(III) addition, but only one type that can be formed from turnover. Note that in the uncoupled reaction of 2OG with O_2 to give succinate, CO_2 consumes only one of the oxygen atoms of O_2; reduction of the other oxygen atom of O_2 to give water requires two electrons (along with two protons). One of the electrons may come from Fe(II) to give a PHD2:Fe(III) species, which can then bind another 2OG to give the stable PHD2:Fe(III):2OG complex; the other species formed in this reaction is unclear, but it may, in turn, cause the blue colour observed. This hypothesis needs further exploration.

Another interesting observation was that FG-4592 binding was poor in the presence of Fe(III). In the anoxic PHD2:Fe(III):FG-4592 complex (**Figure 2.85** c), there

are two peaks in the shielded methyl region: one in the -0.4 ppm region that may be PHD2:Fe(III), PHD2:Fe(III):FG-4592, or a mixture, and one in the position where the oxic/anoxic PHD2:Fe(II):FG-4592 peak is typically found (**Figure 2.67** c-d). In the oxic PHD2:Fe(III):FG-4592 complex (**Figure 2.85** d), the shielded methyl peak that is found in the same position as the shielded methyl for the PHD2:Fe(II):FG-4592 complex is not observed. One possible explanation is the existence of a reducing agent in the protein solution at low concentration, creating a small concentration of Fe(II) in the anoxic sample. The presence of a reducing agent in solution was not indicated by ^{1}H NMR but is still a possibility (a protein-bound reducing agent would give peaks too broad to observe). It is also possible that PHD2 itself—or Fe(II) in solution, or PHD2-bound Fe(II)—acts as a reducing agent. This set of experiments (**Figure 2.85** c-d) was repeated yielding the same results. Further consideration of the potential cause of these observations was explored in the following experiments.

When FG-4592 was added to the oxic/anoxic PHD2:Fe(III):2OG complexes (**Figure 2.85** e-f), the resultant spectra seemed to best match the oxic/anoxic PHD2:Fe(III):2OG complexes, as analysed by the region between 9 and 12 ppm. Therefore, it is proposed that the oxic/anoxic PHD2:Fe(III):2OG complexes are stable against FG-4592 binding in a similar way to the oxic PHD2:Fe(II):2OG complex (**Figure 2.67** f). This observation further supports the theory that the oxic PHD2:Fe(II):2OG complex is an Fe(III) complex.

When these complexes were left for ~15 hours, the oxic/anoxic PHD2:Fe(III):2OG complexes were partially disrupted by FG-4592, as evidenced by the shielded methyl peak appearing around -0.8 ppm (**Figure 2.85** g-h). Both the oxic and anoxic spectra experienced the same level of displacement by FG-4592. It is still possible that the -0.8 ppm peak belongs to the oxic/anoxic PHD2:Fe(II):FG-4592 complexes

(**Figure 2.67** c-d) from reduction of the active-site metal through catalysis, but for now it will be assumed to be evidence of oxic/anoxic PHD2:Fe(III):FG-4592 complex formation, as this seems like the most likely cause.

From these studies, it was determined that the oxic/anoxic PHD2:Fe(III):2OG complexes are resistant to FG-4592 binding (**Figure 2.85** e-h), but to a lesser extent than the oxic PHD2:Fe(II):2OG (**Figure 2.67** f, h) complex (likely a different PHD2:Fe(III):2OG complex, as discussed above). This observation supports the hypothesis that the oxic PHD2:Fe(II):2OG complex is an Fe(III) complex (from oxidation of the Fe(II)), but the Fe(III) formed at the active site of PHD2 is more tightly bound than in the case where Fe(III) is added to solution.. Another hypothesis is that FG-4592 is less able to bind to Fe(III), a possibility which was explored in work described further in this section.

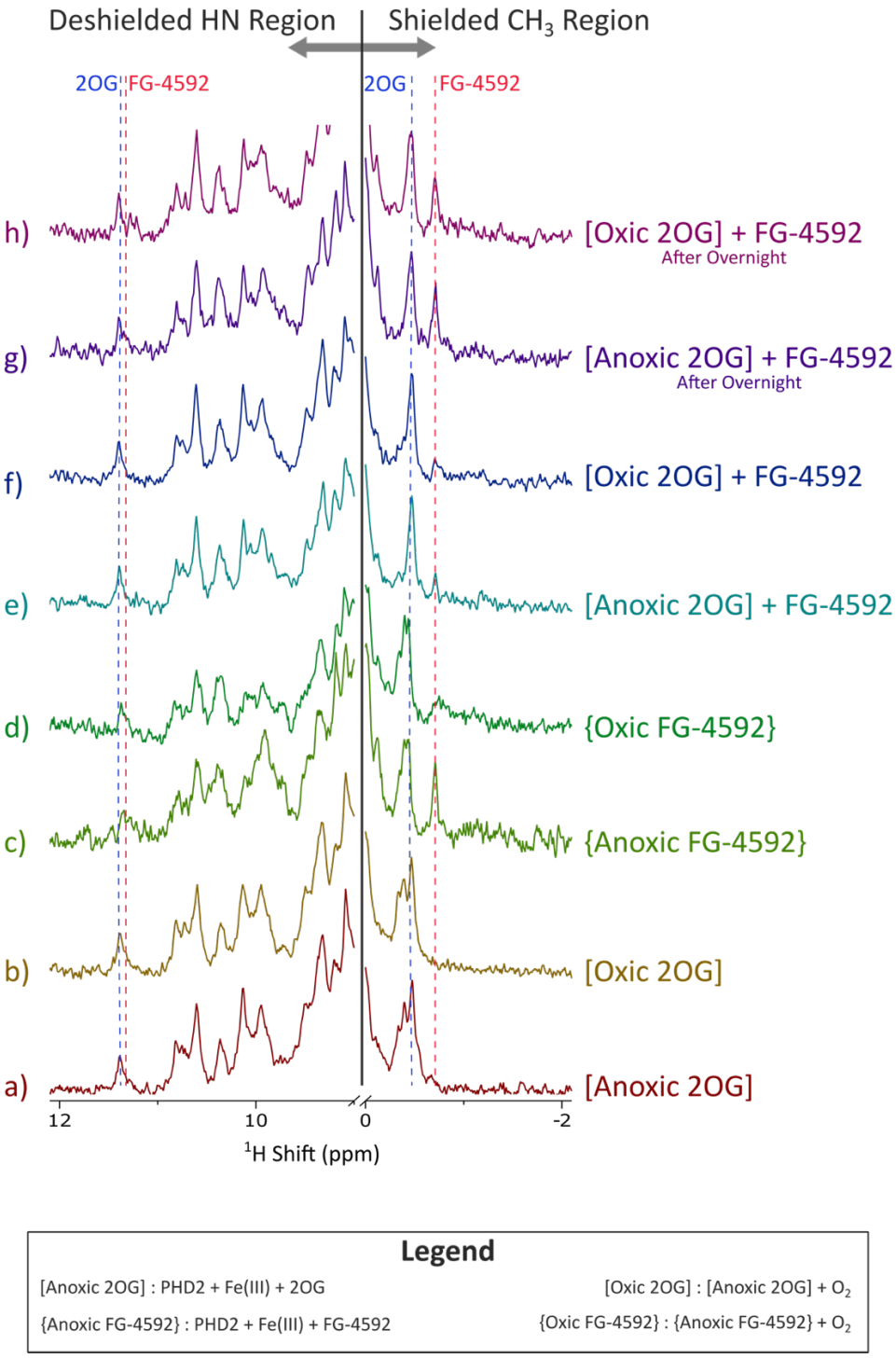


Figure 2.85 *^{1}H NMR spectra of the competition between 2OG and FG-4592 for PHD2:Fe(III) binding. The labels in the figure above each spectrum indicates the starting complex. Each component after a "+" was added to solution in the order written from left to right. Controls: a) PHD2:Fe(III):2OG, b) PHD2:Fe(III):2OG + O_2, c) PHD2:Fe(III):FG-4592, d) PHD2:Fe(III):FG-4592 + O_2. Inhibitor competition: e) PHD2:Fe(III):2OG + FG-4592 → PHD2:Fe(III):2OG, f) PHD2:Fe(III):2OG + O_2 +*

FG-4592 → PHD2:Fe(III):2OG + O_2. Inhibitor binding over time: g) PHD2:Fe(III):2OG + FG-4592 → PHD2:Fe(III):2OG + PHD2:Fe(III):FG-4592 after ~15 hours at room temperature, h) PHD2:Fe(III):2OG + O_2 + FG-4592 → PHD2:Fe(III):2OG + O_2 + PHD2:Fe(III):FG-4592 after ~15 hours at room temperature. The dotted red lines indicate the characteristic shifts of the FG-4592 complex (though the position of the deshielded peak is inexact in this spectrum) and the dotted blue lines indicate the characteristic shifts of the 2OG complex. These shifts were used to investigate the identity of the bound species (ligand or inhibitor). The black, vertical separating line indicates the position where the region from 0 to 9 ppm of the spectrum was removed for simplicity. The oxic and anoxic PHD2:Fe(III):2OG complexes have been found to be more stable against FG-4592 binding than the anoxic PHD2:Fe(II):2OG complex but less stable than the PHD2:Fe(II):2OG complex. Standard concentrations of each component were: 100 μM unlabelled PHD2, 300 μM Fe(III), 500 μM 2OG, 500 μM FG-4592, <2 ppm O_2 pressure (anoxic), and room pressure O_2 (oxic). Buffer conditions were 135 mM NaCl, 10% D_2O, and 90% 50 mM Tris-d_{11} pH 7.5.

Next, the Fe(III) complexes of NOG were evaluated for complex stability. On addition of FG-4592 to the oxic/anoxic PHD2:Fe(III):NOG complexes (**Figure 2.86** e-f), a minor peak indicating FG-4592 binding was observed. This indicates that the oxic/anoxic PHD2:Fe(III):NOG complexes (**Figure 2.86** e-f) are more stable than the oxic/anoxic PHD2:Fe(II):NOG complexes (**Figure 2.69** e-f). Again, it is uncertain if this stability is due to Fe(III) being a weaker binder of FG-4592 than Fe(II), or if the PHD2 complexes in the presence of ligand are stabilised by Fe(III). The ligand does seem to have an impact, since initial displacement of the ligand complex by FG-4592 was slower with 2OG than NOG.

After ~15 hours, the oxic/anoxic PHD2:Fe(III):NOG complexes had been further displaced by FG-4592 (**Figure 2.86** g-h). This observation is along similar lines to what had been observed for the 2OG complexes.

From these studies, it was found that the presence of Fe(III) seems to help stabilise the oxic/anoxic PHD2:Fe(III):NOG complexes against FG-4592 binding, but to a lesser extent than oxic PHD2:Fe(II):2OG (which is in the Fe(III) form) was stabilised.

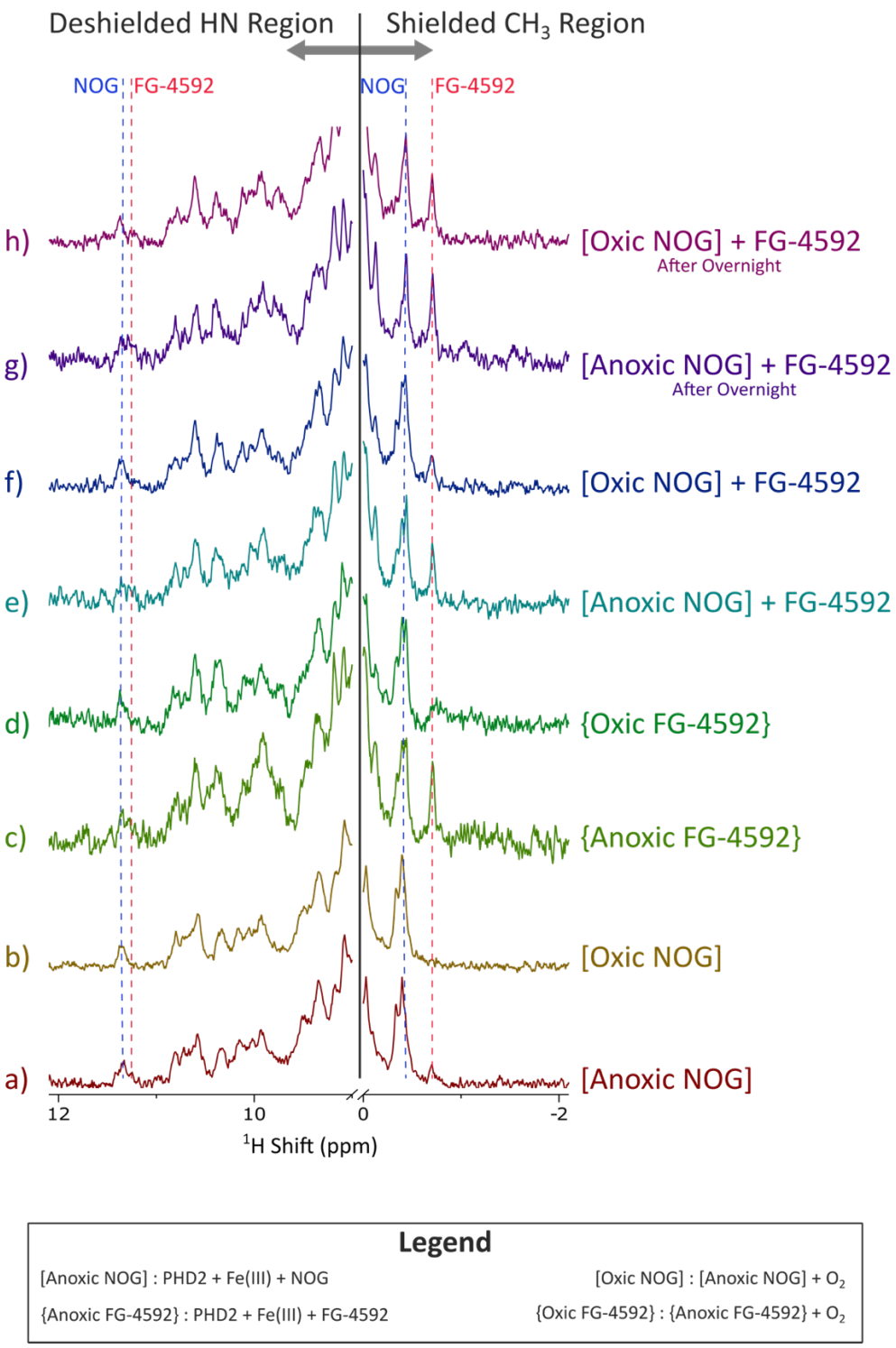


Figure 2.86 *^{1}H spectra of the competition between NOG and FG-4592 for PHD2:Fe(III) binding. The labels in the figure above each spectrum indicates the starting complex. Each component after a "+" was added to solution in the order written from left to right. Controls: a) PHD2:Fe(III):NOG, b) PHD2:Fe(III):NOG + O_2, c) PHD2:Fe(III):FG-4592, d) PHD2:Fe(III):FG-4592 + O_2. Inhibitor competition: e) PHD2:Fe(III):NOG +*

FG-4592 → PHD2:Fe(III):NOG + PHD2:Fe(III):FG-4592 (minor), f) PHD2:Fe(III):NOG + O_2 + FG-4592 → PHD2:Fe(III):NOG + O_2 + PHD2:Fe(III):FG-4592 + O_2 (minor). Inhibitor binding over time: g) PHD2:Fe(III):NOG + FG-4592 → PHD2:Fe(III):NOG + PHD2:Fe(III):FG-4592 after ~15 hours at room temperature, h) PHD2:Fe(III):NOG + O_2 + FG-4592 → PHD2:Fe(III):NOG + O_2 + PHD2:Fe(III):FG-4592 after ~15 hours at room temperature. The dotted red lines indicate the characteristic shifts of the FG-4592 complex (though the position of the deshielded peak is inexact in this spectrum) and the dotted blue lines indicate the characteristic shifts of the NOG complex. These shifts were used to investigate the identity of the bound species (ligand or inhibitor). The black, vertical separating line indicates the position where the region from 0 to 9 ppm of the spectrum was removed for simplicity. The oxic and anoxic PHD2:Fe(III):NOG complexes are more stable against FG-4592 binding than the PHD2:Fe(II):NOG complexes. Standard concentrations of each component were: 100 μM unlabelled PHD2, 300 μM Fe(III), 1 mM NOG, 500 μM FG-4592, <2 ppm O_2 pressure (anoxic), and room pressure O_2 (oxic). Buffer conditions were 135 mM NaCl, 10% D_2O, and 90% 50 mM Tris-d_{11} pH 7.5.

Analysis of the PHD2:Fe(III):2HG complexes yielded surprising results. On addition of FG-4592 to the oxic/anoxic PHD2:Fe(III):2HG complexes (**Figure 2.87** e-f), almost no 2HG was displaced by FG-4592 binding. This appears to be along the same pattern of stability as observed for the 2OG complexes. After ~15 hours, FG-4592 mediated displacement of the oxic/anoxic PHD2:Fe(III):2HG complexes (**Figure 2.87** g-h) occurred to a similar extent as observed in the oxic/anoxic PHD2:Fe(III):2OG (**Figure 2.85** g-h) and oxic/anoxic PHD2:Fe(III):NOG (**Figure 2.86** g-h) complexes. The level of stability of the PHD2:Fe(III):2HG complexes against FG-4592 binding matched the stability observed in the 2OG complexes more closely than that observed for the NOG complexes. This may be due to NOG binding more weakly to the PHD2:Fe(III) complex than either 2OG or 2HG. This observation hints that the behaviour of each ligand in the Fe(III) complexes does not necessarily mirror what was observed for Fe(II) complexes.

From these studies it was found that the stability behaviour of the oxic/anoxic PHD2:Fe(III):2HG complexes (**Figure 2.87** e-h) is similar to that of the oxic/anoxic PHD2:Fe(III):2OG complexes (**Figure 2.85** e-h).

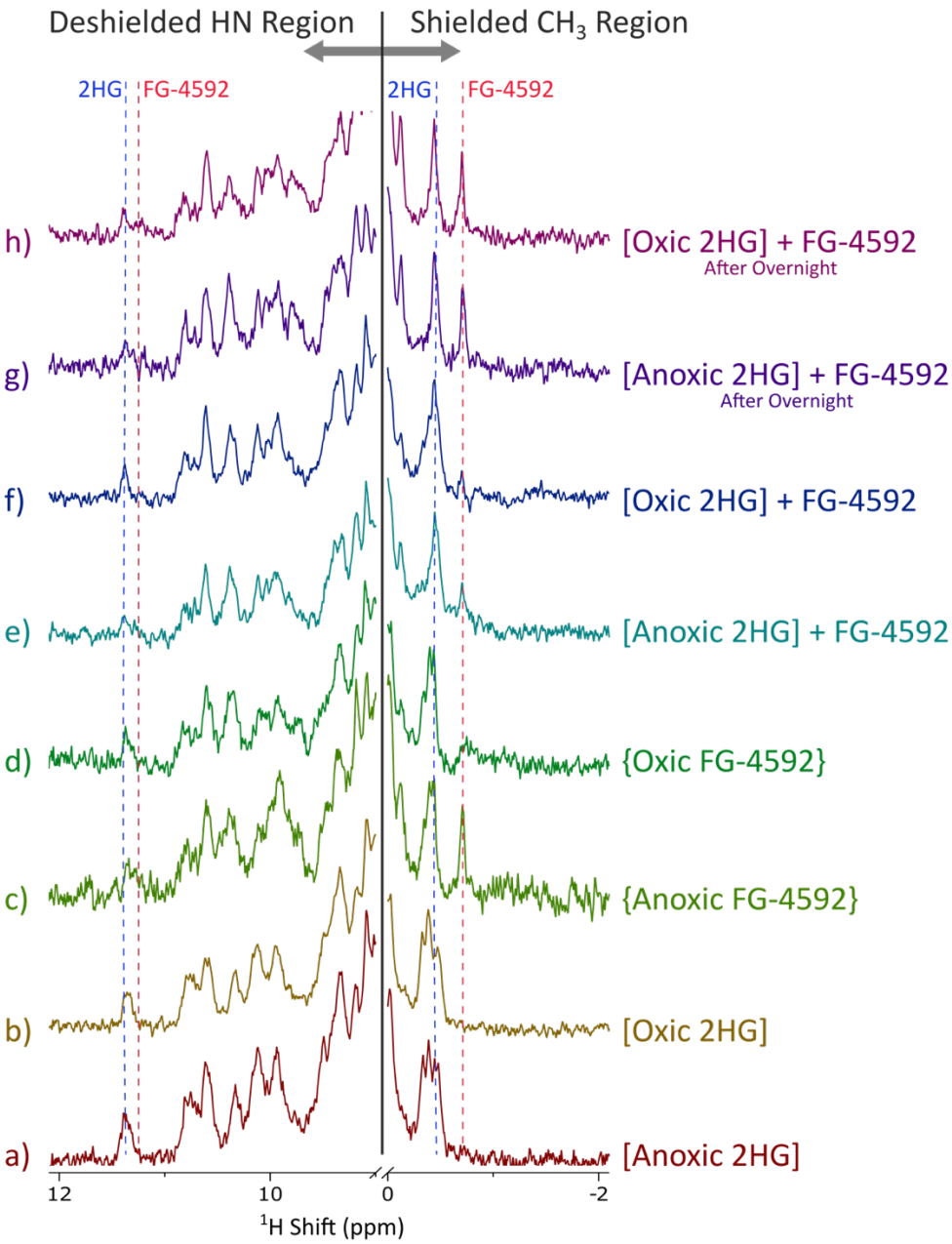


Figure 2.87 *^{1}H spectra of the competition between 2HG and FG-4592 for PHD2:Fe(III) binding. The labels in the figure above each spectrum indicates the starting complex. Each component after a "+" was added to solution in the order written from left to right. Controls: a) PHD2:Fe(III):2HG, b) PHD2:Fe(III):2HG + O_2, c) PHD2:Fe(III):FG-4592, d) PHD2:Fe(III):FG-4592 + O_2. Inhibitor competition: e) PHD2:Fe(III):2HG + FG-4592 → PHD2:Fe(III):2HG, f) PHD2:Fe(III):2HG + O_2 + FG-4592 →*

PHD2:Fe(III):2HG + O_2. Inhibitor binding over time: g) PHD2:Fe(III):2HG + FG-4592 → PHD2:Fe(III):2HG + PHD2:Fe(III):FG-4592 after ~15 hours at room temperature, h) PHD2:Fe(III):2HG + O_2 + FG-4592 → PHD2:Fe(III):2HG + O_2 + PHD2:Fe(III):FG-4592 after ~15 hours at room temperature. The dotted red lines indicate the characteristic shifts of the FG-4592 complex (though the position of the deshielded peak is inexact in this spectrum) and the dotted blue lines indicate the characteristic shifts of the 2HG complex. These shifts were used to investigate the identity of the bound species (ligand or inhibitor). The black, vertical separating line indicates the position where the region from 0 to 9 ppm of the spectrum was removed for simplicity. The level of displacement observed for the oxic and anoxic PHD2:Fe(III):2HG complexes closely matched what was observed for oxic and anoxic PHD2:Fe(III):2OG complexes. Standard concentrations of each component were: 100 μM unlabelled PHD2, 300 μM Fe(III), 1 mM 2HG, 500 μM FG-4592, <2 ppm O_2 pressure (anoxic), and room pressure O_2 (oxic). Buffer conditions were 135 mM NaCl, 10% D_2O, and 90% 50 mM Tris-d_{11} pH 7.5.

The next cosubstrate mimic to be investigated was succinate. As mentioned in the Fe(II) complex studies of succinate, Fe(III) studies were of interest since they could help to elucidate how succinate release occurs during catalysis.

On addition of FG-4592 to the oxic/anoxic PHD2:Fe(III):succinate complexes (**Figure 2.88** e-f), there was substantial displacement of succinate from the anoxic complex, but no displacement in the oxic complex. Considering the pattern of peaks in the 9-12 ppm region of these spectra, it is possible that there is no succinate binding and, therefore, the observed spectra are the oxic/anoxic PHD2:Fe(III):FG-4592 spectra (**Figure 2.88** c-d). Surprisingly, after ~15 hours, the anoxic PHD2:Fe(III):succinate complex was further displaced by FG-4592 (**Figure 2.88** g), but the oxic PHD2:Fe(III):succinate complex was minimally/not displaced (**Figure 2.88** h). The lack of displacement in the oxic complex is to a greater degree than is observed for Fe(III) 2OG complexes. This would suggest that succinate is playing an active role in stabilising

the oxic complex, despite it appearing as if succinate is not bound (from 9-12 ppm spectral analysis). These results should be repeated in case of error.

From these studies it was found that succinate may not bind to the PHD2:Fe(III) complex in a way that effects the structure but may have some role in stabilising the Fe(III) complex, though further analysis is needed.

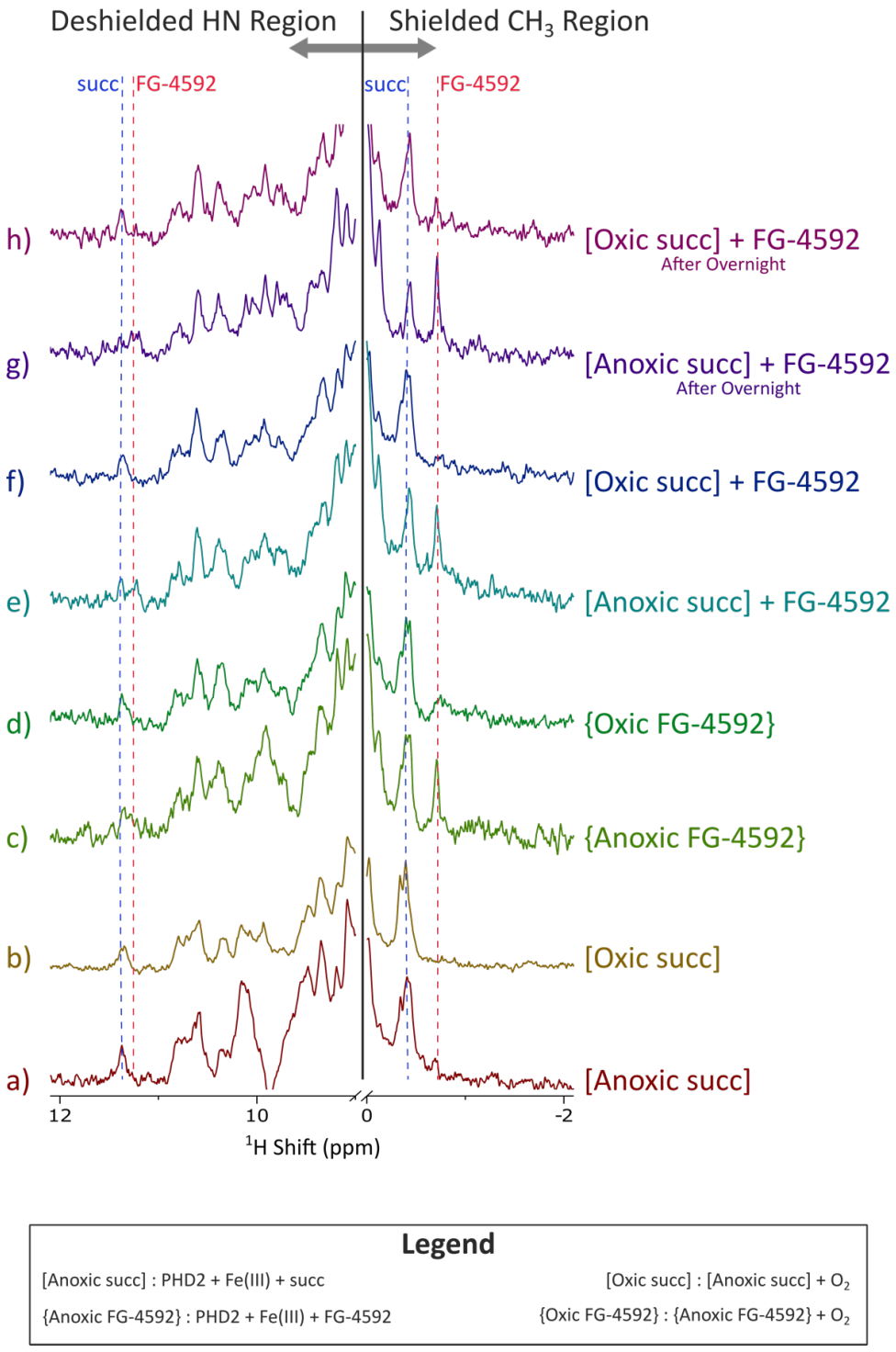


Figure 2.88 *^{1}H spectra of the competition between succinate (succ) and FG-4592 for PHD2:Fe(III) binding. The labels in the figure above each spectrum indicates the starting complex. Each component after a "+" was added to solution in the order written from left to right. Controls: a) PHD2:Fe(III):succ, b) PHD2:Fe(III):succ + O_2, c) PHD2:Fe(III):FG-4592, d) PHD2:Fe(III):FG-4592 + O_2. Inhibitor competition: e) PHD2:Fe(III):succ + FG-4592 → PHD2:Fe(III):succ + PHD2:Fe(III):FG-4592, f)*

PHD2:Fe(III):succ + O_2 + FG-4592 → PHD2:Fe(III):succ + O_2. Inhibitor binding over time: g) PHD2:Fe(III):succ + FG-4592 → PHD2:Fe(III):succ + PHD2:Fe(III):FG-4592 after ~15 hours at room temperature, h) PHD2:Fe(III):succ + O_2 + FG-4592 → PHD2:Fe(III):succ + O_2 after ~15 hours at room temperature. The dotted red lines indicate the characteristic shifts of the FG-4592 complex (though the position of the deshielded peak is inexact in this spectrum) and the dotted blue lines indicate the characteristic shifts of the succ complex. These shifts were used to investigate the identity of the bound species (ligand or inhibitor). The black, vertical separating line indicates the position where the region from 0 to 9 ppm of the spectrum was removed for simplicity. Minimal displacement of the oxic PHD2:Fe(III):succinate complex was observed. Standard concentrations of each component were: 100 μM unlabelled PHD2, 300 μM Fe(III), 1 mM succinate, 500 μM FG-4592, <2 ppm O_2 pressure (anoxic), and room pressure O_2 (oxic). Buffer conditions were 135 mM NaCl, 10% D_2O, and 90% 50 mM Tris-d_{11} pH 7.5.

Next, the fumarate complexes were analysed. Initial analysis of the oxic/anoxic PHD2:Fe(III):fumarate complexes (**Figure 2.89** a-b) revealed that the anoxic complex has hints of an Fe(II) complex peak present. On repetition of this experiment, this peak remained (and the rest of the results were also identical). The cause of this anomaly is still unclear but appears to be a genuine facet of the anoxic PHD2:Fe(III):fumarate complex under these conditions. This peak can also be seen in small quantities for the anoxic PHD2:Fe(III):succ complex (**Figure 2.88** a). The presence of this peak shouldn't affect the experiment as the Fe(II) will get quickly oxidised.

Addition of FG-4592 to the oxic/anoxic PHD2:Fe(III):fumarate complexes (**Figure 2.89** e-f) gave results similar to those observed for succinate. The oxic and anoxic spectra matched the pattern expected of FG-4592 binding (**Figure 2.89** c-d). Over a ~15 hour period, the relative displacement of FG-4592 in the oxic/anoxic PHD2:Fe(III):fumarate complexes (**Figure 2.89** g-h) was similar to what had been

observed for succinate under similar conditions (**Figure 2.88** g-h, which was slight further displacement of fumarate by FG-4592).

This observation has two likely possible causes: 1) succinate binding to Fe(III) under oxic conditions is stronger than would be expected, or 2) the PHD2:Fe(III) complex does not efficiently bind succinate or fumarate, but instead other ligands may destabilise the Fe(III) complexes more than weak ligands such as succinate. The second suggestion is probably more likely.

From these studies it has been found that fumarate interacts with the PHD2:Fe(III) complex in a similar way to succinate, likely, at least in part, because both exhibit the same weakly binding monodentate Fe-binding mode. These observations should be further studied.

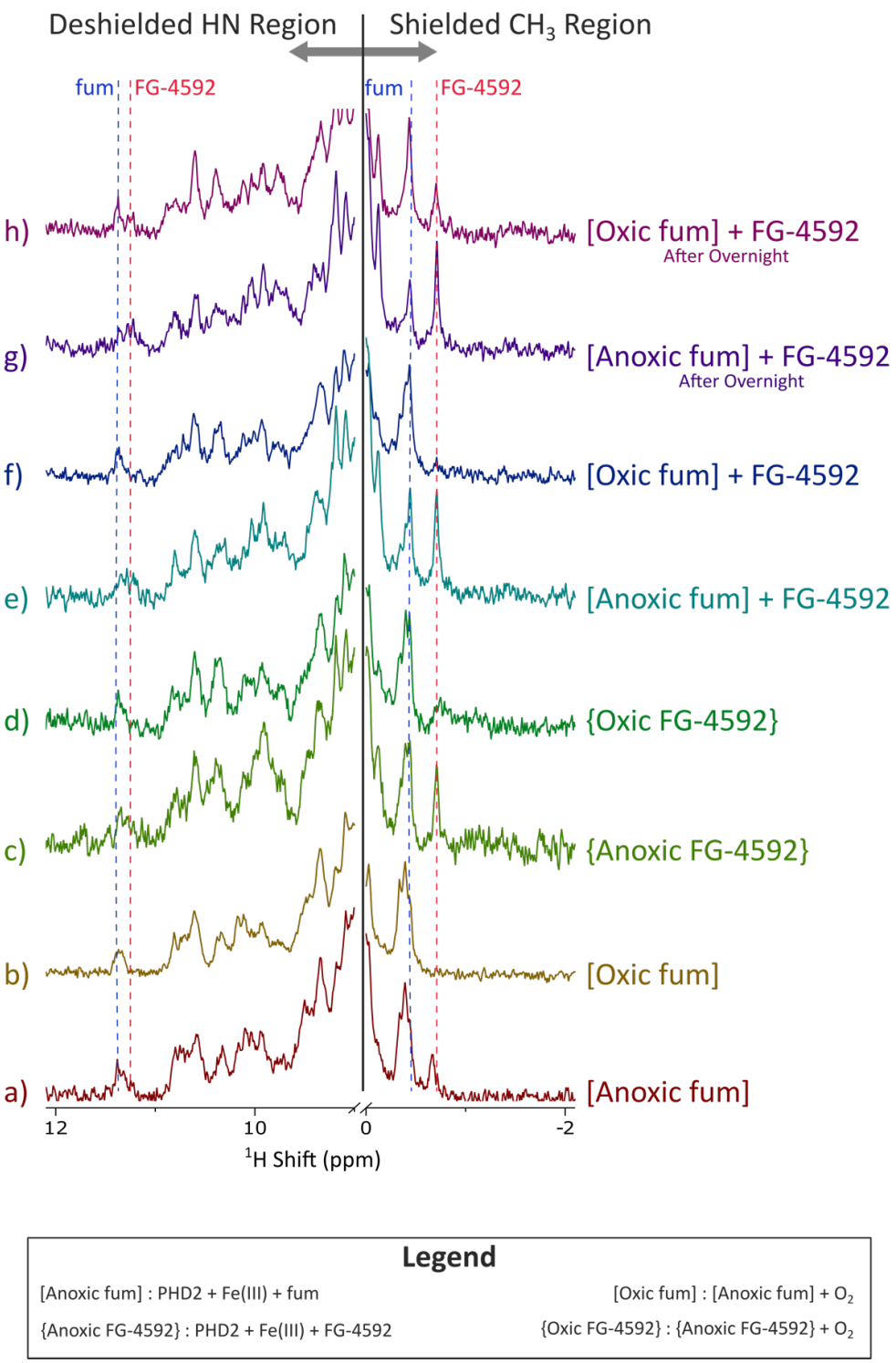


Figure 2.89 *^{1}H spectra of the competition between fumarate (fum) and FG-4592 for PHD2:Fe(III) binding. The labels in the figure above each spectrum indicates the starting complex. Each component after a "+" was added to solution in the order written from left to right. Controls: a) PHD2:Fe(III):fum, b) PHD2:Fe(III):fum:O_2, c) PHD2:Fe(III):FG-4592, d) PHD2:Fe(III):FG-4592:O_2. Inhibitor competition: e)*

PHD2:Fe(III):fum + FG-4592 → PHD2:Fe(III):fum + PHD2:Fe(III):FG-4592, f) PHD2:Fe(III):fum:O_2 + FG-4592 → PHD2:Fe(III):fum:O_2. Inhibitor binding over time: g) PHD2:Fe(III):fum + FG-4592 → PHD2:Fe(III):fum + PHD2:Fe(III):FG-4592 after ~15 hours at room temperature, h) PHD2:Fe(III):fum:O_2 + FG-4592 → PHD2:Fe(III):fum:O_2 + PHD2:Fe(III):FG-4592:O_2 after ~15 hours at room temperature. The dotted red lines indicate the characteristic shifts of the FG-4592 complex (though the position of the deshielded peak is inexact in this spectrum) and the dotted blue lines indicate the characteristic shifts of the succ complex. These shifts were used to investigate the identity of the bound species (ligand or inhibitor). The black, vertical separating line indicates the position where the region from 0 to 9 ppm of the spectrum was removed for simplicity. The PHD2:Fe(III):fum spectra match what was observed for the PHD2:Fe(III):succ spectra. Standard concentrations of each component were: 100 μM unlabelled PHD2, 300 μM Fe(III), 1 mM fumarate, 500 μM FG-4592, <2 ppm O_2 pressure (anoxic), and room pressure O_2 (oxic). Buffer conditions were 135 mM NaCl, 10% D_2O, and 90% 50 mM Tris-d_{11} pH 7.5.

Key results arising from these studies are: 1) Fe(III) is challenging to work with as it exbibits more overlapping peaks than had been observed with other compositions, 2) the stability of weakly binding, 2OG-dissimilar ligands is improved by Fe(III) over Fe(II) binding, 3) overall complex stability is improved by Fe(III), 4) 2OG is not necessarily the strongest binder under the Fe(III) conditions (when the Fe(III) is not produced enzymatically), and 5) FG-4592 binds better to PHD2:Fe(II) than PHD2:Fe(III).

Fe(III) Ligand Complexes				
Ligand	*Oxygen?*	*PHD2:Fe(III):L*	*PHD2:Fe(III):L + I*	*PHD2:Fe(III):L +I (overnight)*
2OG	anoxic	100% L	95% L, 5% I	60% L, 30% I
	oxic	100% L	95% L, 5% I	60% L, 30% I
NOG	anoxic	100% L	60% L, 30% I	50% L, 50% I
	oxic	100% L	95% L, 5% I	60% L, 30% I
2HG	anoxic	100% L	95% L, 5% I	50% L, 50% I
	oxic	100% L	95% L, 5% I	50% L, 50% I
succ	anoxic	100% L	50% L, 50% I	50% L, 50% I
	oxic	100% L	100% L	95% L, 5% I
fum	anoxic	100% L	50% L, 50% I	60% L, 30% I
	oxic	100% L	100% L	90% L 10% I

Table 2.4 *Compiled description of PHD2:Fe(III):ligand complex stabilities against inhibitor binding. Green indicates almost full retention of the ligand complex, yellow indicates approximately equal retention of the ligand complex and displacement by inhibitor, and red indicates almost complete ligand displacement by inhibitor. Oxic and anoxic results are differentiated.*

2.2.4.4 Studies on the Stabilities of PHD2:Fe(III):Ligand:Substrate Complexes

The last set of data needed to complete the oxic/anoxic Fe(II)/Fe(III) ligand +/- substrate studies of the stability of PHD2 complexes was the Fe(III):ligand:substrate complexes. It was envisaged that these studies would indicate: 1) if PHD2:Fe(III):ligand:substrate complexes were more stable than their corresponding PHD2:Fe(II):ligand:substrate complexes and PHD2:Fe(III):ligand complexes (as may be expected since generally both Fe(III) and substrate appear to stabilise PHD2 complexes), 2) if substrate binds to the PHD2:Fe(III):ligand complexes, and 3) if Fe(III) complexes were more stable in the presence or absence of substrate.

Starting with the 2OG:CODD complexes, the addition of CODD to the oxic/anoxic PHD2:Fe(III):2OG complexes appeared to give distinct peaks in the 9-12 ppm region of the spectra (**Figure 2.90** g-h). This observation seems to suggest CODD is binding these complexes. On addition of FG-4592 to the complexes, no displacement of 2OG:CODD was observed (**Figure 2.90** i-j). After ~ 15 hours, the oxic/anoxic

PHD2:Fe(III):2OG:CODD complexes still appeared not to have been displaced (**Figure 2.90** k-l).

Comparison of these behaviours to the oxic/anoxic PHD2:Fe(II):2OG:CODD complexes (**Figure 2.80** i-l) under similar conditions indicates similar initial stability against FG-4592 binding, but even greater binding stability in the anoxic PHD2:Fe(III):2OG:CODD complex over time than in the anoxic PHD2:Fe(III):2OG:CODD complex. This observation supports the hypothesis that the oxic PHD2:Fe(II):2OG:CODD complex (**Figure 2.80** h) is actually an Fe(III) complex, as it exhibits the same behaviour as the Fe(III) complexes discussed here. It should be noted that, as was observed when comparing the oxic PHD2:Fe(II):2OG complex (**Figure 2.67** b) to the oxic/anoxic PHD2:Fe(III):2OG complexes (**Figure 2.85** a-b), the oxic/anoxic PHD2:Fe(III):2OG:CODD complexes (**Figure 2.90** g-h) have more/overlapped peaks in the shielded methyl region than is observed in the oxic PHD2:Fe(II):2OG:CODD spectrum (**Figure 2.80** h).

If we then compare the stability of the oxic/anoxic PHD2:Fe(III):2OG complexes (**Figure 2.85** e-h) to the oxic/anoxic PHD2:Fe(III):2OG:CODD complexes (**Figure 2.90** i-l), it is apparent that the addition of CODD increases the stability of the Fe(III) complexes.

From these studies, it was found that: 1) Fe(III) confers more stability to the 2OG:CODD complexes than Fe(II), 2) the presence of CODD further stabilises the oxic/anoxic PHD2:Fe(III):2OG complexes, and 3) the oxic and anoxic PHD2:Fe(III):2OG:CODD complexes behave similarly.

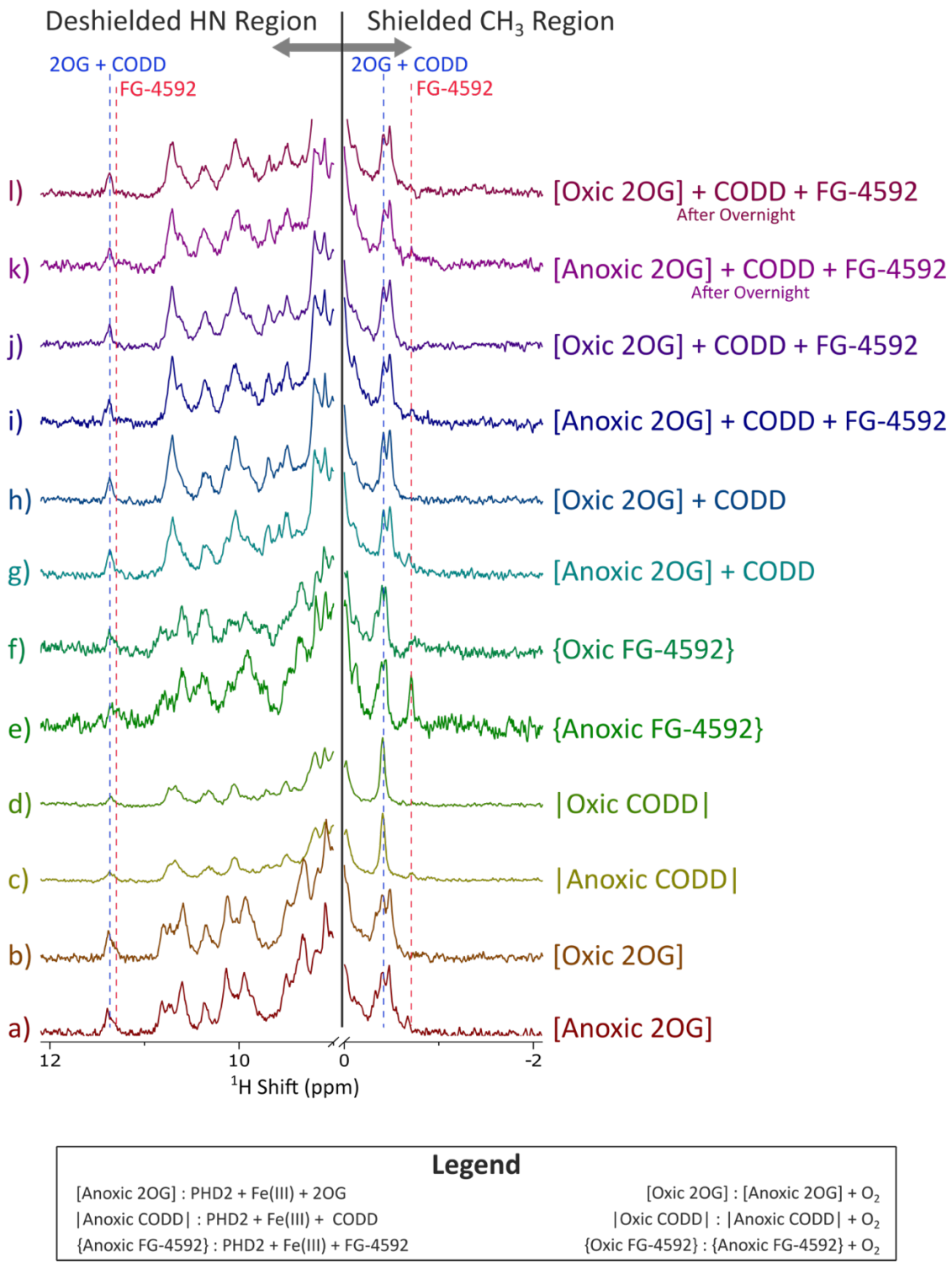


Figure 2.90 *^{1}H spectra of the competition between 2OG:CODD and FG-4592 for PHD2:Fe(III) binding. The labels in the figure above each spectrum indicates the starting complex. Each component after a "+" was added to solution in the order written from left to right. Controls: a) PHD2:Fe(III):2OG, b) PHD2:Fe(III):2OG:O_2, c) PHD2:Fe(III):CODD, d) PHD2:Fe(III):CODD:O_2 e) PHD2:Fe(III):FG-4592, f)*

PHD2:Fe(III):FG-4592:O_2, g) PHD2:Fe(III):2OG + CODD → PHD2:Fe(III):2OG:CODD, h) PHD2:Fe(III):2OG:O_2 + CODD → PHD2:Fe(III):2OG:CODD:O_2. Inhibitor competition: i) PHD2:Fe(III):2OG:CODD + FG-4592 → PHD2:Fe(III):2OG:CODD, j) PHD2:Fe(III):2OG:CODD:O_2 + FG-4592 → PHD2:Fe(III):2OG:CODD:O_2. Inhibitor binding over time: k) PHD2:Fe(III):2OG:CODD + FG-4592 → PHD2:Fe(III):2OG:CODD after ~15 hours at room temperature, and l) PHD2:Fe(III):2OG:CODD:O_2 + FG-4592 → PHD2:Fe(III):2OG:CODD:O_2 after ~15 hours at room temperature. The dotted red lines indicate the characteristic shifts of the FG-4592 complex (though the position of the deshielded peak is inexact in this spectrum) and the dotted blue lines indicate the characteristic shifts of the 2OG:CODD complex. These shifts were used to investigate the identity of the bound species (ligand:substrate or inhibitor). The black, vertical separating line indicates the position where the region from 0 to 9 ppm of the spectrum was removed for simplicity. The oxic and anoxic PHD2:Fe(III):2OG:CODD complexes have been found to be even more stable against displacement by FG-4592 than the oxic and anoxic PHD2:Fe(III):2OG complexes. Standard concentrations of each component were: 100 μM unlabelled PHD2, 300 μM Fe(III), 500 μM 2OG, 500 μM CODD, 500 μM FG-4592, <2 ppm O_2 pressure (anoxic), and room pressure O_2 (oxic). Buffer conditions were 135 mM NaCl, 10% D_2O, and 90% 50 mM Tris-d_{11} pH 7.5.

Next, the stability of the NOG:CODD complex was evaluated in the presence of Fe(III). On CODD addition to the oxic/anoxic PHD2:Fe(III):NOG complexes (**Figure 2.91** g-h), the anoxic spectrum appeared to have 2 extra peaks in the shielded methyl region than the oxic spectrum. This is likely due to the broadening of the weaker peaks in the oxic sample due to paramagnetic effects. If the oxic/anoxic PHD2:Fe(III):NOG complexes (**Figure 2.91** a-b) were compared to the complexes in the presence of CODD (**Figure 2.91** g-h), there are clear changes in the shielded methyl region, indicating CODD binding.

FG-4592 was then added to the oxic/anoxic PHD2:Fe(III):NOG:CODD complexes (**Figure 2.91** i-j). FG-4592 addition did not disrupt binding of the

PHD2:Fe(III):NOG:CODD complex. After ~15 hours, the oxic PHD2:Fe(III):NOG:CODD complex (**Figure 2.91** l) remained stable against FG-4592 binding, but the anoxic complex (**Figure 2.91** k) was partially displaced. This observation differs from what was observed in the anoxic PHD2:Fe(III):2OG:CODD complex which showed complete stability against FG-4592 binding (**Figure 2.90** i).

On comparison of the oxic/anoxic PHD2:Fe(II):NOG:CODD complexes (**Figure 2.81** i-l) with the oxic/anoxic PHD2:Fe(III):NOG:CODD complexes (**Figure 2.91** i-l) there is a substantial discrepancy in complex stability. In the Fe(II) studies, the PHD2:Fe(II):NOG:CODD complexes are about 50% displaced on initial addition of FG-4592 and are completely displaced after ~15 hours. In the Fe(III) studies, only minor displacement of the PHD2:Fe(III):NOG:CODD complex occurs in the anoxic complex, over ~15 hours.

This increased stability is also seen when comparing the oxic/anoxic PHD2:Fe(III):NOG complexes (**Figure 2.86** e-h) to the oxic/anoxic PHD2:Fe(III):NOG:CODD complexes (**Figure 2.91** i-l). In the absence of CODD, displacement by FG-4592 was observed almost immediately in both oxic and anoxic PHD2:Fe(III):NOG complexes, and displacement continues over time. On the other hand, only the anoxic PHD2:Fe(III):NOG:CODD complex is displaced, although to a small degree. This observation is further evidence that both the Fe(II) and Fe(III) ligand complexes are stabilised by CODD binding.

From these studies, it was found that: 1) Fe(III) seems to afford more stability to the NOG:CODD complexes than does Fe(II), 2) the presence of CODD further stabilises the oxic/anoxic PHD2:Fe(III):NOG complexes, and 3) the anoxic

PHD2:Fe(III):NOG:CODD complex has additional peaks in the shielded methyl region that are broadened out by the presence of paramagnetic species in the oxic complex.

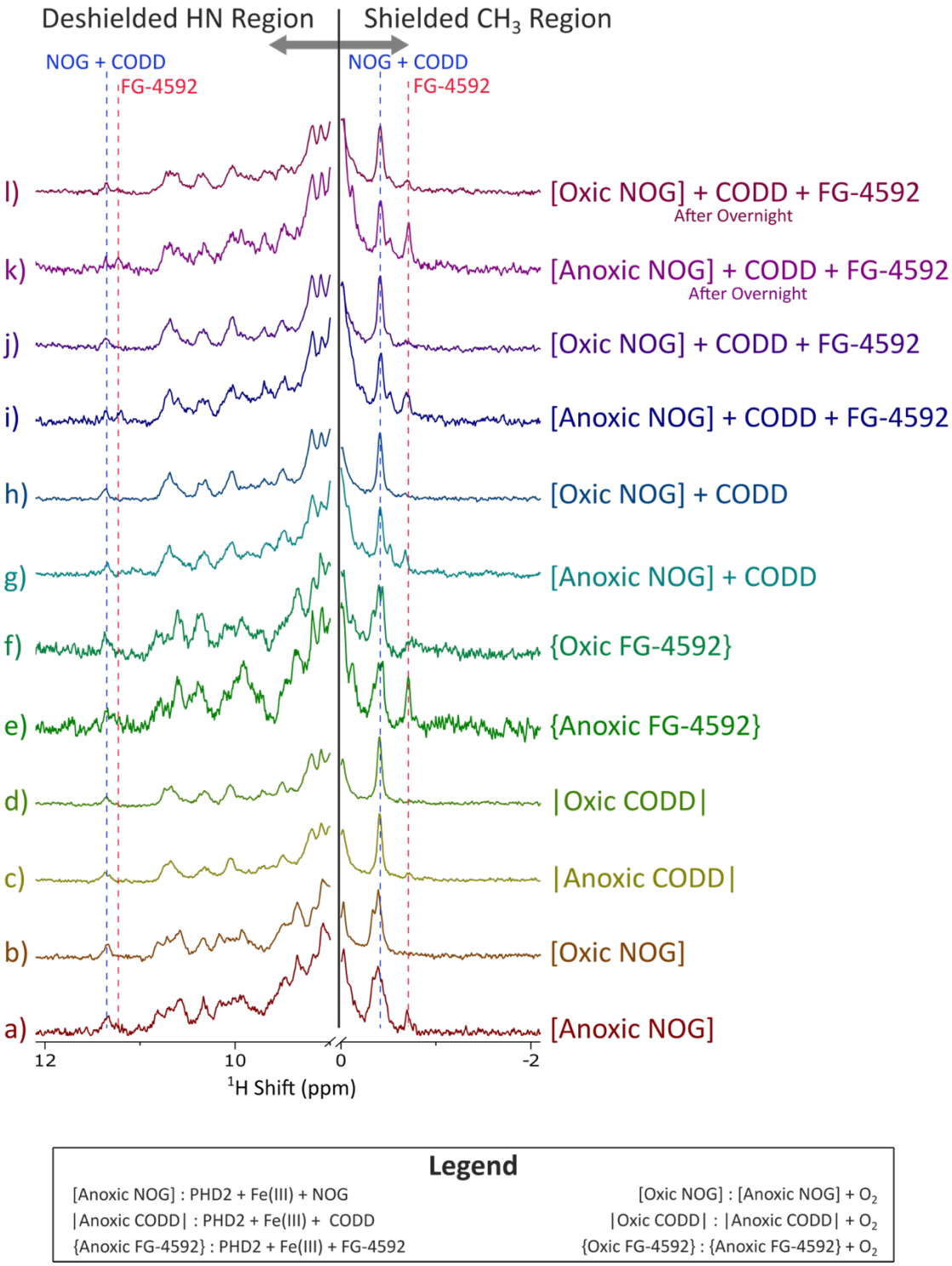


Figure 2.91 *^{1}H spectra of the competition between NOG:CODD and FG-4592 for PHD2:Fe(III) binding. The labels in the figure above each spectrum indicates the starting*

complex. Each component after a "+" was added to solution in the order written from left to right. Controls: a) PHD2:Fe(III):NOG, b) PHD2:Fe(III):NOG + O_2, c) PHD2:Fe(III):CODD, d) PHD2:Fe(III):CODD + O_2 e) PHD2:Fe(III):FG-4592, f) PHD2:Fe(III):FG-4592 + O_2, g) PHD2:Fe(III):NOG + CODD → PHD2:Fe(III):NOG:CODD, h) PHD2:Fe(III):NOG + O_2 + CODD → PHD2:Fe(III):NOG:CODD + O_2. Inhibitor competition: i) PHD2:Fe(III):NOG:CODD + FG-4592 → PHD2:Fe(III):NOG:CODD, j) PHD2:Fe(III):NOG:CODD + O_2 + FG-4592 → PHD2:Fe(III):NOG:CODD + O_2. Inhibitor binding over time: k) PHD2:Fe(III):NOG:CODD + FG-4592 → PHD2:Fe(III):NOG:CODD + PHD2:Fe(III):FG-4592 after ~15 hours at room temperature, and l) PHD2:Fe(III):NOG:CODD + O_2 + FG-4592 → PHD2:Fe(III):NOG:CODD + O_2 after ~15 hours at room temperature. The dotted red lines indicate the characteristic shifts of the FG-4592 complex (though the position of the deshielded peak is inexact in this spectrum) and the dotted blue lines indicate the characteristic shifts of the NOG:CODD complex. These shifts were used to investigate the identity of the bound species (ligand:substrate or inhibitor). The black, vertical separating line indicates the position where the region from 0 to 9 ppm of the spectrum was removed for simplicity. The PHD2:Fe(III):NOG complex is stabilised by the presence of CODD binding, and to a greater extent in the oxic complex. Standard concentrations of each component were: 100 μM unlabelled PHD2, 300 μM Fe(III), 1 mM NOG, 500 μM CODD, 500 μM FG-4592, <2 ppm O_2 pressure (anoxic), and room pressure O_2 (oxic). Buffer conditions were 135 mM NaCl, 10% D_2O, and 90% 50 mM Tris-d_{11} pH 7.5.

2HG was then studied under Fe(III) and CODD conditions. On addition of CODD to the oxic/anoxic PHD2:Fe(III):2HG complex (**Figure 2.92** g-h), a subtle difference in the spectra was observed, indicating that a 2HG:CODD complex is formed. On addition of FG-4592 to the oxic/anoxic PHD2:Fe(III):2HG:CODD complexes (**Figure 2.92** i-j), the anoxic complex showed minimal displacement by FG-4592 and the oxic complex showed no displacement. Over time (~15 hours) only the anoxic complex saw further displacement by FG-4592 whereas the oxic complex appeared relatively stable.

Comparison of the stabilities (with respect to FG-4592 binding) of the oxic/anoxic PHD2:Fe(III):2HG complexes (**Figure 2.87** e-h) with those for the oxic/anoxic PHD2:Fe(III):2HG:CODD complexes (**Figure 2.92** i-l) indicated that the oxic PHD2:Fe(III):2HG complex is stabilised by CODD binding over a short timeframe (< 30 minutes). However, both the oxic and anoxic complexes show greater stability in the presence of CODD over a longer time period (~ 15 hours). This stabilisation appears less pronounced than was observed with the PHD2:Fe(III):NOG:CODD and PHD2:Fe(III):2OG:CODD complexes, an observation which may reflect weaker binding of 2HG to PHD2 as compared to 2OG or NOG binding.

When comparing the stabilities of the oxic/anoxic PHD2:Fe(II):2HG:CODD complexes (**Figure 2.82** i-l) with the oxic/anoxic PHD2:Fe(III):2HG:CODD complexes (**Figure 2.92** i-l), the Fe(III) complexes appear to be more stable than the Fe(II) complexes.

From these studies, it was found that: 1) Fe(III) seems to afford more stability to the 2HG:CODD complexes than the corresponding Fe(II) complexes, 2) The presence of CODD further stabilises the oxic/anoxic PHD2:Fe(III):2HG complexes, and 3) the oxic and anoxic PHD2:Fe(III):2HG:CODD complexes are not equally stable.

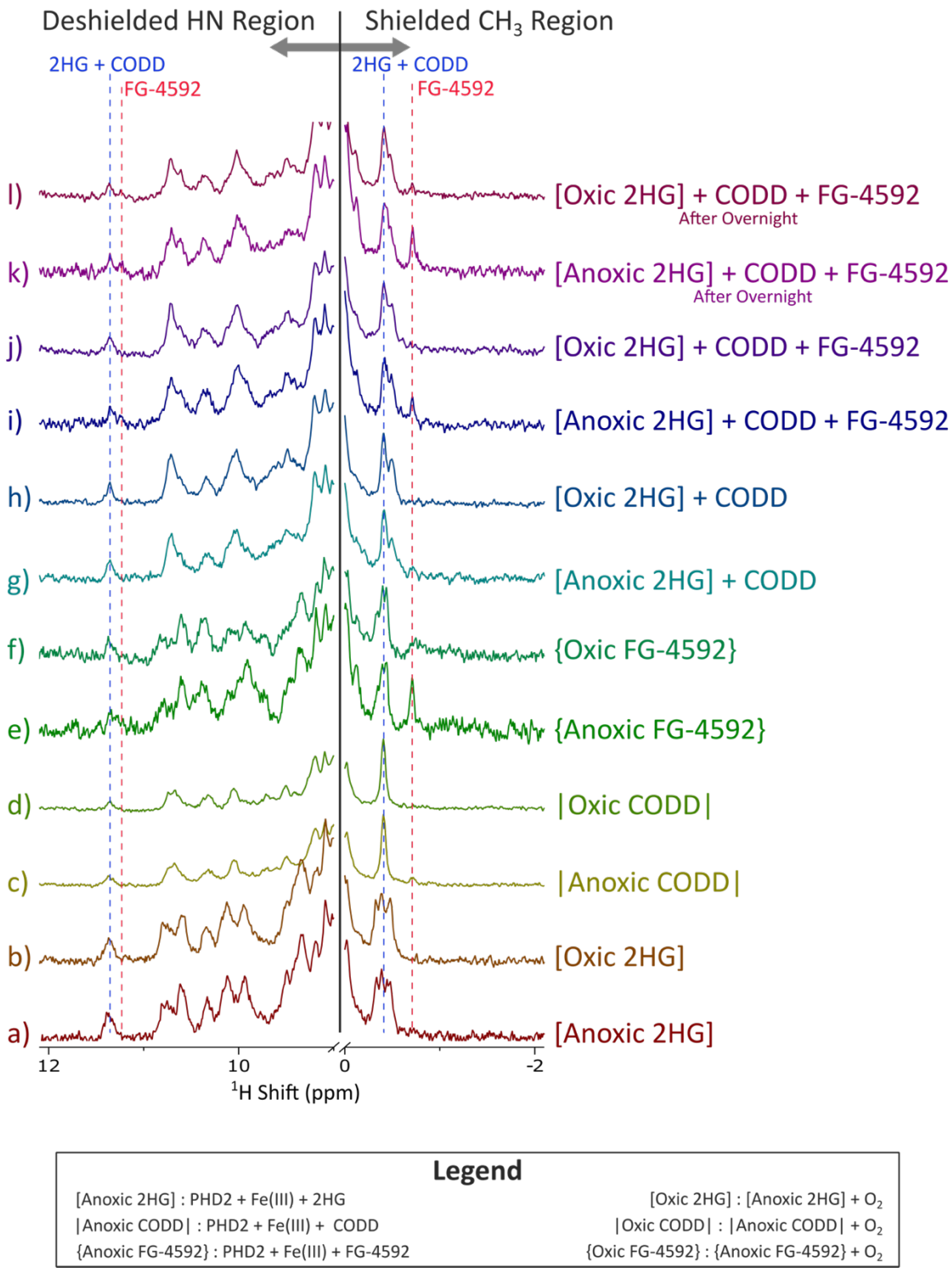


Figure 2.92 *^{1}H spectra of the competition between 2HG:CODD and FG-4592 for PHD2:Fe(III) binding. The labels in the figure above each spectrum indicates the starting complex. Each component after a "+" was added to solution in the order written from left to right. Controls: a) PHD2:Fe(III):2HG, b) PHD2:Fe(III):2HG + O_2, c) PHD2:Fe(III):CODD, d) PHD2:Fe(III):CODD + O_2 e) PHD2:Fe(III):FG-4592, f)*

PHD2:Fe(III):FG-4592 + O_2, g) PHD2:Fe(III):2HG + CODD → PHD2:Fe(III):2HG:CODD, h) PHD2:Fe(III):2HG + O_2 + CODD → PHD2:Fe(III):2HG:CODD + O_2. Inhibitor competition: i) PHD2:Fe(III):2HG:CODD + FG-4592 → PHD2:Fe(III):2HG:CODD + PHD2:Fe(III):FG-4592 (very minor), j) PHD2:Fe(III):2HG:CODD + O_2 + FG-4592 → PHD2:Fe(III):2HG:CODD + O_2. Inhibitor binding over time: k) PHD2:Fe(III):2HG:CODD + FG-4592 → PHD2:Fe(III):2HG:CODD + PHD2:Fe(III):FG-4592 after ~15 hours at room temperature, and l) PHD2:Fe(III):2HG:CODD + O_2 + FG-4592 → PHD2:Fe(III):2HG:CODD + O_2 after ~15 hours at room temperature. The dotted red lines indicate the characteristic shifts of the FG-4592 complex (though the position of the deshielded peak is inexact in this spectrum) and the dotted blue lines indicate the characteristic shifts of the 2HG:CODD complex. These shifts were used to investigate the identity of the bound species (ligand:substrate or inhibitor). The black, vertical separating line indicates the position where the region from 0 to 9 ppm of the spectrum was removed for simplicity. The PHD2:Fe(III):2HG complex is stabilised by the presence of CODD binding, and to a greater extent in the oxic complex. Standard concentrations of each component were: 100 μM unlabelled PHD2, 300 μM Fe(III), 1 mM 2HG, 500 μM CODD, 500 μM FG-4592, <2 ppm O_2 pressure (anoxic), and room pressure O_2 (oxic). Buffer conditions were 135 mM NaCl, 10% D_2O, and 90% 50 mM Tris-d_{11} pH 7.5.

Next, the succinate:CODD complex in the presence of Fe(III) was evaluated. This complex is of interesting because it may give an idea of how succinate escapes the PHD active site after catalysis (CODD may block the exit of succinate).

On addition of CODD to the oxic/anoxic PHD2:Fe(III):succ complex (**Figure 2.93** g-h), the oxic spectrum gives a single peak in the shielded methyl region, whereas the anoxic spectrum gives two peaks. One of these peaks is at a shift of around -0.5 ppm, which is not a commonly observed shift in these studies. Interestingly, on FG-4592 addition to these complexes (**Figure 2.93** i-j), the anoxic complex is partially displaced by FG-4592 binding and, though the peak at -0.4 ppm still partially remains, the peak at -0.5 ppm disappears. The oxic spectrum, on the other hand, shows no displacement by

FG-4592. After additional time (~15 hours), the oxic/anoxic PHD2:Fe(III):succ:CODD complexes manifested no further changes in displacement by FG-4592.

Comparison of the oxic/anoxic PHD2:Fe(III):succ complexes (**Figure 2.88** e-h) with the oxic/anoxic PHD2:Fe(III):succ:CODD complexes (**Figure 2.93** i-l) shows only a minimal increase in stability of the PHD2:Fe(III):succ complexes on CODD addition. Both sets of experiments show similar trends in relative levels of displacement of oxic vs anoxic complexes by FG-4592 binding.

Comparison of oxic/anoxic PHD2:Fe(II):succ:CODD complexes (**Figure 2.83** i-l) with the oxic/anoxic PHD2:Fe(III):succ:CODD complexes (**Figure 2.93** i-l) indicate greater stability of all the Fe(III) complexes over the corresponding Fe(II) complexes; notably, the Fe(II) complex in the presence of CODD showed almost no protection against FG-4592 binding.

From these studies, it was found that: 1) Fe(III) seems to afford more stability to the succ:CODD complexes than Fe(II), 2) The presence of CODD further stabilises the oxic/anoxic PHD2:Fe(III):succ complexes, and 3) the oxic and anoxic PHD2:Fe(III):succ:CODD complexes are not equally stable, as had been observed for the succ complexes. At present the available results do not inform on the mechanism of succinate release, except that succinate likely can bind in the presence of CODD.

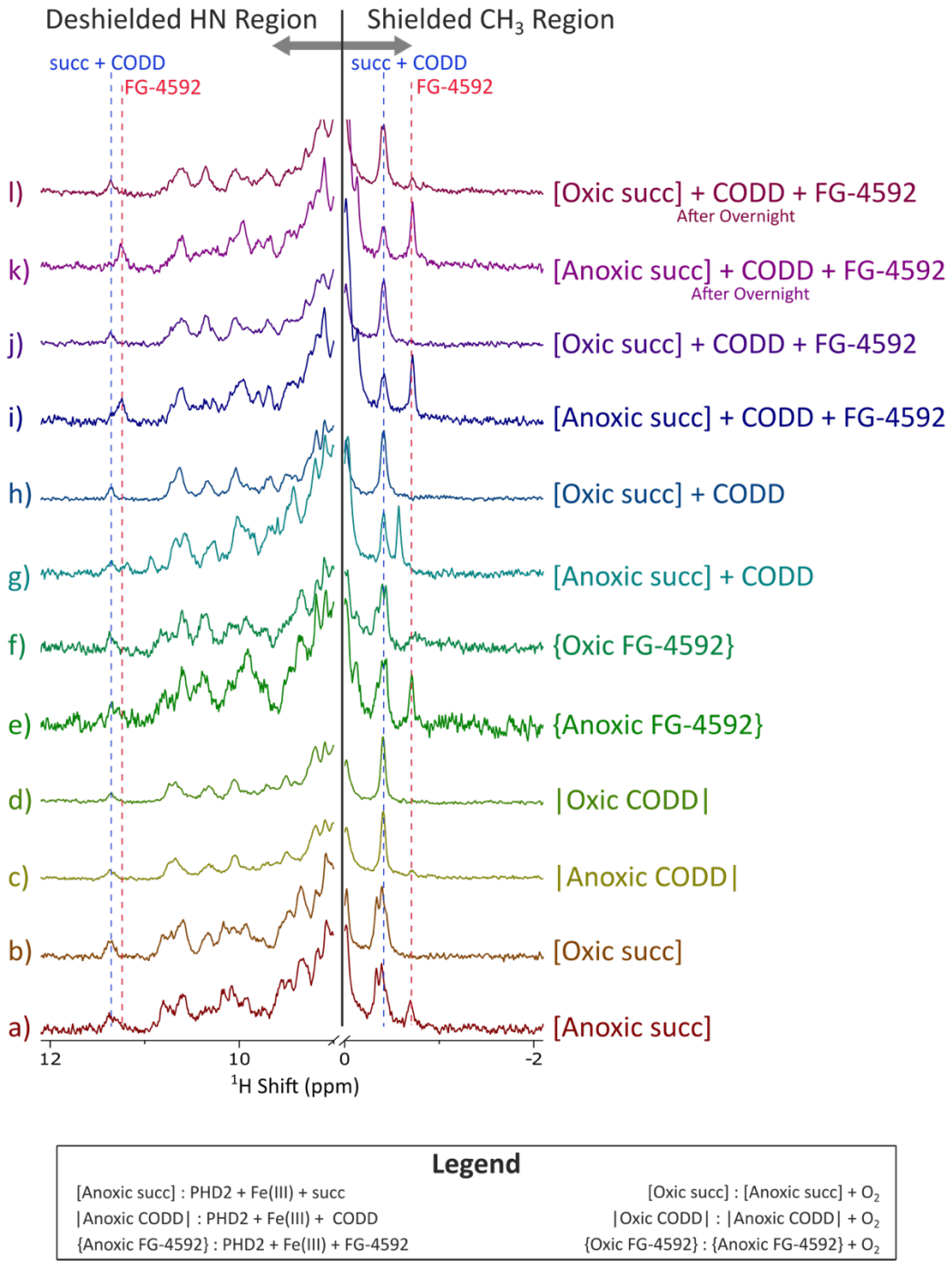


Figure 2.93 *^{1}H NMR spectra of the competition between succinate(succ):CODD and FG-4592 for PHD2:Fe(III) binding. The labels in the figure above each spectrum indicates the starting complex. Each component after a "+" was added to solution in the order written from left to right. Controls: a) PHD2:Fe(III):succ, b) PHD2:Fe(III):succ + O_2, c) PHD2:Fe(III):CODD, d) PHD2:Fe(III):CODD:O_2 e) PHD2:Fe(III):FG-4592, f) PHD2:Fe(III):FG-4592 + O_2, g) PHD2:Fe(III):succ + CODD → PHD2:Fe(III):succ:CODD, h) PHD2:Fe(III):succ + O_2 + CODD →*

PHD2:Fe(III):succ:CODD + O_2. Inhibitor competition: i) PHD2:Fe(III):succ:CODD + FG-4592 → PHD2:Fe(III):succ:CODD + PHD2:Fe(III):FG-4592, j) PHD2:Fe(III):succ:CODD + O_2 + FG-4592 → PHD2:Fe(III):succ:CODD + O_2. Inhibitor binding over time: k) PHD2:Fe(III):succ:CODD + FG-4592 → PHD2:Fe(III):succ:CODD + PHD2:Fe(III):FG-4592 after ~15 hours at room temperature, and l) PHD2:Fe(III):succ:CODD + O_2 + FG-4592 → PHD2:Fe(III):succ:CODD + O_2 after ~15 hours at room temperature. The dotted red lines indicate the characteristic shifts of the FG-4592 complex (though the position of the deshielded peak is inexact in this spectrum) and the dotted blue lines indicate the characteristic shifts of the succ:CODD complex. These shifts were used to investigate the identity of the bound species (ligand:substrate or inhibitor). The black, vertical separating line indicates the position where the region from 0 to 9 ppm of the spectrum was removed for simplicity. The anoxic PHD2:Fe(III):succ:CODD complex exhibits a set of two peaks in the shielded methyl region of the spectrum, one with a unique shift of -0.5 ppm, which has not been observed in other Fe(III) complexes. The PHD2:Fe(III):succ complex was shown to be stabilised by the presence of CODD, and to a greater extent in the oxic spectrum. Standard concentrations of each component were: 100 μM unlabelled PHD2, 300 μM Fe(III), 1 mM succinate, 500 μM CODD, 500 μM FG-4592, <2 ppm O_2 pressure (anoxic), and room pressure O_2 (oxic). Buffer conditions were 135 mM NaCl, 10% D_2O, and 90% 50 mM Tris-d_{11} pH 7.5.

The last set of experiments to be recorded were with fumarate(fum):CODD complexes in the presence of Fe(III). As seen with all previous Fe(III) CODD studies, addition of CODD to the oxic/anoxic PHD2:Fe(III):fum complexes (**Figure 2.94** g-h) led to a unique set of peaks, indicative of a distinct PHD2:Fe(III):fum:CODD complex formation. On addition of FG-4592 to the oxic/anoxic PHD2:Fe(III):fum:CODD complexes (**Figure 2.94** i-j), almost no displacement of the complex by FG-4592 was observed. After ~15 hours (**Figure 2.94** k-l), displacement occurred to a minor extent in the anoxic spectrum, but almost no displacement was observed in the oxic spectrum.

From these studies, it was found that CODD addition causes both initial and long-term stability of the PHD2:Fe(III):fum:CODD complex against displacement by FG-

4592 (as can be observed when comparing **Figure 2.89** e-h to **Figure 2.94** i-j). Further, Fe(III) stabilisation of the complex is observed (comparing **Figure 2.84** i-l to **Figure 2.94** i-j).

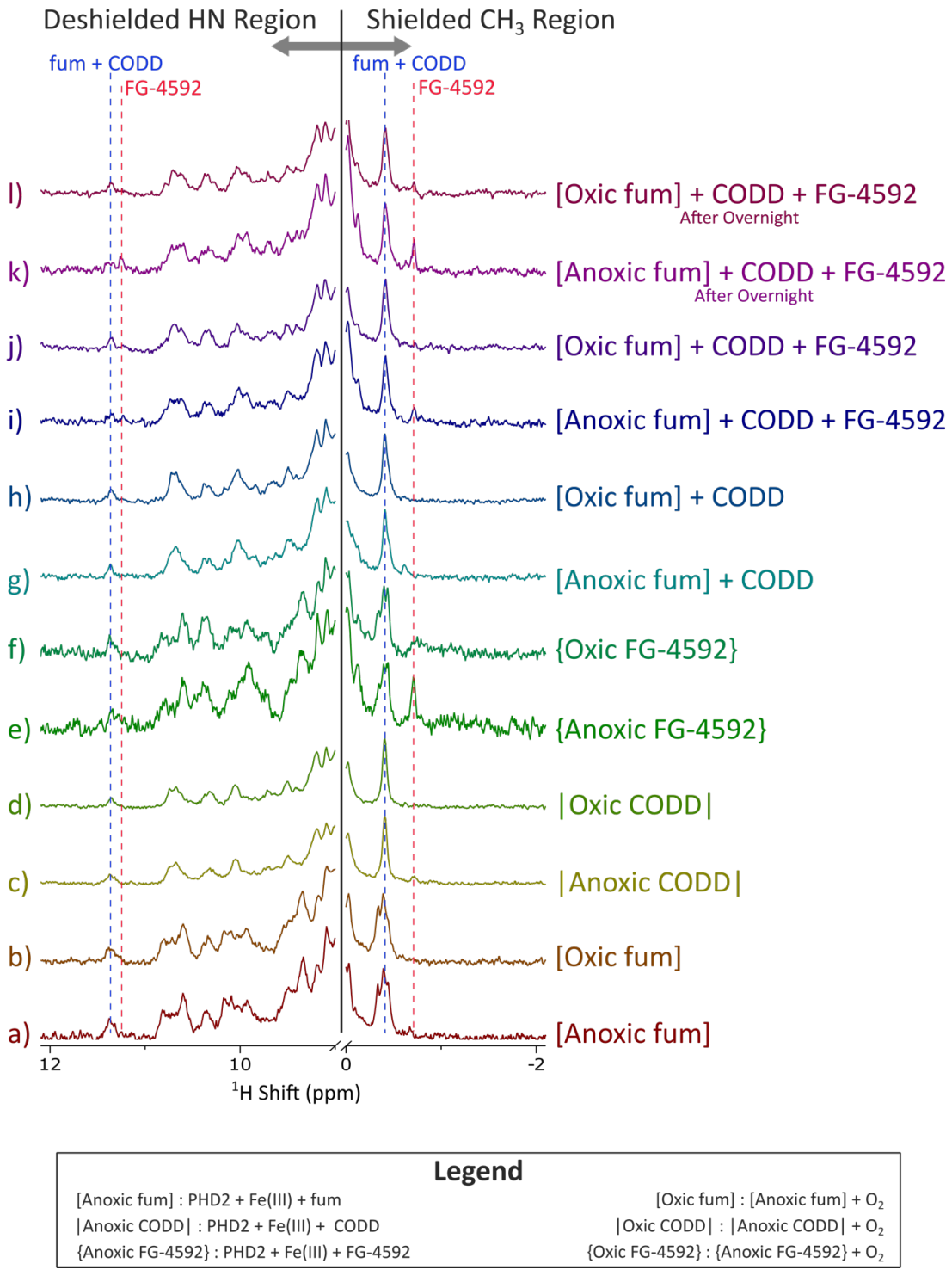


Figure 2.94 *^{1}H spectra of the competition between fumarate(fum):CODD and FG-4592 for PHD2:Fe(III) binding. The labels in the figure above each spectrum indicates the starting complex. Each component after a "+" was added to solution in the order written from left to right. Controls: a) PHD2:Fe(III):fum, b) PHD2:Fe(III):fum + O_2, c) PHD2:Fe(III):CODD, d) PHD2:Fe(III):CODD + O_2 e) PHD2:Fe(III):FG-4592, f)*

PHD2:Fe(III):FG-4592 + O_2, g) PHD2:Fe(III):fum + CODD → PHD2:Fe(III):fum:CODD, h) PHD2:Fe(III):fum + O_2 + CODD → PHD2:Fe(III):fum:CODD + O_2. Inhibitor competition: i) PHD2:Fe(III):fum:CODD + FG-4592 → PHD2:Fe(III):fum:CODD + PHD2:Fe(III):FG-4592, j) PHD2:Fe(III):fum:CODD + O_2 + FG-4592 → PHD2:Fe(III):fum:CODD + O_2. Inhibitor binding over time: k) PHD2:Fe(III):fum:CODD + FG-4592 → PHD2:Fe(III):fum:CODD + PHD2:Fe(III):FG-4592 after ~15 hours at room temperature, and l) PHD2:Fe(III):fum:CODD + O_2 + FG-4592 → PHD2:Fe(III):fum:CODD + O_2 after ~15 hours at room temperature. The dotted red lines indicate the characteristic shifts of the FG-4592 complex (though the position of the deshielded peak is inexact in this spectrum) and the dotted blue lines indicate the characteristic shifts of the fum:CODD complex. These shifts were used to investigate the identity of the bound species (ligand:substrate or inhibitor). The black, vertical separating line indicates the position where the region from 0 to 9 ppm of the spectrum was removed for simplicity. The oxic and anoxic PHD2:Fe(III):fum complexes have been shown to be stabilised against FG-4592 binding by the presence of CODD. Standard concentrations of each component were: 100 μM unlabelled PHD2, 300 μM Fe(III), 1 mM fumarate, 500 μM CODD, 500 μM FG-4592, <2 ppm O_2 pressure (anoxic), and room pressure O_2 (oxic). Buffer conditions were 135 mM NaCl, 10% D_2O, and 90% 50 mM Tris-d_{11} pH 7.5.

From these studies, it was found that: 1) Fe(III) seems to afford more stability (with respect to FG-4592 binding) to the fumarate:CODD complexes than Fe(II), 2) The presence of CODD further stabilises the oxic/anoxic PHD2:Fe(III):2HG complexes, and 3) the oxic and anoxic PHD2:Fe(III):2HG:CODD complexes are not equally stable. As had been observed for the succinate complexes.

Comparisons of the stabilities of the various complexes is given in **Table 2.5**.

Fe(III) Ligand:Substrate Complexes				
Ligand	*Oxygen?*	*PHD2:Fe(III):L:S*	*PHD2:Fe(III):L:S + I*	*PHD2:Fe(III):L:S +I (overnight)*
2OG	anoxic	100% L:S	100% L:S	100% L:S
	oxic	100% L:S	100% L:S	100% L:S
NOG	anoxic	100% L:S	100% L:S	90% L:S, 10% I
	oxic	100% L:S	100% L:S	100% L:S
2HG	anoxic	100% L:S	95% L:S, 5% I	90% L:S, 10% I
	oxic	100% L:S	100% L:S	100% L:S
succ	anoxic	100% L:S	30% L:S, 60% I	30% L:S, 60% I
	oxic	100% L:S	100% L:S	100% L:S
fum	anoxic	100% L:S	95% L:S, 5% I	90% L:S, 10% I
	oxic	100% L:S	100% L:S	100% L:S

Table 2.5 *Compiled description of PHD2:Fe(III):ligand:substrate complex stabilities against inhibitor binding. Green indicates full or almost full retention of the ligand complex, yellow indicates approximately equal retention of ligand complex and displacement by inhibitor, and red indicates almost complete ligand displacement by inhibitor. Note that the oxic and anoxic results are differentiated.*

2.2.4.5 Summary of Results

Overall, the results presented imply that, under the tested conditions, oxygen does not form stable PHD2:metal:2OG/NOG complexes in the absence of active site Fe(II). From studies of the stabilities of PHD2 complexes under various conditions, certain conclusions can be drawn.

First, PHD2:metal:2OG complexes are generally the most stable complexes as compared to the analogous complexes with NOG / other 2OG competitors / mimics tested under the same conditions. Second, the tested PHD2 metal ions bind similarly, but with evidence for clear differences in conformational changes observed on their binding. Third, PHD2:Fe(II) reacts with 2OG then oxygen to form a—likely very—stable and inactive PHD2:Fe(III):2OG complex, which can reversibly bind HIF-α. A similar, but not similarly functional, complex is formed by binding of 2OG to the PHD2:Fe(III) complex (formed by mixing PHD2 and Fe(III)). These reactions are of considerable interest in terms of the roles of the PHDs in the hypoxic response. For example, the

PHD2:Fe(III):2OG complex may help in capture of low levels of HIF- α, which can then become activated by reaction with ascorbate prior to oxygen binding.

Fourth, the PHD2:Fe(II):ligand complexes are more stable (with respect to FG-4592 binding) than the PHD2:Fe(III):ligand complexes for the close 2OG mimics, including NOG and 2HG. This observation may reflect the apparent gap between the weak potency of PHD inhibition under standard turnover conditions by 2HG (and other oncometabolites, i.e. succinate/fumarate) and the in-cell strong upregulation of HIF- α.

Fifth, CODD binding generally stabilises the PHD2:Fe:ligand complexes against FG-4592 binding more effectively than without CODD, and to a greater degree than Fe(III). This observation likely reflects capping of the active site region by CODD.

Sixth, FG-4592 appears to bind more potently to PHD2:Fe(II) than the analogous Fe(III) complex. Work on other PHD inhibitors, especially those in clinical use, with respect to PHD2:Fe(II) and PHD2:Fe(III) binding is of interest. One exciting possibility is to identify oxidation state specific inhibitors.

These results (as observed over time) are summarised in **Table 2.6**.

Fe(II)/Fe(III) Ligand/Substrate Complexes Over Time					
Ligand	*Oxygen?*	*PHD2:Fe(II):L +I (overnight)*	PHD2:Fe(II):L:S +I (overnight)	*PHD2:Fe(III):L +I (overnight)*	PHD2:Fe(III):L:S +I (overnight)
2OG	anoxic	100% I	5% L:S, 95% I	60% L, 30% I	100% L:S
	oxic	100% L	95% L:S, 5% I	60% L, 30% I	100% L:S
NOG	anoxic	50% L, 50% I	5% L:S, 95% I	50% L, 50% I	90% L:S, 10% I
	oxic	100% L	5% L:S, 95% I	60% L, 30% I	100% L:S
2HG	anoxic	100% I	100% I	50% L, 50% I	90% L:S, 10% I
	oxic	100% I	50% L:S, 50% I	50% L, 50% I	100% L:S
succ	anoxic	100% I	100% I	50% L, 50% I	30% L:S, 60% I
	oxic	100% I	100% I	95% L, 5% I	100% L:S
fum	anoxic	100% I	100% I	60% L, 30% I	90% L:S, 10% I
	oxic	100% I	10% L:S, 90% I	90% L, 10% I	100% L:S

Table 2.6 *Compiled description of PHD2:Fe(II):ligand:substrate complex stabilities against inhibitor binding. Green indicates almost full retention of the ligand complex, yellow indicates approximately equal retention of ligand complex and displacement by inhibitor, and red indicates almost complete ligand displacement by inhibitor. Oxic and anoxic results are differentiated.*

2.3 Conclusions

In conclusion, the combined results demonstrate how detailed NMR studies involving careful examination of changes in spectra observed on binding of ligands can provide new mechanistic insight. The value of NMR as a dynamic, in solution, and real-time probe of the state of a protein and its environment has been demonstrated in this chapter. Unique PHD2 complexes have been identified through paramagnetic effects such as shifts and paramagnetic relaxation enhancements present in the newly explored PHD2:metal complexes (**Sections 2.2.2.1.1** and **2.2.2.1.2**). The results demonstrate that small changes in ligand binding can have substantial consequences for active site chemistry. In particular, the results show how analysis of the normally uncrowded shielded methyl region may be an especially useful tool for analyzing ligand binding, at least in the case of PHD2.

Most notably, this lead to the discovery of the unusual $^{1}H,^{15}N$-HSQC and spectra of the oxic and anoxic PHD2:Fe(II):2OG complexes (**Figure 2.17** and **Figure 2.18**). The oxic spectrum contains peaks closely matched to other PHD2:metal:2OG complexes and the anoxic spectrum contains two sets of peaks: one nearly matched to the oxic spectrum and the other unique. It has been hypothesised that the two sets of peaks in the anoxic spectrum may be attributed to two different oxidation or spin states, possibly relating to two different conformations. If two different spin states are present, these are likely the low spin (diamagnetic) and high spin (paramagnetic) Fe(II) oxidation states, as has been supported by EPR studies (**Figure 2.45**). The flipping of spin states in the anoxic PHD2:Fe(II):2OG complex may reflect flipping between monodentate and bidentate binding of 2OG to the Fe(II) centre, although there are other possibilities. Though 2OG is traditionally believed to bind the Fe(II) centre in a bidentate manner, molecular

simulation studies hint at the possibility of 2OG adopting both of these states, [5] where monodentate binding occurs similarly to how succinate is thought to bind the PHD2:Fe(II):succinate complex. It should be noted that the oxic and anoxic PHD2:Fe(II):NOG complexes (**Figure 2.21**) show a similar two sets of peaks with similar shifts to the anoxic PHD2:Fe(II):2OG complex, reflecting the lack of reaction of the complex with O_2.

With knowledge of the distinct reaction of the oxic and anoxic PHD2:Fe:2OG complexes, the goal was to better understand how and if the difference in spectra translates to unique properties and small-molecule ligand interactions. From these studies it was found that the oxic PHD2:Fe(II):2OG complex and the oxic PHD2:Fe(II):2OG:HIF-1α CODD complex are both significantly more stable against 2OG displacement by inhibitors than the other studied oxic/anoxic PHD2:metal:ligand:substrate complexes.

The combined results show that there is more than one type of Fe(III) complex; for example, the PHD2:Fe(III):2OG complex formed by Fe(III) addition differs from that formed from oxic PHD2:Fe(II):2OG complex turnover. Interestingly, the oxic PHD2:Fe(II):2OG complex (which is thought to be an oxic PHD2:Fe(III):2OG complex, as shown by EPR) formed from coupled or uncoupled turnover is the more stable complex. This observation indicates that the formation of the Fe(III) at the PHD2:Fe(III):2OG complex active site may be essential to its stability. It should also be noted that the stability of the anoxic PHD2:Fe(II):2OG complex can be improved by CODD substrate binding.

As described above—in the uncoupled reaction of 2OG with O_2 to give succinate—CO_2 consumes only one of the oxygen atoms of O_2; reduction of the other

oxygen atom of O_2 to give water requires two electrons (along with two protons). One of the electrons may come from Fe(II) to give a PHD2:Fe(III) species which can then bind another 2OG to give the stable PHD2:Fe(III):2OG complex. What happens to the oxygen radical anion that is formally formed is unclear.

These findings lead to a hypothesis for a new, or additional, role for PHD2 in cells (**Figure 2.95**). This new role proposes HIF sequestering by the oxic PHD:Fe(II):2OG complex (which is thought to be PHD:Fe(III):2OG complex) to give the oxic PHD:Fe(II):2OG:HIF-α complex (which is thought to be PHD:Fe(III):2OG:HIF-α complex) on interaction with oxygen. This sequestered complex can then continue turnover upon reduction of Fe(III) to Fe(II) by reaction with ascorbate or other reducing agent. [70]

Importantly, this mechanism opens up the possibility for two direct interfaces between PHD2 and O_2, one involving formation of the PHD:Fe(III):2OG:HIF complex and one involving typical 2OG-dependent dioxygenase catalysed HIF-α hydroxylation after reduction of the former complex. These two O_2 interfaces are linked by reduction of the inactive—with regard to HIF-α hydroxylation—PHD:Fe(III):2OG:HIF-α / PHD:Fe(III):2OG complexes to give the active analogous PHD:Fe(II):2OG:HIF-α / PHD:Fe(II):2OG complexes. Both may occur simultaneously. The presence of the second O_2 interface may help to make the hypoxia sensing process more robust or help to tune it in different contexts. It may be argued that there is no evidence for the second interface of the PHDs in cells, but other than the strong evidence that the PHDs catalyse HIF-α hydroxylation, this is also the case for the accepted mechanism. Studying exactly how the PHDs work within cells can be the subject of future work, possibly involving mutagenesis studies.

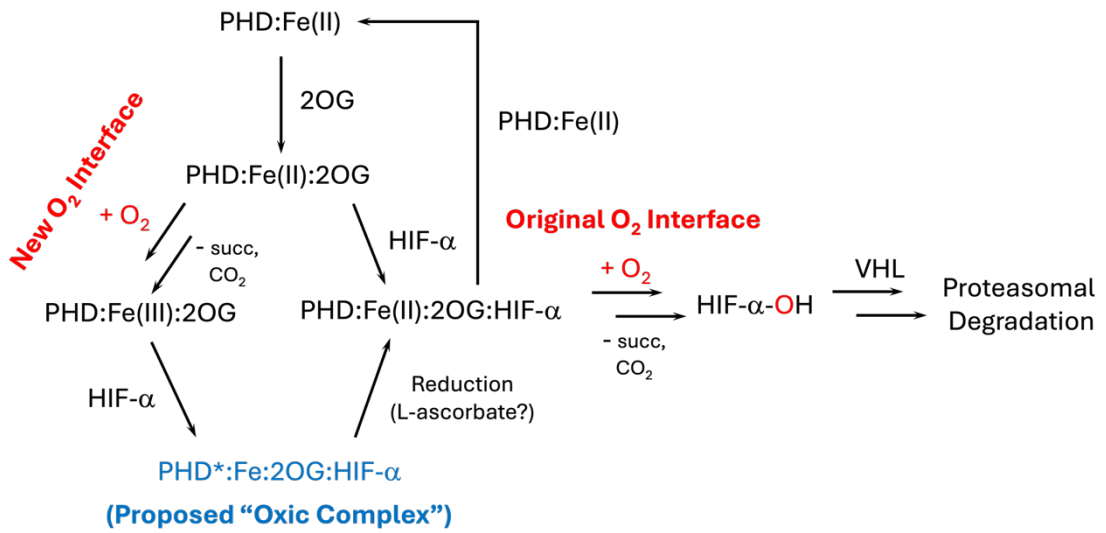


Figure 2.95 *Proposed modified roles of PHD2 in oxygen sensing showing a new second interface between PHD2 (and by implication other PHDs) and O_2. This mechanism builds on the consensus mechanism of PHD2 found in Chapter 1,* ***Figure 1.2****, which is denoted as the "original O_2 interface" in this figure. In the new O_2 interface, the PHD:Fe(II) complex reacts with 2OG and O_2 in the absence of HIF-α to give a PHD*:Fe:2OG:HIF-α "oxic" complex, where * indicates an unassigned modification, which undergoes reduction to give the catalytically active PHD:Fe(II):2OG:HIF-α complex. The new interface offers a mechanism for PHD2 to capture HIF-α and may serve to increase robustness of the hypoxic response.*

2.4 References

[1] C. Liao and Q. Zhang, "Understanding the Oxygen-Sensing Pathway and Its Therapeutic Implications in Diseases," *American Journal of Pathology,* vol. 190, no. 8, pp. 1584-1595, 2020.

[2] S. E. Wilkins, M. I. Abboud, R. L. Hancock and C. J. Schofield, "Targeting Protein–Protein Interactions in the HIF System," *ChemMedChem,* vol. 11, no. 8, pp. 773-786, 2016.

[3] A. M. Menses and B. Wielockx, "PHD2: from hypoxia regulation to disease progression," *Hypoxia,* vol. 4, pp. 53-67, 2016.

[4] H. Tarhonskaya, R. Chowdhury, I. K. H. Leung, N. D. Loik, J. S. O. McCullagh, T. D. W. Claridge, C. J. Schofield and E. Flashman, "Investigating the contribution of the active site environment to the slow reaction of hypoxia-inducible factor prolyl hydroxylase domain 2 with oxygen," *Biochemical Journal,* vol. 463, no. 3, pp. 363-372, 2014.

[5] C. Domene, C. Jorgensen and C. Schofield, "Mechanism of Molecular Oxygen Diffusion in a Hypoxia-Sensing Prolyl Hydroxylase Using Multiscale Simulation," *Journal of the American Chemical Society,* vol. 142, no. 5, pp. 2253-2263, 2020.

[6] M. Abboud, *Using NMR to study protein-ligand interactions,* Oxford: University of Oxford, 2016.

[7] I. Leung, *NMR studies on 2-oxoglutarate oxygenases,* Oxford: University of Oxford, 2013.

[8] M. Mobli and J. C. Hoch, "Nonuniform sampling and non-Fourier signal processing methods in multidimensional NMR," *Progress in Nuclear Magnetic Resonance Spectroscopy,* vol. 83, pp. 21-41, 2014.

[9] M. Mayzel, K. Kazimierczukb and V. Y. Orekhov, "The causality principle in the reconstruction of sparse NMR spectra," *Chemical Communications,* vol. 50, pp. 8947-8950, 2014.

[10] M. Mobli, M. W. Maciejewski, A. D. Schuyler, A. S. Stern and J. C. Hoch, "Sparse Sampling Methods In Multidimensional NMR," *Physical Chemistry Chemical Physics,* vol. 14, no. 31, p. 10835–10843, 2012.

[11] Á. Szigetvári and C. Szántay, "On the utility of nonuniformly sampled two-dimensional NMR spectra in the pharmaceutical industry," *Magnetic Resonance in Chemistry,* vol. 59, p. 264–286, 2021.

[12] F. Delaglio, G. S. Walker, K. A. Farley, R. Sharma, J. C. Hoch, L. W. Arbogast, R. G. Brinson and J. P. Marino, "Non-Uniform Sampling for All: More NMR Spectral

Quality, Less Measurement Time," *American Pharmaceutical Review,* vol. 20, no. 4, p. 339681, 2017.

[13] J. Cavanagh, N. J. Skelton, W. J. Fairbrother, M. Rance and A. G. P. III, Protein NMR Spectroscopy, Academic Press, 2006.

[14] D. Nguyen, C. Chen, M. Pettitt and J. Iwahara, "NMR Methods for Characterizing the Basic Side Chains of Proteins: Electrostatic Interactions, Hydrogen Bonds, and Conformational Dynamics," *Methods in Enzymology,* vol. 615, p. 285–332, 2018.

[15] K. Trainor, J. A. Palumbo, D. W. S. MacKenzie and E. M. Meiering, "Temperature dependence of NMR chemical shifts: Tracking and statistical analysis," *Protein Science,* vol. 29, no. 1, pp. 306-314, 2020.

[16] A. Bax, "Two Dimensional NMR and Protein Structure," *Annual Review of Biochemistry,* vol. 58, pp. 223-256, 1989.

[17] X. Yi, L. Zhang, R. A. Friesner and A. McDermott, "Predicted and Experimental NMR Chemical Shifts at Variable Temperatures: The Effect of Protein Conformational Dynamics," *The Journal of Physical Chemistry Letters,* vol. 15, no. 8, p. 2270–2278, 2024.

[18] H. Okazaki, N. Matsuo, T. Tenno, N. Goda, Y. Shigemitsu, M. Ota and H. Hiroaki, "Using 1HN amide temperature coefficients to define intrinsically disordered regions: An alternative NMR method," *Protein Science,* vol. 27, no. 10, pp. 1821-1830, 2018.

[19] M. I. Abboud, T. E. McAllister, I. K. H. Leung, R. Chowdhury, C. Jorgensen, C. Domene, J. Mecinović, K. Lippl, R. L. Hancock, R. J. Hopkinson, A. Kawamura, T. D. W. Claridge and C. J. Schofield, "2-Oxoglutarate regulates binding of hydroxylated hypoxia-inducible factor to prolyl hydroxylase domain 2," *Chemical Communications,* vol. 54, no. 25, pp. 3130-3133, 2018.

[20] R. Chowdhury, I. K. H. Leung, Y.-M. Tian, M. I. Abboud, W. Ge, C. Domene, F.-X. Cantrelle, I. Landrieu, A. P. Hardy, C. W. Pugh, P. J. Ratcliffe, T. D. W. Claridge and C. J. Schofield, "Structural basis for oxygen degradation domain selectivity of the HIF prolyl hydroxylases," *Nature Communications,* vol. 7, p. 12673, 2016.

[21] E. Flashman, E. A. Bagg, R. Chowdhury, J. Mecinović, C. L. M. A. McDonough, K. S. Hewitson and C. J. Schofield, "Kinetic Rationale for Selectivity toward N- and C-terminal Oxygen-dependent Degradation Domain Substrates Mediated by a Loop Region of Hypoxia-Inducible Factor Prolyl," *Journal of Biological Chemistry,* vol. 283, no. 7, pp. 3808-3815.

[22] R. Chowdhury, M. A. McDonough, J. Mecinović, C. Loenarz, E. Flashman, K. S. Hewitson, C. Domene and C. J. Schofield, "Structural Basis for Binding of Hypoxia-Inducible Factor to the Oxygen-Sensing Prolyl Hydroxylases," *Structure,* vol. 17, no. 7, pp. 981-989.

[23] P. Rabe, C. C. Walla, N. K. Goodyear, J. Welsh, R. Southwart, I. Clifton, J. D. Linyard, A. Tumber, T. D. Claridge, W. K. Myers and C. J. Schofield, "Spectroscopic studies reveal details of substrate-induced conformational changes distant from the active site in isopenicillin N synthase," *Journal of Biological Chemistry,* vol. 298, no. 9, p. 102249, 2022.

[24] W. G. Kaelin and P. J. Ratcliffe, "Oxygen Sensing by Metazoans: The Central Role of the HIF Hydroxylase Pathway," *Molecular Cell,* vol. 30, no. 4, pp. 393-402, 2008.

[25] C. J. Schofield and P. J. Ratcliffe, "Signalling hypoxia by HIF hydroxylases," *Biochemical and Biophysical Research Communications,* vol. 338, no. 1, pp. 617-626, 2005.

[26] G. L. Semenza, "Hypoxia-Inducible Factors in Physiology and Medicine," *Cell,* vol. 148, no. 3, p. 399–408, 2012.

[27] W. D. Figg, G. Fiorini, R. Chowdhury, Y. Nakashima, A. Tumber, M. A. McDonough and C. J. Schofield, "Structural basis for binding of the renal carcinoma target hypoxia-inducible factor 2α to prolyl hydroxylase domain 2," *Proteins,* vol. 91, no. 11, pp. 1510-1524, 2023.

[28] Y.-Z. Gu, S. M. Moran, J. B. Hogenesch, L. Wartman and C. A. Bradfield, "Molecular Characterization and Chromosomal Localization of a Third α-Class Hypoxia Inducible Factor Subunit, HIF3α," *Gene Expression,* vol. 7, no. 3, p. 205–213, 2018.

[29] H. Tarhonskaya, A. P. Hardy, E. A. Howe, N. D. Loik, H. B. Kramer, J. S. O. McCullagh, C. J. Schofield and E. Flashman, "Kinetic Investigations of the Role of Factor Inhibiting Hypoxia-inducible Factor (FIH) as an Oxygen Sensor," *Journal of Biological Chemistry,* vol. 290, no. 32, pp. 19726-19742, 2015.

[30] E. Flashman, L. M. Hoffart, R. B. Hamed, J. M. Bollinger, C. Krebs and C. J. Schofield, "Evidence for the slow reaction of hypoxia-inducible factor prolyl hydroxylase 2 with oxygen," *The FEBS Journal,* vol. 277, no. 19, pp. 4089-4099, 2010.

[31] G. Fiorini and C. J. Schofield, "Biochemistry of the hypoxia-inducible factor hydroxylases," *Current Opinion in Chemical Biology,* vol. 79, p. 102428, 2024.

[32] M. S. Islam, T. M. Leissing, R. Chowdhury, R. J. Hopkinson and C. J. Schofield, "2-Oxoglutarate-Dependent Oxygenases," *Annual Review of Biochemistry,* vol. 87, pp. 585-620, 2018.

[33] M. W. Thompson, "Regulation of zinc-dependent enzymes by metal carrier proteins," *BioMetals,* vol. 35, p. 187–213, 2022.

[34] M. Keith, H. Chih-chin and F. Carol, "Function and Mechanism of Zinc Metalloenzymes," *The Journal of Nutrition,* vol. 130, no. 5, pp. 1437S-1446S, 2000.

[35] J. Dong, K. L. Callahan, N. B. Borotto and R. W. Vachet, "Identifying Zn-bound histidine residues in metalloproteins using hydrogen deuterium exchange mass spectrometry," *Analytical Chemistry,* vol. 86, no. 1, p. 766–773, 2013.

[36] I. B. Trindade, A. Coelho, F. Cantini, M. Piccioli and R. O. Louro, "NMR of paramagnetic metalloproteins in solution: Ubi venire, quo vadis?," *Journal of Inorganic Biochemistry,* vol. 234, p. 111871, 2022.

[37] R. Cammack, "Nickel in Metalloproteins," *Advances in Inorganic Chemistry,* vol. 32, pp. 297-333, 1988.

[38] J. L. Boer, S. B. Mulrooney and R. P. Hausinger, "Nickel-Dependent Metalloenzymes," *Archives of Biochemistry and Biophysics,* vol. 544, p. 142–152, 2014.

[39] S. W. Ragsdale, "Nickel-based Enzyme Systems," *Journal of Biological Chemistry,* vol. 284, no. 28, pp. 18571-18575, 2009.

[40] M. Alfano and C. Cavazza, "Structure, function, and biosynthesis of nickel-dependent enzymes," *Protein Science,* vol. 29, no. 5, p. 1071–1089, 2020.

[41] M. A. Goldberg, S. P. Dunning and H. F. Bunn, "Regulation of the Erythropoietin Gene: Evidence That the Oxygen Sensor Is a Heme Protein," *Science,* vol. 242, no. 4884, pp. 1412-1415, 1988.

[42] K. Gersonde, "Reversible Dioxygen Binding," in *Biological Oxidations. Colloquium der Gesellschaft für Biologische Chemie 14–16*, Berlin, 1983.

[43] B. M. Hoffman and D. H. Petering, "Coboglobins: Oxygen-Carrying Cobalt-Reconstituted Hemoglobin and Myoglobin," *Proceedings of the National Academy of Sciences of the United States of America,* vol. 67, no. 2, p. 637–643, 1970.

[44] M. Ikeda-Saito, H. Yamamoto, K. Imai, F. J. Kayne and T. Yonetani, "Studies on cobalt myoglobins and hemoglobins. Preparation of isolated chains containing cobaltous protoporphyrin IX and characterization of their equilibrium and kinetic properties of oxygenation and EPR spectra," *Journal of Biological Chemistry,* vol. 252, no. 2, pp. 620-624, 1977.

[45] E. K. Barefield, D. H. Busch and S. M. Nelson, "Iron, Cobalt, and Nickel Complexes having Anomalous Magnetic Moments," *Quarterly Reviews, Chemical Spciety,* vol. 22, pp. 457-498, 1968.

[46] J. S. Griffith and L. E. Orgel, "The residual paramagnetism and nuclear magnetic resonance spectra of cobaltic complexes," *Transactions of the Faraday Society,* vol. 53, pp. 601-606, 1957.

[47] Y. Wu, N. Wang, Y. Lei, T. Hu, Q. You and X. Zhang, "Small-molecule inhibitors of HIF-PHD2: a valid strategy to renal anemia treatment in clinical therapy," *MedChemComm,* vol. 7, pp. 1271-1284, 2016.

[48] R. P. Hausinger, "Fe(II)/α-Ketoglutarate-Dependent Hydroxylases and Related Enzymes," *Critical Reviews in Biochemistry and Molecular Biology ,* vol. 39, pp. 21-68, 2008.

[49] D. A. Quist, D. E. Diaz, J. J. Liu and K. D. Karlin, "Activation of dioxygen by copper metalloproteins and insights from model complexes," *Journal of biological inorganic chemistry,* vol. 22, no. 2-3, p. 253–288, 2017.

[50] I. B. Butler, M. A. Schoonen and D. T. Rickard, "Removal of dissolved oxygen from water: A comparison of four common techniques," *Talanta,* vol. 41, no. 2, pp. 211-215, 1994.

[51] A. B. Sahakyan, W. F. Vranken, A. Cavalli and M. Vendruscolo, "Structure-based prediction of methyl chemical shifts in proteins," *Journal of Biomolecular NMR,* vol. 50, no. 4, pp. 331-346, 2011.

[52] B. Bleijlevens, T. Shivarattan, K. S. v. d. Boom, A. d. Haan, G. v. d. Zwan, P. J. Simpson and S. J. Matthews, "Changes in Protein Dynamics of the DNA Repair Dioxygenase AlkB upon Binding of Fe2+ and 2-Oxoglutarate," *Biochemistry,* vol. 51, no. 16, p. 3334–3341, 2012.

[53] C. Lai, Z. Tang, Z. Liu, P. Luo, W. Zhang, T. Zhang, W. Zhang, Z. Dong, X. Liu, X. Yang and F. Wang, "Probing the functional hotspots inside protein hydrophobic pockets by in situ photochemical trifluoromethylation and mass spectrometry," *Chemical Science,* vol. 15, no. 7, p. 2545–2557, 2024.

[54] L. Young, R. Jernigan and D. Covell, "A role for surface hydrophobicity in protein-protein recognition," *Protein Science,* vol. 3, no. 5, pp. 717-729, 1994.

[55] M. D. Kelly and R. L. Mancera, "A New Method for Estimating the Importance of Hydrophobic Groups in the Binding Site of a Protein," *Journal of Medicinal Chemistry,* vol. 48, no. 4, p. 1069–1078, 2005.

[56] B. Bleijlevens, T. Shivarattan, E. Flashman, Y. Yang, P. J. Simpson, P. Koivisto, B. Sedgwick, C. J. Schofield and S. J. Matthews, "Dynamic states of the DNA repair enzyme AlkB regulate product release," *EMBO Reports,* vol. 9, no. 9, p. 872–877, 2008.

[57] C. E. Cooper, "Nitric oxide and iron proteins," *Biochimica et Biophysica Acta (BBA) - Bioenergetics,* vol. 1411, no. 2–3, pp. 290-309, 1999.

[58] R. Chowdhury, E. Flashman, J. Mecinović, H. B. Kramer, B. M. Kessler, Y. M. Frapart, J.-L. Boucher, I. J. Clifton, M. A. McDonough and C. J. Schofield, "Studies on the reaction of nitric oxide with the hypoxia-inducible factor prolyl hydroxylase

domain 2 (EGLN1)," *Journal of Molecular Biology,* vol. 410, no. 2, pp. 268-279, 2011.

[59] A. Weidemann and R. Johnson, "Biology of HIF-1a," *Cell Death & Differentiation,* vol. 15, p. 621–627, 2008.

[60] B. Han, Y. Liu, S. W. Ginzinger and D. S. Wishart, "SHIFTX2: significantly improved protein chemical shift prediction," *Journal of biomolecular NMR,* vol. 50, no. 1, p. 43–57, 2011.

[61] G. Fiorini, *Mechanistic studies on human prolyl hydroxylase domain 2,* Oxford: University of Oxford, 2024.

[62] D. P. Stiehl, R. Wirthner, J. Köditz, P. Spielmann, G. Camenisch and R. H. Wenger, "Increased Prolyl 4-Hydroxylase Domain Proteins Compensate for Decreased Oxygen Levels: EVIDENCE FOR AN AUTOREGULATORY OXYGEN-SENSING SYSTEM," *Journal of Biological Chemistry,* vol. 281, no. 33, pp. 23482-23491, 2006.

[63] L. D. Jong, S. Albracht and A. Kemp, "Prolyl 4-hydroxylase activity in relation to the oxidation state of enzyme-bound iron: The role of ascorbate in peptidyl proline hydroxylation," *Biochimica et Biophysica Acta,* vol. 704, no. 2, pp. 326-332, 1982.

[64] E. Flashman, S. L. Davies, K. K. Yeoh and C. J. Schofield, "Investigating the dependence of the hypoxia-inducible factor hydroxylases (factor inhibiting HIF and prolyl hydroxylase domain 2) on ascorbate and other reducing agents," *Biochemical Journal,* vol. 427, no. 1, pp. 135-142, 2010.

[65] I. Degtyarenko, R. M. Nieminen and C. Rovira, "Structure and dynamics of dioxygen bound to cobalt and iron heme," *Biophysical Journal,* vol. 91, no. 6, pp. 2024-2034, 2006.

[66] T.-L. Yeh, T. M. Leissing, M. I. Abboud, C. C. Thinnes, O. Atasoylu, J. P. Holt-Martyn, D. Zhang, A. Tumber, K. Lippl and C. T. Lohans, "Molecular and cellular mechanisms of HIF prolyl hydroxylase inhibitors in clinical trials," *Chemical Science,* vol. 8, no. 11, pp. 7651-7668, 2017.

[67] F.-J. Chou, Y. Liu, F. Lang and C. Yang, "D-2-Hydroxyglutarate in Glioma Biology," *Cells,* vol. 10, no. 9, p. 2345, 2021.

[68] L. Valcarcel-Jimenez and C. Frezza, "Fumarate hydratase (FH) and cancer: a paradigm of oncometabolism," *British Journal of Cancer,* vol. 129, p. 1546–1557, 2023.

[69] J. E. Longbotham, C. Levy, L. O. Johannissen, H. Tarhonskaya, S. Jiang, C. Loenarz, E. Flashman, S. Hay, C. J. Schofield and N. S. Scrutton, "Structure and Mechanism of a Viral Collagen Prolyl Hydroxylase," *Biochemistry,* vol. 54, no. 39, p. 6093–6105, 2015.

[70] A. Khan, C. J. Schofield and T. D. W. Claridge, "Reducing Agent-Mediated Nonenzymatic Conversion of 2-Oxoglutarate to Succinate: Implications for Oxygenase Assays," *Chembiochem,* vol. 21, no. 20, pp. 2898-2902, 2020.

[71] B. Han, Y. Liu, S. W. Ginzinger and D. S. Wishart, "SHIFTX2: significantly improved protein chemical shift prediction," *Journal of biomolecular NMR,* vol. 50, no. 1, pp. 43-57, 2011.

[72] R. Chowdhury, M. A. McDonough, a. Mecinović, C. Loenarz, E. Flashman, K. S. Hewitson, C. Domene and C. J. Schofield, "Structural Basis for Binding of Hypoxia-Inducible Factor to the Oxygen-Sensing Prolyl Hydroxylases," *Structure,* vol. 17, no. 7, pp. 913-914, 2009.

[73] S. Martinez and R. P. Hausinger, "Catalytic Mechanisms of Fe(II)- and 2-Oxoglutarate-dependent Oxygenases," *Journal of Biological Chemistry,* vol. 290, no. 34, pp. 20702-20711, 2015.

Chapter 3:

Studies on the Structure and Dynamics of WelO5

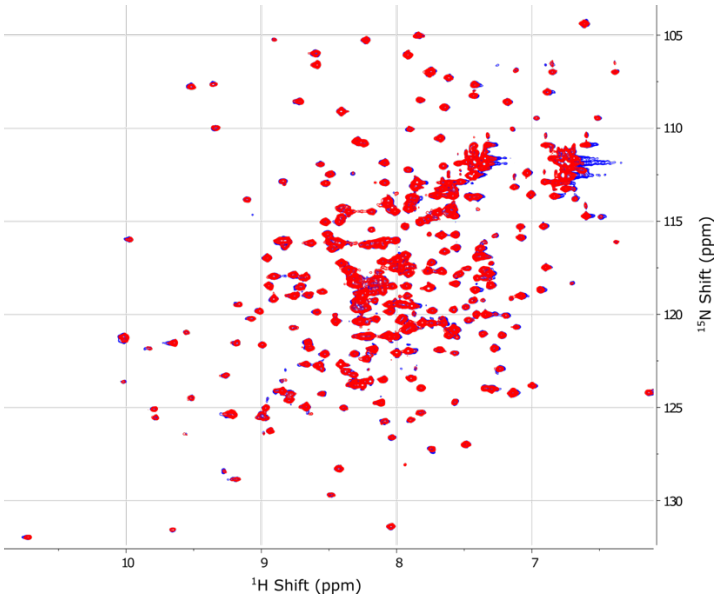


Table of Contents

Chapter 3: 3-1

3.1 Introduction 3-3

3.2 Results 3-3

3.2.1 Discussion of Active Site Ligand Coordination of WelO5 and PHD2 3-4

3.2.2 Metal Analysis Studies 3-5

3.2.3 Optimisation of $^{1}H,^{15}N$-HSQC Conditions/Parameters for 3-D Studies 3-16

3.2.3.1 His-Tag Studies 3-16

3.2.3.2 Degradation Studies 3-17

3.2.3.3 Expanded Window Spectral Studies 3-18

3.2.3.4 Temperature Studies 3-21

3.2.3.5 Non-uniform Sampling Studies 3-22

3.2.3.6 Summary of Analyses 3-23

3.2.4 Studies on the WelO5:Zn(II):2OG Complex for $^{1}H,^{15}N$-HSQC Spectral Assignment 3-24

3.2.5 3-D NMR Experiments 3-26

3.2.6 Studies of Oxic and Anoxic Complexes 3-31

3.2.6.1 Study of Fe(II), 2OG, and Substrate Binding to WelO5 3-31

3.2.6.2 Oxic and Anoxic Complex Comparison Studies 3-36

3.3 Summary 3-40

3.4 References 3-43

3.1 Introduction

The biocatalytic potential of WelO5 has garnered interest for the production of halogenated molecules with a wide scope of applications, including in medicinal chemistry. [1] Biocatalytic methods are being used in synthesis in order to reduce cost, improve stereoselectivity, increase efficiency and safety, and reduce environmental impact. [2] [3] WelO5 catalyses the chlorination of unactivated, sp^3 hybridised carbons without the aid of a carrier protein. [4] Biophysical studies, including X-ray crystallography and small-molecule screening employing mass spectrometry (Ellen Gallimore, D. Phil thesis, University of Oxford), [5] have been used to investigate how WelO5 functions and how it may be modified for expanded uses in synthesis. There are no reported studies on WelO5 solution dynamics—internal protein motions, conformational substates, atomic scale molecular motions, etc.—in particular using NMR. The studies described in this chapter aimed to use ^{1}H,^{15}N-HSQC spectra to study WelO5 dynamics in water. WelO5 and PHD2 will be compared to further study if the oxygen sensing role of the latter is manifested in atypical properties.

3.2 Results

Unlike previous work on PHD2, WelO5 had little to no precedent for optimal conditions for NMR studies (see work done in Ellen Gallimore's D. Phil thesis). [5] Rather than evaluating all relevant inactive WelO5 complexes as was carried out with PHD2—which involved probing each of the essential components of the active PHD2 complex including active site metal, ligand, gas molecule, and substrate—a few complexes of interest were chosen based on relevance to PHD2. If WelO5 exhibited

unique interactions with oxygen, as had been the case for PHD2, further experiments could be explored.

3.2.1 Discussion of Active Site Ligand Coordination of WelO5 and PHD2

Comparison of the active sites of PHD2 and WelO5 reveals interesting differences (**Figure 3.1**). The overall active sites are similar, both containing a single Fe(II), which is ligated by two histidine residues and, in both cases, 2OG binds to the Fe(II) in a bidentate binding mode, as observed by crystallography. Key differences include an Fe(II)-coordinating chloride ion in the case of WelO5 and an Fe(II)-coordinating aspartate residue in the case of PHD2.

There is also a difference in 2OG binding at the active site Fe(II) and how it is oriented relative to the substrate, as shown in crystal structure derived views (**Figure 3.1**). As observed by crystallography, the 2OG C1 carboxylate coordinates trans to His374 in the case of PHD2 and trans to His164 in the case of WelO5 **(Figure 3.1**). [6] [7] The substrate of WelO5 is oriented at the open coordination site of the active site Fe(II). By contrast, the substrate of PHD2 is oriented close to where the 2OG C1 carboxylate is coordinated (**Figure 3.1**). In previous discussions of 2OG coordination at the PHD2 active site Fe(II), it was suggested that exchange between bidentate and monodentate coordination modes, or flipping of 2OG binding between two bidentate coordination modes (a second possible orientation of 2OG at the PHD2 active site could be with the C1 carboxylate trans to His313) may be possible explanations for the two sets of peaks observed during solution studies on the anoxic, but not the oxic, PHD2:Fe(II):2OG spectrum (Chapter 2, **Figure 2.17**, **Figure 2.18**, and **Section 2.3**). [8] It was considered that studies of the interaction of the WelO5:Fe(II):2OG complex with and without oxygen may inform on whether PHD2 is special in this regard.

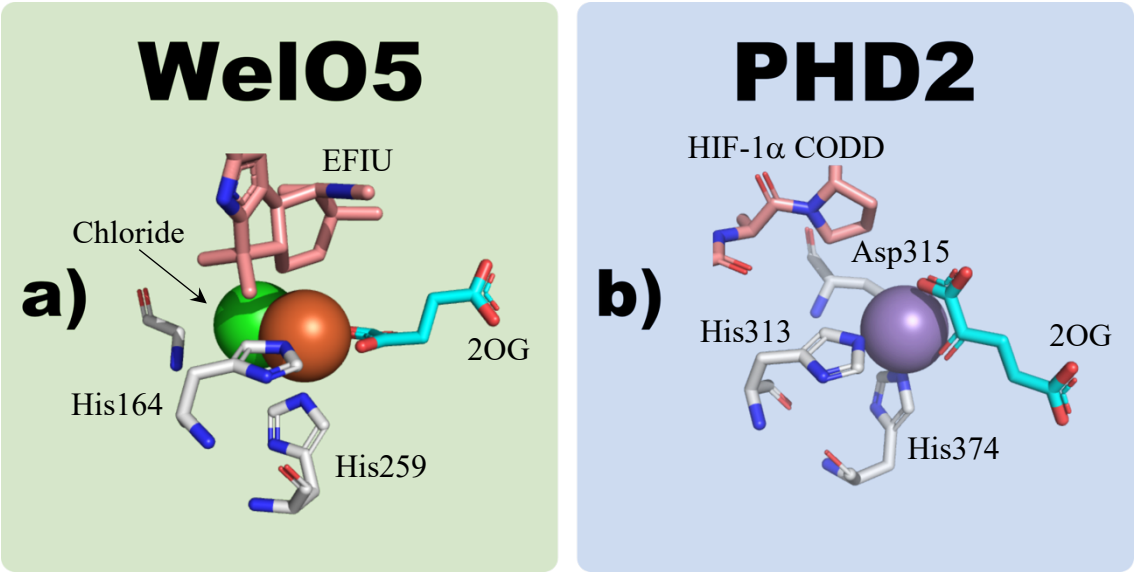


Figure 3.1 *Comparison of the active sites of WelO5 and PHD2 based on crystal structures. The conformations shown are of the substrate-bound complexes: a) WelO5 view showing the Fe-binding residues, the Fe-chelating chloride, 2OG, and the EFIU substrate (PDB: 5IQT) and b) PHD2 showing the Fe-binding residues (Mn(II) substituting for Fe(II) in the crystal structure), 2OG, and HIF-1α CODD (PDB: 5L9B). Note for PHD2: a water molecule (not shown) also coordinates the metal. Differences in 2OG binding at the WelO5 and PHD2 active sites should be noted and that WelO5 only has two coordinating residues, whereas PHD2 has three.*

3.2.2 Metal Analysis Studies

As discussed previously with PHD2, Zn(II) is often the metal of choice for initial structural studies on non-heme Fe-metalloproteins, due to its diamagnetic nature and single protein bound oxidation state. [9] [10] [11] No previous $^{1}H,^{15}N$-HSQC spectra of WelO5 in the presence of Zn(II) have been reported. It was envisaged that the WelO5:Zn(II):2OG spectrum may provide a useful diamagnetic baseline for NMR studies comparing the shifts and broadening of various WelO5:metal:cofactor:substrate complexes.

Interestingly, similar patterns in the peak shape and intensity were observed for the WelO5:Zn(II):2OG complex (**Figure 3.2**) as had been observed for the

PHD2:Zn(II):2OG complex (Chapter 2, **Figure 2.11**). In both protein complexes, the peaks were found to be considerably more asymmetrical and broader than other metal complexes. This asymmetry may be attributed to a difference in protein dynamics or stability of the Zn(II) complex. This should be further explored with other methods such as B-factor analysis and temperature studies (Chapter 2, **Figure 2.4**). [12]

One major problem with the WelO5:Zn(II):2OG complex was greater instability compared to the other studied WelO5:metal:2OG complexes and the PHD2:Zn(II):2OG complex (**Figure 3.3**, **Figure 3.6**, **Figure 3.8**, and Chapter 2 **Figure 2.11** respectively). Another feature to note was the spectral crowding observed around 8 ppm, which is likely due in part to the destabilisation of the complex and its large molecular weight (**Figure 3.2**). These features were considered to make 3-D spectral data collection and ^{1}H,^{15}N-HSQC assignment difficult for the PHD2:Zn(II):2OG complex.

Further optimisation may be needed to make this a viable system of study. Otherwise, other WelO5:metal:2OG complexes should be considered for assignment of the ^{1}H,^{15}N-HSQC spectrum.

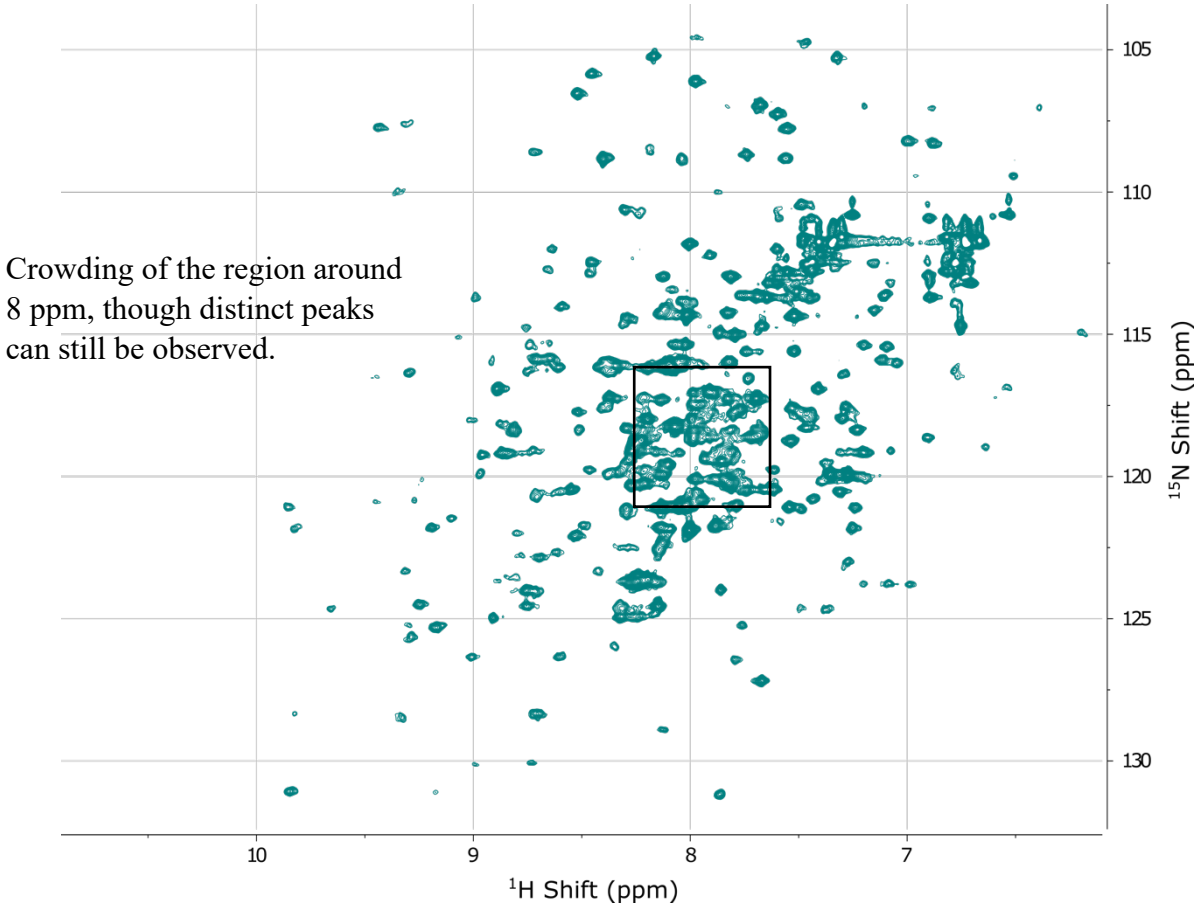


Figure 3.2 *^{1}H,^{15}N-HSQC spectrum of the oxic WelO5:Zn(II):2OG complex. Due to the size of the WelO5 protein and lack of stability of the WelO5:Zn(II):2OG complex, greater crowding was observed in regions around 8 ppm, as indicated by the black box. This may complicate ^{1}H,^{15}N-HSQC spectral assignment by 3-D NMR. Standard concentrations of each component were: 100 μM ^{15}N-labelled WelO5, 300 μM Zn(II), 500 μM 2OG, and room pressure O_2. Buffer conditions were 10% D_2O, and 90% 50 mM Tris-d_{11} pH 6.5.*

The next complex studied was WelO5:Ni(II):2OG (**Figure 3.3**), which had been previously studied by ^{1}H,^{15}N-HSQC NMR. [5] Protein-bound Ni has three possible oxidation states (Ni(I), Ni(II), and Ni(III), with Ni(II) the most common in proteins), making it desirable as an inactive Fe(II) surrogate (Chapter 1, **Table 1.1**). But unlike other inactive metal surrogates like Zn(II), Ni(II) is slightly paramagnetic. This slight paramagnetism is thought to increase the strength of interaction between Ni(II) and paramagnetic oxygen—which is involved in the catalytic mechanism of WelO5—as well as have the potential to induce paramagnetic shifts and/or broadening on nearby residues

(see Chapter 1, **Section 1.2.5**). Since oxygen is also paramagnetic, it may be difficult to distinguish the paramagnetic effects of Ni(II) from oxygen gas.

As had been observed with the PHD2:Ni(II):2OG complex (Chapter 2, **Figure 2.12**), WelO5:Ni(II):2OG complex peaks were more symmetrical and intense than the analogous Zn(II) complex peaks. This difference was especially prevalent in the region between 9-10 ppm, which has often correlated with more ordered protein peak regions in the PHD2 and WelO5 studies discussed in this thesis. In contrast with the analogous Zn(II) complex, the Ni(II) complex was found to be exceptionally stable over time and at temperatures up to 308K (see **Section 3.2.3.4**). These observations indicate Ni(II) stabilises the protein and may be a better target for dynamics studies than the more commonly used Zn(II). It was considered that the stability of the WelO5:Ni(II):2OG complex and intensity of its peaks (without evidence for paramagnetic broadening) would make the WelO5:Ni(II):2OG complex a viable option for 3-D NMR analysis, though caution still must be taken when considering the paramagnetic effects.

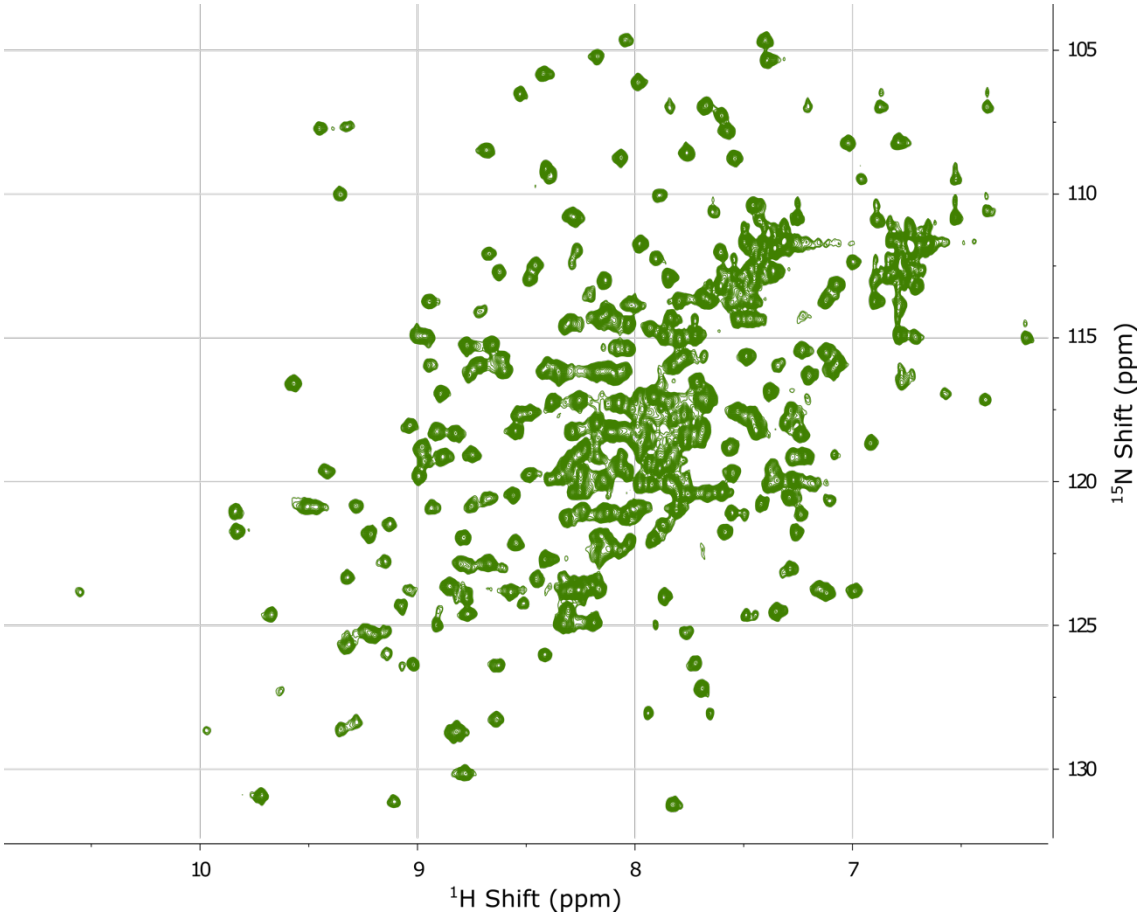


Figure 3.3 *^{1}H,^{15}N-HSQC spectrum of the oxic WelO5:Ni(II):2OG complex. The peaks of the WelO5:Ni(II):2OG complex are relatively intense and uniform, with minor paramagnetic shifts and no visible paramagnetic broadening, making it a useful complex for further studies. Standard concentrations of each component were: 100 µM ^{15}N-labelled WelO5, 300 µM Ni(II), 500 µM 2OG, and room pressure O_2. Buffer conditions were 10% D_2O, and 90% 50 mM Tris-d_{11} pH 6.5.*

Comparison between the WelO5:Zn(II):2OG and WelO5:Ni(II):2OG complexes indicated similar peak shifts, which would make the nearest neighbour approach a viable method for assignment across these spectra (**Figure 3.4**). [13] Slight shift differences are likely attributable to the paramagnetism of the metal. The similarity between the WelO5:Zn(II):2OG complex and the WelO5:Ni(II):2OG complex with slight shift differences mirrors what was observed in the case of PHD2 (Chapter 2, **Figure 2.11** and **Figure 2.12**). This may be due to the similarities in the active site conformations of PHD2 and WelO5 (**Figure 3.1**) or properties of the metals.

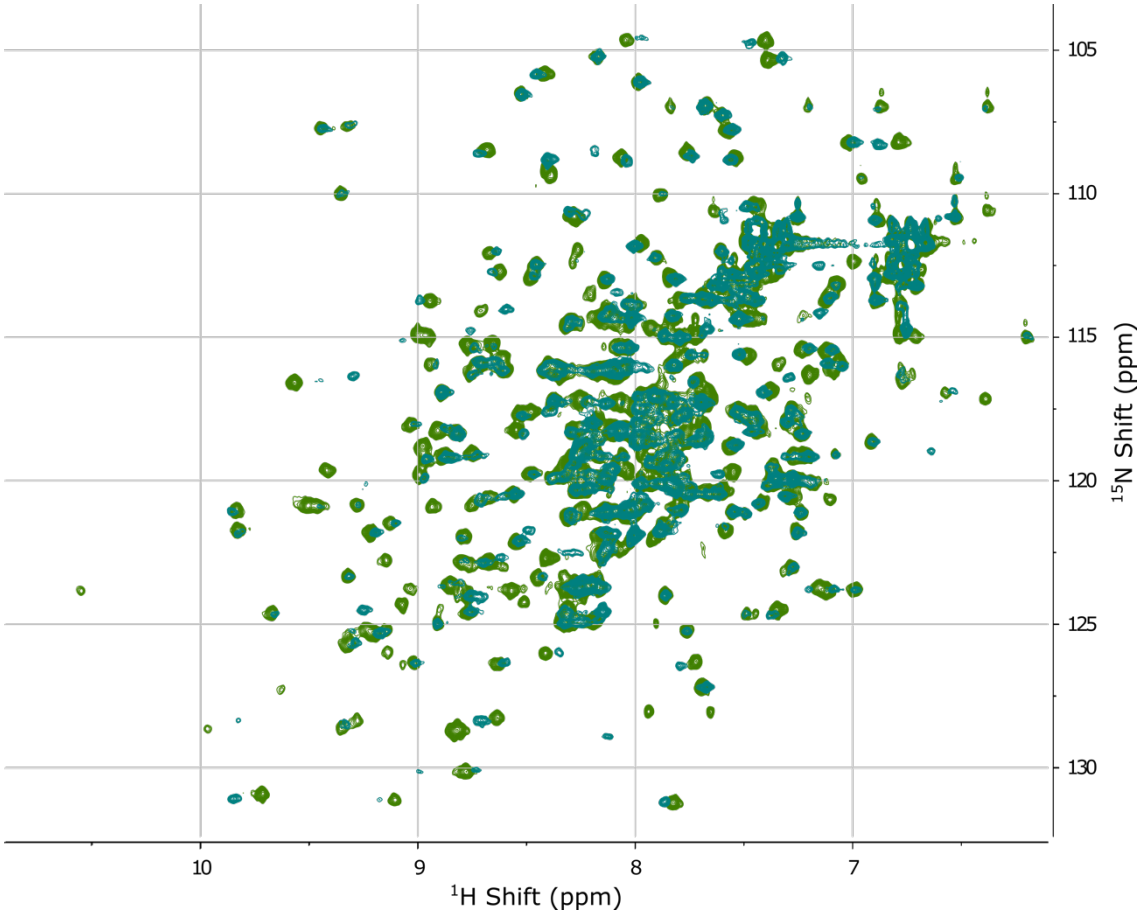


Figure 3.4 *Comparison of the $^{1}H,^{15}N$-HSQC spectra of the oxic WelO5:Zn(II):2OG (teal) and WelO5:Ni(II):2OG (green) complexes. Peaks from the Ni(II)-containing complex were found to be sharper and more regularly shaped than peaks from the Zn(II) complex. Shift differences between the two complexes were minor and can be attributed to paramagnetic effects. Standard concentrations of each component were: 100 μM ^{15}N-labelled WelO5, 300 μM Ni(II), 500 μM 2OG, and room pressure O_2. Buffer conditions were 10% D_2O, and 90% 50 mM Tris-d_{11} pH 6.5.*

In order to investigate the binding affinity of Zn(II) metal in the WelO5:Zn(II):2OG complex, Ni(II) was titrated into the WelO5:Zn(II):2OG complex (**Figure 3.5**). On Ni(II) addition, very few spectral shifts were observed, indicating that the complex remained Zn(II) bound. Some peaks disappeared or were shifted at higher Ni(II) concentrations, which may be due to minor displacement of Zn(II) by Ni(II) and due to destabilisation of the complex at high metal ion concentrations. [14]

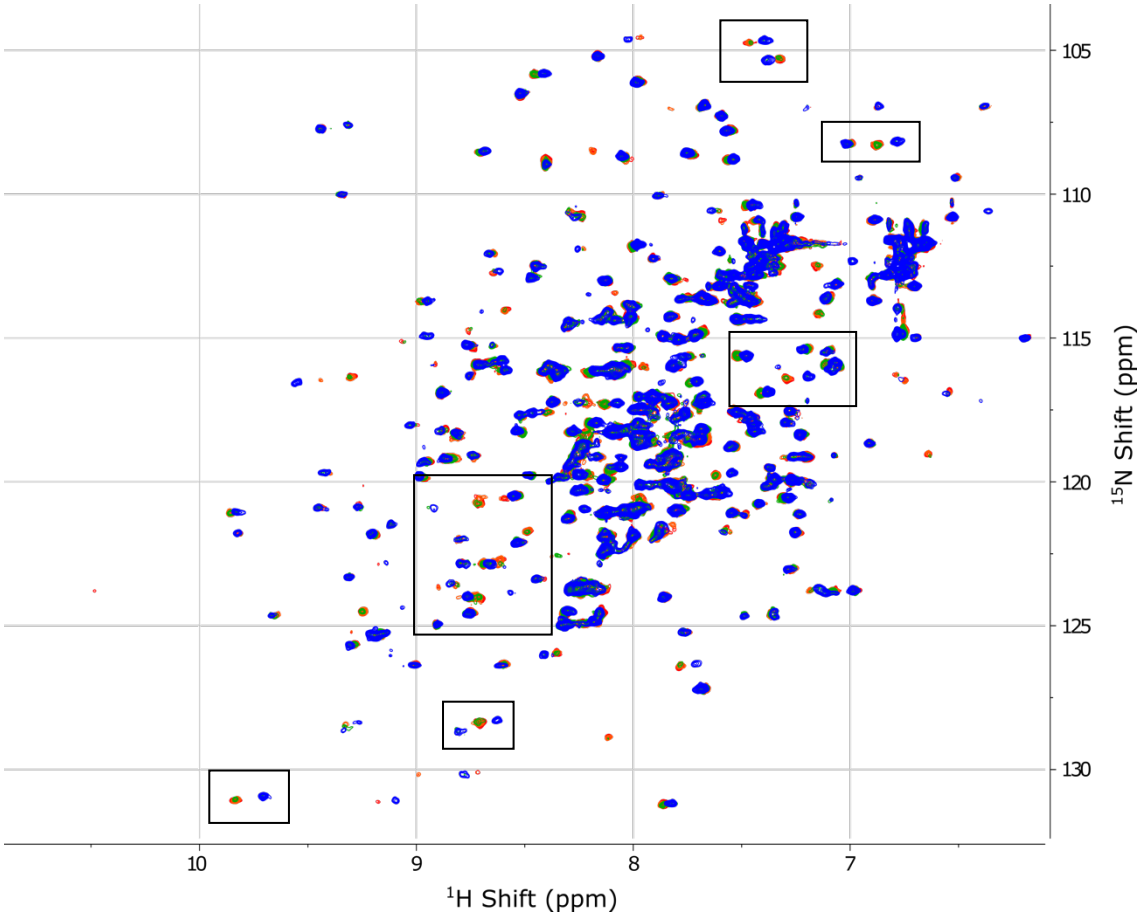


Figure 3.5 *^{1}H,^{15}N-HSQC spectrum of WelO5:Zn(II):2OG (red) with Ni(II) titrations: 1 eq. Zn(II):1 eq. Ni(II) (green), 1 eq. Zn(II):2 eq. Ni(II) (blue). Addition of Ni(II) to the WelO5:Zn(II):2OG complex lead to minor displacement of the Zn(II) complex and possible destabilisation of the protein. Example regions where peak disappearance or shifts are observed are shown within black boxes. Standard concentrations of each component were: 100 µM ^{15}N-labelled WelO5, 300 µM Zn(II), 500 µM 2OG, and room pressure O_2. Buffer conditions were 10% D_2O, and 90% 50 mM Tris-d_{11} pH 6.5.*

Next, the ^{1}H,^{15}N-HSQC spectrum of the WelO5:Co(II):2OG complex was collected (**Figure 3.6**). As a metal ion with two different accessible oxidation states at the protein active site (Co(II) and Co(III)) [15] [16] along with strong paramagnetism (Chapter 1, **Table 1.1**), Co may be a useful Fe mimic for understanding changes in WelO5 on oxygen interaction. Co(II) has been used as an Fe(II) mimic when studied with other metalloproteins and has been found to act as an inhibitor to the catalytic mechanism of Fe(II)-based metalloproteins like PHD2. [17] Co(II) has the additional benefits of high

functional similarity to Fe(II), both in its position on the periodic table as well as the value of its spin-only magnetic moment. [18] [19]

The WelO5:Co(II):2OG complex, much like the PHD2:Co(II):2OG complex (Chapter 2, **Figure 2.13**), showed large peak shifts with minimal broadening as a result of paramagnetic effects. This may make peak assignment by the nearest neighbour approach difficult in the case of Co(II) complexes. Unlike the PHD2:Co(II):2OG spectrum, the WelO5:Co(II):2OG spectrum does not have significantly more peaks than the WelO5:Zn(II):2OG spectrum (**Figure 3.2**), indicating that the way Co(II) binds to the active site of these two proteins may vary. The higher complexity of the PHD2:Co(II):2OG spectrum as compared to the WelO5:Co(II):2OG spectrum may hint at a role for Co(II) in oxygen interaction with PHD2 and may be of relevance to inhibition of PHD2 by Co(II), though these findings are in early stages and should be evaluated further.

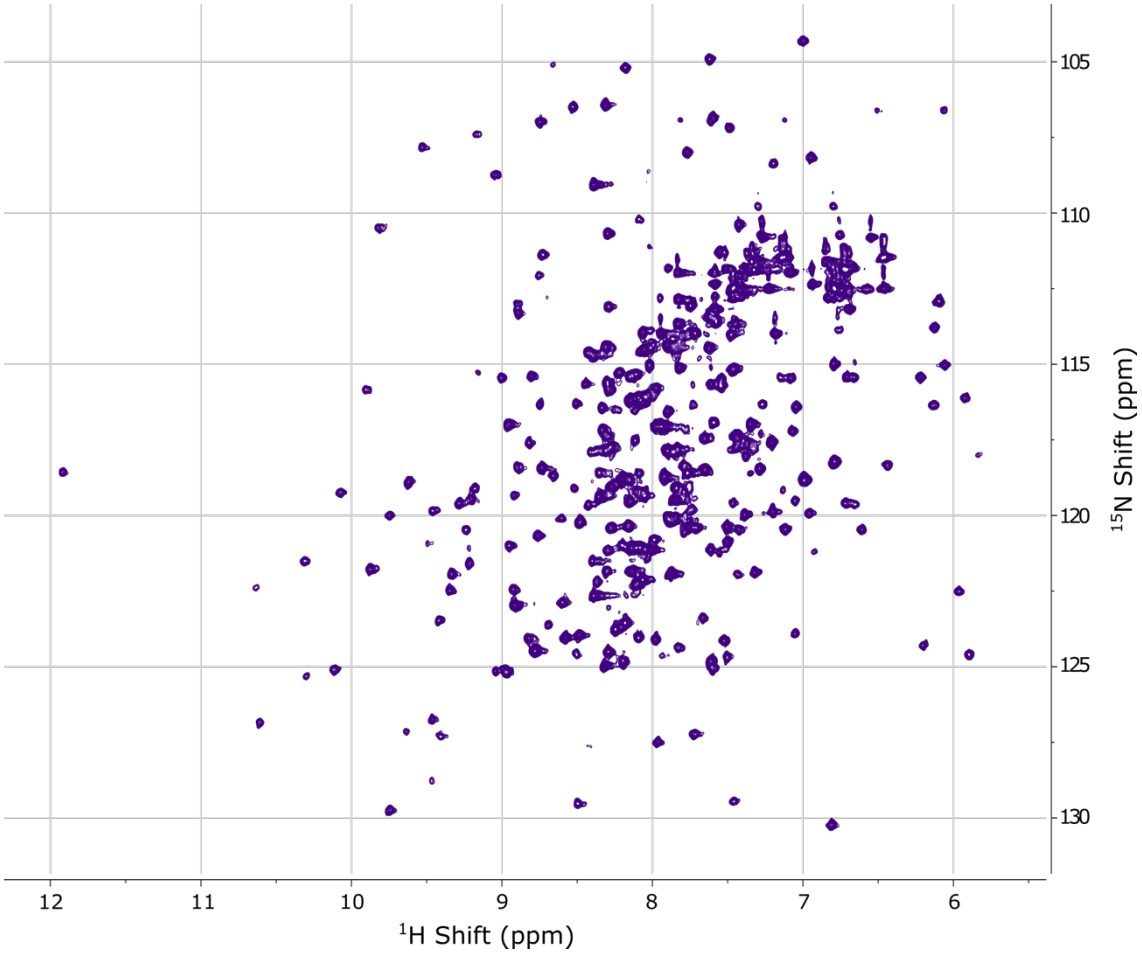


Figure 3.6 *^{1}H,^{15}N-HSQC spectrum of the oxic WelO5:Co(II):2OG complex. Large paramagnetic peak shifts were observed. Standard concentrations of each component were: 100 µM ^{15}N-labelled WelO5, 300 µM Co(II), 500 µM 2OG, and room pressure O_2. Buffer conditions were 10% D_2O, and 90% 50 mM Tris-d_{11} pH 6.5.*

The last complex of interest in the oxic WelO5:metal:2OG studies was the WelO5:Fe(II):2OG complex (**Figure 3.8**), as Fe(II) is the natural cofactor of WelO5 catalysis. As with PHD2, the WelO5:Fe(II):2OG complex in the presence of oxygen is complicated by the substrate uncoupled turnover of 2OG, which may form Fe(III) at the active site, as was proposed for the PHD2:Fe(II):2OG complex (Chapter 2, **Section 2.3**).

Unlike the PHD2 complex, formation of a new complex following exposure of WelO5, Fe(II), and 2OG to oxygen was slow. After components of the complex were mixed, a disordered protein ^{1}H,^{15}N-HSQC spectrum was observed: most peaks start out

around 8 ppm but the spectrum slowly develops into a more complex spectrum over several hours (**Figure 3.7**). The resultant complex spectrum was significantly broader and had a narrower range of peak shifts than had been observed in previous WelO5:metal:2OG complexes. This may make the oxic WelO5, Fe(II), and 2OG product complex(es) difficult to study.

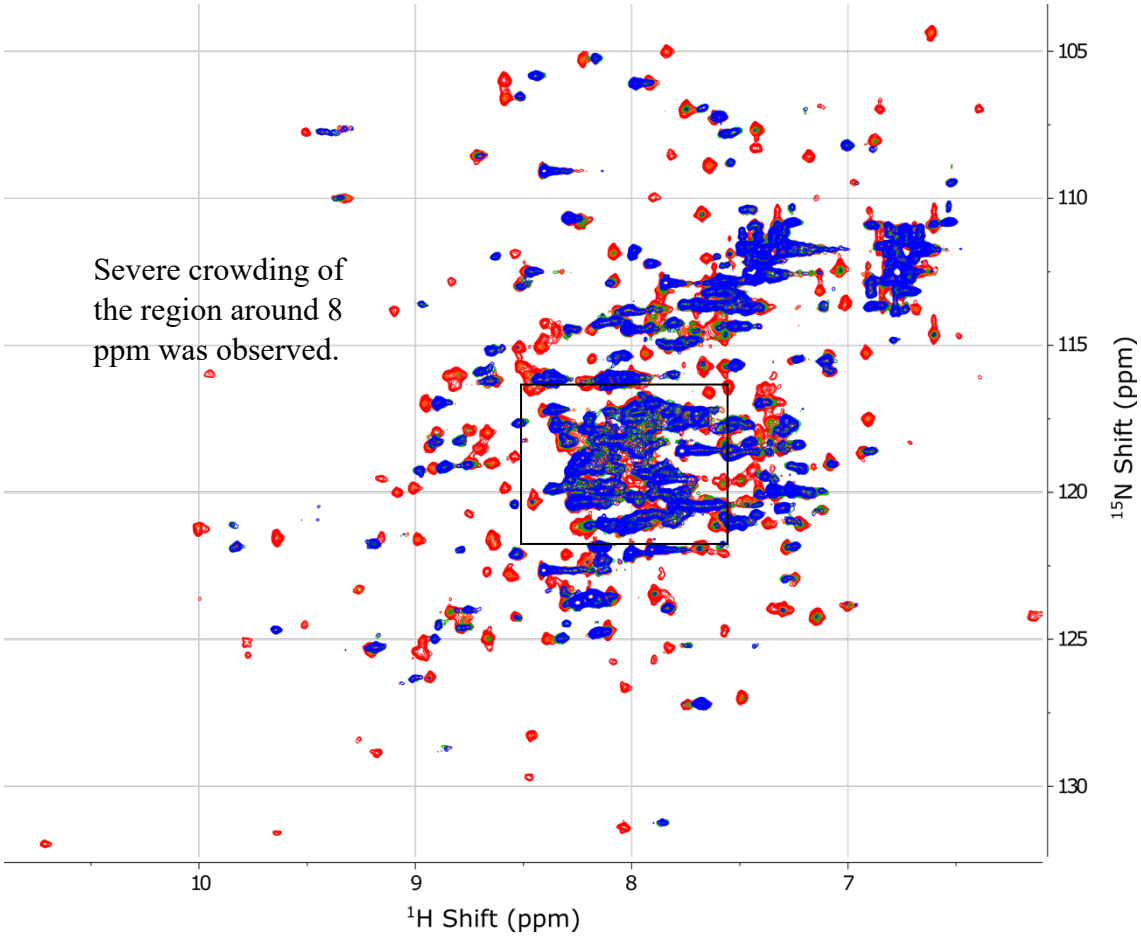


Figure 3.7 *^{1}H,^{15}N-HSQC spectra timecourse of the oxic WelO5:Fe(II):2OG complex at: 3 hours (blue), 6 hours (green), and 9 hours (red) of complex formation. The spectrum developed from an initially disordered spectrum with most peak shifts falling around 8 ppm to a more ordered spectrum with more diverse peak shifts over time. Crowding in the 8 ppm region is shown within the black box. Standard concentrations of each component were: 100 µM ^{15}N-labelled WelO5, 300 µM Fe(II), 500 µM 2OG, and room pressure O_2. Buffer conditions were 10% D_2O, and 90% 50 mM Tris-d_{11} pH 6.5.*

It is uncertain what causes the slower WelO5:Fe(II) complex formation, or more likely a mixture of complexes, from the addition of WelO5, Fe(II), and 2OG to an oxic solution, but further studies are needed. Some possible explanations could be that the fewer metal-interacting residues or the interaction with a chloride ion at the active site of WelO5 makes the Fe(II) binding less stable than in the PHD2 active site. Alternatively, the patch of hydrophobic residues at the PHD2 active site (Chapter 2, **Section 2.2.2.2.1**) may have a stabilising effect on the active site Fe(II) that is not available to the Fe(II) of WelO5.

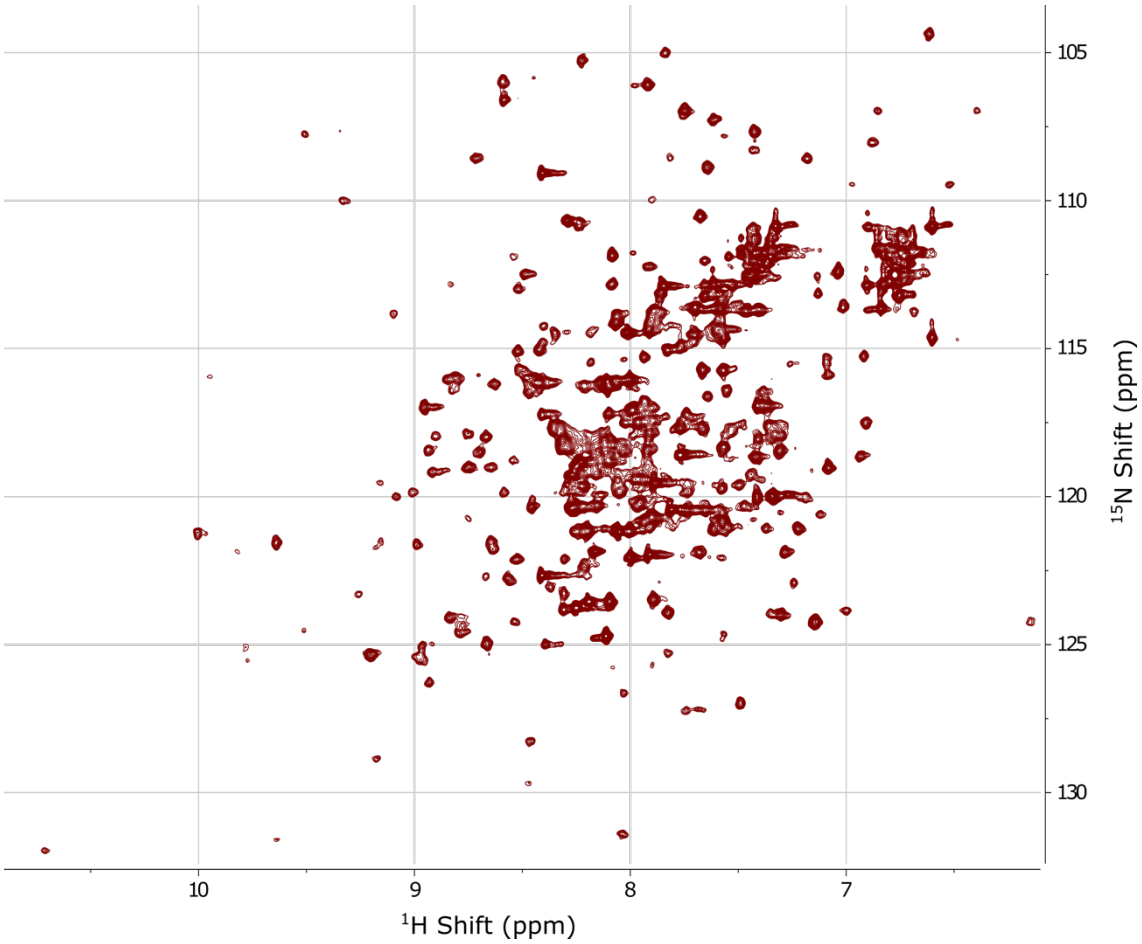


Figure 3.8 *^{1}H,^{15}N-HSQC spectrum of the oxic WelO5:Fe(II):2OG complex. A more complex spectrum with a greater range of peak shifts develops over several hours. Standard concentrations of each component were: 100 µM ^{15}N-labelled WelO5, 300 µM Fe(II), 500 µM 2OG, and room pressure O_2. Buffer conditions were 10% D_2O, and 90% 50 mM Tris-d_{11} pH 6.5.*

From these studies, it was determined that $^{1}H,^{15}N$-HSQC spectral assignment should be viable with the WelO5:Zn(II):2OG or WelO5:Ni(II):2OG complexes, though issues of stability with the former may arise. Analysis of the oxic WelO5:Fe(II):2OG complex and its interaction with oxygen gas at the active site (in comparison to PHD2) may be difficult due to the slow formation of a stable complex.

3.2.3 Optimisation of $^{1}H,^{15}N$-HSQC Conditions/Parameters for 3-D Studies

3.2.3.1 His-Tag Studies

As some protein samples in these experiments retained their polyhistidine-tag (His-tag) to avoid the instability observed in the mutation studies (not described in this thesis; proposed future experiments outlined in Chapter 6, **Section 6.1.2**), the effects on the protein structure in the presence of a His-tag was studied. All 3-D and the majority of the 2-D NMR studies described in this thesis were done in the absence of a His-tag. Comparison of the His-tagged and untagged protein samples (**Figure 3.9**, blue and red respectively) revealed no major changes in the spectra. Additional peaks, however, were observed with the His-tagged WelO5 sample, likely belonging to the His-tag resonances. Since these may complicate the spectrum, His-tagged samples were not generally used for observing site-specific shifts, but may have a purpose in 1-D spectral studies.

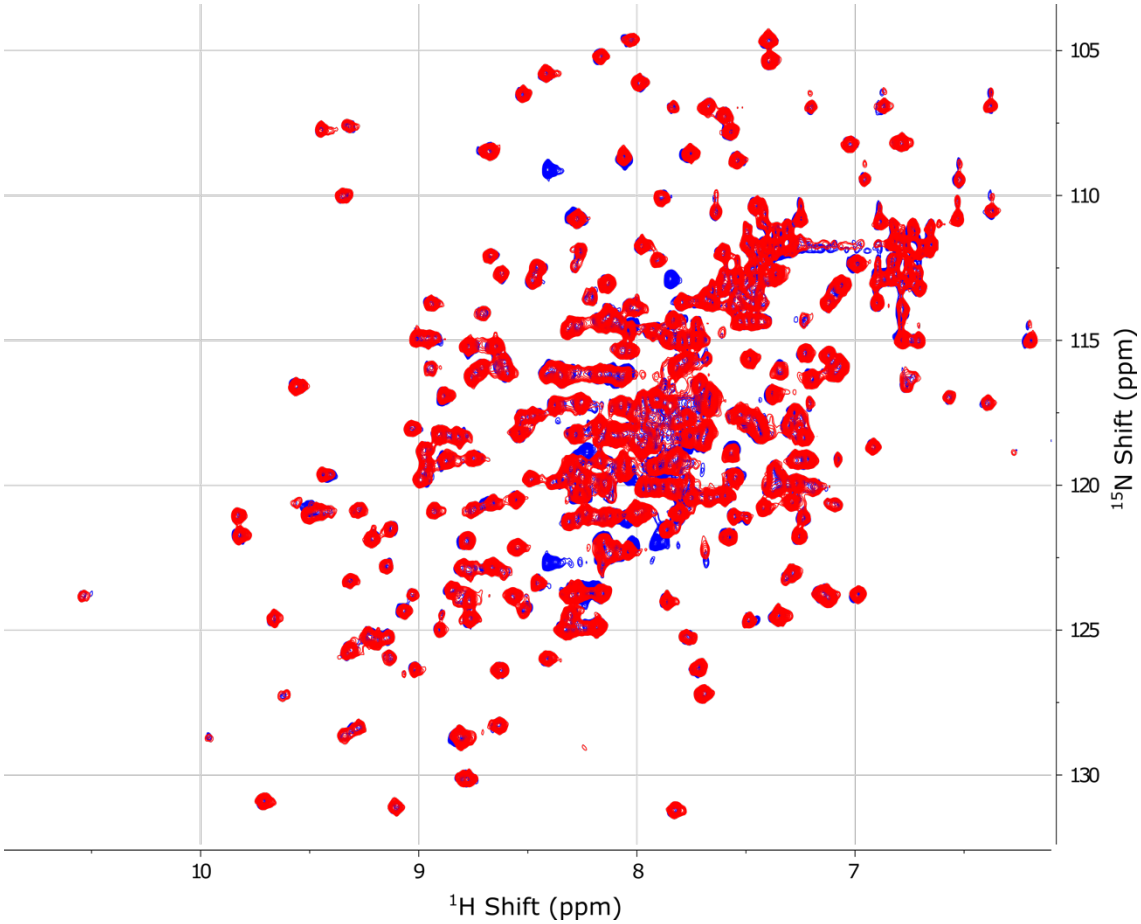


Figure 3.9 *^{1}H,^{15}N-HSQC spectrum of the oxic WelO5:Ni(II):2OG complex in the presence (blue) or absence (red) of a polyhistidine-tag. His resonances are observed as blue peaks without equivalent peaks in the red spectrum. Standard concentrations of each component were: 50 µM ^{15}N-labelled WelO5, 100 µM Fe(II), 200 µM 2OG, and room pressure O_2. Buffer conditions were 10% D_2O, and 90% 50 mM Tris-d_{11} pH 6.5.*

3.2.3.2 Degradation Studies

Next, the stability of the WelO5:Ni(II):2OG complex was analysed after 2 months at 4° C. Very little degradation was observed, with slightly weaker peaks and slightly more crowding in the 8 ppm ^{1}H,^{15}N-HSQC spectral region (**Figure 3.10**). This observation indicates that the complex is relatively stable over time and may be a viable alternative to the WelO5:Zn(II):2OG complex, which has less regular peak shapes and less intense signals.

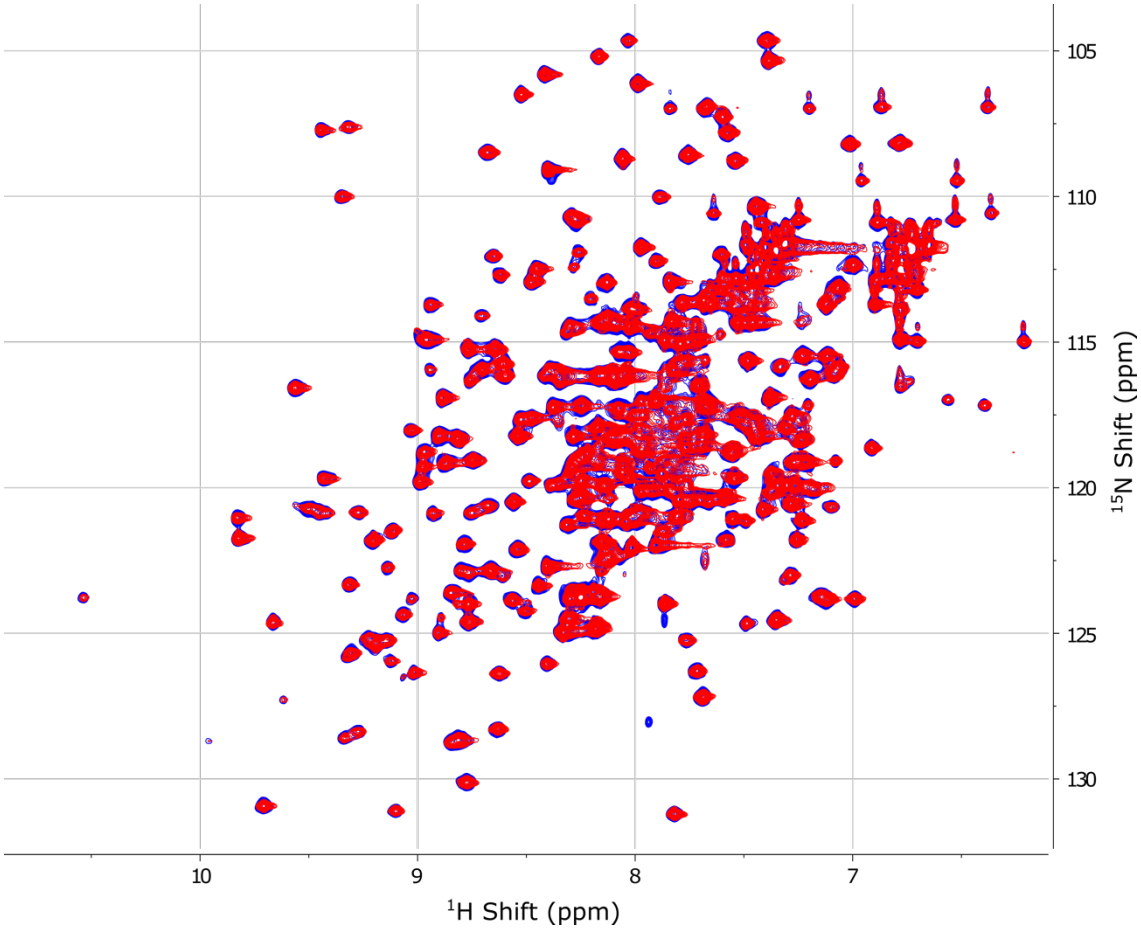


Figure 3.10 *^{1}H,^{15}N-HSQC spectrum of the oxic WelO5:Ni(II):2OG complex before (blue) and after 2 months at 4° C (red). Standard concentrations of each component were: 50 µM ^{15}N-labelled WelO5, 100 µM Ni(II), 100 µM 2OG, and room pressure O_2. Buffer conditions were 10% D_2O, and 90% 50 mM Tris-d_{11} pH 6.5.*

3.2.3.3 Expanded Window Spectral Studies

On initial studies of the triple-^{2}H,^{13}C,^{15}N-labelled complex for 3-D NMR studies, with the ^{15}N-^{1}H peaks remaining protonated, the position of side-chain N-H peaks were determined by expanding the spectral window for the WelO5:Zn(II):2OG complex, as previously carried out on the single-labelled PHD2 (Chapter 2, **Figure 2.2**). The majority of side-chain aliased peaks appear to be in the region of 125 ppm in the ^{15}N dimension (**Figure 3.11**). This information will be useful later when assigning the ^{1}H,^{15}N-HSQC spectrum as it will indicate which resonances don't belong to the protein backbone. Interestingly, the side-chain peaks were more visible in the WelO5 spectrum than they

had been in the PHD2 spectrum, and were in regions of minimal crowding, making them easier to distinguish from other residues in this region.

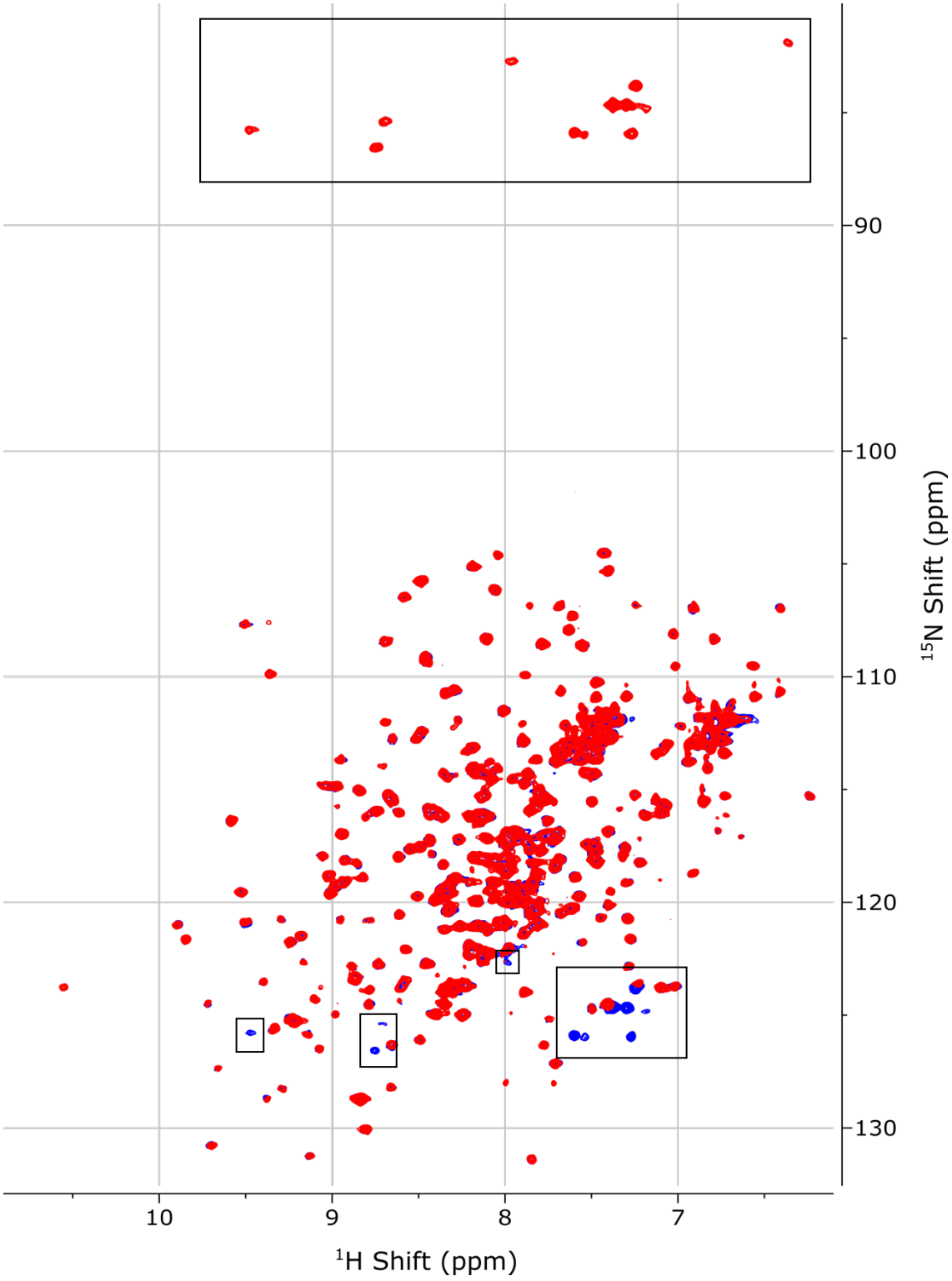


Figure 3.11 *^{1}H,^{15}N-HSQC spectrum of the oxic WelO5:Ni(II):2OG complex with (red) and without (blue) an expanded spectral window. Peaks that were unaliased by expansion of the spectral window are shown with ^{15}N shifts around 80-90 ppm as shown in the large black box. Peaks in the spectrum with a normal spectral window are blue and are shown*

in the smaller black boxes around 120-130 ppm in the ^{15}N dimension. These side-chain peaks will be easy to characterise going forward as they are in regions of minimal spectral overlap. Standard concentrations of each component were: 160.6 μM $^{2}H,^{13}C,^{15}N$-labelled WelO5, 600 μM Ni(II), 600 μM 2OG, and room pressure O_2. Buffer conditions were 5% D_2O, and 95% 50 mM Tris-d_{11} pH 6.5.

3.2.3.4 Temperature Studies

Temperature studies on the WelO5:Ni(II):2OG complex were carried out as a comparison to the PHD2:Zn(II):2OG data (Chapter 2, **Figure 2.4**) since optimisation was still needed to form a stable enough WelO5:Zn(II):2OG complex to run long term, high temperature studies.

From these experiments, it was found that signals for WelO5:Ni(II):2OG were stronger and much more uniform in temperature-dependent peak shifts in the WelO5 spectrum than had been seen in the PHD2:Zn(II):2OG spectrum. This observation follows the general trend that PHD2 seems to give more unique shifts and more complex spectra than WelO5. Difference in choice of surrogate active site metal may also play a role.

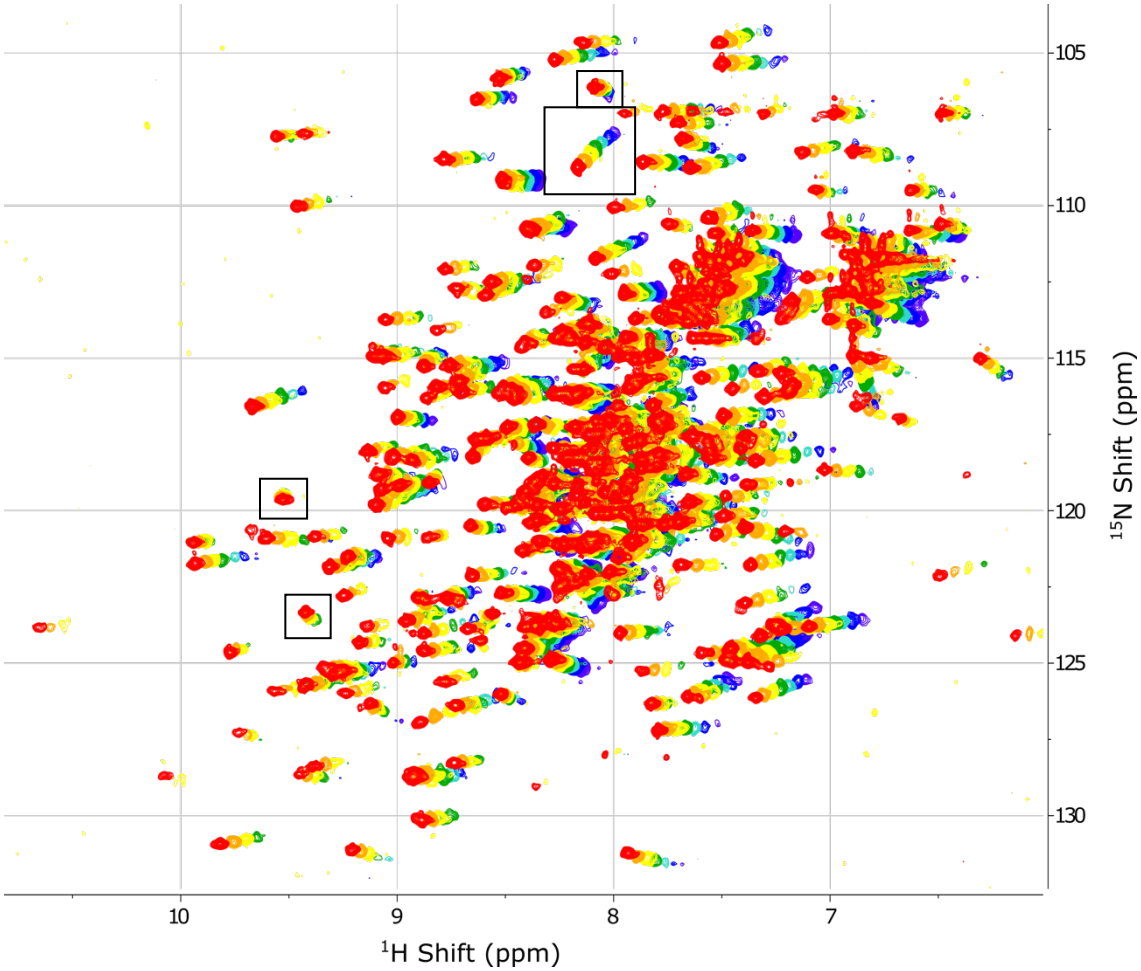


Figure 3.12 *^{1}H,^{15}N-HSQC spectra of the oxic WelO5:Ni(II):2OG complex at various temperatures. The temperatures explored were 278 K (black), 283 K (purple), 288 K (blue), 293 K (cyan), 298 K (green), 303 K (yellow), 308 K (orange), and 310 K (red). Some example peaks with unique shifts over temperature variation are indicated within the black boxes. Greater uniformity of peak shifts are observed in the WelO5 temperature studies as compared to PHD2. Standard concentrations of each component were: 50 µM ^{15}N-labelled WelO5, 100 µM Ni(II), 100 µM 2OG, and room pressure O_2. Buffer conditions were 10% D_2O, and 90% 50 mM Tris-d_{11} pH 6.5.*

3.2.3.5 Non-uniform Sampling Studies

As with PHD2 (Chapter 2, **Figure 2.1**), non-uniform sampling (NUS) acquisition was carried out to investigate if it would be a viable data acquisition method for 3-D NMR experiments. WelO5:Zn(II):2OG samples were run at 0% and 25% NUS (**Figure 3.13**, blue and red respectively) on a 950 MHz instrument. The data showed strong overlap between the two spectra, indicating that 25% NUS should be viable. A few peaks

in the 9 ppm region of the ^{1}H dimension were lost to the NUS acquisition method, which should be taken into consideration. From this experiment, NUS was determined to be a viable method of data acquisition for 3-D NMR experiments.

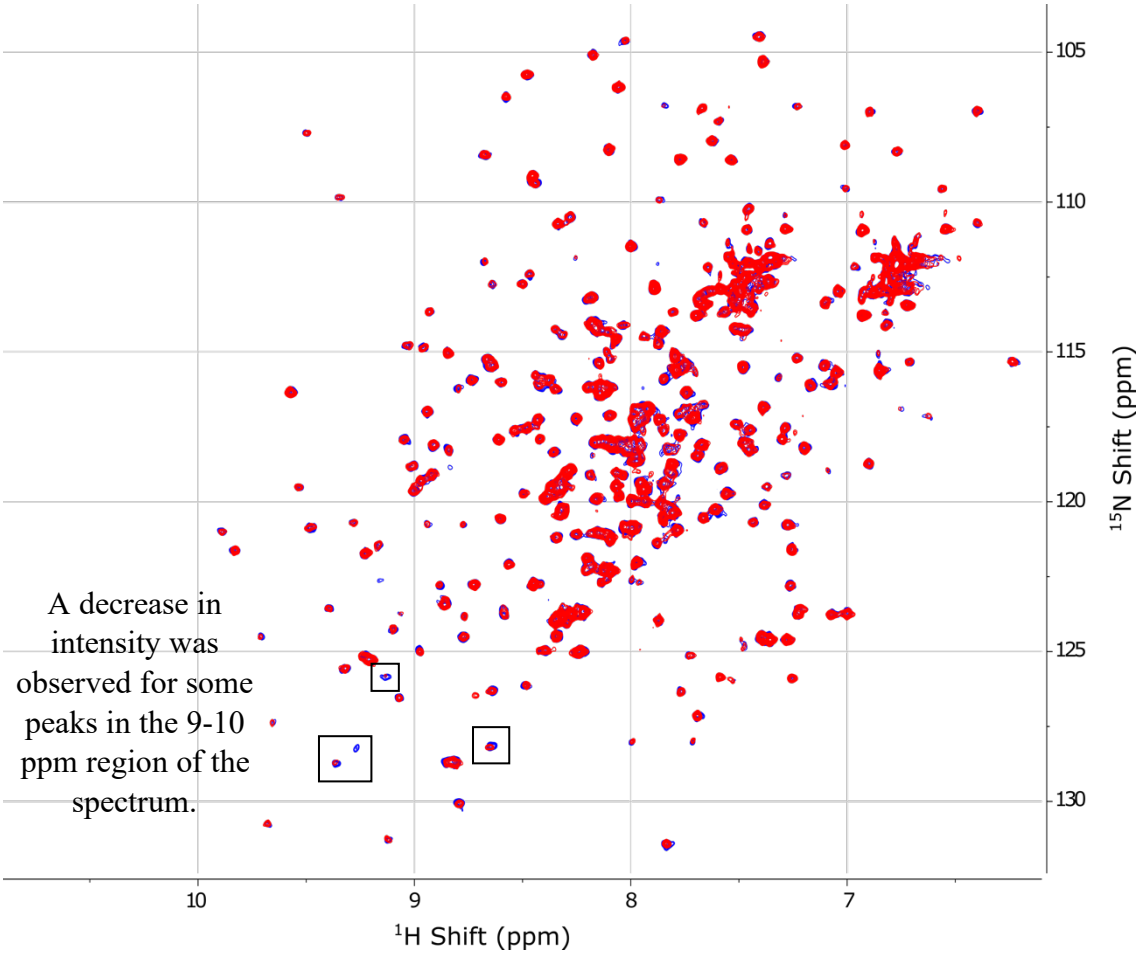


Figure 3.13 *^{1}H,^{15}N-HSQC spectrum of the oxic WelO5:Zn(II):2OG complex at 0% (blue) and 25% (red) NUS sampling. At 25% sampling, NUS appears to be a viable method of data acquisition. Peaks with lower intensities after NUS sampling are indicated within the black boxes. Standard concentrations of each component were: 100 µM ^{15}N-labelled WelO5, 300 µM Zn(II), 200 µM 2OG, and room pressure O_2. Buffer conditions were 10% D_2O, and 90% 50 mM Tris-d_{11} pH 6.5.*

3.2.3.6 Summary of Analyses

From these studies, it was discovered that: 1) WelO5 has generally more uniform and stronger peaks in the ^{1}H,^{15}N-HSQC spectrum than PHD2; 2) the WelO5:Co(II):2OG complex does not have more than one set of peaks in the ^{1}H,^{15}N-HSQC spectrum, in

contrast to what has been observed with the PHD2:Co(II):2OG complex; 3) the WelO5:Fe(II):2OG complex was found to form slowly over several hours; 4) changes in the active-site metal caused minimal changes in peak shifts for WelO5 complexes compared to PHD2 complexes; 5) variable temperature studies revealed less deviation from the standard peak shift than in the case of PHD2, with relatively uniform shifts; and 6) NUS acquisition methods should be viable for 3-D spectral acquisition.

Despite the stability of the WelO5:Ni(II):2OG complex, the WelO5:Zn(II):2OG complex was chosen for 3-D NMR experiments in order to avoid paramagnetic broadening or shifting at active site residues. The WelO5:Ni(II):2OG complex may be used in future 3-D NMR studies to make up for the lack of stability of the WelO5:Zn(II):2OG complex, as described in **Section 3.2.5**.

3.2.4 Studies on the WelO5:Zn(II):2OG Complex for $^{1}H,^{15}N$-HSQC Spectral Assignment

Studies were carried out to optimise conditions for 3-D NMR analysis of the WelO5:Zn(II):2OG complex, including to investigate the best conditions for protein stability. The first step was to observe the WelO5:Zn(II) complex in the absence of 2OG (**Figure 3.14**). This revealed a substantially disordered protein spectrum that had partially precipitated from solution. It's interesting to note that WelO5:Zn(II) is less stable than PHD2:Zn(II), where *apo*-WelO5 has been found to be destabilised by the presence of the Zn(II) ion and is more stable as an *apo* protein, whereas PHD2 tends to require a metal and cofactor for stability.

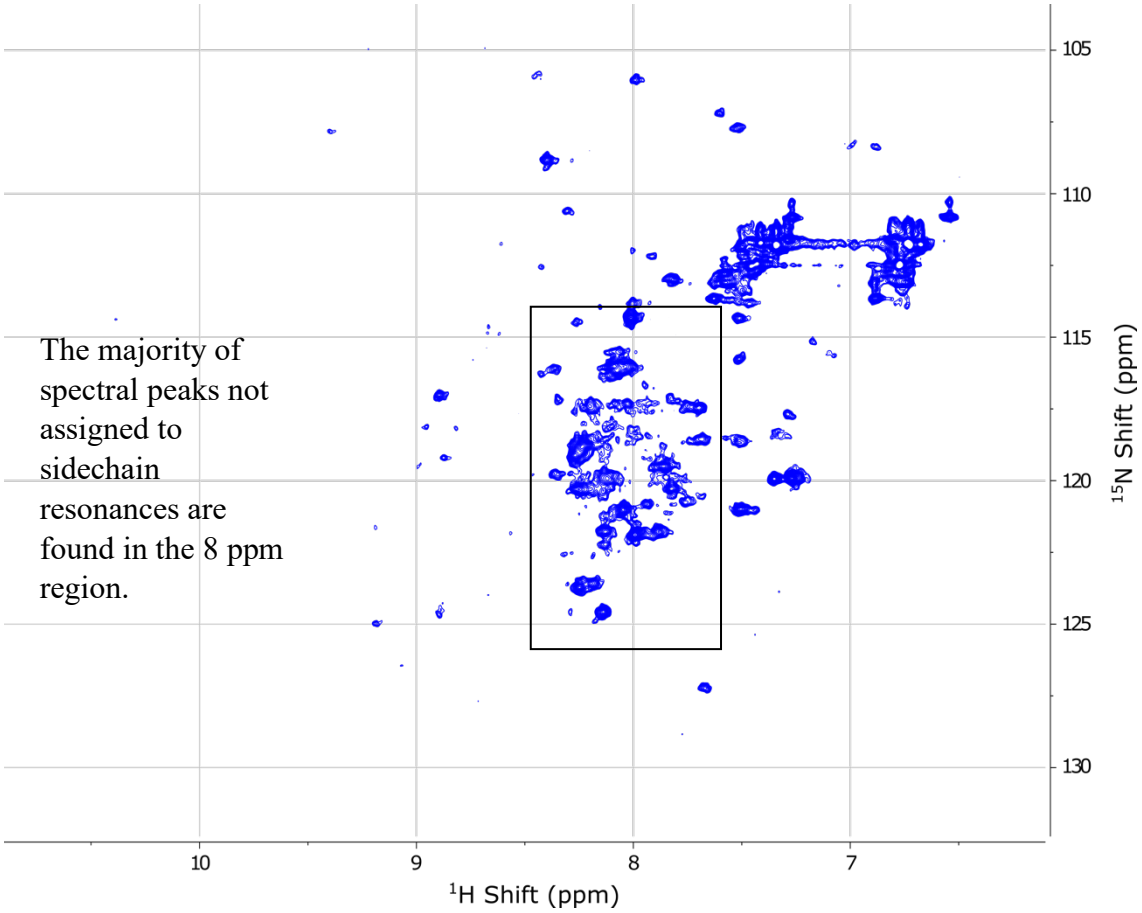


Figure 3.14 *$^{1}H,^{15}N$-HSQC spectrum of the oxic WelO5:Zn(II) complex. In the absence of cofactor, the WelO5:Zn(II) complex is unstable. The major region for the aggregation of peaks is indicated within the black box. Standard concentrations of each component were: 100 μM ^{15}N-labelled WelO5, 300 μM Zn(II), and room pressure O_2. Buffer conditions were 10% D_2O, and 90% 50 mM Tris-d_{11} pH 6.5.*

Next, a WelO5:Zn(II):2OG sample was run with both $^{1}H,^{15}N$-HSQC and $^{1}H,^{15}N$-TROSY pulse sequences (**Figure 3.15**, blue and red respectively) with the same number of scans and increments. These studies showed similar spectral quality with the two pulse sequences, with slightly higher resolution in the 8 ppm region of the $^{1}H,^{15}N$-TROSY spectrum. It was concluded that either $^{1}H,^{15}N$-HSQC or $^{1}H,^{15}N$-TROSY pulse sequences would be viable for 3-D spectral acquisition, though $^{1}H,^{15}N$-TROSY experiments were preferred.

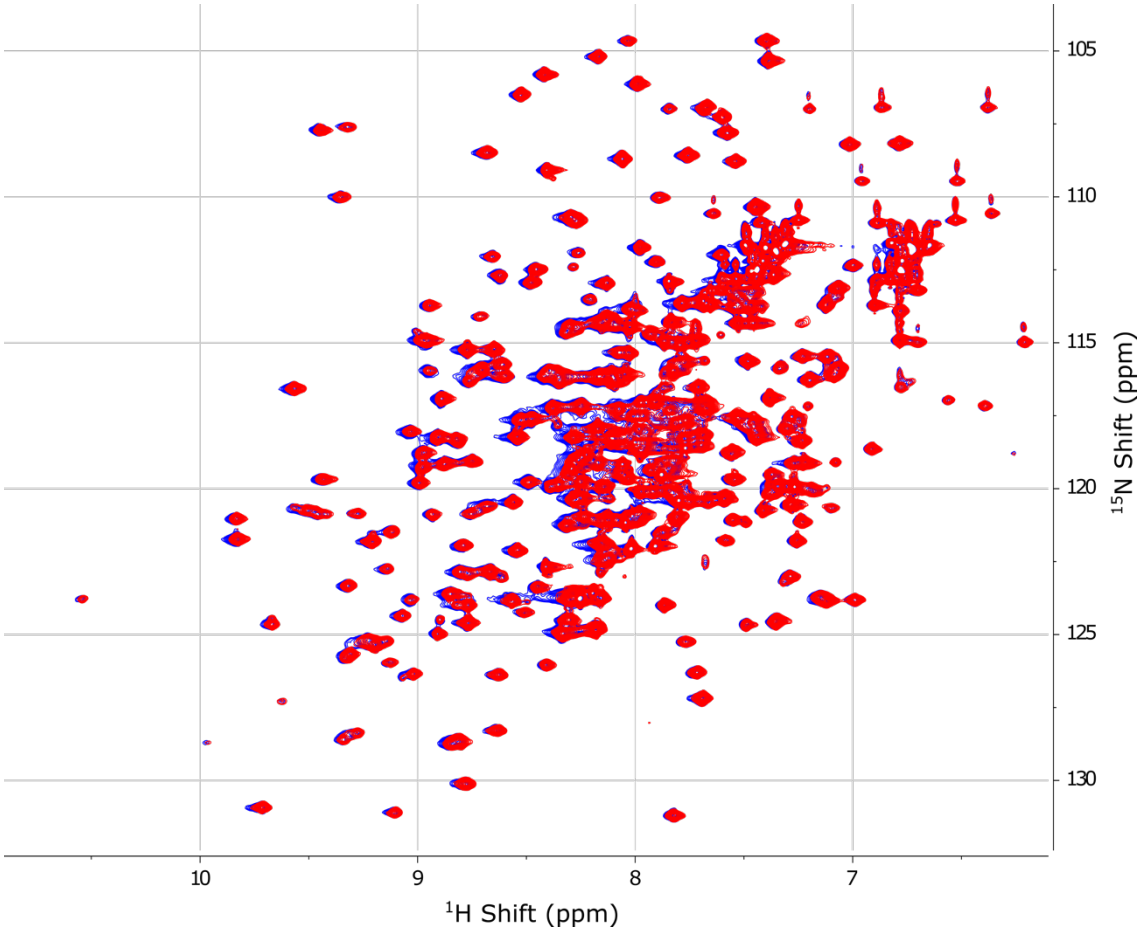


Figure 3.15 *$^{1}H,^{15}N$ spectrum of the oxic WelO5:Zn(II):2OG complex using $^{1}H,^{15}N$-HSQC (blue) and $^{1}H,^{15}N$-TROSY (red) pulse sequences. The peak positions are identical for the two experiment types, with slightly less separation in peaks in the 8 ppm region of the $^{1}H,^{15}N$-HSQC spectrum. Standard concentrations of each component were: 100 µM ^{15}N-labelled WelO5, 300 µM Zn(II), 200 µM 2OG, and room pressure O_2. Buffer conditions were 10% D_2O, and 90% 50 mM Tris-d_{11} pH 6.5.*

From these experiments, $^{1}H,^{15}N$-TROSY was chosen as the preferred experimental method for 3-D spectral acquisition.

3.2.5 3-D NMR Experiments

For 3-D NMR protein sample preparation, the initial goal was to incrementally transfer the $^{2}H,^{13}C,^{15}N$-labelled protein sample into a buffer composed of 600 µM 2OG, 600 µM $Zn(II)Cl_2$, 95% Tris-D_{11}, and 5% D_2O by adding the buffer to the diluted protein

solution, mixing, removing the eluent by centrifugation, then adding additional buffer solution until the protein sample was approximately 500 μM, 600 μM Zn(II)Cl_2, 600 μM 2OG, 95% Tris-D_{11} buffer, and 5% D_2O. On buffer addition, *apo*-WelO5 immediately precipitated, and the highest protein concentration achieved was 168 μM. This sample was run on a 950 MHz instrument (with the help of Prof. Christina Redfield, Department of Biochemistry, University of Oxford). Despite relatively strong ^{1}H,^{15}N-TROSY spectra and 3-D (HNCO, HNCA, HNCOCACB, HNCACO, and HNCACAB) spectra, too many peaks were missing from the 3-D spectra to allow for ^{1}H,^{15}N-HSQC assignment. The initial assumption was that precipitation of the protein led to loss of crucial peaks, so new protein sample conditions would need to be proposed.

Further optimisation of sample conditions was carried out. It was found that the protein exhibited increased stability on 1) addition of Zn(II) acetate (Zn(II)Ac) in place of $ZnCl_2$ and 2) addition of the metal cofactor for an extended time before addition of 2OG. Tests were carried out for protein buffer solutions containing either 50 mM NaCl (**Figure 3.16**) or 25 mM L-glutamic acid / 25 mM L-arginine (Glu/Arg) (**Figure 3.17**) with Zn(II)Ac as the metal cofactor to observe changes in WelO5 complex stability under these conditions. These experiments showed substantial stabilisation by the Glu/Arg addition.

In the WelO5:Zn(II)Ac:2OG spectrum with NaCl addition, there was substantial signal overlap and crowding in the region around 118 ppm in the ^{15}N dimension and 8.0 ppm in the ^{1}H dimension of the spectrum (**Figure 3.16**), making assignment of the spectrum difficult.

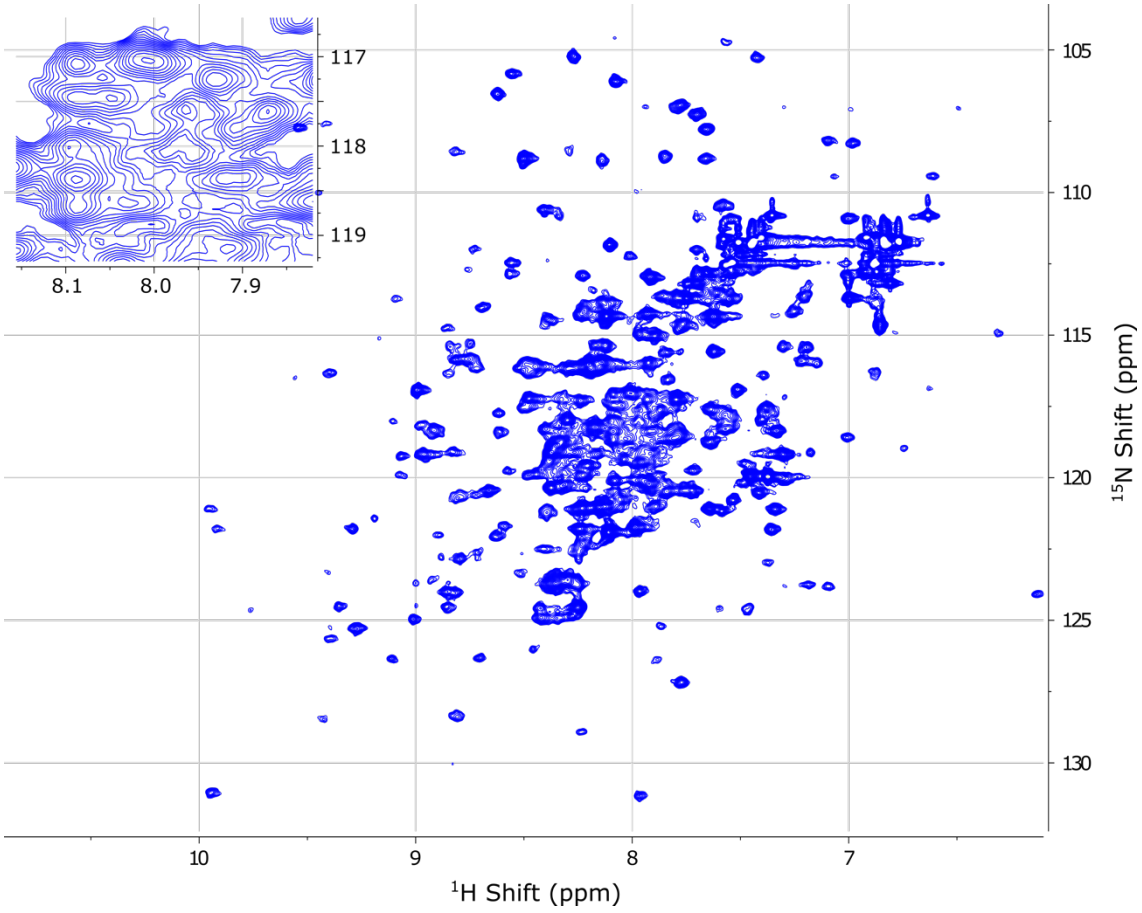


Figure 3.16 *$^{1}H,^{15}N$-HSQC spectrum of the oxic WelO5:Zn(II)Ac:2OG complex in the presence of NaCl. Substantial signal overlap was observed in the 8 ppm region of the ^{1}H dimension, as shown in the top left corner of the figure. Standard concentrations of each component were: 260 µM ^{15}N-labelled WelO5, 440 µM Zn(II), 880 µM 2OG, and room pressure O_2. Buffer conditions were 50 mM NaCl, 5% D_2O, and 95% 50 mM Tris-d_{11} pH 6.50.*

In contrast, the WelO5:Zn(II)Ac:2OG complex in the presence of Glu/Arg appeared less crowded in the region around 118 ppm in the ^{15}N dimension and 8.0 ppm in the ^{1}H dimension of the spectrum (**Figure 3.17**)), likely making it easier to assign with 3-D NMR experiments. WelO5 samples in the presence of Glu/Arg also exhibited less precipitation. The preferred conditions were determined to be WelO5:Zn(II)Ac:2OG in the presence of Glu/Arg; therefore, these conditions were used on a second run of the 3-D NMR experiments.

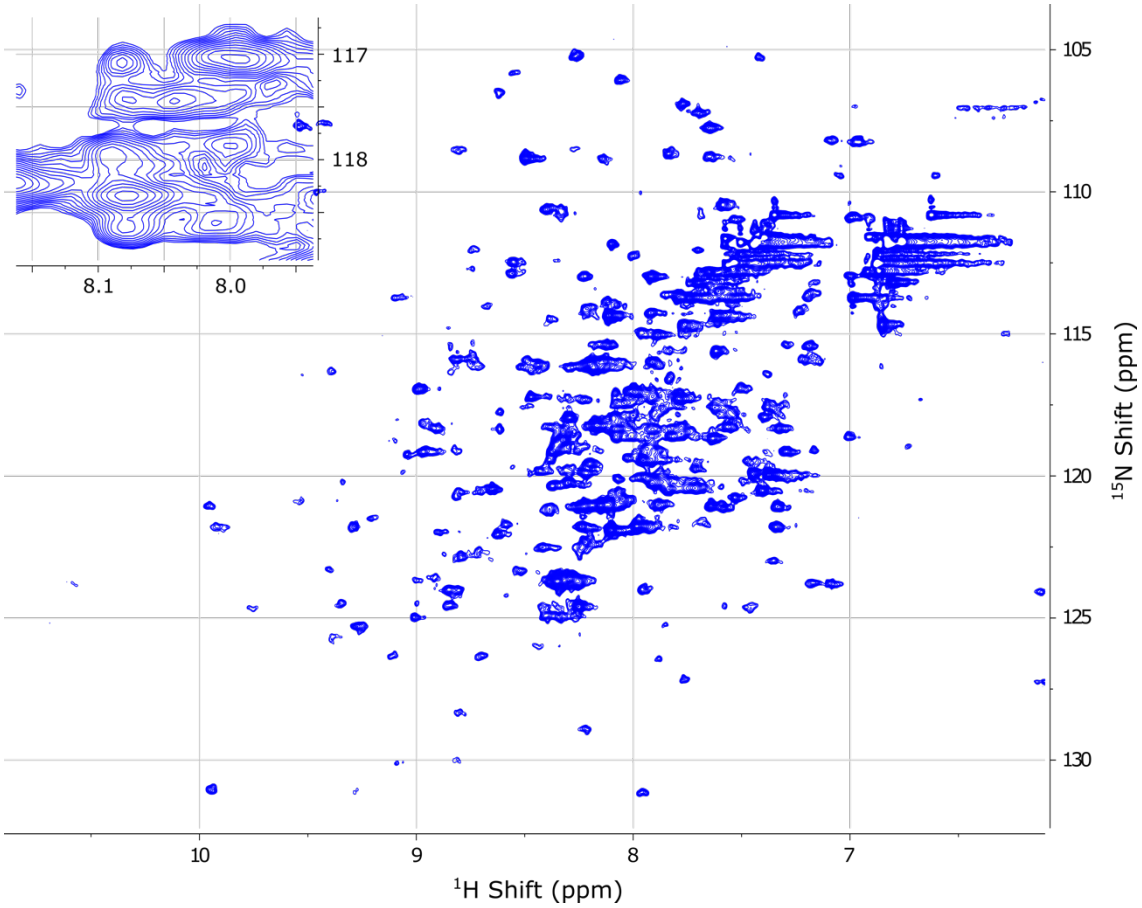


Figure 3.17 *^{1}H,^{15}N-HSQC spectrum of the oxic WelO5:Zn(II)Ac:2OG complex in the presence of Glu/Arg. Better resolution of peaks in the 8 ppm region of the spectrum was achieved, as shown in the top left of the figure. Standard concentrations of each component were: 257 µM ^{15}N-labelled WelO5, 440 µM Zn(II), 880 µM 2OG, and room pressure O_2. Buffer conditions were 25 mM L-glutamic acid, 25 mM L-arginine, 5% D_2O, and 95% 50 mM Tris-d_{11} pH 6.50.*

The first step of the new 3-D NMR setup was stepwise addition of concentrated metal and 2OG in small volumes to the dilute protein solution, as had been shown by optimisation studies, to lead to less protein precipitation. This sample was then concentrated to the desired concentration. The final sample concentrations were approximately 450 µM deuterated ^{2}H,^{13}C,^{15}N-WelO5, 1 mM Zn(II)Ac, 2 mM 2OG, 25 mM L-glutamic acid, and 25 mM L-arginine. This was a much higher WelO5 protein concentration than had previously been achieved. Again, the sample was run on the 950 MHz NMR spectrometer. The spectra obtained from these set of experiments gave very

strong peaks with little indication of degradation/precipitation by the end of the experimental runs (**Figure 3.18**). The additional 3-D datasets included HNCOCACB and HNCACB. Despite strong peaks in the ^{1}H and ^{15}N dimensions of the ^{1}H,^{15}N-HSQC spectrum, some peaks from the 3-D datasets were missing. It was unclear why peaks could not be correlated across all spectra. Assignment could not be carried out.

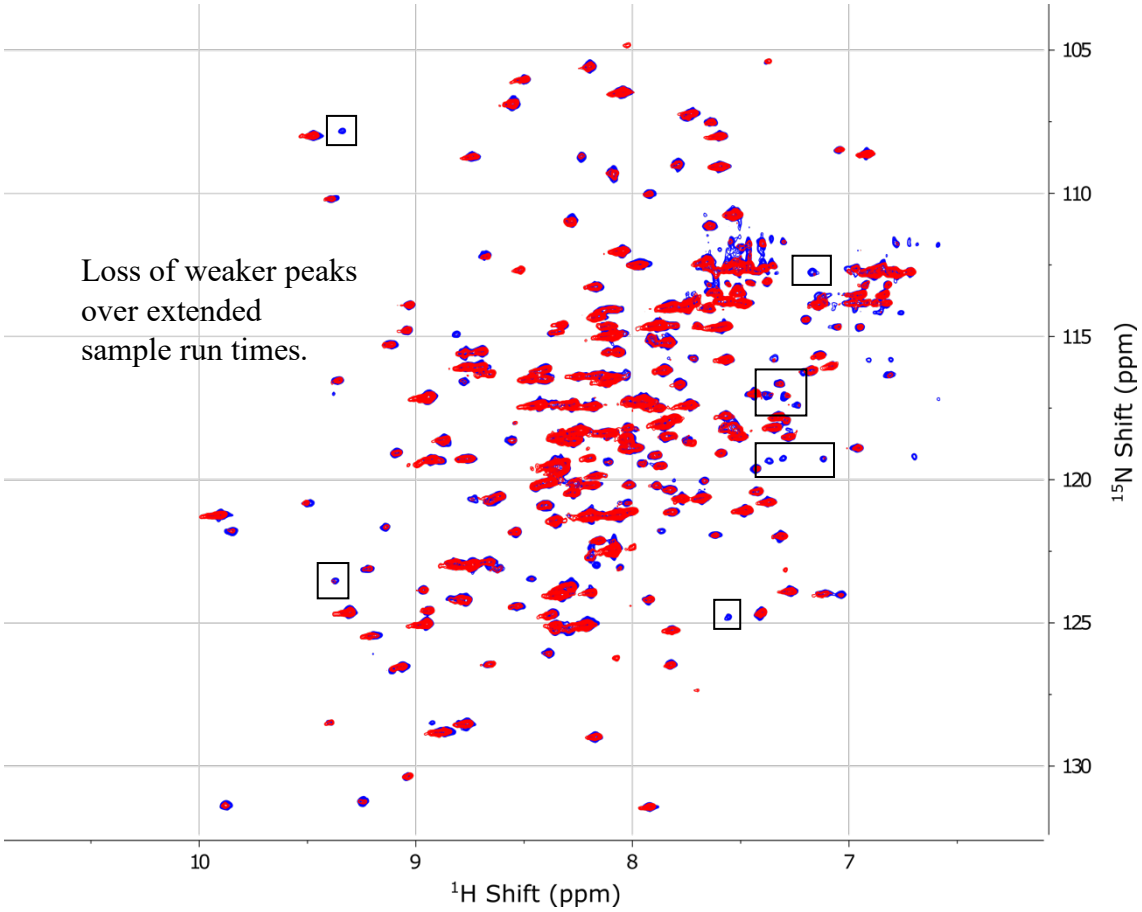


Figure 3.18 *^{1}H,^{15}N-BTROSY spectrum of the oxic, triple-labelled WelO5:Zn(II)Ac:2OG complex before (blue) and after (red) 11 days at 308 K. The sample degradation was minimal over the timespan of the experiments. Standard concentrations of each component were: 450 µM ^{13}C,^{15}N-WelO5, 1 mM Zn(II)Ac, 2 mM 2OG, 25 mM L-glutamic acid, and 25 mM L-arginine, and room pressure O_2. Buffer conditions were 5% D_2O, and 95% 50 mM Tris-d_{11} pH 6.5.*

3.2.6 Studies of Oxic and Anoxic Complexes

3.2.6.1 Study of Fe(II), 2OG, and Substrate Binding to WelO5

As with PHD2 (Chapter 2, **Section 2.2.2.1**), oxic and anoxic experiments were collected for the WelO5:Fe(II):2OG complex. These studies are both important to understand WelO5 and for a better understanding of the unique properties of PHD2-oxygen interactions, as WelO5 has a similar active site but is a functionally distinct Fe(II)- and 2OG-dependent dioxygenase.

From the previous WelO5:Fe(II):2OG studies indicating slow complex formation (**Figure 3.7**), it was of interest to investigate the delay. This required acquisition of the *apo*-WelO5 and WelO5:Fe(II) spectra (**Figure 3.19**), in which the previously studied WelO5:Zn(II) complex (**Figure 3.14**) could be used as a control. Interestingly, both the *apo*-WelO5 (**Figure 3.19**, blue) and the WelO5:Fe(II) (**Figure 3.19**, red) spectra appeared to exhibit more distinct peak shifts than the WelO5:Zn(II) spectrum, but WelO5 in the presence of Fe(II) showed little indication of Fe(II) binding.

This finding may indicate that the WelO5:Fe(II):2OG complex formation may be delayed by the WelO5:Fe(II) complex formation. Since *apo*-WelO5 is stable over the course of the $^{1}H,^{15}N$-HSQC spectral acquisition, the instability of the WelO5:Zn(II) and the WelO5:Zn(II):2OG complexes may be attributed to destabilisation of *apo*-WelO5 by Zn(II). Therefore, future 3-D NMR experiments may benefit from the use of the WelO5:Ni(II):2OG complex, which has consistently been found to be stable.

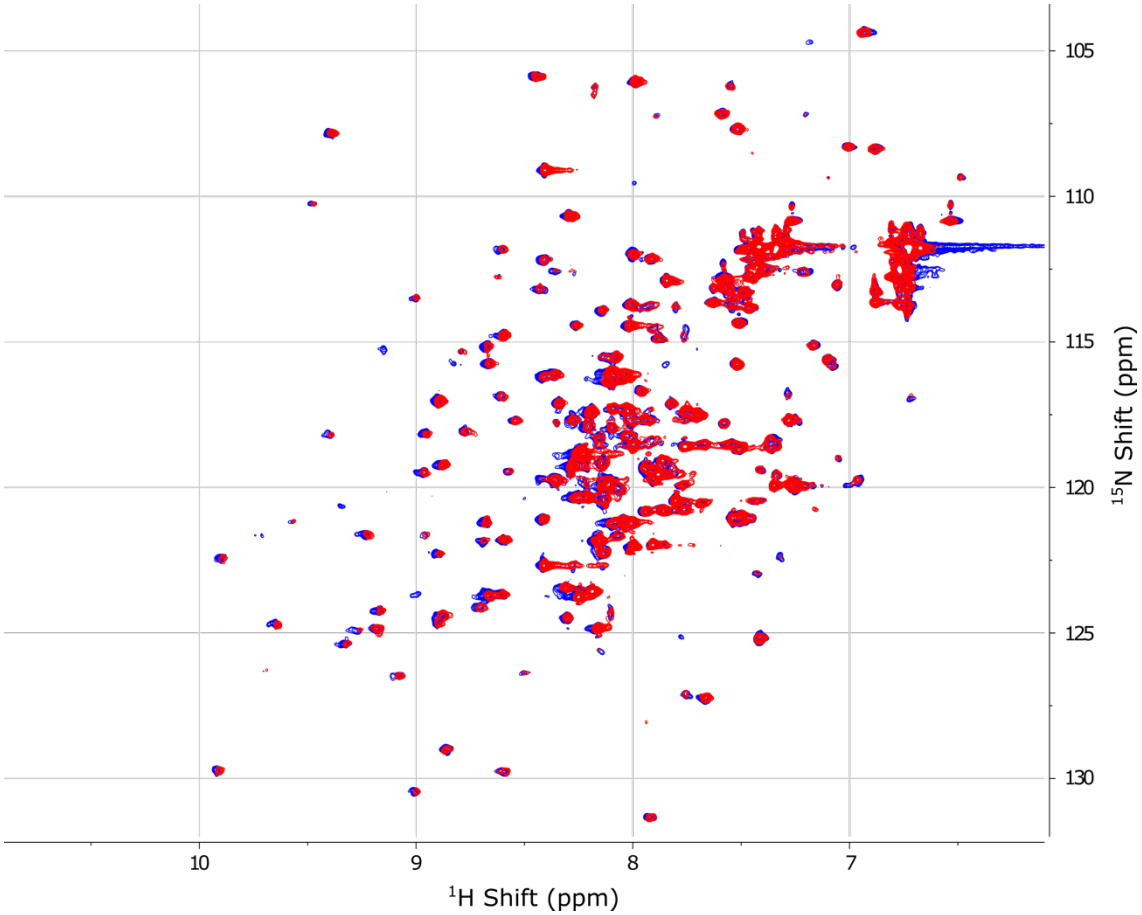


Figure 3.19 *^{1}H,^{15}N-HSQC spectrum of the oxic WelO5 complex in the presence (red) and absence (blue) of Fe(II). Peak positions in the presence and absence of Fe(II) are very similar at these initial timepoints. Standard concentrations of each component were: 100 µM ^{15}N-labelled WelO5, 300 µM Fe(II), and room pressure O_2. Buffer conditions were 10% D_2O, and 90% 50 mM Tris-d_{11} pH 6.5.*

As with the WelO5:Fe(II):2OG complex, the WelO5:Fe(II) complex forms over an extended time period. (**Figure 3.20**). The complex that is formed strongly resembles the WelO5:Fe(II):2OG complex, which may indicate that 2OG has a weaker impact on the structure of WelO5 than is observed for PHD2.

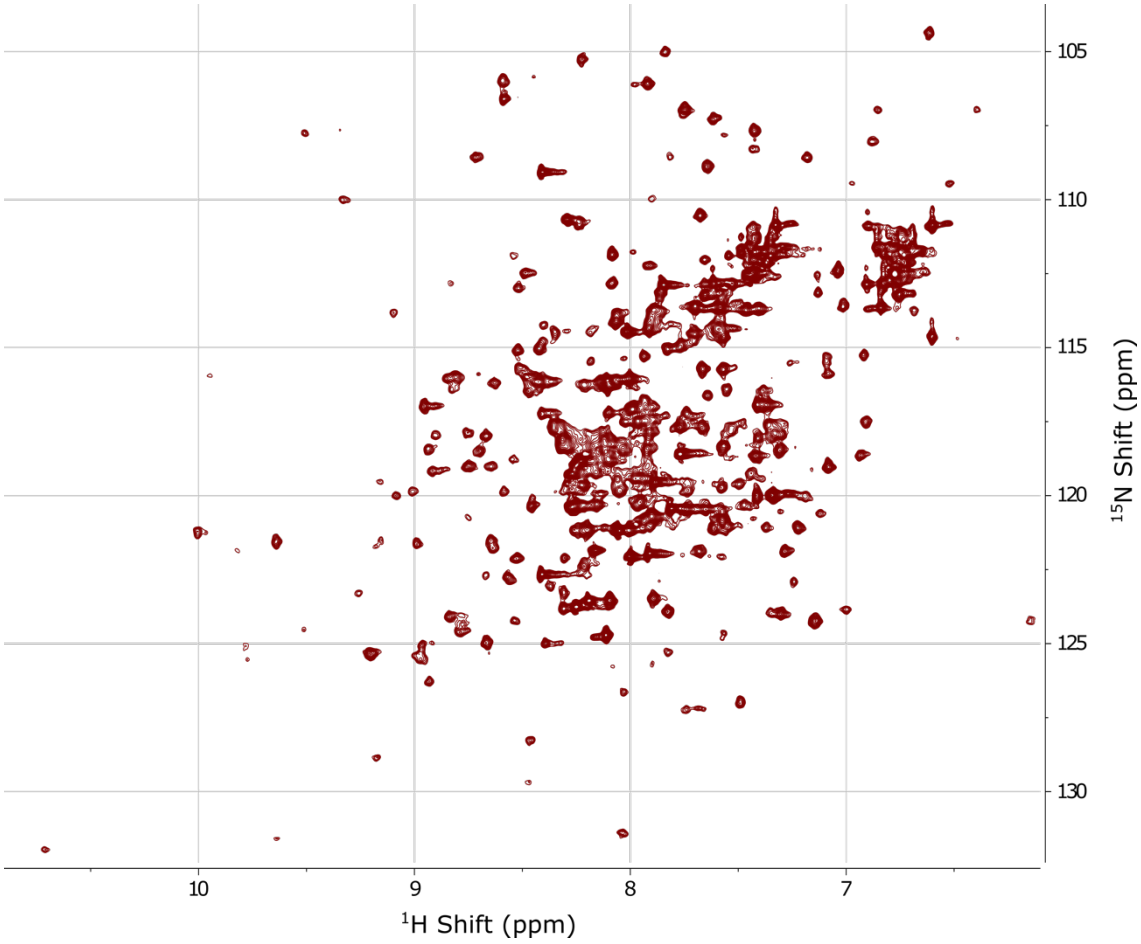


Figure 3.20 *^{1}H,^{15}N-HSQC spectrum of the oxic WelO5:Fe(II) complex. Interestingly, in the absence of cofactor, the WelO5:Fe(II) complex resembles the WelO5:Fe(II):2OG complex, both in its delayed formation and its ^{1}H,^{15}N-HSQC spectral shifts. Standard concentrations of each component were: 100 μM ^{15}N-labelled WelO5, 300 μM Fe(II), and room pressure O_2. Buffer conditions were 10% D_2O, and 90% 50 mM Tris-d_{11} pH 6.5.*

On addition of 2OG to the WelO5:Fe(II) complex that has been left for an extended time to form (**Figure 3.21**), very few changes were observed in the ^{1}H,^{15}N-HSQC spectrum, with minor shift differences but no indication of substantial structural changes. It's notable that the ^{1}H,^{15}N-HSQC spectrum of the WelO5:Fe(II):2OG complex has fewer peaks when 2OG is added after the WelO5:Fe(II) complex has been formed for several hours. This may indicate that oxidation of the active site Fe(II) to Fe(III) occurs, inhibiting the ability of 2OG to bind. It may also be due to degradation of the sample.

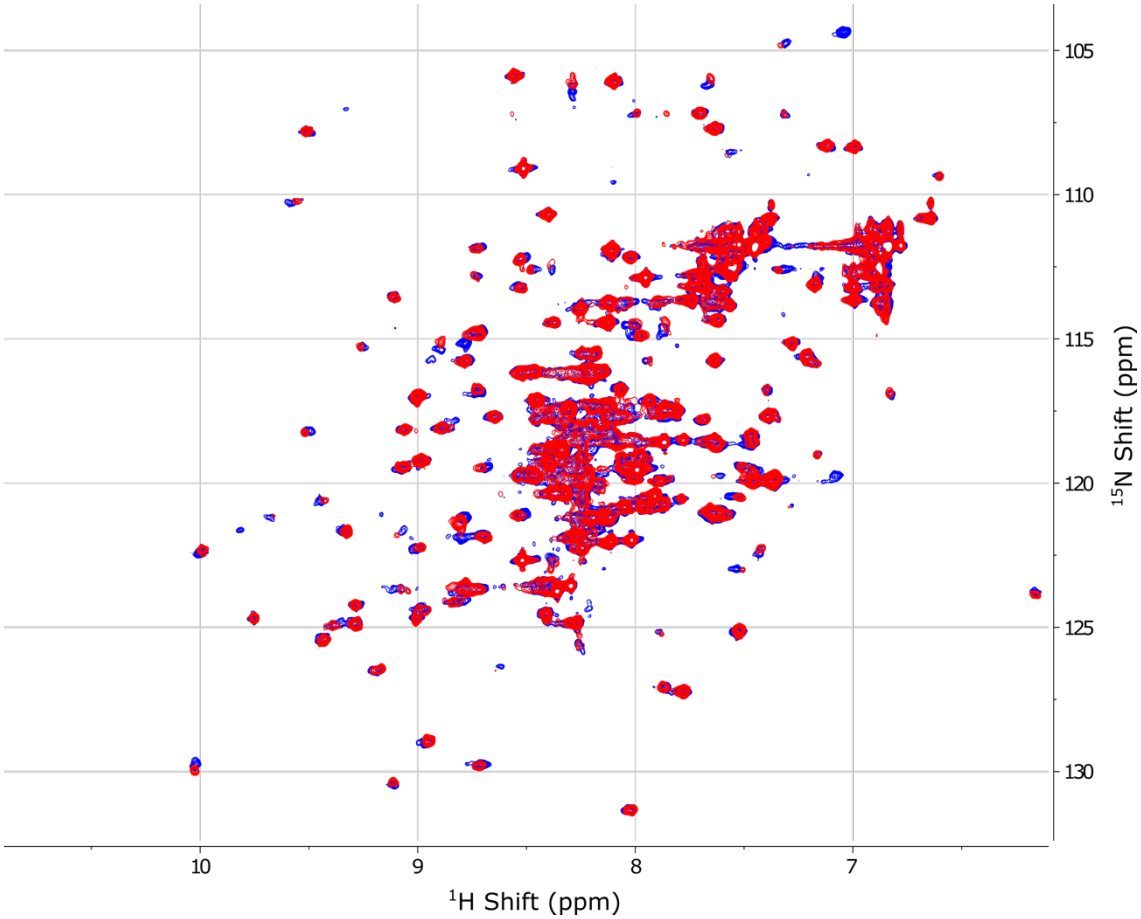


Figure 3.21 *^{1}H,^{15}N-HSQC spectrum of the oxic WelO5:Fe(II) complex in the presence (red) and absence (blue) of 2OG. Few peak shifts are observed on addition of 2OG to the WelO5:Fe(II) complex. Standard concentrations of each component were: 100 µM ^{15}N-labelled WelO5, 300 µM Fe(II), 500 µM 2OG, and room pressure O_2. Buffer conditions were 10% D_2O, and 90% 50 mM Tris-d_{11} pH 6.5.*

With this data in mind, as well as the WelO5:Fe(II):2OG complex formation studies (**Figure 3.7**), the oxic WelO5:Fe(II):2OG complex was subsequently kept at 4 °C overnight to fully form the complex before starting any experiments (**Figure 3.22**, blue). This resulted in a much more ordered spectrum that resembled other WelO5:metal:2OG complexes, though substantial crowding in the 8 ppm region was still observed.

The substrate, 12-epi-fischerindole U (EFIU), was then added to the WelO5:Fe(II):2OG complex and the sample was left for 2 hours to equilibrate (**Figure 3.22**, red). The complex that was formed showed only minor peak shifts over time, with

evidence of both EFIU and WelO5 protein precipitation. This may indicate 1) poor EFIU binding to the WelO5:Fe(II):2OG complex, 2) little to no change in the structure of the protein when substrate binds, or 3) a slow binding interaction between the WelO5:Fe(II):2OG complex and EFIU, as has been seen with other components of the WelO5 complex.

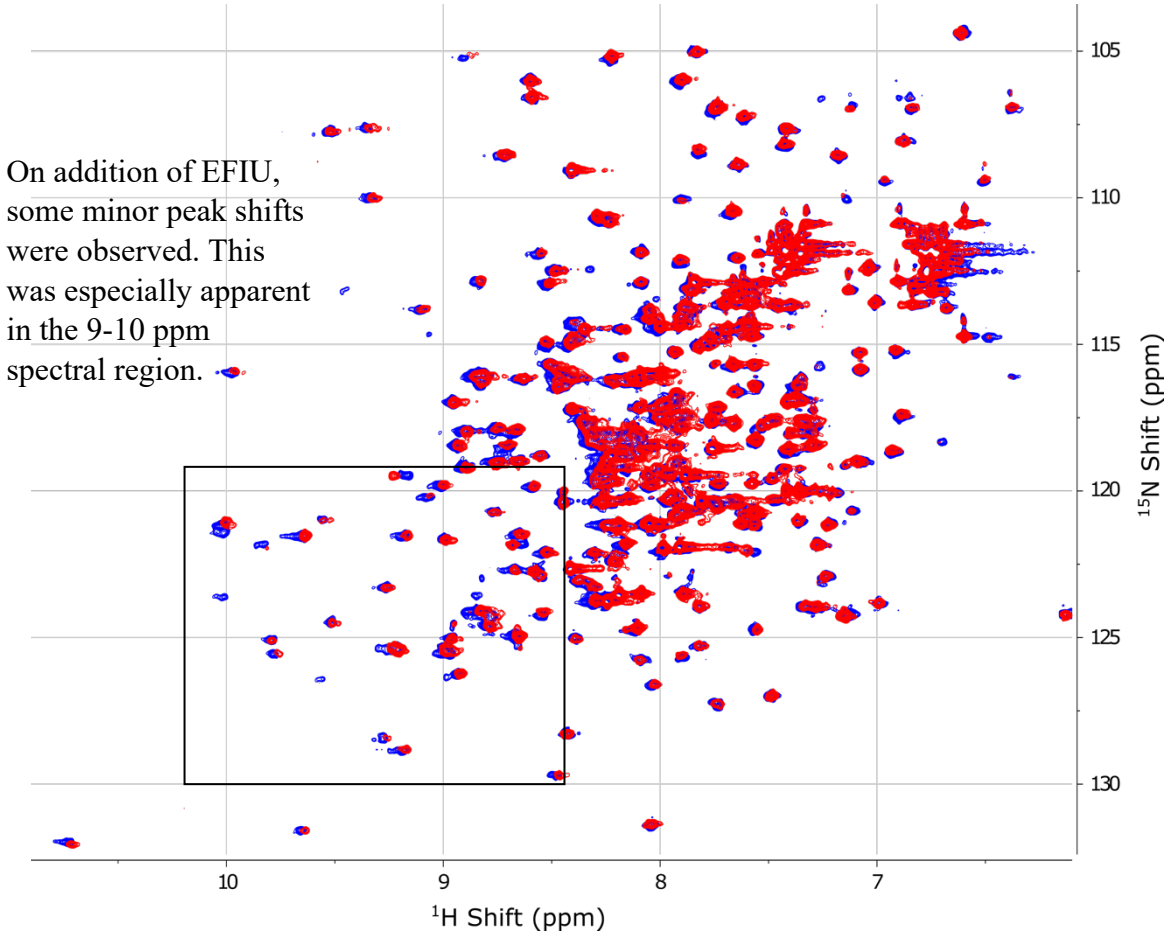


Figure 3.22 *^{1}H,^{15}N-HSQC spectrum of the oxic WelO5:Fe(II):2OG complex in the presence (red) or absence (blue) of EFIU substrate. Small changes in WelO5:Fe(II):2OG peaks are observed on EFIU binding. Peak shifts were most obvious in the region of the spectrum between 9-10 ppm, as shown within the black box. Standard concentrations of each component were: 100 µM ^{15}N-labelled WelO5, 300 µM Fe(II), 500 µM 2OG, 500 µM EFIU, and room pressure O_2. Buffer conditions were 10% D_2O, and 90% 50 mM Tris-d_{11} pH 6.5.*

Studies on the *apo*-WelO5, WelO5:Fe(II), WelO5:Fe(II):2OG, and WelO5:Fe(II):2OG:EFIU complexes have shown slow binding of each component of the WelO5 active/native complex. Evidence for EFIU substrate binding to the WelO5:Fe(II):2OG complex is unclear. Due to the difficulty of forming WelO5:Fe(II) complexes, oxygen studies may be difficult. Further optimisation may be needed.

3.2.6.2 Oxic and Anoxic Complex Comparison Studies

After observing the drawbacks of the oxic WelO5:Fe(II) complexes, it was of interest to determine if these same qualities can be observed in the anoxic WelO5:Fe(II) complexes. These complexes may be informative on the cause of the oxic WelO5:Fe(II) complex instability.

Interestingly, the anoxic WelO5:Fe(II):2OG complex gave a relatively strong spectrum with only minor crowding of peaks in the 8 ppm region (**Figure 3.23**, blue). As with the oxic WelO5:Fe(II):2OG complex (**Figure 3.8**), only one set of signals was observed.

When nitric oxide (NO) was added to the anoxic WelO5:Fe(II):2OG complex, no changes in the spectrum were observed. This result is similar to what had been observed with the anoxic PHD2:Fe(II):2OG complex on NO addition (Chapter 2, **Figure 2.28**), though dissimilar to what has been seen with some other 2OG-dependent dioxygenases, including clavaminate synthase, which has been observed to bind NO in crystallographic studies. [20]

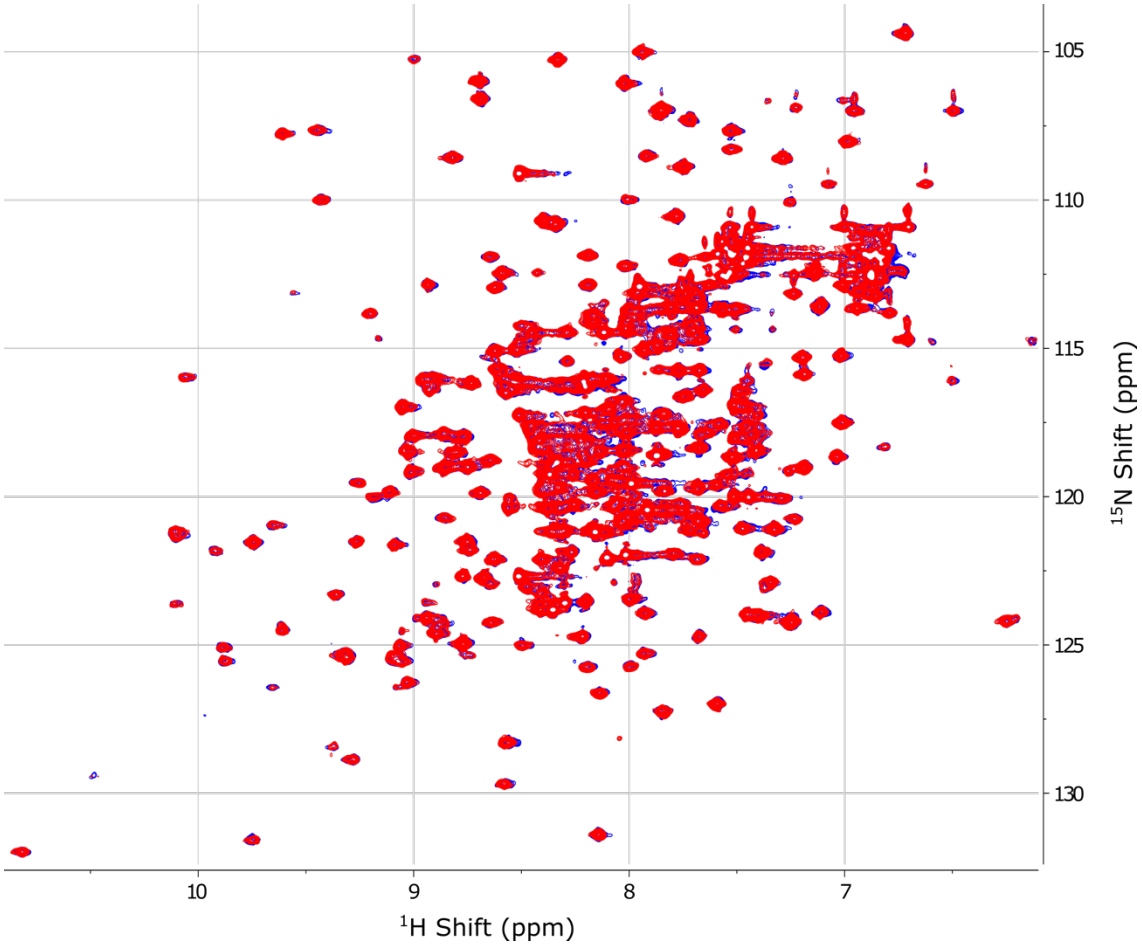


Figure 3.23 *^{1}H,^{15}N-HSQC spectrum of the anoxic WelO5:Fe(II):2OG complex in the presence (red) or absence (blue) of nitric oxide (NO). No changes in the spectrum were observed on addition of NO. Standard concentrations of each component were: 100 µM ^{15}N-labelled WelO5, 200 µM Fe(II), 400 µM 2OG, and 1000 ppm of NO. Buffer conditions were 10% D_2O, and 90% 50 mM Tris-d_{11} pH 6.5.*

These experiments were repeated with addition of succinate in place of the 2OG, potentially to form WelO5:Fe(II):succinate and WelO5:Fe(II):succinate:NO complexes (**Figure 3.24**). This was, in part, to see if the addition of a monodentate binding ligand would better allow for nitric oxide binding. The WelO5:Fe(II):succinate complex exhibited a highly crowded spectrum with peaks falling mostly in the region of 7-9 ppm. On NO addition, no change in the spectrum was observed except for some loss in peak intensity, likely due to protein precipitation over time due to the instability of the complex. This result aligns with previous studies that indicated succinate exhibits weak

cosubstrate binding at the active site metal due to its monodentate binding mode (Chapter 2, **Figure 2.73**). [21]

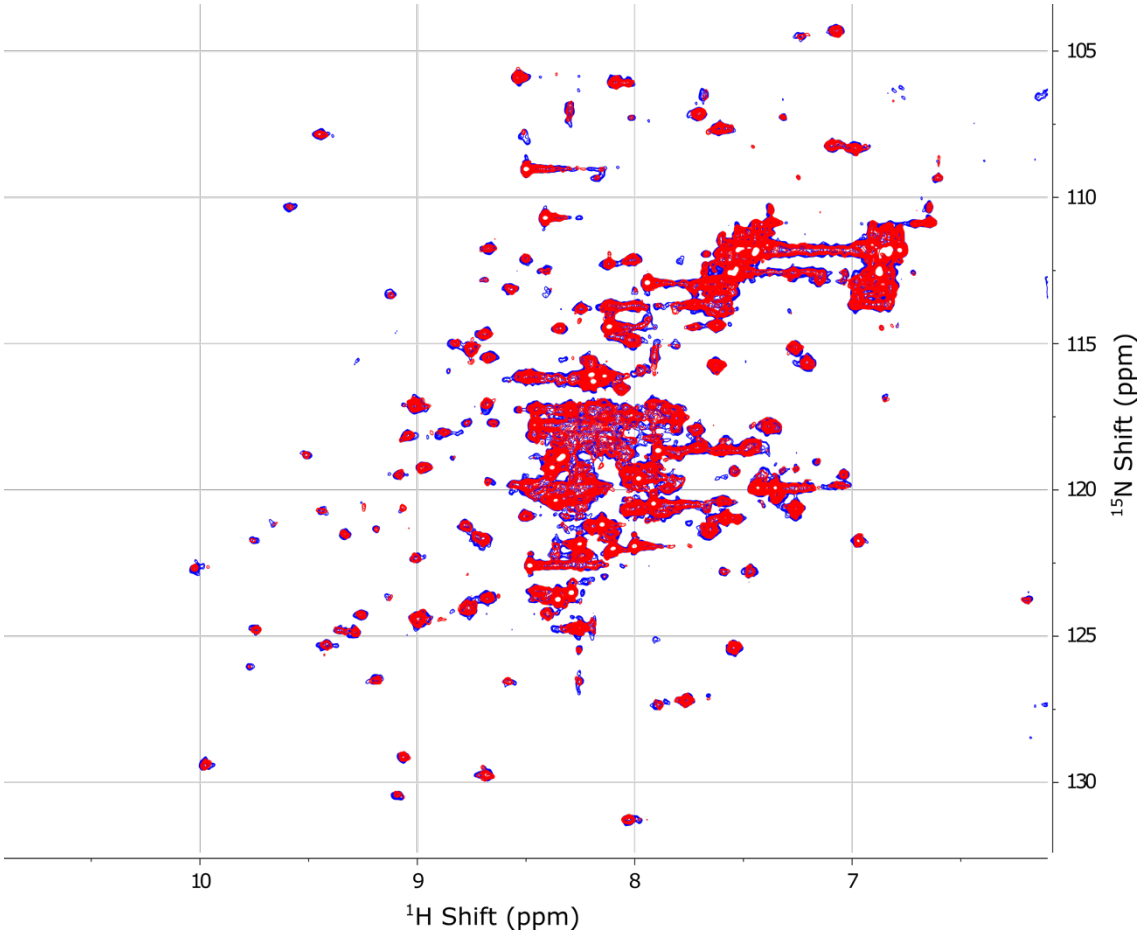


Figure 3.24 *^{1}H,^{15}N- spectrum of the anoxic WelO5:Fe(II):succinate complex in the presence (red) or absence (blue) of nitric oxide (NO). No significant changes were observed on NO addition. Standard concentrations of each component were: 100 µM ^{15}N-labelled WelO5, 200 µM Fe(II), 800 µM succinate, and 1000 ppm of NO. Buffer conditions were 10% D_2O, and 90% 50 mM Tris-d_{11} pH 6.5.*

Comparison of the anoxic WelO5:Fe(II):2OG complex (**Figure 3.23** and **Figure 3.24)** with the oxic WelO5:Fe(II):2OG complex (**Figure 3.8**) showed no change in the ^{1}H,^{15}N-HSQC spectrum on addition of O_2. Thus, this contrasts drastically with what had been observed in the case of the oxic and anoxic PHD2:Fe(II):2OG complexes (as seen in **Figure 2.17**, **Figure 2.18**, and **Figure 2.19**). The lack of spectral change on addition of oxygen to the WelO5:Fe(II):2OG complex, but not the PHD2:Fe(II):2OG complex

supports the proposal that PHD2 may be special in its reaction with oxygen. Further studies will be needed to explore the differences between the PHD2 and WelO5 complexes and their interactions with oxygen.

As has been discussed in **Section 2.3** of Chapter 2, the unique oxic complex of PHD2 (thought to be a sequestered PHD:Fe(III):2OG:HIF complex) can be reversed by the addition of ascorbate. Therefore, studies of the effect of ascorbate on WelO5 were of interest. Addition of ascorbate to the oxic WelO5:Fe(II):2OG complex lead to no change in the spectrum (**Figure 3.25**). Analysis of the ^{1}H spectrum within the timeframe of the ^{1}H,^{15}N-HSQC experiment indicated that consumption of ascorbate was occurring alongside uncoupled turnover. This indicates that uncoupled 2OG turnover did not cause unique changes in the WelO5 structure or the active site metal, in contrast to what had been observed in the case of PHD2 (Chapter 2, **Figure 2.17** and **Figure 2.90**). This may be further evidence for the unique oxygen interaction mechanism of PHD2.

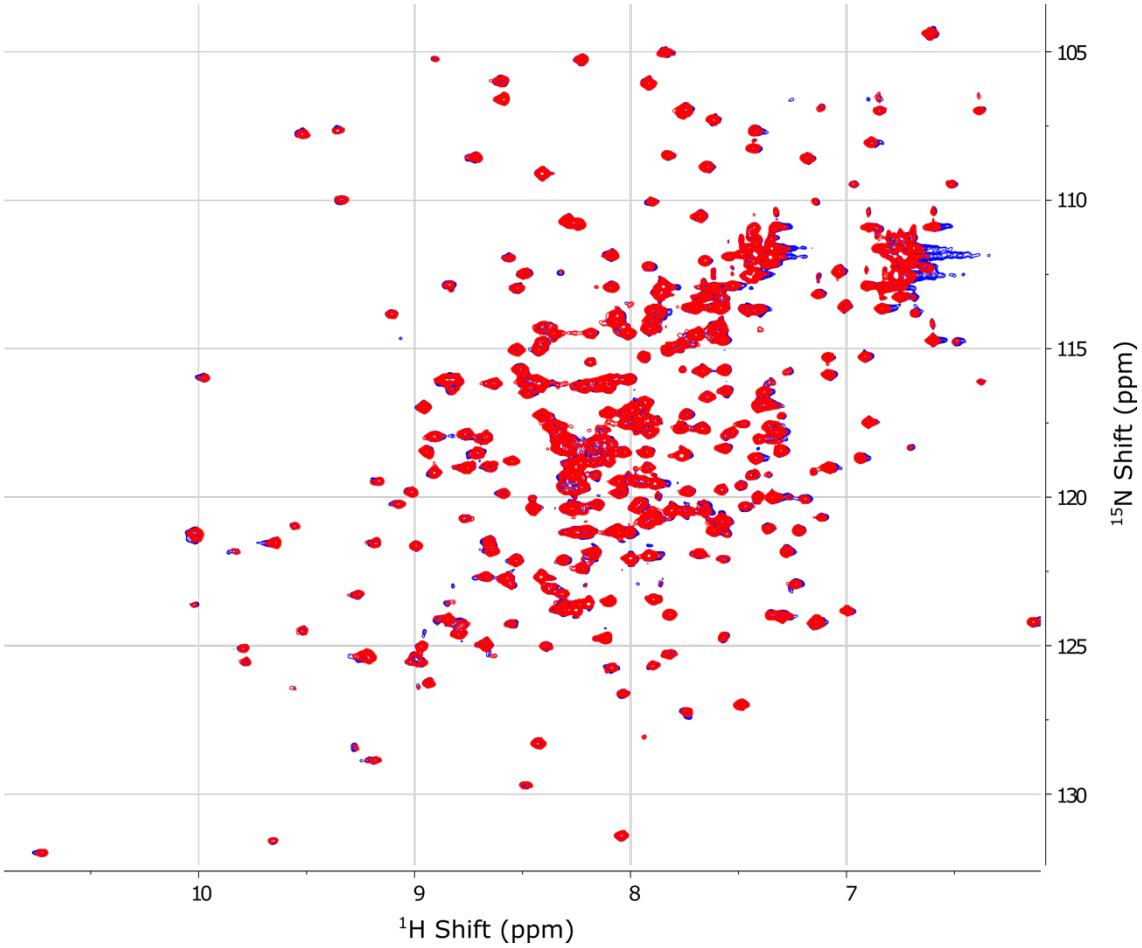


Figure 3.25 *$^{1}H,^{15}N$-HSQC spectrum of the oxic WelO5:Fe(II):2OG complex in the presence (red) or absence (blue) of ascorbate. No change was observed on ascorbate addition. Standard concentrations of each component were: 100 µM ^{15}N-labelled WelO5, 150 µM Fe(II), 400 µM 2OG, 500 µM ascorbate, and room pressure O_2. Buffer conditions were 10% D_2O, and 90% 50 mM Tris-d_{11} pH 6.5.*

3.3 Summary

NMR studies on WelO5 were carried out with the intent to investigate features of WelO5 that promote halogenation over hydroxylation and the seemingly unique structural features of PHD2. While WelO5 has been previously studied, little is known about its dynamics, so the first goal of this research was to acquire 3-D NMR spectral data for assignment of the $^{1}H,^{15}N$-HSQC spectrum, which would be a useful tool in site-specifically tracking structural changes in WelO5.

Conditions were developed for 3D studies, starting with analysis of metal binding. Some key findings were: 1) the WelO5:Co(II):2OG complex exhibits strong paramagnetic peak shifts, as had previously been observed with the PHD2:Co(II):2OG complex, but does not similarly exhibit doubling of number of peaks, 2) the oxic WelO5:Fe(II), WelO5:Fe(II):2OG, and WelO5:Fe(II):2OG:EFIU complexes are slow to form, and 3) most WelO5 complexes in the presence of Zn(II) are unstable. Studies on oxygen interaction with WelO5 revealed no change in $^{1}H,^{15}N$-HSQC spectra on introduction of oxygen or the surrogate molecule NO to the protein solution: 1) the anoxic and oxic WelO5:Fe(II):2OG spectra were identical, with a single set of peaks, 2) NO did not cause changes in the anoxic WelO5:Fe(II):2OG or anoxic WelO5:Fe(II):succinate complex spectra, 3) and addition of ascorbate did not change the $^{1}H,^{15}N$-HSQC spectrum of the oxic WelO5:Fe(II):2OG complex, despite evidence of uncoupled turnover. This further supports the idea that the unique doubling of peaks and shift differences observed in some PHD2 complexes under various metal and oxic/anoxic conditions may be evidence of the unusual nature of PHD2.

Despite high quality 2-D and 3-D spectra collected from the WelO5:Zn(II):2OG complex, enough peaks were missing so that the $^{1}H,^{15}N$-HSQC spectrum could not be assigned. Future work may involve attempting to collect 3-D spectra of the WelO5:Ni(II):2OG complex, since the $^{1}H,^{15}N$-HSQC spectrum of the WelO5:Zn(II):2OG complex could be assigned from this data by nearest neighbour approach due to the similarity in the spectra.

The work described in this chapter has helped to lay a foundation for future detailed studies on WelO5 in solution. Unfortunately, my studies were curtailed due to the COVID-19 pandemic. Some interesting conclusions can, however, be drawn from the results, including with respect to comparison for the studies on PHD2 described in

Chapter 2. In particular, the NMR studies imply important differences in the reactivity of the two 2OG-dependent dioxygenases with Fe(II), O_2, and 2OG. In the absence of O_2, the PHD2:Fe(II) complex binds 2OG to form an PHD2:Fe(II):2OG complex, which manifests conformational mobility, as evidenced by the observation of two sets of NMR signals. The PHD2:Fe(II):2OG complex then reacts with O_2 to give a stable "oxic" PHD2:Fe(III):2OG complex, which is less conformationally mobile. Although further work is required, the apparent difference in conformational mobility may reflect a difference in coordination chemistry at the active site. By contrast, the WelO5, Fe(II), and 2OG NMR studies imply formation of the same complex under anoxic and oxic conditions—this is most likely the WelO5:Fe(II):2OG complex, something that can be tested by EPR and other spectroscopic analyses. This complex was slower to form in the presence of O_2, possibly because the oxidation of the active site Fe(II) to Fe(III) blocked its formation. Although further work is required, the results for WelO5 and PHD2, combined with those for other 2OG-dependent dioxygenases, are consistent with the proposal that PHD2 is an unusual 2OG-dependent dioxygenase, in particular with respect to its slow reaction with O_2 and, as shown here, by the formation of a stable inactive PHD2:Fe(II):2OG complex, which can reversibly bind HIF-α.

3.4 References

[1] M. Z. Hernandes, S. M. T. Cavalcanti, D. R. M. Moreira, W. F. d. Azevedo and A. C. L. Leite, "Halogen Atoms in the Modern Medicinal Chemistry: Hints for the Drug Design, Current Drug Targets," *Current Drug Targets,* vol. 11, no. 3, pp. 303-314, 2010.

[2] P. N. Devine, R. M. Howard, R. Kumar, M. P. Thompson, M. D. Truppo and N. J. Turner, "Extending the application of biocatalysis to meet the challenges of drug development," *Nature Reviews Chemistry,* vol. 2, pp. 409-421, 2018.

[3] A. Fryszkowska and P. N. Devine, "Biocatalysis in drug discovery and development," *Current Opinion in Chemical Biology,* vol. 55, pp. 151-160, 2020.

[4] A. J. Mitchell, Q. Zhu, A. O. Maggiolo, N. R. Ananth, M. L. Hillwig, X. Liu and A. K. Boal, "Structural basis for halogenation by iron- and 2-oxo-glutarate-dependent enzyme WelO5," *Nature Chemical Biology,* vol. 12, p. 636–640, 2016.

[5] E. Gallimore, *Evaluating the biocatalytic potential of a small molecule 2-oxoglutarate dependent halogenase,* Oxford: University of Oxford, 2018.

[6] W. D. Figg, M. A. McDonough, R. Chowdhury, Y. Nakashima, Z. Zhang, J. P. Holt-Martyn, A. Krajnc and C. J. Schofield, "Structural Basis of Prolyl Hydroxylase Domain Inhibition by Molidustat," *ChemMedChem,* vol. 16, no. 13, p. 2082–2088, 2021.

[7] R. Chowdhury, M. A. McDonough, J. Mecinović, C. Loenarz, E. Flashman, K. S. Hewitson, C. Domene and C. J. Schofield, "Structural Basis for Binding of Hypoxia-Inducible Factor to the Oxygen-Sensing Prolyl Hydroxylases," *Structure,* vol. 17, no. 7, pp. 981-989, 2009.

[8] C. Domene, C. Jorgensen and C. J. Schofield, "Mechanism of Molecular Oxygen Diffusion in a Hypoxia-Sensing Prolyl Hydroxylase Using Multiscale Simulation," *Journal of the American Chemical Society,* vol. 142, no. 5, pp. 2253-2263, 2020.

[9] M. W. Thompson, "Regulation of zinc-dependent enzymes by metal carrier proteins," *BioMetals,* vol. 35, p. 187–213, 2022.

[10] M. Keith, H. Chih-chin and F. Carol, "Function and Mechanism of Zinc Metalloenzymes," *The Journal of Nutrition,* vol. 130, no. 5, pp. 1437S-1446S, 2000.

[11] J. Dong, K. L. Callahan, N. B. Borotto and R. W. Vachet, "Identifying Zn-bound histidine residues in metalloproteins using hydrogen deuterium exchange mass spectrometry," *Analytical Chemistry,* vol. 86, no. 1, p. 766–773, 2013.

[12] Z. Sun, Q. Liu, G. Qu, Y. Feng and M. T. Reetz, "Utility of B-Factors in Protein Science: Interpreting Rigidity, Flexibility, and Internal Motion and Engineering Thermostability," *Chemical Reviews,* vol. 119, no. 3, p. 1626–1665, 2019.

[13] M. P. Williamson, "Using chemical shift perturbation to characterise ligand binding," *Progress in Nuclear Magnetic Resonance Spectroscopy,* vol. 73, pp. 1-16, 2013.

[14] M. J. Tamás, S. K. Sharma, S. Ibstedt, T. Jacobson and P. Christen, "Heavy Metals and Metalloids As a Cause for Protein Misfolding and Aggregation," *Biomolecules,* vol. 4, no. 1, p. 252–267, 2014.

[15] B. M. Hoffman and D. H. Petering, "Coboglobins: Oxygen-Carrying Cobalt-Reconstituted Hemoglobin and Myoglobin," *Proceedings of the National Academy of Sciences of the United States of America,* vol. 67, no. 2, p. 637–643, 1970.

[16] M. Ikeda-Saito, H. Yamamoto, K. Imai, F. J. Kayne and T. Yonetani, "Studies on cobalt myoglobins and hemoglobins. Preparation of isolated chains containing cobaltous protoporphyrin IX and characterization of their equilibrium and kinetic properties of oxygenation and EPR spectra," *Journal of Biological Chemistry,* vol. 252, no. 2, pp. 620-624, 1977.

[17] Y. Fang, H. Zhang, Y. Zhong and X. Ding, "Prolyl hydroxylase 2 (PHD2) inhibition protects human renal epithelial cells and mice kidney from hypoxia injury," *Oncotarget,* vol. 7, no. 34, pp. 54317-54328, 2016.

[18] E. K. Barefield, D. H. Busch and S. M. Nelson, "Iron, Cobalt, and Nickel Complexes having Anomalous Magnetic Moments," *Quarterly Reviews, Chemical Spciety,* vol. 22, pp. 457-498, 1968.

[19] J. S. Griffith and L. E. Orgel, "The residual paramagnetism and nuclear magnetic resonance spectra of cobaltic complexes," *Transactions of the Faraday Society,* vol. 53, pp. 601-606, 1957.

[20] Z. Zhang, J. s. Ren, K. Harlos, C. H. McKinnon, I. J. Clifton and C. J. Schofield, "Crystal structure of a clavaminate synthase-Fe(II)-2-oxoglutarate-substrate-NO complex: evidence for metal centered rearrangements," *FEBS Letters,* vol. 517, no. 1-3, pp. 7-12, 2022.

[21] M. I. Abboud, T. E. McAllister, I. K. H. Leung, R. Chowdhury, C. Jorgensen, C. Domene, J. Mecinović, K. Lippl, R. L. Hancock, R. J. Hopkinson, A. Kawamura, T. D. W. Claridge and C. J. Schofield, "2-Oxoglutarate regulates binding of hydroxylated hypoxia-inducible factor to prolyl hydroxylase domain 2," *Chemical Communications,* vol. 54, no. 25, pp. 3130-3133, 2018.

Chapter 4:

Appendix

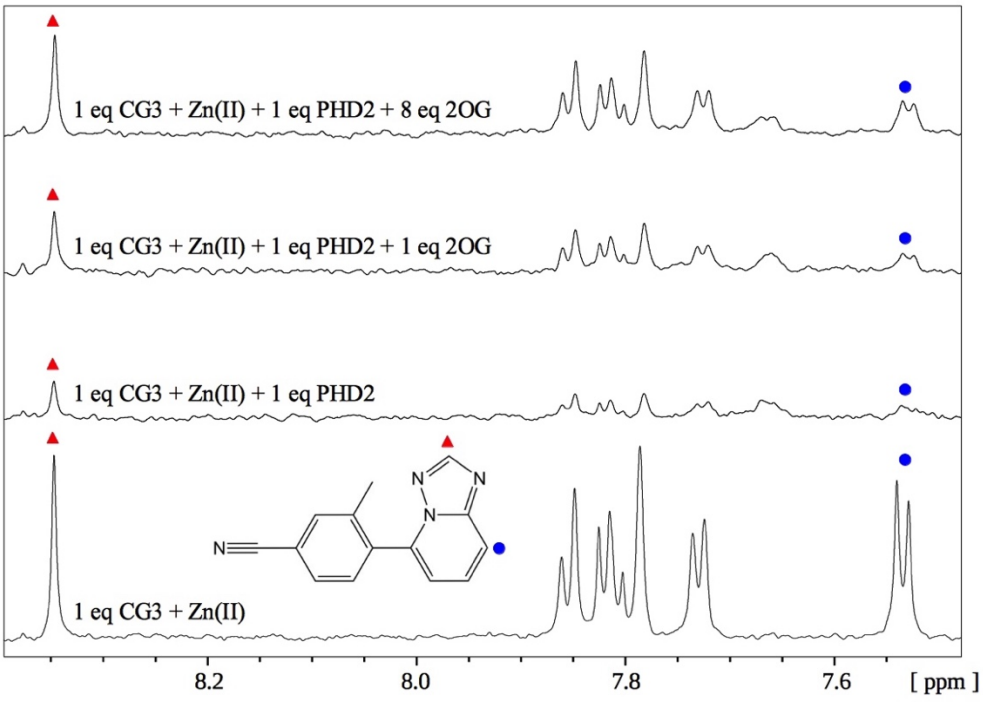


Table of Contents

Chapter 4: 1

4.1 Collaborative Work with IPNS 3

4.2 Studies of ZPR2, VRN2, and RAP2 3

4.3 PHD2 6

4.3.1 Inhibitor Studies 6

4.3.1.1 Takeda-like CG Compounds 6

4.3.1.1.1 Turnover Studies 7

4.3.1.1.2 Binding and Competition Studies 7

4.4 References 14

4.1 Collaborative Work with IPNS

^{19}F-NMR studies were carried out with Patrick Rabe for the paper: *Spectroscopic studies reveal details of substrate-induced conformational changes distant from the active site in isopenicillin N synthase.* [1] In this study, single and doubly labelled (^{19}F) IPNS mutants on the α3, α6, and α10 helices were perturbed by Fe(II), ACV, or nitric oxide (NO, a mimic of dioxygen) binding and observed through ^{19}F-NMR spectra. Cd(II) and Zn(II) in place of Fe(II) were used as controls. Additionally, the broadening and shifting of ^{19}F peaks were observed by varying temperature (information on variable temperature studies can be found in Chapter 2, **Section 2.2.1.3** and Chapter 3, **Section 3.2.3.4** of this thesis).

4.2 Studies of ZPR2, VRN2, and RAP2

NMR experiments to measure pKa values of ZPR2, VRN2, and RAP2 plant protein substrates were carried out in collaboration with Brian White at the University of Oxford. These proteins are of interest in the adaptation of plants to low oxygen conditions that may be a result of factors such as environmental conditions—flooding, ice, etc—or endogenously generated oxygen gradients within plants, [2] where oxygen concentrations within the plants can range from 2-9% relative to 21% ambiently. [3] ZPR2, VRN2, and RAP2 have been found to be involved in the regulation of genes related to shoot apical meristem (SAM) activity and leaf development, [3] flowering, [4] and the plant stress response to submergence [5] respectively. In this study, three substrates of plant oxygenases of interest were observed by ^{1}H NMR at the following pH values: 6.00, 6.19, 6.38, 6.62, 6.80, 6.98, 7.20, 7.58, and 7.78. Observation of the effects of pH variation on

oxygen-sensing proteins and substrates may mimic hypoxia stressors [6] and inform on the pKa of residues of interest, which can lead to better understanding of related function.

From these studies, the predicted pKa values for the proteins were as follows: 6.9 for ZPR2 (**Figure 4.1**), 6.7 for each of the VRN2 peaks measured (**Figure 4.2**), and 6.8 for RAP2 (**Figure 4.3**). The set of VRN2 experiments were repeated with a new batch of protein with the same results. Further analysis is needed.

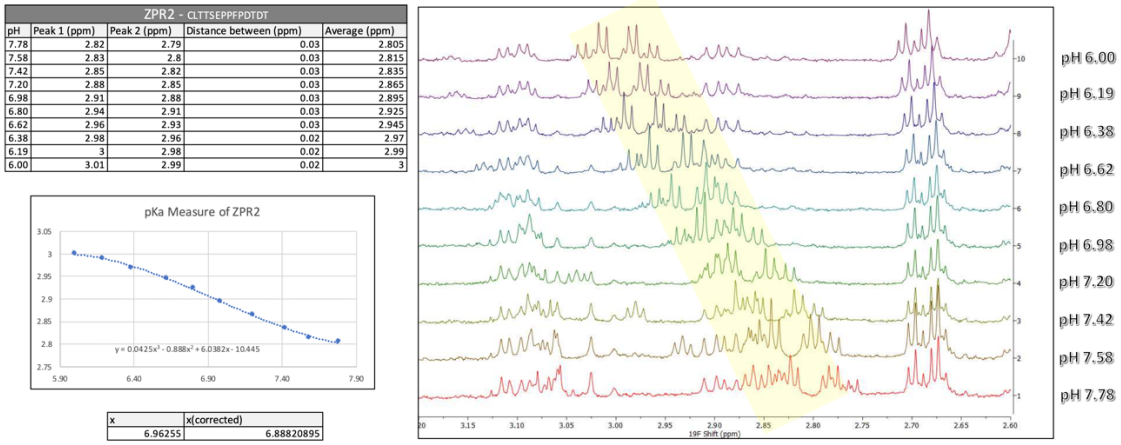


Figure 4.1 *^{1}H NMR spectral analysis of the pKa of ZPR2. Peak shift analysis gives a pKa of approximately 6.9.*

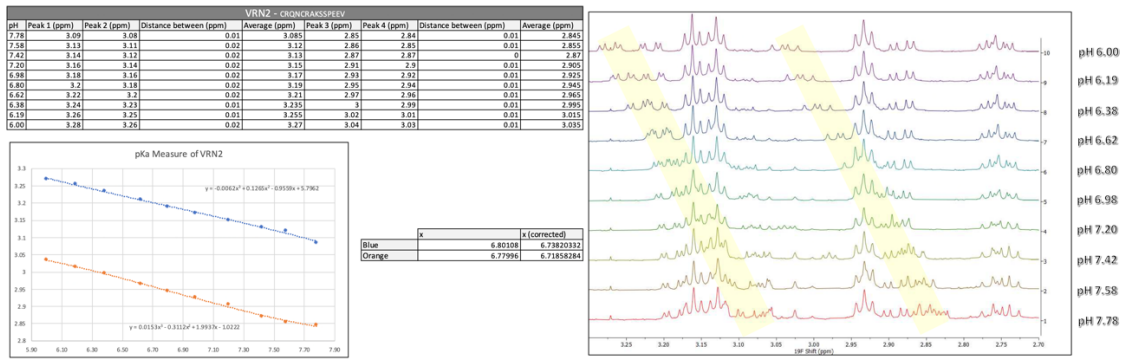
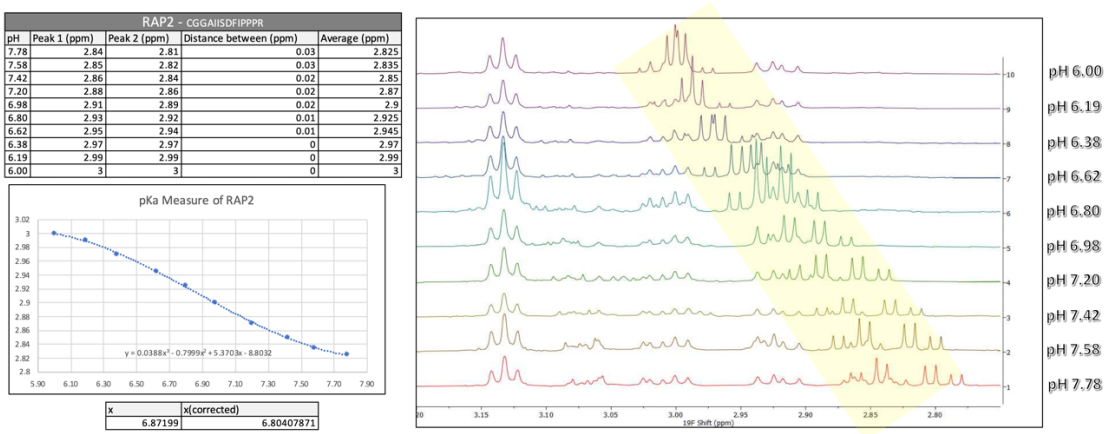


Figure 4.2 *^{1}H NMR spectral analysis of the pKa of VRN2. Peak shift analysis gives a pKa of approximately 6.7 for each of the peaks of interest. This experiment was repeated with the same results. Further analysis is needed.*



RAP2 - CGGAIISDFIPPPR

pH	Peak 1 (ppm)	Peak 2 (ppm)	Distance between (ppm)	Average (ppm)
7.78	2.84	2.81	0.03	2.825
7.58	2.85	2.82	0.03	2.835
7.42	2.86	2.84	0.02	2.85
7.20	2.88	2.86	0.02	2.87
6.98	2.91	2.89	0.02	2.9
6.80	2.93	2.92	0.01	2.925
6.62	2.95	2.94	0.01	2.945
6.38	2.97	2.97	0	2.97
6.19	2.99	2.99	0	2.99
6.00	3	3	0	3

x	x(corrected)
6.87199	6.80407871

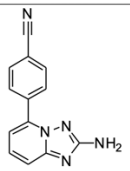
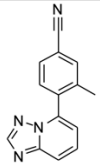
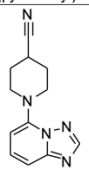
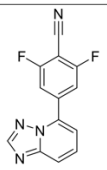
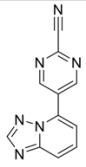
Figure 4.3 *^{1}H NMR spectral analysis of the pKa of RAP2. Peak shift analysis gives a pKa of approximately 6.8.*

4.3 PHD2

4.3.1 Inhibitor Studies

4.3.1.1 Takeda-like CG Compounds

The compounds discussed here were based on a molecule originally reported by researchers at Takeda pharmaceuticals, prepared in Oxford by Caitlin Gold (Department of Chemistry). [7]

CG1 **MW =235.25**	 4-(2-amino-[1,2,4]triazolo[1,5- *a*]pyridin-5-yl)benzonitrile
CG3 **MW= 234.26**	 4-([1,2,4]triazolo[1,5- *a*]pyridin-5-yl)-3-methylbenzonitrile
CG4 **MW = 227.27**	 1-([1,2,4]triazolo[1,5- *a*]pyridin-5-yl)piperidine-4-carbonitrile
CG6 **MW = 256.22**	 4-([1,2,4]triazolo[1,5-*a*]pyridin-5-yl)-2,6-difluorobenzonitrile
CG10 **MW = 222.21**	 5-([1,2,4]triazolo[1,5-*a*]pyridin-5-yl)pyrimidine-2-carbonitrile

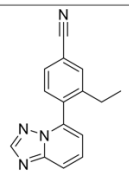
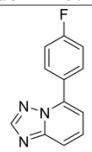
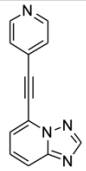
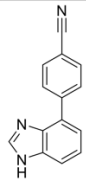
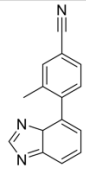
CG16 **MW= 248.29**	 4-([1,2,4]triazolo[1,5-*a*]pyridin-5-yl)-3-ethylbenzonitrile
CG17 **MW= 213.22**	 5-(4-fluorophenyl)-[1,2,4]triazolo[1,5-*a*]pyridine
CG22 **MW = 220.24**	 5-(pyridin-4-ylethynyl)-[1,2,4]triazolo[1,5- *a*]pyridine
CG25 **MW = 219.25**	 4-(1*H*-benzo[*d*]imidazol-4-yl)benzonitrile
CG27 **MW = 233.27**	 4-(3a*H*-benzo[*d*]imidazol-4-yl)-3-methylbenzonitrile

Figure 4.4 *A list of compounds prepared by Caitlin Gold (Department of Chemistry, University of Oxford).*

4.3.1.1.1 Turnover Studies

Each of the inhibitors was added to a solution containing PHD2, Fe(II), ascorbate, 2OG, and HIF-1α CODD (as described in Chapter 5, **Section 5.2.4.1**) and turnover was followed by ^{1}H NMR spectroscopy (**Figure 4.5**). From these studies, it was found that the inhibitor with the greatest inhibitory potential, even greater than the optimal Takeda compound, [7] was CG3 (**Figure 4.5**, dark blue).

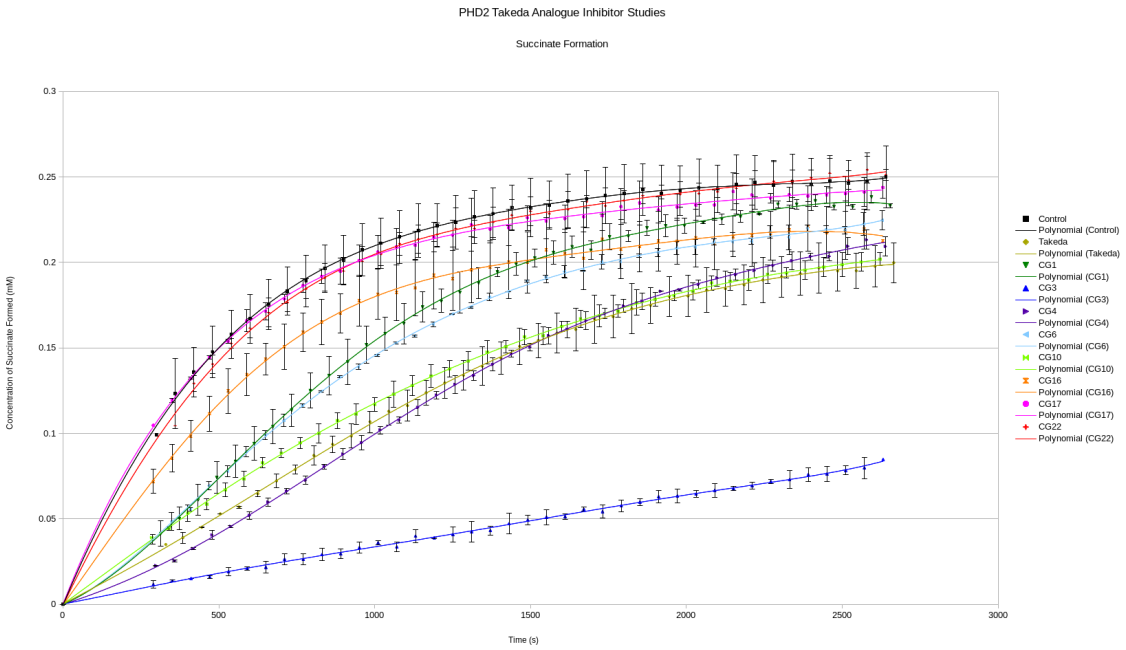


Figure 4.5 *Comparison of turnover of 2OG in the presence of CG compounds. The rate of 2OG turnover in the presence of various CG inhibitors was observed by ^{1}H NMR time-course experiments. From these studies, the CG compound that showed the most inhibition was CG3. All other compounds showed no/limited inhibition.*

4.3.1.1.2 Binding and Competition Studies

Next, binding and competition studies between inhibitors of interest and 2OG were carried out to determine the relative affinities of each inhibitor candidate to PHD2 (**Figure 4.6**). 1 equivalent of 2OG was added to a PHD2:Zn(II) complex, where Zn(II) is used as a diamagnetic mimic of Fe(II). On addition of a single equivalent of CG3, approximately half of the PHD2:Zn(II):2OG complex was lost. On addition of 7

equivalents of CG3, most of the PHD2:Zn(II):2OG complex was lost, indicating that CG3 may inhibit PHD2.

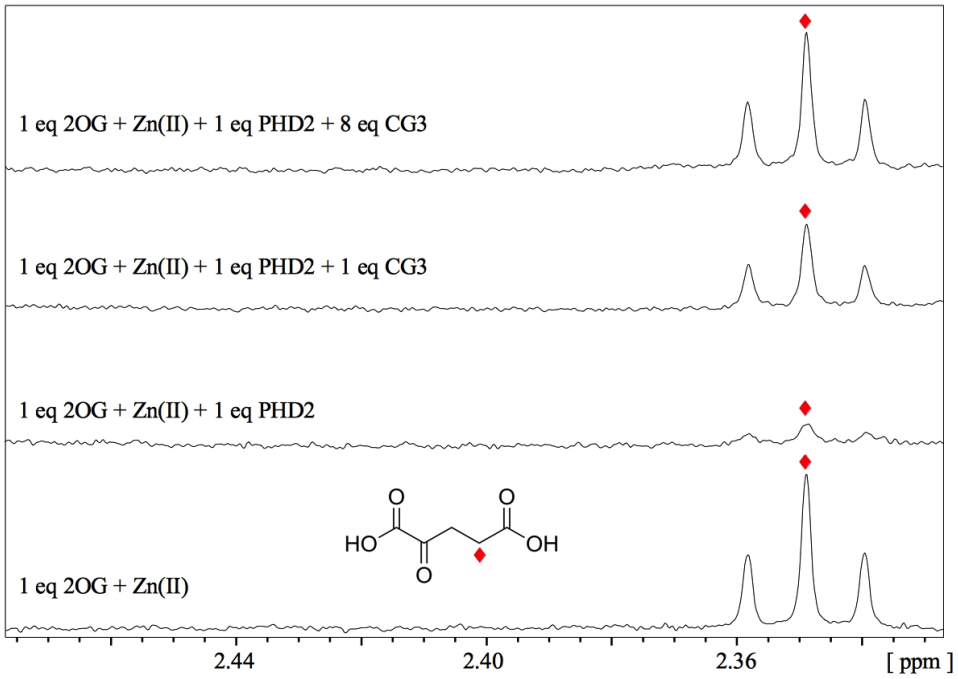


Figure 4.6 *CG3 competition assay. At 1 equivalent of PHD2 and 1 equivalent of 2OG, most of the 2OG is bound, as shown by the disappearance of the 2OG triplet peak. When 1 equivalent of CG3 is added, approximately half of the intensity of the 2OG triplet peak is restored, indicating that 2OG was displaced from binding to PHD2 by CG3. 7 more equivalents of CG3 were added and most of 2OG was displaced from binding with PHD2. This likely indicates that CG3 can readily displace 2OG binding at the PHD2 active site and may be useful as an inhibitor.*

The PHD2:Zn(II):CG3 complex was then mixed with 1 equivalent of 2OG to observe competition of 2OG with this inhibited complex (**Figure 4.7**). Minimal displacement of the PHD2:Zn(II):CG3 complex was observed. On addition of 7 more equivalents of 2OG, only approximately a third of the CG3 complex was displaced. This indicates that CG3 binding of PHD2:Zn(II) is not easily displaced by 2OG.

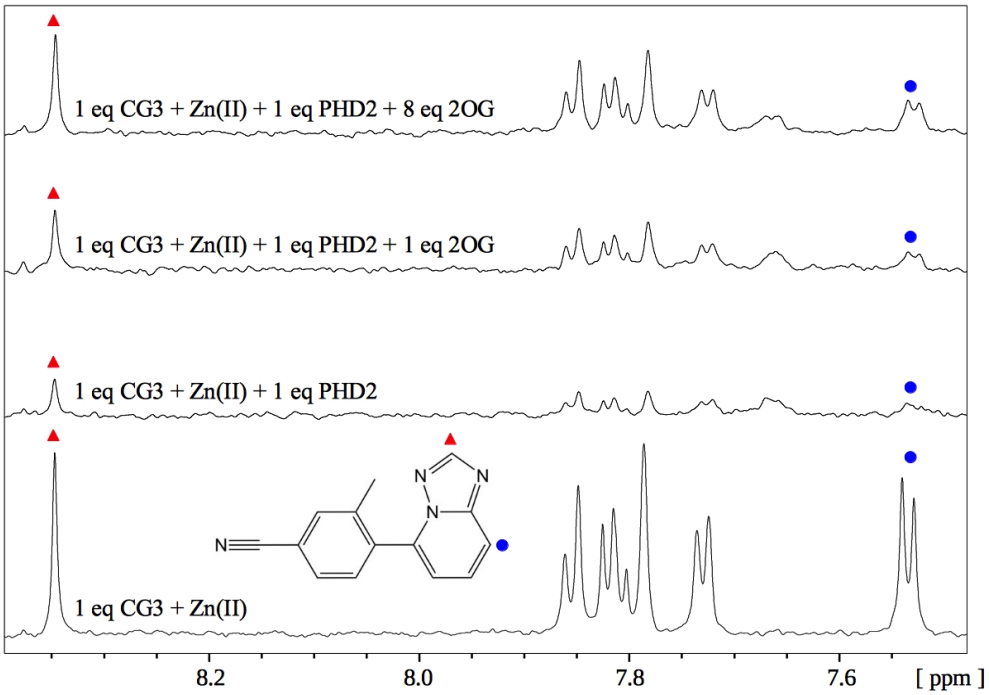


Figure 4.7 *CG3 binding assay. At 1 equivalent of PHD2 and 1 equivalent of CG3, most of the CG3 is bound to PHD2, as shown by the disappearance of the CG3 peaks. When 1 equivalent of 2OG is added, some of the intensity of the CG3 peaks was restored, indicating that some CG3 was displaced from binding to PHD2 by 2OG. 7 more equivalents of 2OG were added and the intensity of the free CG3 peaks approximately doubled. These observations imply CG3 may be a strong binder to PHD2.*

Analogous experiments with CG6 and CG22 indicated they are weaker binders to PHD2 (**Figure 4.8**, **Figure 4.9**, **Figure 4.10**, and **Figure 4.11**) and exhibit both weaker abilities to displace 2OG from the PHD2:Zn(II):2OG complex and are more easily displaced by 2OG binding from the PHD2:Zn(II):CG complexes than the related CG3 complex. Overall, these studies indicate that further exploration of Takeda-like compounds should focus on inhibitor structures similar to CG3, which has been shown to: 1) inhibit PHD2 more efficiently than the Takeda compound, 2) shows strong ability to displace 2OG from the PHD2:Zn(II):2OG complex, and 3) has a strong binding affinity for the PHD2:Zn(II) complex.

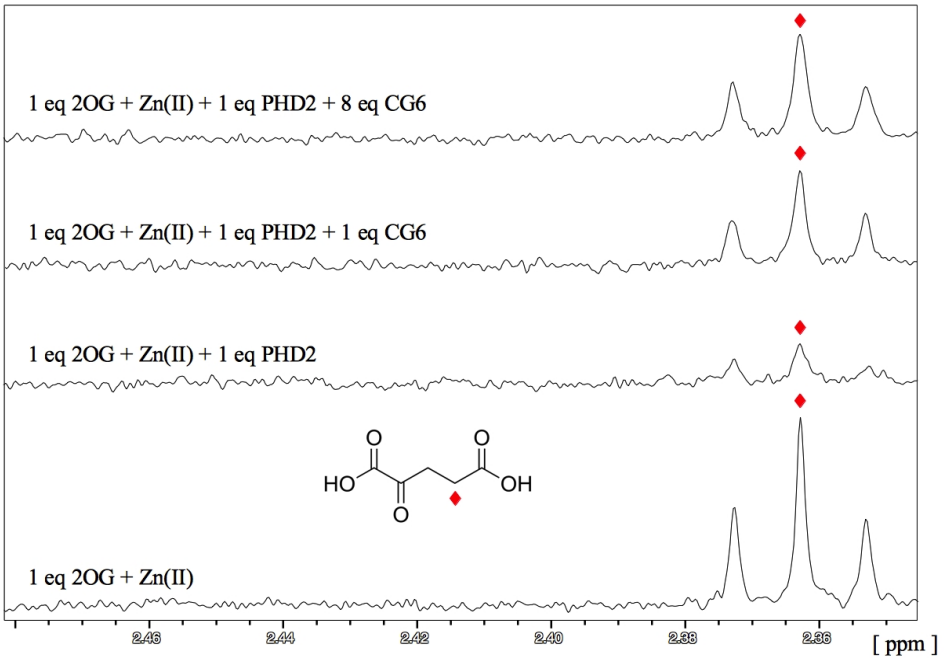


Figure 4.8 *CG6 competition assay. At 1 equivalent of PHD2 and 1 equivalent of 2OG, most of the 2OG is bound, as shown by the disappearance of the 2OG triplet peak. When 1 equivalent of CG6 is added, approximately half of the intensity of the 2OG triplet peak is restored, indicating that 2OG was displaced from binding to PHD2 by CG6. 7 more equivalents of CG6 were added, but no significant change in 2OG binding was observed. This may indicate that CG6 can displace 2OG binding at the PHD2 active site, but the effect is likely weaker than observed with CG3.*

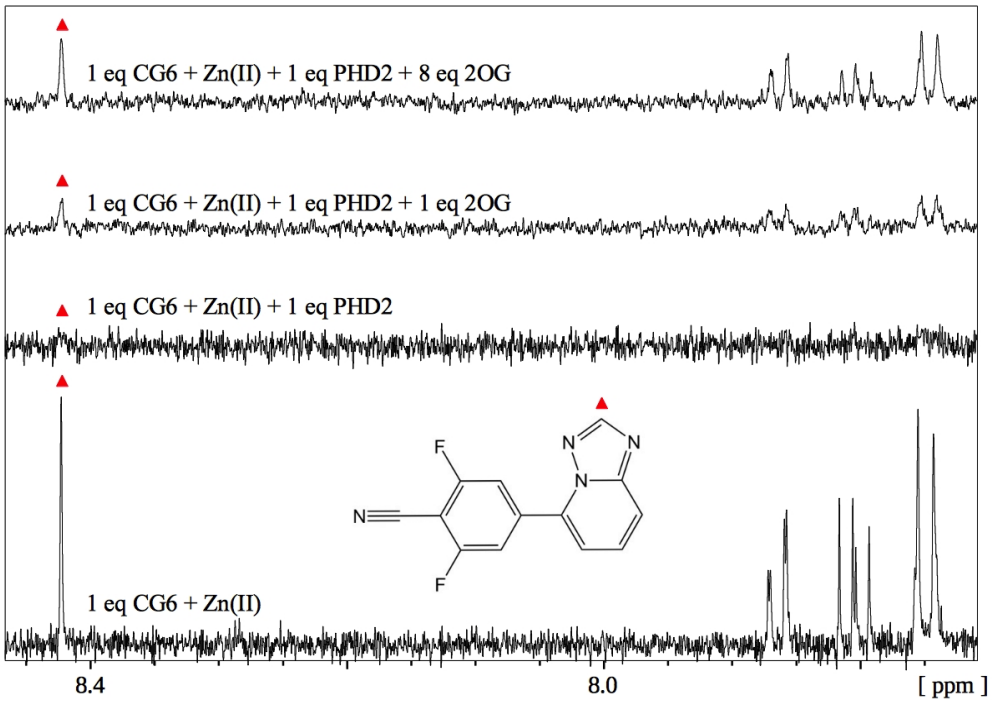


Figure 4.9 *CG6 binding assay. At 1 equivalent of PHD2 and 1 equivalent of CG6, most of the CG6 is bound to PHD2, as shown by the disappearance of the CG6 peaks. When 1 equivalent of 2OG was added, a small amount of the intensity of the CG6 peaks was restored, indicating that minimal CG6 was displaced from binging to PHD2 by 2OG. 7 more equivalents of 2OG were added and the intensity of the free CG6 peaks approximately doubled. Minimal displacement of CG6 may indicate that CG6 is a strong binder.*

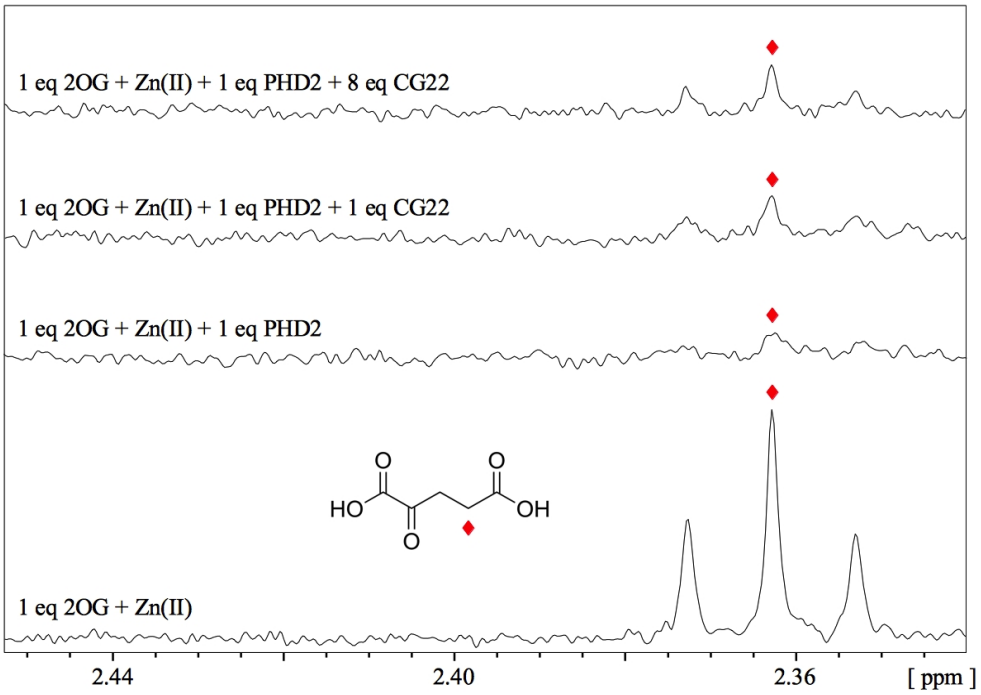


Figure 4.10 *CG22 competition assay. At 1 equivalent of PHD2 and 1 equivalent of 2OG, most of the 2OG is bound, as shown by the disappearance of the 2OG triplet peak. 1 equivalent of CG22 is added, but there is minimal displacement of 2OG binding to PHD2. Similarly, after adding 7 additional equivalents of CG22 there is little displacement of 2OG. From this assay it appears that CG22 is not efficient at displacing 2OG from PHD2 binding.*

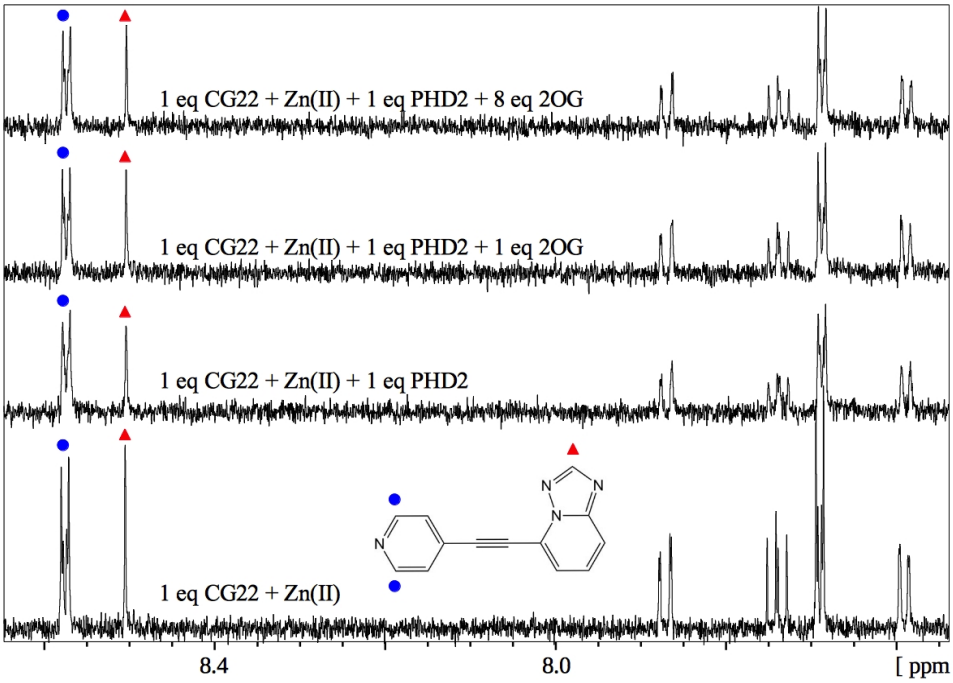


Figure 4.11 *CG22 binding assay. At 1 equivalent of PHD2 and 1 equivalent of CG22, less than half of the CG22 is bound to PHD2, as shown by the minimal decrease in signal intensity of the CG22 peaks. When 1 and 8 equivalents of 2OG were added, minimal changes in free CG22 peak intensity were observed. This may indicate that CG22 is not a strong binder.*

4.4 References

[1] P. Rabe, C. C. Walla, N. K. Goodyear, J. Welsh, R. Southwart, I. Clifton, J. D. Linyard, A. Tumber, T. D. Claridge, W. K. Myers and C. J. Schofield, "Spectroscopic studies reveal details of substrate-induced conformational changes distant from the active site in isopenicillin N synthase," *Journal of Biological Chemistry,* vol. 298, no. 9, p. 102249, 2022.

[2] D. A. Weits, J. T. v. Dongen and F. Licausi, "Molecular oxygen as a signaling component in plant development," *New Phytologist,* vol. 229, no. 1, pp. 24-35, 2020.

[3] A.-L. L. Gac and T. Laux, "Hypoxia Is a Developmental Regulator in Plant Meristems," *Molecular Plant,* vol. 12, no. 11, pp. 1422-1424, 2019.

[4] L. Yan, A. Loukoianov, A. Blechl, G. Tranquilli, W. Ramakrishna, P. SanMiguel, J. L. Bennetzen, V. Echenique and J. Dubcovsky, "The Wheat VRN2 Gene Is a Flowering Repressor Down-Regulated by Vernalization," *Science,* vol. 303, no. 5664, p. 1640–1644, 2016.

[5] C. Papdi, I. Pérez-Salamó, M. P. Joseph, B. Giuntoli, L. Bögre, C. Koncz and L. Szabados, "The low oxygen, oxidative and osmotic stress responses synergistically act through the ethylene response factor VII genes RAP2.12,RAP2.2 and RAP2.3," *The Plant Journal,* vol. 82, no. 5, pp. 772-784, 2015.

[6] H. H. Felle, "pH Regulation in Anoxic Plants," *Annals of Botany,* vol. 96, no. 4, p. 519–532, 2005.

[7] S. Ahmed, A. Ayscough, G. R. Barker, H. E. Canning, R. Davenport, R. Downham, D. Harrison, K. Jenkins, N. Kinsella, D. G. Livermore, S. Wright, A. D. Ivetac, R. Skene, S. J. Wilkens, N. A. Webster and A. G. Hendrick, "1,2,4-Triazolo-[1,5-a]pyridine HIF Prolylhydroxylase Domain-1 (PHD-1) Inhibitors With a Novel Monodentate Binding Interaction," *Journal of Medicinal Chemistry,* vol. 60, no. 13, 2017.

Chapter 5:

Methods

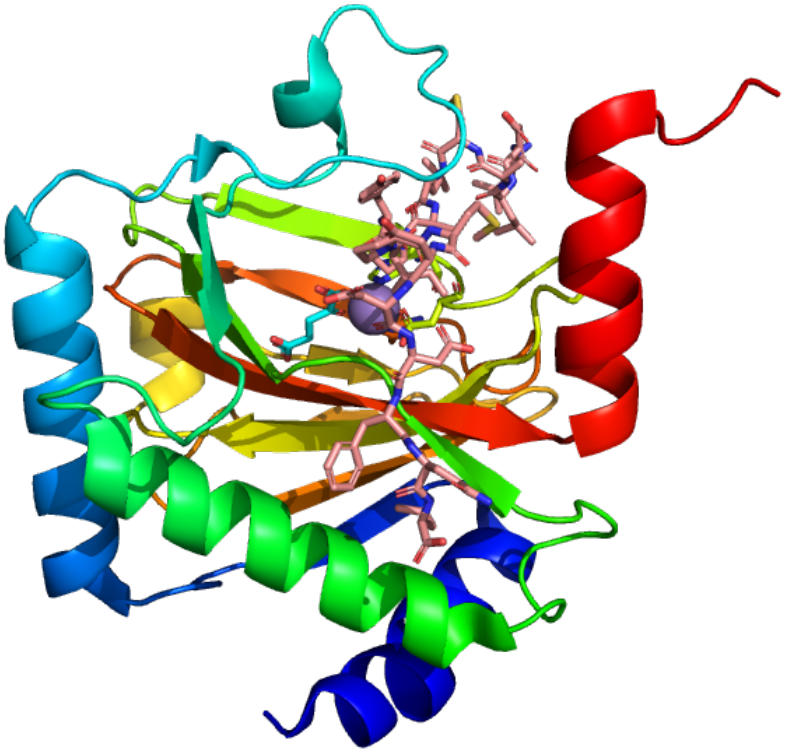


Table of Contents

Chapter 5: 5-1

5.1 Protein Production Procedures 5-4

5.1.1 Solution Preparations 5-4

5.1.1.1 30 mg/mL kanamycin sulphate ($C_{18}H_{36}N_4O_{11}$ x H_2SO_4) solution 5-4

5.1.1.2 50 mg/mL kanamycin sulphate ($C_{18}H_{36}N_4O_{11}$ x H_2SO_4) solution 5-4

5.1.1.3 1 M Isopropyl β-D-1-thiogalactopyranoside (IPTG, $C_9H_{18}O_5S$) solution 5-4

5.1.1.4 0.5 % thiamine hydrochloride ($C_{12}H_{17}ClN_4OS \cdot HCl$) solution 5-5

5.1.1.5 20 % (w/v) glucose ($C_6H_{12}O_6$) solution 5-5

5.1.1.6 1 M $MgSO_4$ solution 5-5

5.1.2 Transformation, Expression, and Purification of PHD2 5-5

5.1.2.1 Agar Plate Preparation 5-5

5.1.2.2 Transformation of PHD2 Plasmid 5-6

5.1.2.2.1 Transformation into Ultra-Competent XL10-Gold® or 10-β® E. coli Cells (Stratagene) 5-6

5.1.2.2.2 Mini-prep 5-7

5.1.2.2.3 Transformation into BL21(DE3)® E. Coli Cells 5-7

5.1.2.3 Expression Studies of PHD2 5-8

5.1.2.3.1 Starter Culture and Glycerol Stock Preparation 5-8

5.1.2.3.2 Large-Scale Growths 5-8

5.1.2.3.3 Purification of PHD2 5-10

5.1.2.4 Transformation, Expression, and Purification of WelO5 5-12

5.1.2.4.1 Transformation of WelO5 Plasmid 5-12

5.1.2.5 Expression Studies of WelO5 5-12

5.1.2.5.1 Starter Culture and Glycerol Stock Preparation 5-12

5.1.2.5.2 Large-Scale Growth 5-12

5.1.2.5.3 Purification of WelO5 5-14

5.1.2.6 SDS-PAGE Gel Preparation 5-16

5.1.2.6.1 SDS-PAGE Solution Preparation 5-16

5.1.2.6.2 SDS-PAGE Gel Preparation 5-17

5.1.2.6.3 SDS-PAGE Protein Loading 5-18

5.2 NMR Sample Procedures 5-19

5.2.1 Solution Preparations 5-19

5.2.1.1 Tris-D_{11} buffer preparation (pH 7.5) 5-19

5.2.1.2 Tris-D_{11} buffer preparation (pH 6.6) 5-19

5.2.1.3 10 mM $(NH_4)_2Fe(SO_4)_2 \cdot 6H_2O$ solution 5-19

5.2.1.4 10 mM $NiO_4S \cdot 6H_2O$ solution 5-19

5.2.1.5 10 mM $ZnCl_2$ solution 5-20

5.2.1.6 10 mM 2OG solution 5-20

5.2.1.7 10 mM sodium L-ascorbate (C6H7NaO6) solution 5-20

5.2.1.8 10 mM CODD solution 5-20

5.2.2 Buffer Exchange 5-20

5.2.3 Anoxic NMR Sample Preparation 5-21

5.2.4 NMR Experiments 5-21

5.2.4.1 2OG Turnover Assays for PHD2 5-22

5.2.4.2 Competition and Binding Assays for PHD2 5-23

5.2.4.2.1 Binding Experiments 5-23

5.2.4.2.2 Competition Experiments 5-25

5.2.4.2.3 ^{15}N-HSQC for PHD2 5-26

5.2.4.2.4 ^{15}N-HSQC for WelO5 5-27

5.2.4.2.5 ^{1}H,^{13}C,^{15}N-PHD2 3-D Experiments 5-28

5.3 Non-Denaturing Mass Spectrometry Sample Procedures 5-28

5.4 Parallel Mode EPR Sample Procedures 5-29
5.4.1 Sample preparation..... 5-29
5.4.2 EPR experimental procedures..... 5-30

5.1 Protein Production Procedures

Chemicals were from Sigma-Aldrich unless otherwise stated. The HIF-1α CODD peptide was purchased from Severn Biotech Ltd. and Tris-D_{11} from Cambridge Isotope Laboratories. PHD2 plasmids 1-426, 181-407, and 181-426 were provided by Martine Abboud. All WelO5 plasmids were provided by Ellen Gallimore. *E. coli* (XL10-Gold®, 10-β®, and BL21(DE3)®) cells were obtained commercially: stored at –80°C in glycerol stock.

5.1.1 Solution Preparations

5.1.1.1 30 mg/mL kanamycin sulphate ($C_{18}H_{36}N_4O_{11}$ x H_2SO_4) solution

Kanamycin sulphate (300 mg) was added to autoclaved, deionised water (10 mL). The solution was mixed until clear by vortexing. The solution was then passed through a pipette filter (0.22 µm) into a sterile falcon tube. The solution was fractioned into 1 mL aliquots and stored in a -20°C freezer for up to 1 month.

5.1.1.2 50 mg/mL kanamycin sulphate ($C_{18}H_{36}N_4O_{11}$ x H_2SO_4) solution

The same procedure as the 30 mg/mL kanamycin solution was used except with 500 mg of kanamycin sulphate.

5.1.1.3 1 M Isopropyl β-D-1-thiogalactopyranoside (IPTG, $C_9H_{18}O_5S$) solution

IPTG (2.38 g) was added to autoclaved, deionised water (10 mL). The solution was mixed until it was clear by vortexing. The solution was then passed through a pipette filter (0.22 µm) into a sterile falcon tube. The solution was used within 2 hours of preparation.

5.1.1.4 0.5 % thiamine hydrochloride ($C_{12}H_{17}ClN_4OS \cdot HCl$) solution

Thiamine hydrochloride (50 mg) was mixed with autoclaved, deionised water (10 mL). The solution was mixed until clear by vortexing. The solution was then passed through a pipette filter (0.22 µm) into a sterile falcon tube. The solution was fractioned into 50 µL aliquots and stored in a 4°C cold room to use within the week.

5.1.1.5 20 % (w/v) glucose ($C_6H_{12}O_6$) solution

$C_6H_{12}O_6$ (100 g) was added to autoclaved, deionised water (500 mL). The solution was mixed until clear by vortexing. The solution was then passed through a membrane filter (0.22 µm) into a sterile, autoclaved glass bottle. The solution was stored in a 4°C cold room to use within the week.

5.1.1.6 1 M $MgSO_4$ solution

Anhydrous $MgSO_4$ (2.4g) was added to autoclaved, deionised water (20 mL). The solution was mixed until clear by vortexing. The solution was then passed through a pipette filter (0.22 µm) into a sterile falcon tube. The solution was fractioned into 1 mL aliquots and stored in a 4°C cold room to use within the month.

5.1.2 Transformation, Expression, and Purification of PHD2

5.1.2.1 Agar Plate Preparation

Carried out in a Safe 2020 Class II Microbiological Safety Cabinet (Thermo Fisher Scientific)):

NaCl (2.5 g), tryptone (2.5 g), yeast extract (1.25 g), agar (3.75 g), and distilled water (250 mL) were added to a 500 mL glass bottle. The bottle was loosely capped and autoclaved in a Crystal Autoclave (Rodwell) for 12 minutes (sterilization time) at 3.6 bar and 135°C. The bottle was removed from the autoclaved and cooled to around 55°C in a

45°C hot bath. Kanamycin solution (50 µL; 30 mg/mL for PHD2, or 50 mg/mL for WelO5) and agar solution (50 mL) were added to the falcon tube and mixed thoroughly by capping and inverting the tube (as many tubes were made as plates needed). Agar (25 mL) including the antibiotic mixture was poured into each Petri dish and the plates were left—with the lid half covering the top—to cool for 10 minutes. Once cooled, the lids were placed on the plates, the plates were inverted and sealed with parafilm, and the plates were stored in a 4°C cold room until use (discarded after 20 days without use). The remaining agar solution (without antibiotic) was capped and sealed with parafilm before storage in the cold room for up to 20 days.

5.1.2.2 Transformation of PHD2 Plasmid

5.1.2.2.1 Transformation into Ultra-Competent XL10-Gold® or 10-β® E. coli Cells (Stratagene)

An Eppendorf tube containing *E. coli* cells (one of the two strains listed above) was placed on ice for 20 minutes to defrost. An Eppendorf tube containing PHD2 plasmid solution was heated to 85°C for 20 minutes (to ensure no phage contamination) and cooled for 1 minute on ice. In a new Eppendorf tube, plasmid solution (4 µL) was added to cells (50 µL) and the mixture was gently mixed by drawing in and out of a pipette. The mixture was left for 30 minutes on ice to equilibrate. The mixture was then placed in a 42°C water bath (45 seconds for XL10-Gold® cells or 30 seconds for 10-β cells). The tube was then placed on ice for 2 minutes. Room-temperature SOC media (250 µL; prepared next to a flame by mixing 2YT media (38.8 mL), 2M glucose solution (800 µL), and 1M $MgCl_2$ solution (400 µL)) was added to the Eppendorf tube and the mixture was mixed gently by drawing in and out of a pipette. The solution was placed in a Eppendorf Thermomixer Compact with a 1.5 mL block (Sigma-Aldrich) at 220 rpm and 37°C for 45-70 minutes (until the formation of a cell pellet was visible). The remaining steps were

carried out inside a Safe 2020 Class II Microbiological Safety Cabinet (Thermo Fisher Scientific). The transformation solution (200 µL) was spread onto a 37°C agar plate (with a kanamycin concentration of 30 µg/mL) with an L-shaped spreader. The plate was left to dry for 10 minutes before it was inverted and placed in a 37°C Heraeus microbiological incubator (Thermo Scientific) overnight. The plate was sealed with parafilm and stored at 4°C.

5.1.2.2.2 Mini-prep

A colony was picked from the transformation plate with a sterile pipette tip and placed in a falcon tube containing 2YT media (10 mL; provided by Manso Jubier (Department of Chemistry, University of Oxford); kanamycin concentration of 30 µg/mL). This process was repeated 3 additional times. The falcon tubes were capped and placed in a 37°C shaking incubator overnight. The next morning the falcon tubes were removed from the shaking incubator, the pipette tips were removed from the tubes, and the tubes were centrifuged in an Allegra™ X-30R centrifuge with a SX4750 rotor (Beckman Coulter) at 4,000 rpm and 4°C for 20 minutes. The tubes were then removed from the rotor and the supernatant was discarded. The mini-prep protocol and reagents found in GeneJET Plasmid Mini-prep Kit (Thermo Scientific) was used on all four cultures and the plasmids were sequenced by Eurofins Genomics.

5.1.2.2.3 Transformation into BL21(DE3)® E. Coli Cells

The transformation steps were repeated with the freshly-prepared plasmids and transformed into BL21(DE3)® *E. coli* cells with the following revisions: plasmid (1 µL) and cells (20 µL) were used; heat-shock was carried out for 45 seconds; the transformation mixture (100 µL) was plated.

5.1.2.3 Expression Studies of PHD2

5.1.2.3.1 Starter Culture and Glycerol Stock Preparation

Procedures were carried out in a Safe 2020 Class II Microbiological Safety Cabinet (Thermo Fisher Scientific)). 30 mg/mL kanamycin solution (100 µL; 300 mg of kanamycin sulphate and 10 mL of Milli-Q water was passed through a 0.20 µm pipette filter) was added to 2YT solution (100 mL; prepared by Manso Jubier (Department of Chemistry, University of Oxford)) in an Erlenmeyer culture flask (500 mL; Schott). The solution was swirled until uniform. A colony from the BL21(DE3)® transformation plate was picked with a sterile pipette tip and added to the flask. The flask was topped with a foam stopper and placed in an Incubator Shaker Series (Brunswick Scientific) incubator at 220 rpm and 37°C overnight. The flask was stored at 4°C for 0-6 hours until use.

The starter culture (800 µL) and 50 % glycerol solution (500 µL) were mixed in a cryovial (1.8 mL) until uniform. The solution was immediately capped and placed in dry ice before long-term storage at -80°C. This glycerol stock was used in the preparation of starter cultures with the following procedure:

The glycerol stock was removed from the -80°C freezer and immediately placed on dry ice. A sterile loop was used to scrape the top of the glycerol stock and the loop was swirled inside the 2YT media flask containing 30 µg/mL kanamycin. The rest of the previous starter culture protocol was followed.

5.1.2.3.2 Large-Scale Growths

5.1.2.3.2.1 Unlabelled Protein Production

Five PYREX® narrow-mouth graduated Erlenmeyer culture flasks (2 L each) were filled with 2YT media (1L: tryptone (16 g), yeast extract (10 g), and NaCl (5 g) in deionised water (1 L)) and capped with a foam stopper and aluminium foil. The flasks

were autoclaved in a Crystal Autoclave (Rodwell) for 2 hours. The flasks were left to cool until they reached 25-29°C (room temperature). 30 mg/mL kanamycin solution (1 mL) and starter culture (15 mL) were added to each flask. The flasks were placed in an Incubator Shaker Series (Brunswick Scientific) incubator at 150 rpm and 22°C overnight. The flasks were each induced with 1 M IPTG solution (600 µL; isopropyl β-D-1-thiogalactopyranoside (1.19 g) mixed with Milli-Q water (5 mL) and filtered through a pipette filter (0.20 µL), freshly prepared) and placed back in the shaking incubator at 150 rpm and 16°C. The flasks were incubated for 20 hours before pelleting the cells with an Avanti™ J-25 centrifuge and JLA 16.250 rotor (Beckman Coluter) at 8,000 rpm and 4°C for 10 minute cycles. The cell pellets were bagged and weighed before storage at -80°C.

5.1.2.3.2.2 Labelled Protein Production

Five PYREX® narrow-mouth graduated Erlenmeyer culture flasks (2 L each) were filled with M9 media (1 L: Na_2HPO_4 heptahydrous (11.3 g), KH_2PO_4 (3 g), ^{15}N-labelled NH_4Cl (1 g), NaCl (0.5 g), and $CaCl_2$ (0.4 mg) were mixed with deionised water (1 L)) and capped with a foam stopper and aluminium foil. The flasks were autoclaved in a Crystal Autoclave (Rodwell) for 2 hours. The flasks were left to cool until they reached 25-29°C (room temperature). The flasks were each supplemented with 1 M $MgSO_4$ solution (1 mL), 20 % glucose solution (100 mL), and 0.5 % *(w/v)* thiamine sulphate solution (100 µL). All solutions were freshly prepared and sterilized by passing through a pipette filter (0.20 µm). 30 mg/mL kanamycin solution (1 mL) and starter culture (25 mL) were added to each flask (to give an initial OD of approximately 0.1). The same incubation, induction, and harvesting steps were used for preparation of the unlabelled media.

5.1.2.3.3 Purification of PHD2

The cell pellet (20-30 g) was resuspended in binding buffer (100 mL) and the following (approximately 1 mg each) were added: DNase I, egg-white lysozyme, PMSF, and TCEP. The mixture was stirred at 4°C until uniform. The mixture was then placed on ice and sonicated with a Vibra-Cell™ Ultrasonic Liquid Processor VC 505 (Sonics) at 60 % power, for 9.9 second pulse and delay cycles, and for a total of 14 minutes. The mixture was centrifuged at 24,000 rpm and 4°C for 35 minutes with an Avanti™ J-26S XP centrifuge and JA 25.50 rotor (Beckman Coulter) to pellet out the cell debris. The supernatant was passed through a pipette filter (0.20 μm) into a narrow, graduated cylinder in preparation for purification.

The purification was initially carried out through a 5 mL settled-bed volume Novagen His·Bind® resin nickel-affinity column with a 1 mL/min flowrate connected to an ÄKTAdesign FPLC system (Amersham Biosciences, GE Healthcare) at 4°C. The FPLC machine was pump/line primed with Milli-Q water and binding buffer and the column was washed with 3 column volumes of Milli-Q water and 3 column volumes of binding buffer. The method was run at 1 mL/min with 100 % binding buffer while loading the lysate (approximately 120 mL). After 21 column volumes of binding buffer, gradient elution was set to reach 100 % elution buffer after 60 column volumes. Fractionation was set to 5 mL fractions. The gradient was held at 100 % elution buffer for 5 additional column volumes then 100 % binding buffer for 5 additional column volumes before ending the method. The location and purity of the protein was determined by analysis of the fractions by SDS-PAGE.

The fractions containing protein were collected in a falcon tube and the concentration (mg/mL) was determined by NanoDrop™ One (Thermo Scientific) using

the molecular weight and molar extinction coefficient. A 0.5 M solution of EDTA (passed through a membrane filter (0.20 μm) and prepared in Milli-Q water) was added until the molar ratio of protein to EDTA was approximately 1:6,000. The falcon tube was sealed with parafilm and placed on a Stuart™ Scientific roller mixer SRT1 (Sigma-Aldrich) overnight.

The EDTA-treated protein solution was concentrated to 2 mL with Amicon Ultra-15 centrifugal filter units (molecular weight cut-off 10 kDa; Millipore) in an Allegra™ X-30R Centrifuge with a SX4750 rotor (Beckman Coulter). The FPLC system was pump/line primed with Milli-Q water and gel-filtration buffer. A Superdex 200 Prep-Grade XK16 Column (GE Healthcare; provided by Adam Hardy) was attached to the system and equilibrated with 1 column volume of Milli-Q and 1 column volume of gel-filtration buffer. The protein was loaded onto the column with a 2 mL injection loop and eluted with 1 column volume of gel-filtration buffer, collecting in 5 mL fractions. The fractions were concentrated down to approximately 10 mg/mL (as determined by the NanoDrop specified above) by Allegra™ X-30R Centrifuge with a SX4750 rotor (Beckman Coulter) and stored in aliquots of 75 μL at -80°C.

Buffer Compositions (all buffers were adjusted to pH 7.5, made with Milli-Q water, and filtered through a 0.20 μm membrane filter):

- Binding buffer: 50 mM Trizma® Base, 200 mM NaCl, 5 mM imidazole.
- Elution buffer: 50 mM Trizma® Base, 200 mM NaCl, 500 mM imidazole.
- Gel-filtration buffer: 20 mM Trizma® Base, 150 mM NaCl.

5.1.2.4 Transformation, Expression, and Purification of WelO5

5.1.2.4.1 *Transformation of* WelO5 *Plasmid*

Wt WelO5, WelO5 G166D, WelO5 I161A, and WelO5 I161A-G166D plasmids were provided by Ellen Gallimore (Department of Chemistry, University of Oxford). Expression steps were performed the same for all plasmid constructs. All transformation and mini-prep steps were identical to those carried out with PHD2: reference above for the details.

5.1.2.5 Expression Studies of WelO5

5.1.2.5.1 Starter Culture and Glycerol Stock Preparation

Procedures were carried out in a Safe 2020 Class II Microbiological Safety Cabinet (Thermo Fisher Scientific)). The steps used for starter culture and glycerol stock preparation were identical to those carried out for PHD2 with the following exception: the antibiotic solution used was 50 mg/mL kanamycin solution (kanamycin sulphate (500 mg) and Milli-Q water (10 mL), passed through a pipette filter (0.20 μm)).

5.1.2.5.2 Large-Scale Growth

5.1.2.5.2.1 Unlabelled Protein Production:

Five PYREX® narrow-mouth graduated Erlenmeyer culture flasks (2 L each) were filled with 2YT media (1 L: tryptone (16 g), yeast extract (10 g), and NaCl (5 g) in deionised water (1 L)) and capped with a foam stopper and aluminium foil. The flasks were autoclaved in a Crystal Autoclave (Rodwell) for 2 hours. The flasks were left to cool until they reached 25-29°C (room temperature). 50 mg/mL kanamycin solution (1 mL) and starter culture (5 mL) were added to each flask. The flasks were placed in an Incubator Shaker Series (Brunswick Scientific) incubator at 150 rpm and 37°C for about 4 hours (until the flask reached an OD of approximately 0.8). The flasks were cooled to

30°C in the shaking incubator for 30 minutes before inducing with 1 M IPTG solution (600 µL: isopropyl β-D-1-thiogalactopyranoside (1.19 g) and Milli-Q water (5 mL) filtered through a pipette filter (0.20 µL), freshly prepared). The flasks were placed back in the shaking incubator at 150 rpm and 30°C and incubated for 20 hours before pelleting the cells with an Avanti™ J-25 centrifuge and JLA 16.250 rotor (Beckman Coluter) at 6,000 xg and 4°C for 10 minute cycles. The cell pellets were bagged and weighed before storage at -80°C.

5.1.2.5.2.2 Labelled Protein Production:

Five PYREX® narrow-mouth graduated Erlenmeyer culture flasks (2 L each) were filled with M9 media (1 L: Na_2HPO_4 dihydrate (7.6 g), KH_2PO_4 (3 g), ^{15}N-labelled NH_4Cl (2 g), and NaCl (0.5 g) were mixed with deionised water (1 L)) and capped with a foam stopper and aluminium foil. The flasks were autoclaved using a Crystal Autoclave (Rodwell) for 2 hours. The flasks were left to cool until they reached 25-29°C (room temperature). The flasks were each supplemented with glucose (4 g), $MnCl_2$ tetrahydrate (16 mg), $MgSO_4$ (120.4 mg), thiamine (1 mg), Na_2SO_4 (42.6 mg), $FeCl_3$ (5 mg), biotin (1 mg), and $CaCl_2$ dihydrate (65.7 mg). The solution was passed through a sterile membrane filter (0.20 µm) that was sealed inside a Safe 2020 Class II Microbiological Safety Cabinet (Thermo Fisher Scientific) before exposure to air. 50 mg/mL kanamycin solution (1 mL), 10 mg/mL ZnCl2 solution (50 µL), 10 mg/mL $CuCl_2$ solution (10 µL), 10 mg/mL $CoCl_2$ solution (10 µL), and 5 mg/mL H_3BO_3 solution (20 µL). All solutions were prepared with autoclaved, deionised water and filtered through a pipette filter (0.20 µm)). Once the solution was mixed thoroughly, starter culture (25 mL) was added to each flask (to give an initial OD of approximately 0.1). The same incubation, induction, and harvesting steps were used as the unlabelled media.

5.1.2.5.3 Purification of WelO5

The cell pellet (20-30 g) was resuspended in binding buffer (100 mL) and DNase I (approximately 1 mg) was added. The mixture was stirred at 4°C until uniform. The mixture was then placed on ice and sonicated with a Vibra-Cell™ Ultrasonic Liquid Processor VC 505 (Sonics) at 60 % power, for 9.9 second pulse and delay cycles, and for a total of 8 minutes. The mixture was centrifuged at 40,000 xg and 4°C for 30 minutes with an Avanti™ J-26S XP centrifuge and JA 25.50 rotor (Beckman Coulter) to remove the cell debris. The resultant supernatant was passed through a pipette filter (0.20 µm) into a narrow, graduated cylinder in preparation for purification.

The purification was initially carried out through a 5 mL settled-bed volume Novagen His·Bind® resin nickel-affinity column with a 1 mL/min flowrate connected to an ÄKTAdesign FPLC system (Amersham Biosciences, GE Healthcare) at 4°C. The FPLC was pump/line primed with Milli-Q water and binding buffer and the column was washed with 3 column volumes of Milli-Q water and 3 column volumes of binding buffer. The method was run at 1 mL/min with 100 % binding buffer while loading the lysate (approximately 120 mL). After loading the lysate, elution buffer was added stepwise to the system starting with 20 % elution buffer for 15 column volumes. Fractionation was set to 5 mL fractions. For 20 column volumes the system is set to 100 % elution buffer in which the protein elutes. For 5 column volumes the column is reset to 100 % binding buffer. The location and purity of the protein was determined by analysis of the fractions by SDS-PAGE.

The fractions containing protein were collected in a falcon tube and the concentration (mg/mL) was determined by NanoDrop One (Thermo Scientific). A 0.5 M solution of EDTA (passed through a membrane filter (0.20 µm) and prepared in Milli-Q

water) was added until the molar ratio of protein to EDTA was approximately 1:6,000 (1:145 for the triple-labelled protein). The falcon tube was sealed with parafilm and placed on a Stuart™ Scientific roller mixer SRT1 (Sigma-Aldrich) overnight.

For studies on unlabelled and ^{15}N-labelled WelO5, the concentration and gel-filtration steps were carried out as for the protocol for PHD2, with adjustments for use of a Superdex 200 Prep-Grade XK26 Column (GE Healthcare) during gel-filtration.

For ^{2}H-^{13}C-^{15}N-labelled WelO5, after EDTA treatment, a dialysis cassette (15 mL) was hydrated in gel-filtration buffer for 2 minutes. The protein solution was added to the cassette with a metal syringe and air was removed from the cassette. The cassette was placed in a beaker (600 mL) containing gel-filtration buffer (500 mL) and a stir bar. The cassette was slowly stirred overnight at 4°C. The next morning, freshly prepared gel-filtration buffer (500 mL) was added to the beaker and the old buffer was discarded. The solution was stirred for an hour at 4°C. The cassette was removed from the beaker and the sample was collected with a syringe and stored in a falcon tube on ice. The solution was then concentrated and aliquoted as described in the PHD2 protocol.

Buffer Compositions (all buffers were adjusted to pH 7.5, made with Milli-Q water, and filtered through a membrane filter (0.20 μm)):

- Binding buffer: 50 mM Trizma® Base, 500 mM NaCl, 5 mM imidazole, 1 mM TCEP (added directly before use).
- Elution buffer: 50 mM Trizma® Base, 500 mM NaCl, 500 mM imidazole, 1 mM TCEP (added directly before use).
- Gel-filtration buffer: 50 mM Trizma® Base, 500 mM NaCl, 1 mM TCEP (added directly before use).

5.1.2.6 SDS-PAGE Gel Preparation

All gels were either prepared through this method or bought from ThermoFisher Scientific (NuPAGE Bis-Tris Gels).

5.1.2.6.1 *SDS-PAGE Solution Preparation*

- Running Buffer (1 L) x20
    - Trizma base (30 g), glycine (144 g), and SDS (10 g) were added to a glass bottle (1 L).
    - The bottle was topped up to 1 L with deionised water and mixed until it was uniform.
- Gel Stain (1 L)
    - Acetic acid (100 mL), methanol (300 mL), and Coomassie brilliant blue stain (2.5 mL) was added to a 1 L glass bottle.
    - The bottle was topped up to 1 L with deionised water and mixed until it was uniform.
- Destain Solution (1 L)
    - Acetic acid (100 mL) and methanol (300 mL) were added to a glass bottle (1 L).
    - The bottle was topped up to 1 L with deionised water and mixed until it was uniform.

- Sample Loading Buffer (10 mL)
    - 0.5 M Tris-HCl (1 mL) at pH 6.8, 0.2 % *(w/v)* bromophenol blue (20 mg), 10 % SDS solution (2 mL), glycerol (1.2 mL), and β-mercaptoethanol (0.5 mL) were added to a small falcon tube.
    - The tube was inverted several times until uniform.
- 10 % SDS solution
    - SDS (1 g) was added to deionised water (10 mL) and the solution was mixed until uniform.

5.1.2.6.2 *SDS-PAGE Gel Preparation*

Three equivalents of resolving gel and three equivalents of stacking gel were prepared (for 2 gels and a test gel).

Preparation of 3 resolving gel equivalents (12.5 % acrylamide)

- Tris-HCl (3.75 mL; 1.5 M, pH 8.8), deionised water (4.71 mL), 30 % (w/v) acrylamide / 1.034 % (w/v) bis-acrylamide stock (6.24 mL), and 10 % (w/v) SDS solution (150 µL) were added to a falcon tube and the tube was inverted several times until the mixture was uniform.
- 10 % (w/v) APS solution (150 µL) and TEMED (12 µL) were quickly added and the falcon tube was capped and inverted several times to mix the sample.

The solution was added into 2 glass gel molds until the molds were filled approximately 2 cm from the tops. Ethanol was immediately added to the top of each gel and the gels were left to solidify for 20 minutes (solidity was determined by the remaining gel solution in the falcon tube). Excess ethanol was poured off and the top of the gel was dried with Western blotting paper.

3 stacking gels were prepared as follows (3.0 % acrylamide):

- 0.5 M Tris-HCl (1.89 mL; pH 6.8), Milli-Q water (4.71 mL), 30 % (w/v) acrylamide / 1.034 % (w/v) bis-acrylamide stock (0.75 mL), and 10 % (w/v) SDS solution (75 µL) were added to a falcon tube and the tube was capped and inverted several times to mix the sample.
- 10 % (w/v) APS solution (150 µL) and TEMED (15 µL) were quickly added and the falcon tube was capped and inverted several times to mix the sample.

A stacking gel was added to the top of each gel until they overflowed the molds and a comb was placed in the top of each. The gels were left for an hour to solidify (solidity was determined by the remaining gel solution in the falcon tube). Once solidified, The gels were either used immediately or wrapped with a wet paper towel and ciran wrap and stored for up to a day in a 4°C cold room

5.1.2.6.3 *SDS-PAGE Protein Loading*

Each protein fraction (7 µL) and sample loading buffer (7 µL; containing a stain) were added to an Eppendorf tube boiled at 95°C on a hot block for 10 minutes. The gels were loaded into the protein loader and the combs were removed from the tops.

The following were loaded into each lane:

- Lane 1: Thermo Scientific PageRuler Prestained Protein Ladder (7 µL; 10-170 kDa)
- Remaining lanes: protein samples (7 µL)

The samples were run at 180 V for about 40 minutes (until the blue stain reached the bottom of the gels). The gels were then removed from the moulds and placed in the gel stain for 10 minutes. After staining, the gels were rinsed gently with deionised water

and soaked in destain solution for 1 hour while rocking. The gels were imaged with Image Lab Software (Life Science Research, Bio-Rad).

5.2 NMR Sample Procedures

5.2.1 Solution Preparations

5.2.1.1 Tris-D_{11} buffer preparation (pH 7.5)

The buffer was prepared at 50 mM Tris-D_{11} and 150 mM NaCl. Tris-D_{11} (331 mg) and NaCl (438 mg) were added to autoclaved, deionised water (50 mL). The solution was then mixed until clear by vortexing. The solution was adjusted to pH 7.5 with concentrated HCl and 5 M NaOH (the pH was adjusted with the solution at room temperature). It was then passed through a membrane filter (0.22 µm) into a sterile falcon tube. The solution was stored in a 4°C cold room.

5.2.1.2 Tris-D_{11} buffer preparation (pH 6.6)

The conditions used were identical to those described for the solution at pH 7.5 except the solution was adjusted to pH 6.6 and no NaCl was added.

5.2.1.3 10 mM $(NH_4)_2Fe(SO_4)_2 \cdot 6H_2O$ solution

$(NH_4)_2Fe(SO_4)_2 \cdot 6H_2O$ (39 mg) was added to 20 mM HCl (10 mL) in deionised water. The solution was mixed until clear by vortexing and used immediately.

5.2.1.4 10 mM $NiO_4S \cdot 6H_2O$ solution

$NiO_4S \cdot 6H_2O$ (15 mg) was added to deionised water (10 mL). The solution was mixed until clear by vortexing. The solution was stored at 4°C until use.

5.2.1.5 10 mM $ZnCl_2$ solution

$ZnCl_2$ (14 mg) was added to deionised water (10 mL). The solution was mixed until clear by vortexing. The solution was stored at 4°C until use.

5.2.1.6 10 mM 2OG solution

Disodium 2OG (19 mg) was added to deionised water (10 mL). The solution was mixed until clear by vortexing. The solution was used within 10 hours of preparation.

5.2.1.7 10 mM sodium L-ascorbate (C6H7NaO6) solution

$C_6H_7NaO_6$ (20 mg) was added to deionised water (10 mL). The solution was mixed until clear by vortexing. The solution was used within 10 hours of preparation.

5.2.1.8 10 mM CODD solution

CODD (4.5 mg) was added to deuterated DMSO (200 mL). The solution was mixed with a pipette and stored at -20°C.

5.2.2 Buffer Exchange

A Mini Bio-Spin® chromatography column with Bio-Gel® P-6 (Bio-Rad) was removed from the 4°C fridge, inverted a few times, then placed over a microcentrifuge tube (2 mL). The tip and cap were removed and the column was drained until it stopped dripping. The column was capped and placed in a Microfuge 22R Centrifuge (Beckman Coulter) at 1000 xg and 4°C for 2 minutes. The eluent was discarded. Solvent (500 µL; Tris-D_{11} buffer at pH 6.6 or 7.5 or 200 mM ammonium acetate solution depending on the experiment) was added to the top of the column and the column was centrifuged at 1000x g and 4°C for 1 minute. The buffer exchange process was repeated 3 more times and the eluent was discarded. Protein solution (20-75 µL: 20 for native mass spectrometry and

75 for NMR) was added to the top of the column, the column was placed over an Eppendorf tube (1.5 mL), and the column was spun for another 4 minutes under the same conditions. The eluent was collected and the concentration was determined by NanoDrop One (Therm Scientific) analysis using extinction coefficient and molecular weight.

5.2.3 Anoxic NMR Sample Preparation

In order to ensure a dioxygen-free environment, all equipment was placed in a glovebox overnight. Samples of protein, buffer, ligands, substrates, and metals were placed in the glovebox in small volumes and purged by mixing with a pipette every 20 minutes for 2 hours. Once the samples had been sufficiently purged of dioxygen, they were added to an Eppendorf tube and mixed thoroughly before transferring into a 3 mm NMR MATCH tube with a long, thin tipped pipette (when the sample will not run down the side of the tube, the tube is lightly tapped until it does). Any fingerprints were wiped from the outside of the NMR tube, then the 3 mm tube was then placed in a 5 mm medium pressure tube, sealed, and removed from the glovebox. The tube could be lightly swung downwards to remove any bubbles.

If additions were needed, the sample was placed back in the glovebox, carefully removed with a needle (a small amount of volume will be lost), and placed in an Eppendorf for further additions. Use of a needle for removal of the NMR sample should be avoided if other options are available.

5.2.4 NMR Experiments

All experiments were carried out using an Avance III 700 NMR spectrometer (Bruker) with an inverse TCI $^{1}H/^{13}C/^{15}N$ cryoprobe. Before acquisition of ^{15}N-HSQC, 1 aliquot (75 µL) of the protein was buffer-exchanged with a Mini Bio-Spin®

chromatography column with Bio-Gel® P-6 (Bio-Rad) into Tris-D_{11} buffer at pH 6.6 (protocol described above). Before all other experiments, the protein was exchanged by the same method into Tris-D_{11} buffer at pH 7.5 (50 mM Tris-D_{11} and 150 mM NaCl). 3-D experiment protein preparation is described separately.

5.2.4.1 2OG Turnover Assays for PHD2

To determine the turnover rate of 2OG to succinate by PHD2, the following solutions were prepared:

- 10 mM Fe(II) solution (in 20 mM HCl), 10 mM 2OG, 10 mM ascorbate, 10 mM CODD, and Tris-D11 buffer (50 mM Tris(hydroxymethyl-d3)amino-d2-methane (tris), 150 mM NaCl, pH 7.5 at room temperature).

The desired concentrations in the 5 mm NMR tubes were as follows:

- 10 µM PHD2, 100 µM Fe(II), 400 µM CODD, 500 µM 2OG, 500 µM ascorbate, 10 % D_2O, and 90 % Tris-D11 buffer

A sample containing all components except the protein and substrate was used to tune, match, and 3-D shim before the run. Tris-D_{11} buffer, D_2O, ascorbate, and Fe(II) were added to an Eppendorf tube and the solution was mixed thoroughly by drawing in and out of a pipette. PHD2 was added to the solution and the solution was again mixed thoroughly. The solution was incubated at room temperature (with the Eppendorf tube cap opened) for 5 minutes. CODD was added to the solution, the solution was mixed, and the solution was again incubated at room temperature for 5 minutes. 2OG was added and the solution was mixed and incubated at room temperature for 30 seconds. The solution was then pipetted into a 5 mm economy NMR tube and the tube was centrifuged for a few seconds. The tube was then capped and placed in the AVIII 700 at 298 K. After

locking and a quick 1-D shim along the z-direction, the sample was run on a standard Bruker pulse program, zgesgp, with the multi_zgvd command at 0 seconds fixed delay and 40 experiments. Automatic shimming was turned on during the series of runs.

After the runs finished, The first spectrum was processed with exponential multiplication, phased, baseline corrected, and integrated at the low-field 2OG triplet peak and the succinate singlet peak separately. These commands were carried over to the remaining spectra with "multicmd" and "multi_integ3" (after creation of an integral file). The intensities of the peaks relative to the number of protons each peak represented was used to determine the relative concentrations of 2OG and succinate, and the data was plotted as a decay in 2OG concentration and increase of succinate concentration.

5.2.4.2 Competition and Binding Assays for PHD2

To investigate the strength of binding of an inhibitor to PHD2, the following solutions were prepared:

- 10 mM 2OG, 10 mM metal solution, 10 mM of inhibitor (compound of interest), and Tris-D11 buffer (50 mM Tris(hydroxymethyl-d3)amino-d2-methane (tris), 150 mM NaCl, pH 7.5 at room temperature).

5.2.4.2.1 Binding Experiments

The desired concentrations in the 3 mm NMR tubes for the binding experiments were as follows (each number represents an experiment that was run):

- 50 µM inhibitor and 10 % D_2O, and 90 % Tris-D11 buffer
- 50 µM inhibitor, 200 µM metal ion solution, and 10 % D_2O, and 90 % Tris-D_{11} buffer

- 50 μM inhibitor, 200 μM metal ion solution, 50 μM PHD2, and 10 % D_2O, and 90 % Tris-D_{11} buffer
- 50 μM inhibitor, 200 μM metal ion solution, 50 μM PHD2, 50 μM 2OG, and 10 % D_2O, and 90 % Tris-D11 buffer
- 50 μM inhibitor, 200 μM metal ion solution, 50 μM PHD2, 400 μM 2OG, and 10 % D_2O, and 90 % Tris-D_{11} buffer

Tris-D_{11} buffer and 50 μM inhibitor were added to an Eppendorf tube and the solution was mixed thoroughly by drawing in and out of a pipette. The solution was transferred to a 3mm MATCH NMR tube and placed in the AVIII 700 NMR instrument at 298 K and left to equilibrate. The solution was tuned, matched, and shimmed. A CPMG-edited ^1H and a spin echo ^1H experiment were each carried out.

The sample was removed from the instrument and 200 μM metal ion solution was added to the top of the tube. The tube was capped and inverted several times until mixed. The sample was placed back in the instrument—tuned, matched, and shimmed—and CPMG-edited ^1H and spin echo ^1H experiments were again carried out.

A new sample was prepared with 50 μM inhibitor, 200 μM metal ion solution, 50 μM PHD2, and Tris-D_{11} buffer. The steps of mixing, equilibrating, tuning, matching, shimming, and acquiring CPMG-edited ^1H and spin echo ^1H experiments were carried out for all experiments in this set and will be assumed to be part of the sample run. After this sample was run, it was removed from the instrument and 50 μM 2OG was added to the top of the sample. The tube was capped and inverted several times until mixed. The sample was placed back in the instrument and run. Again these steps were repeated for the addition of 350 μM 2OG to the sample.

5.2.4.2.2 Competition Experiments

The desired concentrations in the 3 mm NMR tubes for the competition experiments were (each number represents an experiment that was run):

- 50 µM 2OG and 10 % D_2O, and 90 % Tris-D_{11} buffer
- 50 µM 2OG, 200 µM metal solution, and 10 % D_2O, and 90 % Tris-D_{11} buffer
- 50 µM 2OG, 200 µM metal solution, 50 µM PHD2, and 10 % D_2O, and 90 % Tris-D_{11} buffer
- 50 µM 2OG, 200 µM metal solution, 50 µM PHD2, 50 µM inhibitor, and 10 % D2O, and 90 % Tris-D_{11} buffer
- 50 µM 2OG, 200 µM metal solution, 50 µM PHD2, 400 µM inhibitor, and 10 % D_2O, and 90 % Tris-D_{11} buffer

The following steps are similar to the binding experiment studies except that the roles of inhibitor and 2OG are reversed:

Tris-D_{11} buffer and 50 µM 2OG were added to an Eppendorf tube and the solution was mixed thoroughly by drawing in and out of a pipette. The solution was transferred to a 3mm MATCH NMR tube and placed in the AVIII 700 NMR instrument at 298 K and left to equilibrate. The solution was tuned, matched, and shimmed. A CPMG-edited ^1H (Bruker: cpmg_project with presaturation; D20 = 0.001 s and L4 ~ 20-50) and a spin echo ^1H experiment were each carried out.

The sample was removed from the instrument and 200 µM Zn(II) solution was added to the top of the tube. The tube was capped and inverted several times until mixed. The sample was placed back in the instrument—tuned, matched, and shimmed—and CPMG-edited ^1H and spin echo ^1H experiments were again carried out.

A new sample was prepared with 50 µM 2OG, 200 µM metal solution, 50 µM PHD2, and Tris-D_{11} buffer. The steps of mixing, equilibrating, tuning, matching, shimming, and acquiring CPMG-edited ^{1}H and spin echo ^{1}H experiments were carried out for all experiments in this set. After this sample was run, it was removed from the instrument and 50 µM inhibitor was added to the top of the sample. The tube was capped and inverted several times until mixed. The sample was placed back in the instrument and run. Again, these steps were repeated for the addition of 350 µM inhibitor to the sample.

5.2.4.2.3 *^{15}N-HSQC for PHD2*

The following solutions were prepared:

- 10 mM Fe(II) in 20 mM HCl, 10 mM Zn(II), 10 mM 2OG, 10 mM CODD, and Tris-D11 buffer (50 mM Tris(hydroxymethyl-d3)amino-d2-methane (tris), pH 6.6 at room temperature).

The desired concentrations in the NMR tubes were as follows (+/- indicates that depending on the experiment, different conditions were used):

- 50 µM PHD2, 100 µM Zn(II) or Fe(II), +/- 200 µM CODD, +/- 100 µM 2OG, 10 % D_2O, and 90 % Tris-D_{11} buffer at pH 6.6.

For most experiments, the temperature was adjusted to 308K.

Tris-D_{11} buffer, D_2O, and Fe(II) or Zn(II) were added to an Eppendorf tube and the solution was mixed thoroughly by drawing in and out of a pipette. PHD2 was added to the solution and the solution was again mixed thoroughly. Depending on the experimental conditions, 2OG then CODD were added and the solution was incubated at

room temperature (with the Eppendorf tube cap opened) for 20 minutes. The solution was pipetted into a 3 mm MATCH NMR tube and the tube was centrifuged for a few seconds.

The sample was placed in the AVIII 700 instrument. The temperature of the sample was equilibrated in the instrument for 10 to 20 minutes. The instrument was then locked, tuned, and 3-D shimmed. Three different pulse sequences were generally used: *HSQCETFPF3GPSI, HSQCETFPF3GPSI, or TROSYETF3GPSI*. The sample was run at 2048 F2 increments, 128 to 512 F1 increments, and 16 to 64 scans. The proton spectrum was recorded before and after each run to determine the loss of sample during the run.

The experiments were run, processed, and analysed using Topspin 4.0.6 software (Bruker) or CCPNmr Analysis software.

5.2.4.2.4 *^{15}N-HSQC for WelO5*

The following solutions were prepared:

- 10 mM Ni(II), 10 mM 2OG, and Tris-D11 buffer (50 mM Tris(hydroxymethyl-d3)amino-d2-methane, pH 6.6 at room temperature).

The desired concentrations in the NMR tubes were as follows (+/- indicates that depending on the experiment, different conditions were used):

- 50 µM WelO5, 83.3 µM Ni(II), +/- 66.7 µM 2OG, 10 % D_2O, and 90 % Tris-D_{11} buffer at pH 6.6.

The remaining conditions and protocol are the same as in the ^{15}N-HSQC for PHD2.

5.2.4.2.5 *$^{1}H,^{13}C,^{15}N$-PHD2 3-D Experiments*

The following experiments were carried out using a 950 MHz NMR Instrument:

Experiment Type	Pulse Sequence (Bruker)	# Scans	H	N	C
HNCA	hncagp2h3d	64	1024	64	128
HNCO	hncogp3d	16	1024	64	96
HNCOCA	-	-	-	-	-
HNCACO	hncacogp2h3d	64	1024	64	96
HNCACB	hncacbgp2h3d	80	1024	64	128
HNCOCACB	hncocacbgp2h3d	80	1024	64	128

5.3 Non-Denaturing Mass Spectrometry Sample Procedures

The protein samples were often prepared by mixing ~10 mg/mL protein solution (5 mL) with 200 mM ammonium acetate solution (15 mL). The protein sample (20 µL) was then buffer exchanged by a Mini Bio-Spin® chromatography column with Bio-Gel® P-6 (Bio-Rad) into 200 mM ammonium acetate solution. 10 mM Fe(II), 10 mM Ni(II), and protein stock solutions were diluted down to 20 µM with 200 mM ammonium acetate buffer.

All non-denaturing mass spectrometry runs were performed on a quadrupole time-of-flight (qTOF) mass spectrometer (Synapt HD MS, Waters, Wilmslow, Manchester, UK). Solutions containing 10 µM protein, 10 µM metal (if needed), and 200 µM ammonium acetate were pipetted in the wells on a sample plate of an automated chip-based nano-electrospray ion source (TriVersa Nanomate, Advion, Ithaka, NY, USA). The solution was then sprayed through a nozzle in a Nanomate chip. Data collection and analysis were carried out using Waters MassLynx™ software. Mass spectra were calibrated externally using CsI solution to produce CsI cluster ions.

5.4 Parallel Mode EPR Sample Procedures

5.4.1 Sample preparation

A 10 mM solution of ammonium Fe(II) sulphate in 20 mM HCl Milli-Q and a 10 mM solution of 2OG in Milli-Q were freshly prepared and placed on ice along with protein sample. The following concentrations were typically used:

- For control samples: oxic and anoxic preparations of 200 µM Fe(II), 600 µM 2OG, 100% Tris-D11, pH 7.5
- For protein samples: oxic and anoxic preparations of 200 µM PHD2, 200 µM Fe(II), 600 µM 2OG, 70% Tris-D_{11}, 20% D_2O, pH 7.5

The samples were added to EPR tubes via metal syringes. The oxic samples were mixed first in order to allow some time to equilibrate before freezing. A dewar flask filled with liquid nitrogen was then introduced into the anoxic chamber with a falcon tube towards the top that was full of holes for liquid nitrogen penetration. The anoxic samples were slowly lowered into the liquid nitrogen. When the bottom of the tube touched the liquid nitrogen (indicated by a fizzle noise) the sample was lowered at about 2 mm/s to allow for ice expansion, so as to not shatter the tube. Once the tube was mostly submerged, it was placed in the falcon tube inside the liquid nitrogen. The dewar flask was removed from the anoxic chamber and the same procedures were carried out on the oxic samples. The lid of the falcon tube was sealed and the falcon tube with samples was transferred into a larger liquid nitrogen dewar for overnight storage.

The samples were removed from the large liquid nitrogen dewar and placed in a small liquid nitrogen bowl. Remaining liquid nitrogen was removed from the top of the tube, and a similar tube was taped to the tube opening (in order to make the tube long enough that it could be easily removed from the instrument.

5.4.2 EPR experimental procedures

The parameters for the EPR analysis were optimised before each experiment and run with both parallel and perpendicular measurements. Experiments were run at the University of Oxford CAESR EPR Facility on the EMX instrument in parallel-mode EPR operated by Dr. William Myers (Department of Chemistry, University of Oxford).

Chapter 6:

Summary and Future Work

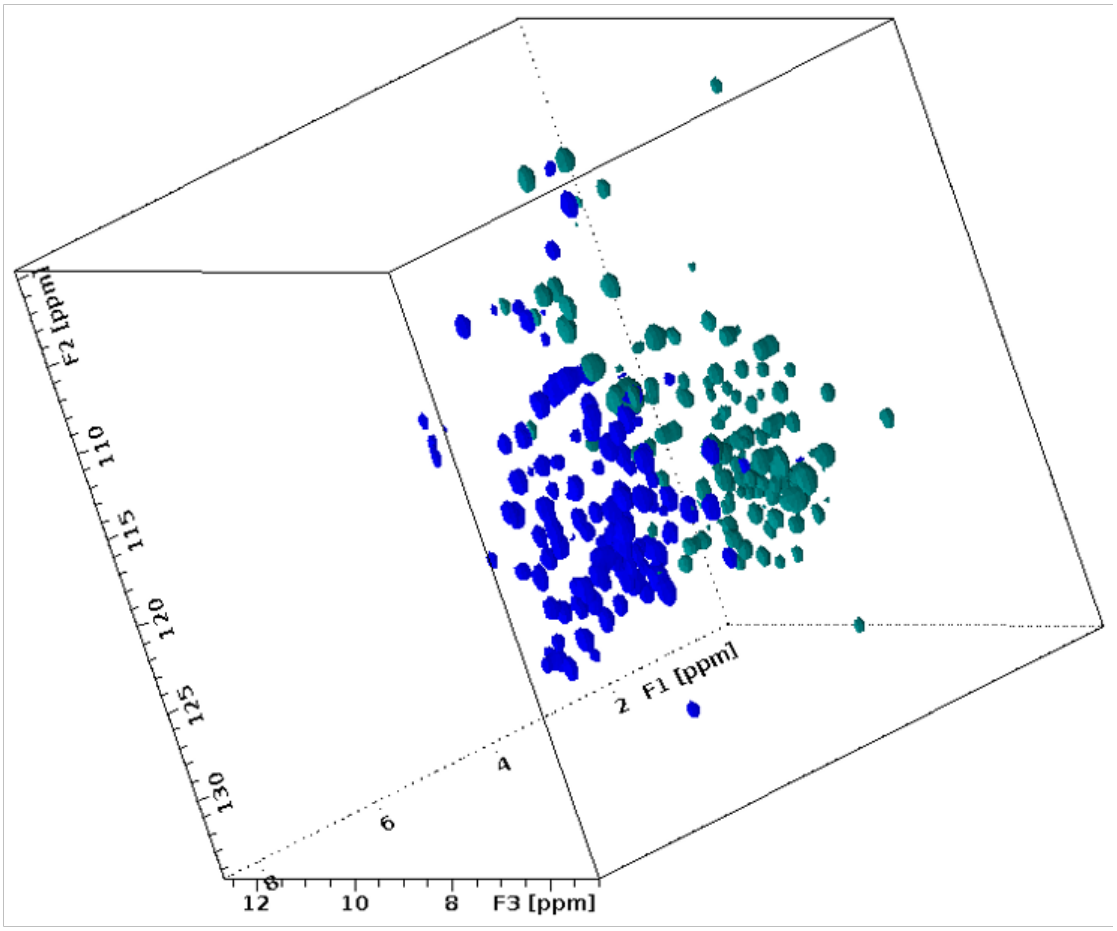


Table of Contents

Chapter 6: 6-1

6.1 Summary and Future Work 6-3

6.1.1 PHD2 6-3

6.1.2 WelO5 6-9

6.2 References 6-11

6.1 Summary and Future Work

6.1.1 PHD2

In **Chapter 2** of this thesis, methods for probing the interactions between O_2 and the PHD2 active site were described (outlined in **Chapter 2, Section 2.3**; the conclusions are summarised below). The results indicated differences in the magnetic environment experienced by both the PHD2:Fe(II):2OG and PHD2:Fe(II):2OG:CODD complexes when exposed to ambient oxygen levels. The observations can be attributed to one or more of the following: structural changes in the protein, changes in the oxidation state or spin state of the active site metal, or paramagnet-induced changes on stable and orientation-specific interactions between 2OG/oxygen and the protein. The PHD2:Fe(II):2OG (and possibly the PHD2:Fe(II):2OG:CODD) complex, in the absence of oxygen, exhibits two unique sets of peaks, whereas only one set of peaks—which correlated well with one set of peaks in the anoxic spectrum—is visible in the presence of oxygen. Studies analysing the stability of these complexes, along with studies analysing inhibitor binding in the presence and absence of oxygen (studied by ^{1}H NMR of the shielded methyl resonances), show that the PHD2:Fe(II):2OG and PHD2:Fe(II):2OG:CODD complexes formed in the presence of oxygen are exceptionally stable. The evidence presented indicates that these oxic complexes reflect PHD:Fe(III):2OG +/- CODD complexes, which do not react with O_2 once in a steady state. The stable oxic complexes can be recycled back into the catalytically active—likely Fe(II)—complexes by reducing agents such as ascorbate. In this section, further potential studies into the hypoxia-sensitive properties of PHD2 and its oxygen reactivity are described.

Recent research into the rate limiting step of PHD2-oxygen interactions using molecular dynamics simulations have implied that access of oxygen to the PHD2 active

site may be regulated by the movement of oxygen from the junction between an internal, hydrophobic channel (formed from the interaction between PHD2 and the HIF substrate) and the active site pocket. [1] Related hydrophobic pockets involved in oxygen movement within proteins have been explored by methods such as X-ray crystallography, NMR, computational chemistry, and activity assays, [2] in some cases utilising a variety of noble gases, including argon and xenon, as stable probes. [3] [4] Utilising noble gases as gas probes for hydrophobic pockets within PHD2 may provide insight into oxygen-protein interactions and enable studies of the apparently slow oxygen reaction of PHD2. At high gas pressures, it may also be possible to force gas-protein interactions at the active site, as has been shown for deoxyhaemoglobin at high nitrogen pressures. [5]

Of the noble gases, xenon appears to be the most useful probe of the hydrophobic pockets of PHD2, in part because: xenon has been shown to exhibit greater gas occupancy at hydrophobic sites than either krypton or argon, [6] can be directly observed by NMR through its stable ^{129}Xe and ^{131}Xe isotopes, [2] and is highly polarisable. [2] Xenon is particularly useful in NMR analysis of gas-protein interactions due to: the high sensitivity of xenon chemical shifts to changes in local environment and protein conformational states, [7] the relatively strong impact of xenon interactions on nearby ^{1}H, ^{15}N, and ^{13}C chemical shifts relative to those of other noble gases, [3] [8] the ability to probe exchange rates and binding affinities by examining xenon line widths, [2] the chemical shift differences between protein free and bound xenon resonances, [9] the site-specificity with which chemical shifts can be observed, [8] and the high degree of agreement between NMR results and those from X-ray crystallography. [9] Additionally, xenon chemical shifts alone have been found to be enough to infer xenon binding sites within a protein. [7] Future work may, thus, involve analysis of the anoxic PHD2:Fe(II):2OG and anoxic PHD2:Fe(II):2OG:CODD complexes under various xenon gas pressures using ^{129}Xe

NMR and $^{1}H,^{15}N$-HSQC NMR methods. Together these experiments may help to determine the number and types of gas binding pockets within the hydrophobic channels and active site of PHD2 as well as the residues directly interacting with gas molecules. These studies may provide new information on overall structural changes induced by gas binding, as it is notable that there are few studies on how nitrogen gas (N_2) interacts with enzymes (other than those directly producing or reacting with it) and the PHDs are candidates for such studies.

Noble gases are useful probes for the exploration of gas-protein interactions by NMR and other techniques but may not fully imitate the enzymatically relevant gas of interest (in this case, oxygen). An alternative approach may be to directly probe the interactions of PHD2 with oxygen at the active site and hydrophobic channels. For these studies, use of an inhibitor or catalytically inert metal ion will likely be required. As oxygen has been found to preferentially interact with hydrophobic regions of proteins, [10] [11] probing PHD2-oxygen interactions directly may provide useful clues into the slow reaction of PHD2 with oxygen. As with studies on noble gas / protein interactions, NMR may well be an ideal method for such research.

High pressure NMR techniques, with incremental increases in oxygen pressures, can lead to notable shifts or broadening in ^{1}H, ^{15}N, or ^{13}C resonances due to the paramagnetic effects of oxygen. [10] Paramagnetic effects induced by oxygen interaction with hydrophobic pockets within the protein may, however, be difficult to distinguish from pressure-induced structural changes, [11] [12] and oxygen interactions with protein residues may also be difficult to identify due to their transient nature [10] [11] [13] as well as the likely need for oxygen to adopt a preferential orientation within the hydrophobic region of interest to induce oxygen anisotropy for sufficient pseudocontact shifts. [13] When appropriately aligned, paramagnetic effects can be observed by NMR

for oxygen populations in the hydrophobic regions of the protein at as little as 1% occupancy. [10] With increasing oxygen pressures, shifts in the $^{1}H,^{15}N$-HSQC spectrum have been observed up to 1 ppm from the initial peak, with no significant changes at similar nitrogen or argon gas pressures, indicating that teasing out structural changes induced by gas pressure from those caused by paramagnetic oxygen may be viable for some proteins. [10] Similar large, selective peak shifts and broadening have been reported in the case of $^{1}H,^{15}N$-TROSY experiments (which can be treated similar to the $^{1}H,^{15}N$-HSQC spectrum for these purposes). [11]

Continuing from the research carried out in this thesis, $^{1}H,^{15}N$-HSQC experiments at variable oxygen pressures would be useful for probing the hydrophobic channel—and possibly active site—of PHD2 to better understand PHD2-oxygen interactions, with complimentary experiments carried out under various xenon and nitrogen gas pressures. These experiments may provide a basis from which further exploration into the slow reaction of oxygen with PHD2 may be explored as well as developing a useful tool for probing gas-protein interactions in general.

One drawback of the use of paramagnetic species in an NMR sample, as discussed previously in **Chapter 1, Section 1.2.5.1**, is the magnitude of paramagnetic relaxation enhancements (PREs) that may lead to severe broadening or complete loss of protein peaks. This may result in difficulties utilising paramagnets (like oxygen) as a probe to track paramagnet-residue interactions. This is especially prevalent when the species of interest—Fe and oxygen for the work in this thesis—are paramagnetic. One solution to this problem is the utilisation of pulse sequences that are designed to ameliorate the effects of paramagnetic relaxation.

An antiphase, inversion recovery $^{1}H,^{15}N$-HSQC (^{15}N-IR-HSQC-AP) is a novel method for suppressing the bulk of NMR signals in order to boost paramagnetically

relaxed signals. [14] The separation of paramagnetically relaxed signals from the bulk of signals occurs by inversion of longitudinal magnetisation along the -z direction, then separation of signals based on T1 relaxation as they equilibrate; paramagnetic signals will relax more quickly. To retain quickly relaxing signals during the coherence transfer step, compared to a standard $^{1}H,^{15}N$-HSQC pulse sequence, the length of insensitive nuclei enhanced by polarisation transfer (INEPT) is reduced. The refocusing step is then removed from the end of the pulse sequence to avoid further loss of quickly relaxing signals, and the resultant antiphase doublet is processed in dispersion mode to regain a pseudo-singlet. [14]

From this method, a $^{1}H,^{15}N$-HSQC spectrum that includes the paramagnetically broadened signals of interest can be obtained. This may be useful in the assignment and tracking of signals in regions of interest that interact with the catalytically relevant Fe(II)/Fe(III) or oxygen in the PHD2:Fe:2OG, PHD2:Fe:2OG:CODD, PHD2:Fe:2OG:O_2, or PHD2:Fe:2OG:CODD:O_2 complexes (see **Chapter 2**), especially at high oxygen concentrations, as has been discussed above. Further research into these essential paramagnetic species and their involvement in the slow reaction of oxygen with PHD2 is needed.

Observation of the shielded methyl region of PHD2 was a cornerstone of the research described in this thesis, as it provided new insight into the stability and conformational variability of various PHD2 complexes of interest (see **Chapter 2, Section 2.3**). PHD2 is unusual in that its structure involves a hydrophobic, shielded methyl patch directly below the proposed binding position of oxygen at the active site. This region of shielded methyl peaks, as described in **Chapter 2, Section 2.2.2.2.1** and **Section 2.3,** may be a useful reporter of changes at the PHD2 active site both due the methyl peaks' unique positions and due to the shielded methyl shifts falling outside of

the typical range of ^{1}H shifts: often below 0 ppm, in a region with no crowding. A computational method useful in predicting methyl ^{1}H chemical shifts of proteins, SHIFTX2, [15] was used for analysis of possible shielded methyls of PHD2 in this thesis (see **Chapter 2, Section 2.2.2.2.1**) but cannot predict resonances below 0 ppm. Further analysis of these peaks may involve assignment of the ^{1}H shielded methyl peaks by NMR.

Methyl ^{1}H chemical shifts are of interest in NMR analyses due to the frequency with which methyl groups are positioned in the hydrophobic core or complex interfaces of the protein, acting as key reporters of changes in structure and dynamics. [16] [17] Methods have been developed to capitalise on the unique features of methyl-containing residues for protein assignment work. In many of these studies, most of protons in the protein are deuterated, with ^{1}H protons being selectively located at methyl-containing residues of interest, with acquisition of ^{1}H-^{13}C correlations through various NMR techniques. [17]

Of the many pulse sequences available, experiments of interest include: 1) 3-D doubly sensitivity-enhanced ^{13}C-TOCSY-CHD_2 for correlation of the ^{1}H-^{13}C methyl resonances with ^{13}C resonances of the side chain for amino acid assignment and the related CHD_2-detected 2-D constant-time (CT) [^{1}H-^{13}C]-HSQC for everyday analysis, [16] 2) assignment of NOEs between methyls of ^{13}C-labelled protein with ^{12}C-labelled phenylalanine and tyrosine residues by ^{13}C-double filtered and ^{13}C-filtered edited experiments, which may give more site-selective information on shielded methyls (methyls adjacent to aromatic groups as labelled in this experimental design), [18] and 3) selective optimised flip angle short transient (SOFAST)-methyl-TROSY, which achieves greater signal to noise within a shorter timeframe than for methyl-TROSY acquisition for larger proteins, as adapted from the SOFAST-HMQC. [19] [20]

From methyl resonance assignment, greater certainty for site-specific effects from oxygen binding or paramagnetic Fe(II)/Fe(III) oxidation/reduction may be achieved, informing on PHD2-oxygen interactions.

6.1.2 WelO5

In **Chapter 3** of this thesis, early-stage studies concerning analysis of the dynamics and conformational flexibility of WelO5 were examined by NMR spectroscopy. Initial studies involved optimisation of $^{1}H,^{15}N$-HSQC sample conditions for 3-D experiments. On application of these optimisation steps to production and analysis of the ^{2}H-^{15}N-^{13}C triple-labelled protein, significant precipitation occurred, though enough of the sample was retained in solution for 3-D data acquisition. The results indicated that the 3D NMR peaks were strong enough for amino acid residue assignment, yet there was complete apparent loss of some peaks vital to the assignment steps. 3-D experiments were repeated after further protein stability optimisation and the resultant spectra gave strong signals yet still lacked peaks in positions vital to protein assignment (see **Chapter 3, Section 3.2.5**). Further analysis is needed to determine the cause of the apparent loss of these signals.

There are overall similarities between the proposed catalytic mechanism and active site coordination chemistry of WelO5 and PHD2 (see **Chapter 3, Figure 3.1**), but there are also key differences, hence comparison between the hydroxylase (PHD2) and halogenase (WelO5) enzymes is of interest. Initial comparative studies into the overlap of structural and dynamic properties of PHD2 and WelO5 yielded interesting results. Despite the larger size of the WelO5, the $^{1}H,^{15}N$-HSQC spectra of WelO5 gave sharper and more regularly shaped peaks than had been observed with PHD2 (see **Chapter 3**), possibly hinting at greater PHD2 dynamics. WelO5 was also shown to exhibit fewer chemical shifts and broadening due to changes in chemical/magnetic environment

compared to PHD2, most notably spectral changes were not observed when comparing the oxic and anoxic WelO5:Fe(II):2OG complexes. The shielded methyl region of WelO5 was found to be less informative than in the case of PHD2: with fewer peaks that are less responsive to changes in the chemical/magnetic environment. This may distinguish the characteristic properties of the PHD2:Fe(II):2OG on oxygen binding/interaction that is linked to the slow oxygen reaction.

As discussed previously, the halogenation activity of WelO5 may provide a useful tool for functionalisation during medicinal chemistry optimisation involving halogenation in order to improve metabolic and pharmacokinetic properties. [21] Despite the potential for WelO5-catalysed halogenation of drug molecules, the substrate specificity which non-heme iron halogenases—including WelO5—exhibit limits functionalisation to indole-alkaloid type substrates. [21] Mutagenesis has, therefore, been useful in both expanding the substrate scope of WelO5 and exploring further possibilities for functionalisation, including hydroxylation. [21] [22] [23] Understanding the details of the preference of WelO5 for catalytic halogenation over hydroxylation, and how the active site of WelO5 influences product structure, is essential to developing WelO5 as a tool for synthesis.

Future research on WelO5 may involve studies of mutants of interest—with respect to altered substrate and product selectivity—by NMR to understand their structure and function. The catalytic mechanism of WelO5 that has been selectively mutated at the active site residues I161A and G166D, as described in a recent PhD thesis, [23] produced modified products that are not halogenated. Further studies into the identities of these enzymatic products as well as the structurally and functionally unique properties of the mutant proteins by ^{1}H and $^{1}H,^{15}N$-HSQC NMR methods may provide new insight into the preference of WelO5 for halogenation over hydroxylation.

6.2 References

[1] C. Domene, C. Jorgensen and C. J. Schofield, "Mechanism of Molecular Oxygen Diffusion in a Hypoxia-Sensing Prolyl Hydroxylase Using Multiscale Simulation," *Journal of the American Chemical Society,* vol. 142, no. 5, p. 2253–2263, 2020.

[2] B. W. Roose, S. D. Zemerov and I. J. Dmochowski, "Xenon-Protein Interactions: Characterization by X-Ray Crystallography and Hyper-CEST NMR," *Methods in Enzymology,* vol. 602, pp. 249-272, 2018.

[3] L. Nisius, M. Stadler, H. R. Kalbitzer and E. Brunner, "NMR spectroscopic study of noble gas binding into the engineered cavity of HPr(I14A) from Staphylococcus carnosus," *Journal of Physical Chemistry B,* vol. 109, no. 38, pp. 17795-17798, 2005.

[4] N. Colloc'h, P. Carpentier, L. C. Montemiglio, B. Vallone and T. Prangé, "Mapping Hydrophobic Tunnels and Cavities in Neuroglobin with Noble Gas under Pressure," *Biophysical Journal,* vol. 113, no. 10, pp. 2199-2206, 2017.

[5] W. A. Gerth, "Nitrogen binding to deoxyhemoglobin at high pressures and its relation to changes in hemoglobin-oxygen affinity," *Journal of Biological Chemistry,* vol. 263, no. 27, pp. 13515-13521, 1988.

[6] M. L. Quillin, W. A. Breyer, I. J. Griswold and B. W. Matthews, "Size versus polarizability in protein-ligand interactions: binding of noble gases within engineered cavities in phage T4 lysozyme," *Journal of Molecular Biology,* vol. 302, no. 4, pp. 955-977, 2000.

[7] S. M. Rubin, S.-Y. Lee, E. J. Ruiz, A. Pines and D. E. Wemmer, "Detection and characterization of xenon-binding sites in proteins by 129Xe NMR spectroscopy," *Journal of Molecular Biology,* vol. 322, no. 2, pp. 425-440, 2002.

[8] R. Anedda, B. Era, M. Casu, A. Fais, M. Ceccarelli, M. Corda and P. Ruggerone, "Evidences of Xenon-Induced Structural Changes in the Active Site of Cyano-MetMyoglobins: A 1H NMR Study," *The Journal of Physical Chemistry B,* vol. 112, no. 49, p. 15856–15866, 2008.

[9] H. Desvaux, L. Dubois, G. Huber, M. L. Quillin, P. Berthault and B. W. Matthews, "Dynamics of Xenon Binding Inside the Hydrophobic Cavity of Pseudo-Wild-type Bacteriophage T4 Lysozyme Explored through Xenon-Based NMR Spectroscopy," *Journal of the American Chemical Society,* vol. 127, no. 33, p. 11676–11683, 2005.

[10] R. Kitahara, Y. Yoshimura, M. Xue, T. Kameda and F. A. A. Mulder, "Detecting O2 binding sites in protein cavities," *Scientific Reports,* vol. 6, p. 20534, 2016.

[11] T. Kawamura, T. Wakamoto, S. Kitazawa, S. Sakuraba, T. Kameda and R. Kitahara, "Analysis of O2-binding Sites in Proteins Using Gas-Pressure NMR Spectroscopy: Outer Surface Protein A," *Biophysical Journal,* vol. 112, no. 9, pp. 1820-1828, 2017.

[12] M. Sakakura, S. Noba, P. A. Luchette, I. Shimada and R. S. Prosser, "An NMR Method for the Determination of Protein-Binding Interfaces Using Dioxygen-Induced Spin−Lattice Relaxation Enhancement," *Journal of the American Chemical Society,* vol. 127, no. 16, p. 5826–5832, 2005.

[13] T. S. Ulmer, I. D. Campbell and J. Boyd, "The Effects of Dissolved Oxygen upon Amide Proton Relaxation and Chemical Shift in a Perdeuterated Protein," *Journal of Magnetic Resonance,* vol. 157, no. 2, pp. 181-189, 2002.

[14] I. B. Trindade, M. Invernici, F. Cantini, R. O. Louro and M. Piccioli, "PRE-driven protein NMR structures: an alternative approach in highly paramagnetic systems," *The FEBS Journal,* vol. 288, no. 9, pp. 3010-3023, 2020.

[15] B. Han, Y. Liu, S. W. Ginzinger and D. S. Wishart, "SHIFTX2: significantly improved protein chemical shift prediction," *Journal of Biomolecular NMR,* vol. 50, no. 1, p. 43–57, 2011.

[16] R. Otten, B. Chu, K. D. Krewulak, H. J. Vogel and F. A. A. Mulder, "Comprehensive and Cost-Effective NMR Spectroscopy of Methyl Groups in Large Proteins," *Journal of the American Chemical Society,* vol. 132, no. 9, p. 2952–2960, 2010.

[17] V. Tugarinov, V. Kanelis and L. E. Kay, "Isotope labeling strategies for the study of high-molecular-weight proteins by solution NMR spectroscopy," *Nature Protocols,* vol. 1, no. 2, pp. 749-754, 2006.

[18] N. K. Goto and L. E. Kay, "New developments in isotope labeling strategies for protein solution NMR spectroscopy," *Current Opinion in Structural Biology,* vol. 10, no. 5, pp. 585-592, 2000.

[19] C. Amero, P. Schanda, M. A. Durá, I. Ayala, D. Marion, B. Franzetti, B. Brutscher and J. Boisbouvier, "Fast Two-Dimensional NMR Spectroscopy of High Molecular Weight Protein Assemblies," *Journal of the American Chemical Society,* vol. 131, no. 10, p. 3448–3449, 2009.

[20] P. Schanda, Ē. Kupče and B. Brutscher, "SOFAST-HMQC Experiments for Recording Two-dimensional Deteronuclear Correlation Spectra of Proteins within a Few Seconds," *Journal of Biomolecular NMR,* vol. 33, p. 199–211, 2005.

[21] T. Hayashi, M. Ligibel, E. Sager, M. Voss, J. Hunziker, K. Schroer, R. Snajdrova and R. Buller, "Evolved Aliphatic Halogenases Enable Regiocomplementary C−H Functionalization of a Pharmaceutically Relevant Compound," *Angewandte Chemie International Edition,* vol. 58, no. 51, pp. 18535-18539, 2019.

[22] M. L. Matthews, C. S. Neumann, L. A. Miles and J. M. Bollinger, "Substrate positioning controls the partition between halogenation and hydroxylation in the aliphatic halogenase, SyrB2," *Proceedings of the National Academy of Sciences of the United States of America,* vol. 106, no. 42, pp. 17723-17728, 2009.

[23] E. Gallimore, *Evaluating the biocatalytic potential of a small molecule 2-oxoglutarate dependent halogenase,* University of Oxford, 2018.